SHAPING THE BRAIN BY NEURONAL CYTOSKELETON: FROM DEVELOPMENT TO DISEASE AND REGENERATION

EDITED BY: C. Laura Sayas, Monica Mendes Sousa and Jesus Avila

PUBLISHED IN: Frontiers in Cellular Neuroscience and
Frontiers in Molecular Neuroscience

frontiers Research Topics

ISSN 1664-8714
ISBN 978-2-88963-552-8
DOI 10.3389/978-2-88963-552-8

About Frontiers

Frontiers is more than just an open-access publisher of scholarly articles: it is a pioneering approach to the world of academia, radically improving the way scholarly research is managed. The grand vision of Frontiers is a world where all people have an equal opportunity to seek, share and generate knowledge. Frontiers provides immediate and permanent online open access to all its publications, but this alone is not enough to realize our grand goals.

Frontiers Journal Series

The Frontiers Journal Series is a multi-tier and interdisciplinary set of open-access, online journals, promising a paradigm shift from the current review, selection and dissemination processes in academic publishing. All Frontiers journals are driven by researchers for researchers; therefore, they constitute a service to the scholarly community. At the same time, the Frontiers Journal Series operates on a revolutionary invention, the tiered publishing system, initially addressing specific communities of scholars, and gradually climbing up to broader public understanding, thus serving the interests of the lay society, too.

Dedication to Quality

Each Frontiers article is a landmark of the highest quality, thanks to genuinely collaborative interactions between authors and review editors, who include some of the world's best academicians. Research must be certified by peers before entering a stream of knowledge that may eventually reach the public - and shape society; therefore, Frontiers only applies the most rigorous and unbiased reviews.
Frontiers revolutionizes research publishing by freely delivering the most outstanding research, evaluated with no bias from both the academic and social point of view. By applying the most advanced information technologies, Frontiers is catapulting scholarly publishing into a new generation.

What are Frontiers Research Topics?

Frontiers Research Topics are very popular trademarks of the Frontiers Journals Series: they are collections of at least ten articles, all centered on a particular subject. With their unique mix of varied contributions from Original Research to Review Articles, Frontiers Research Topics unify the most influential researchers, the latest key findings and historical advances in a hot research area! Find out more on how to host your own Frontiers Research Topic or contribute to one as an author by contacting the Frontiers Editorial Office: researchtopics@frontiersin.org

SHAPING THE BRAIN BY NEURONAL CYTOSKELETON: FROM DEVELOPMENT TO DISEASE AND REGENERATION

Topic Editors:
C. Laura Sayas, University of La Laguna, Spain
Monica Mendes Sousa, University of Porto, Portugal
Jesus Avila, Severo Ochoa Molecular Biology Center (CSIC-UAM), Spain

Citation: Sayas, C. L., Sousa, M. M., Avila, J., eds. (2020). Shaping the Brain by Neuronal Cytoskeleton: From Development to Disease and Regeneration. Lausanne: Frontiers Media SA. doi: 10.3389/978-2-88963-552-8

Table of Contents

frontiers in Cellular Neuroscience

EDITORIAL
published: 31 January 2020
doi: 10.3389/fncel.2020.00012

Editorial: Shaping the Brain by Neuronal Cytoskeleton: From Development to Disease and Degeneration

Jesús Avila[1,2], *Monica M. Sousa*[3] *and Carmen Laura Sayas*[4]*

[1] Centro de Biología Molecular "Severo Ochoa" (CSIC-UAM), Universidad Autónoma de Madrid, Madrid, Spain, [2] Centro de Investigación Biomédica en Red de Enfermedades Neurodegenerativas (CIBERNED), Madrid, Spain, [3] Nerve Regeneration Group, Instituto de Biologia Molecular e Celular-IBMC and Instituto de Inovação e Investigação em Saúde, Universidade Do Porto, Porto, Portugal, [4] Departamento de Ciencias Médicas Básicas, Instituto de Tecnologías Biomédicas (ITB), Universidad de La Laguna (ULL), Tenerife, Spain

Keywords: neuronal cytoskeleton, astrocyte cytoskeleton, microtubules (MTs), actin cytoskeleton, tau, neuron

Editorial on the Research Topic

Shaping the Brain by Neuronal Cytoskeleton: From Development to Disease and Degeneration

The brain is the most complex organ in nature, which receives and process external information and controls most body vital functions. Brain functional complexity correlates with an intricate architecture formed by networks of millions of neurons and supporting glial cells. Achieving and maintaining these complicated structures relies on the coordinated action and reorganization of the different cytoskeletal filaments that conform the brain cytoskeleton. In this Frontiers Research Topic, we present a selection of reviews, opinion, and original research articles mainly focused on the diverse and key roles of actin and tubulin cytoskeleton in neuronal biology, from neuronal migration, and differentiation during development to axon diameter regulation or dendritic spine formation and plasticity. The role of microtubular proteins in neurodegeneration and the potential therapeutic action of cytoskeletal stabilizers in different brain disorders is also discussed. The function of cytoskeleton in astrocytes biology is further reviewed.

OPEN ACCESS

Edited and reviewed by:
Enrico Cherubini, European Brain Research Institute, Italy

***Correspondence:**
Carmen Laura Sayas
csayasca@ull.edu.es

Specialty section:
This article was submitted to Cellular Neurophysiology, a section of the journal Frontiers in Cellular Neuroscience

Received: *30 December 2019*
Accepted: *15 January 2020*
Published: *31 January 2020*

Citation:
Avila J, Sousa MM and Sayas CL (2020) Editorial: Shaping the Brain by Neuronal Cytoskeleton: From Development to Disease and Degeneration. Front. Cell. Neurosci. 14:12. doi: 10.3389/fncel.2020.00012

ROLES OF ACTIN AND TUBULIN CYTOSKELETON IN NEURONAL BIOLOGY

Actin Cytoskeleton

Actin-Spectrin Skeleton and Axon Diameter

The nerve impulse is transmitted along neuronal axons. Axon diameter, which influences the transmission of electric signals, varies depending on different aspects such as neuronal type, organelles distribution, activation state of the neuron, or circumferential tension and contractility. Changes in axon caliber rely on axonal cytoskeleton. Costa et al. review here the current knowledge on the molecular mechanisms involved in the regulation of axon diameter, with special focus on the role of the actin-spectrin-based membrane periodic skeleton and non-muscle myosin II present in axons. They summarize the known contribution of different factors to the regulation of axon tension and contractility, including adducin -an actin capping protein-, Ca^{2+} levels, or activity-dependent mechanisms. Authors emphasize that the development of novel cell biology tools, such as new actin probes, state-of-the-art live imaging and super-resolution microscopy, has made possible the discovery of these previously unidentified actin rings. They highlight that this periodic actin-spectrin cytoskeleton is more dynamic than initially expected and might play important roles in the maintenance of neuronal architecture and function.

Actin Cytoskeleton and Dendritic Spines: From Long-term Learning to ASD

Dendritic spines are small actin-rich dendritic protrusions where the postsynaptic part of most excitatory synapses is located. Spine density, morphology, and size are crucial for learning and long-term memory acquisition and consolidation. Basu and Lamprecht review the role of actin in dendritic spine formation and stabilization during these processes. Based on published observations, the authors further propose a model to describe how actin and its regulatory proteins, with relatively short half-lives and fast dynamics, might contribute to the stabilization of dendritic spine morphology. They focus on different molecular mechanisms that lead to the reduction of actin dynamics and to the formation of a stable actin cytoskeleton scaffold in spines that contribute to preserve and consolidate long-term memory.

Changes in dendritic spine shape, number and size also underly synaptic perturbations that occur during the pathogenesis of neuropsychiatric disorders such as autism spectrum disorder (ASD). Here Hlushchenko et al. investigate how different actin regulators that had been related to ASD contribute to the regulation of dendritic spine morphology and density as well as to the size, density, and localization of inhibitory synapses. For this purpose, authors induced ASD-associated *de novo* missense mutations in five actin-regulatory proteins and analyzed the subcellular localization and the effects of the overexpressed wild-type and mutated proteins on dendritic spines and inhibitory synapses. They showed that ASD-associated mutations in actin regulators induce significant alterations in dendritic spine morphology, leading to a shift from mushrooms to thin spines, and promote variable changes in inhibitory synapses.

Microtubules (MTs)

MT Reorganization During CNS Development

Neurons are highly polarized cells with a complex architecture that is accomplished through dramatic morphological changes during development. Achieving and maintaining neuronal morphology is crucial for the proper functioning of Central Nervous System (CNS). Microtubular cytoskeleton plays crucial roles during neuronal development, supporting stem cell proliferation and neuronal migration, contributing to neuronal differentiation, axon guidance and dendrite arborization, and providing structural integrity to maintain neuronal connections once formed. The participation of MTs and their interacting regulatory proteins in neuronal development is analyzed in different articles of this Research Topic. The contribution by Sayas et al. concerns the roles of neuronal CLASPs, which are MT plus-end tracking proteins (+TIPs), during neuronal differentiation. By using stable neuroblastoma cell lines deficient in either CLASP1 or CLASP2 and primary hippocampal neurons from CLAS2-KO mice, authors show that CLASP1 and CLASP2 have opposite roles during neurite and axon extension. Their data point to CLASPs participation in different feedback loops that control the signaling of upstream kinases. In their article, Gorelik et al., investigate the relationship between Rac1, a well-known regulator of actin and tubulin cytoskeletons, and the C3 complement molecule, which belongs to the innate immune system, during brain development. By using C3 deficient mice, authors show the effects of C3 on Rac1 activity, and on the phosphorylation state of cofilin, one of its downstream effectors. Based on their data, authors point to Rac1 GTPase as an important signaling mediator downstream of complement activation in the developing mouse brain. Here, Xu et al. identify a new interaction between the ion and metabolite channel Pannexin 1(Panx1) and the MT regulator CRMP2 and suggest that this interaction might inhibit neuritogenesis. The authors describe how probenecid, a Panx1 inhibitor, disrupts the Panx1-CRMP2 interaction and further propose that released CRMP2 promotes MT polymerization, stabilization and bundling, thereby inducing neurite extension. The review of Lasser et al. synthesizes a broad range of research on the role of MT cytoskeleton in neuronal development, focusing on mutations that affect different tubulin isotypes and microtubular regulators, leading to the pathogenesis of several neurodevelopmental disorders, such as ASD, microcephaly, polymicrogyria, lyssencephaly, and intellectual disabilities.

MT-Stabilizing Drugs as Potential Therapeutic Agents for Brain Disorders

In mature neurons, MTs play fundamental roles in the maintenance of neuronal architecture and intracellular transport of cargoes. Since neuronal axons can be 1 m long, maintaining proper transport is crucial for neuronal viability. Neurons are thus particularly susceptible to MT defects, which are involved in the pathogenesis of several brain disorders. The article by Varidaki et al. reviews published data on MT-stabilizing agents used as chemotherapies to treat cancer and the efforts being made to reposition them as potential treatments for neurodegenerative and psychiatric disorders. The authors outline the brain penetrance properties and side effects of different MT-targeting agents, and finish by summarizing the underway current clinical trials to evaluate the potential therapeutic potential of these compounds in the treatment of different brain disorders. MTs are also involved in the adaptive plasticity response of damaged neurons and glial cells upon traumatic brain injury (TBI). In this collection, Chuckowree et al. evaluate the potential therapeutic effects of a brain-penetrant MT-stabilizing agent, epothilone D, in a clinically relevant model of mild TBI (mTBI) in mice. Unexpectedly, they found that epothilone D induces alterations in dendritic spines, leading to a reduction in spine length and an increase in mushroom spine density, with no obvious effects on astroglial response, and axonal pathology. They propose to investigate further the possible use of MT-stabilizing drugs as potential therapeutic agents against TBI.

Tau Protein, Neurodegeneration, and Neuroprotection

In the present Research Topic, different articles focus on tau protein, a structural neuronal MT-associated protein (MAP) that induces MT polymerization and stabilization and plays crucial roles in several neurodegenerative disorders, including Alzheimer's disease (AD), and other tauopathies.

Using biochemical and immunohistochemical assays, Ritter et al. analyze the localization of human N279K tau, a mutation highly prevalent in a tauopathy named frontotemporal dementia with parkinsonism-17 (FTDP-17), finding that the mutant tau localizes more prominently in the nucleus than wild type tau protein. Moosecker et al. investigate the molecular mechanisms through which pioglitazone (Pio), a pharmacological agonist of the peroxisome proliferator activated receptor g (PPARg), might prevent AD symptoms by reducing synaptic malfunction and loss. The authors show that Pio reduces amyloid precursor protein (APP) processing and tau hyperphosphorylation and missorting to synapses and the subsequent synaptic loss. They conclude that activated PPARg exerts neuroprotection by acting on Aβ and tau. In an opinion article, Gozes et al. discuss their findings on the neuroprotective actions of Activity-Dependent Neuroprotective Protein (ADNP) and its derived peptide, NAP, through NAP binding to tau and EBs (a MT protein from the +TIP family). Authors finish their article commenting on the ADNP syndrome, a type of ASD (neurodevelopmental disorder) induced by *de novo* mutations in ADNP, and the use of NAP as a potential treatment. Finally, in an up-to-date review, Alonso et al. discuss how tau phosphorylation affects tau function, changing it from a MT stabilizer to a MT disrupter, contributing to tau prion-like nature and leading to tau aggregation and its eventual involvement in neurodegenerative diseases such as AD and other tauopathies.

ROLES OF CYTOSKELETON IN ASTROCYTE BIOLOGY

Astrocytes, the most abundant glial cells with several key roles in CNS, possess also a highly intricate architecture that varies in response to different physiological and pathological conditions. In this collection, Schiweck et al. summarize current knowledge about the mechanisms that regulate changes in astrocyte morphology during CNS development, injury and disease, with special focus on cytoskeleton rearrangement. The authors start by reviewing how astrocytes acquire their complex star-like shape during development and then they describe how astrocytes modulate the formation and activity of synapses in mature CNS, through their perisynaptic astrocytic processes (PSPs). The article finishes reviewing how astrocytes undergo dramatic shape changes and become "reactive" upon astrogliosis that occur in response to pathological conditions such as traumatic brain injury or degenerative disorders.

AUTHOR CONTRIBUTIONS

JA, MS, and CS read all the articles to confirm their quality and interest for the present Research Topic. JA, MS, and CS then sent them out for assessment by expert reviewers, and made final decisions for publication, based on reviewers comments. CS wrote the editorial article. JA and MS revised it and gave their feedback comments.

Conflict of Interest: The authors declare that the research was conducted in the absence of any commercial or financial relationships that could be construed as a potential conflict of interest.

frontiers in Molecular Neuroscience

MINI REVIEW
published: 01 May 2018
doi: 10.3389/fnmol.2018.00143

The Role of Actin Cytoskeleton in Dendritic Spines in the Maintenance of Long-Term Memory

*Sreetama Basu and Raphael Lamprecht**

Sagol Department of Neurobiology, Faculty of Natural Sciences, The Integrated Brain and Behavior Research Center, University of Haifa, Haifa, Israel

Evidence indicates that long-term memory formation involves alterations in synaptic efficacy produced by modifications in neural transmission and morphology. However, it is not clear how such alterations induced by learning, that encode memory, are maintained over long period of time to preserve long-term memory. This is especially intriguing as the half-life of most of the proteins that underlie such changes is usually in the range of hours to days and these proteins may change their location over time. In this review we describe studies that indicate the involvement of dendritic spines in memory formation and its maintenance. These studies show that learning leads to changes in the number and morphology of spines. Disruption in spines morphology or manipulations that lead to alteration in their number after consolidation are associated with impairment in memory maintenance. We further ask how changes in dendritic spines morphology, induced by learning and reputed to encode memory, are maintained to preserve long-term memory. We propose a mechanism, based on studies described in the review, whereby the actin cytoskeleton and its regulatory proteins involved in the initial alteration in spine morphology induced by learning are also essential for spine structural stabilization that maintains long-term memory. In this model glutamate receptors and other synaptic receptors activation during learning leads to the creation of new actin cytoskeletal scaffold leading to changes in spines morphology and memory formation. This new actin cytoskeletal scaffold is preserved beyond actin and its regulatory proteins turnover and dynamics by active stabilization of the level and activity of actin regulatory proteins within these memory spines.

Keywords: actin cytoskeleton, dendritic spines, long term memory, memory maintenance, structural plasticity, neuronal morphology

OPEN ACCESS

Edited by:
C. Laura Sayas,
Universidad de La Laguna, Spain

Reviewed by:
Jacek Jaworski,
International Institute of Molecular and Cell Biology in Warsaw (IIMCB), Poland
Christian Gonzalez-Billault,
Universidad de Chile, Chile

****Correspondence:***
Raphael Lamprecht
rlamp@research.haifa.ac.il

Received: *08 December 2017*
Accepted: *09 April 2018*
Published: *01 May 2018*

Citation:
Basu S and Lamprecht R (2018) The Role of Actin Cytoskeleton in Dendritic Spines in the Maintenance of Long-Term Memory. Front. Mol. Neurosci. 11:143. doi: 10.3389/fnmol.2018.00143

Evidence suggests that long-term memory is formed by enduring alterations in synaptic efficacy and connectivity between neurons (Konorski, 1948; Hebb, 1949; Dudai, 1989; Bliss and Collingridge, 1993; Martin et al., 2000; Tsien, 2000; Kandel, 2001; Lamprecht and LeDoux, 2004; Caroni et al., 2012; Bailey et al., 2015). However, it is not clear how such changes induced by learning that encode memory are maintained over long period of time to preserve long-term memory especially since the half-life of the proteins that underlie such changes is relatively short (Hanus and Schuman, 2013; Alvarez-Castelao and Schuman, 2015) and these proteins may change their location over time. In this review we will explore the roles of dendritic spines in long-term memory maintenance and examine the possibility

that morphological changes that are induced by learning and that are hypothesized to encode memory are maintained to preserve long-term memory without significant decay. We will further describe how the actin cytoskeleton may be involved in preserving the morphology of dendritic spines after learning to maintain long-term memory.

SPINE MORPHOLOGY AFFECTS NEURONAL FUNCTION

Dendritic spines receive excitatory synaptic inputs and confine local synaptic signaling and the diffusion of postsynaptic molecules (Nimchinsky et al., 2002; Lamprecht and LeDoux, 2004; Newpher and Ehlers, 2009; Nishiyama and Yasuda, 2015). Alterations in spine morphology may be involved in neuronal functions that subserve memory formation. For example, it was revealed that spines with large postsynaptic densities (PSDs) tend to have a higher level of α-amino-3-hydroxy-5-methyl-4-isoxazolepropionic acid receptors (AMPARs) than spines with smaller PSDs (e.g., Takumi et al., 1999). Since the area of PSDs is correlated with that of the dimensions of the spine head (Harris and Stevens, 1989), it is implied that spines with larger head express more glutamate receptors than spines with smaller head. In addition, a study found a correlation between the amplitudes of currents in the spine and the spine head volume showing that the distribution of functional AMPARs is approximately proportional to the spine head volume (Noguchi et al., 2011). Thus, synaptic efficacy mediated by AMPA receptors is correlated with spine head volume from silent synapses in small spines to highly responsive larger spines. AMPA receptors trafficking into the synapse is involved in memory formation. For example, fear conditioning drives glutamate receptor 1 (GluA1)-containing AMPARs into synapses in lateral amygdala (LA) neurons (Rumpel et al., 2005; Yeh et al., 2006; Nedelescu et al., 2010; Ota et al., 2010). Moreover, fear memory is impaired if GluA1-AMPAR insertion is blocked (Rumpel et al., 2005).

The geometry of the spine neck may also affect synaptic efficacy. Spine neck plasticity appears to mainly affect local voltage amplification in spines and biochemical compartmentalization, such as of Ca^{2+}, within the spine head (Noguchi et al., 2005) that may affect signal transduction and bidirectional diffusion of material from dendrite to spines (Bloodgood and Sabatini, 2005; Gray et al., 2006; Santamaria et al., 2006). Spines with longer thinner spine necks confine more molecules. Thus, changes in spine neck may affect synaptic efficacy and also neuronal function (Araya et al., 2006, 2014). For example, spines with long neck have small somatic voltage contributions. Synaptic stimulation paired with postsynaptic activity can lead to shortening of spines necks and to change in the input/output gain of pyramidal neurons and to increase in synaptic efficacy (Araya et al., 2014).

LEARNING LEADS TO SPINES MORPHOGENESIS

It has been shown that changes in dendritic spines morphology and number are associated with memory formation (Lamprecht and LeDoux, 2004; Bailey et al., 2015). For example, contextual fear conditioning leads to an increase in the density of dendritic spines in hippocampal CA1 and the anterior cingulate cortex (Restivo et al., 2009; Vetere et al., 2011). Auditory fear conditioning increases the rate of spines elimination in layer-V pyramidal neurons in the mouse frontal association cortex whereas fear extinction induces spines formation in this brain region (Lai et al., 2012). Fear conditioning leads to an increase in postsynaptic density (PSD) area in smooth endoplasmic reticulum (sER)-free spines and to decrease in spines head volume in LA (Ostroff et al., 2010). Intense training with high footshock during inhibitory avoidance, that induced higher resistance to extinction and thus suggests an enhanced learning, led to an increase in mushroom shaped spines along with a decrease in thin spines in the dorsomedial striatum (Bello-Medina et al., 2016). Auditory fear conditioning leads to increase in pathway-specific formation of LA axons boutons in auditory cortex (ACx), dendritic spines of pyramidal cells in layer 5 of ACx, and putative LA–ACx synaptic pairs (Yang et al., 2016).

SPINES STABILITY AND LONG-TERM MEMORY

A key question that arises from the above observations is whether spines formation and morphogenesis induced by learning are stable for a long period of time to maintain long-term memory. Evidence indicates that this may be the case. First, there are ample observations showing that spines are stable for days to years. For example, the structure of dendritic spines is stable for days in cultured hippocampal slices (De Roo et al., 2008) and for years in the cortex *in vivo* (Grutzendler et al., 2002; Trachtenberg et al., 2002; Zuo et al., 2005). Second, spine stability is associated with long-term memory persistence. For example, a fraction of newly formed spines persist over weeks and the amount of stable spines correlates with performance after learning (Yang et al., 2009). New dendritic spines are grown following training for a forelimb reaching task and are preferentially stabilized by subsequent training sessions (Xu et al., 2009). Acquired motor task is disrupted by post learning optical activation of Rac1 GTPase and shrinkage of the learning-potentiated spines a day after training indicating that preserving the spines morphology is necessary for memory maintenance and that their shrinkage leads to memory erasure (Hayashi-Takagi et al., 2015). Interfering with actin cytoskeleton polymerization in basolateral amygdala complex (BLC) during the maintenance phase of conditioned place preference (CPP) memory led to the impairment in maintenance of CPP memory and to decrease in spines density in BLC suggesting that dendritic spines persistence supports the maintenance of the memory trace (Young et al., 2014).

The above observations show that spines are formed by learning and last for days to weeks and potentially more after behavioral training and that disruption in spines morphology after memory consolidation is associated with impairment in memory maintenance suggesting that spines persistence is essential for memory maintenance. However, it is not clear how these spines are stabilized in the face of the short life and dynamics of the molecules that build them. Below we

suggest that the actin cytoskeleton which is intimately involved in spine formation and morphogenesis also stabilizes its structure under certain conditions, a stabilization that is necessary for maintaining long-term memory.

ACTIN CYTOSKELETON IS INVOLVED IN SPINE MORPHOGENESIS AND MEMORY FORMATION

Actin and Spine Morphology

Actin cytoskeleton is involved in the morphogenesis of dendritic spines. Mature spines contain a mixture of branched and linear actin filaments at their base, neck, and head. The spine neck contains both linear and branched filaments whereas branched actin filament network is a dominant feature of the spine head (Korobova and Svitkina, 2010). The actin cytoskeleton is intimately involved in the formation and elimination, stability, motility, and morphology of dendritic spines (Halpain et al., 1998; Matus, 2000; Schubert and Dotti, 2007; Honkura et al., 2008; Hotulainen and Hoogenraad, 2010; Chazeau et al., 2014). The shape and dynamics of mature spines are regulated by two distinct pools of actin filaments (Honkura et al., 2008). The stable pool of F-actin has a turnover rate of minutes and is mainly found at the base of the spine head whereas the dynamic pool has a turnover rate of seconds. It is suggested that the volume of spines is maintained actively and continuously by an exact balance between the pressure generated by the surrounding tissue and the expansive force created by the dynamic F-actin pool. Changes in spine structure depend on actin polymerization. For example, spine head enlargement by glutamate stimulation is dependent on actin polymerization (Matsuzaki et al., 2004).

In addition to stabilization of spine head morphology actin may be involved also in spine neck stabilization. A biophysical model suggests that constriction of the spine neck assists in the stabilization of spines, thus pointing to a role in stabilization and maintenance of ring-like F-actin structures that are consistently found in spine neck (Miermans et al., 2017).

Actin cytoskeleton polymerization, depolymerization and branching leading to changes in spine morphology are closely controlled by small GTPases Rac1, Cdc42 and Rho GTPases and their downstream effectors such as Arp2/3 and formins (e.g., Luo, 2000; Woolfrey and Srivastava, 2016). These actin regulatory proteins are functionally linked with synaptic receptors, such as glutamate receptors, Eph receptors, and adhesion molecules (e.g., cadherin), that participate in spine morphogenesis and memory formation (e.g., Woolfrey and Srivastava, 2016). In addition, actin filaments dynamics may be also coupled with microtubules dynamics for temporal and local regulation of dendritic spines (Shirao and González-Billault, 2013).

Actin and Memory

It has been shown that actin cytoskeleton is essential for memory formation. Interfering with proper actin cytoskeleton polymerization impairs the formation of long-term memory (e.g., Mantzur et al., 2009; Rehberg et al., 2010; Gavin et al., 2011). Moreover, regulation of actin polymerization is important for spine morphology and memory formation. For example, deletion of the actin filament depolymerizing protein n-cofilin or its regulator LIM kinase (LIMK-1) leads to alterations in spines morphology, synaptic plasticity and learning and memory (Meng et al., 2002; Rust et al., 2010). In addition, interfering with cofilin function impaired spines shrinkage induced by LTD and memory extinction (Zhou et al., 2004; Wang et al., 2013). In addition, actin-regulatory proteins that control actin filaments network and affect spine morphology are also involved in memory formation. For example, the WAVE isoforms (WAVE-1, WAVE-2, and WAVE-3) allow the assembly of multiprotein complexes that include regulatory proteins that affect actin structure and branching (e.g., Arp2/3) (Pollard, 2007; Takenawa and Suetsugu, 2007; Pollitt and Insall, 2009). This Wave Regulatory Complex (WRC) is functionally linked to synaptic receptors to affect actin cytoskeleton and spine morphology. For example, BDNF signaling may activate Rac1, that in turn leads to relocation of CYFIP1 (cytoplasmic FMRP-interacting protein 1) to affect the WRC, actin cytoskeleton and spine morphology (De Rubeis et al., 2013). Loss of WAVE-1 reduces spines density and leads to impairment in Morris water maze memory retention (Soderling et al., 2007). Arp2/3 is concentrated in spines and is needed for spine head growth and for activity-dependent spine enlargement (Kim et al., 2006, 2013; Rácz and Weinberg, 2008; Wegner et al., 2008; Hotulainen et al., 2009). Deletion of ArpC3, an essential Arp2/3 subunit, leads to defects in actin turnover in spine and spine formation and morphology (Kim et al., 2013). ArpC3f/f:CamKIIα-Cre mice are impaired in Y-maze (working memory) and novel object recognition (episodic memory) tests. Inhibition of Arp2/3, in LA during auditory fear conditioning impaired the formation of long-term, but not short-term, fear memory (Basu et al., 2016).

Thus, actin cytoskeleton and its regulatory proteins are involved in spine morphogenesis and memory formation. However, for memory to persist these structural changes need to be maintained over long-period of time. Can actin cytoskeleton maintain long-lasting changes in spine morphogenesis observed after learning?

EVIDENCE FOR A ROLE FOR ACTIN CYTOSKELETON AND ITS REGULATORY PROTEINS IN MAINTAINING SPINE MORPHOLOGY AND MEMORY

There are several observations that show that actin and its regulatory proteins are involved in maintaining spines morphology and the persistence of long–term memory. The maintenances of long-term conditioned place preference (CPP) memory, formed through association with methamphetamine (METH), is impaired by infusion of Latrunculin A (LatA), into basolateral amygdala complex (BLC) 2 days after training (Young et al., 2014) (LatA prevents the incorporation of G-actin into dynamic F-actin, Morton et al., 2000). Inhibition of non-muscle myosin II also impaired CPP memory maintenance. The investigators further revealed that spines density in BLC increased with CPP training and that LatA infusion into BLC

2 days following training reduced spines density in CPP-paired animals, with no effect on spines in control animals. Thus, the study implies that maintenance of memories is supported by a constitutive cycling of filament actin that maintains spine stability.

Actin regulatory proteins are also involved in maintaining long-term memory. Activation of Rac1, a GTPase that affects actin regulatory proteins, in activated synapses in motor cortex leads to spine shrinkage (Hayashi-Takagi et al., 2015). Activation of Rac1 a day after training also impaired motor task memory. Since activation of Rac1 leads to disruption of actin cytoskeleton and spine shrinkage (Hayashi-Takagi et al., 2015) the study indicates that the integrity of spines structure is important for maintaining motor task memory. In this context it is worth noting that loss of Rac1 leads to increase in mean PSD length and mean spine head area and impairment in working/episodic-like memory in the delayed matching-to-place (DMP) task (Haditsch et al., 2009). Thus, alteration in Rac1 activity leads to abnormal spine morphology and affects memory formation and maintenance.

Rac1 is also involved in forgetting. Inhibition of Rac1 activity in hippocampal neurons form extended object recognition memory and impairs the forgetting of contextual fear memory (Jiang et al., 2016; Liu et al., 2016). Rac1 activation on the other hand accelerated memory decay within 24 h. Moreover, expression of active Rac1 produced more lamellipodia-like synapses with a large spine head and overexpression of Rac1-DN led to a reduced spine density, with more long and thin filopodia-like spines. Activation of Rac1 in LA impaired long- but not short-term memory formation (Das et al., 2017). In Drosophila, Rac1 also mediates forgetting (Shuai et al., 2010; Dong et al., 2016).

Cdc42 is also involved in synaptic and structural plasticity of spines and in memory formation (Kim et al., 2014; Hedrick et al., 2016). Cdc42 cKO affects spine morphology, synaptic plasticity, and remote memory in mice (Kim et al., 2014). Cdc42 is also implicated in forgetting. Single-session training of Drosophila leads to anesthesia-resistant memory (ARM) formation and Cdc42 activation. Repeated learning extends ARM by inhibition of Cdc42-mediated forgetting. Inhibition of Cdc42 prolongs ARM retention and increased Cdc42 activity abolishes repetition-induced ARM extension (Zhang et al., 2016).

Forgetting is also regulated by Arp2/3 complex in C. elegans (Hadziselimovic et al., 2014). Upregulation of the Arp2/3 complex in AVA interneuron prevents forgetting. In contrast, downregulation of the Arp2/3 complex accelerates forgetting. Interestingly, it was shown that ArpC3 is needed for maintaining normal spine morphology in mice as ArpC3 deletion has no effect on spines morphology 1–2 weeks after ArpC3 knock down but at the 4 and 8 weeks time points the fraction of mushroom type spines decreased while filopodia-like spines increased in dendrites from ArpC3 KO compared to control (Kim et al., 2013).

Profilin is an actin regulatory protein that can mediate stabilization of spine morphology (Ackermann and Matus, 2003; Michaelsen et al., 2010; Michaelsen-Preusse et al., 2016). Profilin is translocated into dendritic spines after various stimulation such as stimuli leading to LTP or LTD and NMDA receptors stimulation (Ackermann and Matus, 2003; Michaelsen et al., 2010; Bosch et al., 2014; Michaelsen-Preusse et al., 2016). Profilin translocation into spines starts minutes after stimulation and lasted for many hours leading to suppression of actin dynamics and stabilization of spine morphology. Profilin–G-actin complex binds to VASP through its poly-proline segment ($G(GP_5)_3$) (Reinhard et al., 1995; Ferron et al., 2007) and such binding is needed for glutamate-induced translocation of profilin into spines and for consolidation and stabilization of spine morphology (Ackermann and Matus, 2003). It has been shown that fear conditioning leads to the translocation of profilin into dendritic spines in LA (Lamprecht et al., 2006) and that these profilin-containing spines in LA are larger than spines that do not contain profilin. Microinjection of $G(GP_5)_3$, that binds profilin and thus competes with its binding to VASP, but not the control peptide $G(GA_5)_3$, impaired the formation of long- but not short-term fear memory in LA (Basu et al., 2016). These results indicate that VASP-profilin binding in LA is essential for the formation of long-term fear memory. Moreover, it suggests that profilin translocation into spines, that leads to suppression of actin dynamics and stabilization of spine structure (Ackermann and Matus, 2003), is essential for the formation of long-term fear memory in LA.

The above observations indicate that the actin cytoskeleton and its regulatory proteins are involved in spine stabilization and in the maintenance of long-term memory. However, it is not clear how actin preserves spine stability that may mediate the maintenance of long-term memory. This is especially puzzling in light of the relatively short half-life of actin and its regulatory proteins and in the fast dynamic of the actin cytoskeleton and associated proteins network that support spine morphology.

A MODEL FOR ACTIN CYTOSKELETON MAINTENANCE OF SPINE STRUCTURE AND LONG-TERM MEMORY

The above observations indicate that spines morphogenesis followed by their stabilization are involved in long-term memory formation and maintenances, respectively. Moreover, the actin cytoskeleton and its regulatory proteins are involved in spine morphogenesis and stabilization and in memory consolidation and maintenances. However, these observations beg the question: How spine structure stability involved in memory maintenance last beyond actin and its regulatory proteins turnover and dynamics to preserve enduring memories? Below are observations that collectively form a model to describe the function of actin cytoskeleton in spine stabilization and memory endurance.

The model includes two aspects that interact with each other- the spontaneous activation of glutamate receptor during the maintenance phase of memory to reduce actin dynamic and to tag the memory trace spines for delivery of proteins and mRNAs into spines and the maintenance of the actin network in spines in a steady state structure to preserve spines morphology.

Spontaneous Glutamate Activity Maintains Actin Structure, Spine Morphology and Memory

It has been shown that actin dynamics in spines and actin-based protrusive activity from the spine head are potently inhibited by activation of either AMPA or NMDA receptors (Fischer et al., 2000). This blockade of motility causes spines to round up and to be more stable and regular. The authors further show results suggesting that low-voltage-activated Ca^{2+} channels mediate the inhibitory effects of AMPARs on actin dynamics in spine. The effect on reduction of actin dynamics could be mediated by Ca^{2+}-responsive actin binding proteins. The authors suggest two distinct types of morphological plasticity in spines, the first leading to formation of new spines by stimulation such as LTP operating through NMDA receptors, and a second where AMPAR activation at established synapses stabilizes spine morphology. The differential involvement of glutamate in various stages of synapse formation may be related to the different conditions appropriate for spine formation and morphogenesis and for those required for spines maintenance. For example, newly formed synapses may exhibit only NMDA receptor-mediated currents followed by insertion of AMPA receptors (Liao et al., 1999; Petralia et al., 1999). As mentioned above learning leads to the insertion of AMPA receptors into synapses (e.g., Rumpel et al., 2005). Maintenance of established spine structure is suggested to require continual activation of AMPA receptors involving miniature synaptic events resulting from spontaneous vesicle fusion to prevent spine loss in the absence of action potentials (McKinney et al., 1999). Thus, miniature synaptic events at specific spines where responses to glutamate is enhanced during learning (e.g., by insertion of AMPA receptors) may lead to the maintenance of dendritic spines and their morphology needed for the persistence of long-term memory. Indeed, increase in miniature synaptic events is detected following learning during memory maintenance period (e.g., Ghosh et al., 2015). Thus, it could be that larger spines that contain more AMPA receptors are more sensitive to release of glutamate, and thus more stable, than smaller spines that are less sensitive and more dynamic. Indeed, larger spines are resistant to LTP and suggested to form the physical trace of long-term memory (Matsuzaki et al., 2004). Thus, the aforementioned observations suggest that glutamate receptors and calcium channels activation during learning leads to changes in actin structure and neuronal morphogenesis in specific activated spines. Subsequently, AMPA receptors activation by spontaneous release of glutamate in these synapses is involved in suppressing actin dynamic and preserving the new actin structure.

Activation of glutamate receptors can also lead to recruitment of actin capping proteins, known to stabilize F-actin, into spine head and can serve to stabilize spine morphology. Selective activation of synaptic glutamate receptors can lead to translocation of the actin filament barbed-end capping proteins Eps8, that stabilizes F-actin (Disanza et al., 2004), to the spine head (Menna et al., 2013). Eps8 is needed for proper spine morphology (Menna et al., 2013) and mice lacking Eps8 exhibit immature spines. These Eps8 KO mice are also impaired in passive avoidance long-term memory (Menna et al., 2013).

Reduction in actin dynamics induced by glutamate can support the stabilization of spines but it does not solve the problem of how actin cytoskeleton structure in spine, that mediates spine morphology, is preserved for long time despite actin protein turnover and dynamics. A self-perpetuating mechanism that maintains the structure of actin in spines is required to preserve spine morphology after learning.

Learning Leads to the Formation of New Scaffold of Actin Cytoskeletal Structure That Is Preserved to Maintain Spine Structure and Long-Term Memory

As described above the structure of dendritic spines may be stable after learning for months or years. However, the actin filaments that support spines structure turn over in minutes to hours. Over 80% of F-actin in spines turns over every minute (e.g., Star et al., 2002). How therefore does the spine structure remain stable in light of the rapid turnover of actin cytoskeleton that supports its structure?

It is possible that the altered actin cytoskeleton that supports the newly shaped spines after learning serves as a blueprint where the newly actin monomers and nucleation proteins replenish the network continuously keeping the general structure intact based on the initial (post-learning) structure. In that manner the rapid turnover of F-actin does not affect the general structure of actin filaments in spine and therefore spine structure remains stable. Mature spines consist of a mixture of branched and linear actin filaments in their base, neck, and head that determines their structure. Thus, the length and network structure of the actin filaments should be in a steady state to maintain spines morphology. In this model (**Figure 1**) we suggest several conditions that can contribute to the maintenance of the actin network structure and consequently to preserving the stability of spine morphology: (1) Actin filaments length stays intact after learning by balancing the rate of actin polymerization and depolymerization. This could be achieved by controlling the activity of actin polymerization (e.g., formins) and depolymerization (e.g., cofilin) regulatory proteins as well as of capping proteins. (2) The branching of actin by Arp2/3, localized in spines (Kim et al., 2006, 2013; Rácz and Weinberg, 2008; Wegner et al., 2008; Hotulainen et al., 2009), is on these preexisting F-actins (F-actin in condition #1) keeping the actin network structure. This requires that Arp2/3 will recognize the targeted filament to be branched and that Wasp will be activated during the maintenance phase so that Arp2/3 can be assembled. (3) Alternatively, the structure of the actin network may be maintained en masse by keeping the concentration of actin regulatory proteins in stable balance. For example, the structure of the actin network is determined by the ratio between capping proteins and Arp2/3. Increasing the concentration of the capping proteins leads to an increase in the Arp2/3 mediated branching of the actin cytoskeleton network

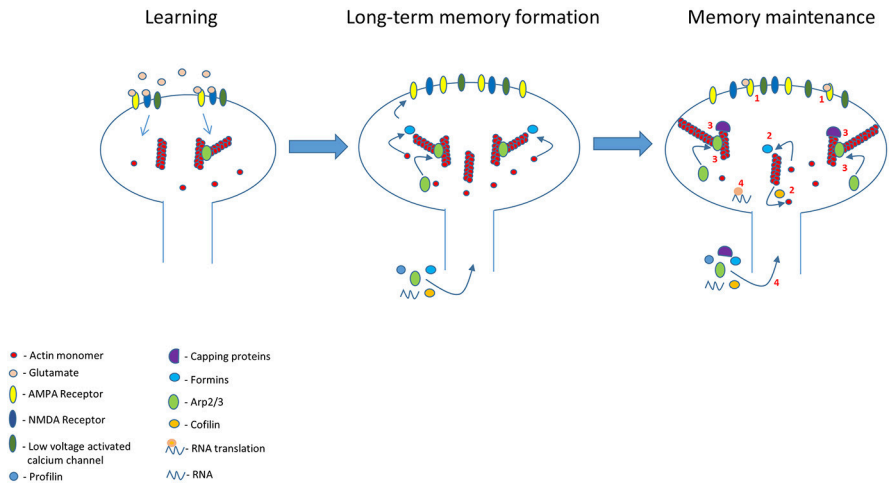

FIGURE 1 | Glutamate receptors and other synaptic receptors (e.g., Eph receptor) activation during learning leads to build up of new actin cytoskeletal scaffold leading to changes in spines morphology and memory formation. This new actin cytoskeletal scaffold is preserved in the memory spines to maintain spine morphology and long-term memory. This actin cytoskeleton structure lasts beyond actin and its regulatory proteins turnover and dynamics by several molecular activities (see numbers in figure): (1) Continued synaptic receptors (e.g., AMPA receptor) and channels activation during memory maintenance in the memory spines to regulate molecules that control actin dynamics and branching. (2) Stable actin polymerization and depolymerization ratio by actin regulatory proteins. (3) Capping proteins contribute to reduction in actin dynamics. In addition, a steady balance between capping and Arp2/3 proteins concentrations preserves a steady state structure of the branched network by controlling the number of branch points. (4) The balanced activation of actin regulatory proteins is kept steady by the receptors activation-mediated stabilization of actin regulatory proteins activity and levels in spines. The level of the proteins can be controlled by regulating trafficking and *in situ* proteins synthesis.

(Akin and Mullins, 2008). Such a balance may be achieved by a molecular mechanism that keeps the concentrations of the various actin regulatory proteins in spines constant. Keeping a stable concentration of a protein in spines could be achieved by: (1) *In situ* constant synthesis or suppression of synthesis of specific proteins in spines. The protein synthesis machinery exists in spines (e.g., Pierce et al., 2000; Ostroff et al., 2002) and active synapses may attract mRNAs (Kosik, 2016). Active suppression of dendritic protein synthesis is involved in miniature synaptic transmission induced stabilization of synaptic function (Sutton et al., 2006). (2) Actively controlling the translocation of specific proteins into specific spines. For example, myosin can deliver proteins into spines and may distribute distinct cargoes by using specific receptors (Kneussel and Wagner, 2013). Moreover, it has been shown that proteins can be translocated into specific spines after synaptic activation or learning (Matsuo et al., 2008; Bosch et al., 2014). Thus, learning induced continuous activation of specific spines (see above) can contribute to delivery of specific proteins and mRNAs into these spines keeping the concentrations of actin regulatory proteins in spines at steady state and thus preserving the actin cytoskeleton structure. Indeed, altering the concentration or activity of actin regulatory proteins can affect spines stability. For example, the stability of mature dendritic spines is controlled by cofilin activity and affecting this activity disrupts spines stability (e.g., Shi et al., 2009). Deletion of ArpC3 leads to a loss of large mushroom-shaped spines and an increase in filopodial-like spines indicating that conserved level of Arp2/3 may be crucial for long-term stabilization of spines *in vivo* (Kim et al., 2013).

Spines may also shrink after stimulation leading to long-term depression (LTD) that may be involved in experience-based neuronal network refinement (Nägerl et al., 2004; Zhou et al., 2004). LTD induced shrinkage of spines may lead to a new steady state with less complexed branched F-actin network and less F-actin (Okamoto et al., 2004). This may also be accompanied by reduction of AMPA receptors in synapse (Shepherd and Huganir, 2007). The stabilization of thinner spines may still be dependent on glutamate receptors or/and other synaptic receptors activities such as Eph receptors (e.g., Shi et al., 2009) balancing the new actin dynamics and branching by maintaining the concentrations and activities of actin regulatory proteins in the spine. Since there might be a decrease in calcium influx in response to synaptic stimulation, stabilizing the structure of actin cytoskeleton network may be dependent on maintaining actin regulatory proteins concentrations and activities using other signaling pathways.

SUMMARY AND CONCLUSIONS

Long-term memories last for years. The neuronal processes that encode memories last as long as memory exists. Alterations in neuronal morphology especially of dendritic spines have been suggested to underlie the formation of memory and their stabilization the maintenance of memory. In this review we show evidence indicating that changes in actin cytoskeleton subserves spine morphogenesis induced by learning and that preserving these actin cytoskeleton alterations is involved in maintaining spine morphology and memory for a long period of time. We

suggest mechanisms that include reduction in actin dynamics and the formation of a stable blue print of actin cytoskeleton structure in spines to preserve actin cytoskeleton scaffold, spine morphology and memory.

AUTHOR CONTRIBUTIONS

All authors listed have made a substantial, direct and intellectual contribution to the work, and approved it for publication.

REFERENCES

Ackermann, M., and Matus, A. (2003). Activity-induced targeting of profilin and stabilization of dendritic spine morphology. *Nat. Neurosci.* 6, 1194–1200. doi: 10.1038/nn1135

Akin, O., and Mullins, R. D. (2008). Capping protein increases the rate of actin-based motility by promoting filament nucleation by the Arp2/3 complex. *Cell* 133, 841–851. doi: 10.1016/j.cell.2008.04.011

Alvarez-Castelao, B., and Schuman, E. M. (2015). The regulation of synaptic protein turnover. *J. Biol. Chem.* 290, 28623–28630. doi: 10.1074/jbc.R115.657130

Araya, R., Jiang, J., Eisenthal, K. B., and Yuste, R. (2006). The spine neck filters membrane potentials. *Proc. Natl. Acad. Sci. U.S.A.* 103, 17961–17966. doi: 10.1073/pnas.0608755103

Araya, R., Vogels, T. P., and Yuste, R. (2014). Activity-dependent dendritic spine neck changes are correlated with synaptic strength. *Proc. Natl. Acad. Sci. U.S.A.* 111, E2895–E2904. doi: 10.1073/pnas.1321869111

Bailey, C. H., Kandel, E. R., and Harris, K. M. (2015). Structural components of synaptic plasticity and memory consolidation. *Cold Spring Harb. Perspect. Biol.* 7:a021758. doi: 10.1101/cshperspect.a021758

Basu, S., Kustanovich, I., and Lamprecht, R. (2016). Arp2/3 and VASP are essential for fear memory formation in lateral amygdala. *eNeuro* 29:3. doi: 10.1523/ENEURO.0302-16.2016

Bello-Medina, P. C., Flores, G., Quirarte, G. L., McGaugh, J. L., and Prado Alcalá R. A. (2016). Mushroom spine dynamics in medium spiny neurons of dorsal striatum associated with memory of moderate and intense training. *Proc. Natl. Acad. Sci. U.S.A.* 113, E6516–E6525. doi: 10.1073/pnas.1613680113

Bliss, T. V., and Collingridge, G. L. (1993). A synaptic model of memory: long-term potentiation in the hippocampus. *Nature* 361, 31–39. doi: 10.1038/361031a0

Bloodgood, B. L., and Sabatini, B. L. (2005). Neuronal activity regulates diffusion across the neck of dendritic spines. *Science* 310, 866–869. doi: 10.1126/science.1114816

Bosch, M., Castro, J., Saneyoshi, T., Matsuno, H., Sur, M., and Hayashi, Y. (2014). Structural and molecular remodeling of dendritic spine substructures during long-term potentiation. *Neuron* 82, 444–459. doi: 10.1016/j.neuron.2014.03.021

Caroni, P., Donato, F., and Muller, D. (2012). Structural plasticity upon learning: regulation and functions. *Nat. Rev. Neurosci.* 13, 478–490. doi: 10.1038/nrn3258

Chazeau, A., Mehidi, A., Nair, D., Gautier, J. J., Leduc, C., Chamma, I., et al. (2014). Nanoscale segregation of actin nucleation and elongation factors determines dendritic spine protrusion. *EMBO J.* 33, 2745–2764. doi: 10.15252/embj.201488837

Das, A., Dines, M., Alapin, J. M., and Lamprecht, R. (2017). Affecting long-term fear memory formation through optical control of Rac1 GTPase and PAK activity in lateral amygdala. *Sci Rep.* 7:13930. doi: 10.1038/s41598-017-13674-9

De Roo, M., Klauser, P., and Muller, D. (2008). LTP promotes a selective long-term stabilization and clustering of dendritic spines. *PLoS Biol.* 6:e219. doi: 10.1371/journal.pbio.0060219

De Rubeis, S., Pasciuto, E., Li, K. W., Fernández, E., Di Marino, D., Buzzi, A., et al. (2013). CYFIP1 coordinates mRNA translation and cytoskeleton remodeling to ensure proper dendritic spine formation. *Neuron* 79, 1169–1182. doi: 10.1016/j.neuron.2013.06.039

Disanza, A., Carlier, M. F., Stradal, T. E., Didry, D., Frittoli, E., Confalonieri, S., et al. (2004). Eps8 controls actin-based motility by capping the barbed ends of actin filaments. *Nat. Cell. Biol.* 6, 1180–1188. doi: 10.1038/ncb1199

Dong, T., He, J., Wang, S., Wang, L., Cheng, Y., and Zhong, Y. (2016). Inability to activate Rac1-dependent forgetting contributes to behavioral inflexibility in mutants of multiple autism-risk genes. *Proc. Natl. Acad. Sci. U.S.A.* 113, 7644–7649. doi: 10.1073/pnas.1602152113

Dudai, Y. (1989). *The Neurobiology of Memory*. New York, NY: Oxford University Press.

Ferron, F., Rebowski, G., Lee, S. H., and Dominguez, R. (2007). Structural basis for the recruitment of profilin-actin complexes during filament elongation by Ena/VASP. *EMBO J.* 26, 4597–4606. doi: 10.1038/sj.emboj.7601874

Fischer, M., Kaech, S., Wagner, U., Brinkhaus, H., and Matus, A. (2000). Glutamate receptors regulate actin-based plasticity in dendritic spines. *Nat. Neurosci.* 3, 887–894. doi: 10.1038/78791

Gavin, C. F., Rubio, M. D., Young, E., Miller, C., and Rumbaugh, G. (2011). Myosin II motor activity in the lateral amygdala is required for fear memory consolidation. *Learn. Mem.* 19, 9–14. doi: 10.1101/lm.024042.111

Ghosh, S., Reuveni, I., Barkai, E., and Lamprecht, R. (2015). CaMKII activity is required for maintaining learning-induced enhancement of AMPAR-mediated synaptic excitation. *J. Neurochem.* 136, 1168–1176. doi: 10.1111/jnc.13505

Gray, N. W., Weimer, R. M., Bureau, I., and Svoboda, K. (2006). Rapid redistribution of synaptic PSD-95 in the neocortex *in vivo*. *PLoS Biol.* 4:e0040370. doi: 10.1371/journal.pbio.0040370

Grutzendler, J., Kasthuri, N., and Gan, W. B. (2002). Long-term dendritic spine stability in the adult cortex. *Nature* 420, 812–816. doi: 10.1038/nature01276

Haditsch, U., Leone, D. P., Farinelli, M., Chrostek-Grashoff, A., Brakebusch, C., Mansuy, I. M., et al. (2009). A central role for the small GTPase Rac1 in hippocampal plasticity and spatial learning and memory. *Mol. Cell. Neurosci.* 41, 409–419. doi: 10.1016/j.mcn.2009.04.005

Hadziselimovic, N., Vukojevic, V., Peter, F., Milnik, A., Fastenrath, M., Fenyves, B. G., et al. (2014). Forgetting is regulated via Musashi-mediated translational control of the Arp2/3 complex. *Cell* 156, 1153–1166. doi: 10.1016/j.cell.2014.01.054

Halpain, S., Hipolito, A., and Saffer, L. (1998). Regulation of F-actin stability in dendritic spines by glutamate receptors and calcineurin. *J. Neurosci.* 18, 9835–9844. doi: 10.1523/JNEUROSCI.18-23-09835.1998

Hanus, C., and Schuman, E. M. (2013). Proteostasis in complex dendrites. *Nat. Rev. Neurosci.* 14, 638–648. doi: 10.1038/nrn3546

Harris, K. M., and Stevens, J. K. (1989). Dendritic spines of CA1pyramidal cells in the rat hippocampus: serial electron microscopy with reference to their biophysical characteristics. *J. Neurosci.* 9, 2982–2997. doi: 10.1523/JNEUROSCI.09-08-02982.1989

Hayashi-Takagi, A., Yagishita, S., Nakamura, M., Shirai,. F., Wu, Y. I., Loshbaugh, A. L., et al. (2015). Labelling and optical erasure of synaptic memory traces in the motor cortex. *Nature* 525, 333–338. doi: 10.1038/nature15257

Hebb, D. O. (1949). *The Organization of Behavior: A Neuropsychological Theory*. New York, NY: Wiley.

Hedrick, N. G., Harward, S. C., Hall, C. E., Murakoshi, H., McNamara, J. O., and Yasuda, R. (2016). Rho GTPase complementation underlies BDNF-dependent homo- and heterosynaptic plasticity. *Nature* 538, 104–108. doi: 10.1038/nature19784

Honkura, N., Matsuzaki, M., Noguchi, J., Ellis-Davies, G. C., and Kasai, H. (2008). The subspine organization of actin fibers regulates the structure and plasticity of dendritic spines. *Neuron* 57, 719–729. doi: 10.1016/j.neuron.2008.01.013

Hotulainen, P., and Hoogenraad, C. C. (2010). Actin in dendritic spines: connecting dynamics to function. *J. Cell Biol.* 189, 619–629. doi: 10.1083/jcb.201003008

Hotulainen, P., Llano, O., Smirnov, S., Tanhuanpää, K., Faix, J., Rivera, C., et al. (2009). Defining mechanisms of actin polymerization and depolymerization during dendritic spine morphogenesis. *J. Cell. Biol.* 185, 323–339. doi: 10.1083/jcb.200809046

Jiang, L., Mao, R., Zhou, Q., Yang, Y., Cao, J., Ding, Y., et al. (2016). Inhibition of Rac1 activity in the hippocampus impairs the forgetting of contextual fear memory. *Mol. Neurobiol.* 53, 1247–1253 doi: 10.1007/s12035-015-9093-6

Kandel, E. R. (2001). The molecular biology of memory storage: a dialogue between genes and synapses. *Science* 294, 1030–1038. doi: 10.1126/science.1067020

Kim, I. H., Racz, B., Wang, H., Burianek, L., Weinberg, R., Yasuda, R., et al. (2013). Disruption of Arp2/3 results in asymmetric structural plasticity of dendritic

spines and progressive synaptic and behavioral abnormalities. *J. Neurosci.* 33, 6081–6092. doi: 10.1523/JNEUROSCI.0035-13.2013

Kim, I. H., Wang, H., Soderling, S. H., and Yasuda, R. (2014). Loss of Cdc42 leads to defects in synaptic plasticity and remote memory recall. *Elife* 8:3. doi: 10.7554/elife.02839.001

Kim, Y., Sung, J. Y., Ceglia, I., Lee, K. W., Ahn, J. H., Halford, J. M., et al. (2006). Phosphorylation of WAVE1 regulates actin polymerization and dendritic spine morphology. *Nature* 442, 814–817. doi: 10.1038/nature04976

Kneussel, M., and Wagner, W. (2013). Myosin motors at neuronal synapses: drivers of membrane transport and actin dynamics. *Nat. Rev. Neurosci.* 14, 233–247. doi: 10.1038/nrn3445

Konorski, J. (1948). *Conditioned Reflexes and Neuron Organization*. Cambridge: Cambridge University Press.

Korobova, F., and Svitkina, T. (2010). Molecular architecture of synaptic actin cytoskeleton in hippocampal neurons reveals a mechanism of dendritic spine morphogenesis. *Mol. Biol. Cell*, 21, 165–176. doi: 10.1091/mbc.E09-07-0596

Kosik, K. S. (2016). Life at low copy number: how dendrites manage with so few mRNAs. *Neuron* 92, 1168–1180. doi: 10.1016/j.neuron.2016.11.002

Lai, C. S., Franke, T. F., and Gan, W. B. (2012). Opposite effects of fear conditioning and extinction on dendritic spine remodelling. *Nature* 48, 87–91. doi: 10.1038/nature10792

Lamprecht, R., and LeDoux, J. (2004). Structural plasticity and memory. *Nat. Rev. Neurosci.* 5, 45–54. doi: 10.1038/nrn1301

Lamprecht, R., Farb, C. R., Rodrigues, S. M., and LeDoux, J. E. (2006). Fear conditioning drives profilin into amygdala dendritic spines. *Nat. Neurosci*, 9, 481–483. doi: 10.1038/nn1672

Liao, D., Zhang, X., O'Brien, R., Ehlers, M. D., and Huganir, R. L. (1999). Regulation of morphological postsynaptic silent synapses in developing hippocampal neurons. *Nat. Neurosci.* 2, 37–43. doi: 10.1038/4540

Liu, Y., Du, S., Lv, L., Lei, B., Shi, W., Tang, Y., et al. (2016). Hippocampal activation of Rac1 regulates the forgetting of object recognition memory. *Curr. Biol.* 26, 2351–2357. doi: 10.1016/j.cub.2016.06.056

Luo, L. (2000). Rho GTPases in neuronal morphogenesis. *Nat. Rev. Neurosci.* 1, 173–180. doi: 10.1038/35044547

Mantzur, L., Joels, G., and Lamprecht, R. (2009). Actin polymerization in lateral amygdala is essential for fear memory formation. *Neurobiol. Learn. Mem.* 91, 85–88. doi: 10.1016/j.nlm.2008.09.001

Martin, S. J., Grimwood, P. D., and Morris, R. G. (2000). Synaptic plasticity and memory: an evaluation of the hypothesis. *Annu. Rev. Neurosci.* 23, 649–711. doi: 10.1146/annurev.neuro.23.1.649

Matsuo, N., Reijmers, L., and Mayford, M. (2008). Spine-type-specific recruitment of newly synthesized AMPA receptors with learning. *Science* 319, 1104–1107. doi: 10.1126/science.1149967

Matsuzaki, M., Honkura, N., Ellis-Davies, G. C., and Kasai, H. (2004). Structural basis of long-term potentiation in single dendritic spines. *Nature* 429, 761–766. doi: 10.1038/nature02617

Matus, A. (2000). Actin-based plasticity in dendritic spines. *Science* 290, 754–758. doi: 10.1126/science.290.5492.754

McKinney, R. A., Capogna, M., Dürr, R., Gähwiler, B. H., and Thompson, S. M. (1999). Miniature synaptic events maintain dendritic spines via AMPA receptor activation. *Nat. Neurosci.* 2, 44–49. doi: 10.1038/4548

Meng, Y., Zhang, Y., Tregoubov, V., Janus, C., Cruz, L., Jackson, M., et al. (2002). Abnormal spine morphology and enhanced LTP in LIMK-1 knockout mice. *Neuron* 35, 121–133. doi: 10.1016/S0896-6273(02)00758-4

Menna, E., Zambetti, S., Morini, R., Donzelli, A., Disanza, A., Calvigioni, D., et al. (2013). Eps8 controls dendritic spine density and synaptic plasticity through its actin-capping activity. *EMBO J.* 32, 1730–1744. doi: 10.1038/emboj.2013.107

Michaelsen, K., Murk, K., Zagrebelsky, M., Dreznjak, A., Jockusch, B. M., Rothkegel, M., et al. (2010). Fine-tuning of neuronal architecture requires two profilin isoforms. *Proc. Natl. Acad. Sci. U.S.A.* 107, 15780–15785. doi: 10.1073/pnas.1004406107

Michaelsen-Preusse, K., Zessin, S., Grigoryan, G., Scharkowski, F., Feuge, J., Remus, A., et al. (2016). Neuronal profilins in health and disease: Relevance for spine plasticity and Fragile X syndrome. *Proc. Natl. Acad. Sci. U.S.A.* 113, 3365–3370. doi: 10.1073/pnas.1516697113

Miermans, C. A., Kusters, R. P., Hoogenraad, C. C., and Storm, C. (2017). Biophysical model of the role of actin remodeling on dendritic spine morphology. *PLoS ONE* 12:e0170113. doi: 10.1371/journal.pone.0170113

Morton, W. M., Ayscough, K. R., and McLaughlin, P. J. (2000). Latrunculin alters the actin-monomer subunit interface to prevent polymerization. *Nat. Cell. Biol.* 2, 376–378. doi: 10.1038/35014075

Nägerl, U. V., Eberhorn, N., Cambridge, S. B., and Bonhoeffer, T. (2004). Bidirectional activity-dependent morphological plasticity in hippocampal neurons. *Neuron* 44, 759–767. doi: 10.1016/j.neuron.2004.11.016

Nedelescu, H., Kelso, C. M., Lázaro-Muñoz, G., Purpura, M., Cain, C. K., Ledoux, J. E., et al. (2010). Endogenous GluR1-containing AMPA receptors translocate to asymmetric synapses in the lateral amygdala during the early phase of fear memory formation: an electron microscopic immunocytochemical study. *J. Comp. Neurol.* 518, 4723–4739. doi: 10.1002/cne.22472

Newpher, T. M., and Ehlers, M. D. (2009). Spine microdomains for postsynaptic signaling and plasticity. *Trends Cell. Biol.* 19, 218–222. doi: 10.1016/j.tcb.2009.02.004

Nimchinsky, E. A., Sabatini, B. L., and Svoboda, K. (2002). Structure and function of dendritic spines. *Annu. Rev. Physiol.* 64, 313–353. doi: 10.1146/annurev.physiol.64.081501.160008

Nishiyama, J., and Yasuda, R. (2015). Biochemical computation for spine structural plasticity. *Neuron* 87, 63–75. doi: 10.1016/j.neuron.2015.05.043

Noguchi, J., Matsuzaki, M., Ellis-Davies, G. C. R., and Kasai, H. (2005). Spine-neck geometry determines NMDA receptor-dependent Ca^{2+} signaling in dendrites. *Neuron* 46, 609–622. doi: 10.1016/j.neuron.2005.03.015

Noguchi, J., Nagaoka, A., Watanabe, S., Ellis-Davies, G. C., Kitamura, K., Kano, M., et al. (2011). *In vivo* two-photon uncaging of glutamate revealing the structure-function relationships of dendritic spines in the neocortex of adult mice. *J. Physiol.* 589, 2447–2457. doi: 10.1113/jphysiol.2011.207100

Okamoto, K., Nagai, T., Miyawaki, A., and Hayashi, Y. (2004). Rapid and persistent modulation of actin dynamics regulates postsynaptic reorganization underlying bidirectional plasticity. *Nat. Neurosci* 7, 1104–1112. doi: 10.1038/nn1311

Ostroff, L. E., Fiala, J. C., Allwardt, B., and Harris, K. M. (2002). Polyribosomes redistribute from dendritic shafts into spines with enlarged synapses during LTP in developing rat hippocampal slices. *Neuron* 35, 535–545. doi: 10.1016/S0896-6273(02)00785-7

Ostroff, L. E., Cain, C. K., Bedont, J., Monfils, M. H., and Ledoux, J. E. (2010). Fear and safety learning differentially affect synapse size and dendritic translation in the lateral amygdala. *Proc. Natl. Acad. Sci. U.S.A.* 107, 9418–9423. doi: 10.1073/pnas.0913384107

Ota, K. T., Monsey, M. S., Wu, M. S., and Schafe, G. E. (2010). Synaptic plasticity and NO-cGMP-PKG signaling regulate pre- and postsynaptic alterations at rat lateral amygdala synapses following fear conditioning. *PLoS ONE* 5:e11236. doi: 10.1371/journal.pone.0011236

Petralia, R. S., Esteban, J. A., Wang, Y. X., Partridge, J. G., Zhao, H. M., Wenthold, R. J., et al. (1999). Selective acquisition of AMPA receptors over postnatal development suggests a molecular basis for silent synapses. *Nat. Neurosci.* 2, 31–36. doi: 10.1038/4532

Pierce, J. P. 1., van Leyen, K., and McCarthy, J. B. (2000). Translocation machinery for synthesis of integral membrane and secretory proteins in dendritic spines. *Nat. Neurosci.* 3, 311–313. doi: 10.1038/73868

Pollard, T. D. (2007). Regulation of actin filament assembly by Arp2/3 complex and formins. *Annu. Rev. Biophys. Biomol. Struct.* 36, 451–477. doi: 10.1146/annurev.biophys.35.040405.101936

Pollitt, A. Y., and Insall, R. H. (2009). WASP and SCAR/WAVE proteins: the drivers of actin assembly. *J. Cell. Sci.* 122, 2575–2578. doi: 10.1242/jcs.023879

Rácz, B., and Weinberg, R. J. (2008). Organization of the Arp2/3 complex in hippocampal spines. *J. Neurosci.* 28, 5654–5659. doi: 10.1523/JNEUROSCI.0756-08.2008

Rehberg, K., Bergado-Acosta, J. R., Koch, J. C., and Stork, O. (2010). Disruption of fear memory consolidation and reconsolidation by actin filament arrest in the basolateral amygdala. *Neurobiol. Learn. Mem.* 94, 117–126. doi: 10.1016/j.nlm.2010.04.007

Reinhard, M., Giehl, K., Abel, K., Haffner, C., Jarchau, T., Hoppe, V., et al. (1995). The proline-rich focal adhesion and microfilament protein VASP is a ligand for profilins. *EMBO J.* 14, 1583–1589.

Restivo, L., Vetere, G., Bontempi, B., and Ammassari-Teule, M. (2009). The formation of recent and remote memory is associated with time-dependent formation of dendritic spines in the hippocampus and anterior cingulate cortex. *J. Neurosci.* 29, 8206–8214. doi: 10.1523/JNEUROSCI.0966-09.2009

Rumpel, S., LeDoux, J., Zador, A., and Malinow, R. (2005). Postsynaptic receptor trafficking underlying a form of associative learning. *Science* 308, 83–88. doi: 10.1126/science.1103944

Rust, M. B., Gurniak, C. B., Renner, M., Vara, H., Morando, L., Görlich, A., et al. (2010). Learning, AMPA receptor mobility and synaptic plasticity depend on n-cofilin-mediated actin dynamics. *EMBO J.* 29, 1889–1902. doi: 10.1038/emboj.2010.72

Santamaria, F., Wils, S., De Schutter, E., and Augustine, G. J. (2006). Anomalous diffusion in Purkinje cell dendrites caused by spines. *Neuron* 52, 635–648. doi: 10.1016/j.neuron.2006.10.025

Schubert, V., and Dotti, C. G. (2007). Transmitting on actin: synaptic control of dendritic architecture. *J. Cell. Sci.* 120, 205–212. doi: 10.1242/jcs.03337

Shepherd, J. D., and Huganir, R. L. (2007). The cell biology of synaptic plasticity: AMPA receptor trafficking. *Annu. Rev. Cell Dev. Biol.* 23, 613–643. doi: 10.1146/annurev.cellbio.23.090506.123516

Shi, Y., Pontrello, C. G., DeFea, K. A., Reichardt, L. F., and Ethell, I. M. (2009). Focal adhesion kinase acts downstream of EphB receptors to maintain mature dendritic spines by regulating cofilin activity. *J. Neurosci.* 29, 8129–8142. doi: 10.1523/JNEUROSCI.4681-08.2009

Shirao, T., and González-Billault, C. (2013). Actin filaments and microtubules in dendritic spines. *J. Neurochem.* 126, 155–164. doi: 10.1111/jnc.12313

Shuai, Y., Lu, B., Hu, Y., Wang, L., Sun, K., and Zhong, Y. (2010). Forgetting is regulated through Rac activity in Drosophila. *Cell* 140, 579–589. doi: 10.1016/j.cell.2009.12.044

Soderling, S. H., Guire, E. S., Kaech, S., White, J., Zhang, F., Schutz, K., et al. (2007). A WAVE-1 and WRP signaling complex regulates spine density, synaptic plasticity, and memory. *J. Neurosci.* 27, 355–365. doi: 10.1523/JNEUROSCI.3209-06.2006

Star, E. N., Kwiatkowski, D. J., and Murthy, V. N. (2002). Rapid turnover of actin in dendritic spines and its regulation by activity. *Nat. Neurosci.* 5, 239–246. doi: 10.1038/nn811

Sutton, M. A., Ito, H. T., Cressy, P., Kempf, C., Woo, J. C., and Schuman, E. M. (2006). Miniature neurotransmission stabilizes synaptic function via tonic suppression of local dendritic protein synthesis. *Cell* 125, 785–799. doi: 10.1016/j.cell.2006.03.040

Takenawa, T., and Suetsugu, S. (2007). The WASP-WAVE protein network: connecting the membrane to the cytoskeleton. *Nat. Rev. Mol. Cell. Biol.* 8, 37–48. doi: 10.1038/nrm2069

Takumi, Y., Ramírez-León, V., Laake, P., Rinvik, E., and Ottersen, O. P. (1999). Different modes of expression of AMPA and NMDA receptors in hippocampal synapses. *Nat. Neurosci.* 2, 618–624. doi: 10.1038/10172

Trachtenberg, J. T., Chen, B. E., Knott, G. W., Feng, G., Sanes, J. R., Welker, E., et al. (2002). Long-term *in vivo* imaging of experience-dependent synaptic plasticity in adult cortex. *Nature* 420, 788–794. doi: 10.1038/nature01273

Tsien, J. Z. (2000). Linking Hebb's coincidence-detection to memory formation. *Curr. Opin. Neurobiol.* 10, 266–273. doi: 10.1016/S0959-4388(00)00070-2

Vetere, G., Restivo, L., Cole, C. J., Ross, P. J., Ammassari-Teule, M., Josselyn, S. A., et al. (2011). Spine growth in the anterior cingulate cortex is necessary for the consolidation of contextual fear memory. *Proc. Natl. Acad. Sci. U.S.A.* 108, 8456–8460. doi: 10.1073/pnas.1016275108

Wang, Y., Dong, Q., Xu, X. F., Feng, X., Xin, J., Wang, D. D., et al. (2013). Phosphorylation of cofilin regulates extinction of conditioned aversive memory via AMPAR trafficking. *J. Neurosci.* 33, 6423–6433. doi: 10.1523/JNEUROSCI.5107-12.2013

Wegner, A. M., Nebhan, C. A., Hu, L., Majumdar, D., Meier, K. M., Weaver, A. M., et al. (2008). N-wasp and the arp2/3 complex are critical regulators of actin in the development of dendritic spines and synapses. *J. Biol. Chem.* 283, 15912–15920. doi: 10.1074/jbc.M801555200

Woolfrey, K. M., and Srivastava, D. P. (2016). Control of dendritic spine morphological and functional plasticity by small GTPases. *Neural Plast.* 2016:3025948. doi: 10.1155/2016/3025948

Xu, T., Yu, X., Perlik, A. J., Tobin, W. F., Zweig, J. A., Tennant, K., et al. (2009). Rapid formation and selective stabilization of synapses for enduring motor memories. *Nature* 462, 915–919. doi: 10.1038/nature08389

Yang, G., Pan, F., and Gan, W. B. (2009). Stably maintained dendritic spines are associated with lifelong memories. *Nature* 462, 920–924. doi: 10.1038/nature08577

Yang, Y., Liu, D. Q., Huang, W., Deng, J., Sun, Y., Zuo, Y., et al. (2016). Selective synaptic remodeling of amygdalocortical connections associated with fear memory. *Nat. Neurosci.* 19, 1348–1355. doi: 10.1038/nn.4370

Yeh, S. H., Mao, S. C., Lin, H. C., and Gean, P. W. (2006). Synaptic expression of glutamate receptor after encoding of fear memory in the rat amygdala. *Mol. Pharmacol.* 69, 299–308. doi: 10.1124/mol.105.017194

Young, E. J., Aceti, M., Griggs, E. M., Fuchs, R. A., Zigmond, Z., Rumbaugh, G., et al. (2014). Selective, retrieval-independent disruption of methamphetamine-associated memory by actin depolymerization. *Biol. Psychiatry* 75, 96–104. doi: 10.1016/j.biopsych.2013.07.036

Zhang, X., Li, Q., Wang, L., Liu, Z. J., and Zhong, Y. (2016). Cdc42-Dependent forgetting regulates repetition effect in prolonging memory retention. *Cell Rep.* 16, 817–825. doi: 10.1016/j.celrep.2016.06.041

Zhou, Q., Homma, K. J., and Poo, M. M. (2004). Shrinkage of dendritic spines associated with long-term depression of hippocampal synapses. *Neuron* 44, 749–757. doi: 10.1016/j.neuron.2004.11.011

Zuo, Y., Lin, A., Chang, P., and Gan, W. B. (2005). Development of long-term dendritic spine stability in diverse regions of cerebral cortex. *Neuron* 46, 181–189. doi: 10.1016/j.neuron.2005.04.001

Conflict of Interest Statement: The authors declare that the research was conducted in the absence of any commercial or financial relationships that could be construed as a potential conflict of interest.

frontiers in Molecular Neuroscience

OPINION
published: 01 May 2018
doi: 10.3389/fnmol.2018.00151

ADNP, a Microtubule Interacting Protein, Provides Neuroprotection Through End Binding Proteins and Tau: An Amplifier Effect

Illana Gozes[1]*, *Yanina Ivashko-Pachima*[1] and *Carmen L. Sayas*[2]

[1] *The Lily and Avraham Gildor Chair for the Investigation of Growth Factors, Dr. Diana and Zelman Elton (Elbaum) Laboratory for Molecular Neuroendocrinology, Department of Human Molecular Genetics and Biochemistry, Sackler Faculty of Medicine, Sagol School of Neuroscience and Adams Super Center for Brain Studies, Tel Aviv University, Tel Aviv, Israel,* [2] *Centre for Biomedical Research of the Canary Islands, Institute for Biomedical Technologies, Universidad de La Laguna, Tenerife, Spain*

Keywords: microtubules, microtubule-associated proteins, ADNP, tau, microtubule end binding proteins

ACTIVITY-DEPENDENT NEUROPROTECTIVE PROTEIN (ADNP) INTERACTS WITH MICROTUBULES

Neuronal plasticity, key to brain function in health, is impaired in neurodevelopmental, neuropsychiatric and neurodegenerative diseases. Neuronal plasticity depends on an intact cytoskeletal system. Here, we focus on recently discovered as well as "classical" cytoskeletal proteins including activity-dependent neuroprotective protein (ADNP), Tau and microtubule end binding proteins (EBs), impacting neuroplasticity and neuropathology.

Original structure-function analysis of astrocyte-secreted protein fragments identified femtomolar-acting neuroprotective peptide moieties VLGGGSALLRSIPA (Brenneman and Gozes, 1996), SALLRSIPA (Brenneman et al., 1998) and NAPVSIPQ (Bassan et al., 1999), with NAPVSIPQ (NAP) being a fragment of ADNP (Bassan et al., 1999). However, ADNP does not only provide neuroprotection through the NAP motif, but is essential for brain formation, with complete *Adnp* gene knockout in mice resulting in neural tube closure failure and fetal death. Furthermore, NAP promotes neural tube closure in the face of alcohol intoxication (Chen et al., 2005). Thus, the mechanism of ADNP protection, potentially through the potent NAP motif, is of interest.

In search for NAP binding partners, we subjected mouse brain protein extracts to affinity chromatography with NAP as a ligand and identified tubulin as an interacting partner (Divinski et al., 2004, 2006). These results were coupled to NAP promoting changes in microtubule structure and protecting against microtubule disassembly induced by nocodazole *in vitro* (Gozes and Divinski, 2007) and colchicine *in vivo* (Jouroukhin et al., 2013). Further data suggested NAP protection against Zinc intoxication, which was originally linked to microtubule disruption (Divinski et al., 2004, 2006) and increased specificity to beta III tubulin, or to neuronal cells (Divinski et al., 2006; Holtser-Cochav et al., 2006). Parallel studies identified reduced axonal transport (Amram et al., 2016), increased tau hyperphosphorylation and tau depositions as a consequence of *Adnp* haploinsufficiency (Vulih-Shultzman et al., 2007). However, direct interaction of NAP with pure tubulin was not confirmed (Yenjerla et al., 2010). Thus, the discovery of (1) the requirement for the SIP motif on NAPVSIPQ and related peptides for neuroprotection (Wilkemeyer et al., 2003), (2) the SxIP microtubule end binding protein 1 (EB1) interacting motif as a microtubule tip localization signal (Honnappa et al., 2009; Jiang et al., 2012), and (3) EB3 as essential for dendritic spine formation(Jaworski et al., 2009), directed research toward ADNP-NAP-EB1/3 interactions. EB1/3 proteins are the master regulators of the microtubule plus-end tracking proteins (+TIPs), which accumulate at the growing ends of microtubules, showing a "comet" pattern at microtubule tips (Lansbergen and Akhmanova, 2006).

OPEN ACCESS

Edited by:
Christian Gonzalez-Billault, Universidad de Chile, Chile

Reviewed by:
Ioannis Sotiropoulos, University of Minho, Portugal
Alain Buisson, Université Grenoble Alpes, France
Eva Maria Jimenez-Mateos, Royal College of Surgeons in Ireland, Ireland

***Correspondence:**
Illana Gozes
igozes@tauex.tau.ac.il

Received: *17 January 2018*
Accepted: *17 April 2018*
Published: *01 May 2018*

Citation:
Gozes I, Ivashko-Pachima Y and Sayas CL (2018) ADNP, a Microtubule Interacting Protein, Provides Neuroprotection Through End Binding Proteins and Tau: An Amplifier Effect. Front. Mol. Neurosci. 11:151. doi: 10.3389/fnmol.2018.00151

THE IDENTIFICATION OF THE NAP/ADNP EB-DIRECT INTERACTION AND EB REQUIREMENT FOR NAP ACTIVITY

To establish a direct connection between ADNP and the EB family of proteins, specific immunoprecipitation experiments were carried out, showing direct interactions and enhancement of EB3-ADNP as well as other microtubule plus-end protein interactions by NAP (Oz et al., 2014). Further affinity chromatography with NAPVSIPQ and recombinant EB proteins (Oz et al., 2014) showed direct interaction with NAP and identified displacement with NAPVSKIPQ (SxIP=SKIP), but not with NAPVAAAAQ. These studies were further elaborated to show direct interactions in COS-7 cells expressing fluorescent EB3 and subject to fluorescent-NAP. Finally, silencing of EB1 and EB3, but not of EB2, abolished NAP protection in the neuronal model pheochromocytoma (PC12) against Zinc intoxication (Oz et al., 2014), and NAP increased PSD-95 expression in dendritic spines, which was inhibited by EB3 silencing (Oz et al., 2014). Together, these studies implicate ADNP/NAP in synaptic plasticity, involving EB proteins (Jaworski et al., 2009; Oz et al., 2014). While these results explained the previously observed NAP interaction with microtubules, bringing into focus the SIP motif (Gozes et al., 2016; Quraishe et al., 2016) and suggesting an amplifier effect at the microtubule tip, the molecular mechanism of increased Tau hyperphosphorylation, as a consequence of ADNP deficiency and protection by NAP against tauopathy (Vulih-Shultzman et al., 2007; Matsuoka et al., 2008; Shiryaev et al., 2009; Jouroukhin et al., 2013), still required further investigations.

TAU REGULATES THE LOCALIZATION AND FUNCTION OF EB1 AND EB3 IN DEVELOPING NEURONAL CELLS AND ANTAGONIZES EB TRACKING AT MICROTUBULE ENDS THROUGH A PHOSPHORYLATION-DEPENDENT MECHANISM

Tau and EBs were shown to partially co-localize at extending neurites of N1E-115 neuroblastoma cells and axons of primary hippocampal neurons, confirmed by immunoprecipitation and by tau/EB1 direct *in vitro* pull-down assays (Sayas et al., 2015). Fluorescence recovery after photobleaching assays performed in neuroblastoma cells corroborated tau modulation of EB3 cellular mobility (Sayas et al., 2015). Another excellent report shows that Tau and EBs form a complex via the C-terminal region of EBs and the microtubule-binding sites of Tau and further show that these two domains are required for the inhibitory activity of Tau on EB localization to microtubule ends. Additionally, their results show that the phosphomimetic mutation S262E within Tau microtubule-binding sites impairs EB/Tau interaction and prevents the inhibitory effect of Tau on EB comets (Ramirez-Rios et al., 2016). The question then arose if there is an EBs/Tau-ADNP/NAP connection.

ADNP/NAP DRAMATICALLY INCREASE MICROTUBULE END-BINDING PROTEIN-TAU INTERACTION: A NOVEL AVENUE FOR PROTECTION AGAINST TAUOPATHY

We have recently demonstrated that NAP augmented EB1 and EB3 comet density, amounts, length and speed in the N1E-115 neuroblastoma neuronal model. NAP enhanced EB3 homodimer formation, while decreasing EB1-EB3 heterodimer content and driving EB1- and EB3-Tau interactions (dramatic 20-fold increases), leading to recruitment of EB1/EB3 and Tau to microtubules under zinc intoxication, which has previously been shown to be linked to Tau hyperphosphorylation (Ivashko-Pachima et al., 2017). As indicated above, our previous results showed that while NAP protected neuronal-like cells against oxidative stress, it did not protect NIH3T3 fibroblasts (Divinski et al., 2004). Indeed, NAP did not protect NIH3T3 cells against zinc intoxication, unless these cells were transfected with Tau. Interestingly, other microtubule-associated proteins (MAPs) may replace Tau; thus, EB-Tau (MAPs) interaction is identified as a novel target for endogenous ADNP neuroprotection (Ivashko-Pachima et al., 2017). Importantly, as indicated, phosphorylation of S262 impaired EB/Tau interactions and our previous data have directly shown that NAP inhibits tau hyperphosphorylation at the S262 site (Jouroukhin et al., 2013) in multiple tauopathy models (Magen et al., 2014), with this phosphorylation site being linked to impaired axonal transport and neurodegeneration (Iijima-Ando et al., 2012), partially solving the NAP/ADNP protective activity against tauopathy (**Figure 1**). Future studies encompassing the impact of the NAP-EBs-Tau interaction on Tau aggregation (Gozes et al., 2014a,b), mitochondrial function (Esteves et al., 2014) and autophagy (Sragovich et al., 2017) are planned and will contribute to clarify the relevance of this protein complex in neuroprotection in the context of tauopathies and other neurodegenerative diseases.

THE ADNP SYNDROME

The ADNP syndrome (Helsmoortel et al., 2014), a recently described autism spectrum disorder syndrome driven by heterozygous, mostly protein truncating, *de novo* mutations in ADNP (Gozes et al., 2015, 2017a,b), is a subject of our future studies. These studies are aimed at connecting protein structure to function, with the human condition being characterized with intellectual disability, global developmental delays (including motor delays) and facial dimorphisms. Interestingly, ∼80% of the ADNP children can be identified by premature deciduous tooth eruption, a unique early diagnostic marker. Teething and bone/brain formation converge on mechanisms linked to ubiquitin impacted by the cytoskeleton, paving the path to future research. From a clinical perspective, Coronis Neurosciences

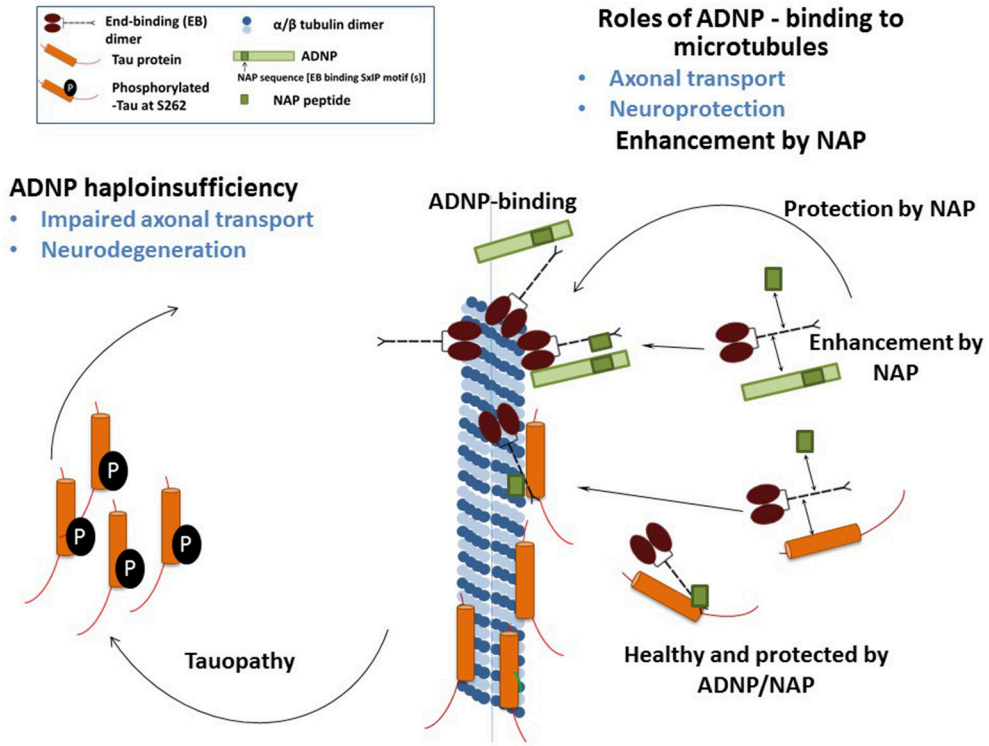

FIGURE 1 | The illustration shows the mechanism of NAP/ADNP neuroprotection against tauopathy in the disease state. In the healthy state, ADNP enhances axonal transport and synaptic plasticity. ADNP has two adjacent SIP motifs, one within the NAP sequence and one upstream (Bassan et al., 1999; Zamostiano et al., 2001). A NAP—related peptide SKIP (encompassing the SxIP motif), enhances axonal transport in *Adnp* haploinsufficient mice, probably through the same mechanism (Amram et al., 2016). In tissue culture cells, NAP also enhances dendritic spine formation (synaptic plasticity) through an EB3-depedent mechanism (Oz et al., 2014).

(www.coronisns.com) is developing NAP (CP201) (Magen and Gozes, 2013, 2014) for the ADNP syndrome.

AUTHOR CONTRIBUTIONS

All authors listed, have made substantial, direct and intellectual contribution to the work, and approved it for publication.

FUNDING

YI-P was partly supported by a scholarship from the Dr. Miriam and Sheldon G. Adelson Graduate School of the Faculty of Medicine at Tel Aviv University (IG) and this paper is part of the graduation requirements. The research was further supported by funds from the Israel Science Foundation (ISF) grant (1424/14), ERA-NET neuron AUTYSM, AMN Foundation, Drs. Ronith and Armand Stemmer and Mr. Arthur Gerbi (French Friends of Tel Aviv University), as well as Canadian (Mrs. Anne and Mr. Alex Cohen) and Spanish Friends of Tel Aviv University. CS research was supported first by CSIC and CIBERNED, in the group of Prof. J. Avila (CBM Severo Ochoa, CSIC-UAM, Madrid), and then as PI by the IMBRAIN project [(FP7-REGPOT-2012-CT2012-31637-IMBRAIN), Framework Programme 7 (Capacities)], awarded to the ITB and CIBICAN at ULL. CS is currently supported by ULL and Cabildo de Tenerife, under the Programa Agustín de Betencourt.

REFERENCES

Amram, N., Hacohen-Kleiman, G., Sragovich, S., Malishkevich, A., Katz, J., Touloumi, O., et al. (2016). Sexual divergence in microtubule function: the novel intranasal microtubule targeting SKIP normalizes axonal transport and enhances memory. *Mol. Psychiatry* 21, 1467–1476. doi: 10.1038/mp.2015.208

Bassan, M., Zamostiano, R., Davidson, A., Pinhasov, A., Giladi, E., Perl, O., et al. (1999). Complete sequence of a novel protein containing a femtomolar-activity-dependent neuroprotective peptide. *J. Neurochem.* 72, 1283–1293. doi: 10.1046/j.1471-4159.1999.0721283.x

Brenneman, D. E., and Gozes, I. (1996). A femtomolar-acting neuroprotective peptide. *J. Clin. Invest.* 97, 2299–2307. doi: 10.1172/JCI118672

Brenneman, D. E., Hauser, J., Neale, E., Rubinraut, S., Fridkin, M., Davidson, A., et al. (1998). Activity-dependent neurotrophic factor: structure-activity relationships of femtomolar-acting peptides. *J. Pharmacol. Exp. Ther.* 285, 619–627.

Chen, S. Y., Charness, M. E., Wilkemeyer, M. F., and Sulik, K. K. (2005). Peptide-mediated protection from ethanol-induced neural tube defects. *Dev. Neurosci.* 27, 13–19. doi: 10.1159/000084528

Divinski, I., Holtser-Cochav, M., Vulih-Schultzman, I., Steingart, R. A., and Gozes, I. (2006). Peptide neuroprotection through specific interaction with brain tubulin. *J. Neurochem.* 98, 973–984. doi: 10.1111/j.1471-4159.2006.03936.x

Divinski, I., Mittelman, L., and Gozes, I. (2004). A femtomolar acting octapeptide interacts with tubulin and protects astrocytes against zinc intoxication. *J. Biol. Chem.* 279, 28531–28538. doi: 10.1074/jbc.M403197200

Esteves, A. R., Gozes, I., and Cardoso, S. M. (2014). The rescue of microtubule-dependent traffic recovers mitochondrial function in Parkinson's disease. *Biochim. Biophys. Acta* 1842, 7–21. doi: 10.1016/j.bbadis.2013.10.003

Gozes, I., and Divinski, I. (2007). NAP, a neuroprotective drug candidate in clinical trials, stimulates microtubule assembly in the living cell. *Curr. Alzheimer Res.* 4, 507–509. doi: 10.2174/156720507783018208

Gozes, I., Helsmoortel, C., Vandeweyer, G., N., Van der Aa, Kooy, F., and Sermone, S. B. (2015). The compassionate side of neuroscience: tony sermone's undiagnosed genetic Journey–ADNP mutation. *J. Mol. Neurosci.* 56, 751–757. doi: 10.1007/s12031-015-0586-6

Gozes, I., Iram, T., Maryanovsky, E., Arviv, C., Rozenberg, L., Schirer, Y., et al. (2014a). Novel tubulin and tau neuroprotective fragments sharing structural similarities with the drug candidate NAP (Davuentide). *J. Alzheimer's Dis.* 40(Suppl. 1):S23–S36. doi: 10.3233/JAD-131664

Gozes, I., Patterson, M. C., Van Dijck, A., Kooy, R. F., Peeden, J. N., Eichenberger, J. A., et al. (2017a). The eight and a half year journey of undiagnosed AD: gene sequencing and funding of advanced genetic testing has led to hope and new beginnings. *Front. Endocrinol.* 8:107. doi: 10.3389/fendo.2017.00107

Gozes, I., Schirer, Y., Idan-Feldman, A., David, M., and Furman-Assaf, S. (2014b). NAP alpha-aminoisobutyric acid (IsoNAP). *J. Mol. Neurosci.* 52, 1–9. doi: 10.1007/s12031-013-0103-8

Gozes, I., Sragovich, S., Schirer, Y., and Idan-Feldman, A. (2016). D-SAL and NAP: two peptides sharing a SIP domain. *J. Mol. Neurosci.* 59, 220–231. doi: 10.1007/s12031-015-0701-8

Gozes, I., Van Dijck, A., Hacohen-Kleiman, G., Grigg, I., Karmon, G., Giladi, E., et al. (2017b). Premature primary tooth eruption in cognitive/motor-delayed ADNP-mutated children. *Transl. Psychiatry* 7:e1043. doi: 10.1038/tp.2017.27

Helsmoortel, C., Vulto-van Silfhout, A. T., Coe, B. P., Vandeweyer, G., Rooms, L., van den Ende, J., et al. (2014). A SWI/SNF-related autism syndrome caused by de novo mutations in ADNP. *Nat. Genet.* 46, 380-384. doi: 10.1038/ng.2899

Holtser-Cochav, M., Divinski, I., and Gozes, I. (2006). Tubulin is the target binding site for NAP-related peptides: ADNF-9, D-NAP, and D-SAL. *J. Mol. Neurosci.* 28, 303–307. doi: 10.1385/JMN:28:3:303

Honnappa, S., Gouveia, S. M., Weisbrich, A., Damberger, F. F., Bhavesh, N. S., Jawhari, H., et al. (2009). An EB1-binding motif acts as a microtubule tip localization signal. *Cell* 138, 366–376. doi: 10.1016/j.cell.2009.04.065

Iijima-Ando, K., Sekiya, M., Maruko-Otake, A., Ohtake, Y., Suzuki, E., Lu, B., et al. (2012). Loss of axonal mitochondria promotes tau-mediated neurodegeneration and Alzheimer's disease-related tau phosphorylation via PAR-1. *PLoS Genet.* 8:e1002918. doi: 10.1371/journal.pgen.1002918

Ivashko-Pachima, Y., Sayas, C. L., Malishkevich, A., and Gozes, I. (2017). ADNP/NAP dramatically increase microtubule end-binding protein-Tau interaction: a novel avenue for protection against tauopathy. *Mol. Psychiatry* 22, 1335–1344. doi: 10.1038/mp.2016.255

Jaworski, J., Kapitein, L. C., Gouveia, S. M., Dortland, B. R., Wulf, P. S., Grigoriev, I., et al. (2009). Dynamic microtubules regulate dendritic spine morphology and synaptic plasticity. *Neuron* 61, 85–100. doi: 10.1016/j.neuron.2008.11.013

Jiang, K., Toedt, G., Montenegro Gouveia, S., Davey, N. E., Hua, S., van der Vaart, B., et al. (2012). A Proteome-wide screen for mammalian SxIP motif-containing microtubule plus-end tracking proteins. *Curr. Biol.* 22, 1800–1807. doi: 10.1016/j.cub.2012.07.047

Jouroukhin, Y., Ostritsky, R., Assaf, Y., Pelled, G., Giladi, E., and Gozes, I. (2013). NAP (davunetide) modifies disease progression in a mouse model of severe neurodegeneration: protection against impairments in axonal transport. *Neurobiol. Dis.* 56, 79–94. doi: 10.1016/j.nbd.2013.04.012

Lansbergen, G., and Akhmanova, A. (2006). Microtubule plus end: a hub of cellular activities. *Traffic* 7, 499–507. doi: 10.1111/j.1600-0854.2006.00400.x

Magen, I., and Gozes, I. (2013). Microtubule-stabilizing peptides and small molecules protecting axonal transport and brain function: focus on davunetide (NAP). *Neuropeptides* 47, 489–495. doi: 10.1016/j.npep.2013.10.011

Magen, I., and Gozes, I. (2014). Davunetide: Peptide therapeutic in neurological disorders. *Curr. Med. Chem.* 21, 2591–2598. doi: 10.2174/0929867321666140217124945

Magen, I., Ostritsky, R., Richter, F., Zhu, C., Fleming, S. M., Lemesre, V., et al. (2014). Intranasal NAP (davunetide) decreases tau hyperphosphorylation and moderately improves behavioral deficits in mice overexpressing alpha-synuclein. *Pharmacol. Res. Perspect.* 2:e00065. doi: 10.1002/prp2.65

Matsuoka, Y., Jouroukhin, Y., Gray, A. J., Ma, L., Hirata-Fukae, C., Li, H. F., et al. (2008). A neuronal microtubule-interacting agent, NAPVSIPQ, reduces tau pathology and enhances cognitive function in a mouse model of Alzheimer's disease. *J. Pharmacol. Exp. Ther.* 325, 146–153. doi: 10.1124/jpet.107.130526

Oz, S., Kapitansky, O., Ivashco-Pachima, Y., Malishkevich, A., Giladi, E., Skalka, N., et al. (2014). The NAP motif of activity-dependent neuroprotective protein (ADNP) regulates dendritic spines through microtubule end binding proteins. *Mol. Psychiatry* 19, 1115–1124. doi: 10.1038/mp.2014.97

Quraishe, S., Sealey, M., Cranfield, L., and Mudher, A. (2016). Microtubule stabilising peptides rescue tau phenotypes *in-vivo*. *Sci. Rep.* 6:38224. doi: 10.1038/srep38224

Ramirez-Rios, S., Denarier, E., Prezel, E., Vinit, A., Stoppin-Mellet, V., Devred, F., et al. (2016). Tau antagonizes end-binding protein tracking at microtubule ends through a phosphorylation-dependent mechanism. *Mol. Biol. Cell* 27, 2924–2934. doi: 10.1091/mbc.E16-01-0029

Sayas, C. L., Tortosa, E., Bollati, F., Ramírez-Ríos, S., Arnal, I., and Avila, J. (2015). Tau regulates the localization and function of End-binding proteins 1 and 3 in developing neuronal cells. *J. Neurochem.* 133, 653–667. doi: 10.1111/jnc.13091

Shiryaev, N., Jouroukhin, Y., Giladi, E., Polyzoidou, E., Grigoriadis, N. C., Rosenmann, H., et al. (2009). NAP protects memory, increases soluble tau and reduces tau hyperphosphorylation in a tauopathy model. *Neurobiol. Dis.* 34, 381–388. doi: 10.1016/j.nbd.2009.02.011

Sragovich, S., Merenlender-Wagner, A., and Gozes, I. (2017). ADNP plays a key role in autophagy: from autism to schizophrenia and Alzheimer's disease. *Bioessays* 39:1700054. doi: 10.1002/bies.201700054

Vulih-Shultzman, I., Pinhasov, A., Mandel, S., Grigoriadis, N., Touloumi, O., Pittel, Z., et al. (2007). Activity-dependent neuroprotective protein snippet NAP reduces tau hyperphosphorylation and enhances learning in a novel transgenic mouse model. *J. Pharmacol. Exp. Ther.* 323, 438–449. doi: 10.1124/jpet.107.129551

Wilkemeyer, M. F., Chen, S. Y., Menkari, C. E., Brenneman, D. E., Sulik, K. K., and Charness, M. E. (2003). Differential effects of ethanol antagonism and neuroprotection in peptide fragment NAPVSIPQ prevention of ethanol-induced developmental toxicity. *Proc. Natl. Acad. Sci. U.S.A.* 100, 8543–8548. doi: 10.1073/pnas.1331636100

Yenjerla, M., LaPointe, N. E., Lopus, M., Cox, C., Jordan, M. A., Feinstein, S. C., et al. (2010). The neuroprotective peptide NAP does not directly affect polymerization or dynamics of reconstituted neural microtubules. *J. Alzheimer's Dis.* 19, 1377–1386. doi: 10.3233/JAD-2010-1335

Zamostiano, R., Pinhasov, A., Gelber, E., Steingart, R. A., Seroussi, E., Giladi, E., et al. (2001). Cloning and characterization of the human activity-dependent neuroprotective protein. *J. Biol. Chem.* 276, 708–714. doi: 10.1074/jbc.M007416200

Conflict of Interest Statement: The authors declare that the research was conducted in the absence of any commercial or financial relationships that could be construed as a potential conflict of interest.

frontiers in Molecular Neuroscience

ORIGINAL RESEARCH
published: 07 May 2018
doi: 10.3389/fnmol.2018.00150

Complement C3 Affects Rac1 Activity in the Developing Brain

*Anna Gorelik, Tamar Sapir, Lihi Ben-Reuven and Orly Reiner**

Department of Molecular Genetics, Weizmann Institute of Science, Rehovot, Israel

The complement system, which is part of the innate immune response system, has been recently shown to participate in multiple key processes in the developing brain. Here we aimed to elucidate downstream signaling responses linking complement C3, a key molecule of the pathway, to small GTPases, known to affect the cytoskeleton. The expression pattern of the activated small GTPase Rac1 resembled that of complement C3. C3-deficient mice exhibited reduced Rac1 and elevated RhoA activity in comparison with control mice. The most pronounced reduction of Rac1 activity occurred at embryonic day 14. Rac1 has been implicated in neuronal migration as well as neuronal stem cell proliferation and differentiation. Consistent with the reduction in Rac1 activity, the expression of phospho-cofilin, decreased in migrating neurons. Reduced Rac1-GTP was also correlated with a decrease in the expression of progenitor markers (Nestin, Pax6 and Tbr2) and conversely the expression of neuronal markers (Dcx and NeuN) increased in C3 knockout (KO) cortices in comparison with wild-type (WT) cortices. More specifically, C3 deficiency resulted in a reduction in the number of the cells in S-phase and an elevation in the number of cells that precociously exited the cell cycle. Collectively, our findings suggest that C3 impacts the activity of small GTPases resulting in cell cycle defects and premature neuronal differentiation.

Keywords: complement C3, cortical development, neuronal stem cells, cell cycle, Rac1

OPEN ACCESS

Edited by:
Jesus Avila,
Universidad Autonoma de Madrid, Spain

Reviewed by:
Gavin John Clowry,
Newcastle University, United Kingdom
Tobias Engel,
Royal College of Surgeons in Ireland, Ireland

***Correspondence:**
Orly Reiner
orly.reiner@weizmann.ac.il

Received: *06 February 2018*
Accepted: *16 April 2018*
Published: *07 May 2018*

Citation:
Gorelik A, Sapir T, Ben-Reuven L and Reiner O (2018) Complement C3 Affects Rac1 Activity in the Developing Brain. Front. Mol. Neurosci. 11:150. doi: 10.3389/fnmol.2018.00150

INTRODUCTION

Complement acts as a rapid and efficient immune surveillance system that has distinct effects on healthy and altered host cells and foreign intruders (reviews Walport, 2001a,b; Zipfel et al., 2007; Ricklin et al., 2010; Hawksworth et al., 2017). The complement system is composed of a large family of proteins, which are either secreted or membrane bound. These proteins are usually inactive until the system is triggered by stimuli. Complement is activated by three major routes: the classical, the alternative and the lectin pathways, all of which converge on complement component C3, a central molecule in the system that ultimately drives complement effector functions, including the elimination of pathogens, debris and cellular structures. Several complement proteins are cleaved during activation of the system; for example, C3 is cleaved into two fragments, C3a and C3b.

During recent years, the notion that the immune system participates in regulation of complex behavior has emerged and it has been proposed to be malfunctioning in diseases as diverse as autism spectrum disorder (Hsiao et al., 2012; Onore et al., 2012), as well as late onset diseases such as Alzheimer's (review Veerhuis et al., 2011). Mutations in members of the lectin arm of the complement pathway have been previously implicated in 3MC syndrome (Degn et al., 2011; Rooryck et al., 2011), in which intellectual impairment is part of the complex syndrome.

C3 regulates the number and function of glutamatergic synapses in the hippocampus and exerts negative effects on hippocampus-dependent cognitive performance (Perez-Alcazar et al., 2014). C3 deficiency spared age dependent synaptic and neuronal loss in a region-specific manner and protected against cognitive impairment in normal aging of wild-type (WT) mice (Shi et al., 2015). Furthermore, it was shown that C3 deficiency is beneficial in Alzheimer's disease model as it protected against age- and plaque related synapse and neuron loss, decreased glial reactivity and spared cognitive decline in APP/PS1mice despite an increased plaque burden in the mouse brain (Shi et al., 2017). Innate immune molecules have been found participate in regulation of synaptic plasticity (review Boulanger and Shatz, 2004). The activity of the complement pathway has been implicated in developmental pruning of synapses refinement of the mouse visual system (Stevens et al., 2007; Schafer et al., 2012; Bialas and Stevens, 2013).

Our recent research has shown that immune signaling plays a role in early neural brain development, which includes neuronal stem cell proliferation and neuronal migration (Gorelik et al., 2017a,b). In particular, we have shown that key proteins in the lectin arm of this pathway, MASP1, MASP2 and C3, are expressed in the developing cortex and that neuronal stem cell proliferation and neuronal migration is affected in KO and knockdown mice. Molecular mimics of C3 cleavage products rescued the migration defects that have been seen following knockdown of *C3* or *Masp2*. Pharmacological activation of the downstream receptors rescued *Masp2* and *C3* knockdown as well as *C3* KO (Gorelik et al., 2017a). An additional study investigated the complex developmental roles of *Serping1* or C1 inhibitor, which is known to inhibit the initiation of the complement cascade (Gorelik et al., 2017b). Knockdown or KO of *Serping1* affected neuronal stem cell proliferation and impaired neuronal migration in mice both in a cell-autonomous and non-cell autonomous manner. Most importantly, expression of protein components mimicking cleaved C3 rescued the knockdown of *Serping1*, indicating complement pathway functionality. Despite compelling evidence for the complement functions in the developing brain, the molecular mechanisms that allow these secreted molecules to exert their function is unknown. C3a and C5a receptors are G-protein coupled, which are involved in a wide repertoire of cellular signaling. Activation of G-proteins may induce cytoskeletal rearrangement, which is required for cell division and radial neuronal migration. As key regulators of actin and microtubule cytoskeletons, cell polarity and adhesion, the Rho GTPases play critical roles in CNS neuronal migration (reviews Govek et al., 2011; Evsyukova et al., 2013). Furthermore, activation of the C3a receptor by C3a induced the activity of Rac1, a Rho GTPase, in migrating crest cells (Carmona-Fontaine et al., 2011). Moreover, when Rac1 was inhibited, neural crest cell explants lost their coattraction, supporting the idea that this mechanism occurs by mutual chemoattraction, possibly via Rac1 activated by C3aR upon binding to C3a. Rho family GTPases function as molecular switches and cycle between an active, GTP-bound state, and an inactive, GDP-bound state (review Iden and Collard, 2008). In this current study, we demonstrated the effect of C3 deficiency on the activity of small GTPases, in particular Rac1, and revealed how this affects neuronal stem cell cycle and cell fate determination.

MATERIALS AND METHODS

Antibodies

Mouse anti RAC1 (Millipore, 1:1000), rabbit anti RHOA (Cell Signaling, 1:1000), mouse anti CDC42 (Cytoskeleton, 1:1000), rabbit anti Glutathione-S-Transferase (GST; Santa Cruz, 1:2000) and rabbit anti EMERIN (Santa Cruz, Miami, FL, USA-254 1:1000) were used for western blotting.

The following antibodies were used for immunostainings: mouse anti RAC1 (Millipore, 1:200), mouse anti active RAC1 (NewEast Biosciences, 1:200), rabbit anti C3 (Antibody Verify, 1:400), mouse anti Phospho-COFILIN (Santa Cruz, 1:200), mouse anti iododeoxyuridine (IdU)-B44 (BD Biosciences, 1:200, 347580).

Animals

Animal protocols were approved by the Weizmann Institute IACUC and were carried out in accordance with their approved guidelines (approval number 34400317-2). *C3* KO mice were obtained from the Jackson Laboratory. Male and female embryos were used in the study.

Small GTPases Activation Assay

GST-P21 activated kinase (GST-PAK), GST-RHOTEKIN (GST-RTKN) and GST were purified in NETN buffer (0.5% NP-40, 20 mM Tris-HCl pH 8, 100 mM NaCl, 1 mM EDTA) supplemented with PMSF and incubated with glutathione-agarose beads.

Cortices (two brains per tube) from *C3* KO or WT embryos (E16) were collected on ice, immediately dissociated in the lysis buffer (50 mM Tris-HCl pH 7.5; 150 mM NaCl; 1 mM EDTA; 1 mM EGTA; 1% Triton X-100 supplemented with aprotinin, leupeptin, NaF, sodium orthovanadate and protease inhibitor cocktail) and centrifuged at 13,000 rpm. 0.5% of the resulted soup was used directly for western blot analysis to determine the general levels of small GTPases. The rest of the soup from each condition was divided to three equal parts and incubated overnight in 4°C with GST-PAK, GST-RTKN or GST treated beads. The beads were washed three times with NETN buffer. The pelleted beads were eluted by heating in 2× SDS-buffer. The samples were separated by SDS-PAGE and subjected to western blot analysis with the indicated antibodies. The relative quantification of the protein bands was performed with ImageJ "Gels" measurements. The intensity measurements of the bands of the small GTPases from the pull down were normalized to the intensity of the GST bands and to the level of the relevant small GTPase in the brain lysates. Emerin intensity served as the loading control of the lysates. The resulted data from six independent biological repeats of the WT and *C3* KO were analyzed with the *Student t*-test. The averages are presented in the graphs.

IdU/EdU Labeling

The thymidine analogs IdU (0.01 ml of 5 mg/ml IdU solution per gram body weight) and 5-ethynyl-2′-deoxyuridine (EdU, 50 mg per gram body weight) were injected intraperitoneally to pregnant *C3* KO and WT mice (E14) 3 h and 30 min respectively before sacrifice. The brains were removed and fixed in 2.5% PFA-PBS overnight, washed and cryoprotected by immersion in 30% sucrose-PBS solution. The cryosections (10 μm) were pretreated in boiling sodium citrate buffer (10 mM, pH 6) for 30 min. The click reaction was performed with Cy3 azide (2.5 μM) in the PBS-based buffer containing 100 mM Tris-HCl, 1 mM $CuSO_4$ and 100 mM ascorbic acid. To block EdU epitopes before immunostaining with anti IdU antibodies the reaction was followed by a click reaction with a non-fluorescent molecule (Phenylthiomethyl-Azide 20 mM, Sigma). After treatment with 10 mM ascorbic acid and 4 mM $CuSO_4$, followed by incubation with 20 mM EDTA, the immunostainings with anti-IdU-B44 were performed. The length of S phase was calculated $T_{s\text{-}phase} = \frac{Ti}{L/S}$, given i = labeling interval 2.5 h, $L_{(leaving)} = Idu^{+}EdU^{-}$, $S_{(currently\ at\ S\text{-}phase)} = IdU^{+}EdU^{+}$. This protocol was adapted from a previously published procedure (Nowakowski et al., 1989). Overall, click reactions can be successfully combined with immunostainings (Kalveram et al., 2013).

Immunocytochemistry

Floating vibratome sections (60 μm) or cryosections (10 μm) were permeabilized using 0.1% Triton X-100 and blocked in blocking solution (PBS, 0.1% Triton X-100, 10% HS; 10% FBS) for 60 min. Antibodies were incubated in blocking solution over night at 4°C. After washing, appropriate secondary antibodies (Jackson ImmunoResearch) were diluted in blocking solution, and incubated for 2 h at room temperature. Slices were mounted onto glass slides using Aqua Polymount (Polysciences). Brains of embryos treated with EdU/IdU were fixed in 2.5% PBS-PFA, cryoprotected in 20% sucrose and cryo-sectioned to 14 μm thick slices before further processing.

Microscopy, Quantification and Statistical Analyses

Images were taken using confocal microscopy (LSM800 Zeiss), equipped with Axio Observer Z1 microscope, and imaged with either Plan-apochromat 20×/0.8, or Plan-apochromat 63×/1.4 oil objectives. The scaling data are 0.624 × 0.624 μm per pixel for 20× magnification, and 0.198 × 0.198 × 0.51 μm per voxol for 60× magnification. The images were processed by ZEN software and/or Imaris software. Cell count and colocalization analyses were performed using Imaris software (Bitplane Inc., Zurich, Switzerland, Imaris core module). Three brains were analyzed for each treatment. Four representative slices from each brain were chosen for analysis. The size of the area of interest was determined and preserved per each experiment. For the cell counts the relevant channel of an area of interest was analyzed with "Spots" module of Imaris, every spot labeling approximate center of the cell body. For double-labeling the new channel was created with Imaris channel mixer and this channel was analyzed with "Spots" module. For the intensity analysis, the mean gray values (ImageJ) of the relevant channel of the identical areas of the cortex were compared. Comparisons of intensities were conducted using the whole width of the imaged cortex. Statistical analysis was performed by *t*-test or *t*-test with Bonferroni correction. Error bars represent standard error.

Real-Time qRT-PCR

E14 cortices (two brains for each repeat, $N = 4$) from *C3* KO and WT were dissected in cold PBS and RNA isolation was performed according with Sigma protocol (TRI reagent, Sigma). After Dnase treatment (Sigma), first-strand cDNA synthesis was done using M-MLV RT (Promega). Relative levels of expression (three technical repeats for each sample) were normalized to the *29rps* gene. Real-time PCR with SYBR FAST ABI qPCR kit (Kapa Biosystems) was performed using (Quant Studio 5). The following sets of primers were used for Real-time PCR reactions: 29rps: 5′-TCGTTGGGCGTCTGAAGGCAA and 5′-CGGAAG CACTGGCGGCACAT; C3aR: 5′-GGTGAGATGGAGGAACC AGA and 5′-ATTGGGACTGCTAGGCAATG; Nestin: 5′-GC AACTGGCACACCTCAAGA and 5′-AGCAGAGTCCTGTAT GTAGCC; Pax6: 5′-CTTTGAGAAGTGTGGGAACCAG and 5′-TGGTTAAAGTCTTCTGCCTGTGAG; Sox2: 5′-TTCGCA GGGAGTTCGCAAAA and 5′-ACCCAGCAAGAACCCTTT CC; Svet1: 5′-GTCGTAGCAACAGGATAGATGAG and 5′-GG CAAACCATTGGGAACTCGTG; NeuroD1: 5′-ACAACAGG AAGTGGAAACATGACC and 5′-CACTCATCTGTCCAGCT TGGG; Tbr2: 5′-GACCTCCAGGGACAATCTGA and 5′-GG CCTACCAAAACACGGATA; Dcx: 5′-GAGTGGGGCTTTCG AGTGAT and 5′-GGAACCACAGCAACTTTTCCAA; NeuN: 5′-GCGGAAACCTCCTCGGACAG and 5′-TTTTCAACGGG TTCAGCGTTCC; Satb2: 5′-CAGCCAGCCAAGTTTCAGAC and 5′-GGAATCATCAAACCTCCCACGG.

RESULTS

The Activity of Small GTPases in C3 Brain Lysates

As mentioned above, previous studies have demonstrated that Rac1 is activated following the binding of C3a to the C3a receptor (Carmona-Fontaine et al., 2011), therefore, we examined the activity of the small GTPases Rac1, RhoA and Cdc42 in the developing brains of WT and *C3* KO mice (**Figure 1**). The activity of these proteins is regulated by the interaction of Rho family GTPases with guanine-nucleotide exchange factors (GEFs) and GTPase-activating proteins (GAPs). The activated small GTPases bind to their effectors. For example, the GTP-bound Rac1 bind to p21 protein (Cdc42/Rac)-activated kinase 1 (PAK) protein through its Cdc42-Rac-interactive-binding (CRIB) domain (Frost et al., 1997). This property enabled measuring the activity of the small GTPases in brain lysates using pull-down experiments with recombinant proteins expressing the binding domains (from PAK1 for Cdc42 and Rac1 and from Rhotekin (RTKN) for RhoA; **Figure 1**). The activity was determined by the ratio of the signal of active pulled-down proteins (Rac1, RhoA, or Cdc42) vs. the amount of

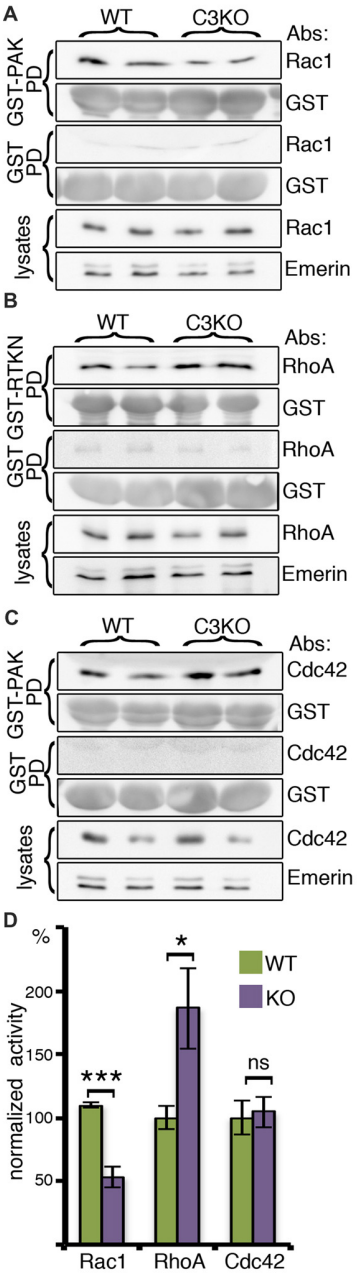

FIGURE 1 | The activity of the small Rho GTPases, RAC1, RHOA and CDC42, in brain lysates. Protein extracts from *C3* knockout (KO; $N = 6$) and wild-type (WT; $N = 6$) E16 cortices were incubated with glutathione-agarose beads pretreated with GST-P21 activated kinase Glutathione-S-Transferase-P21 activated kinase (GST-PAK; **A,C**), GST-Rhotekin Rhotekin (RTKN; **B**) or GST as control for all conditions **(A–C)**. The amount of activated RAC1 **(A)** was determined as a ratio of the amount of RAC1 bound to GST-PAK normalized to the amount of GST-PAK in the reaction and to the total amount of RAC1 in the brain lysate (RAC1/EMERIN in lysates). In a similar way, the activity of RHOA **(B)** and CDC42 was quantified **(C)**. All three proteins did not bind to GST. **(D)** Comparison of the normalized activity is shown. Student's *t*-test, $^{***}p < 0.001$, $^{*}p < 0.05$, ns, $p = 0.81$.

the relevant recombinant protein in reaction, normalized by the total amount of the small GTPases in the lysate (**Figures 1A–C**). *C3* KO mice exhibited a significant reduction in Rac1 activity and a significant elevation in RhoA activity, while no change was observed in the activity of Cdc42 (**Figure 1D**).

In Situ Localization of Rac1-GTP

To better understand how the reduction in Rac1 activity in C3 KO impacts brain development, immunostainings with anti-Rac1 and anti-C3 antibodies were conducted on E14 embryonic brain slices (**Figures 2A,B**). The distribution of the active Rac1 signal was most pronounced in the area which is in between the intermediate zone and the cortical plate, the subplate, and in the marginal zone. Prior to entering the cortical plate migrating neurons usually change their polarity (Tabata and Nakajima, 2003). Interestingly, immunostainings with anti-C3 antibodies demonstrate an increased signal in the same domain (**Figure 2A**). Higher magnification images reveal that in many cases the C3 signal is juxtaposed to active Rac1, which could be expected from an extracellular secreted molecule and an intracellular signaling molecule, respectively (**Figure 2B**). We next proceeded to examine whether the expression of total Rac1 differs from that of active Rac1. At E16, Rac1 is widely expressed in the developing brain and a more pronounced signal can be seen in the intermediate zone and the cortical plate. Active Rac1 strongest signal was observed in the subplate similar to E14 (**Figure 2C**). Then, we examined how active Rac1 is modulated in embryonic C3 KO brain (**Figures 2D–G**). At embryonic day 14 and 16, Rac1 activity was markedly and significantly reduced in C3 deficient brain sections (**Figures 2D,E,G**). Rac1 activity at embryonic day 18 did not differ between the C3 KO and the WT brains (**Figures 2F,G**). Rac1 has multiple downstream targets, amongst them it is known to induce the phosphorylation of Cofilin, which promotes actin polymerization (Delorme et al., 2007). Furthermore, previous studies have demonstrated that Cofilin is phosphorylated in migrating neurons, downstream to the Reelin pathway, and this activity is important to promote neuronal migration (Chai et al., 2009; Frotscher et al., 2017). Therefore, E16 brain sections were immunostained with anti-phospho-Cofilin antibodies (**Figure 2H**). The sections from C3 KO mice displayed significantly reduced levels of phospho-Cofilin, which mirrored the reduction in activated Rac1 (**Figure 2I**). Interestingly, the reduction in Rac1 activity was temporal and correlated well with the developmental peak in neuronal stem cell proliferation and neuronal migration. We speculate that at least part of the neuronal migration impairments observed in the developing C3 deficient mice are due to the reduction in active Rac1 and consequently phosphorylated Cofilin (Gorelik et al., 2017a).

Rac1-GTP in the VZ and SVZ

Next, the proliferative zones, which include the ventricular zone (VZ) and subVZ (SVZ) were examined more closely (**Figure 3**). Rac1-GTP is localized mainly to the apical membrane in the VZ (**Figure 3A** and insert), with some cells showing a signal in the cell soma (**Figure 3A**). Rac1 activity is significantly and markedly reduced in the same areas in C3 KO mice (**Figures 3A,B**). Reduced Rac1 activity within these stem cell niches may affect

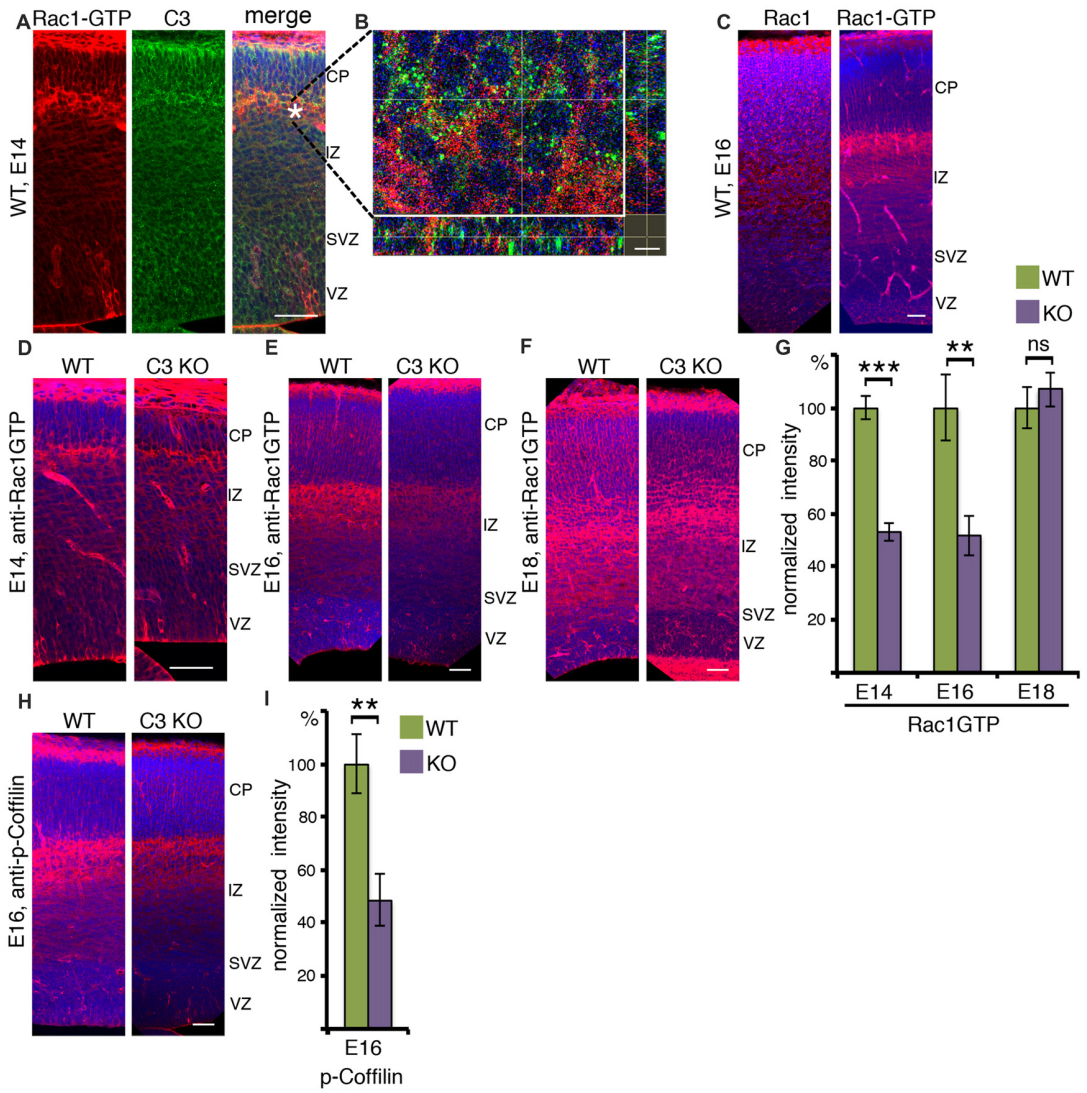

FIGURE 2 | Activated RAC1 in the developing cortex. **(A)** E14 brain sections were immunostained with anti-RAC1-GTP and anti-C3 antibodies. RAC1-GTP shows the highest intensity on the entrance to the cortical plate (CP). The scale bar is 50 μm. **(B)** High-magnification shows that in this area the signal of C3 is in close vicinity to that of RAC1-GTP. The scale bar is 5 μm. **(C)** E16 brain sections were immunostained with anti-RAC1 or anti-RAC1-GTP antibodies. Total RAC1 was evenly distributed all over the cortex, whereas the intensity of RAC1-GTP immunostaining signal was the highest between intermediate zone (IZ) and CP. The scale bar is 50 μm. **(D–F)** Comparison of anti-RAC1-GTP immunostaining in WT and *C3* KO on different embryonic days: E14 (**D**, $N = 6$), E16 (**E**, $N = 6$), E18 (**F**, $N = 6$). **(G)** The normalized intensity of RAC1-GTP is presented as percentage of WT levels. **(H)** WT and *C3* KO E16 brain sections ($N = 6$) were immunostained with anti-phospho-COFILIN antibodies. The scale bars are 50 μm. **(I)** The normalized intensity of phospho-COFILIN is presented as percentage of WT levels. Student's *t*-test, $^{***}p < 0.001$, $^{**}p < 0.01$.

neuronal cell fate decision as well as cell cycle parameters. Therefore, we examined the steady state mRNA status of a battery of genes using RNA extracted from WT and C3 KO E14 cortices (**Figure 3C**). The expression of the C3a receptor C3aR, increased in more than 25% in the C3 KO, probably reflecting some compensatory pathways due to the absence of C3 and its cleavage products C3a and C3b. This finding may suggest that in C3 KO there may be alterations in other complement-related genes. Next we proceeded to investigate the expression of a battery of progenitor markers by means of real-time qPCR. A significant reduction was noted in the expression of two progenitor markers, Nestin and Pax6. However, the expression of Sox2, which labels preferentially radial glia, but also intermediate progenitor cells (Hutton and Pevny, 2011) and Svet1, which labels multipolar cells in the SVZ (Tarabykin et al., 2001; Sasaki et al., 2008) did not vary between the WT and the control brains. In a similar manner, the expression of NeuroD1, which is highly expressed in the VZ, is upregulated several fold in the SVZ, and then is downregulated in the CP (Pataskar et al., 2016), was similar between the two genotypes. The expression of the intermediate progenitor marker, Tbr2 (Kowalczyk et al., 2009), was significantly reduced in the C3 KO mice. In a converse

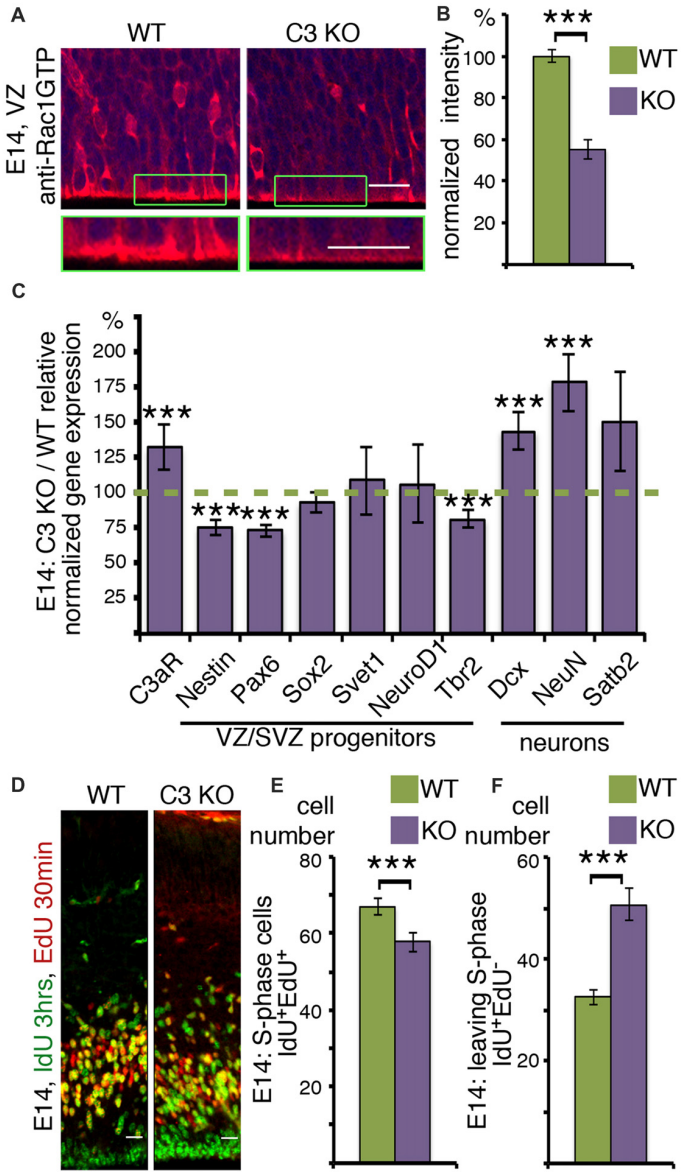

FIGURE 3 | *C3* KO affects neuronal cell fate decisions and stem cell porliferation. **(A,B)** Ventricular zone (VZ) area of E14 WT and C3 KO brain sections ($N = 6$) immunostained with anti-RAC1-GTP antibodies. A higher magnification is shown in the green boxed insert. **(B)** The intensity of RAC1-GTP was measured and shown as percentage of WT levels. Student's *t*-test, $^{***}p < 0.001$ **(C)** Results of real-time qRT-PCR are presented as the ratio of mRNA expression levels of *C3* KO to the WT. Two technical repeats of four brains for each genotype were used for analysis. *Student's t*-test with Bonferroni correction, $^{***}p < 0.001$. **(D)** *C3* KO and WT embryonic brains were labeled at E14 with IdU (3 h) and EdU (30 min). The brains were cryosectioned, EdU was detected by Cu(I)-catalyzed [3 + 2] cycloaddition reaction followed by immunostainings with anti-IdU antibodies. The scale bar is 20 μm. The number of cells per equal area which are actively in S-phase (IdU^+EdU^+; **E**) and leaving the cell cycle (IdU^+EdU^-; **F**) compared between *C3* KO ($N = 17$) and WT ($N = 22$), Student's *t*-test, $^{***}p < 0.001$.

fashion, there was a significant increase in the expression of two early neuronal markers, Dcx (Francis et al., 1999) and NeuN (Mullen et al., 1992). Changes in the expression of the neuronal upper layer marker Satb2 (Britanova et al., 2008) were not significant. The observed decrease in some of the progenitor markers and the increase in some of the neuronal markers suggest that in C3 KO there may be a reduction in some of the neuronal progenitors which results in premature differentiation.

To gain a direct insight on cell cycle parameters, the progenitors were double labeled with two thymidine analogs, which are incorporated into the DNA during S-phase. The first label was done with IdU, followed by a second label with EdU. IdU was detected by immunostaining and EdU incorporation was visualized by click chemistry. The nuclei which are double labeled with both analogs either remained in S-phase for the duration of the combined labeling time or re-entered S-phase. The number of double positive cells decreased in the C3 KO

mice (**Figure 3E**). Conversely, the number of cells that exited S-phase and were exclusively labeled by IdU, was higher in the C3 deficient embryos (**Figure 3F**). The duration of S-phase was 5.24 ± 0.75 h in the WT animals and only 2.96 ± 0.64 h in the C3 KO mice. In summary, C3 KO mice exhibited significant deviations in S-phase duration from the WT mice. Collectively, our study demonstrates that deficiency of C3 affected not only neuronal migration (Gorelik et al., 2017a) but also impaired cell cycle progression and the expression of cell fate markers.

DISCUSSION

Our current study suggests that the small GTPase Rac1 may be participating in mediating the signaling following complement activation in the developing brain. Small Rho GTPases are known to mediate cytoskeletal changes involving both the actin and the microtubule cytoskeleton, both of which are important for CNS development (reviews Govek et al., 2011; Evsyukova et al., 2013). Our study detected that *C3* KO mice exhibit a significant reduction in Rac1 activity and a significant elevation in RhoA activity, while no change was observed in the activity of Cdc42. The reduction in Rac1 and elevation in RhoA fits with the known activities of these small GTPases. From the perspective of cell morphology, Rac1 and RhoA oppose each other. Canonical descriptions of cell migration place active Rac1 at the front of a migrating cell and active RhoA at its rear. Biochemically, Rac1 and RhoA are generally found to interact in mutually antagonistic ways, playing opposing roles in cell migration (review Guilluy et al., 2011). These opposing activities, as well as a negative feedback loop, lead to bistability in the signals regulating the dynamic cytoskeleton (Byrne et al., 2016). The availability of antibodies which recognize the active, GTP-bound form of Rac1 activation enabled the visualization of the temporal and spatial specific activity in the developing brain. Rac1 activity peaked at E14, coinciding with active neuronal migration and neuroblast proliferation. Migrating neurons entering the cortical plate demonstrated a strong Rac1-GTP signal which was reduced in C3 KO. The documented role of C3 in refinement of synaptic connections (Stevens et al., 2007) and the pattern of active Rac1 localization may point at additional and yet unexplored roles of C3 in early synaptogenesis. We found a particular high Rac1 GTP in the subplate, a transient zone that is located below the cortical plate and above the intermediate zone in the rodent developing cortex. The marginal zone and subplate neurons are among the first to be become post mitotic and they contribute to axon pathfinding and to circuits establishment (Balslev et al., 1996; López-Bendito and Molnár, 2003).

We further investigated the phosphorylation status of Cofilin, which is one of the downstream targets of Rac1. Cofilin is also known to promote neuronal migration and acts downstream to the Reelin pathway (Chai et al., 2009; Frotscher et al., 2017). The phosphorylation of Cofilin in C3 KO brains, was markedly reduced. Rac1 conditional KO mice exhibited delayed neuronal migration of pyramidal neurons (Chen et al., 2007). The phenotype observed in these Rac1 conditional KO mice was similar to that documented in *C3* KO, where neuronal migration was hindered but not completely halted (Gorelik et al., 2017a). Our previous studies have shown that the active lectin/MASP arm of the complement pathway, leading to cleavage of C3, and activating the complement peptide receptors for C3a and C5a, is required for proper migration of neurons in the developing brain (Gorelik et al., 2017a). Furthermore, we suggested that functional activation of the pathway, resulting in C3 cleavage and production of C3 and C5 bioactive mediators, may be an important step in shaping the journey of neurons on their way to the cortical plate. Based on our current findings, we propose that Rac1 is one of the mediators of the complement signaling and that Rac1 facilitates transmission of the signal to the cytoskeleton, which will in turn mobilize the migrating neurons.

The possible effect on Rac1 activity was further investigated in the VZ and SVZ zones. A prominent signal of Rac1-GTP was noticed in the apical domain of neuroblasts in the VZ, which confirms previous studies (Minobe et al., 2009). In that study, addition of a Rac inhibitor or forced expression of a dominant-negative Rac1 significantly retarded interkinetic nuclear migration, and resulted in cytokinesis failures (Minobe et al., 2009). A role for Rac1 in the production of neuronal progenitors and cell fate specification was shown using a conditional allele (Chen et al., 2009). Rac1 deletion in the telencephalic VZ progenitors resulted in reduced sizes of both the striatum and cerebral cortex. Neuronal progenitors exhibited accelerated cell-cycle exit and increased apoptosis during early corticogenesis, leading to a decrease of the neural progenitor pool in mid-to-late telencephalic development (E16.5 to E18.5; Chen et al., 2009). Here, we have demonstrated a significant reduction in the length of S-phase and an increased exit from the cell cycle in the *C3* deficient mice. We propose that complement C3 KO resulted in modified expression of some key progenitor genes. Recent studies demonstrate that at the single cell level there is a huge variability in gene expression levels, therefore, it is possible that the lack of C3 affects different progenitor populations in diverse manners. The expression of *Nestin* was significantly reduced following C3 KO; *Nestin* mRNA expression correlates with many, but not all, regions of proliferating CNS progenitor cells. In addition to its temporal and spatial regulation, *Nestin* expression is also regulated at the level of subcellular mRNA localization: in columnar neuroepithelial and radial glial cells *Nestin* mRNA was predominantly localized to the pial endfeet where most of the active Rac1 signal was localized to (Dahlstrand et al., 1995). In a similar manner, the expression of the key progenitor maker *Pax6* was reduced in C3 KO brains. The levels of *Pax6* are known to be essential for controlling the balance between neural stem cell self-renewal and neurogenesis (Sansom et al., 2009). However, the expression of *Sox2* did not vary. Within the second population of progenitors, the intermediate progenitors, a reduction in the expression of the transcription factor Tbr2 (Kowalczyk et al., 2009), was noted, but no changes were noted in the expression of *Svet1*. One consequence of the reduced expression of some progenitor gene makers, shortening of S-phase and an increased exit from S-phase could be premature differentiation and depletion of the pool

of progenitors. Indeed, we noted increased expression of the neuronal markers *Dcx* and *NeuN*, and in our previous studies we detected a reduction in the width of *C3* KO cortices (Gorelik et al., 2017a). Collectively, our findings implicate Rac1 as one of the important downstream mediators of complement activity within the developing brain of the mouse embryo.

AUTHOR CONTRIBUTIONS

AG planned, conducted and analyzed most of the experiments. TS and LB-R planned, conducted and analyzed some of the experiments. OR planned and analyzed the experiments. All the authors participated in writing of the manuscript. All authors agree to be accountable for the content of the work.

FUNDING

The research has been supported by the Israel Science Foundation (Grant No. 347/15), the Legacy Heritage Biomedical Program of the Israel Science Foundation (Grant No. 2041/16), ERA-NET Neuron with support of the IMOH (Grant No. 3-0000-12276), by the European Cooperation on Science and Technology (COST Action CA16118), Weizmann-FAPESP supported by a research grant from Sergio and Sonia Lozinsky, Nella and Leon Benoziyo Center for Neurological Diseases, Jeanne and Joseph Nissim Foundation for Life Sciences Research, Wohl Biology Endowment Fund, Lulu P. and David J. Levidow Fund for Alzheimers Diseases and Neuroscience Research, the Helen and Martin Kimmel Stem Cell Research Institute, the Kekst Family Institute for Medical Genetics, the David and Fela Shapell Family Center for Genetic Disorders Research.

ACKNOWLEDGMENTS

We are grateful for the help of Ofira Higfa, Yehuda Melamed, Osnat Amram and Oz Yirmiyahu from the Weizmann Institute of Science. OR is the incumbent of the Bernstein-Mason Chair of Neurochemistry. TS is an Incumbent of the Leir Research Fellow Chair in Autism Spectrum Disorder Research.

REFERENCES

Balslev, Y., Saunders, N. R., and Mollgard, K. (1996). Synaptogenesis in the neocortical anlage and early developing neocortex of rat embryos. *Acta Anat.* 156, 2–10. doi: 10.1159/000147822

Bialas, A. R., and Stevens, B. (2013). TGF-β signaling regulates neuronal C1q expression and developmental synaptic refinement. *Nat. Neurosci.* 16, 1773–1782. doi: 10.1038/nn.3560

Boulanger, L. M., and Shatz, C. J. (2004). Immune signalling in neural development, synaptic plasticity and disease. *Nat. Rev. Neurosci.* 5, 521–531. doi: 10.1038/nrn1428

Britanova, O., de Juan Romero, C., Cheung, A., Kwan, K. Y., Schwark, M., Gyorgy, A., et al. (2008). Satb2 is a postmitotic determinant for upper-layer neuron specification in the neocortex. *Neuron* 57, 378–392. doi: 10.1016/j.neuron.2007.12.028

Byrne, K. M., Monsefi, N., Dawson, J. C., Degasperi, A., Bukowski-Wills, J. C., Volinsky, N., et al. (2016). Bistability in the Rac1, PAK, and RhoA signaling network drives actin cytoskeleton dynamics and cell motility switches. *Cell Syst.* 2, 38–48. doi: 10.1016/j.cels.2016.01.003

Carmona-Fontaine, C., Theveneau, E., Tzekou, A., Tada, M., Woods, M., Page, K. M., et al. (2011). Complement fragment C3a controls mutual cell attraction during collective cell migration. *Dev. Cell* 21, 1026–1037. doi: 10.1016/j.devcel.2011.10.012

Chai, X., Förster, E., Zhao, S., Bock, H. H., and Frotscher, M. (2009). Reelin stabilizes the actin cytoskeleton of neuronal processes by inducing n-cofilin phosphorylation at serine3. *J. Neurosci.* 29, 288–299. doi: 10.1523/JNEUROSCI.2934-08.2009

Chen, L., Liao, G., Waclaw, R. R., Burns, K. A., Linquist, D., Campbell, K., et al. (2007). Rac1 controls the formation of midline commissures and the competency of tangential migration in ventral telencephalic neurons. *J. Neurosci.* 27, 3884–3893. doi: 10.1523/JNEUROSCI.3509-06.2007

Chen, L., Melendez, J., Campbell, K., Kuan, C. Y., and Zheng, Y. (2009). Rac1 deficiency in the forebrain results in neural progenitor reduction and microcephaly. *Dev. Biol.* 325, 162–170. doi: 10.1016/j.ydbio.2008.10.023

Dahlstrand, J., Lardelli, M., and Lendahl, U. (1995). Nestin mRNA expression correlates with the central nervous system progenitor cell state in many, but not all, regions of developing central nervous system. *Dev. Brain Res.* 84, 109–129. doi: 10.1016/0165-3806(94)00162-s

Degn, S. E., Jensenius, J. C., and Thiel, S. (2011). Disease-causing mutations in genes of the complement system. *Am. J. Hum. Genet.* 88, 689–705. doi: 10.1016/j.ajhg.2011.05.011

Delorme, V., Machacek, M., DerMardirossian, C., Anderson, K. L., Wittmann, T., Hanein, D., et al. (2007). Cofilin activity downstream of Pak1 regulates cell protrusion efficiency by organizing lamellipodium and lamella actin networks. *Dev. Cell* 13, 646–662. doi: 10.1016/j.devcel.2007.08.011

Evsyukova, I., Plestant, C., and Anton, E. S. (2013). Integrative mechanisms of oriented neuronal migration in the developing brain. *Annu. Rev. Cell Dev. Biol.* 29, 299–353. doi: 10.1146/annurev-cellbio-101512-122400

Francis, F., Koulakoff, A., Boucher, D., Chafey, P., Schaar, B., Vinet, M. C., et al. (1999). Doublecortin is a developmentally regulated, microtubule-associated protein expressed in migrating and differentiating neurons. *Neuron* 23, 247–256. doi: 10.1016/s0896-6273(00)80777-1

Frost, J. A., Steen, H., Shapiro, P., Lewis, T., Ahn, N., Shaw, P. E., et al. (1997). Cross-cascade activation of ERKs and ternary complex factors by Rho family proteins. *EMBO J.* 16, 6426–6438. doi: 10.1093/emboj/16.21.6426

Frotscher, M., Zhao, S., Wang, S., and Chai, X. (2017). Reelin signaling inactivates cofilin to stabilize the cytoskeleton of migrating cortical neurons. *Front. Cell. Neurosci.* 11:148. doi: 10.3389/fncel.2017.00148

Gorelik, A., Sapir, T., Haffner-Krausz, R., Olender, T., Woodruff, T. M., and Reiner, O. (2017a). Developmental activities of the complement pathway in migrating neurons. *Nat. Commun.* 8:15096. doi: 10.1038/ncomms15096

Gorelik, A., Sapir, T., Woodruff, T. M., and Reiner, O. (2017b). Serping1/C1 inhibitor affects cortical development in a cell autonomous and non-cell autonomous manner. *Front. Cell. Neurosci.* 11:169. doi: 10.3389/fncel.2017.00169

Govek, E. E., Hatten, M. E., and Van Aelst, L. (2011). The role of Rho GTPase proteins in CNS neuronal migration. *Dev. Neurobiol.* 71, 528–553. doi: 10.1002/dneu.20850

Guilluy, C., Garcia-Mata, R., and Burridge, K. (2011). Rho protein crosstalk: another social network? *Trends Cell Biol.* 21, 718–726. doi: 10.1016/j.tcb.2011.08.002

Hawksworth, O. A., Coulthard, L. G., and Woodruff, T. M. (2017). Complement in the fundamental processes of the cell. *Mol. Immunol.* 84, 17–25. doi: 10.1016/j.molimm.2016.11.010

Hsiao, E. Y., McBride, S. W., Chow, J., Mazmanian, S. K., and Patterson, P. H. (2012). Modeling an autism risk factor in mice leads to permanent immune dysregulation. *Proc. Natl. Acad. Sci. U S A* 109, 12776–12781. doi: 10.1073/pnas.1202556109

Hutton, S. R., and Pevny, L. H. (2011). SOX2 expression levels distinguish between neural progenitor populations of the developing dorsal telencephalon. *Dev. Biol.* 352, 40–47. doi: 10.1016/j.ydbio.2011.01.015

Iden, S., and Collard, J. G. (2008). Crosstalk between small GTPases and polarity proteins in cell polarization. *Nat. Rev. Mol. Cell Biol.* 9, 846–859. doi: 10.1038/nrm2521

Kalveram, B., Lihoradova, O., Indran, S. V., Head, J. A., and Ikegami, T. (2013). Using click chemistry to measure the effect of viral infection on host-cell RNA synthesis. *J. Vis. Exp.* 78:e50809. doi: 10.3791/50809

Kowalczyk, T., Pontious, A., Englund, C., Daza, R. A., Bedogni, F., Hodge, R., et al. (2009). Intermediate neuronal progenitors (basal progenitors) produce pyramidal-projection neurons for all layers of cerebral cortex. *Cereb. Cortex* 19, 2439–2450. doi: 10.1093/cercor/bhn260

López-Bendito, G., and Molnár, Z. (2003). Thalamocortical development: how are we going to get there? *Nat. Rev. Neurosci.* 4, 276–289. doi: 10.1038/nrn1075

Minobe, S., Sakakibara, A., Ohdachi, T., Kanda, R., Kimura, M., Nakatani, S., et al. (2009). Rac is involved in the interkinetic nuclear migration of cortical progenitor cells. *Neurosci. Res.* 63, 294–301. doi: 10.1016/vj.neures.2009.01.006

Mullen, R. J., Buck, C. R., and Smith, A. M. (1992). NeuN, a neuronal specific nuclear protein in vertebrates. *Development* 116, 201–211.

Nowakowski, R. S., Lewin, S. B., and Miller, M. W. (1989). Bromodeoxyuridine immunohistochemical determination of the lengths of the cell cycle and the DNA-synthetic phase for an anatomically defined population. *J. Neurocytol.* 18, 311–318. doi: 10.1007/bf01190834

Onore, C., Careaga, M., and Ashwood, P. (2012). The role of immune dysfunction in the pathophysiology of autism. *Brain Behav. Immun.* 26, 383–392. doi: 10.1016/j.bbi.2011.08.007

Pataskar, A., Jung, J., Smialowski, P., Noack, F., Calegari, F., Straub, T., et al. (2016). NeuroD1 reprograms chromatin and transcription factor landscapes to induce the neuronal program. *EMBO J.* 35, 24–45. doi: 10.15252/embj.201591206

Perez-Alcazar, M., Daborg, J., Stokowska, A., Wasling, P., Björefeldt, A., Kalm, M., et al. (2014). Altered cognitive performance and synaptic function in the hippocampus of mice lacking C3. *Exp. Neurol.* 253, 154–164. doi: 10.1016/j.expneurol.2013.12.013

Ricklin, D., Hajishengallis, G., Yang, K., and Lambris, J. D. (2010). Complement: a key system for immune surveillance and homeostasis. *Nat. Immunol.* 11, 785–797. doi: 10.1038/ni.1923

Rooryck, C., Diaz-Font, A., Osborn, D. P., Chabchoub, E., Hernandez-Hernandez, V., Shamseldin, H., et al. (2011). Mutations in lectin complement pathway genes COLEC11 and MASP1 cause 3MC syndrome. *Nat. Genet.* 43, 197–203. doi: 10.1038/ng.757

Sansom, S. N., Griffiths, D. S., Faedo, A., Kleinjan, D. J., Ruan, Y., Smith, J., et al. (2009). The level of the transcription factor Pax6 is essential for controlling the balance between neural stem cell self-renewal and neurogenesis. *PLoS Genet.* 5:e1000511. doi: 10.1371/journal.pgen.1000511

Sasaki, S., Tabata, H., Tachikawa, K., and Nakajima, K. (2008). The cortical subventricular zone-specific molecule Svet1 is part of the nuclear RNA coded by the putative netrin receptor gene Unc5d and is expressed in multipolar migrating cells. *Mol. Cell. Neurosci.* 38, 474–483. doi: 10.1016/j.mcn.2008.04.002

Schafer, D. P., Lehrman, E. K., Kautzman, A. G., Koyama, R., Mardinly, A. R., Yamasaki, R., et al. (2012). Microglia sculpt postnatal neural circuits in an activity and complement-dependent manner. *Neuron* 74, 691–705. doi: 10.1016/j.neuron.2012.03.026

Shi, Q., Chowdhury, S., Ma, R., Le, K. X., Hong, S., Caldarone, B. J., et al. (2017). Complement C3 deficiency protects against neurodegeneration in aged plaque-rich APP/PS1 mice. *Sci. Transl. Med.* 9:eaaf6295. doi: 10.1126/scitranslmed.aaf6295

Shi, Q., Colodner, K. J., Matousek, S. B., Merry, K., Hong, S., Kenison, J. E., et al. (2015). Complement C3-deficient mice fail to display age-related hippocampal decline. *J. Neurosci.* 35, 13029–13042. doi: 10.1523/JNEUROSCI.1698-15.2015

Stevens, B., Allen, N. J., Vazquez, L. E., Howell, G. R., Christopherson, K. S., Nouri, N., et al. (2007). The classical complement cascade mediates CNS synapse elimination. *Cell* 131, 1164–1178. doi: 10.1016/j.cell.2007.10.036

Tabata, H., and Nakajima, K. (2003). Multipolar migration: the third mode of radial neuronal migration in the developing cerebral cortex. *J. Neurosci.* 23, 9996–10001. doi: 10.1523/JNEUROSCI.23-31-09996.2003

Tarabykin, V., Stoykova, A., Usman, N., and Gruss, P. (2001). Cortical upper layer neurons derive from the subventricular zone as indicated by Svet1 gene expression. *Development* 128, 1983–1993.

Veerhuis, R., Nielsen, H. M., and Tenner, A. J. (2011). Complement in the brain. *Mol. Immunol.* 48, 1592–1603. doi: 10.1016/j.molimm.2011.04.003

Walport, M. J. (2001a). Complement. First of two parts. *N. Engl. J. Med.* 344, 1058–1066. doi: 10.1056/NEJM200104053441406

Walport, M. J. (2001b). Complement. Second of two parts. *N. Engl. J. Med.* 344, 1140–1144. doi: 10.1056/NEJM200104123441506

Zipfel, P. F., Wurzner, R., and Skerka, C. (2007). Complement evasion of pathogens: common strategies are shared by diverse organisms. *Mol. Immunol.* 44, 3850–3857. doi: 10.1016/j.molimm.2007.06.149

Conflict of Interest Statement: The authors declare that the research was conducted in the absence of any commercial or financial relationships that could be construed as a potential conflict of interest.

frontiers in Cellular Neuroscience

ORIGINAL RESEARCH
published: 11 May 2018
doi: 10.3389/fncel.2018.00124

Probenecid Disrupts a Novel Pannexin 1-Collapsin Response Mediator Protein 2 Interaction and Increases Microtubule Stability

*Xiaoxue Xu[1†], Leigh E. Wicki-Stordeur[1†], Juan C. Sanchez-Arias[1], Mei Liu[1,2], Maria S. Weaver[1], Catherine S. W. Choi[1] and Leigh A. Swayne[1,3,4]**

[1]Division of Medical Sciences, University of Victoria, Victoria, BC, Canada, [2]Key Laboratory of Neuroregeneration of Jiangsu and Ministry of Education, Co-Innovation Center of Neuroregeneration, Nantong University, Nanjing, China, [3]Department of Biology, University of Victoria, Victoria, BC, Canada, [4]Island Medical Program and Department of Cellular and Physiological Sciences, University of British Columbia, Vancouver, BC, Canada

Neurite formation relies on finely-tuned control of the cytoskeleton. Here we identified a novel protein-protein interaction between the ion and metabolite channel protein Pannexin 1 (Panx1) and collapsin response mediator protein 2 (Crmp2), a positive regulator of microtubule polymerization and stabilization. Panx1 and Crmp2 co-precipitated from both Neuro-2a (N2a) cells and mouse ventricular zone (VZ) tissue. *In vitro* binding assays between purified proteins revealed the interaction occurs directly between the Panx1 C-terminus (Panx1 CT) and Crmp2. Because Crmp2 is a well-established microtubule-stabilizing protein, and we previously observed a marked increase in neurite formation following treatment with the Panx1 blocker, probenecid, in N2a cells and VZ neural precursor cells (NPCs), we investigated the impact of probenecid on the Panx1-Crmp2 interaction. Probenecid treatment significantly disrupted the Panx1-Crmp2 interaction by both immunoprecipitation (IP) and proximity ligation analysis, without altering overall Crmp2 protein expression levels. In the presence of probenecid, Crmp2 was concentrated at the distal ends of growing neurites. Moreover, probenecid treatment increased tubulin polymerization and microtubule stability in N2a cells. These results reveal that probenecid disrupts a novel interaction between Panx1 and the microtubule stabilizer, Crmp2, and also increases microtubule stability.

Keywords: cytoskeleton, Crmp2, microtubules, neurite, neurodevelopment, neuronal polarity, Pannexin 1, probenecid

OPEN ACCESS

Edited by:
C. Laura Sayas,
Universidad de La Laguna, Spain

Reviewed by:
Rajesh Khanna,
University of Arizona, United States
Georg Zoidl,
York University, Canada

****Correspondence:***
Leigh A. Swayne
lswayne@uvic.ca

[†]These authors have contributed equally to this work.

Received: *02 January 2018*
Accepted: *17 April 2018*
Published: *11 May 2018*

Citation:
Xu X, Wicki-Stordeur LE, Sanchez-Arias JC, Liu M, Weaver MS, Choi CSW and Swayne LA (2018) Probenecid Disrupts a Novel Pannexin 1-Collapsin Response Mediator Protein 2 Interaction and Increases Microtubule Stability. Front. Cell. Neurosci. 12:124. doi: 10.3389/fncel.2018.00124

INTRODUCTION

Pannexin 1 (Panx1) was first discovered about 20 years ago (Panchin et al., 2000) and forms large-pore membrane channels that mediate passage of ions and metabolites (reviewed in Chiu et al., 2018; Whyte-Fagundes and Zoidl, 2018). Panx1 channels facilitate ATP release from cells, implicating them in many physiological and pathophysiological contexts (reviewed in Velasquez and Eugenin, 2014; Dahl, 2015; Lapato and Tiwari-Woodruff, 2018). Although widely expressed throughout the body, Panx1 is enriched in the brain (Penuela et al., 2007) where it is linked to synaptic plasticity, and learning and memory (reviewed in Boyce et al., 2018).

Previous work from our lab identified Panx1 as a new player in the regulation of neurites (Wicki-Stordeur and Swayne, 2013). We discovered the expression of Panx1 in neural precursor cells (NPCs) and developing neurons of the postnatal ventricular zone (VZ; Wicki-Stordeur et al., 2012; Wicki-Stordeur and Swayne, 2013). Using a combination of models, mouse neuroblastoma Neuro-2a (N2a) cells and VZ NPCs, we made several key observations suggesting Panx1 is a negative regulator of neurite formation (Wicki-Stordeur and Swayne, 2013). Firstly, we found that endogenous N2a cell Panx1 expression levels undergo a striking reduction over the course of retinoic acid differentiation, during which these cells also form long neurites. We further observed that direct reduction of Panx1 activity or expression increased neurite formation, while Panx1 overexpression inhibited neurite formation under retinoic acid stimulation. More recently, work from another group supported these findings, demonstrating that disruption of Panx1 (block or KO) increased axonal caliber and growth rate in dorsal root ganglion neurons (Horton et al., 2017). Together these data from others and us suggest that Panx1 is a negative regulator of neurite extension and/or stability, however the underlying mechanism has not yet been resolved.

To shed light on the molecular processes involved, we turned to Panx1 protein interaction partners. We previously conducted a study to identify novel Panx1-interacting proteins and found that many of these were cytoskeleton associated proteins, including components of the Arp2/3 complex (Wicki-Stordeur and Swayne, 2013). Another key regulator of neurite formation identified in this screen, but not previously validated, was collapsin response mediator protein 2 (Crmp2; *Dpysl2)*. Crmp2 is a microtubule-associated protein that plays a key role in neurite formation (Gu and Ihara, 2000; Fukata et al., 2002; Suzuki et al., 2003; Crews et al., 2011; Lin et al., 2011; Higurashi et al., 2012; Wilson et al., 2014; reviewed in Quach et al., 2015; Takano et al., 2015) by enhancing microtubule polymerization and by directly binding to tubulin dimers at the plus-end of microtubules (Niwa et al., 2017). Capitalizing on the striking neurite outgrowth we observed in the presence of probenecid, a Panx1 blocker (Silverman et al., 2008), here we investigated whether probenecid modulates the Panx1-Crmp2 interaction and microtubule stability.

MATERIALS AND METHODS

Animals

All procedures were carried out in accordance with the recommendations of the Canadian Council for Animal Care and the University of Victoria Animal Care Committee. The protocol was approved by the University of Victoria Animal Care Committee. For Western blot time course analyses of Panx1 and Crmp2 expression in the VZ, C57BL/6J mice were sacrificed at P0, P7, P10, P28 and P60. The VZ were removed by dissection and processed for SDS-PAGE/Western blot analysis as indicated below.

Cell Culture

Wildtype N2a cells (ATCC, CCL-131) and N2a cells stably expressing Panx1-EGFP (described previously in Boyce et al., 2015; Boyce and Swayne, 2017) were cultured in DMEM/F12 (Thermo Fisher Scientific, 11330-032) supplemented with 10% fetal bovine serum (Thermo Fisher Scientific, 12483-020), 100 U/mL penicillin and 100 μg/mL streptomycin (Thermo Fisher Scientific, 15140-122). For probenecid assays, wildtype N2a cells were seeded at 2.1×10^4 cells/cm^2, and 24 h later the (complete) culture medium was supplemented with 1 mM probenecid (Thermo Fisher Scientific, P36400) or vehicle control for 16 h. Where indicated, wildtype N2a cells were transfected using jetPEI (Polyplus-transfection, 101-10N), according to the manufacturer's instructions with Panx1EGFP (generously provided by Drs. Dale Laird and Silvia Penuela, University of Western Ontario, London, ON, Canada) or pEGFP-N1 control plasmid to express EGFP.

Antibodies

Primary antibodies used in this study were mouse anti-Crmp2 monoclonal (1:100 [immunostaining] or 1:6000–1:8000 [Western blotting]; Novus, NBP1-50580), rabbit anti-Crmp2/Toad64 polyclonal (1:4000–1:10,000 [Western blotting]; Bioss Antibodies, BS-1790R), mouse anti-GFP monoclonal (1:1000; MilliporeSigma, 11814460001 ROCHE), rabbit anti-GFP polyclonal (1:10,000; Thermo Fisher Scientific, A6455), rabbit anti-Panx1 CT395 (1:500–1:4000; a generous gift from Drs. Dale Laird and Silvia Penuela, University of Western Ontario, London, ON, Canada), rabbit anti-Panx1 (D9M1C) monoclonal antibody (Cell Signaling Technology, 91137S), rabbit anti-Panx1 EL2 (a generous gift from Drs. Dale Laird and Silvia Penuela), sheep polyclonal anti-alpha/beta tubulin (1:1500; Cytoskeleton Inc., ATN02), mouse anti-acetylated tubulin monoclonal (1:2000; MilliporeSigma, T6793), rat anti-tyrosinated tubulin polyclonal (1:1000; EMD Millipore, MAB1864-I). Secondary antibodies were Alexa Fluor 488-conjugated AffiniPure Donkey Anti-Mouse IgG (1:300, Jackson Immunoresearch, 715-545-151), horseradish peroxidase (HRP)-conjugated AffiniPure donkey anti-rabbit IgG (1:2000–1:4000, Jackson Immunoresearch, 711-035-152), HRP-conjugated AffiniPure donkey anti-mouse IgG (1:2000–1:4000, Jackson Immunoresearch, 715-035-150), HRP-conjugated AffiniPure donkey anti-sheep (1:1500, Jackson Immunoresearch, 713-035-147), and HRP-conjugated donkey anti-rat (1:3000, Jackson Immunoresearch, 712-035-153).

Western Blot Analysis

Samples were homogenized in either PBS (150 mM NaCl, 9.1 mM Na_2HPO_4, 1.7 mM NaH_2PO_4) or TBS (50 mM Tris, pH 8.0, 150 mM NaCl) based RIPA buffer (1% IGEPAL, 0.5% sodium deoxycholate, 0.1% SDS) supplemented with protease inhibitor cocktail at 1 μL/10^6 cells (stock: 104 mM 4-(2-aminoethyl)benzenesulfonyl fluoride hydrochloride, 0.08 mM aprotinin, 4 mM bestatin hydrochloride, 1.4 mM N-(trans-epoxysuccinyl)-L-leucine 4-guanidinobutylamide, 2 mM leupeptin hemisulfate salt, 1.5 mM pepstatin-A; MilliporeSigma, P8340), PMSF at 2 μL/10^6 cells, 10 μM sodium orthovanadate and 1 mM EDTA for 30 min, and centrifuged at 4°C for 20 min at 12,000 rpm to remove debris. Samples were heated to 95–100°C for 5–20 min in SDS-PAGE

loading dye under reducing conditions (dithiothreitol and β-mercaptoethanol) before loading onto gels. Gels were transferred to 0.2 μm polyvinyldene fluoride (PVDF; Bio-rad, 162-0177) membrane for 1 h at 85–95 V, or 16–18 h at 22 V. Transfer was confirmed by Ponceau S (MilliporeSigma, P7170) total protein staining. Blocking and antibody incubations were performed in 5% skim milk, or 5% bovine serum albumin (BSA; MilliporeSigma, A2153), both with 0.1% Tween 20. Immunoreactive bands were visualized via enhanced chemiluminescence imaging using a G:BOX Chemi XR5 (Syngene) and quantified by densitometry measurements using ImageJ[1].

Tubulin Polymerization *in Cellulo*

Assessment of tubulin polymerization (stability) in cells was performed as described previously (Wang et al., 2010) with modifications. Following probenecid or vehicle control treatments, N2a cells were rinsed twice at 37°C with pre-warmed PME buffer (100 mM PIPES, pH 6.9, 1 mM $MgCl_2$, 2 mM EGTA), then harvested in PME buffer supplemented with 0.05% TritonX-100 and protease inhibitors. The lysates were centrifuged at 13,000× *g* for 20 min at 20°C. The supernatant (S fraction) containing solubilized tubulin and the pellet (P fraction) containing polymerized tubulin were collected separately and processed for analysis by Western blotting. Equal loading of fractions was determined by Ponceau S staining of the PVDF membrane.

Tubulin Polymerization *in Vitro*

Tubulin polymerization *in vitro* was measured using the Tubulin Polymerization Assay kit (Cytoskeleton, BK011P) according to the manufacturer's instructions. Concentrations of probenecid used were 200 μM and 1 mM.

GFP Immunoprecipitations

These experiments were performed as previously described (Wicki-Stordeur and Swayne, 2013). Briefly, Panx1EGFP and EGFP expressing N2a cells were collected 96 h following transfection. Approximately 4.5×10^7 cells per condition were homogenized on ice in RIPA buffer supplemented with protease inhibitor cocktail and PMSF for 30 min, followed by centrifugation at 4°C for 20 min at 12,000 rpm to remove debris. Lysates were pre-cleared for 45–60 min with protein-G agarose beads (MilliporeSigma, 11243233001 ROCHE) at 4°C with shaking, then added to 200 μL protein-G bead suspension cross-linked with 5 μg of GFP monoclonal antibody (MilliporeSigma, 11814460001 ROCHE), and incubated overnight at 4°C with shaking. Beads were washed once with RIPA buffer and twice with PBS, then eluted in two bead volumes of 0.5 M ammonium hydroxide/0.5 mM EDTA for 30 min at room temperature with shaking. Probenecid treatment details are provided in the figure legends and text.

Endogenous Immunoprecipitations

N2a cells (4.5×10^7 cells/immunoprecipitation (IP)), or VZ tissue dissected from pooled P0–P10 or P60 C57BL/6J mice were homogenized in TBS lysis buffer (10 mM Tris base, pH 7.4, 150 mM NaCl, 1% IGEPAL), supplemented with protease inhibitor cocktail, PMSF, and sodium orthovanadate, for 30 min on ice, followed by centrifugation at 4°C for 20 min at 12,000 rpm to remove debris. The supernatant was pre-cleared for 45–60 min with protein-A agarose beads (MilliporeSigma, 11134515001 ROCHE) cross-linked to ChromPure rabbit IgG (Jackson ImmunoResearch, 011-000-003) at 4°C with shaking. Pre-cleared lysate (1.5–2.5 mg) was added to 200 μL protein-A bead suspension cross-linked with 5 μg of Panx1-EL2 antibody (generously provided by Drs. Dale Laird and Silvia Penuela, University of Western Ontario, Canada), Crmp2 polyclonal antibody (Bioss Antibodies, BS-1790R), or ChromPure rabbit IgG control, and incubated 1.5 h at 4°C with shaking. Beads were washed 2–3 times with TBS/0.5% IGEPAL and four times with TBS, then eluted in two bead volumes of 0.5 M ammonium hydroxide/0.5 mM EDTA for 30 min at room temperature with shaking. The eluent was dried and rehydrated in TBS lysis buffer with SDS-PAGE loading dye under reducing conditions to analyze by Western blotting.

In Vitro Binding Assays

To generate Panx1 C-terminus (Panx1CT)-GST plasmid, Panx1CT sequence (amino acids 299–426) was cloned from the Panx1-EGFP plasmid (forward primer: ACTTTGGAA TTCTCGGCAGAAAACGGAC, reverse primer: TGCTATCT CGAGTTAGCAGGACGGAT). The Panx1CT sequence and pGEX-4T-3 plasmid (GE Healthcare Lifesciences, 27-4583) were digested with EcoRI and XhoI, gel purified (Qiagen, 28704), and ligated overnight. All recombinant proteins for *in vitro* binding assays were generated in BL21 *Escherichia coli* (*E. coli*; New England Biolabs, C2527I). BL21 *E. coli* were transformed with plasmids encoding Panx1CT-GST, Crmp2-GST (a generous gift from Dr. Rajesh Khanna, University of Arizona, Tucson, AZ, USA), or GST control plasmid (pGEX-4T-3) according to the manufacturer's instructions, and grown up overnight on LB agar at 37°C. The following day, single colonies were picked and grown in 50 mL LB broth at 37°C overnight. LB broth was added (200 mL) and the cultures were grown 2 h at 37°C, then induced with IPTG (1 mM) at 37°C for 4 h. The bacteria were pelleted and re-suspended in 10 mL cold re-suspension buffer (PBS, 0.05% Tween 20, 2 mM EDTA, 0.1% β-mercaptoethanol) before being lysed by 2–3 passages through a French press at ∼1100 psi. GST fusion proteins were recovered by binding with glutathione-sepharose beads (Thermo Fisher Scientific, G4510) overnight at 4°C, then washed three times with 0.5 mL RIPA, twice with 0.5 mL RIPA without the SDS, three times with 0.5 mL PBS, and then re-suspended to 50% with PBS. To estimate protein concentration, the final products were compared with BSA standards of known microgram amounts on Colloidal Blue-stained (Thermo Fisher Scientific, LC6025) SDS-PAGE gels. Purified Panx1CT and Crmp2 were removed from the beads by cleavage with thrombin (GE Healthcare Lifesciences, 27-0846-01), or Factor Xa (New England Biolabs, P8010L), respectively. The beads were washed twice in thrombin cleavage buffer (50 mM Tris-HCl pH 8.0, 150 mM NaCl, 2.5 mM $CaCl_2$, 0.1% β-mercaptoethanol), or Factor Xa cleavage buffer

[1]http://imagej.nih.gov/ij/

(20 mM Tris-HCl, pH 8.0, 100 mM NaCl, 2 mM $CaCl_2$) then incubated in 250 μL buffer with 10 μL thrombin or Factor Xa at room temperature for 2 h (thrombin) or 4 h (Factor Xa). PMSF (15 μL) was added to the beads, incubated for 15 min, and repeated once more. The supernatants were removed and analyzed by SDS-PAGE for concentration (against BSA standards) and confirmation of cleavage. For the *in vitro* binding assay, purified Crmp2 (0.03 nmol) or Panx1CT (0.3 nmol) was incubated with 0.034 nmol Panx1CT-GST or Crmp2-GST coupled to glutathione agarose beads at 4°C for 1 h with shaking. Beads were washed 2–3 times with RIPA buffer, two times with TBS/1% IGEPAL and three times with TBS, eluted by boiling at 100°C in SDS-PAGE loading dye under reducing conditions, and analyzed by Western blotting.

PNGase F Deglycosylation

Panx1EGFP transfected N2a cells were lysed in TBS- or PBS-RIPA. 10–15 μg total protein underwent PNGase F (New England Biolabs, P0704) reaction, according to the manufacturer's manual. Samples were analyzed by Western Blot probed with anti-Panx1 (D9M1C) rabbit monoclonal antibody (Cell Signaling Technology, 91137S) and rabbit anti-GFP polyclonal antibody (Thermo Fisher Scientific, A6455).

Confocal Immunofluorescence Microscopy

N2a cells plated on poly-D-lysine (PDL; MilliporeSigma, P6407)-coated coverslips were fixed with 4% paraformaldehyde for 10 min, then washed three times with PBS before immunostaining. Antibodies were diluted in 10 mM PBS supplemented with 0.3% Triton-X-100 and 3% normal donkey serum (Jackson Immunoresearch, 017-000-121). Confocal imaging and analysis were performed blind to the treatment conditions using a Leica SP8 confocal microscope and Leica Application Suite Software version 3.1.3.16308. Images were imported to ImageJ (Schneider et al., 2012[2]), and the background was subtracted uniformly from each channel prior to analysis. Representative images were uniformly adjusted using Adobe Photoshop CS5 Extended software (Adobe Systems Incorporated). Neurites were defined as extensions from the cell body equal to or greater than one corresponding cell body diameter in length (Wicki-Stordeur and Swayne, 2013), and traced from their place of origin at the soma to their tips; only the longest neurite was included for subsequent analysis. In order to quantify the localization of Crmp2 following probenecid treatment, line scans were performed on each traced neurite, and mean fluorescence intensities were grouped in four equal neurite segments: the first three segments, closest to the soma, were defined as the neurite "shaft", while the last segment, farthest from the soma, was defined as the neurite "tip". A ratio was then calculated for each neurite between the average intensity in the neurite tip and the average intensity in the corresponding neurite shaft. These ratio data were grouped by total neurite length (10–30 μm, 30–50 μm, >50 μm) and graphed against a hypothetical value of 1. Data were obtained from 126 neurites (n), obtained from 75 cells from three independent cultures, for a total of 75 traced cells.

Proximity Ligation Assay

Proximity ligation assay (PLA) was carried out with the Duolink PLA kit (MilliporeSigma, DUO92013) according to the manufacturer's instructions. N2a cells stably expressing Panx1-EGFP (described previously in Boyce and Swayne, 2017) were plated on PDL-coated coverslips with selection antibiotic geneticin 418, grown for 24 h, and treated with 1 mM probenecid or vehicle control for 16 h. Cells were fixed for 10 min in 4% paraformaldehyde. After several rinses in PBS, coverslips were incubated with a mixture of rabbit polyclonal anti-GFP (1:500, Thermo Fisher Scientific, A6455) and monoclonal anti-Crmp2 (1:100, Novus Biologicals, NBP1-50580) antibodies, rabbit polyclonal anti-GFP and mouse anti-GFP monoclonal (1:50, MilliporeSigma, 11814460001 ROCHE) antibodies (positive control), or in antibody buffer alone (negative control) at 4°C overnight. The coverslips were incubated with PLA probe anti-rabbit PLUS and PLA probe anti-mouse MINUS (each at 1:5 dilution) for 60 min at 37°C in a humid chamber. Image acquisition and analysis were performed blind to the treatment conditions. Confocal z-stacks of randomly selected ROIs were acquired on a Leica TCS SP8 confocal microscope using the "Mark and Find" and "Autofocus" tools of the Leica Application Suite Software, version 3.1.3.16308. Image files were imported into Fiji for subsequent analysis (Schindelin et al., 2012[3]). We used a semi-automated protocol to generate regions of interest (ROIs) consisting of cell somas together with their respective neurites. In brief ROI masks were obtained using, maximum intensity projections of the EGFP signal that were thresholded and binarized. These were subjected to automatic detection of particles with size = 10,000–300,000 pixels (1 pixel = 0.076 μm) and a circularity of 0.1–1.0. These parameters identified individual cellular ROIs for the majority of cells and were further curated for inaccuracies (e.g., large cell clumps were excluded; while still blinded to the treatment conditions). Neurites traced manually and were combined to their respective soma(s) to create complete individual cellular ROIs (neurite + soma). The fluorescence intensity (mean gray value, arbitrary unit, arb.u.) within each of these ROIs was calculated and normalized to its respective ROI area. This value was then multiplied by 100 to obtain the PLA fluorescence intensity per 100 μm^2. All cells included in the analysis were evaluated for their wellness status and signs of stress (e.g., blebbing, large vacuoles; Frigault et al., 2009) using transmitted light microscopy (while blinded to the treatment conditions). Data were obtained from $n = 77$ cells (vehicle group) and $n = 70$ cells (probenecid group) from three independent passages.

Statistical Analysis

Statistical analyses were performed using Prism Windows v5.01 and Mac OS X v5.0d software (GraphPad Software[4]),

[2]https://imagej.nih.gov/ij/

[3]https://imagej.net/Fiji

[4]http://www.graphpad.com

and SPSS Statistics for Windows (v25, IBM) For statistical analysis, variables and their residuals were tested for normality using the Shapiro-Wilk test (null hypothesis: data follow a normal distribution; alternative hypothesis: data do not follow a normal distribution). For variables that fit a normal distribution, parametric tests were used for comparisons, while non-parametric tests were performed for variables that rejected the null hypothesis (i.e., data are not normally distributed). The complete description of the normality tests are found in the Supplementary Material. Statistical tests are reported in each figure legend. All variances are reported as standard error of the mean. Significance is denoted as $P < 0.05$ (*), $P < 0.01$ (**), $P < 0.001$ (***), $P < 0.0001$ (****). Exact P values and sample sizes are provided in the Figure legends.

RESULTS

Panx1 Interacts Directly With the Microtubule Stabilizer Crmp2 Via the Panx1CT

We previously identified Panx1 as a negative regulator of neurite outgrowth in N2a cells and primary VZ NPCs (Wicki-Stordeur and Swayne, 2013); however, the underlying mechanisms remained unknown. To gain further insight, we mined our previously described Panx1 interactome (Wicki-Stordeur and Swayne, 2013) for proteins with established role(s) in neurite outgrowth or stabilization. Based on a substantial body of evidence that has established it as a microtubule-associated protein that plays a critical role in neurite stability (reviewed in Ip et al., 2014; Quach et al., 2015), we decided to focus our attention on Crmp2 (*Dpysl2*; **Figure 1A**).

Reciprocal IPs with antibodies for Panx1 and Crmp2 confirmed the endogenous co-precipitation of these proteins (**Figure 1B**). Crmp2 co-enriched with antibodies to Panx1 but not control IgG. Similarly, Panx1 co-precipitated specifically with antibodies to Crmp2. In order to determine whether the Panx1-Crmp2 interaction was direct, we performed *in vitro* binding assays using purified epitope-tagged proteins (**Figure 1C**). We found that the Panx1CT enriched specifically with purified Crmp2-GST bound to glutathione-agarose beads, but not to control GST. Similarly, Crmp2 was enriched by Panx1CT-GST but did not interact with control GST. Taken together, these data confirm that Panx1 and Crmp2 interact directly through the Panx1CT.

The Panx1/Crmp2 Interaction Occurs in the VZ *in Vivo*

We next investigated postnatal co-expression of Panx1 and Crmp2 in the mouse VZ *in vivo*. Western blotting demonstrated the two proteins were present in VZ tissue across a range of ages (P0–P60; **Figure 2A**). While Crmp2 expression remained relatively constant across the time range analyzed, Panx1 expression levels peaked close to birth, then dramatically decreased with age. Reciprocal IP experiments in VZ tissues from both young and old mice (**Figure 2B**) confirmed the Panx1-Crmp2 interaction also occurred *in vivo*.

Probenecid Treatment Decreases Crmp2 Association With Panx1, Without Altering Crmp2 Expression Levels

Our previous work demonstrated that Panx1 negatively regulates neurite outgrowth (Wicki-Stordeur and Swayne, 2013). Knockdown of Panx1 expression with siRNA and Panx1 block with probenecid (Silverman et al., 2008) increased neurite outgrowth; conversely, Panx1 overexpression decreased neurite outgrowth. Because Crmp2 is a positive regulator of microtubule stabilization and neurite extension, we hypothesized that probenecid promotes neurite outgrowth by releasing Crmp2 from its direct interaction with Panx1. In support of this hypothesis, we found that 16 h probenecid treatment (the treatment time for which we observed marked increased neurite outgrowth in our previous report) significantly (∼60%) decreased the relative amount of Crmp2 co-precipitating with Panx1 compared to vehicle control treatment (**Figure 3A**). Importantly, we observed no change in overall Crmp2 expression levels as demonstrated by intensity analysis of the inputs. Further, short term probenecid treatment (30 min) was sufficient to produce a ∼30% decrease that approached statistical significance ($p = 0.085$).

We next used PLA to confirm the effects of probenecid treatment on the Panx1-Crmp2 interaction (**Figure 4**). We employed N2a cells stably expressing low levels of Panx1-EGFP (Boyce et al., 2015; Boyce and Swayne, 2017) in order to use anti-GFP and anti-Crmp2 antibodies for the assessment of proximity between the two proteins. The PLA signal (bright white dots) is generated where Panx1EGFP and Crmp2 are within 40 nm (Söderberg et al., 2006), and these dots can therefore be interpreted as the subcellular loci of their interaction. The distribution pattern of Panx1EGFP was consistent with our previous reports (Boyce et al., 2015; Boyce and Swayne, 2017), with enrichment at the plasma membrane, but also an intracellular punctate population that we recently demonstrated is due to constitutive ATP release and ATP-induced internalization of Panx1 to endosomal compartments (note that these are maximum intensity projections shown in contrast to confocal z-sections shown in our previous reports). Cells treated with probenecid (16 h) extended long neurites, much longer than those spontaneously arising in vehicle-treated cells, as previously reported and quantified in our original report (Wicki-Stordeur and Swayne, 2013). In vehicle-treated cells, the PLA signal was observed throughout the cell, from the plasma membrane, where Panx1 is relatively enriched (as per the green EGFP signal), to the peri-nuclear region, where Crmp2 is relatively enriched (as demonstrated by confocal immunocytochemistry in **Figure 5**). In probenecid-treated cells, PLA signal was observed in both cell body and neurites. Probenecid treatment (16 h) significantly reduced the intensity of the PLA signal compared with vehicle controls, in agreement with our IP results.

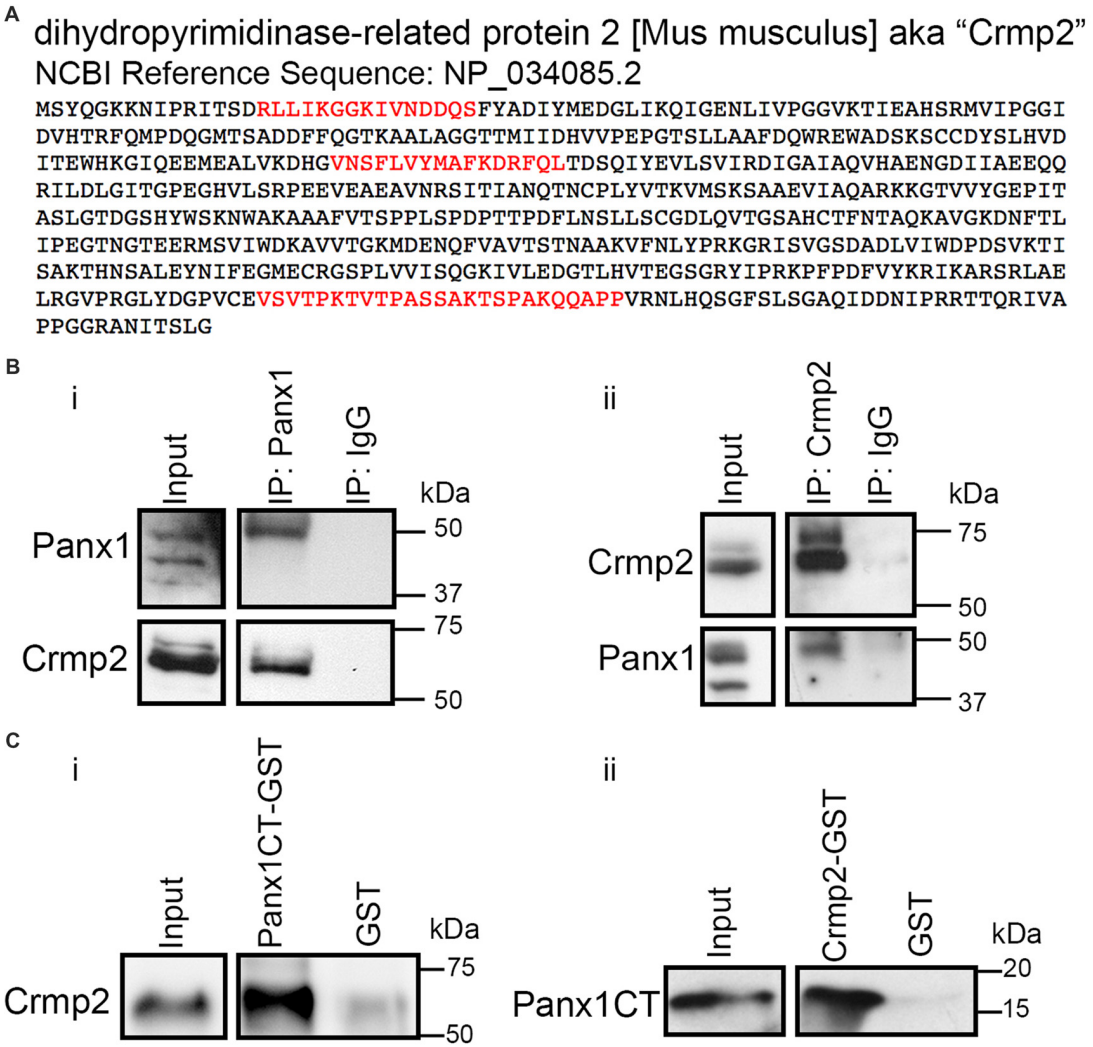

FIGURE 1 | Pannexin 1 (Panx1) and collapsin response mediator protein 2 (Crmp2) interact. **(A)** Crmp2 peptides (red) identified previously by immunoprecipitation (IP) coupled to LC-MS/MS in Wicki-Stordeur and Swayne (2013). Peptides were identified specifically in IPs from Panx1-EGFP expressing Neuro-2a (N2a) cells, and not EGFP controls. **(B)** Western blot of endogenous IPs from N2a cell lysates. **(i)** Crmp2 precipitates specifically with Panx1 compared with IgG control. **(ii)** Panx1 precipitates specifically with Crmp2 compared with IgG control. **(C)** Western blots of an *in vitro* binding assay using purified Crmp2 and Panx1 C-terminus (Panx1CT). **(i)** The Panx1CT enriches with immobilized Crmp2-GST compared with GST control. **(ii)** Crmp2 enriches with Panx1CT-GST compared with GST control. These results are representative of three independent replicates. For the complete blots of parts **(B,C)**, see Supplementary Material. This data was previously included in the PhD thesis of LWS (link: https://dspace.library.uvic.ca/handle/1828/6938).

Probenecid Treatment Leads to Concentration of Crmp2 at Microtubule Plus Ends and Increases Microtubule Polymerization and Stability

We then examined the distribution of Crmp2 in vehicle-treated and probenecid-treated N2a cells using confocal immunocytochemistry (**Figure 5A**). In control, vehicle-treated cells, Crmp2 was enriched in the peri-nuclear region. In the presence of probenecid, Crmp2 immunoreactivity was concentrated at the distal tips of the probenecid-induced neurites. Next, based on the well-documented role of Crmp2 as a microtubule stabilizing protein, we predicted that release of Crmp2 from Panx1 and its observed concentration at distal neurite tips would likely lead to increased microtubule stability. To first test this hypothesis, we treated N2a cells with probenecid or vehicle control, then analyzed the amount of polymerized and soluble tubulin within each sample (**Figure 6A**). Probenecid treatment significantly increased the ratio of polymerized:soluble tubulin within N2a cells, suggesting that probenecid increased microtubule stability. In order to determine whether this was due to a direct impact of probenecid on tubulin polymerization, we carried out an *in vitro* tubulin polymerization assay. Our results (**Figure 6B**) showed that probenecid did not directly promote the assembly of tubulin to MTs *in vitro*, supporting the idea that probenecid's impact on MT stability in cells occurred

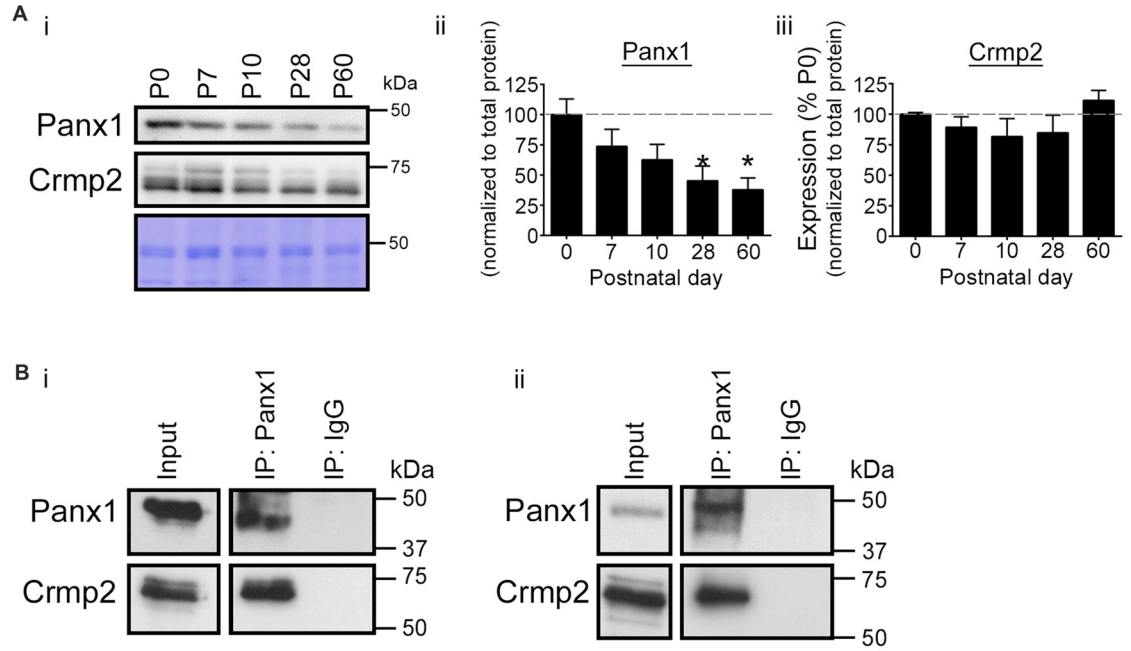

FIGURE 2 | Validation of the Panx1-Crmp2 interaction in the mouse ventricular zone (VZ). **(Ai)** Western blot of a time course of Panx1 and Crmp2 expression in the VZ. **(ii)** Panx1 expression peaked within the early postnatal period (P0–P7), and dramatically decreased with age (P28–P60; $p = 0.0365$ by one-way analyses of variance (ANOVA); $F_{(4,10)} = 3.9$; Dunnett's multiple comparison test *post hoc*, P28 $p = 0.0352$, and P60, $p = 0.0177$; $n = 3$). Coomassie Blue was employed as a loading control. **(iii)** Crmp2 expression remained relatively constant across this time course ($F_{(4,10)} = 1.3$; $p = 0.3333$, one-way ANOVA; $n = 3$). **(B)** Western blot of endogenous Panx1 IPs from mouse brain VZ tissue. Crmp2 co-precipitated specifically with Panx1 from young (P10; **i**) and adult (P60; **ii**) mouse VZ. For the complete blots of part **(B)**, see Supplementary Material. This data was previously included in the PhD thesis of LWS (link: https://dspace.library.uvic.ca/handle/1828/6938).

through an indirect mechanism. To further validate the impact of probenecid on microtubule stability, we examined two tubulin post-translational modifications (**Figure 6C**): tyrosination, an indicator of dynamic tubulin, and acetylation, an indicator of stable tubulin (Kollins et al., 2009). Probenecid treatment decreased tyrosinated tubulin, and increased acetylated tubulin compared to vehicle control. Together these results suggest that probenecid enhances microtubule stability through an indirect mechanism.

DISCUSSION

Our previous work (Wicki-Stordeur and Swayne, 2013) demonstrated that Panx1 acts as a negative regulator of neurite outgrowth in N2a cells and primary VZ NPCs. Here we expand on that work, focusing on our discovery of an interaction between Panx1 and a microtubule-associated protein, Crmp2, and the robust induction of neurite outgrowth in the presence of the Panx1 blocker, probenecid. Crmp2 is largely restricted to the nervous system (Goshima et al., 1995; Wang and Strittmatter, 1996; Charrier et al., 2003), and acts as a microtubule-stabilizer (Gu and Ihara, 2000; Fukata et al., 2002; Lin et al., 2011) in part via promoting α/β-tubulin dimer assembly onto growing microtubule plus-ends (Niwa et al., 2017), thereby playing a key role in promoting neurite outgrowth (e.g., Suzuki et al., 2003; Crews et al., 2011; Higurashi et al., 2012; Wilson et al., 2014; reviewed in Ip et al., 2014; Quach et al., 2015).

We observed a postnatal decline in Panx1 expression in the VZ, reminiscent of the decrease in Panx1 levels across postnatal neuronal differentiation and neuritogenesis that we previously observed *in vitro* (Wicki-Stordeur and Swayne, 2013). This time course of reduction in Panx1 expression levels corresponds with critical periods of increased neuritogenesis, neurite stabilization, and network development, which roughly occur across similar postnatal time-courses in the developing cortex, cerebellum and eye (Heng et al., 2010; Kato et al., 2012). Given our recent findings demonstrating a key role for Panx1 in NPC maintenance *in vivo* (Wicki-Stordeur et al., 2016), this decrease in expression could also be associated with the age-dependent decrease in the number of VZ NPCs observed in mice and humans (Sanai et al., 2011; Wang et al., 2011; Shook et al., 2012; Daynac et al., 2016; reviewed in Apple et al., 2017; Conover and Todd, 2017).

In our earlier study using probenecid, we observed a remarkable induction of neurite outgrowth in both N2a cells and primary VZ NPC cultures (Wicki-Stordeur and Swayne, 2013). Because Crmp2 is a microtubule-stabilizer, we wondered whether this effect of probenecid could be due to modulation of the Panx1-Crmp2 interaction. Since probenecid is a small molecule with a hydrophobic core, it is reasonable for us to suspect that it readily crosses cell membranes disrupting both plasma membrane and intracellular Panx1-Crmp2 interactions.

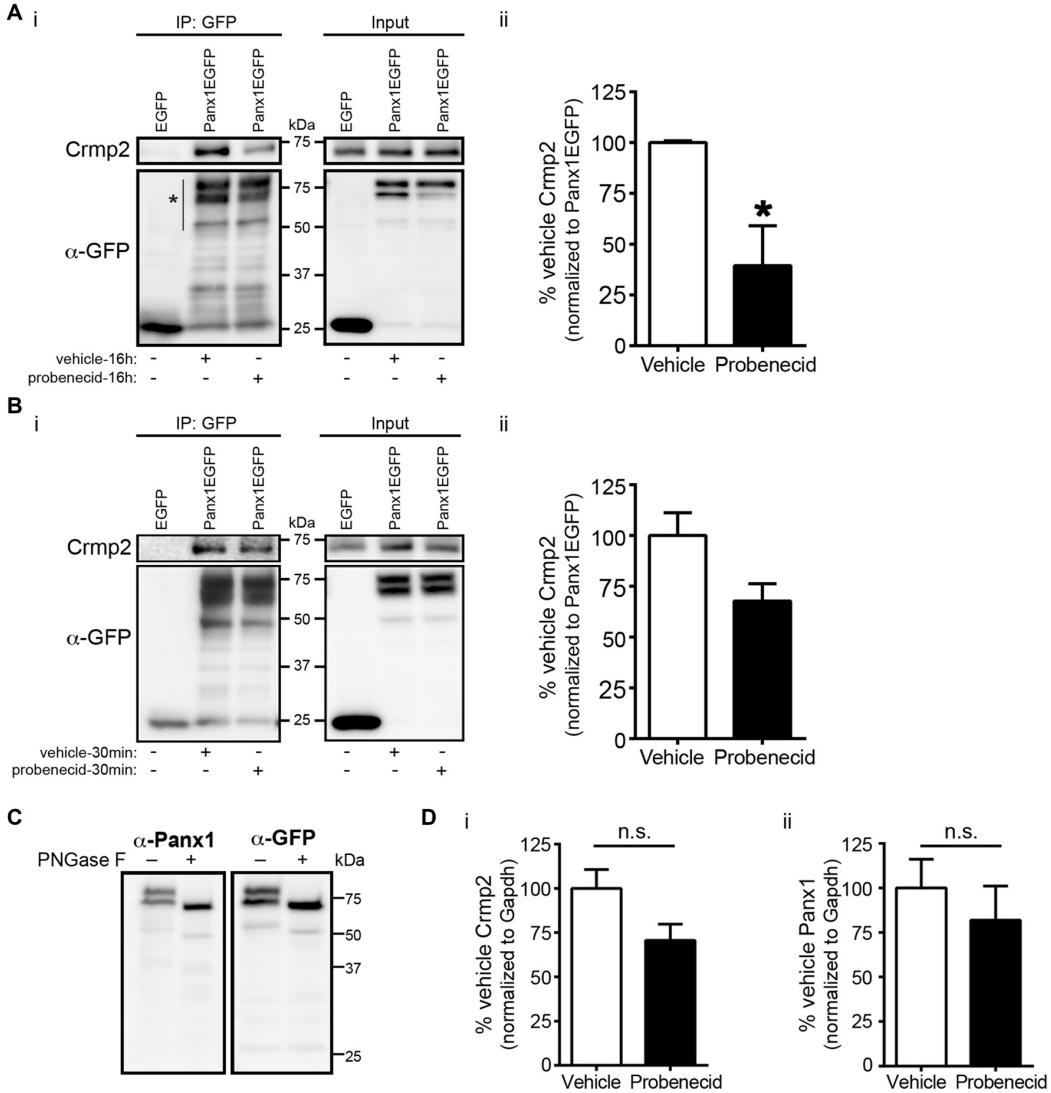

FIGURE 3 | Probenecid treatment decreases Crmp2 co-precipitation with Panx1. **(Ai)** Western blot of a GFP IP from N2a cells expressing Panx1-EGFP, or EGFP control, treated (16 h) with probenecid or vehicle control. **(ii)** Probenecid treatment (16 h) significantly decreased the amount of Crmp2 that precipitated with Panx1-EGFP. Crmp2 signal in the IP fraction was normalized to GFP signal intensity from the same lane (Panx1-EGFP [vehicle] vs. Panx1-EGFP [probenecid]: 100.0 ± 0.8 vs. 39.4 ± 19.6, $p = 0.0368$, $n = 3$, unpaired t-test). **(B)** The same assay was performed with a shorter 30 min treatment **(i)**. **(ii)** Short probenecid treatment (30 min) revealed a ∼30% decrease in Crmp2 co-precipitation (Panx1-EGFP [vehicle] vs. Panx1-EGFP [probenecid]: 100.0 ± 11.1 vs. 67.7 ± 19.6, $p = 0.0826$, $n = 3$, unpaired t-test). **(C)** PNGase F treatment was performed to confirm the upper Panx1EGFP immunoreactive band was indeed glycosylated Panx1 and assessed by Western blotting. Note that both immunoreactive bands shifted in response to N-glycosidase F treatment, suggesting that both major bands are mature glycosylated Panx1EGFP of differing molecular weights. **(D)** Analysis of the input intensities revealed that probenecid treatment did not change the overall expression of **(i)** Crmp2 ($p = 0.2000$, Mann-Whitney test, $n = 3$) or **(ii)** Panx1 ($p = 0.578$, unpaired t-test, $n = 3$). Normalized to Gapdh (not shown), n.s., non-significant.

Remarkably, probenecid exposure indeed decreased the amount of Crmp2 co-precipitating with Panx1, without affecting total Crmp2 expression (**Figure 3**). Taken together with our data demonstrating a direct interaction between the purified Panx1CT and Crmp2 (**Figure 1**), these results suggest that binding of probenecid at the first extracellular loop (Michalski and Kawate, 2016) allosterically disrupts the Crmp2 interaction at the Panx1CT. Notably, the Panx1CT has been reported to be involved in blocking the Panx1 pore (Chekeni et al., 2010; Sandilos et al., 2012; Dourado et al., 2014; Chiu et al., 2017), therefore it is tempting to speculate based on our findings, that its stimulation of allosteric communication between the EL1 and the C-terminus (CT) could underlie probenecid-mediated Panx1 inhibition.

Complementary PLA confirmed a decrease in the Panx1-Crmp2 association in the presence of probenecid. It is important to note that the intensity of the PLA signal does not reflect the actual number of interacting molecules, and

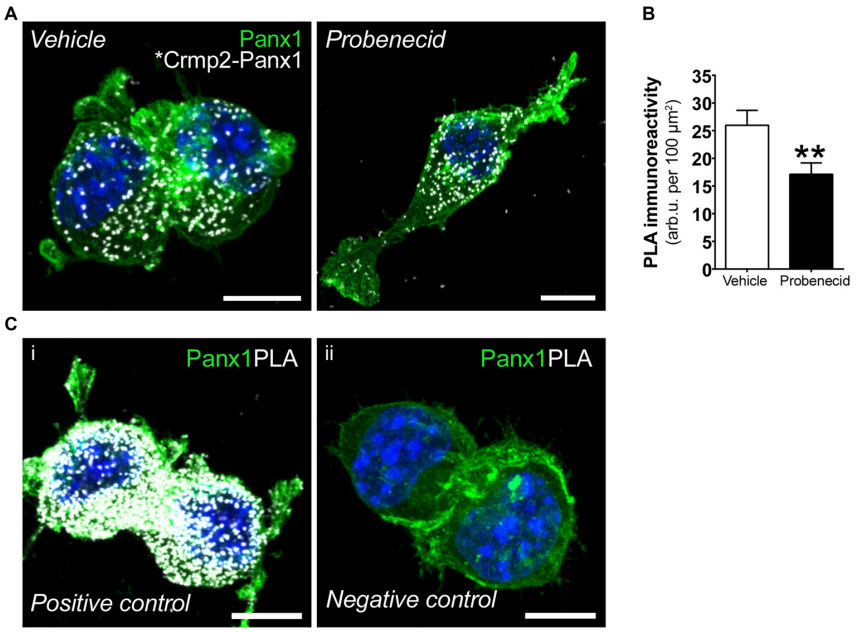

FIGURE 4 | Probenecid decreases proximity ligation assay (PLA) between Panx1EGFP and Crmp2. **(A)** Representative confocal maximum intensity projections of vehicle- (left) and probenecid-treated (right) Panx1-EGFP-expressing N2a cells demonstrating PLA-positive Crmp2-Panx1 clusters (white). **(B)** Probenecid treatment significantly decreased mean fluorescence intensity of the PLA signal (vehicle: 26.0 ± 2.7 arb.u. per 100 μm^2 vs. probenecid: 17.1 ± 2.1 arb.u. per 100 μm^2, $p = 0.0037$, $n = 77$ cells and $n = 70$ cells, respectively, Mann-Whitney test). **(C)** Controls for PLA included **(i)** cells were incubated with α-GFP anti-mouse and α-GFP anti-rabbit to serve as a positive control. **(ii)** No primary antibodies were included to serve as a negative control. Hoechst 33342 was used as a nuclear counterstain. Scale bars, 10 μm.

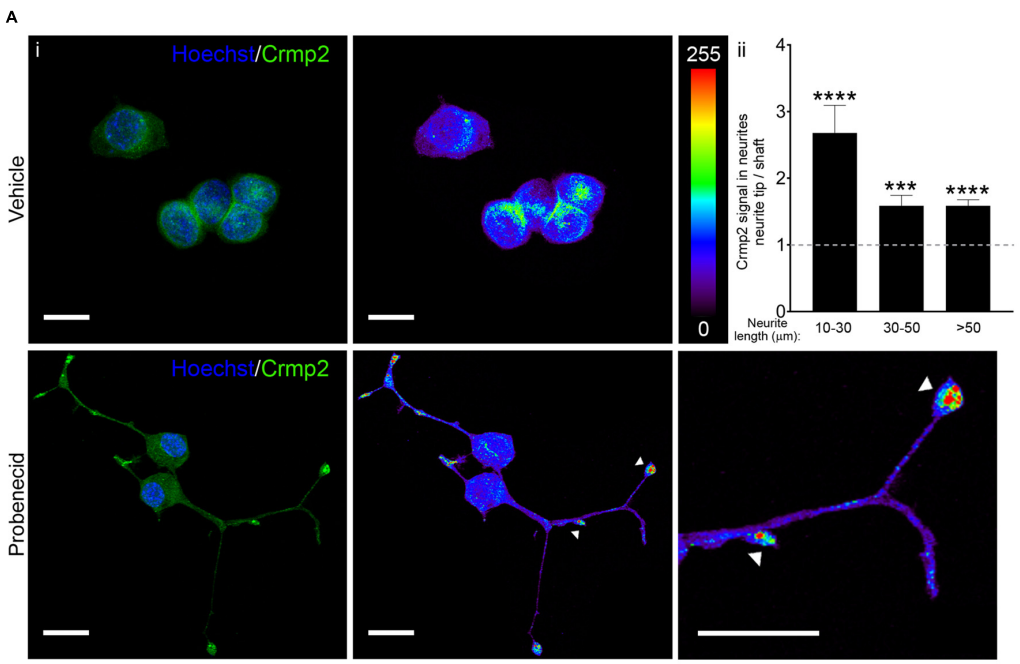

FIGURE 5 | Probenecid treatment results in Crmp2 concentration at neurite tips. **(Ai)** Representative confocal images from N2a cells treated with vehicle (upper panels) or probenecid (lower panels) and immunostained for Crmp2. Crmp2 signal intensity is indicated in the heat maps. Hoechst 33342 was used as a nuclear counterstain. Scale bars: 20 μm. **(ii)** Crmp2 signal in probenecid-induced neurites was more abundant in neurite tips compared to the shaft, regardless of neurite length (10–30 μm, $p < 0.0001$, $n = 38$ neurites; 30–50 μm, $p = 0.0003$, $n = 40$ neurites; >50 μm, $p < 0.0001$, $n = 48$ neurites; Wilcoxon signed-rank test against a hypothetical median value of 1.0).

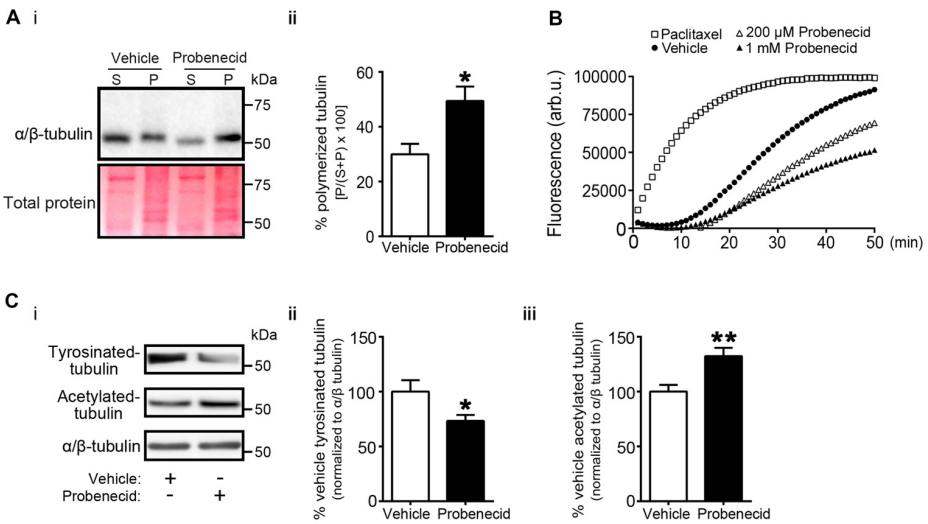

FIGURE 6 | Probenecid treatment increases microtubule stability in cells. **(Ai)** N2a cells were treated with vehicle control or probenecid and then fractionated to obtain polymerized and soluble microtubule fractions. P (pellet) contains the polymerized microtubule fraction and S (supernatant) contains the soluble tubulin fraction. Ponceau S staining was employed as a loading control. **(ii)** Probenecid enhanced the percentage of polymerized microtubules to soluble tubulin (vehicle: 29.9 ± 3.8% vs. probenecid: 49.4 ± 5.2%, $p = 0.0107$ by unpaired *t*-test; $n = 7$). **(B)** Tubulin polymerization assays *in vitro*. Paclitaxel (3 μM) and vehicle were employed as positive and negative controls, respectively. The experiment was performed three times, with the replicates as follows: paclitaxel $n = 5$; Vehicle $n = 5$; 200 μM Probenecid $n = 5$; 1 mM Probenecid $n = 7$. **(Ci)** Western blot of post-translationally modified tubulin species from N2a cells treated with probenecid or vehicle control. Tyrosinated-tubulin represents the dynamic population, and acetylated-tubulin represents the stable population. Total α/β-tubulin was used for normalization. Probenecid treatment **(ii)** decreased tyrosinated-tubulin (100.0 ± 10.5% vs. 73.3 ± 5.5%, $p = 0.0377$ by unpaired *t*-test; $n = 9$) and **(iii)** increased acetylated-tubulin (100.0 ± 6.1% vs. 132.0 ± 7.6%, $p = 0.0043$ by unpaired *t*-test; $n = 9$).

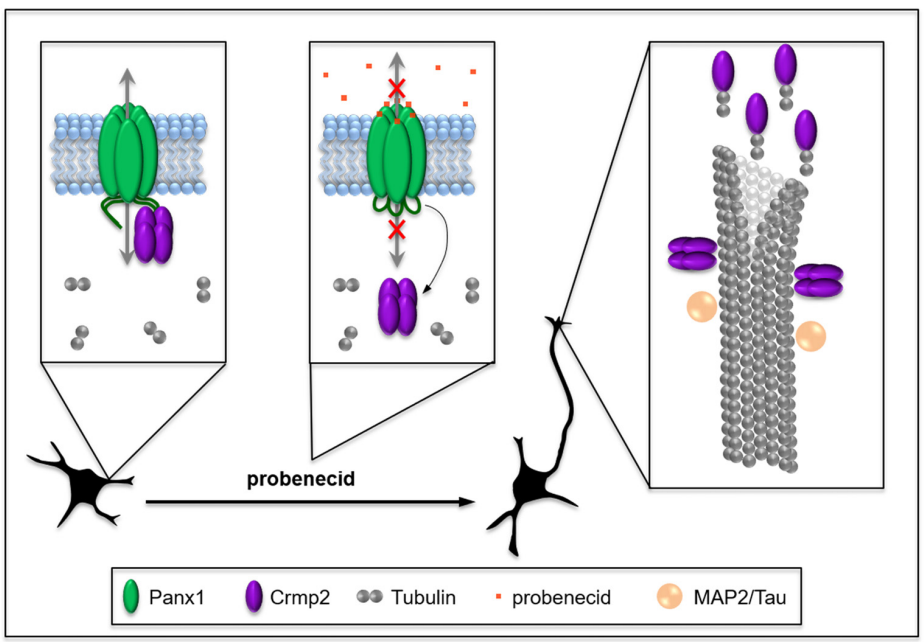

FIGURE 7 | Working model: probenecid promotes neurite outgrowth by releasing Crmp2 thereby stabilizing microtubules. Panx1, which is developmentally regulated at a cellular and tissue level in neural precursor cells (NPCs), physically sequesters Crmp2, thereby inhibiting neuritogenesis until appropriate connections can be made. Probenecid binds to the first extracellular loop causing allosteric disruption of Crmp2 binding to the CT and resulting in a "release" of Crmp2 from the Panx1/Crmp2 complex. Free Crmp2 facilitates tubulin polymerization, and microtubule stabilization and bundling, thereby promoting neurite extension. MAP2 and Tau are microtubule-associated proteins that also contribute to microtubule stabilization in different types of neurites in the CNS and are included for context.

a large signal can be generated by a very small number of interacting molecules. This is because the PLA signal is generated by a process called rolling circle DNA synthesis, which occurs when oligonucleotide probes connected to the secondary antibodies towards each primary antibody are in close proximity or part of a protein complex; the reaction results in several hundred-fold amplification of the DNA circle.

Immunocytochemistry further revealed that Crmp2 was concentrated at the tips of neurites in probenecid treated cells. This is consistent with another study demonstrating concentration of Crmp2 on the distal region of growing axons in primary hippocampal neurons (Inagaki et al., 2001). Interestingly, we noted that Crmp2 signal in the neurite tip vs. shaft was significantly higher in short neurites (10–30 μm) compared to the longer ones (30–50 μm and >50 μm). Assuming that the shorter neurites are at an earlier stage of formation, this finding suggests that Crmp2 may be more heavily involved in microtubule assembly during the initial stages of neurite formation.

It is reasonable to hypothesize that this increase in free Crmp2 would impact on microtubule stability. Supporting this prediction, probenecid also significantly increased microtubule polymerization, as well as post-translational modifications associated with microtubule stability. Because of Crmp2's well-documented role in stabilizing microtubules through binding to microtubule-plus ends (Niwa et al., 2017), these novel findings by our group suggest that probenecid-mediated neurite outgrowth could result from release of Crmp2 from Panx1. Importantly, our *in vitro* microtubule polymerization assay results support the idea that probenecid's enhancement of microtubule stability in cells occurs though an indirect mechanism. **Figure 7** demonstrates our working model, in which probenecid binding to Panx1 results in release of Crmp2, which then concentrates at microtubule plus-ends to promote neurite stability and elongation.

Our discovery of the interaction between Panx1 and Crmp2 expands our understanding of Panx1 interactions with the cytoskeleton. Bhalla-Gehi et al. (2010) first reported an interaction between actin and ectopically expressed Panx1, and demonstrated that actin filament (not microtubule) dynamics were critical for Panx1 trafficking and stability at the plasma membrane. We also previously identified several cytoskeletal proteins as potential Panx1 interaction partners, and validated an interaction between endogenous Panx1, actin and Arp3, a component of the actin-associated Arp2/3 complex, in N2a cells (Wicki-Stordeur and Swayne, 2013). Our novel data presented here additionally links Panx1 to the microtubule cytoskeleton. Notably, in addition to regulating microtubule stability, Crmp2 also acts as a bridge between microtubule and actin networks (Tan et al., 2015). Therefore, the potential role of Panx1 in regulating microtubule and actin filament crosstalk during neuritogenesis will be the focus of future work.

Overall this work identifies a new protein-protein interaction implicated in regulation of the cytoskeleton. These data are especially relevant in the context of neuroplasticity, with important implications for crosstalk between ion and metabolite channels like Panx1 and the cytoskeleton.

AUTHOR CONTRIBUTIONS

LEW-S, XX, JCS-A and LAS designed research and wrote the manuscript. LEW-S, XX, JCS-A, ML, MSW and CC performed research. LEW-S, XX, JCS-A, ML, MSW, CSWC and LAS analyzed data.

FUNDING

This project was supported by operating grants from the Canadian Institutes of Health Research (MOP142215), the Natural Sciences and Engineering Research Council of Canada (NSERC; 402270-2011), the Scottish Rite Charitable Foundation of Canada (15118) and the University of Victoria Division of Medical Sciences to LAS. LAS is also supported by a Michael Smith Foundation for Health Research and British Columbia Schizophrenia Society Foundation Scholar Award (5900). LEW-S was supported by a Vanier Canada Graduate Scholarship (NSERC), and MSW was supported by a University of Victoria Summer Undergraduate Student Award. ML received partial salary support from the Key Laboratory of Neuroregeneration of Jiangsu and Ministry of Education, Co-innovation Center of Neuroregeneration, Nantong University, China. LAS is also grateful for infrastructure support from the Canada Foundation for Innovation (29462) and the BC Knowledge Development Fund (804754) for the Leica SP8 confocal microscope system.

SUPPLEMENTARY MATERIAL

The Supplementary Material for this article can be found online at: https://www.frontiersin.org/articles/10.3389/fncel.2018.00124/full#supplementary-material

REFERENCES

Apple, D. M., Solano-Fonseca, R., and Kokovay, E. (2017). Neurogenesis in the aging brain. *Biochem. Pharmacol.* 141, 77–85. doi: 10.1016/j.bcp.2017.06.116

Bhalla-Gehi, R., Penuela, S., Churko, J. M., Shao, Q., and Laird, D. W. (2010). Pannexin1 and pannexin3 delivery, cell surface dynamics, and cytoskeletal interactions. *J. Biol. Chem.* 285, 9147–9160. doi: 10.1074/jbc.M109.082008

Boyce, A. K. J., Epp, A. L., Nagarajan, A., and Swayne, L. A. (2018). Transcriptional and post-translational regulation of pannexins. *Biochim. Biophys. Acta* 1860, 72–82. doi: 10.1016/j.bbamem.2017.03.004

Boyce, A. K. J., Kim, M. S., Wicki-Stordeur, L. E., and Swayne, L. A. (2015). ATP stimulates pannexin 1 internalization to endosomal compartments. *Biochem. J.* 470, 319–330. doi: 10.1042/bj20141551

Boyce, A. K. J., and Swayne, L. A. (2017). P2X7 receptor cross-talk regulates ATP-induced pannexin 1 internalization. *Biochem. J.* 474, 2133–2144. doi: 10.1042/BCJ20170257

Charrier, E., Reibel, S., Rogemond, V., Aguera, M., Thomasset, N., and Honnorat, J. (2003). Collapsin response mediator proteins (CRMPs): involvement in nervous system development and adult neurodegenerative disorders. *Mol. Neurobiol.* 28, 51–64. doi: 10.1385/mn:28:1:51

Chekeni, F. B., Elliott, M. R., Sandilos, J. K., Walk, S. F., Kinchen, J. M., Lazarowski, E. R., et al. (2010). Pannexin 1 channels mediate 'find-me' signal release and membrane permeability during apoptosis. *Nature* 467, 863–867. doi: 10.1038/nature09413

Chiu, Y. H., Jin, X., Medina, C. B., Leonhardt, S. A., Kiessling, V., Bennett, B. C., et al. (2017). A quantized mechanism for activation of pannexin channels. *Nat. Commun.* 8:14324. doi: 10.1038/ncomms14324

Chiu, Y. H., Schappe, M. S., Desai, B. N., and Bayliss, D. A. (2018). Revisiting multimodal activation and channel properties of Pannexin 1. *J. Gen. Physiol.* 150, 19–39. doi: 10.1085/jgp.201711888

Conover, J. C., and Todd, K. L. (2017). Development and aging of a brain neural stem cell niche. *Exp. Gerontol.* 94, 9–13. doi: 10.1016/j.exger.2016.11.007

Crews, L., Ruf, R., Patrick, C., Dumaop, W., Trejo-Morales, M., Achim, C. L., et al. (2011). Phosphorylation of collapsin response mediator protein-2 disrupts neuronal maturation in a model of adult neurogenesis: implications for neurodegenerative disorders. *Mol. Neurodegener.* 6:67. doi: 10.1186/1750-1326-6-67

Dahl, G. (2015). ATP release through pannexon channels. *Philos. Trans. R. Soc. Lond. B Biol. Sci.* 370:20140191. doi: 10.1098/rstb.2014.0191

Daynac, M., Morizur, L., Chicheportiche, A., Mouthon, M. A., and Boussin, F. D. (2016). Age-related neurogenesis decline in the subventricular zone is associated with specific cell cycle regulation changes in activated neural stem cells. *Sci. Rep.* 6:21505. doi: 10.1038/srep21505

Dourado, M., Wong, E., and Hackos, D. H. (2014). Pannexin-1 is blocked by its C-terminus through a delocalized non-specific interaction surface. *PLoS One* 9:e99596. doi: 10.1371/journal.pone.0099596

Frigault, M. M., Lacoste, J., Swift, J. L., and Brown, C. M. (2009). Live-cell microscopy—tips and tools. *J. Cell Sci.* 122, 753–767. doi: 10.1242/jcs.033837

Fukata, Y., Itoh, T. J., Kimura, T., Ménager, C., Nishimura, T., Shiromizu, T., et al. (2002). CRMP-2 binds to tubulin heterodimers to promote microtubule assembly. *Nat. Cell Biol.* 4, 583–591. doi: 10.1038/ncb825

Goshima, Y., Nakamura, F., Strittmatter, P., and Strittmatter, S. M. (1995). Collapsin-induced growth cone collapse mediated by an intracellular protein related to UNC-33. *Nature* 376, 509–514. doi: 10.1038/376509a0

Gu, Y., and Ihara, Y. (2000). Evidence that collapsin response mediator protein-2 is involved in the dynamics of microtubules. *J. Biol. Chem.* 275, 17917–17920. doi: 10.1074/jbc.C000179200

Heng, J. I., Chariot, A., and Nguyen, L. (2010). Molecular layers underlying cytoskeletal remodelling during cortical development. *Trends Neurosci.* 33, 38–47. doi: 10.1016/j.tins.2009.09.003

Higurashi, M., Iketani, M., Takei, K., Yamashita, N., Aoki, R., Kawahara, N., et al. (2012). Localized role of CRMP1 and CRMP2 in neurite outgrowth and growth cone steering. *Dev. Neurobiol.* 72, 1528–1540. doi: 10.1002/dneu.22017

Horton, S. M., Luna Lopez, C., Blevins, E., Howarth, H., Weisberg, J., Shestopalov, V. I., et al. (2017). Pannexin 1 modulates axonal growth in mouse peripheral nerves. *Front. Cell. Neurosci.* 11:365. doi: 10.3389/fncel.2017.00365

Inagaki, N., Chihara, K., Arimura, N., Ménager, C., Kawano, Y., Matsuo, N., et al. (2001). CRMP-2 induces axons in cultured hippocampal neurons. *Nat. Neurosci.* 4, 781–782. doi: 10.1038/90476

Ip, J. P., Fu, A. K., and Ip, N. Y. (2014). CRMP2: functional roles in neural development and therapeutic potential in neurological diseases. *Neuroscientist* 20, 589–598. doi: 10.1177/1073858413514278

Kato, Y., Kaneko, N., Sawada, M., Ito, K., Arakawa, S., Murakami, S., et al. (2012). A subtype-specific critical period for neurogenesis in the postnatal development of mouse olfactory glomeruli. *PLoS One* 7:e48431. doi: 10.1371/journal.pone.0048431

Kollins, K. M., Bell, R. L., Butts, M., and Withers, G. S. (2009). Dendrites differ from axons in patterns of microtubule stability and polymerization during development. *Neural Dev.* 4:26. doi: 10.1186/1749-8104-4-26

Lapato, A. S., and Tiwari-Woodruff, S. K. (2018). Connexins and pannexins: at the junction of neuro-glial homeostasis and disease. *J. Neurosci. Res.* 96, 31–44. doi: 10.1002/jnr.24088

Lin, P. C., Chan, P. M., Hall, C., and Manser, E. (2011). Collapsin response mediator proteins (CRMPs) are a new class of microtubule-associated protein (MAP) that selectively interacts with assembled microtubules via a taxol-sensitive binding interaction. *J. Biol. Chem.* 286, 41466–41478. doi: 10.1074/jbc.M111.283580

Michalski, K., and Kawate, T. (2016). Carbenoxolone inhibits Pannexin1 channels through interactions in the first extracellular loop. *J. Gen. Physiol.* 147, 165–174. doi: 10.1085/jgp.201511505

Niwa, S., Nakamura, F., Tomabechi, Y., Aoki, M., Shigematsu, H., Matsumoto, T., et al. (2017). Structural basis for CRMP2-induced axonal microtubule formation. *Sci. Rep.* 7:10681. doi: 10.1038/s41598-017-11031-4

Panchin, Y., Kelmanson, I., Matz, M., Lukyanov, K., Usman, N., and Lukyanov, S. (2000). A ubiquitous family of putative gap junction molecules. *Curr. Biol.* 10, R473–R474. doi: 10.1016/s0960-9822(00)00576-5

Penuela, S., Bhalla, R., Gong, X. Q., Cowan, K. N., Celetti, S. J., Cowan, B. J., et al. (2007). Pannexin 1 and pannexin 3 are glycoproteins that exhibit many distinct characteristics from the connexin family of gap junction proteins. *J. Cell Sci.* 120, 3772–3783. doi: 10.1242/jcs.009514

Quach, T. T., Honnorat, J., Kolattukudy, P. E., Khanna, R., and Duchemin, A. M. (2015). CRMPs: critical molecules for neurite morphogenesis and neuropsychiatric diseases. *Mol. Psychiatry* 20, 1037–1045. doi: 10.1038/mp.2015.77

Sanai, N., Nguyen, T., Ihrie, R. A., Mirzadeh, Z., Tsai, H. H., Wong, M., et al. (2011). Corridors of migrating neurons in the human brain and their decline during infancy. *Nature* 478, 382–386. doi: 10.1038/nature10487

Sandilos, J. K., Chiu, Y. H., Chekeni, F. B., Armstrong, A. J., Walk, S. F., Ravichandran, K. S., et al. (2012). Pannexin 1, an ATP release channel, is activated by caspase cleavage of its pore-associated C terminal autoinhibitory region. *J. Biol. Chem.* 287, 11303–11311. doi: 10.1074/jbc.M111.323378

Schindelin, J., Arganda-Carreras, I., Frise, E., Kaynig, V., Longair, M., Pietzsch, T., et al. (2012). Fiji: an open-source platform for biological-image analysis. *Nat. Methods* 9, 676–682. doi: 10.1038/nmeth.2019

Schneider, C. A., Rasband, W. S., and Eliceiri, K. W. (2012). NIH Image to ImageJ: 25 years of image analysis. *Nat. Methods* 9, 671–675. doi: 10.1038/nmeth.2089

Shook, B. A., Manz, D. H., Peters, J. J., Kang, S., and Conover, J. C. (2012). Spatiotemporal changes to the subventricular zone stem cell pool through aging. *J. Neurosci.* 32, 6947–6956. doi: 10.1523/JNEUROSCI.5987-11.2012

Silverman, W., Locovei, S., and Dahl, G. (2008). Probenecid, a gout remedy, inhibits pannexin 1 channels. *Am. J. Physiol. Cell Physiol.* 295, C761–C767. doi: 10.1152/ajpcell.00227.2008

Söderberg, O., Gullberg, M., Jarvius, M., Ridderstråle, K., Leuchowius, K. J., Jarvius, J., et al. (2006). Direct observation of individual endogenous protein complexes *in situ* by proximity ligation. *Nat. Methods* 3, 995–1000. doi: 10.1038/nmeth947

Suzuki, Y., Nakagomi, S., Namikawa, K., Kiryu-Seo, S., Inagaki, N., Kaibuchi, K., et al. (2003). Collapsin response mediator protein-2 accelerates axon regeneration of nerve-injured motor neurons of rat. *J. Neurochem.* 86, 1042–1050. doi: 10.1046/j.1471-4159.2003.01920.x

Takano, T., Xu, C., Funahashi, Y., Namba, T., and Kaibuchi, K. (2015). Neuronal polarization. *Development* 142, 2088–2093. doi: 10.1242/dev.114454

Tan, M., Cha, C., Ye, Y., Zhang, J., Li, S., Wu, F., et al. (2015). CRMP4 and CRMP2 interact to coordinate cytoskeleton dynamics, regulating growth cone development and axon elongation. *Neural Plast.* 2015:947423. doi: 10.1155/2015/947423

Velasquez, S., and Eugenin, E. A. (2014). Role of Pannexin-1 hemichannels and purinergic receptors in the pathogenesis of human diseases. *Front. Physiol.* 5:96. doi: 10.3389/fphys.2014.00096

Wang, G., Gao, X., Huang, Y., Yao, Z., Shi, Q., and Wu, M. (2010). Nucleophosmin/B23 inhibits Eg5-mediated microtubule depolymerization by inactivating its ATPase activity. *J. Biol. Chem.* 285, 19060–19067. doi: 10.1074/jbc.M110.100396

Wang, C., Liu, F., Liu, Y. Y., Zhao, C. H., You, Y., Wang, L., et al. (2011). Identification and characterization of neuroblasts in the subventricular zone and rostral migratory stream of the adult human brain. *Cell Res.* 21, 1534–1550. doi: 10.1038/cr.2011.83

Wang, L. H., and Strittmatter, S. M. (1996). A family of rat CRMP genes is differentially expressed in the nervous system. *J. Neurosci.* 16, 6197–6207. doi: 10.1523/JNEUROSCI.16-19-06197.1996

Whyte-Fagundes, P., and Zoidl, G. (2018). Mechanisms of pannexin1 channel gating and regulation. *Biochim. Biophys. Acta* 1860, 65–71. doi: 10.1016/j.bbamem.2017.07.009

Wicki-Stordeur, L. E., Dzugalo, A. D., Swansburg, R. M., Suits, J. M., and Swayne, L. A. (2012). Pannexin 1 regulates postnatal neural stem and progenitor cell proliferation. *Neural Dev.* 7:11. doi: 10.1186/1749-8104-7-11

Wicki-Stordeur, L. E., Sanchez-Arias, J. C., Dhaliwal, J., Carmona-Wagner, E. O., Shestopalov, V. I., Lagace, D. C., et al. (2016). Pannexin 1 differentially affects neural precursor cell maintenance in the ventricular zone and peri-infarct cortex. *J. Neurosci.* 36, 1203–1210. doi: 10.1523/JNEUROSCI.0436-15.2016

Wicki-Stordeur, L. E., and Swayne, L. A. (2013). Panx1 regulates neural stem and progenitor cell behaviours associated with cytoskeletal dynamics and interacts with multiple cytoskeletal elements. *Cell Commun. Signal.* 11:62. doi: 10.1186/1478-811x-11-62

Wilson, S. M., Moutal, A., Melemedjian, O. K., Wang, Y., Ju, W., Francois-Moutal, L., et al. (2014). The functionalized amino acid (S)-Lacosamide subverts CRMP2-mediated tubulin polymerization to prevent constitutive and activity-dependent increase in neurite outgrowth. *Front. Cell. Neurosci.* 8:196. doi: 10.3389/fncel.2014.00196

Conflict of Interest Statement: The authors declare that the research was conducted in the absence of any commercial or financial relationships that could be construed as a potential conflict of interest.

frontiers in Cellular Neuroscience

REVIEW
published: 14 June 2018
doi: 10.3389/fncel.2018.00165

The Role of the Microtubule Cytoskeleton in Neurodevelopmental Disorders

*Micaela Lasser, Jessica Tiber and Laura Anne Lowery**

Department of Biology, Boston College, Chestnut Hill, MA, United States

Neurons depend on the highly dynamic microtubule (MT) cytoskeleton for many different processes during early embryonic development including cell division and migration, intracellular trafficking and signal transduction, as well as proper axon guidance and synapse formation. The coordination and support from MTs is crucial for newly formed neurons to migrate appropriately in order to establish neural connections. Once connections are made, MTs provide structural integrity and support to maintain neural connectivity throughout development. Abnormalities in neural migration and connectivity due to genetic mutations of MT-associated proteins can lead to detrimental developmental defects. Growing evidence suggests that these mutations are associated with many different neurodevelopmental disorders, including intellectual disabilities (ID) and autism spectrum disorders (ASD). In this review article, we highlight the crucial role of the MT cytoskeleton in the context of neurodevelopment and summarize genetic mutations of various MT related proteins that may underlie or contribute to neurodevelopmental disorders.

Keywords: cytoskeleton, microtubule dynamics, MAPs, neuronal migration, neurodevelopmental disorders

OPEN ACCESS

Edited by:
C. Laura Sayas,
Universidad de La Laguna, Spain

Reviewed by:
Marina Mikhaylova,
Universitätsklinikum Hamburg-Eppendorf, Germany
Roland Brandt,
University of Osnabrück, Germany
Illana Gozes,
Tel Aviv University, Israel

****Correspondence:***
Laura Anne Lowery
laura.lowery@bc.edu

Received: *23 February 2018*
Accepted: *28 May 2018*
Published: *14 June 2018*

Citation:
Lasser M, Tiber J and Lowery LA (2018) The Role of the Microtubule Cytoskeleton in Neurodevelopmental Disorders.
Front. Cell. Neurosci. 12:165.
doi: 10.3389/fncel.2018.00165

INTRODUCTION

The development of the central nervous system (CNS) and wiring of the brain is an extremely complex process, governed by the communication and careful coordination of the neuronal cytoskeleton, comprised of microtubule (MT), actin and intermediate filament networks (Menon and Gupton, 2016; Pacheco and Gallo, 2016; Kirkcaldie and Dwyer, 2017). Newly formed neurons face many challenges as they undergo dramatic changes in shape and migrate their way through the extracellular terrain in order to establish connections with other cells. Specifically, dynamic MTs play pivotal roles in creating cell polarity, as well as aiding in neural migration in order to establish appropriate neural connectivity throughout development and into adulthood. The elaborate MT network is integral to facilitate numerous morphological and functional processes during neurodevelopment, including cell proliferation, differentiation and migration, as well as accurate axon guidance and dendrite arborization. The organization and remodeling of the MT network is also essential for developing neurons to form axons, dendrites and assemble synapses. Moreover, in mature neurons, MTs continue to maintain the structure of axons and dendrites, and serve as tracks for intracellular trafficking, allowing motor proteins to deliver specific cargoes within the cell.

As brain development relies heavily on proper MT function, defects in the MT cytoskeleton can lead to detrimental effects on neural proliferation, migration and connectivity. Over the last several

years, numerous studies have identified mutations within genes coding for proteins that interact with and directly modulate the structure and function of the MT cytoskeleton. Many of these MT-associated mutations have been linked to various neurodevelopmental disorders including lissencephaly, polymicrogyria, autism spectrum disorders (ASD) and intellectual disabilities (ID; Srivastava and Schwartz, 2014; Chakraborti et al., 2016; Stouffer et al., 2016). The regulation of the MT cytoskeleton during specific stages of brain development still remains an active topic of research. In this review article, we highlight various studies that illustrate important functions of the MT cytoskeleton that contribute to proper neural development and how genetic mutations within MT-related proteins can alter these crucial functions that may lead to disorders of neural development.

THE ROLE OF THE MICROTUBULE CYTOSKELETON DURING NEURAL DEVELOPMENT

MTs are one of the major cytoskeletal components present in all eukaryotic cell types. They are composed of α- and β-tubulin heterodimers, which bind to form 13 polarized linear protofilaments that associate laterally together to create the MT (**Figure 1**; Akhmanova and Steinmetz, 2008). MTs are extremely dynamic structures, existing in either a growing state (polymerization) or shrinking state (depolymerization). The plus ends of MTs can rapidly switch between these two states, going from growth to shrinkage (catastrophe), or from shrinkage to growth (rescue), a process called "dynamic instability" (Mitchison and Kirschner, 1984). Developing neurons depend on this stochastically dynamic nature of the MT cytoskeleton in order to remodel their shape, proliferate and migrate, as well as other processes during different phases of neural development, as described in more detail below.

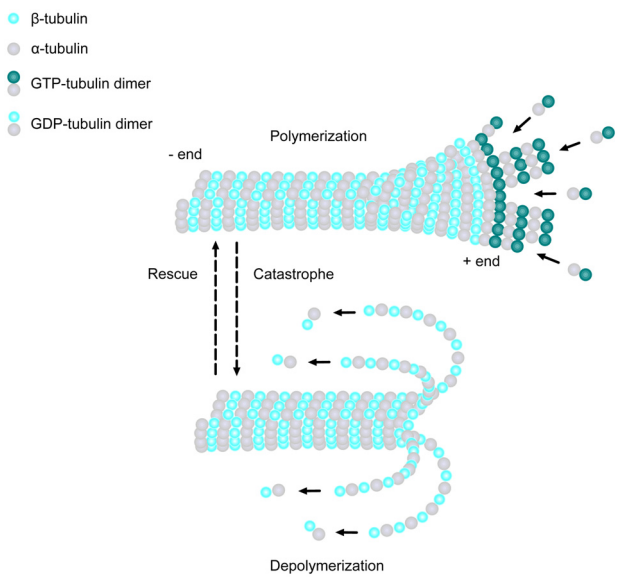

FIGURE 1 | Microtubule (MT) basics. MTs are linear structures comprised of α-tubulin and β-tubulin heterodimers. MTs are extremely dynamic, existing in either a growing state (polymerization) or shrinking state (depolymerization), and can rapidly switch from growth to shrinkage (catastrophe) or from shrinkage to growth (rescue). Addition of new GTP-bound heterodimers occurs at the MT plus end during polymerization. Shortly thereafter, the tubulin subunits hydrolyze their bound GTP to GDP. When the addition of GTP-bound heterodimers slows and the MT lattice is composed of predominantly GDP-tubulin, the protofilaments splay apart and the MT depolymerizes.

Neurite Formation and Axon Specification

Neurons begin their development as spherical, unpolarized cells, with MTs emanating from MT organizing centers (MTOCs), such as the centrosome, and are nucleated by the γ-tubulin ring complex (γ-TuRC; Kuijpers and Hoogenraad, 2011). This structure acts as a template for the α- and β-tubulin dimers to begin polymerization and is the cap of the minus end as the MT plus end grows away from the MTOC (Kuijpers and Hoogenraad, 2011). Once differentiation occurs, neurons form multiple processes, termed neurites, which extend from the spherical cell body and elongate to form thin protrusions (Götz and Huttner, 2005). MTs are one of the major players which influence the formation of neurites by creating small bundles that invade lamellipodia in multiple directions (Götz and Huttner, 2005). It has been suggested that MT sliding may play a key role in initiating neurite formation. One study demonstrated that MT-associated protein 2c (MAP2c) could stabilize MT bundles *in vitro*, which then rapidly move toward the cell periphery, prompting protrusions via a dynein-driven force (Dehmelt et al., 2006). It has also been shown that neurite formation can be induced by the MT motor protein, kinesin-1, which drives MT sliding and generates a mechanical force on the cell membrane (Lu et al., 2013; Winding et al., 2016). Studies have also demonstrated that actin filaments contribute to membrane protrusions, working in combination with stable MTs to initiate neurite outgrowth (Dent et al., 2011; Sainath and Gallo, 2015). Together, these results suggest that the local increase in actin dynamics, as well as the mechanical forces produced by MT sliding, all play key roles in stimulating neurite formation.

After neurite extension, one of the multiple processes becomes the axon, while the others later develop into dendrites (Menon and Gupton, 2016). Stable MTs are essential in axon specification and actively determine the polarity of developing neurons (Conde and Cáceres, 2009; Hoogenraad and Bradke, 2009). Interestingly, the ratio of stable to dynamic MTs was found to be significantly higher in one specific neurite compared to other neurites during this stage of neural development (Witte et al., 2008). Furthermore, axon formation was induced in unpolarized neurons following the addition of a photoactivatable analog of the MT-stabilizing drug taxol, while the addition of low doses of taxol led to the formation of multiple axons (Witte et al., 2008). These results suggest that in unpolarized neurons, the stabilization of MTs within one specific neurite occurs before axon formation begins. Once neurons begin to establish a distinct polarity, the centrosome progressively loses its function as an MTOC, with MTs beginning to nucleate from non-centrosomal MTOCs, such as Gogli outposts

(Stiess et al., 2010; Stiess and Bradke, 2011; Ori-McKenney et al., 2012; Yau et al., 2014). Moreover, the stabilization of non-centrosomal MTs by the minus-end binding protein, calmodulin-regulated spectrin-associated protein 2 (CAMSAP2), was shown to be required for the establishment of neuronal polarity and axon formation (Yau et al., 2014). Reduction of CAMSAP2 inhibited both proper polarization and axon formation *in vitro*, and led to defects in neural migration *in vivo*, providing further evidence that MT stabilization is critical for these processes during neural development (Yau et al., 2014). Increased MT stabilization may also provide tracks for selective targeting of MT motor proteins to aid in the transportation of various organelles and proteins that are necessary for the eventual formation of axonal segments (Kapitein and Hoogenraad, 2011). Kinesin-1 has been shown to preferentially bind to stabilized MTs and accumulate in the future axon, contributing to early polarized trafficking, suggesting that an increase of stable MTs may lead to increased kinesin-mediated transport, driving both neuronal polarization and eventual axon specification (Nakata and Hirokawa, 2003; Jacobson et al., 2006).

Axon Elongation and Branching

A major change that occurs, following axon specification, is the formation and enlargement of the growth cone, a dynamic structure at the tip of the growing axon responsible for driving axon elongation and branching (Kahn and Baas, 2016). Neuronal growth cones probe the extracellular environment and come into contact with various external stimuli, thus steering the axon in a particular direction (Lowery and Van Vactor, 2009). The growth cone uses the cytoskeletal machinery to progress through three distinct morphological stages, termed protrusion, engorgement and consolidation (Lowery and Van Vactor, 2009). To progress through these stages, an array of dynamic MTs penetrate into the central and peripheral domains of the growth cone, and can display different behaviors which include splaying, looping and bundling (Tanaka and Kirschner, 1991). This remodeling is essential for MTs to probe the growth cone periphery in search of guidance cues, which prompt growth cone advancement and turning. Additionally, growth cone formation and advancement require the interaction between actin filaments and dynamic MTs, which work in combination to promote the extension of lamellipodia and filopodia at the tip of the axon (Dent et al., 2011).

Cytoskeletal remodeling must also occur during axon branching, which involves an accumulation of actin filaments that will form axonal filopodia along the axon shaft (Mattila and Lappalainen, 2008). Shortly thereafter, MTs begin to invade the actin-rich filopodia with localized splaying of the normally bundled MT array (Dent et al., 1999; Gallo and Letourneau, 1999). This invasion by the axonal MTs into the filopodia allows their maturation into collateral branches as they continue extending. Early studies showed that there was an increase in the number of MTs at regions that eventually become axon branches, suggesting that MTs within the parent axon undergo fragmentation, and a portion of these fragments are then translocated to the developing branches (Yu et al., 1994; Kalil and Dent, 2014; Armijo-Weingart and Gallo, 2017). Thus, MT fragmentation and transportation appear to be key mechanisms which regulate the beginning of axon branch formation. Crosstalk between actin and MTs also seems to be required during the initial steps of axon branching (Dent and Kalil, 2001; Kalil and Dent, 2014; Gallo, 2016; Pacheco and Gallo, 2016). Dynamic MTs colocalize with F-actin in regions of axon branching, whereas stable MTs are excluded from these regions (Dent and Kalil, 2001). Moreover, when MT dynamics were dampened in neurons treated with either taxol or nocodazole, invasion of MTs into filopodia was reduced and they were unable to interact with actin-filament bundles, which resulted in decreased neurite formation (Dent et al., 2007). Recently, the cytoskeleton-associated protein, drebrin, was shown to regulate both actin filaments and MTs to initiate the formation of axon branches (Ketschek et al., 2016; Zhao et al., 2017). Endogenous drebrin was found to localize to axon actin patches *in vivo*, which eventually form axonal filopodia, suggesting that drebrin may contribute to the development of these precursor structures before axon branching (Ketschek et al., 2016). Additionally, reduction of drebrin severely inhibited axonal filopodia formation and the number of collateral branches *in vitro*, further demonstrating an essential role for drebrin in regulating these processes (Ketschek et al., 2016). Expression of drebrin also increased the number of axonal filopodia that contained end-binding protein 3 (EB3) comets, indicating that drebrin can promote the entry of dynamic MTs into axonal filopodia during the formation of axon branches (Ketschek et al., 2016). Thus, dynamic MTs and their interactions with actin filaments are crucial for the establishment and formation of collateral branches during neuronal development.

Dendritogenesis and Synapse Formation

Following axon formation, other neurites begin to develop into dendrites, prompting dramatic changes to the MT network. While dendrites branch more extensively than axons, the behavior of MTs during this process has not yet been fully elucidated. One of the most striking features that distinguishes dendrites from axons is the orientation of their MTs. Axons display uniform plus-end distal MTs, while dendrites harbor a population of MTs with mixed polarity, where both plus and minus ends are oriented towards the cell body (Kapitein and Hoogenraad, 2015; Tas et al., 2017). These distinct polarity patterns are essential for determining the directionality of intracellular cargo transport, which maintains both the composition and morphological differences between axons and dendrites. Several studies have suggested that the translocation of MTs of differing orientations within dendrites plays a key role in establishing their mixed polarity (Sharp et al., 1995, 1997; Yu et al., 2000; Zheng et al., 2008; Rao et al., 2017). When MT assembly was inhibited with low levels of vinblastine, dendritic elongation was reduced, however MT reorientation was not hindered, suggesting that transport of MTs from the cell body is a possible mechanism for creating the non-uniform orientation of dendritic MTs (Sharp et al., 1995). Moreover, several studies have shown that neurons use distinct motor proteins to engage in specific transportation events that may

drive this difference in MT orientation between axons and dendrites (Sharp et al., 1997; Yu et al., 2000; Zheng et al., 2008; Rao et al., 2017). Reduction of the kinesin-related motor protein CHO1 (also known as KIF23) from cultured neurons inhibited the movement of minus-end distal MTs into nascent dendrites and these processes failed to differentiate (Sharp et al., 1997; Yu et al., 2000). Likewise, reduction of kinesin-12 (also known as KIF15) produced similar phenotypic results (Lin et al., 2012). The abnormalities observed with depletion of kinesin-6 could be rescued by overexpression of kinesin-12, indicating that these two motor proteins may share functional redundancy within dendrites (Lin et al., 2012). Similarly, neurons treated with the dynein inhibitor, Ciliobrevin D, displayed a decrease in MT transport and abnormal MT orientation in the axon, which could be rescued after Ciliobrevin D washout (Rao et al., 2017). Thus, active MT transport by specific motor proteins is essential for both establishment and maintenance of MT bi-directionality during dendritic development.

The next steps in neuronal development are the formation and maturation of dendritic spines, which represent postsynaptic sites of excitatory synapses. The connections between an axon and a dendrite of neighboring neurons is a process that continuously occurs throughout development and into adulthood, as the brain rewires these connections in response to novel stimuli. For some time, it was thought that dendritic spines were devoid of dynamic MTs, and that actin was the main regulator of spine morphology and dynamics associated with synaptic plasticity. However, within the last decade, the use of new visualization techniques has revealed that MT dynamics do play an essential role in dendritic spine development (Yau et al., 2016; Dent, 2017). In concert with MT transport, MT polymerization actively occurs and contributes to the development of the dendritic branches. MT assembly occurs within the cell body, and after transport, these newly formed MTs are incorporated into the dendrite (Dent, 2017). Dynamic MTs can penetrate into dendritic spines of different shapes, including mushroom, stubby and thin, and can modulate their morphology by interacting with F-actin via +TIPs, such as EB3 (Gu et al., 2008; Jaworski et al., 2009; Dent, 2017). Furthermore, reduction of EB3 impairs spine development, and pharmacological manipulation of MT dynamics severely decreases the total number of spines and inhibits the formation of spines that are induced by brain-derived neurotrophic factor (BDNF; Gu et al., 2008; Jaworski et al., 2009). Interestingly, N-methyl-D-aspartate receptor (NMDAR)-dependent synaptic activation in hippocampal cell cultures increases the proportion of dendritic spines containing dynamic MTs, which contributes to spine enlargement, and this increase in MT invasion is inhibited by either blocking action potential activity or by dampening MT dynamics (Merriam et al., 2011). Additionally, dendritic spines exhibiting elevations in calcium signaling contain increased amounts of F-actin, and these spines are preferentially targeted by dynamic MTs, which interact with F-actin in a drebrin-dependent manner (Merriam et al., 2013). Moreover, studies have shown that the invasion of dynamic MTs into dendritic spines provide tracks for MT-dependent motors to deliver specific cargoes that are essential for synaptic plasticity (McVicker et al., 2016). It has also been demonstrated that the severing of dynamic MTs by the MT-severing proteins, katanin and fidgetin, are essential for dendrite development and synapse formation (Mao et al., 2014; Leo et al., 2015), which will be discussed in greater detail in subsequent sections. Together, these results strongly indicate that dynamic MTs are key regulators of dendritic spine formation, maintenance and synaptic activity, and that +TIPs play a role in this dynamicity to modulate spine morphology during neural development.

Microtubules Guide Intracellular Transport During Axon and Dendrite Maintenance

MT-dependent cargo transport is an essential process that regulates the unique composition of both axons and dendrites and aids in maintaining their polarized morphology. This active transport mechanism is also necessary to accurately distribute specific cargoes and establish particular signaling pathways throughout the neuron. Neuronal intracellular transport is driven by the MT-dependent motors, kinesin and dynein, which move in opposite directions to deliver various cargo such as organelles, neurotransmitter receptors, cell signaling molecules and mRNAs, to the correct location within the cell (Hirokawa et al., 2010). Moreover, adaptor proteins and local signaling pathways regulate proper cargo delivery by aiding in cargo loading, anchoring and motility (Maday et al., 2014). The specific orientations of MTs are critical in determining the routes in which cargoes will travel throughout the neuron. For example, studies have demonstrated that dynein selectively transports cargoes along minus-end out oriented MTs found within dendrites (Kapitein et al., 2010; Tas et al., 2017). It has also been shown that kinesin-1 preferentially transports cargoes along MTs in axons, whereas kinesin-3 exhibits no selectivity, delivering cargoes to both axons and dendrites. It has been reported that specific post translational modifications of MTs are recognized by various kinesin superfamily members, which can regulate their localization and functions within neurons (Kapitein et al., 2010; Tas et al., 2017). As mentioned previously, it has been suggested that kinesin-1 preferentially binds to stabilized MTs that have either been acetylated or detyrosinated (Nakata et al., 2011), while kinesin-3 prefers to bind to tyrosinated MTs (Tas et al., 2017). However, the exact mechanisms which govern MT properties within axons and dendrites that subsequently guide specific motor proteins still remain unknown.

REGULATORS OF THE NEURONAL MICROTUBULE NETWORK

The essential remodeling and organization of the MT cytoskeleton during neuronal morphogenesis relies on a vast array of MT-regulating proteins that have been identified over the last few decades (**Figure 2**). These proteins carry out specific functions to control MT dynamicity, fragmentation, stabilization, and intracellular transport. Many act directly on MTs to affect their nucleation, assembly, or stability,

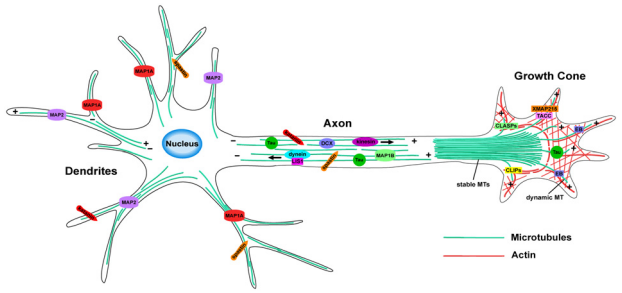

FIGURE 2 | MT organization and MT-associated proteins (MAPs) in axons and dendrites. In axons, MTs form stable, polarized bundles, which provide structural integrity and serve as tracks to guide MT-dependent motor proteins. Axonal MTs are stabilized by several MAPs including Tau, MAP1B and DCX. The growth cone contains an array of both stable and dynamic MTs, which prompt growth cone advancement and turning. Various +TIPs accumulate at the growing MT plus ends in the growth cone, where they regulate MT dynamics during axon outgrowth and guidance. MTs of mixed polarity are located within dendrites where MAP1A and MAP2 aid in MT stabilization. The MT-severing proteins, katanin and spastin, are critical for reorganizing the MT network in both axons and dendrites.

while others act indirectly by modulating tubulin levels or intracellular transport, producing downstream effects on neuronal differentiation. The combined efforts of MT-regulating proteins such as MT associated proteins (MAPs), +TIPs and MT motor proteins, provide the mechanisms by which the MT network reshapes its architecture during neuronal development. Here, we highlight several groups of MT regulators and their respective functions that control the assembly of new MTs and their dynamicity, as well as how they regulate MT stability, fragmentation and intracellular trafficking within neurons.

Microtubule Plus End Tracking Proteins (+TIPs)

+TIPs are proteins which accumulate at growing MT plus-ends where they regulate MT dynamics, as well as facilitate their interactions with other proteins, organelles, and actin (Akhmanova and Steinmetz, 2008). Many families of +TIPs have been found to be crucial for different neurodevelopmental processes, specifically during neurite extension and axon outgrowth. For example, adenomatous polyposis coli (APC) is enriched in the nervous system where it plays a significant role in establishing neuronal polarity, as well as aiding in migration and axon navigation by stabilizing MTs (Shi et al., 2004; Koester et al., 2007; Eom et al., 2014). Other core regulators of the +TIP network involved in neural development are the EBs. EBs autonomously recognize the growing MT plus end, functioning as a scaffold for other +TIPs to associate and interact with the plus end, thereby regulating MT dynamics (Akhmanova and Steinmetz, 2008). Additionally, several studies suggest differential roles of EB proteins during neurodevelopment, demonstrating that the mechanisms underlying their regulation of the MT cytoskeleton are quite complex. For instance, as mentioned previously, EB3 expression is upregulated during neurodevelopment and is important for regulating MT dynamicity during dendritic spine development (Jaworski et al., 2008). Interestingly, this increase in EB3 expression coincides with a decrease in EB1 expression (Jaworski et al., 2008). However, EB1 is specifically upregulated during axon extension and has been shown to be critical for proper MT organization, as depletion of EB1 in *Drosophila* leads to abnormalities in MT architecture leading to aberrant axon outgrowth (Alves-Silva et al., 2012).

Cytoplasmic linker proteins (CLIPs) are another group of +TIPs that participate in several neural developmental processes including axon formation and outgrowth, as well as dendrite arborization (van de Willige et al., 2016). CLIPs are enriched in axonal growth cones, where they stabilize MTs invading the growth cone leading edge, and in dendritic spines, where they regulate the crosstalk between actin and dynamic MTs (Neukirchen and Bradke, 2011; Swiech et al., 2011). Additionally, mutations within CLIPs have been associated with ID (Larti et al., 2015), which will be discussed further in subsequent sections. Similar to CLIPs, cytoplasmic linker associated proteins (CLASPs) also regulate MT dynamics during axon outgrowth where they accumulate along MTs at the leading edge of the growth cone, suggesting a role in facilitating axon navigation during development (Lee et al., 2004; Marx et al., 2013). Additional +TIPs found to be important for regulating MT dynamics during neural development include the MT polymerase XMAP215 (Lowery et al., 2013), the XMAP215-interactor, TACC3 (Nwagbara et al., 2014; Bearce et al., 2015; Cammarata et al., 2016; Erdogan et al., 2017), as well as the other TACC family members, TACC1 and TACC2 (Lucaj et al., 2015; Rutherford et al., 2016).

Microtubule Lattice-Binding Proteins

Remodeling of MTs within neurons is essential for the establishment and maintenance of neuronal polarity, axon outgrowth and guidance, synapse formation and migration. There are numerous MAPs that can bind along the MT lattice and regulate MT dynamics in order to properly organize and remodel the MT cytoskeleton during neural development. The most widely studied and best-characterized group of MT lattice-binding proteins are structural MAPs, which are comprised of three distinct groups including MAP1, MAP2 and tau.

There are three members of the MAP1 family found in vertebrates, MAP1A, MAP1B and MAP1S. MAP1B is highly expressed during early neuronal development and is found to be enriched at growing axons, where it regulates axon outgrowth via its interaction with the MT cytoskeleton (Bouquet et al., 2004; Jayachandran et al., 2016). Neuronal subtypes derived from *map1b*−/− mice revealed several defects including higher collateral axon branching, improper growth cone turning, as well as abnormalities in synaptic vesicle fusion and synaptic plasticity, suggesting that MAP1B is necessary during these processes (Bouquet et al., 2004; Bodaleo et al., 2016). Furthermore, reduction of MAP1B was also shown to decrease MT growth speed in the proximal and distal axon shaft, suggesting that MAP1B may function as a regulator of MT dynamics during axon outgrowth (Tymanskyj et al., 2012). Less is currently known about MAP1A, but it appears to participate in dendritic

remodeling and preferentially localizes to postsynaptic densities (PSD) where it interacts with PSD proteins to support synaptic function (Koleske, 2013; Takei et al., 2015). It has also been shown that expression of MAP1A increases MT stability *in vitro* (Vaillant et al., 1998) and *Map1a* mutant mouse Purkinje neurons were shown to have abnormal MT networks, demonstrating an important role for MAP1A in MT organization and stabilization (Liu et al., 2015).

Similar to MAP1A, the MAP2 family of proteins are also enriched within dendrites and they have been shown to increase MT stability by rescuing catastrophes (Dehmelt and Halpain, 2005). Furthermore, they are important for regulating MT organization in dendrites by participating in MT bundling, as well as creating the proper spacing between MTs (Teng et al., 2001; Dehmelt and Halpain, 2005). Moreover, it was recently demonstrated that MAP2 can interact with both kinesin-1 and kinesin-3 motors to regulate their distribution of specific cargoes throughout the neuron (Gumy et al., 2017). MAP2-deficient mice show no overt neurological abnormalities, though they do display a reduction in MT density and dendrite length (Harada et al., 2002). However, mice deficient in both MAP2 and MAP1B have severe cortical defects, suggesting there may be a compensatory mechanism between these two proteins (Teng et al., 2001).

Tau is the most widely studied MT lattice binding protein due to its implication in neurodegenerative diseases (Matamoros and Baas, 2016). It is expressed in the brain throughout development into adulthood and appears to have several different functions in relation to MTs. Tau has been shown to increase MT polymerization, prevent MT depolymerization, and regulate MT organization (Wang and Mandelkow, 2016). Additionally, it has been demonstrated that tau dynamically interacts with MTs through a kiss-and-hop mechanism, where it remains associated with a single MT filament for only milliseconds before rapidly dissociating (Janning et al., 2014). Moreover, axonal transport rates are not significantly affected by either the elimination or overexpression of tau, further supporting the kiss-and-hop mechanism, as MT-dependent motor proteins would be impeded by tau if it associated with MTs for longer periods of time (Yuan et al., 2008; Janning et al., 2014). Tau is also expressed within axonal growth cones where it co-localizes with both MTs and actin filaments, and it can influence the organization of dynamic MTs to facilitate axon outgrowth and turning mediated by guidance cues (Li et al., 2014; Biswas and Kalil, 2018). Furthermore, tau seems to be critical for neuronal migration during brain development, as reduction of tau impaired the radial migration of cortical neurons, in addition to causing morphological abnormalities of the leading edge in these cells (Sapir et al., 2012). Interestingly, there may be functional redundancy between tau and MAP1B, as both have been shown to act synergistically to promote axon outgrowth and neuronal migration (Takei et al., 2000).

Microtubule Severing Proteins

The reorganization of MTs depends on the process of MT severing, accomplished by enzymes such as katanin, spastin and fidgetin, which act to cut MTs into small pieces so that they can be transported to other locations within the cell in order to form a new MT array. Katanin consists of a P60 subunit, encoded by KATNA1, which functions to sever MTs, and a P80 subunit, encoded by KATNB1, which regulates the ATPase activity and localizes the protein primarily to centrosomes (McNally et al., 2000). In addition to the centrosome, katanin has been found to be highly expressed in growing axons (Karabay et al., 2004). Proper function of katanin within neurons seems to be dosage-dependent. Expression of a dominant-negative P60-katanin construct inhibited MT severing leading to abnormal axon outgrowth in cultured rat sympathetic neurons (Karabay et al., 2004). Conversely, overexpression of the P60-katanin construct led to increased MT severing, which was also detrimental to axon outgrowth (Karabay et al., 2004). More recently, katanin-mediated severing has been shown to regulate the development of dendrites and synapses at the neuromuscular junction (NMJ). The loss of the katanin P60 subunit in *Drosophila* resulted in abnormal synapse morphology at the NMJ, including an increased number of small boutons, more stable MT loops and dendritic overgrowth (Mao et al., 2014). Moreover, genetic mutations within several katanin-associated proteins have been linked to microcephaly, suggesting that proper function of katanin is important during early brain development (Bartholdi et al., 2014).

Similar to katanin, spastin is another MT severing protein that is highly enriched in developing axons and is thought to be involved in promoting axon outgrowth (Yu et al., 2008). Reduction of spastin function in zebrafish caused severe defects in motor axon outgrowth, as well as abnormalities in neuronal connectivity (Wood et al., 2006). Additionally, knockdown of spastin in cultured neurons reduced axonal branching, whereas overexpression increased the number of branches and filopodia, indicating that spastin also functions in a dosage-dependent manner (Yu et al., 2008). Furthermore, mutations within spastin cause autosomal dominant hereditary spastic paraplegia, which is a disease characterized by axonal degeneration that leads to a progressive gait disorder (Hazan et al., 1999). Therefore, the regulation of MT severing by spastin is vital for axon outgrowth that is necessary to establish proper neural connectivity.

Less is currently known about the precise functions of fidgetin, however it has been associated with various aspects of vertebrate embryonic development (Cox et al., 2000). It has been demonstrated that fidgetin can depolymerize and sever MTs *in vitro*, as well as regulate MT dynamics at mitotic centrosomes (Mukherjee et al., 2012). Moreover, knocking down fidgetin in *Drosophila* disrupts normal axon development by causing an increase in the number of synaptic boutons, as well as an increase in stable MTs (Leo et al., 2015). Interestingly, these results are similar to the phenotypes previously observed with the reduction of katanin, suggesting that fidgetin behaves in a similar fashion to other MT-severing enzymes (Mao et al., 2014). However, axons in cultured vertebrate neurons are significantly longer with more minor processes and contain an increase in labile MT mass when fidgetin is depleted, suggesting that fidgetin regulates axon elongation by severing MT labile domains during neurodevelopment (Leo et al., 2015).

THE MAJOR PLAYERS OF NEURONAL MOVEMENT: MICROTUBULE-ASSOCIATED GENES LINKED TO DISORDERS OF NEURONAL MIGRATION

Development of the brain requires extensive neuronal proliferation and migration. This orchestrated movement of neurons to their final destination within the brain relies heavily on the support and coordination of the MT cytoskeleton, along with various MT-associated proteins. Abnormalities in proliferation or migration can lead to downstream defects in neural connectivity and various neurodevelopmental disorders. Human and mouse genetic studies have been instrumental in understanding the dynamic nature and function of the MT cytoskeleton and its associated regulators during neuronal migration. In the following sections, we discuss several well-characterized neuronal migration disorders and the various MT-associated genetic mutations that lead to these disorders during brain development (**Table 1**).

Type I Lissencephaly

One of the most widely known neuronal migration disorders is type I lissencephaly ("smooth brain"), also known as classic lissencephaly. This malformation is characterized by a spectrum of cortical abnormalities, which are defined by the absence or reduction of cortical folds (gyri) and grooves (sulci), making parts of the surface of the brain appear smooth. More severe forms of type I lissencephaly result in the complete loss of cortical folds (agyria), while milder forms result in the reduction of cortical folds (pachygyria), or areas of heterotopic bands of gray matter within the cortex (subcortical band heterotopia (SBH); Forman et al., 2005; Barkovich et al., 2012). Agyria and pachygyria arise from post-mitotic neurons failing to reach their proper positions, leading to a disorganized and thickened four-layer cortex instead of the normal six-layered cortex. In SBH, neurons migrate abnormally and form an extra layer of cells underneath the gray matter within the cortex. Type I lissencephaly is typically diagnosed in children within the first few months of life and patients often have many other symptoms including epilepsy, ID, developmental delays and motor function impairments.

Over the last few decades, studies of families with one or multiple individuals affected by type I lissencephaly led to the discovery of several mutations associated with MT-related genes (Kerjan and Gleeson, 2007). The first two genes to be identified were lissencephaly 1 (LIS1; Reiner et al., 1993), located on the short arm of chromosome 17, and doublecortin (DCX; Gleeson et al., 1998; des Portes et al., 1998), located on the X-chromosome. Human mutations of LIS1 (also known as PAFAH1B1, platelet-activating factor acetylhydrolase 1b, regulatory subunit 1) are heterozygous, affecting both males and females, while mutations of DCX are hemizygous, occurring on the X-chromosome, and largely affect only males. Mutations within LIS1 tend to be associated with a more severe phenotype in posterior brain regions, whereas mutations within DCX have the reverse effect with a more severe phenotype in frontal brain regions (Pilz et al., 1998). Both of these genes account for most cases of type I lissencephaly and code for MAPs that are necessary for neuronal differentiation and migration due to their essential interactions with the MT cytoskeleton (Pilz et al., 1998; Stouffer et al., 2016).

In migrating neurons, LIS1 predominately localizes to the centrosome where it aids in nuclear movement and acts as an adaptor protein to stabilize MTs by minimizing catastrophe (Sapir et al., 1997; Shu et al., 2004). LIS1 has also been shown to regulate the MT minus end directed motor, dynein (Smith et al., 2000; Rehberg et al., 2005), by increasing its localization and stabilization at MT plus ends (Li et al., 2005; DeSantis et al., 2017), and assisting in its transport of cargo along the MT (Egan et al., 2012; Moughamian et al., 2013; Vagnoni et al., 2016). DCX has been shown to be highly expressed in the growing axon, where it directly nucleates and stabilizes MTs by supporting their 13 protofilament structure and participates in promoting growth cone formation (Burgess and Reiner, 2000; Tint et al., 2009; Bechstedt and Brouhard, 2012; Jean et al., 2012). The interactions of LIS1 and DCX with MTs are regulated by numerous phosphorylation events (Sapir et al., 1999; Schaar et al., 2004). However, the specific sites of phosphorylation, as well as the kinases and phosphatases which regulate this activity, have still not been fully elucidated in relation to classic lissencephaly. It is possible that genetic mutations at specific phosphorylation sites may alter the interaction between LIS1 and DCX with the MT cytoskeleton, thereby changing their functions and producing variable phenotypic outcomes.

The creation of several mouse models of classic lissencephaly have been instrumental in investigating the cellular and molecular irregularities that occur due to the implicated genetic mutations of this disorder. Homozygous *Lis1* knockout (KO) mice die prenatally, indicating that LIS1 is absolutely essential for normal embryonic development (Hirotsune et al., 1998). Lis1-null heterozygous mice display motor coordination and cognition deficits, as well as severe disorganization of the cortical layers, hippocampus, and other areas within the brain (Paylor et al., 1999; Fleck et al., 2000; Youn et al., 2009). Moreover, overexpression of LIS1 caused severe structural brain abnormalities, including smaller brain size, distorted cellular organization and an increase in apoptotic cells, suggesting proper function of LIS1 is required in a dose-dependent manner (Bi et al., 2009). Inhibition of dynein results in a similar phenotype, further supporting the role of LIS1 in dynein function (Shu et al., 2004; Grabham et al., 2007; Tsai et al., 2007). Additional studies using histological analysis and BrdU labeling experiments have also provided strong evidence towards *in vivo* migrational defects in mice with reduced *Lis1* dosage, demonstrating that LIS1 is necessary for proper neuronal migration (Hirotsune et al., 1998; Gambello et al., 2003). Interestingly, mice with mutations in *Dcx* only display mild disordered neuronal migration phenotypes, mostly occurring in the hippocampus of both heterozygous females and hemizygous males (Corbo et al., 2002). In contrast, RNAi-directed depletion of Dcx showed abnormal radial migration of neurons in rat neocortex (Bai et al., 2003). It is possible that this variability of phenotypic severity may be due to compensation

TABLE 1 | Microtubule (MT)-associated genes linked to neurodevelopmental diseases.

Disease	Gene	Major pathways/roles	Additional phenotypes	References
Intellectual disabilities (ID)	KIF1A	Kinesin; MT-dependent motor		Willemsen et al. (2014)
	KIF4A	Kinesin; MT-dependent motor		Kondo et al. (2012), Lee et al. (2015), Ohba et al. (2015) and McVicker et al. (2016)
	CLIP1	MT binding; +TIP; MT dynamics		Coquelle et al. (2002), Jaworski et al. (2008), Swiech et al. (2011) and Larti et al. (2015)
	KATNAL1	MT severing	Microcephaly	Bartholdi et al. (2014) and Banks et al. (2018)
	MID2	Ubiquitin ligase; MT binding		Geetha et al. (2014) and Gholkar et al. (2016)
Autism spectrum disorders (ASD)	AUTS2	Cytoskeletal remodeling		Kawauchi et al. (2003), Kalscheuer et al. (2007), Oksenberg et al. (2013) and Hori et al. (2014)
	ADNP	Chromatin remodeling	ID, developmental delay, motor delay	Mandel et al. (2007), Vulih-Shultzman et al. (2007), Oz et al. (2012), Helsmoortel et al. (2014), Schirer et al. (2014), Gozes et al. (2017a,b), Ivashko-Pachima et al. (2017), Gozes et al. (2018) and Van Dijck et al. (2018)
	JAKMIP1	MT-associated kinase; MT dynamics; GABA receptor trafficking		Couve et al. (2004), Steindler et al. (2004), Vidal et al. (2007), Kaminsky et al. (2011), Hedges et al. (2012), Poultney et al. (2013) and Berg et al. (2015)
	MARK1	MT-associated kinase; MT dynamics; mitochondrial trafficking		Drewes et al. (1997), Mandelkow et al. (2004), Maussion et al. (2008) and Sapir et al. (2008)
Microcephaly	ASPM	Mitotic spindle protein; cell division	ID, speech delay, seizures, short stature	Kouprina et al. (2005), Jiang et al. (2017) and Duerinckx and Abramowicz (2018)
	MCPH1	Mitotic spindle protein; DNA damage response; chromosome condensation	ID, seizures, short stature	Trimborn et al. (2004) and Gruber et al. (2011)
	STIL	Mitotic spindle checkpoint protein; centriole amplification	ID, seizures, short stature	Kumar et al. (2009), Kitagawa et al. (2011) and Vulprecht et al. (2012)
	CDK5RAP2	Centrosome integrity; spindle pole morphology	ID	Bond et al. (2005), Choi et al. (2010) and Lizarraga et al. (2010)
	CENPJ	Centrosome integrity; spindle pole morphology	ID, seizures	Kitagawa et al. (2011) and Garcez et al. (2015)
	PRUNE1	Cell motility; MT dynamics		Zollo et al. (2017)
	KIF20B	Kinesin; MT-dependent motor; cell polarity; cytokinesis		McNeely et al. (2017)
Polymicrogyria (PMG)	TUBA8	MT component		Abdollahi et al. (2009), Jaglin et al. (2009) and Poirier et al. (2010)
	TUBB2B	MT component	ID, epilepsy	Abdollahi et al. (2009), Jaglin et al. (2009), Jaglin and Chelly (2009), Poirier et al. (2010), Cushion et al. (2013) and Stouffer et al. (2016)
	TUBB3	MT component		Abdollahi et al. (2009), Jaglin et al. (2009), Poirier et al. (2010), Tischfield et al. (2010) and Whitman et al. (2016)
	KIF5C	Kinesin; MT-dependent motor	ID, seizures	Kanai et al. (2000), Homma et al. (2003), Poirier et al. (2013a) and Willemsen et al. (2014)
	KIF2A	Kinesin; MT-dependent motor	ID, epilepsy, developmental delay	Kanai et al. (2000), Homma et al. (2003) and Poirier et al. (2013a)
	DYNC1H1	Dynein; MT-dependent motor		Hafezparast et al. (2003), Shu et al. (2004), Ori-McKenney and Vallee (2011), Poirier et al. (2013a) and Zhao et al. (2016)
Lissencephaly	LIS1 (PAFAH1B1)	MT binding; dynein binding; MT stability; neuronal migration	ID, epilepsy	Reiner et al. (1993), Sapir et al. (1997), Hirotsune et al. (1998), Paylor et al. (1999), Smith et al. (2000), Fleck et al. (2000), Gambello et al. (2003), Shu et al. (2004), Li et al. (2005), Rehberg et al. (2005), Tsai et al. (2007), Bi et al. (2009), Youn et al. (2009), Egan et al. (2012), Moughamian et al. (2013), Vagnoni et al. (2016) and DeSantis et al. (2017)
	DCX	MT stability; promotes growth cone formation; neuronal migration	ID, epilepsy	Gleeson et al. (1998), des Portes et al. (1998), Pilz et al. (1998), Burgess and Reiner (2000), Corbo et al. (2002), Bai et al. (2003), Moores et al. (2004), Deuel et al. (2006), Tanaka et al. (2006), Bechstedt and Brouhard (2012) and Stouffer et al. (2016)
	TUBA1A	MT component	ID, PMG, epilepsy, motor delay	Poirier et al. (2007), Keays et al. (2007), Abdollahi et al. (2009), Jaglin et al. (2009), Jaglin and Chelly (2009), Poirier et al. (2010), Cushion et al. (2013), Fry et al. (2014), Bahi-Buisson et al. (2014) and Stouffer et al. (2016)

by other members of the DCX superfamily. For example, doublecortin-like kinase-1 (DCLK1) is a closely related gene to DCX, and *Dcx/Dckl1* KO mice display a more severe phenotype of cortical development, supporting the idea of genetic redundancy (Deuel et al., 2006; Tanaka et al., 2006). Together, *in vivo* and *in vitro* studies have confirmed that these two proteins are critical regulators of proper neuronal migration by working in combination, potentially in similar molecular pathways, to stabilize the MT cytoskeleton throughout neurodevelopment.

More recently, another genetic mutation linked to classic lissencephaly has been identified, occurring in the TUBA1A gene locus (Poirier et al., 2007). TUBA1A is an α-tubulin isotype specifically expressed in the developing nervous system and is required for proper MT structure and function (Keays et al., 2007; Poirier et al., 2007; Fry et al., 2014). Mice with heterozygous mutations of TubA1A were shown to have abnormal neuronal migration and lamination defects similar to the human phenotype (Keays et al., 2007, 2010). Subsequent patient studies revealed several TUBA1A mutations in locations that are predicted to interfere with the interactions between known binding partners, like DCX and other tubulins, suggesting that this may be a possible mechanism to explain how the mutations lead to cortical migration defects (Poirier et al., 2007; Bahi-Buisson et al., 2014), however, the molecular basis of these alterations still remains unclear. In addition to causing symptoms associated with classic lissencephaly, mutations within this gene have also been shown to cause a wide range of other cortical malformations, which will be discussed further in subsequent sections.

Polymicrogyria

Another well-known neuronal migration disorder is Polymicrogyria (PMG), which is a spectrum of disorders characterized by excessive cerebral cortex folding and malformations of cortical layering. It has been described that hypoxia, congenital infections, inflammation of the microvasculature, as well as mitochondrial diseases are among the non-genetic causes that may lead to the cortical abnormalities related to PMG during early embryonic development (Gressens, 2000; Stutterd and Leventer, 2014). Clinical manifestations of PMG are heterogeneous and cause a wide range of developmental disabilities, making a uniform classification of this disorder difficult. Both environmental and genetic causes have been implicated in PMG; however, our current understanding of this cortical malformation still remains incomplete. Defining features of PMG are controversial, as some sources debate whether this disorder is truly due to a neuronal migration defect or a post-migrational defect, with abnormalities occurring after neurons are properly positioned to form the cortical layers (Judkins et al., 2011; Barkovich et al., 2012). These ambiguities make the need for more pathological and molecular studies essential in order to determine the mechanisms that lead to this developmental disorder.

Genetic studies have implicated numerous candidate genes associated with PMG, including transcription factors, signaling molecules and various cytoskeletal components, such as multiple tubulin isotypes and kinesin family members. The α-tubulin genes, TUBA1A and TUBA8, as well as the β-tubulin genes, TUBB2B and TUBB3, have all been identified in connection with PMG (Abdollahi et al., 2009; Jaglin et al., 2009; Poirier et al., 2010, 2013b). Mutations within these neuronally-expressed genes occur in a heterozygous fashion, with the exception of TUBA8 mutations, which are homozygous. Alterations within any of these genes can lead to structural and functional defects of the MT cytoskeleton, as well as interfere with the interactions between the MT cytoskeleton and other MT-related proteins. The abnormalities which arise from mutations of these tubulin isotypes are subtle yet distinct, indicating that they each play a unique role in regulating the MT cytoskeleton. For example, PMG patients harboring a mutation within TUBA8 have been shown to also have optic nerve hypoplasia and callosal dysgenesis (Abdollahi et al., 2009), whereas patients with a mutation in TUBB2B have asymmetrical PMG, dysmorphic basal ganglia, as well as heterotopic neuronal cells in the white matter areas of the cortex (Jaglin et al., 2009; Cushion et al., 2013). Additionally, axonal defects are present in all known TUBB3 mutations, which create abnormalities in axon targeting of the oculomotor muscles, leading to eye movement disorders such as congenital fibrosis of the external ocular muscles (CFEOM; Tischfield et al., 2010; Whitman et al., 2016). PMG patients with either TUBA1A or TUBB2B mutations have been found to display overlapping cortical malformations, possibly due to their similar roles in the formation of tubulin heterodimers, suggesting that MT stability may underlie some of the clinical phenotypes (Jaglin and Chelly, 2009; Cushion et al., 2013; Stouffer et al., 2016).

Within the last several years, studies have identified additional PMG-associated mutations within genes encoding several MT motor proteins including kinesin family members KIF5C and KIF2A, and a dynein-associated protein, DYNC1H1 (Poirier et al., 2013a; Fiorillo et al., 2014). Each mutation results in varying phenotypes, however, all of these genes play pivotal roles in regulating the MT cytoskeleton within neurons. KIF5C and KIF2A encode members of the kinesin superfamily, both of which are highly expressed in the developing nervous system and are involved in the intracellular transport of cargo along MTs (Kanai et al., 2000; Homma et al., 2003). *Kif2a* KO mice die shortly after birth and display numerous brain abnormalities including aberrant axon outgrowth and collateral branching, as well as delayed neuronal migration (Homma et al., 2003). Additionally, the MT-depolymerizing activity in neuronal growth cones was found to be reduced, indicating that KIF2A mechanistically regulates the growth cone via its interactions with the MT cytoskeleton during axon outgrowth. In contrast, Kif5C KO mice are viable and do not display any gross malformations within the CNS, aside from smaller brain size and a reduction of motor neurons (Kanai et al., 2000). This drastic difference in phenotype could be due to compensation by other closely related genes, suggesting that there may be functional redundancy among the kinesin family members. DYNC1H1 is a large subunit of the cytoplasmic dynein complex and various mouse models indicate that this gene is also vital for cortical development. Inactivation of the mouse homolog causes embryonic lethality, and

N-ethyl-N-nitrosourea (ENU)-induced heterozygous missense mutations result in neurodegenerative diseases, as well as abnormal neuronal migration and retrograde axonal transport (Hafezparast et al., 2003; Ori-McKenney and Vallee, 2011; Zhao et al., 2016). Moreover, RNAi-directed reduction of *Dync1h1* similarly resulted in impaired neuronal migration (Shu et al., 2004). Taken together, these results highlight the importance of MT-dependent intracellular trafficking during early neural development.

Microcephaly

Primary microcephaly (MCPH) is a neurodevelopmental disorder characterized by a smaller-than-normal head size arising from abnormal prenatal brain growth. This reduced head size occurs due to insufficient proliferation or increased apoptosis of neural stem cells, leading to a reduction in the number of neurons and impaired neurogenesis during development (Barkovich et al., 2012). Often, individuals with this disorder also present with ID, poor motor function, abnormal craniofacial features and seizures. A wide range of factors have been linked to cases of microcephaly such as genetic mutations, chromosomal abnormalities, vertically transmitted infections and other environmental factors (Barkovich et al., 2012).

Several genes have been discovered to be associated with MCPH, many of which code for proteins that localize to the centrosome and play a significant role in regulating MT dynamics. Mutations in abnormal spindle-like microcephaly-associated (ASPM) have been found to be the most common cause of MCPH (Duerinckx and Abramowicz, 2018). ASPM is essential for normal function and organization of mitotic spindle poles specifically within the developing brain (Kouprina et al., 2005). A recent study showed that ASPM can also recruit Katanin to promote MT severing and disassembly, suggesting that misregulation of this process may lead to microcephaly (Jiang et al., 2017). Likewise, microcephalin 1 (MCPH1), a gene which regulates DNA-damage responses, has also been found to be crucial for proper mitotic spindle alignment within neuroprogenitors (Gruber et al., 2011). Reduction of MCPH1 results in an imbalance between mitosis and the centrosome cycle, causing asymmetric cell division and dysregulation of chromosome condensation (Trimborn et al., 2004; Gruber et al., 2011). Another gene, SCL-TAL1 interrupting locus (STIL), encodes a cytoplasmic centriole duplication factor that is required for centriole formation and proper spindle positioning during embryonic brain development (Kumar et al., 2009; Kitagawa et al., 2011). Depletion of STIL results in a loss of centriole amplification, whereas overexpression leads to excess centriole formation (Vulprecht et al., 2012). CDK5 regulatory subunit associated protein 2 (CDK5RAP2) also codes for a protein that localizes to the centrosome and is involved in centrosome function and MT nucleation (Bond et al., 2005; Choi et al., 2010). Mutations of this gene result in cells displaying mitotic delay with abnormal spindle pole number and orientation (Lizarraga et al., 2010). Centromere protein J (CENPJ) is also involved in maintaining centrosome integrity and normal spindle pole morphology. Downregulation or loss of CENPJ leads to centrosome duplication abnormalities which contribute to spindle orientation defects, as well as improper neuronal migration and morphology (Kitagawa et al., 2011; Garcez et al., 2015). Together, these genes code for proteins which all play pivotal roles in regulating centrosome and spindle pole related functions, as well as MT dynamics. Disruptions within any of these genes may lead to defects in the cell cycle, MT nucleation and reduced proliferation of neurons, thus leading to microcephaly. The overlapping functions of these genes in relation to the centrosome are striking and provides strong evidence towards a link between proper centrosome function and MT dynamics during neurogenesis.

More recently, two other genes, PRUNE1 and KIF20B, have been identified in relation to MCPH. Prune exopolyphosphatase 1 (PRUNE1) encodes a member of the DHH (Asp-His-His) phosphoesterase protein superfamily important for cell motility. Genetic studies conducted by Zollo et al. (2017) identified biallelic mutations of PRUNE1 in 13 different individuals with microcephaly and developmental delay. Mutations in PRUNE1 impaired MT polymerization, cell migration and proliferation, suggesting that PRUNE1 may have a fundamental role in regulating these processes throughout cortical development. Kinesin Family Member 20B (KIF20B) is a MT plus end-directed motor that is required for the completion of cytokinesis and regulates cell polarity in neurons (McNeely et al., 2017). Loss of Kif20b disrupts cerebral cortex growth and cell polarization, as well as neurite outgrowth and branching (McNeely et al., 2017). Authors suggest that KIF20B may act to stabilize or bundle MTs in neurites to allow for proper polarization and outgrowth during brain development (McNeely et al., 2017).

MICROTUBULE-ASSOCIATED GENES LINKED TO INTELLECTUAL DISABILITIES AND AUTISM SPECTRUM DISORDERS

Intellectual Disabilities

ID are complex neurodevelopmental disorders that affect a significant portion of the general population and are an immense health issue. ID is defined by an IQ score under 70 and is characterized by impaired intellectual and adaptive functioning that affects everyday living. ID may occur in isolation or it can be accompanied with other medical or behavioral symptoms such as seizures, craniofacial abnormalities, and microcephaly. ID can be caused by both genetic and environmental factors, with genetic causes representing up to 50% of all ID cases (Kaufman et al., 2010). Single gene mutations, as well as pathogenic copy number variants (CNVs), have been associated with ID, several of the implicated genes are involved in MT function.

Whole exome sequencing and next generation sequencing (NGS) studies have identified various mutations within kinesin superfamily members linked to ID. Willemsen et al. (2014) discovered pathogenic mutations in KIF4A and KIF5C in individuals from two different families. *In vivo* studies further confirmed the link between these genes and ID. Knockdown of both KIF4A and KIF5C disrupted the balance between excitatory

and inhibitory synaptic activity, which may be a contributing factor that leads to ID (Willemsen et al., 2014). Furthermore, *de novo* mutations in KIF1A were found in several patients that had a range of cognitive and motor defects, including ID (Lee et al., 2015; Ohba et al., 2015). KIF1A, an anterograde motor protein, transports membranous organelles along MTs within axons and dendrites, and has been shown to be involved in synaptogenesis, as well as learning and memory (Kondo et al., 2012; McVicker et al., 2016). Reduction or loss of this protein results in abnormal interactions with MTs and disruptions in axonal and dendritic transport. Together, these results highlight the importance of the kinesin superfamily members during neural development and how alterations of their MT-dependent functions can lead to a spectrum of neurological defects.

A recent NGS study of large consanguineous Iranian families affected by ID identified a novel mutation in CAP-Gly domain containing linker protein 1 (CLIP1), which encodes a +TIP, CLIP-170, that localizes to the ends of growing MTs (Larti et al., 2015). CLIP1 regulates MT behavior and participates in MT-mediated transport in neurons (Jaworski et al., 2008; Swiech et al., 2011). The protein encoded by CLIP1 was absent from cell lines derived from these ID patients, suggesting that loss of CLIP1 function can lead to cognitive impairments. It has also been shown that CLIP-170 may interact with LIS1 to mediate the recruitment of dynein to MTs and regulate MT dynamics (Coquelle et al., 2002). It is possible that the interaction between CLIP1 and LIS1 may be important for proper neuronal migration during brain development.

Microdeletions on chromosome 13 encompassing several genes, including katanin catalytic subunit A1 like 1 (KATNAL1), were found to result in ID and microcephaly (Bartholdi et al., 2014). KATNAL1 encodes a MT-severing enzyme that regulates the remodeling of cellular MT arrays. Mouse lines carrying a loss-of-function allele in *Katnal1* display defects in learning and memory, as well as abnormal neuronal migration and morphology (Banks et al., 2018). However, there are genetic discrepancies between humans and mice. Human patients are heterozygous for the KATNAL1 deletion, whereas heterozygous mice show no overt phenotypes, suggesting that further investigations are required to understand the causative mechanisms in regards to this genetic mutation (Bartholdi et al., 2014; Banks et al., 2018). Nevertheless, it is evident that KATNAL1 plays an important role during several neuronal processes, and that perturbations of KATNAL1 function can lead to various defects which may eventually contribute to neurodevelopmental disorders.

X-linked ID have been associated with mutations in midline 2 (MID2), a gene that codes for an ubiquitin ligase, which localizes to MTs and regulates their activity during neural tube closure (Geetha et al., 2014). Mid2 was shown to localize and ubiquitinate Astrin, which is a MT organizing protein that regulates MTs during cell division. Loss of Mid2 led to the stabilization of Astrin, causing defects in MT organization, cytokinesis and cell death (Gholkar et al., 2016). This suggests that ubiquitination of Astrin by Mid2 is essential for regulating MT function during cell division and could explain how mutations of MID2 lead to X-linked ID.

Autism Spectrum Disorders

ASD are a heterogeneous group of disorders characterized by a wide range of symptoms and disabilities that can vary in severity. These symptoms include verbal and non-verbal communication deficits, difficulties with social interactions, repetitive behaviors and restrictive interests. Individuals with ASD can also present with additional medical conditions such as epilepsy, motor function impairments, ID, anxiety and sleep disorders. The pathogenesis of ASD is not yet fully understood and a majority of ASD cases do not have a specific known cause. However, increased research efforts have identified various genetic mutations which have been linked to ASD, including several MT-associated genes (Pinto et al., 2014).

One of these genes is autism susceptibility candidate 2 (AUTS2), however the exact functions of AUTS2 have not yet been entirely characterized, though studies suggest that it may play a significant role during early brain development (Kalscheuer et al., 2007). AUTS2 has been found to be highly expressed in the developing brain of zebrafish, and knockdown of this gene resulted in microcephaly along with a reduction in the total number of neurons (Oksenberg et al., 2013). Further studies found that the protein functioned as a regulator of Rac1, a Rho-family GTPase that is crucial for coordinating cytoskeletal rearrangements (Hori et al., 2014). The reduction or loss of Auts2 in mice caused abnormal morphologies of embryonic neurons and impaired their migration (Hori et al., 2014). Knockdown of Auts2 also suppressed the activation of c-Jun N-terminal kinase (JNK). JNK is regulated by Rac1 and is involved in MT formation, as well as MT dynamics at leading processes of migrating neurons (Kawauchi et al., 2003). Taken together, alterations in AUTS2 may inhibit its regulation of Rac1, which then has downstream effects on subsequent target molecules, like JNK, that can lead to defects in cytoskeletal remodeling in migrating neurons.

Another gene implicated in ASD is activity-dependent neuroprotective protein (ADNP; Helsmoortel et al., 2014). This gene is part of the SWI/SNF chromatin remodeling complex and is vital for brain development (Mandel et al., 2007; Helsmoortel et al., 2014). *Adnp*−/− mice die prenatally due to failure of neural tube closure, and *Adnp*+/− mice have increased neuronal death along with abnormal cognitive functioning (Vulih-Shultzman et al., 2007). ADNP was found to be associated with tau mRNA splicing (Schirer et al., 2014), and also participates in the recruitment of Tau to MTs, possibly to prevent free Tau accumulation that eventually leads to neurodegenerative disorders (Oz et al., 2012). Furthermore, ADNP has been shown to directly interact with MT EBs, EB1 and EB3, to promote neurite outgrowth and dendritic spine formation (Oz et al., 2014; Ivashko-Pachima et al., 2017). Together, these findings indicate that mutations of ADNP may alter its interactions with several MT-associated proteins, which have negative downstream effects that alter MT dynamics and hinder different neuronal processes during early development.

Dysregulation of several MT-associated kinases have also been linked to ASD. Janus kinase and MT interacting protein 1

(JAKMIP1) is an RNA binding protein that is highly expressed in glutamatergic neurons (Couve et al., 2004), and has been shown to modify MT polymers and influence MT dynamics (Steindler et al., 2004). Rare deletions of this gene have been found in individuals with ASD (Kaminsky et al., 2011; Hedges et al., 2012; Poultney et al., 2013), and loss of *Jakmip1* in mice results in autistic-like behavior, possibly by affecting the expression of downstream mRNA targets during synaptogenesis (Berg et al., 2015). It has also been suggested that JAKMIP1 modulates intracellular trafficking of GABA receptors via its interaction with the MT cytoskeleton (Vidal et al., 2007). Given these results, it is possible that mutations of JAKMIP1 cause defects in synapse formation, specifically within glutamatergic neurons, that may eventually lead to ASD. Another MT-associated kinase, MT affinity regulating kinase 1 (MARK1), was shown to have altered transcript and protein levels in postmortem brains from patients with ASD (Maussion et al., 2008). MARK1 is a kinase which phosphorylates several MAPs, causing them to dissociate from MTs (Drewes et al., 1997). MARK1 also participates in the regulation of mitochondrial trafficking along MTs in both axons and dendrites and plays a significant role during neuronal polarization and migration (Mandelkow et al., 2004; Maussion et al., 2008). The reduction or overexpression of MARK1 has been shown to cause defects in synaptic function as well as cell migration (Maussion et al., 2008; Sapir et al., 2008). It is possible that mutations within MARK1 modulate its phosphorylation activity of MAPs, leading to aberrant alterations of MT dynamics that disrupt proper neural development.

CONCLUSION

The elaborate MT cytoskeletal network plays many instrumental roles during development of the nervous system. Young neurons rely on the dynamic properties of MTs in order to proliferate and migrate to their final destinations. Moreover, MTs are vital for the formation and extension of both axons and dendrites, which enables the neuron to navigate through the extracellular terrain to create synapses and connections with neighboring cells. Elucidating the molecular mechanisms responsible for regulating the MT cytoskeleton throughout specific stages of neural development still remain an important area of research. In recent years, genetic studies have uncovered numerous mutations within genes that negatively affect the MT cytoskeleton, causing abnormalities in neural migration, proliferation and connectivity. The discovery of mutations occurring within MT-associated genes that lead to neurodevelopmental disorders has provided an opportunity to investigate the functions of MTs at the cellular and molecular level during brain development. Future studies must continue to focus on understanding how these mutations contribute to altered MT function underlying various brain malformations, which will allow insight into the essential roles MTs and their associated proteins play during neural development.

AUTHOR CONTRIBUTIONS

ML and LAL conceived of the manuscript. ML, JT and LAL wrote and edited the manuscript.

FUNDING

LAL is funded by National Institutes of Health (NIH; grant no. R01 MH109651) and ML by NIH grant no. R01 GM121907.

ACKNOWLEDGMENTS

We thank members of the Lowery lab for helpful discussions and suggestions.

REFERENCES

Abdollahi, M. R., Morrison, E., Sirey, T., Molnár, Z., Hayward, B. E., Carr, I. M., et al. (2009). Mutation of the variant α-tubulin TUBA8 results in polymicrogyria with optic nerve hypoplasia. *Am. J. Hum. Genet.* 85, 737–744. doi: 10.1016/j.ajhg.2009.10.007

Akhmanova, A., and Steinmetz, M. O. (2008). Tracking the ends: a dynamic protein network controls the fate of microtubule tips. *Nat. Rev. Mol. Cell Biol.* 9, 309–322. doi: 10.1038/nrm2369

Alves-Silva, J., Sánchez-Soriano, N., Beaven, R., Klein, M., Parkin, J., Millard, T. H., et al. (2012). Spectraplakins promote microtubule-mediated axonal growth by functioning as structural microtubule-associated proteins and EB1-dependent +TIPs (tip interacting proteins). *J. Neurosci.* 32, 9143–9158. doi: 10.1523/JNEUROSCI.0416-12.2012

Armijo-Weingart, L., and Gallo, G. (2017). It takes a village to raise a branch: cellular mechanisms of the initiation of axon collateral branches. *Mol. Cell. Neurosci.* 84, 36–47. doi: 10.1016/j.mcn.2017.03.007

Bahi-Buisson, N., Poirier, K., Fourniol, F., Saillour, Y., Valence, S., Lebrun, N., et al. (2014). The wide spectrum of tubulinopathies: what are the key features for the diagnosis? *Brain* 137, 1676–1700. doi: 10.1093/brain/awu082

Bai, J., Ramos, R. L., Ackman, J. B., Thomas, A. M., Lee, R. V., and LoTurco, J. J. (2003). RNAi reveals doublecortin is required for radial migration in rat neocortex. *Nat. Neurosci.* 6, 1277–1283. doi: 10.1038/nn1153

Banks, G., Lassi, G., Hoerder-Suabedissen, A., Tinarelli, F., Simon, M. M., Wilcox, A., et al. (2018). A missense mutation in Katnal1 underlies behavioural, neurological and ciliary anomalies. *Mol. Psychiatry* 23, 713–722. doi: 10.1038/mp.2017.54

Barkovich, A. J., Guerrini, R., Kuzniecky, R. I., Jackson, G. D., and Dobyns, W. B. (2012). A developmental and genetic classification for malformations of cortical development: update 2012. *Brain* 135, 1348–1369. doi: 10.1093/brain/aws019

Bartholdi, D., Stray-Pedersen, A., Azzarello-Burri, S., Kibaek, M., Kirchhoff, M., Oneda, B., et al. (2014). A newly recognized 13q12.3 microdeletion syndrome characterized by intellectual disability, microcephaly and eczema/atopic dermatitis encompassing the HMGB1 and KATNAL1 genes. *Am. J. Med. Genet. A* 164A, 1277–1283. doi: 10.1002/ajmg.a.36439

Bearce, E. A., Erdogan, B., and Lowery, L. A. (2015). TIPsy tour guides: how microtubule plus-end tracking proteins (+TIPs) facilitate axon guidance. *Front. Cell. Neurosci.* 9:241. doi: 10.3389/fncel.2015.00241

Bechstedt, S., and Brouhard, G. J. (2012). Doublecortin recognizes the 13-protofilament microtubule cooperatively and tracks microtubule ends. *Dev. Cell* 23, 181–192. doi: 10.1016/j.devcel.2012.05.006

Berg, J. M., Lee, C., Chen, L., Galvan, L., Cepeda, C., Chen, J. Y., et al. (2015). JAKMIP1, a novel regulator of neuronal translation, modulates synaptic function and autistic-like behaviors in mouse. *Neuron* 88, 1173–1191. doi: 10.1016/j.neuron.2015.10.031

Bi, W., Sapir, T., Shchelochkov, O. A., Zhang, F., Withers, M. A., Hunter, J. V., et al. (2009). Increased LIS1 expression affects human and mouse brain development. *Nat. Genet.* 41, 168–177. doi: 10.1038/ng.302

Biswas, S., and Kalil, K. (2018). The microtubule-associated protein tau mediates the organization of microtubules and their dynamic exploration of actin-rich

lamellipodia and filopodia of cortical growth cones. *J. Neurosci.* 38, 291–307. doi: 10.1523/JNEUROSCI.2281-17.2017

Bodaleo, F. J., Montenegro-Venegas, C., Henríquez, D. R., Court, F. A., and González-Billault, C. (2016). Microtubule-associated protein 1B (MAP1B)-deficient neurons show structural presynaptic deficiencies *in vitro* and altered presynaptic physiology. *Sci. Rep.* 6:30069. doi: 10.1038/srep32275

Bond, J., Roberts, E., Springell, K., Lizarraga, S. B., Lizarraga, S., Scott, S., et al. (2005). A centrosomal mechanism involving CDK5RAP2 and CENPJ controls brain size. *Nat. Genet.* 37, 353–355. doi: 10.1038/ng1539

Bouquet, C., Soares, S., von Boxberg, Y., Ravaille-Veron, M., Propst, F., and Nothias, F. (2004). Microtubule-associated protein 1B controls directionality of growth cone migration and axonal branching in regeneration of adult dorsal root ganglia neurons. *J. Neurosci.* 24, 7204–7213. doi: 10.1523/JNEUROSCI.2254-04.2004

Burgess, H. A., and Reiner, O. (2000). Doublecortin-like kinase is associated with microtubules in neuronal growth cones. *Mol. Cell. Neurosci.* 16, 529–541. doi: 10.1006/mcne.2000.0891

Cammarata, G. M., Bearce, E. A., and Lowery, L. A. (2016). Cytoskeletal social networking in the growth cone: how +TIPs mediate microtubule-actin cross-linking to drive axon outgrowth and guidance. *Cytoskeleton* 73, 461–476. doi: 10.1002/cm.21272

Chakraborti, S., Natarajan, K., Curiel, J., Janke, C., and Liu, J. (2016). The emerging role of the tubulin code: from the tubulin molecule to neuronal function and disease. *Cytoskeleton* 73, 521–550. doi: 10.1002/cm.21290

Choi, Y.-K., Liu, P., Sze, S. K., Dai, C., and Qi, R. Z. (2010). CDK5RAP2 stimulates microtubule nucleation by the γ-tubulin ring complex. *J. Cell Biol.* 191, 1089–1095. doi: 10.1083/jcb.201007030

Conde, C., and Cáceres, A. (2009). Microtubule assembly, organization and dynamics in axons and dendrites. *Nat. Rev. Neurosci.* 10, 319–332. doi: 10.1038/nrn2631

Coquelle, F. M., Caspi, M., Cordelières, F. P., Dompierre, J. P., Dujardin, D. L., Koifman, C., et al. (2002). LIS1, CLIP-170's key to the dynein/dynactin pathway. *Mol. Cell. Biol.* 22, 3089–3102. doi: 10.1128/mcb.22.9.3089-3102.2002

Corbo, J. C., Deuel, T. A., Long, J. M., LaPorte, P., Tsai, E., Wynshaw-Boris, A., et al. (2002). Doublecortin is required in mice for lamination of the hippocampus but not the neocortex. *J. Neurosci.* 22, 7548–7557. doi: 10.1523/JNEUROSCI.22-17-07548.2002

Couve, A., Restituito, S., Brandon, J. M., Charles, K. J., Bawagan, H., Freeman, K. B., et al. (2004). Marlin-1, a novel RNA-binding protein associates with GABA receptors. *J. Biol. Chem.* 279, 13934–13943. doi: 10.1074/jbc.M311737200

Cox, G. A., Mahaffey, C. L., Nystuen, A., Letts, V. A., and Frankel, W. N. (2000). The mouse fidgetin gene defines a new role for AAA family proteins in mammalian development. *Nat. Genet.* 26, 198–202. doi: 10.1038/79923

Cushion, T. D., Dobyns, W. B., Mullins, J. G. L., Stoodley, N., Chung, S.-K., Fry, A. E., et al. (2013). Overlapping cortical malformations and mutations in TUBB2B and TUBA1A. *Brain* 136, 536–548. doi: 10.1093/brain/aws338

Dehmelt, L., and Halpain, S. (2005). The MAP2/Tau family of microtubule-associated proteins. *Genome Biol.* 6:204. doi: 10.1186/gb-2004-6-1-204

Dehmelt, L., Nalbant, P., Steffen, W., and Halpain, S. (2006). A microtubule-based, dynein-dependent force induces local cell protrusions: implications for neurite initiation. *Brain Cell Biol.* 35, 39–56. doi: 10.1007/s11068-006-9001-0

Dent, E. W. (2017). Of microtubules and memory: implications for microtubule dynamics in dendrites and spines. *Mol. Biol. Cell* 28, 1–8. doi: 10.1091/mbc.E15-11-0769

Dent, E. W., Callaway, J. L., Szebenyi, G., Baas, P. W., and Kalil, K. (1999). Reorganization and movement of microtubules in axonal growth cones and developing interstitial branches. *J. Neurosci.* 19, 8894–8908. doi: 10.1523/JNEUROSCI.19-20-08894.1999

Dent, E. W., Gupton, S. L., and Gertler, F. B. (2011). The growth cone cytoskeleton in axon outgrowth and guidance. *Cold Spring Harb. Perspect. Biol.* 3:a001800. doi: 10.1101/cshperspect.a001800

Dent, E. W., and Kalil, K. (2001). Axon branching requires interactions between dynamic microtubules and actin filaments. *J. Neurosci.* 21, 9757–9769. doi: 10.1523/JNEUROSCI.21-24-09757.2001

Dent, E. W., Kwiatkowski, A. V., Mebane, L. M., Philippar, U., Barzik, M., Rubinson, D. A., et al. (2007). Filopodia are required for cortical neurite initiation. *Nat. Cell Biol.* 9, 1347–1359. doi: 10.1038/ncb1654

DeSantis, M. E., Cianfrocco, M. A., Htet, Z. M., Tran, P. T., Reck-Peterson, S. L., and Leschziner, A. E. (2017). Lis1 has two opposing modes of regulating cytoplasmic dynein. *Cell* 170, 1197.e12–1208.e12. doi: 10.1016/j.cell.2017.08.037

des Portes, V., Francis, F., Pinard, J. M., Desguerre, I., Moutard, M. L., Snoeck, I., et al. (1998). Doublecortin is the major gene causing X-linked subcortical laminar heterotopia (SCLH). *Hum. Mol. Genet.* 7, 1063–1070. doi: 10.1093/hmg/7.7.1063

Deuel, T. A. S., Liu, J. S., Corbo, J. C., Yoo, S.-Y., Rorke-Adams, L. B., and Walsh, C. A. (2006). Genetic interactions between doublecortin and doublecortin-like kinase in neuronal migration and axon outgrowth. *Neuron* 49, 41–53. doi: 10.1016/j.neuron.2005.10.038

Drewes, G., Ebneth, A., Preuss, U., Mandelkow, E. M., and Mandelkow, E. (1997). MARK, a novel family of protein kinases that phosphorylate microtubule-associated proteins and trigger microtubule disruption. *Cell* 89, 297–308. doi: 10.1016/s0092-8674(00)80208-1

Duerinckx, S., and Abramowicz, M. (2018). The genetics of congenitally small brains. *Semin. Cell Dev. Biol.* 76, 76–85. doi: 10.1016/j.semcdb.2017.09.015

Egan, M. J., Tan, K., and Reck-Peterson, S. L. (2012). Lis1 is an initiation factor for dynein-driven organelle transport. *J. Cell Biol.* 197, 971–982. doi: 10.1083/jcb.201112101

Eom, T.-Y., Stanco, A., Guo, J., Wilkins, G., Deslauriers, D., Yan, J., et al. (2014). Differential regulation of microtubule severing by APC underlies distinct patterns of projection neuron and interneuron migration. *Dev. Cell* 31, 677–689. doi: 10.1016/j.devcel.2014.11.022

Erdogan, B., Cammarata, G. M., Lee, E. J., Pratt, B. C., Francl, A. F., Rutherford, E. L., et al. (2017). The microtubule plus-end-tracking protein TACC3 promotes persistent axon outgrowth and mediates responses to axon guidance signals during development. *Neural Dev.* 12:3. doi: 10.1186/s13064-017-0080-7

Fiorillo, C., Moro, F., Yi, J., Weil, S., Brisca, G., Astrea, G., et al. (2014). Novel dynein DYNC1H1 neck and motor domain mutations link distal spinal muscular atrophy and abnormal cortical development. *Hum. Mutat.* 35, 298–302. doi: 10.1002/humu.22491

Fleck, M. W., Hirotsune, S., Gambello, M. J., Phillips-Tansey, E., Suares, G., Mervis, R. F., et al. (2000). Hippocampal abnormalities and enhanced excitability in a murine model of human lissencephaly. *J. Neurosci.* 20, 2439–2450. doi: 10.1523/JNEUROSCI.20-07-02439.2000

Forman, M. S., Squier, W., Dobyns, W. B., and Golden, J. A. (2005). Genotypically defined lissencephalies show distinct pathologies. *J. Neuropathol. Exp. Neurol.* 64, 847–857. doi: 10.1097/01.jnen.0000182978.56612.41

Fry, A. E., Cushion, T. D., and Pilz, D. T. (2014). The genetics of lissencephaly. *Am. J. Med. Genet. C Semin Med. Genet.* 166C, 198–210. doi: 10.1002/ajmg.c.31402

Götz, M., and Huttner, W. B. (2005). The cell biology of neurogenesis. *Nat. Rev. Mol. Cell Biol.* 6, 777–788. doi: 10.1038/nrm1739

Gallo, G. (2016). Coordination of the axonal cytoskeleton during the emergence of axon collateral branches. *Neural Regen. Res.* 11, 709–711. doi: 10.4103/1673-5374.182684

Gallo, G., and Letourneau, P. C. (1999). Different contributions of microtubule dynamics and transport to the growth of axons and collateral sprouts. *J. Neurosci.* 19, 3860–3873. doi: 10.1523/JNEUROSCI.19-10-03860.1999

Gambello, M. J., Darling, D. L., Yingling, J., Tanaka, T., Gleeson, J. G., and Wynshaw-Boris, A. (2003). Multiple dose-dependent effects of Lis1 on cerebral cortical development. *J. Neurosci.* 23, 1719–1729. doi: 10.1523/JNEUROSCI.23-05-01719.2003

Garcez, P. P., Diaz-Alonso, J., Crespo-Enriquez, I., Castro, D., Bell, D., and Guillemot, F. (2015). Cenpj/CPAP regulates progenitor divisions and neuronal migration in the cerebral cortex downstream of Ascl1. *Nat. Commun.* 6:6474. doi: 10.1038/ncomms7474

Geetha, T. S., Michealraj, K. A., Kabra, M., Kaur, G., Juyal, R. C., and Thelma, B. K. (2014). Targeted deep resequencing identifies MID2 mutation for X-linked intellectual disability with varied disease severity in a large kindred from India. *Hum. Mutat.* 35, 41–44. doi: 10.1002/humu.22453

Gholkar, A. A., Senese, S., Lo, Y.-C., Vides, E., Contreras, E., Hodara, E., et al. (2016). The X-linked-intellectual-disability-associated ubiquitin ligase Mid2 interacts with astrin and regulates astrin levels to promote cell division. *Cell Rep.* 14, 180–188. doi: 10.1016/j.celrep.2015.12.035

Gleeson, J. G., Allen, K. M., Fox, J. W., Lamperti, E. D., Berkovic, S., Scheffer, I., et al. (1998). Doublecortin, a brain-specific gene mutated in human X-linked lissencephaly and double cortex syndrome, encodes a putative signaling protein. *Cell* 92, 63–72. doi: 10.1016/s0092-8674(00)80899-5

Gozes, I., Helsmoortel, C., Vandeweyer, G., Van der Aa, N., Kooy, F., and Bedrosian-Sermone, S. (2018). The compassionate side of neuroscience: tony sermone's undiagnosed genetic journey—ADNP mutation. *J. Mol. Neurosci.* 56, 751–757. doi: 10.1007/s12031-018-1028-z

Gozes, I., Patterson, M. C., Van Dijck, A., Kooy, R. F., Peeden, J. N., Eichenberger, J. A., et al. (2017a). The eight and a half year journey of undiagnosed AD: gene sequencing and funding of advanced genetic testing has led to hope and new beginnings. *Front. Endocrinol.* 8:107. doi: 10.3389/fendo.2017.00107

Gozes, I., Van Dijck, A., Hacohen-Kleiman, G., Grigg, I., Karmon, G., Giladi, E., et al. (2017b). Premature primary tooth eruption in cognitive/motor-delayed ADNP-mutated children. *Transl. Psychiatry* 7:e1043. doi: 10.1038/tp.2017.128

Grabham, P. W., Seale, G. E., Bennecib, M., Goldberg, D. J., and Vallee, R. B. (2007). Cytoplasmic dynein and LIS1 are required for microtubule advance during growth cone remodeling and fast axonal outgrowth. *J. Neurosci.* 27, 5823–5834. doi: 10.1523/JNEUROSCI.1135-07.2007

Gressens, P. (2000). Mechanisms and disturbances of neuronal migration. *Pediatr. Res.* 48, 725–730. doi: 10.1203/00006450-200012000-00004

Gruber, R., Zhou, Z., Sukchev, M., Joerss, T., Frappart, P.-O., and Wang, Z.-Q. (2011). MCPH1 regulates the neuroprogenitor division mode by coupling the centrosomal cycle with mitotic entry through the Chk1-Cdc25 pathway. *Nat. Cell Biol.* 13, 1325–1334. doi: 10.1038/ncb2342

Gu, J., Firestein, B. L., and Zheng, J. Q. (2008). Microtubules in dendritic spine development. *J. Neurosci.* 28, 12120–12124. doi: 10.1523/JNEUROSCI.2509-08.2008

Gumy, L. F., Katrukha, E. A., Grigoriev, I., Jaarsma, D., Kapitein, L. C., Akhmanova, A., et al. (2017). MAP2 defines a pre-axonal filtering zone to regulate KIF1- versus KIF5-dependent cargo transport in sensory neurons. *Neuron* 94, 347.e7–362.e7. doi: 10.1016/j.neuron.2017.03.046

Hafezparast, M., Klocke, R., Ruhrberg, C., Marquardt, A., Ahmad-Annuar, A., Bowen, S., et al. (2003). Mutations in dynein link motor neuron degeneration to defects in retrograde transport. *Science* 300, 808–812. doi: 10.1126/science.1083129

Harada, A., Teng, J., Takei, Y., Oguchi, K., and Hirokawa, N. (2002). MAP2 is required for dendrite elongation, PKA anchoring in dendrites, and proper PKA signal transduction. *J. Cell Biol.* 158, 541–549. doi: 10.1083/jcb.200110134

Hazan, J., Fonknechten, N., Mavel, D., Paternotte, C., Samson, D., Artiguenave, F., et al. (1999). Spastin, a new AAA protein, is altered in the most frequent form of autosomal dominant spastic paraplegia. *Nat. Genet.* 23, 296–303. doi: 10.1038/15472

Hedges, D. J., Hamilton-Nelson, K. L., Sacharow, S. J., Nations, L., Beecham, G. W., Kozhekbaeva, Z. M., et al. (2012). Evidence of novel fine-scale structural variation at autism spectrum disorder candidate loci. *Mol. Autism* 3:2. doi: 10.1186/2040-2392-3-2

Helsmoortel, C., Vulto-van Silfhout, A. T., Coe, B. P., Vandeweyer, G., Rooms, L., van den Ende, J., et al. (2014). A SWI/SNF-related autism syndrome caused by *de novo* mutations in ADNP. *Nat. Genet.* 46, 380–384. doi: 10.1038/ng.2899

Hirokawa, N., Niwa, S., and Tanaka, Y. (2010). Molecular motors in neurons: transport mechanisms and roles in brain function, development and disease. *Neuron* 68, 610–638. doi: 10.1016/j.neuron.2010.09.039

Hirotsune, S., Fleck, M. W., Gambello, M. J., Bix, G. J., Chen, A., Clark, G. D., et al. (1998). Graded reduction of Pafah1b1 (Lis1) activity results in neuronal migration defects and early embryonic lethality. *Nat. Genet.* 19, 333–339. doi: 10.1038/1221

Homma, N., Takei, Y., Tanaka, Y., Nakata, T., Terada, S., Kikkawa, M., et al. (2003). Kinesin superfamily protein 2A (KIF2A) functions in suppression of collateral branch extension. *Cell* 114, 229–239. doi: 10.1016/s0092-8674(03)00522-1

Hoogenraad, C. C., and Bradke, F. (2009). Control of neuronal polarity and plasticity—a renaissance for microtubules? *Trends Cell Biol.* 19, 669–676. doi: 10.1016/j.tcb.2009.08.006

Hori, K., Nagai, T., Shan, W., Sakamoto, A., Taya, S., Hashimoto, R., et al. (2014). Cytoskeletal regulation by AUTS2 in neuronal migration and neuritogenesis. *Cell Rep.* 9, 2166–2179. doi: 10.1016/j.celrep.2014.11.045

Ivashko-Pachima, Y., Sayas, C. L., Malishkevich, A., and Gozes, I. (2017). ADNP/NAP dramatically increase microtubule end-binding protein-Tau interaction: a novel avenue for protection against tauopathy. *Mol. Psychiatry* 22, 1335–1344. doi: 10.1038/mp.2016.255

Jacobson, C., Schnapp, B., and Banker, G. A. (2006). A change in the selective translocation of the Kinesin-1 motor domain marks the initial specification of the axon. *Neuron* 49, 797–804. doi: 10.1016/j.neuron.2006.02.005

Jaglin, X. H., and Chelly, J. (2009). Tubulin-related cortical dysgeneses: microtubule dysfunction underlying neuronal migration defects. *Trends Genet.* 25, 555–566. doi: 10.1016/j.tig.2009.10.003

Jaglin, X. H., Poirier, K., Saillour, Y., Buhler, E., Tian, G., Bahi-Buisson, N., et al. (2009). Mutations in the β-tubulin gene TUBB2B result in asymmetrical polymicrogyria. *Nat. Genet.* 41, 746–752. doi: 10.1038/ng.380

Janning, D., Igaev, M., Sündermann, F., Brühmann, J., Beutel, O., Heinisch, J. J., et al. (2014). Single-molecule tracking of tau reveals fast kiss-and-hop interaction with microtubules in living neurons. *Mol. Biol. Cell* 25, 3541–3551. doi: 10.1091/mbc.E14-06-1099

Jaworski, J., Hoogenraad, C. C., and Akhmanova, A. (2008). Microtubule plus-end tracking proteins in differentiated mammalian cells. *Int. J. Biochem. Cell Biol.* 40, 619–637. doi: 10.1016/j.biocel.2007.10.015

Jaworski, J., Kapitein, L. C., Gouveia, S. M., Dortland, B. R., Wulf, P. S., Grigoriev, I., et al. (2009). Dynamic microtubules regulate dendritic spine morphology and synaptic plasticity. *Neuron* 61, 85–100. doi: 10.1016/j.neuron.2008.11.013

Jayachandran, P., Olmo, V. N., Sanchez, S. P., McFarland, R. J., Vital, E., Werner, J. M., et al. (2016). Microtubule-associated protein 1b is required for shaping the neural tube. *Neural Dev.* 11:1. doi: 10.1186/s13064-015-0056-4

Jean, D. C., Baas, P. W., and Black, M. M. (2012). A novel role for doublecortin and doublecortin-like kinase in regulating growth cone microtubules. *Hum. Mol. Genet.* 21, 5511–5527. doi: 10.1093/hmg/dds395

Jiang, K., Rezabkova, L., Hua, S., Liu, Q., Capitani, G., Altelaar, A. F. M., et al. (2017). Microtubule minus-end regulation at spindle poles by an ASPM-katanin complex. *Nat. Cell Biol.* 19, 480–492. doi: 10.1038/ncb3511

Judkins, A. R., Martinez, D., Ferreira, P., Dobyns, W. B., and Golden, J. A. (2011). Polymicrogyria includes fusion of the molecular layer and decreased neuronal populations but normal cortical laminar organization. *J. Neuropathol. Exp. Neurol.* 70, 438–443. doi: 10.1097/NEN.0b013e31821ccf1c

Kahn, O. I., and Baas, P. W. (2016). Microtubules and growth cones: motors drive the turn. *Trends Neurosci.* 39, 433–440. doi: 10.1016/j.tins.2016.04.009

Kalil, K., and Dent, E. W. (2014). Branch management: mechanisms of axon branching in the developing vertebrate CNS. *Nat. Rev. Neurosci.* 15, 7–18. doi: 10.1038/nrn3650

Kalscheuer, V. M., FitzPatrick, D., Tommerup, N., Bugge, M., Niebuhr, E., Neumann, L. M., et al. (2007). Mutations in autism susceptibility candidate 2 (AUTS2) in patients with mental retardation. *Hum. Genet.* 121, 501–509. doi: 10.1007/s00439-006-0284-0

Kaminsky, E. B., Kaul, V., Paschall, J., Church, D. M., Bunke, B., Kunig, D., et al. (2011). An evidence-based approach to establish the functional and clinical significance of copy number variants in intellectual and developmental disabilities. *Genet. Med.* 13, 777–784. doi: 10.1097/GIM.0b013e31822c79f9

Kanai, Y., Okada, Y., Tanaka, Y., Harada, A., Terada, S., and Hirokawa, N. (2000). KIF5C, a novel neuronal kinesin enriched in motor neurons. *J. Neurosci.* 20, 6374–6384. doi: 10.1523/JNEUROSCI.20-17-06374.2000

Kapitein, L. C., and Hoogenraad, C. C. (2011). Which way to go? Cytoskeletal organization and polarized transport in neurons. *Mol. Cell. Neurosci.* 46, 9–20. doi: 10.1016/j.mcn.2010.08.015

Kapitein, L. C., and Hoogenraad, C. C. (2015). Building the neuronal microtubule cytoskeleton. *Neuron* 87, 492–506. doi: 10.1016/j.neuron.2015.05.046

Kapitein, L. C., Schlager, M. A., Kuijpers, M., Wulf, P. S., van Spronsen, M., MacKintosh, F. C., et al. (2010). Mixed microtubules steer dynein-driven cargo transport into dendrites. *Curr. Biol.* 20, 290–299. doi: 10.1016/j.cub.2009.12.052

Karabay, A., Yu, W., Solowska, J. M., Baird, D. H., and Baas, P. W. (2004). Axonal growth is sensitive to the levels of katanin, a protein that severs microtubules. *J. Neurosci.* 24, 5778–5788. doi: 10.1523/JNEUROSCI.1382-04.2004

Kaufman, L., Ayub, M., and Vincent, J. B. (2010). The genetic basis of non-syndromic intellectual disability: a review. *J. Neurodev. Disord.* 2, 182–209. doi: 10.1007/s11689-010-9055-2

Kawauchi, T., Chihama, K., Nabeshima, Y.-I., and Hoshino, M. (2003). The *in vivo* roles of STEF/Tiam1, Rac1 and JNK in cortical neuronal migration. *EMBO J.* 22, 4190–4201. doi: 10.1093/emboj/cdg413

Keays, D. A., Cleak, J., Huang, G.-J., Edwards, A., Braun, A., Treiber, C. D., et al. (2010). The role of Tuba1a in adult hippocampal neurogenesis and the formation of the dentate gyrus. *Dev. Neurosci.* 32, 268–277. doi: 10.1159/000319663

Keays, D. A., Tian, G., Poirier, K., Huang, G.-J., Siebold, C., Cleak, J., et al. (2007). Mutations in α-tubulin cause abnormal neuronal migration in mice and lissencephaly in humans. *Cell* 128, 45–57. doi: 10.1016/j.cell.2006.12.017

Kerjan, G., and Gleeson, J. G. (2007). Genetic mechanisms underlying abnormal neuronal migration in classical lissencephaly. *Trends Genet.* 23, 623–630. doi: 10.1016/j.tig.2007.09.003

Ketschek, A., Spillane, M., Dun, X.-P., Hardy, H., Chilton, J., and Gallo, G. (2016). Drebrin coordinates the actin and microtubule cytoskeleton during the initiation of axon collateral branches. *Dev. Neurobiol.* 76, 1092–1110. doi: 10.1002/dneu.22377

Kirkcaldie, M. T. K., and Dwyer, S. T. (2017). The third wave: intermediate filaments in the maturing nervous system. *Mol. Cell. Neurosci.* 84, 68–76. doi: 10.1016/j.mcn.2017.05.010

Kitagawa, D., Kohlmaier, G., Keller, D., Strnad, P., Balestra, F. R., Flückiger, I., et al. (2011). Spindle positioning in human cells relies on proper centriole formation and on the microcephaly proteins CPAP and STIL. *J. Cell. Sci.* 124, 3884–3893. doi: 10.1242/jcs.089888

Koester, M. P., Müller, O., and Pollerberg, G. E. (2007). Adenomatous polyposis coli is differentially distributed in growth cones and modulates their steering. *J. Neurosci.* 27, 12590–12600. doi: 10.1523/JNEUROSCI.2250-07.2007

Koleske, A. J. (2013). Molecular mechanisms of dendrite stability. *Nat. Rev. Neurosci.* 14, 536–550. doi: 10.1038/nrn3486

Kondo, M., Takei, Y., and Hirokawa, N. (2012). Motor protein KIF1A is essential for hippocampal synaptogenesis and learning enhancement in an enriched environment. *Neuron* 73, 743–757. doi: 10.1016/j.neuron.2011.12.020

Kouprina, N., Pavlicek, A., Collins, N. K., Nakano, M., Noskov, V. N., Ohzeki, J.-I., et al. (2005). The microcephaly ASPM gene is expressed in proliferating tissues and encodes for a mitotic spindle protein. *Hum. Mol. Genet.* 14, 2155–2165. doi: 10.1093/hmg/ddi220

Kuijpers, M., and Hoogenraad, C. C. (2011). Centrosomes, microtubules and neuronal development. *Mol. Cell. Neurosci.* 48, 349–358. doi: 10.1016/j.mcn.2011.05.004

Kumar, A., Girimaji, S. C., Duvvari, M. R., and Blanton, S. H. (2009). Mutations in STIL, encoding a pericentriolar and centrosomal protein, cause primary microcephaly. *Am. J. Hum. Genet.* 84, 286–290. doi: 10.1016/j.ajhg.2009.01.017

Larti, F., Kahrizi, K., Musante, L., Hu, H., Papari, E., Fattahi, Z., et al. (2015). A defect in the CLIP1 gene (CLIP-170) can cause autosomal recessive intellectual disability. *Eur. J. Hum. Genet.* 23, 331–336. doi: 10.1038/ejhg.2014.13

Lee, H., Engel, U., Rusch, J., Scherrer, S., Sheard, K., and Van Vactor, D. (2004). The microtubule plus end tracking protein Orbit/MAST/CLASP acts downstream of the tyrosine kinase Abl in mediating axon guidance. *Neuron* 42, 913–926. doi: 10.1016/j.neuron.2004.05.020

Lee, J.-R., Srour, M., Kim, D., Hamdan, F. F., Lim, S.-H., Brunel-Guitton, C., et al. (2015). *De novo* mutations in the motor domain of KIF1A cause cognitive impairment, spastic paraparesis, axonal neuropathy, and cerebellar atrophy. *Hum. Mutat.* 36, 69–78. doi: 10.1002/humu.22709

Leo, L., Yu, W., D'Rozario, M., Waddell, E. A., Marenda, D. R., Baird, M. A., et al. (2015). Vertebrate fidgetin restrains axonal growth by severing labile domains of microtubules. *Cell Rep.* 12, 1723–1730. doi: 10.1016/j.celrep.2015.08.017

Li, L., Fothergill, T., Hutchins, B. I., Dent, E. W., and Kalil, K. (2014). Wnt5a evokes cortical axon outgrowth and repulsive guidance by tau mediated reorganization of dynamic microtubules. *Dev. Neurobiol.* 74, 797–817. doi: 10.1002/dneu.22102

Li, J., Lee, W.-L., and Cooper, J. A. (2005). NudEL targets dynein to microtubule ends through LIS1. *Nat. Cell Biol.* 7, 686–690. doi: 10.1038/ncb1273

Lin, S., Liu, M., Mozgova, O. I., Yu, W., and Baas, P. W. (2012). Mitotic motors coregulate microtubule patterns in axons and dendrites. *J. Neurosci.* 32, 14033–14049. doi: 10.1523/JNEUROSCI.3070-12.2012

Liu, Y., Lee, J. W., and Ackerman, S. L. (2015). Mutations in the microtubule-associated protein 1A (Map1a) gene cause Purkinje cell degeneration. *J. Neurosci.* 35, 4587–4598. doi: 10.1523/JNEUROSCI.2757-14.2015

Lizarraga, S. B., Margossian, S. P., Harris, M. H., Campagna, D. R., Han, A.-P., Blevins, S., et al. (2010). Cdk5rap2 regulates centrosome function and chromosome segregation in neuronal progenitors. *Development* 137, 1907–1917. doi: 10.1242/dev.040410

Lowery, L. A., Stout, A., Faris, A. E., Ding, L., Baird, M. A., Davidson, M. W., et al. (2013). Growth cone-specific functions of XMAP215 in restricting microtubule dynamics and promoting axonal outgrowth. *Neural Dev.* 8:22. doi: 10.1186/1749-8104-8-22

Lowery, L. A., and Van Vactor, D. (2009). The trip of the tip: understanding the growth cone machinery. *Nat. Rev. Mol. Cell Biol.* 10, 332–343. doi: 10.1038/nrm2679

Lu, W., Fox, P., Lakonishok, M., Davidson, M. W., and Gelfand, V. I. (2013). Initial neurite outgrowth in *Drosophila* neurons is driven by kinesin-powered microtubule sliding. *Curr. Biol.* 23, 1018–1023. doi: 10.1016/j.cub.2013.04.050

Lucaj, C. M., Evans, M. F., Nwagbara, B. U., Ebbert, P. T., Baker, C. C., Volk, J. G., et al. (2015). Xenopus TACC1 is a microtubule plus-end tracking protein that can regulate microtubule dynamics during embryonic development. *Cytoskeleton* 72, 225–234. doi: 10.1002/cm.21224

Maday, S., Twelvetrees, A. E., Moughamian, A. J., and Holzbaur, E. L. F. (2014). Axonal transport: cargo-specific mechanisms of motility and regulation. *Neuron* 84, 292–309. doi: 10.1016/j.neuron.2014.10.019

Mandel, S., Rechavi, G., and Gozes, I. (2007). Activity-dependent neuroprotective protein (ADNP) differentially interacts with chromatin to regulate genes essential for embryogenesis. *Dev. Biol.* 303, 814–824. doi: 10.1016/j.ydbio.2006.11.039

Mandelkow, E.-M., Thies, E., Trinczek, B., Biernat, J., and Mandelkow, E. (2004). MARK/PAR1 kinase is a regulator of microtubule-dependent transport in axons. *J. Cell Biol.* 167, 99–110. doi: 10.1083/jcb.200401085

Mao, C.-X., Xiong, Y., Xiong, Z., Wang, Q., Zhang, Y. Q., and Jin, S. (2014). Microtubule-severing protein Katanin regulates neuromuscular junction development and dendritic elaboration in *Drosophila*. *Development* 141, 1064–1074. doi: 10.1242/dev.097774

Marx, A., Godinez, W. J., Tsimashchuk, V., Bankhead, P., Rohr, K., and Engel, U. (2013). Xenopus cytoplasmic linker-associated protein 1 (XCLASP1) promotes axon elongation and advance of pioneer microtubules. *Mol. Biol. Cell* 24, 1544–1558. doi: 10.1091/mbc.E12-08-0573

Matamoros, A. J., and Baas, P. W. (2016). Microtubules in health and degenerative disease of the nervous system. *Brain Res. Bull.* 126, 217–225. doi: 10.1016/j.brainresbull.2016.06.016

Mattila, P. K., and Lappalainen, P. (2008). Filopodia: molecular architecture and cellular functions. *Nat. Rev. Mol. Cell Biol.* 9, 446–454. doi: 10.1038/nrm2406

Maussion, G., Carayol, J., Lepagnol-Bestel, A.-M., Tores, F., Loe-Mie, Y., Milbreta, U., et al. (2008). Convergent evidence identifying MAP/microtubule affinity-regulating kinase 1 (MARK1) as a susceptibility gene for autism. *Hum. Mol. Genet.* 17, 2541–2551. doi: 10.1093/hmg/ddn154

McNally, K. P., Bazirgan, O. A., and McNally, F. J. (2000). Two domains of p80 katanin regulate microtubule severing and spindle pole targeting by p60 katanin. *J. Cell. Sci.* 113, 1623–1633. Available online at: https://www.ncbi. nlm.nih. gov/pubmed/?term=Two+domains+of+p80+katanin+regulate+microtubule+severing+and+spindle+pole+targeting+by+p60+katanin

McNeely, K. C., Cupp, T. D., Little, J. N., Janisch, K. M., Shrestha, A., and Dwyer, N. D. (2017). Mutation of Kinesin-6 Kif20b causes defects in cortical neuron polarization and morphogenesis. *Neural Dev.* 12:5. doi: 10.1186/s13064-017-0082-5

McVicker, D. P., Awe, A. M., Richters, K. E., Wilson, R. L., Cowdrey, D. A., Hu, X., et al. (2016). Transport of a kinesin-cargo pair along microtubules into dendritic spines undergoing synaptic plasticity. *Nat. Commun.* 7:12741. doi: 10.1038/ncomms12741

Menon, S., and Gupton, S. L. (2016). Building blocks of functioning brain: cytoskeletal dynamics in neuronal development. *Int. Rev. Cell Mol. Biol.* 322, 183–245. doi: 10.1016/bs.ircmb.2015.10.002

Merriam, E. B., Lumbard, D. C., Viesselmann, C., Ballweg, J., Stevenson, M., Pietila, L., et al. (2011). Dynamic microtubules promote synaptic NMDA receptor-dependent spine enlargement. *PLoS One* 6:e27688. doi: 10.1371/journal.pone.0027688

Merriam, E. B., Millette, M., Lumbard, D. C., Saengsawang, W., Fothergill, T., Hu, X., et al. (2013). Synaptic regulation of microtubule dynamics in dendritic spines by calcium, F-actin, and drebrin. *J. Neurosci.* 33, 16471–16482. doi: 10.1523/JNEUROSCI.0661-13.2013

Mitchison, T., and Kirschner, M. (1984). Dynamic instability of microtubule growth. *Nature* 312, 237–242. doi: 10.1038/312237a0

Moughamian, A. J., Osborn, G. E., Lazarus, J. E., Maday, S., and Holzbaur, E. L. F. (2013). Ordered recruitment of dynactin to the microtubule plus-end is required for efficient initiation of retrograde axonal transport. *J. Neurosci.* 33, 13190–13203. doi: 10.1523/JNEUROSCI.0935-13.2013

Moores, C. A., Perdeeriset, M., Francis, F., Chelly, J., Houdusse, A., Milligan, R. A., et al. (2004). Mechanism of microtubule stabilization by doublecortin. *Mol. Cell* 14, 833–839. doi: 10.1016/j.molcel.2004.06.009

Mukherjee, S., Diaz Valencia, J. D., Stewman, S., Metz, J., Monnier, S., Rath, U., et al. (2012). Human Fidgetin is a microtubule severing the enzyme and minus-end depolymerase that regulates mitosis. *Cell Cycle* 11, 2359–2366. doi: 10.4161/cc.20849

Nakata, T., and Hirokawa, N. (2003). Microtubules provide directional cues for polarized axonal transport through interaction with kinesin motor head. *J. Cell Biol.* 162, 1045–1055. doi: 10.1083/jcb.200302175

Nakata, T., Niwa, S., Okada, Y., Perez, F., and Hirokawa, N. (2011). Preferential binding of a kinesin-1 motor to GTP-tubulin-rich microtubules underlies polarized vesicle transport. *J. Cell Biol.* 194, 245–255. doi: 10.1083/jcb.201104034

Neukirchen, D., and Bradke, F. (2011). Cytoplasmic linker proteins regulate neuronal polarization through microtubule and growth cone dynamics. *J. Neurosci.* 31, 1528–1538. doi: 10.1523/JNEUROSCI.3983-10.2011

Nwagbara, B. U., Faris, A. E., Bearce, E. A., Erdogan, B., Ebbert, P. T., Evans, M. F., et al. (2014). TACC3 is a microtubule plus end-tracking protein that promotes axon elongation and also regulates microtubule plus end dynamics in multiple embryonic cell types. *Mol. Biol. Cell* 25, 3350–3362. doi: 10.1091/mbc.E14-06-1121

Ohba, C., Haginoya, K., Osaka, H., Kubota, K., Ishiyama, A., Hiraide, T., et al. (2015). *De novo* KIF1A mutations cause intellectual deficit, cerebellar atrophy, lower limb spasticity and visual disturbance. *J. Hum. Genet.* 60, 739–742. doi: 10.1038/jhg.2015.108

Oksenberg, N., Stevison, L., Wall, J. D., and Ahituv, N. (2013). Function and regulation of AUTS2, a gene implicated in autism and human evolution. *PLoS Genet.* 9:e1003221. doi: 10.1371/journal.pgen.1003221

Ori-McKenney, K. M., Jan, L. Y., and Jan, Y. N. (2012). Golgi outposts shape dendrite morphology by functioning as sites of acentrosomal microtubule nucleation in neurons. *Neuron* 76, 921–930. doi: 10.1016/j.neuron.2012.10.008

Ori-McKenney, K. M., and Vallee, R. B. (2011). Neuronal migration defects in the Loa dynein mutant mouse. *Neural Dev.* 6:26. doi: 10.1186/1749-8104-6-26

Oz, S., Ivashko-Pachima, Y., and Gozes, I. (2012). The ADNP derived peptide, NAP modulates the tubulin pool: implication for neurotrophic and neuroprotective activities. *PLoS One* 7:e51458. doi: 10.1371/journal.pone.0051458

Oz, S., Kapitansky, O., Ivashco-Pachima, Y., Malishkevich, A., Giladi, E., Skalka, N., et al. (2014). The NAP motif of activity-dependent neuroprotective protein (ADNP) regulates dendritic spines through microtubule end binding proteins. *Mol. Psychiatry* 19, 1115–1124. doi: 10.1038/mp.2014.97

Pacheco, A., and Gallo, G. (2016). Actin filament-microtubule interactions in axon initiation and branching. *Brain Res. Bull.* 126, 300–310. doi: 10.1016/j.brainresbull.2016.07.013

Paylor, R., Hirotsune, S., Gambello, M. J., Yuva-Paylor, L., Crawley, J. N., and Wynshaw-Boris, A. (1999). Impaired learning and motor behavior in heterozygous Pafah1b1 (Lis1) mutant mice. *Learn. Mem.* 6, 521–537. doi: 10.1101/lm.6.5.521

Pilz, D. T., Matsumoto, N., Minnerath, S., Mills, P., Gleeson, J. G., Allen, K. M., et al. (1998). LIS1 and XLIS (DCX) mutations cause most classical lissencephaly, but different patterns of malformation. *Hum. Mol. Genet.* 7, 2029–2037. doi: 10.1093/hmg/7.13.2029

Pinto, D., Delaby, E., Merico, D., Barbosa, M., Merikangas, A., Klei, L., et al. (2014). Convergence of genes and cellular pathways dysregulated in autism spectrum disorders. *Am. J. Hum. Genet.* 94, 677–694. doi: 10.1016/j.ajhg.2014.03.018

Poirier, K., Keays, D. A., Francis, F., Saillour, Y., Bahi, N., Manouvrier, S., et al. (2007). Large spectrum of lissencephaly and pachygyria phenotypes resulting from *de novo* missense mutations in tubulin α 1A (TUBA1A). *Hum. Mutat.* 28, 1055–1064. doi: 10.1002/humu.20572

Poirier, K., Lebrun, N., Broix, L., Tian, G., Saillour, Y., Boscheron, C., et al. (2013a). Mutations in TUBG1, DYNC1H1, KIF5C and KIF2A cause malformations of cortical development and microcephaly. *Nat. Genet.* 45, 639–647. doi: 10.1038/ng.2613

Poirier, K., Saillour, Y., Fourniol, F., Francis, F., Souville, I., Valence, S., et al. (2013b). Expanding the spectrum of TUBA1A-related cortical dysgenesis to Polymicrogyria. *Eur. J. Hum. Genet.* 21, 381–385. doi: 10.1038/ejhg.2012.195

Poirier, K., Saillour, Y., Bahi-Buisson, N., Jaglin, X. H., Fallet-Bianco, C., Nabbout, R., et al. (2010). Mutations in the neuronal ß-tubulin subunit TUBB3 result in malformation of cortical development and neuronal migration defects. *Hum. Mol. Genet.* 19, 4462–4473. doi: 10.1093/hmg/ddq377

Poultney, C. S., Goldberg, A. P., Drapeau, E., Kou, Y., Harony-Nicolas, H., Kajiwara, Y., et al. (2013). Identification of small exonic CNV from whole-exome sequence data and application to autism spectrum disorder. *Am. J. Hum. Genet.* 93, 607–619. doi: 10.1016/j.ajhg.2013.09.001

Rao, A. N., Patil, A., Black, M. M., Craig, E. M., Myers, K. A., Yeung, H. T., et al. (2017). Cytoplasmic dynein transports axonal microtubules in a polarity-sorting manner. *Cell Rep.* 19, 2210–2219. doi: 10.1016/j.celrep.2017.05.064

Rehberg, M., Kleylein-Sohn, J., Faix, J., Ho, T.-H., Schulz, I., and Gräf, R. (2005). Dictyostelium LIS1 is a centrosomal protein required for microtubule/cell cortex interactions, nucleus/centrosome linkage, and actin dynamics. *Mol. Biol. Cell* 16, 2759–2771. doi: 10.1091/mbc.E05-01-0069

Reiner, O., Carrozzo, R., Shen, Y., Wehnert, M., Faustinella, F., Dobyns, W. B., et al. (1993). Isolation of a Miller-Dieker lissencephaly gene containing G protein β-subunit-like repeats. *Nature* 364, 717–721. doi: 10.1038/364717a0

Rutherford, E. L., Carandang, L., Ebbert, P. T., Mills, A. N., Bowers, J. T., and Lowery, L. A. (2016). Xenopus TACC2 is a microtubule plus end-tracking protein that can promote microtubule polymerization during embryonic development. *Mol. Biol. Cell* 27, 3013–3020. doi: 10.1091/mbc.E16-03-0198

Sainath, R., and Gallo, G. (2015). Cytoskeletal and signaling mechanisms of neurite formation. *Cell Tissue Res.* 359, 267–278. doi: 10.1007/s00441-014-1955-0

Sapir, T., Cahana, A., Seger, R., Nekhai, S., and Reiner, O. (1999). LIS1 is a microtubule-associated phosphoprotein. *Eur. J. Biochem.* 265, 181–188. doi: 10.1046/j.1432-1327.1999.00711.x

Sapir, T., Elbaum, M., and Reiner, O. (1997). Reduction of microtubule catastrophe events by LIS1, platelet-activating factor acetylhydrolase subunit. *EMBO J.* 16, 6977–6984. doi: 10.1093/emboj/16.23.6977

Sapir, T., Frotscher, M., Levy, T., Mandelkow, E.-M., and Reiner, O. (2012). Tau's role in the developing brain: implications for intellectual disability. *Hum. Mol. Genet.* 21, 1681–1692. doi: 10.1093/hmg/ddr603

Sapir, T., Sapoznik, S., Levy, T., Finkelshtein, D., Shmueli, A., Timm, T., et al. (2008). Accurate balance of the polarity kinase MARK2/Par-1 is required for proper cortical neuronal migration. *J. Neurosci.* 28, 5710–5720. doi: 10.1523/JNEUROSCI.0911-08.2008

Schaar, B. T., Kinoshita, K., and McConnell, S. K. (2004). Doublecortin microtubule affinity is regulated by a balance of kinase and phosphatase activity at the leading edge of migrating neurons. *Neuron* 41, 203–213. doi: 10.1016/s0896-6273(03)00843-2

Schirer, Y., Malishkevich, A., Ophir, Y., Lewis, J., Giladi, E., and Gozes, I. (2014). Novel marker for the onset of frontotemporal dementia: early increase in activity-dependent neuroprotective protein (ADNP) in the face of Tau mutation. *PLoS One* 9:e87383. doi: 10.1371/journal.pone.0087383

Sharp, D. J., Yu, W., and Baas, P. W. (1995). Transport of dendritic microtubules establishes their nonuniform polarity orientation. *J. Cell Biol.* 130, 93–103. doi: 10.1083/jcb.130.1.93

Sharp, D. J., Yu, W., Ferhat, L., Kuriyama, R., Rueger, D. C., and Baas, P. W. (1997). Identification of a microtubule-associated motor protein essential for dendritic differentiation. *J. Cell Biol.* 138, 833–843. doi: 10.1083/jcb.138.4.833

Shi, S.-H., Cheng, T., Jan, L. Y., and Jan, Y. N. (2004). APC and GSK-3β are involved in mPar3 targeting to the nascent axon and establishment of neuronal polarity. *Curr. Biol.* 14, 2025–2032. doi: 10.1016/j.cub.2004.11.009

Shu, T., Ayala, R., Nguyen, M.-D., Xie, Z., Gleeson, J. G., and Tsai, L.-H. (2004). Ndel1 operates in a common pathway with LIS1 and cytoplasmic dynein to regulate cortical neuronal positioning. *Neuron* 44, 263–277. doi: 10.1016/j.neuron.2004.09.030

Smith, D. S., Niethammer, M., Ayala, R., Zhou, Y., Gambello, M. J., Wynshaw-Boris, A., et al. (2000). Regulation of cytoplasmic dynein behaviour and microtubule organization by mammalian Lis1. *Nat. Cell Biol.* 2, 767–775. doi: 10.1038/35041000

Srivastava, A. K., and Schwartz, C. E. (2014). Intellectual disability and autism spectrum disorders: causal genes and molecular mechanisms. *Neurosci. Biobehav. Rev.* 46, 161–174. doi: 10.1016/j.neubiorev.2014.02.015

Steindler, C., Li, Z., Algarté, M., Alcover, A., Libri, V., Ragimbeau, J., et al. (2004). Jamip1 (marlin-1) defines a family of proteins interacting with janus kinases and microtubules. *J. Biol. Chem.* 279, 43168–43177. doi: 10.1074/jbc.M401915200

Stiess, M., and Bradke, F. (2011). Neuronal polarization: the cytoskeleton leads the way. *Dev. Neurobiol.* 71, 430–444. doi: 10.1002/dneu.20849

Stiess, M., Maghelli, N., Kapitein, L. C., Gomis-Rüth, S., Wilsch-Bräuninger, M., Hoogenraad, C. C., et al. (2010). Axon extension occurs independently of centrosomal microtubule nucleation. *Science* 327, 704–707. doi: 10.1126/science.1182179

Stouffer, M. A., Golden, J. A., and Francis, F. (2016). Neuronal migration disorders: focus on the cytoskeleton and epilepsy. *Neurobiol. Dis.* 92, 18–45. doi: 10.1016/j.nbd.2015.08.003

Stutterd, C. A., and Leventer, R. J. (2014). Polymicrogyria: a common and heterogeneous malformation of cortical development. *Am. J. Med. Genet. C Semin Med. Genet.* 166C, 227–239. doi: 10.1002/ajmg.c.31399

Swiech, L., Blazejczyk, M., Urbanska, M., Pietruszka, P., Dortland, B. R., Malik, A. R., et al. (2011). CLIP-170 and IQGAP1 cooperatively regulate dendrite morphology. *J. Neurosci.* 31, 4555–4568. doi: 10.1523/JNEUROSCI.6582-10.2011

Takei, Y., Kikkawa, Y. S., Atapour, N., Hensch, T. K., and Hirokawa, N. (2015). Defects in synaptic plasticity, reduced NMDA-receptor transport and instability of postsynaptic density proteins in mice lacking microtubule-associated protein 1A. *J. Neurosci.* 35, 15539–15554. doi: 10.1523/JNEUROSCI.2671-15.2015

Takei, Y., Teng, J., Harada, A., and Hirokawa, N. (2000). Defects in axonal elongation and neuronal migration in mice with disrupted tau and map1b genes. *J. Cell Biol.* 150, 989–1000. doi: 10.1083/jcb.150.5.989

Tanaka, E. M., and Kirschner, M. W. (1991). Microtubule behavior in the growth cones of living neurons during axon elongation. *J. Cell Biol.* 115, 345–363. doi: 10.1083/jcb.115.2.345

Tanaka, T., Koizumi, H., and Gleeson, J. G. (2006). The doublecortin and doublecortin-like kinase 1 genes cooperate in murine hippocampal development. *Cereb. Cortex* 16, i69–i73. doi: 10.1093/cercor/bhk005

Tas, R. P., Chazeau, A., Cloin, B. M. C., Lambers, M. L. A., Hoogenraad, C. C., and Kapitein, L. C. (2017). Differentiation between oppositely oriented microtubules controls polarized neuronal transport. *Neuron* 96, 1264.e5–1271.e5. doi: 10.1016/j.neuron.2017.11.018

Teng, J., Takei, Y., Harada, A., Nakata, T., Chen, J., and Hirokawa, N. (2001). Synergistic effects of MAP2 and MAP1B knockout in neuronal migration, dendritic outgrowth, and microtubule organization. *J. Cell Biol.* 155, 65–76. doi: 10.1083/jcb.200106025

Tint, I., Jean, D., Baas, P. W., and Black, M. M. (2009). Doublecortin associates with microtubules preferentially in regions of the axon displaying actin-rich protrusive structures. *J. Neurosci.* 29, 10995–11010. doi: 10.1523/JNEUROSCI.3399-09.2009

Tischfield, M. A., Baris, H. N., Wu, C., Rudolph, G., Van Maldergem, L., He, W., et al. (2010). Human TUBB3 mutations perturb microtubule dynamics, kinesin interactions, and axon guidance. *Cell* 140, 74–87. doi: 10.1016/j.cell.2009.12.011

Trimborn, M., Bell, S. M., Felix, C., Rashid, Y., Jafri, H., Griffiths, P. D., et al. (2004). Mutations in microcephalin cause aberrant regulation of chromosome condensation. *Am. J. Hum. Genet.* 75, 261–266. doi: 10.1086/422855

Tsai, J.-W., Bremner, K. H., and Vallee, R. B. (2007). Dual subcellular roles for LIS1 and dynein in radial neuronal migration in live brain tissue. *Nat. Neurosci.* 10, 970–979. doi: 10.1038/nn1934

Tymanskyj, S. R., Scales, T. M. E., and Gordon-Weeks, P. R. (2012). MAP1B enhances microtubule assembly rates and axon extension rates in developing neurons. *Mol. Cell. Neurosci.* 49, 110–119. doi: 10.1016/j.mcn.2011.10.003

Vagnoni, A., Hoffmann, P. C., and Bullock, S. L. (2016). Reducing Lissencephaly-1 levels augments mitochondrial transport and has a protective effect in adult *Drosophila* neurons. *J. Cell. Sci.* 129, 178–190. doi: 10.1242/jcs.179184

Vaillant, A. R., Müller, R., Langkopf, A., and Brown, D. L. (1998). Characterization of the microtubule-binding domain of microtubule-associated protein 1A and its effects on microtubule dynamics. *J. Biol. Chem.* 273, 13973–13981. doi: 10.1074/jbc.273.22.13973

van de Willige, D., Hoogenraad, C. C., and Akhmanova, A. (2016). Microtubule plus-end tracking proteins in neuronal development. *Cell. Mol. Life Sci.* 73, 2053–2077. doi: 10.1007/s00018-016-2168-3

Van Dijck, A., Vulto-van Silfhout, A. T., Cappuyns, E., van der Werf, I. M., Mancini, G. M., Tzschach, A., et al. (2018). Clinical presentation of a complex neurodevelopmental disorder caused by mutations in ADNP. *Biol. Psychiatry* doi: 10.1016/j.biopsych.2018.02.1173 [Epub ahead of print].

Vidal, R. L., Ramírez, O. A., Sandoval, L., Koenig-Robert, R., Härtel, S., and Couve, A. (2007). Marlin-1 and conventional kinesin link GABAB receptors to the cytoskeleton and regulate receptor transport. *Mol. Cell. Neurosci.* 35, 501–512. doi: 10.1016/j.mcn.2007.04.008

Vulih-Shultzman, I., Pinhasov, A., Mandel, S., Grigoriadis, N., Touloumi, O., Pittel, Z., et al. (2007). Activity-dependent neuroprotective protein snippet NAP reduces tau hyperphosphorylation and enhances learning in a novel transgenic mouse model. *J. Pharmacol. Exp. Ther.* 323, 438–449. doi: 10.1124/jpet.107.129551

Vulprecht, J., David, A., Tibelius, A., Castiel, A., Konotop, G., Liu, F., et al. (2012). STIL is required for centriole duplication in human cells. *J. Cell. Sci.* 125, 1353–1362. doi: 10.1242/jcs.104109

Wang, Y., and Mandelkow, E. (2016). Tau in physiology and pathology. *Nat. Rev. Neurosci.* 17, 22–35. doi: 10.1038/nrn.2015.1

Whitman, M. C., Andrews, C., Chan, W.-M., Tischfield, M. A., Stasheff, S. F., Brancati, F., et al. (2016). Two unique TUBB3 mutations cause both CFEOM3 and malformations of cortical development. *Am. J. Med. Genet. A* 170A, 297–305. doi: 10.1002/ajmg.a.37362

Willemsen, M. H., Ba, W., Wissink-Lindhout, W. M., de Brouwer, A. P. M., Haas, S. A., Bienek, M., et al. (2014). Involvement of the kinesin family members KIF4A and KIF5C in intellectual disability and synaptic function. *J. Med. Genet.* 51, 487–494. doi: 10.1136/jmedgenet-2013-102182

Winding, M., Kelliher, M. T., Lu, W., Wildonger, J., and Gelfand, V. I. (2016). Role of kinesin-1-based microtubule sliding in *Drosophila* nervous system development. *Proc. Natl. Acad. Sci. U S A* 113, E4985–E4994. doi: 10.1126/science.353.6302.883-a

Witte, H., Neukirchen, D., and Bradke, F. (2008). Microtubule stabilization specifies initial neuronal polarization. *J. Cell Biol.* 180, 619–632. doi: 10.1083/jcb.200707042

Wood, J. D., Landers, J. A., Bingley, M., McDermott, C. J., Thomas-McArthur, V., Gleadall, L. J., et al. (2006). The microtubule-severing protein Spastin is essential for axon outgrowth in the zebrafish embryo. *Hum. Mol. Genet.* 15, 2763–2771. doi: 10.1093/hmg/ddl212

Yau, K. W., Schätzle, P., Tortosa, E., Pagès, S., Holtmaat, A., Kapitein, L. C., et al. (2016). Dendrites *in vitro* and *in vivo* contain microtubules of opposite polarity and axon formation correlates with uniform plus-end-out microtubule orientation. *J. Neurosci.* 36, 1071–1085. doi: 10.1523/JNEUROSCI.2430-15.2016

Yau, K. W., van Beuningen, S. F. B., Cunha-Ferreira, I., Cloin, B. M. C., van Battum, E. Y., Will, L., et al. (2014). Microtubule minus-end binding protein CAMSAP2 controls axon specification and dendrite development. *Neuron* 82, 1058–1073. doi: 10.1016/j.neuron.2014.04.019

Youn, Y. H., Pramparo, T., Hirotsune, S., and Wynshaw-Boris, A. (2009). Distinct dose-dependent cortical neuronal migration and neurite extension defects in Lis1 and Ndel1 mutant mice. *J. Neurosci.* 29, 15520–15530. doi: 10.1523/JNEUROSCI.4630-09.2009

Yu, W., Ahmad, F. J., and Baas, P. W. (1994). Microtubule fragmentation and partitioning in the axon during collateral branch formation. *J. Neurosci.* 14, 5872–5884. doi: 10.1523/JNEUROSCI.14-10-05872.1994

Yu, W., Cook, C., Sauter, C., Kuriyama, R., Kaplan, P. L., and Baas, P. W. (2000). Depletion of a microtubule-associated motor protein induces the loss of dendritic identity. *J. Neurosci.* 20, 5782–5791. doi: 10.1523/JNEUROSCI.20-15-05782.2000

Yu, W., Qiang, L., Solowska, J. M., Karabay, A., Korulu, S., and Baas, P. W. (2008). The microtubule-severing proteins spastin and katanin participate differently in the formation of axonal branches. *Mol. Biol. Cell* 19, 1485–1498. doi: 10.1091/mbc.E07-09-0878

Yuan, A., Kumar, A., Peterhoff, C., Duff, K., and Nixon, R. A. (2008). Axonal transport rates *in vivo* are unaffected by tau deletion or overexpression in mice. *Mol. Hum. Reprod.* 28, 1682–1687. doi: 10.1523/JNEUROSCI.5242-07.2008

Zhao, B., Meka, D. P., Scharrenberg, R., König, T., Schwanke, B., Kobler, O., et al. (2017). Microtubules modulate F-actin dynamics during neuronal polarization. *Sci. Rep.* 7:9583. doi: 10.1038/s41598-017-09832-8

Zhao, J., Wang, Y., Xu, H., Fu, Y., Qian, T., Bo, D., et al. (2016). Dync1h1 mutation causes proprioceptive sensory neuron loss and impaired retrograde axonal transport of dorsal root ganglion neurons. *CNS Neurosci. Ther.* 22, 593–601. doi: 10.1111/cns.12552

Zheng, Y., Wildonger, J., Ye, B., Zhang, Y., Kita, A., Younger, S. H., et al. (2008). Dynein is required for polarized dendritic transport and uniform microtubule orientation in axons. *Nat. Cell Biol.* 10, 1172–1180. doi: 10.1038/ncb1777

Zollo, M., Ahmed, M., Ferrucci, V., Salpietro, V., Asadzadeh, F., Carotenuto, M., et al. (2017). PRUNE is crucial for normal brain development and mutated in microcephaly with neurodevelopmental impairment. *Brain* 140, 940–952. doi: 10.1093/brain/awx014

Conflict of Interest Statement: The authors declare that the research was conducted in the absence of any commercial or financial relationships that could be construed as a potential conflict of interest.

frontiers in Cellular Neuroscience

ORIGINAL RESEARCH
published: 12 July 2018
doi: 10.3389/fncel.2018.00202

Frontotemporal Dementia-Associated N279K Tau Mutation Localizes at the Nuclear Compartment

Maxi L. Ritter[1], Jesús Avila[2,3], Vega García-Escudero[1], Félix Hernández[2,3]† and Mar Pérez[1]*†*

[1]Departamento de Anatomía Histología y Neurociencia, Facultad de Medicina, Universidad Autonoma de Madrid (UAM), Madrid, Spain, [2]Centro de Biología Molecular Severo Ochoa, Consejo Superior de Investigaciones Científicas (CSIC), Universidad Autonoma de Madrid (UAM), Madrid, Spain, [3]Centro de Investigación Biomédica en Red sobre Enfermedades Neurodegenerativas (CIBERNED), Carlos III Institute of Health, Madrid, Spain

Tau is a microtubule-associated protein that plays an important role in Alzheimer's disease and related tauopathies. Approximately one-half of all cases of Frontotemporal dementia with parkinsonism-17 (FTDP-17) are caused by mutations in the MAPT gene. The N279K mutation is one of the three mutations more prevalent in FTDP-17 cases. Several studies have demonstrated that N279K Tau mutation alters alternative splicing inducing the presence of exon 10. Tau is mainly found in the cytosol of neuronal cells although it has also been localized within the nucleus. Here we demonstrate by biochemical and immunohistochemistry studies in COS-7 cells, that the proportion of mutant N279K Tau increases compared with wild-type at the cell nucleus although cell viability is not affected. These data will provide us with a better outline of the nuclear role of tau protein offering new clues related with this tauopathie.

Keywords: FTDP-17, Alzheimer, tau, transport, nucleus

OPEN ACCESS

Edited by:
José A. G. Agúndez, Universidad de Extremadura, Spain

Reviewed by:
Roland Brandt, University of Osnabrück, Germany
Ana Garcia-Osta, Universidad de Navarra, Spain

***Correspondence:**
Félix Hernández
fhernandez@cbm.csic.es
Mar Pérez
mar.perez@uam.es

†*These authors have contributed equally to this work.*

Received: *01 March 2018*
Accepted: *21 June 2018*
Published: *12 July 2018*

Citation:
Ritter ML, Avila J, García-Escudero V, Hernández F and Pérez M (2018) Frontotemporal Dementia-Associated N279K Tau Mutation Localizes at the Nuclear Compartment. Front. Cell. Neurosci. 12:202. doi: 10.3389/fncel.2018.00202

INTRODUCTION

Tau protein is composed of six different isotypes generated by alternative splicing mechanisms in the central nervous system (CNS) of mammals. Three of these isoforms contain three copies of the microtubule-binding domain (Tau3R) whereas the other three isotypes contain four repeats (Tau4R). The expression of some of these Tau isoforms is developmentally regulated. Thus, mouse isoforms lacking exon 10 (Tau3R) are found at early developmental stages whereas Tau isoforms containing exon 10 (Tau4R) are mainly found in murine neurons at mature developmental stages (Avila et al., 2004; Sergeant et al., 2005). In adult human brain both Tau 3R and Tau 4R are present, although in newborn neurons such as those in the hippocampal dentate gyrus Tau 3R is the main isoform (Bullmann et al., 2007).

Some Tau gene mutations alter proportion Tau4R/Tau3R and this alteration is pathological. The mechanisms regulating the ratio of Tau4R/Tau3R are due to mutations altering splicing in some frontotemporal dementia patients present in exon 10 or intron regions flaking that exon, mainly close to the 5′ splice site of exon 10. N279K mutation (SNP ID number: rs63750756) present in exon 10 is extremely rare among healthy individuals, but it is among most frequent causes of familial frontotemporal dementia[1]. At molecular level, N279K mutation affects exon 10 splicing allowing exon 10 to be incorporated more frequently and

[1]https://www.alzforum.org/mutation/mapt-n279k

causing an increase of Tau4R isoforms (Delisle et al., 1999; Dawson et al., 2007). The N279K mutation strengthens a poly-purine positive cis-element present within exon 10, resulting in increased exon 10 inclusion during splicing process (Hutton, 2001). Consequences of that alteration in Tau 4R/3R proportion is the disruption of subcellular vesicle trafficking and induction of cellular stress at least in iPSC-derived neural stem cells (Wren et al., 2015).

Tau has mainly an axonal localization and can be found associated with microtubules although that interaction is highly dynamic explaining why tau can also be present in other cellular compartments (Janning et al., 2014). Thus, Tau can be also associated with the plasma membrane (Brandt et al., 1995) in an interaction that could be modulated by Tau phosphorylation (Arrasate et al., 2000; Gauthier-Kemper et al., 2018). Also, the presence of a nuclear antigen reacting with several Tau antibodies has been reported, mainly in proliferating cells, demonstrating that Tau is also a nuclear protein (for a review see Bukar Maina et al., 2016).

Nuclear location studies seems to confer Tau an important role in nucleolar structure conformation and heterochromatinization of ribosomal genes (Sjöberg et al., 2006; Rossi et al., 2008). The role that it might play in the nucleus and the physiological consequences derived from its interaction with DNA remains to be elucidated. However, a function related to protection of genomic integrity has been recently suggested to Tau protein (Sjöberg et al., 2006). Interestingly, Tau binding to DNA is modulated by phosphorylation (Camero et al., 2014). However, it is unknown how Tau protein is transported to nucleus as not clear import or export sequences has been described in Tau protein.

Here, we explored the nuclear localization of N279K isoform in order to know the effect of that mutation in nuclear localization. Our data demonstrate that the proportion of mutated Tau, at the cell nucleus, increases compared with wild-type. The consequences of that distribution are discussed.

MATERIALS AND METHODS

Antibodies

List of antibodies used are shown in **Table 1**. The antibodies against Tau used in this study were: Tau 12 (N-terminal, mouse monoclonal); Tau 46 (C-terminal, mouse monoclonal); Tau 1 (unphosphatase-sensitive epitope corresponding to Ser199/202, mouse monoclonal); 7.51 (against microtubule-binding domain); AD2 (Tau phosphorylated at S396/S404, mouse monoclonal); AT-8 (Tau phosphorylated at S202, mouse monoclonal).

The monoclonal antibody directed against β-actin (Sigma St. Louis, MO, USA) was used as internal control for protein quantification. Anti-GADPH (Abcam) and anti-Lamin B1 (Santa Cruz Biotechnology) were used as internal control for nuclear extracts.

Materials

The anti-proteases cocktail and Leptomycin B and the rest of the reagents were purchased from Sigma-Aldrich.

Tau Expression Constructs

The largest CNS isoform of wild-type human Tau was expressed from the SV40 early promoter using the plasmid pSGT42 previously described (Montejo de Garcini et al., 1994). To engineer the N279K mutation, mutagenesis was carried out using the polymerase chain reaction (PCR) with primer N279K forward 5′-GTGCAGATAATTAAGAAGAAGCTGG-3′ and primer N279K reverse 5′-CCAGCTTCTTCTTAATTATCTGCAC-3′ which include the mutated codon. The fragment generated by PCR amplification on pSGT42 using primers described above was digested with *BglII* and *EcoRI* and ligated into the eukaryotic expression vector pSG5 (Stratagene) under the control of SV40 early promoter digested with the same enzymes to obtain pSGTN279K.

Positive clones were analyzed by restriction analysis to test for the proper orientation and correct size of the inserts. Finally,

TABLE 1 | List of antibodies.

Antibody	Epitope	Source, host species, catalog/clone/lot No.,	Dilution
Tau 12	Aminoacids 6–18 of human tau	Abcam; Mouse monoclonal; Cat# ab74137	1/500 (WB)
Tau 46	Aminoacids 404–441 of human tau	Abcam; human; Mouse monoclonal; Cat. #: ab22261	1/1000 (WB)
Tau 1	Unphosphorylated tau in amino acids 198–206	Calbiochem San Diego, CA, USA; Mouse monoclonal	1/5000 (WB); 1/500 (IF)
Tau 5	Amino acids 210–241 of bovine Tau	Abcam; Mouse monoclonal; Cat# ab80579	1/1000
7.51	The microtubule-binding region	Kindly provided by Dr. C. M. Wischik, Aberdeen, UK; Mouse monoclonal	1/100 (WB)
AD2	Phospho tau in S396/404	Biorad Laboratories; Mouse monoclonal; Cat# 56484	1/1000 (WB)
AT8	Phospho tau in S202	Innogenetics. Cat #90206	1/1000 (WB)
Anti-ERK1	C-terminus de ERK 1	Rabbit polyclonal: Santa Cruz Biotechnology; Cat# (C-16): sc-93	1/100 (IF)
Anti-β Actin	Slightly modified β-cytoplasmic actin N-terminal peptide, Ac-Asp-Asp-Asp-Ile-Ala-Ala-Leu-Val-Ile-Asp-Asn-Gly-Ser-Gly-Lys, conjugated to KLH.	Sigma-Aldrich; Monoclonal; Cat# A5441	1/5000 (WB)
Anti-GADPH	Rabbit muscle GAPDH	Abcam; Monoclonal; Cat# AB8245	1/3000 (WB)
Anti-laminin B1	A monoclonal antibody against the C-terminal of Laminin B1	Santa Cruz Biotechnology; Mouse monoclonal; Cat# sc-377000	1/100 (WB)

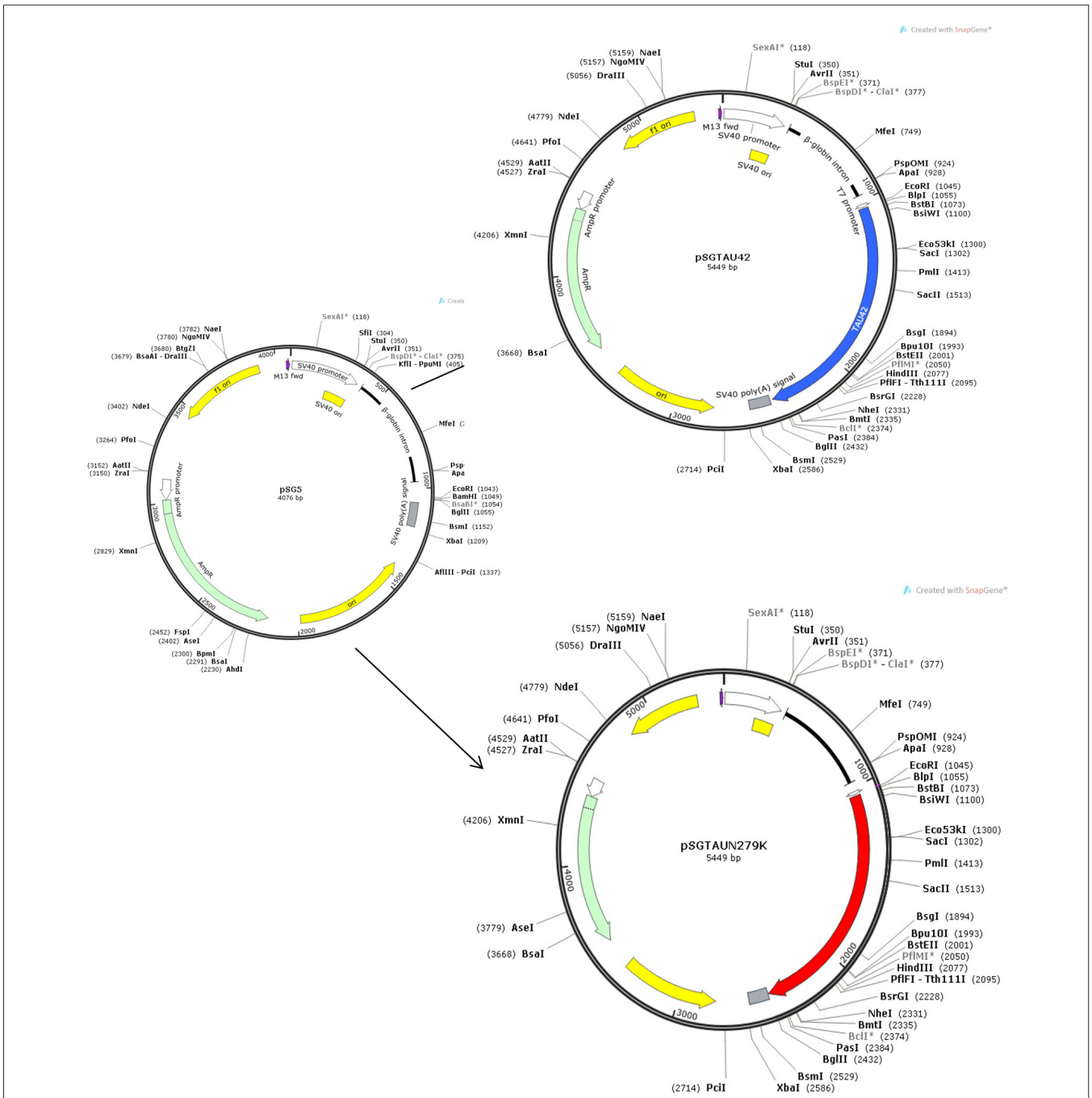

FIGURE 1 | Maps of Tau constructs used in this work.

the constructions were confirmed by DNA- sequencing analysis. **Figure 1** shows the maps of Tau constructs used in this work.

Cell Culture and DNA Transfection

African green monkey kidney fibroblasts (COS-7) cells (Gluzman, 1981) were grown in Dulbecco's modified Eagle's medium supplemented with 10% (vol/vol) fetal bovine serum (FBS). Cells were transfected with the cDNA constructs using PEI reagent (Polysciences, Inc) according to the manufacturer's instructions. The empty vector pSG5 was used to transfect control cells.

Leptomycin B Treatment

One hour before the end of transfection, COS-7 cells were incubated in FBS-free DMEM containing vehicle (methanol) or 20 ng/ml Leptomycin B1.

Toxicity Assays

Cell death was assayed by using the LIVE/DEAD viability/cytotoxicity kit (Invitrogen, Carlsbad, CA, USA) to label live cells and ethidium homodimer-1 to label dead cells. 1×10^5 COS-7 cells were seeded to each well of a 24-well plate and transfected with the plasmids described above. After 48 h postransfection, cell viability was measured using LIVE/DEAD viability kit. Cells were incubated for 20 min with 2 μM propidium iodide and 1 μM calcein. After staining, live cells (green) and dead cells (red) were visualized on a Leica fluorescence microscope and images were taken. Three fields (selected at random) were analyzed per well (100–500 cells/field) and counted with ImageJ software. Cell viability was defined in each condition as the percentage of live cells vs. the total number of cells.

Western Blotting

At 48 h post-transfection, cells were homogenized in lysis buffer (20 mM HEPES pH 7.4, 5 mM EDTA, 100 mM NaCl, 1% Triton X-100, 0.1 mM sodium orthovanadate, protease inhibitor cocktail and 0.1 μM Okadaic acid). Lysates were centrifugated at 10,000 *g* for 15 min at 4°C and protein samples were quantified by the BCA protein assay. Samples were separated on 10% SDS-PAGE and electrophoretically transferred to a nitrocellulose membrane (Schleicher & Schuell GmbH). The membrane was blocked by incubation with 5% semi-fat dried milk in PBS and 0.1% Tween 20 (PBSM), followed by 1-h incubation at room temperature with the primary antibody in PBSM. The following primary antibody dilutions were used: T12 (1/500); T46 (1/1000); Tau5 (1/1000): Tau 1 (1/5000); 7.51 (1/100); AD2 (1/500); anti-GADPH (1/3000); anti-Lamin B1 (1/250) and anti-β actin (1/5000). After three washes, the membrane was incubated with a horseradish peroxidase-anti-mouse Ig conjugate (DAKO), followed by several washes in PBS-Tween 20. The membrane was then incubated for 1 min in Western Lightning reagents (PerkinElmer Life Sciences).

Blots were quantified using the EPSON Perfection 1660 scanner and the ImageJ1.46r image analysis system. The levels of various markers were normalized to the β-actin present in each band.

Nuclear Extracts

Adherent cells were washed with ice-cold PBS and scraped into ice-cold hypotonic Buffer A (20 mM HEPES pH 7, 0.15 mM EDTA, 0.015 mM EGTA, 10 mM KCl, 1% NP-40 supplemented with protease inhibitors), incubated for 30 min on ice in a rotating wheel and pelleted by centrifugation at 2300 rpm for 5 min at 4°C. Supernatant was collected as cytosolic fraction. Nuclear pellet was washed in five volumes of buffer B (10 mM HEPES pH 8, 25% (v/v) Glycerol, 0.1 M NaCl and 0.15 mM EDTA). After centrifugation as above, nuclei in the pellet were resuspended in two cellular volumes of Buffer A.

Immunofluorescence and Confocal Microscopy

For immunofluorescence studies, cells were fixed with 4% formaldehyde. Subsequently, the fixed cells were permeabilized with 0.1% Triton X-100 and Glycine 1 M for 30 min. After fixation, the coverslips were blocked with 1% bovine serum albumin for 30 min and subsequently incubated with primary antibodies in PBS containing 1% bovine serum albumin for 1 h. Coverslips were rinsed three times with PBS and incubated 45 min with Alexa 488-conjugated anti-mouse (diluted 1:400; Thermo Fisher). All the coverslips were finally counterstained for 3 min with 4′,6-Diamidine-2′-phenylindole dihydrochloride (DAPI; 1:1000, Calbiochem-EMD Darmstadt, Germany). After washing with PBS, the coverslips were mounted with FluorosaveTM (Calbiochem, San Diego, CA, USA). Confocal images were obtained using a TCS SP5 Spectral Leica Confocal microscope using an oil-immersion 40× objective with sequential-acquisition setting. The detector pinholes were set to give a 0.3 μm optical slice.

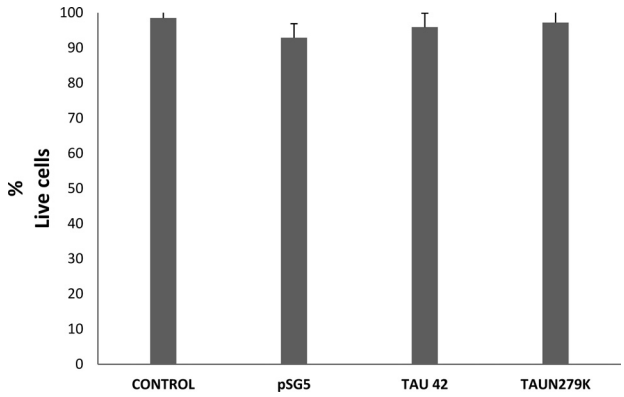

FIGURE 2 | Cell viability of COS-7 cells. Cell viability under control conditions, transfected with empty pSG5 or with pSG5-Tau 42 or with pSG-Tau N279K was measured by labeling with calcein-AM (live cells) and ethidium homodimer-1 (dead cells), 48 h after transfection. Quantification of the percentage of live cells in each condition is shown.

Data Analysis

Data are presented as the mean ± SD. Two group comparisons were made using unpaired Student's two-tailed *t*-test. Significance was accepted at $p < 0.05$.

RESULTS

Overexpression of Tau Without Cell Death

To determine if overexpression of plasmids used in this work was or not toxic for the cells, we performed a toxicity assay. **Figure 2** shows that cell viability under control conditions, transfected with empty pSG5 or with pSG5-Tau 42 or with pSG-Tau N279K plasmid did not correlated with cell death, given the low rate of cell death observed in the cultures of transfected COS-7.

Effect of the N279K Mutation on Tau Phosphorylation in COS-7 Cells

The human wild-type Tau 42 and mutant Tau N279K (**Figure 3A**) plasmids were transfected into COS-7 cells

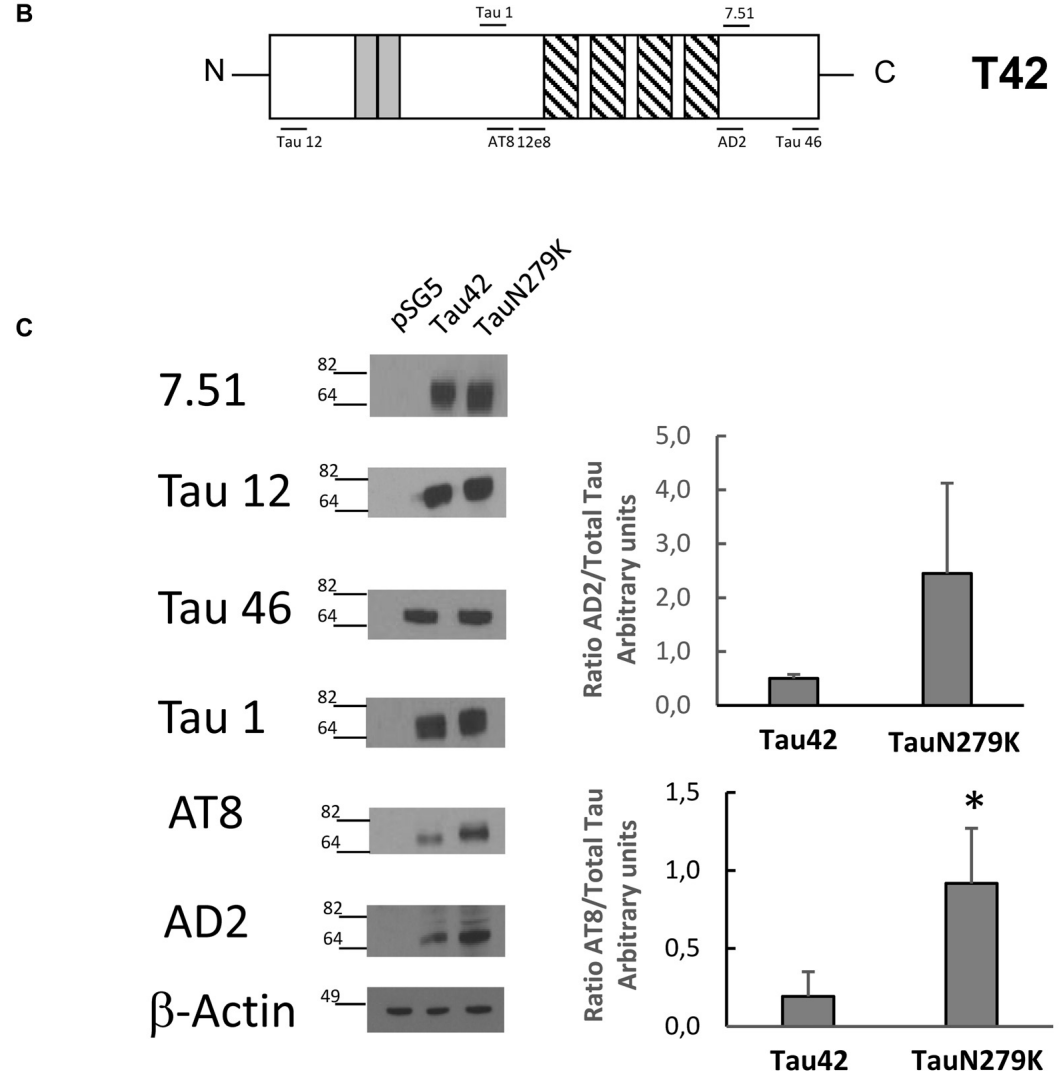

FIGURE 3 | Analysis of human Tau 42 and Tau N279K mutant in COS-7 cells. **(A)** Human Tau 250–300 sequence showing mutated amino acid N279K in red. **(B)** Schematic representation of Tau 42 (T42) correspond to the longest human cDNA isoform of the protein (Goedert et al., 1989). Gray squares indicate the 29-amino acid inserts close to the N-terminal end. Striped square indicates the tubulin binding repeats. Epitopes of antibodies used are indicated. **(C)** Wild-type Tau (Tau 42) and mutant Tau (Tau N279K) were transfected in COS-7 cells. Forty-eight hours after transfection, cell lysates were obtained and analyzed by Western-blot using several anti-Tau antibodies. Actin amount was used in each case as protein loading control. To analyze phosphorylation at AT8 epitope, cells were incubated during 1 h with okadaic acid (0.5 μM). Quantification of AT8 and AD2 antibodies are shown using 7.51 antibody to measure total unphosphorylated tau. AD2 quantification did not show a significant difference, although a tendency toward increase was found. Data are mean ± SD from four separate experiments (*$p < 0.05$).

to explore the effect of the N279K mutation on Tau phosphorylation. The level of Tau was determined by measuring the reactivity of the protein with the monoclonal antibodies T12, T46, 7.51 and Tau 1, which recognize Tau independently of its modification state, and AT8 and AD2, which recognizes phosphoserine 202 and phosphoserines

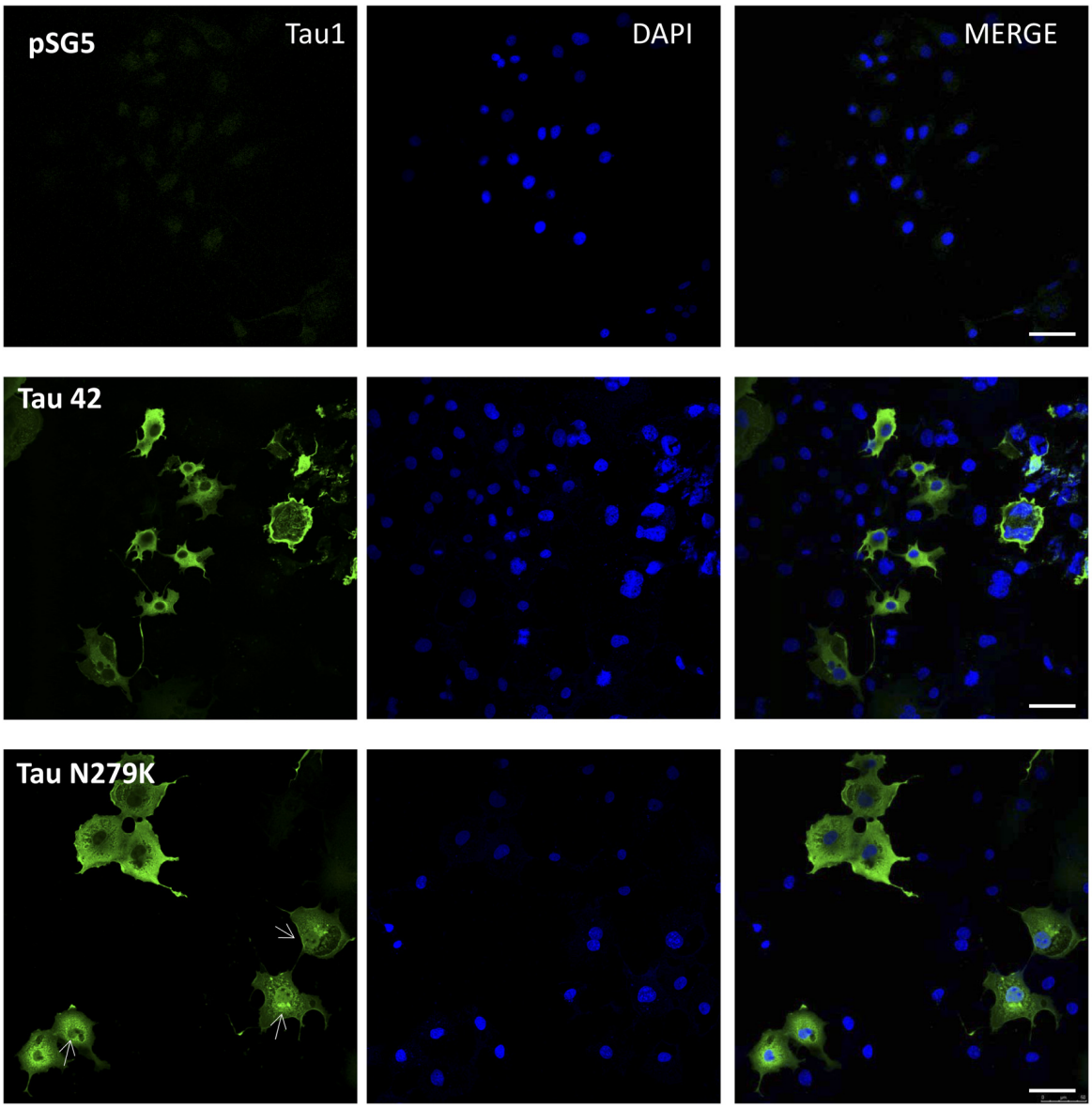

FIGURE 4 | Localization of Tau in COS-7 cells transfected with empty plasmid pSG5, human Tau 42 or Tau N279K. Representative images of localization of Tau 42 and Tau N279K using anti-Tau 1 antibody (green). The localization of nucleus was determined by immunofluorescence with 4′,6-Diamidine-2′-phenylindole dihydrochloride (DAPI). Bar indicates 50 μm. Arrows show nuclear localization of transfected Tau.

396/404 respectively (Buée-Scherrer et al., 1996; **Figure 3B**). AT8 antibody did not recognize phosphorylated human wild-type Tau 42 or mutant Tau N279K (data not shown). However, when transfected cells were incubated during 1 h with okadaic acid (0.5 μM) an increase in phosphorylated tau could be observed. **Figure 3C** shows an increase in the level of phosphorylation at AT-8 epitope of the N279K mutated Tau protein compared with that of wild-type Tau. AD2 signal did not increase at significant levels although an increasing trend was observed. *In vitro* studies have shown that the N279K mutation does not alter the binding of Tau to MTs or decrease the ability of Tau to promote MT assembly (Hong et al., 1998; Barghorn et al., 2000), our results would suggest that phosphorylation of Tau N279K at AT8 epitope could bind to microtubules worse than wild-type Tau.

Effect of the N279K Mutation on Nuclear Localization of Tau in COS-7 Cells

Many studies have indicated that Tau is present in both the cytoplasmic and nuclear compartments (see review Bukar Maina et al., 2016). To analyze the subcellular distribution of Tau N279K, we first performed analysis by

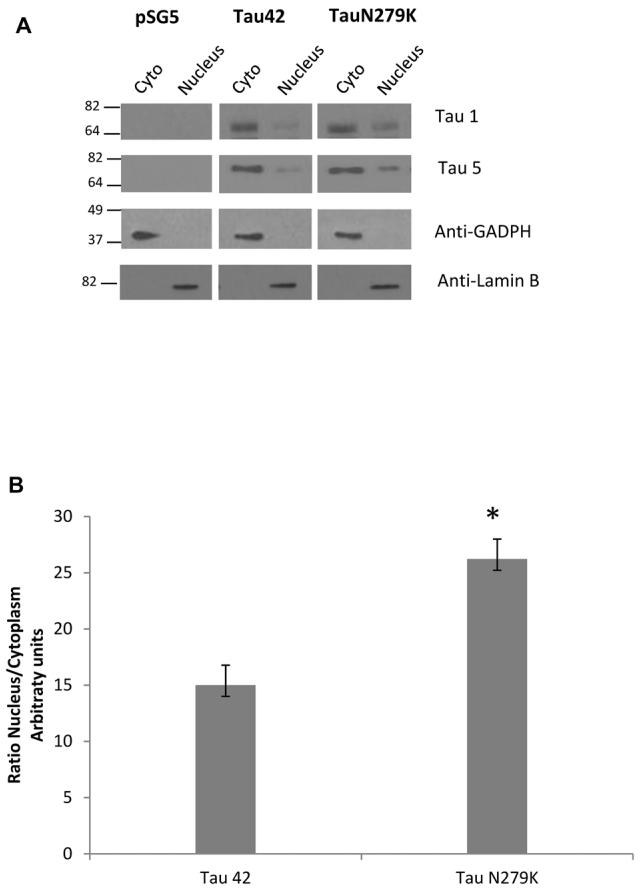

FIGURE 5 | Analysis of Tau localization by Western-blot. **(A)** Representative Western-blot analysis using unphospho-dependent Tau antibody Tau 1 and Tau5. COS-7 cells transfected with both Tau constructs and empty plasmid were subjected to cellular fractionation as described in "Materials and Methods" section. Distribution of Tau was analyzed in cytosolic (Cyto) and nuclear (nucleus) fractions. GADPH and Lamin B were respectively used as specific markers of the cytoplasmic and the nuclear fractions. **(B)** Quantification of ratio Nucleus/Cytoplasm of Tau-1 signal is the mean ± SD ($n = 4$, $^*p < 0.05$).

confocal microscopy for cytoplasmic or nuclear localization of Tau constructs. While Tau 42 showed a preferential cytoplasmic localization, Tau N279K was present in both the cytoplasm and the nucleus (**Figure 4**). To confirm these data obtained by immunofluorescence, we performed subcellular fractionation (see "Materials and Methods" section) on transient transfected COS-7 cells with both plasmids and then analyzed by Western blot analysis with Tau1 antibody (**Figure 5A**). We used anti-GADPH antibody as a cytoplasm marker antibody and the anti-Lamin B1 antibody as a nuclear marker antibody. Tau 42 can be found in the cytosol compartment as well as in the nuclear compartment. This was in agreement with previous results obtained in human neuroblastoma cells (Loomis et al., 1990). Also, we detected Tau N279K in either cytosol as in nucleus fraction, being the levels of Tau N279K in the nucleus slight greater than Tau 42 (approximately it was increased up to 1.5-fold, **Figure 5B**). This result would suggest a role of N279K in subcellular localization of Tau in COS-7 cells.

To confirm that the mutation N279K localizes in the nuclear compartment, we treated COS-7 cells with Leptomycin an inhibitor of nuclear export that blocks the transport of the nuclear export signals (NES)-containing protein from the nucleus to the cytoplasm (Kudo et al., 1998). COS-7 cells were transfected with each of the constructs and cytoplasmic–nuclear Tau localization was analyzed by Western blot (**Figure 6A**). The accumulation of both Tau 42 and Tau N279K was approximately increased up to 2-fold in the nucleus of COS-7 cells after cell treatment with Leptomycin B (**Figure 4B**). Furthermore, transfection of mutant Tau into the cells resulted in a greater nuclear localization respect Tau 42 (**Figure 6B**).

Taken together, data presented in this work suggest that the Tau mutation N279K alters distribution between the cytosol and the nucleus and likely contribute to neurodegeneration.

DISCUSSION

Tau residue N279 has been extensively studied. Thus, this asparagine can be modified by deamination in Alzheimer disease samples (Dan et al., 2013) and it may favor Tau aggregation (Montejo de Garcini et al., 1986). Asparagine-279 can be mutated to lysine causing one of the most frequent causes of familial frontotemporal dementia. That mutation increases Tau4R/Tau3R ratio by altering alternative splicing of exon 10 (Delisle et al., 1999), but has not effects on Tau binding to microtubules or the ability of Tau to promote MT assembly (Hong et al., 1998). In this work, we have analyzed the consequences of that mutation on the subcellular localization of Tau protein.

Our results demonstrate by biochemical and immunohistochemistry studies that N279K mutation alters distribution between the cytosol and the nucleus. We have found that human Tau bearing the mutation N279K is located, in higher proportion than wild-type Tau, at the cell nucleus. Taking into account this, and that NES are domains rich in leucines, we observed that two leucines are found in position 282 and 284. Thus, we wonder if there exist a nuclear export sequence around that epitope. Bioinformatic analysis of all Tau sequence using the neuronal network/hidden Markow model-based prediction method NetNES[2] (la Cour et al., 2004) predicts a NES between residues 277 and 284 in the case of mutant protein. The calculated "NES score" exceeds the threshold between residues 277 and 284 (IIKKKLDL) while wild-type sequence (IINKKLDL) the threshold is only exceeded by the L284 suggesting that N279K mutation participates in generate a stronger nuclear export signal. Interestingly all the sequence is present in exon 10 confirming experimental data suggesting that Tau4R isoforms are found in the nucleus (Liu and Götz, 2013). However, while *in silico* data propose that N279K mutation creates a stronger NES in exon 10,

[2]http://www.cbs.dtu.dk/services/NetNES/

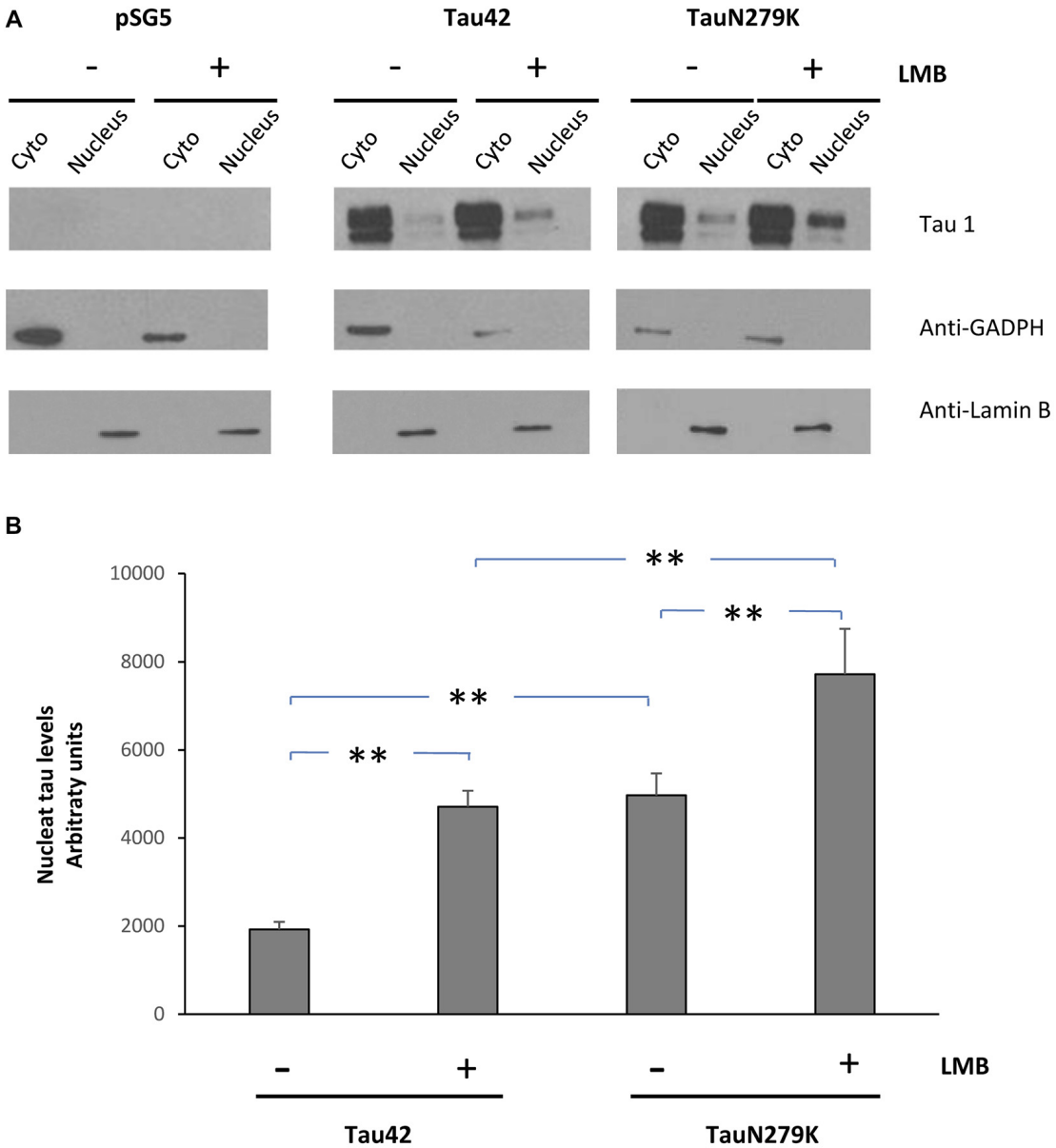

FIGURE 6 | Treatment of cells with an inhibitor of nuclear export, LMB, causes retention of Tau in the nucleus. **(A)** COS-7 cells transfected with empty plasmid, Tau 42 or Tau N279K were incubated with LMB for 1 h. Distribution of Tau was analyzed in cytosolic (Cyto) and nuclear (nucleus) fractions by Western-blot using Tau 1 antibody. GADPH and Lamin B were respectively used as specific markers of the cytoplasmic and the nuclear fractions. **(B)** Quantification of the nucleus intensity of Tau 42 and Tau N279K are shown. Data are mean ± SD ($n = 3$; $^{**}p < 0.01$).

our biochemical data suggested that this is not the case. In fact, overexpression of mutant Tau results in the opposite, an increase in the proportion of mutant Tau presents in the nucleus. In any case, further investigations are necessary in order to know if the export/import nuclear machinery and Tau phosphorylation present in COS-7 cells are different compared with neuronal cells or if the system is saturated in overexpressing cells. It should be taken into account that, as has been recently published (Eftekharzadeh et al., 2017), phosphorylated Tau may disrupt nucleocytoplasmic transport through the binding of phosphoTau to nuclear pore machinery.

We here also show that one of the characteristics of N279K Tau is that is highly phosphorylated compared with wild-type Tau as determined by its interaction with antibody AT8 and AD2. The result of that phosphorylation could be a dysfunction at the nuclear pore, this together with the fact that cytoplasmic aggregates can disrupt nucleocytoplasmic transport of proteins and RNAs (Woerner et al., 2016) could explain to some extent the toxicity of N287K Tau. An additional explanation to the results

obtained would be that taking into account that phosphorylated Tau binds less to microtubules than the unphosphorylated Tau, it is possible that more Tau would be available for redistributing into the nuclear compartment.

It is also possible that other Tau domains could be involved in nuclear Tau localization. Thus, in the adult murine brain, Tau mainly have four microtubule-binding repeats and the presence of only one amino-terminal inserts in the 4R isoform are localized in the nucleus while those 4R isoforms with 0 or 1 amino-terminal inserts N-terminal are hardly localized in the nucleus (Liu and Götz, 2013).

In summary, we like to support the role of exon 10 (Tau 4R) for the presence of Tau at the cell nucleus, a role that could be facilitate by the presence of N279K Tau mutation.

AUTHOR CONTRIBUTIONS

JA, FH and MP conceived and designed the experiments. MR, VG-E and MP performed experiments, analyzed and discussed results. JA, FH and MP wrote the manuscript with feedback from all authors.

FUNDING

This study was funded by grants from the Spanish Ministry of Economy and Competitiveness (Ministerio de Economía y Competitividad; SAF-2014-53040-P (JA) and BFU2016-77885-P (FH)), the Centro de Investigasción Biomédica en Red sobre Enfermedades Neurodegenerativas (CIBERNED, ISCIII; JA).

REFERENCES

Arrasate, M., Pérez, M., and Avila, J. (2000). Tau dephosphorylation at tau-1 site correlates with its association to cell membrane. *Neurochem. Res.* 25, 43–50. doi: 10.1023/A:1007583214722

Avila, J., Lucas, J. J., Perez, M., and Hernandez, F. (2004). Role of tau protein in both physiological and pathological conditions. *Physiol. Rev.* 84, 361–384. doi: 10.1152/physrev.00024.2003

Barghorn, S., Zheng-Fischhöfer, Q., Ackmann, M., Biernat, J., von Bergen, M., Mandelkow, E. M., et al. (2000). Structure, microtubule interactions, and paired helical filament aggregation by tau mutants of frontotemporal dementias. *Biochemistry* 39, 11714–11721. doi: 10.1021/bi000850r

Brandt, R., Leger, J., and Lee, G. (1995). Interaction of tau with the neural plasma membrane mediated by tau's amino-terminal projection domain. *J. Cell Biol.* 131, 1327–1340. doi: 10.1083/jcb.131.5.1327

Buée-Scherrer, V., Condamines, O., Mourton-Gilles, C., Jakes, R., Goedert, M., Pau, B., et al. (1996). AD2, a phosphorylation-dependent monoclonal antibody directed against tau proteins found in Alzheimer's disease. *Mol. Brain Res.* 39, 79–88. doi: 10.1016/0169-328x(96)00003-4

Bukar Maina, M., Al-Hilaly, Y. K., and Serpell, L. C. (2016). Nuclear tau and its potential role in Alzheimer's disease. *Biomolecules* 6:9. doi: 10.3390/biom6010009

Bullmann, T., de Silva, R., Holzer, M., Mori, H., and Arendt, T. (2007). Expression of embryonic tau protein isoforms persist during adult neurogenesis in the hippocampus. *Hippocampus* 17, 98–102. doi: 10.1002/hipo.20255

Camero, S., Benítez, M. J., Cuadros, R., Hernández, F., Avila, J., and Jiménez, J. S. (2014). Thermodynamics of the interaction between Alzheimer's disease related tau protein and DNA. *PLoS One* 9:e104690. doi: 10.1371/journal.pone.0104690

Dan, A., Takahashi, M., Masuda-Suzukake, M., Kametani, F., Nonaka, T., Kondo, H., et al. (2013). Extensive deamidation at asparagine residue 279 accounts for weak immunoreactivity of tau with RD4 antibody in Alzheimer's disease brain. *Acta Neuropathol. Commun.* 1:54. doi: 10.1186/2051-5960-1-54

Dawson, H. N., Cantillana, V., Chen, L., and Vitek, M. P. (2007). The tau N279K exon 10 splicing mutation recapitulates frontotemporal dementia and parkinsonism linked to chromosome 17 tauopathy in a mouse model. *J. Neurosci.* 27, 9155–9168. doi: 10.1523/JNEUROSCI.5492-06.2007

Delisle, M. B., Murrell, J. R., Richardson, R., Trofatter, J. A., Rascol, O., Soulages, X., et al. (1999). A mutation at codon 279 (N279K) in exon 10 of the Tau gene causes a tauopathy with dementia and supranuclear palsy. *Acta Neuropathol.* 98, 62–77. doi: 10.1007/s004010051052

Eftekharzadeh, B., Daigle, J. G., Wegmann, S., Dujardin, S., Schmider, A. B., Godin, M. D., et al. (2017). "Tau protein disrupts nucleocytoplasmic transport in Alzheimer's disease," in *Society for Neuroscience Annual Meeting 2017* 568.11/DP06/L1. Avialable online at: http://www.abstractsonline.com/pp8/#!/4376/presentation/22946

Gauthier-Kemper, A., Suárez Alonso, M., Sündermann, F., Niewidok, B., Fernandez, M. P., Bakota, L., et al. (2018). Annexins A2 and A6 interact with the extreme N terminus of tau and thereby contribute to tau's axonal localization. *J. Biol. Chem.* 293, 8065–8076. doi: 10.1074/jbc.ra117.000490

Gluzman, Y. (1981). SV40-transformed simian cells support the replication of early SV40 mutants. *Cell* 23, 175–182. doi: 10.1016/0092-8674(81)90282-8

Goedert, M., Spillantini, M. G., Potier, M. C., Ulrich, J., and Crowther, R. A. (1989). Cloning and sequencing of the cDNA encoding an isoform of microtubule-associated protein tau containing four tandem repeats: differential expression of tau protein mRNAs in human brain. *EMBO J.* 8, 393–399.

Hong, M., Zhukareva, V., Vogelsberg-Ragaglia, V., Wszolek, Z., Reed, L., Miller, B. I., et al. (1998). Mutation-specific functional impairments in distinct tau isoforms of hereditary FTDP-17. *Science* 282, 1914–1917. doi: 10.1126/science.282.5395.1914

Hutton, M. (2001). Missense and splice site mutations in tau associated with FTDP-17: multiple pathogenic mechanisms. *Neurology* 56, S21–S25. doi: 10.1212/wnl.56.suppl_4.s21

Janning, D., Igaev, M., Sundermann, F., Brühmann, J., Beutel, O., Heinisch, J. J., et al. (2014). Single-molecule tracking of tau reveals fast kiss-and-hop interaction with microtubules in living neurons. *Mol. Biol. Cell* 25, 3541–3551. doi: 10.1091/mbc.E14-06-1099

Kudo, N., Wolff, B., Sekimoto, T., Schreiner, E. P., Yoneda, Y., Yanagida, M., et al. (1998). Leptomycin B inhibition of signal-mediated nuclear export by direct binding to CRM1. *Exp. Cell Res.* 242, 540–547. doi: 10.1006/excr.1998.4136

la Cour, T., Kiemer, L., Mølgaard, A., Gupta, R., Skriver, K., and Brunak, S. (2004). Analysis and prediction of leucine-rich nuclear export signals. *Protein Eng. Des. Sel.* 17, 527–536. doi: 10.1093/protein/gzh062

Liu, C., and Götz, J. (2013). Profiling murine tau with 0N, 1N and 2N isoform-specific antibodies in brain and peripheral organs reveals distinct subcellular localization, with the 1N isoform being enriched in the nucleus. *PLoS One* 8:e84849. doi: 10.1371/journal.pone.0084849

Loomis, P. A., Howard, T. H., Castleberry, R. P., and Binder, L. I. (1990). Identification of nuclear tau isoforms in human neuroblastoma cells. *Proc. Natl. Acad. Sci. U S A* 87, 8422–8426. doi: 10.1073/pnas.87.21.8422

Montejo de Garcini, E., de la Luna, S., Dominguez, J. E., and Avila, J. (1994). Overexpression of tau protein in COS-1 cells results in the stabilization of centrosome-independent microtubules and extension of cytoplasmic processes. *Mol. Cell. Biochem.* 130, 187–196. doi: 10.1007/bf01457399

Montejo de Garcini, E., Serrano, L., and Avila, J. (1986). Self assembly of microtubule associated protein tau into filaments resembling those found in Alzheimer disease. *Biochem. Biophys. Res. Commun.* 141, 790–796. doi: 10.1016/s0006-291x(86)80242-x

Rossi, G., Dalpra, L., Crosti, F., Lissoni, S., Sciacca, F. L., Catania, M., et al. (2008). A new function of microtubule-associated protein tau: involvement in chromosome stability. *Cell Cycle* 7, 1788–1794. doi: 10.4161/cc.7.12.6012

Sergeant, N., Delacourte, A., and Buée, L. (2005). Tau protein as a differential biomarker of tauopathies. *Biochim. Biophys. Acta* 1739, 179–197. doi: 10.1016/j.bbadis.2004.06.020

Sjöberg, M. K., Shestakova, E., Mansuroglu, Z., Maccioni, R. B., and Bonnefoy, E. (2006). Tau protein binds to pericentromeric DNA: a putative role for nuclear tau in nucleolar organization. *J. Cell Sci.* 119, 2025–2034. doi: 10.1242/jcs.02907

Woerner, A. C., Frottin, F., Hornburg, D., Feng, L. R., Meissner, F., Patra, M., et al. (2016). Cytoplasmic protein aggregates interfere with nucleocytoplasmic transport of protein and RNA. *Science* 351, 173–176. doi: 10.1126/science.aad2033

Wren, M. C., Zhao, J., Liu, C. C., Murray, M. E., Atagi, Y., Davis, M. D., et al. (2015). Frontotemporal dementia-associated N279K tau mutant disrupts subcellular vesicle trafficking and induces cellular stress in iPSC-derived neural stem cells. *Mol. Neurodegener.* 10:46. doi: 10.1186/s13024-015-0042-7

Conflict of Interest Statement: The authors declare that the research was conducted in the absence of any commercial or financial relationships that could be construed as a potential conflict of interest.

frontiers in Cellular Neuroscience

ORIGINAL RESEARCH
published: 30 July 2018
doi: 10.3389/fncel.2018.00223

The Microtubule-Modulating Drug Epothilone D Alters Dendritic Spine Morphology in a Mouse Model of Mild Traumatic Brain Injury

*Jyoti A. Chuckowree[1], Zhendan Zhu[1], Mariana Brizuela[1,2], Ka M. Lee[1,3], Catherine A. Blizzard[1] and Tracey C. Dickson[1]**

[1] Menzies Institute for Medical Research, University of Tasmania, Hobart, TAS, Australia, [2] Centre for Neuroscience, School of Medicine, Flinders University, Adelaide, SA, Australia, [3] The Florey Institute of Neuroscience and Mental Health, Parkville, VIC, Australia

Microtubule dynamics underpin a plethora of roles involved in the intricate development, structure, function, and maintenance of the central nervous system. Within the injured brain, microtubules are vulnerable to misalignment and dissolution in neurons and have been implicated in injury-induced glial responses and adaptive neuroplasticity in the aftermath of injury. Unfortunately, there is a current lack of therapeutic options for treating traumatic brain injury (TBI). Thus, using a clinically relevant model of mild TBI, lateral fluid percussion injury (FPI) in adult male Thy1-YFPH mice, we investigated the potential therapeutic effects of the brain-penetrant microtubule-stabilizing agent, epothilone D. At 7 days following a single mild lateral FPI the ipsilateral hemisphere was characterized by mild astroglial activation and a stereotypical and widespread pattern of axonal damage in the internal and external capsule white matter tracts. These alterations occurred in the absence of other overt signs of trauma: there were no alterations in cortical thickness or in the number of cortical projection neurons, axons or dendrites expressing YFP. Interestingly, a single low dose of epothilone D administered immediately following FPI (and sham-operation) caused significant alterations in the dendritic spines of layer 5 cortical projection neurons, while the astroglial response and axonal pathology were unaffected. Specifically, spine length was significantly decreased, whereas the density of mushroom spines was significantly increased following epothilone D treatment. Together, these findings have implications for the use of microtubule stabilizing agents in manipulating injury-induced synaptic plasticity and indicate that further study into the viability of microtubule stabilization as a therapeutic strategy in combating TBI is warranted.

Keywords: traumatic brain injury, fluid percussion injury, neuroplasticity, microtubule stabilization, epothilone D, dendritic spine, cortical projection neuron, mushroom spine

OPEN ACCESS

Edited by:
Jesus Avila, Universidad Autónoma de Madrid, Spain

Reviewed by:
Kevin R. Jones, University of Colorado Boulder, United States
Jennifer Larimore, Agnes Scott College, United States

***Correspondence:**
Tracey C. Dickson
Tracey.Dickson@utas.edu.au

Received: *17 April 2018*
Accepted: *09 July 2018*
Published: *30 July 2018*

Citation:
Chuckowree JA, Zhu Z, Brizuela M, Lee KM, Blizzard CA and Dickson TC (2018) The Microtubule-Modulating Drug Epothilone D Alters Dendritic Spine Morphology in a Mouse Model of Mild Traumatic Brain Injury. Front. Cell. Neurosci. 12:223. doi: 10.3389/fncel.2018.00223

INTRODUCTION

In popular media, mild traumatic brain injury (mTBI) has been referred to as a 'silent epidemic.' Indeed, in a majority of mTBI cases there is distinct absence of clear structural damage alongside normal neuroimaging (Iverson, 2005, 2010; Belanger et al., 2007; Jagoda et al., 2009; Gao and Chen, 2011; Smith et al., 2013). Nevertheless, subtle perturbations in brain structure likely evoke

an insidious cascade of evolving widespread damage to neural circuitry, thought to culminate in long-term and ongoing neurological impairment and associated problems (Büki and Povlishock, 2006; Farkas and Povlishock, 2007; Blyth and Bazarian, 2010; Iverson, 2010; Wang and Ma, 2010; Meaney and Smith, 2011; Johnson et al., 2012a; Hill et al., 2016). This typically incorporates widespread axonal perturbation, known as traumatic axonal injury, throughout the parenchyma and particularly in the white matter tracts. This injury may include changes in the somato-dendritic compartment such as somal atrophy, distorted dendritic arbor geometry and loss of complexity, and decreased dendritic spine density (Chen et al., 2003, 2010; Stone et al., 2004; Spain et al., 2010; Gao and Chen, 2011; Gao et al., 2011; Greer et al., 2011; Campbell et al., 2012).

Data from experimental models shows that mTBI characteristically generates sparse microscopic damage, whereby neural circuits are rendered dysfunctional but not destroyed (Iverson, 2005; DeKosky and Ikonomovic, 2010; Shultz et al., 2016). This highlights an important target for therapeutic intervention. Microtubule disruption and loss is a key ultrastructural hallmark of neuronal injury (Maxwell and Graham, 1997; Tang-Schomer et al., 2012). Moreover, microtubule dynamics are fundamental to a multitude of neuro-glial responses in the aftermath of injury (Chuckowree and Vickers, 2003; Tang-Schomer et al., 2012; Brizuela et al., 2015). Thus, manipulating microtubules provides a novel multi-target approach for intervening in these processes (Brunden et al., 2012; Baas and Ahmad, 2013; Dent, 2016). Of note, microtubule-stabilizing agents of the taxane and epothilone families are used chemotherapeutically at high doses to block the growth of cancerous cells (Goodin, 2004; Michaud, 2009; Zhao et al., 2009; Khrapunovich-Baine et al., 2011). Accumulating data derived from a variety of experimental neural injury and disease paradigms reveals that when used at low doses these drugs have a range of beneficial effects, including dampening detrimental gliotic responses, preventing synapse loss and enhancing adaptive neuronal alterations as well as preserving cognitive and motor functions (Moscarello et al., 2002; Zhang et al., 2005; Andrieux et al., 2006; Ertürk et al., 2007; Brunden et al., 2010, 2011, 2012; Hellal et al., 2011; Sengottuvel et al., 2011; Barten et al., 2012; Tang-Schomer et al., 2012; Baas and Ahmad, 2013; Cartelli et al., 2013; Hur and Lee, 2014; Popovich et al., 2014; Brizuela et al., 2015; Cross et al., 2015; Ruschel et al., 2015; Jang et al., 2016; Penazzi et al., 2016).

The epothilones promote microtubule formation and stabilization, and inhibit microtubule depolymerization (Altmann et al., 2000; Chen et al., 2008). With particular relevance to the brain, epothilones are more water soluble than their taxane counterparts, are blood–brain barrier penetrant, and are retained in the central nervous system for several days after administration (Andrieux et al., 2006; Browne et al., 2011). Importantly, the efficacy of epothilones as a therapeutic strategy in the context of brain injury remains to be elucidated. To address this shortfall we explored the effect of peripherally administered epothilone D following a single mTBI using the clinically relevant lateral fluid percussion brain injury (FPI) model (Thompson et al., 2005). To visualize discrete alterations in the somato-dendritic and axonal compartments of layer 5 cortical excitatory projections neurons we used the Thy1-YFPH mouse, which revealed exquisite neuronal sub-structure (Feng et al., 2000).

MATERIALS AND METHODS

Breeding and Genotyping of Thy1-YFPH Transgenic Mice

All experimental procedures involving animals were approved by the Animal Ethics Committee of the University of Tasmania (ethics approval number A0011076) and are in accordance with the Australian Code of Practice for the Care and Use of Animals for Scientific Purposes. Animals were housed in standard conditions (20°C, 12 h/12 h light/dark cycle) with access to food and water *ad libitum* and monitored daily for signs of stress and illness. Thy1-YFPH line mice [B6.Cg-Tg(Thy1-YFP)HJrs/J, stock number 003782] were obtained from the Jackson Laboratory (Bar Harbor, ME, United States) and maintained as a heterozygous colony. In these animals YFP is expressed under the control of the neuron-specific Thy1 promoter in ∼80% of layer 5 and 2/3 neocortical pyramidal neurons (Feng et al., 2000). Ear punches were taken at weaning (4 weeks) to determine inheritance of the YFP transgene. Tissue was mounted on a glass slide and examined with the 488 nm filter on a Leica DM LB2 microscope (Leica Microsystems Pty Ltd., North Ryde, NSW, Australia). Animals carrying the YFP transgene were identified as possessing YFP-positive (YFP+) axons within their ear clips.

Surgical Preparation

Animals were prepared in groups of four per day. Two animals received FPI while two were sham-operated. Mice were subjected to lateral FPI using an established protocol (Carbonell et al., 1998; Lifshitz et al., 2007; Alder et al., 2011). Briefly, adult male YFP-H mice (10–12 weeks, 25–30 g; n = 12 FPI/brain-injured, n = 12 sham-operated) were anesthetised in a pre-charged induction chamber containing 5% isoflurane (Isoflo, Abbot Australasia Pty Ltd., Botany, NSW, Australia) in 100% O_2. Mice were removed from the induction chamber, pre-emptive analgesia, temgesic (buprenorphine hydrochloride, 0.1 mg/kg; Reckitt Benckiser, West Ryde, NSW, Australia), was administered subcutaneously and the fur covering the scalp was removed. Mice were placed on a homeothermic blanket (Stoelting, Wood Dale, IL, United States) to maintain body temperature at 37°C during surgery and stabilized in a stereotaxic frame (Narishige, Tokyo, Japan) equipped with a nose cone to maintain anesthesia (1–2% isoflurane in 100% O_2). The scalp was cleaned with betadine (Sanofi-aventis Consumer Healthcare, Virginia, QLD, Australia) and 70% ethanol and the topical anesthetic bupivicaine (Bupivicaine hydrochloride, 50 μl 0.25% in sterile saline; Pfizer, West Ryde, NSW, Australia) was administered under the scalp. A midline incision was made to expose the skull from bregma to lambda. The skin was retracted and the fascia covering the skull was removed. A 3.0 mm circular craniectomy was made 2.0 mm posterior and 2.5 mm lateral to bregma on the right hand side of the skull over the somatosensory cortex via manual trephination

with a pin vice equipped with a 2.7 mm trephine drill bit (AgnTho's, Lidingo, Sweden). The underlying dura was left intact. An injury-hub was constructed over the craniectomy – a sterile Luer-Loc syringe hub was cut from a 22-gauge needle, fixed over the craniectomy using Loctite cyanoacrylate (Henkel Australia, Sydney, NSW, Australia), secured to the skull using Paladur dental acrylic (Heraeus Dental Science, Villebon, France), filled with sterile saline and capped with a male Luer-Loc fitting. Pre-, peri-, and post-surgical monitoring was performed to determine respiratory rate, confirm absence of reflexes and monitor mucous membranes/capillary refill time. Following injury-hub placement animals were removed from the stereotaxic frame and allowed to recover in a warmed cage until fully ambulatory (30–60 min) and then placed back in their home cage.

Lateral Fluid Percussion Brain Injury and Drug Treatment

Two hours following application of the injury-hub, once mice had been fully ambulatory for over an hour, each animal was re-anesthetised in a pre-charged induction chamber containing 5% isoflurane in 100% O_2. Following induction of anesthesia, the animal was removed from the induction chamber, the cap was removed from the injury hub and the hub was re-filled with sterile saline and attached to the FP302 Fluid Percussion Device (AmScien Instruments, Richmond, VA, United States) via a 30 cm spacing tube filled with sterile water. The animal was placed on a heated pad and once a normal pattern of breathing resumed, but prior sensitivity to stimulation, an injury of mild severity (1.5 $\pm$ 0.1 atmospheres) was delivered to the intact dura by releasing device's pendulum onto a fluid filled piston, causing transient displacement and deformation of the dura and underlying brain. A transducer incorporated into the device measured the pulse pressure and the peak pressure was recorded within the software. Following injury, animals were placed on their back and visually monitored for recovery of spontaneous breathing. Additionally, the time taken for animals to recover the righting reflex was recorded as a measure of transient unconsciousness/loss of consciousness. Following injury, we did not record any convulsions, mortalities or other complications. Sham-operated animals underwent identical procedures to FPI animals, however, the pendulum was not released. Mice were re-anesthetised, the injury hub was removed and the incision sutured. Immediately following suturing, animals were administered with either epothilone D (2 mg/kg, i.p.; Anita Laboratories, Hangzhou, China; n = 6 FPI and n = 6 sham-operated) or vehicle (equivalent volume DMSO; n = 6 FPI and n = 6 sham-operated). Mice received drug/vehicle treatment within 20 min following completion application of the FPI/Sham-operation. Animals were placed in a heated cage and monitored during the recovery period until fully ambulatory (30–60 min), prior to return to their home cage.

Immunohistochemistry

At 1 week post-injury/sham-operation, mice were intraperitoneally injected with a terminal dose of sodium pentobarbital (300 mg/kg; Troy Laboratories Pty Ltd., Smithfield, NSW, Australia) and transcardially perfused with 4% paraformaldehyde in 0.1 M phosphate buffer. Brains were post-fixed *in vivo* for 24 h at 4°C. Each brain was removed from the skull, embedded in 5% agarose in 0.01 M phosphate buffered saline (PBS) and free-floating coronal sections (50 μm) were cut using a Leica VT1000S vibratome (Leica Biosystems Australia Pty Ltd., Mount Waverly, VIC, Australia) to incorporate the entire injury impact site as well as 0.5–1.0 mm anterior and posterior to this. Sections were serially collected into Costar 24-well culture plates (Corning Life Sciences, New York, NY, United States) containing 0.01M PBS and 0.02% sodium azide and stored until required.

To perform immunohistochemistry, every sixth section from each brain was moved into a fresh culture plate well to represent the injury site. Prior to immunohistochemistry, sections were rinsed in three washes of 0.01 M PBS. Sections then underwent immunofluorescence labeling for glial fibrillary acidic protein (GFAP). Briefly, sections were incubated in rabbit anti-GFAP (1:2000; DAKO, Z0334, Glostrup, Denmark) in diluent (0.01 M PBS with 0.03% Triton X-100) at 4°C for ∼20 h, washed, incubated in goat anti-rabbit Alexa 568 (1:1000; Invitrogen BRL, Life Technologies, Grand Island, NY, United States) and DAPI (1:6000; Invitrogen, D3571) in 0.01M PBS for 1.5 h, washed and mounted serially onto slides (Livingstone International Pty Ltd., Rosebery, NSW, Australia) with Permafluor mounting media (Thermo Scientific, Scoresbury, VIC, Australia).

Microscopy and Image Analysis

Images were collected with an UltraVIEW spinning disk confocal microscope running Volocity Software (PerkinElmer Pty Ltd., Glen Waverley, VIC, Australia), equipped with a 20×/0.5 air, 40×/0.95 air and Plan Apo 60×/1.20 water objective (Nikon, New York, NY, United States). For quantitation of cortical thickness, YFPH cell number and size and degenerated/dystrophic axonal bulb number and size (in the internal and external capsules) the microscope was configured to capture large stitched images of the upper hemispheric quadrant of each brain (20 μm z-stacks, 1 μm slices) with the 20× objective from three representative sections throughout the injury, designated middle, anterior, and posterior representing the middle section (first appearance of two blades of the dentate gyrus) as well as the section 300 μm anterior and 300 μm posterior to this. Using ImageJ freeware (Schneider et al., 2012) the cortex, external and internal capsule were traced in each of the three sections and within these anatomical boarders the individual YFPH+ cells in the cortex and axonal bulbs/dystrophic neurites in the external and internal capsules were traced for quantitation of size and density. To determine the axonal degeneration index (degenerating/beaded YFPH+ axons) single 40× magnification image stacks (20 μm z-stacks, 1 μm slices) were collected from the same three sections as used for the prior analysis. Images for the external capsule were captured from the white matter on the medio-lateral boarder of the lateral ventricle and those for the internal capsule were captured half way between the dorsal and ventral boarder of the internal capsule. For quantification of astrocyte activation (percent area occupied by GFAP expressing astrocytes), 20× single image stacks (20 μm z-stacks, 1 μm slices) were collected from the

same regions used for analysis of axonal denegation, in addition to layer 2/3 of the cortex directly under the impact site. Analysis of percentage area GFAP and YFPH+ axonal degeneration was performed using ImageJ freeware. For dendritic spine analysis, image stacks were captured with the 60× water objective (0.2 μm slices). Image stacks were collected from layer 4/5 directly under the injury site. These included the image in the middle of the impact site as well as an image medial and lateral to this. All layer 5 apical dendrite obliquely projecting branches were traced from each stack and the spines contained on these dendrites were traced in Neurolucida (MBF Biosciences, Williston, VT, United States). Morphology data was generated by allocating each spine to one of three categories, mushroom (prominent head, thin neck), stubby (greater width than length), and thin (greater length than width). Changes in dendritic spine density, length, and morphology were determined by loading Neurolucida data files into Neurolucida Explorer™ (MBF Biosciences).

Statistical Analysis

Data was analyzed (and graphs created) in GraphPad Prism (version 6.0, La Jolla, CA, United States) using unpaired *t*-tests with Welch's correction, or one- or two-way analysis of variance (ANOVA) followed by Tukey's multiple comparison test. Averaged values were expressed as means ± standard error of the mean (SEM). A *p*-value of <0.05, designated *, was considered statistically significant. Figures were prepared in Adobe Illustrator CS6 (version 16.0.0, Adobe Systems, San Jose, CA, United States).

RESULTS

A Single Mild Lateral FPI Caused a Transient Loss of Consciousness in the Absence of Overt Morphological Change

Adult male Thy1-YFPH mice received a single mild lateral FPI or sham-operation followed by epothilone D or vehicle treatment and were perfused 7 days later. In brain-injured mice the acute post-injury period was characterized by a transient loss of consciousness, including a short interval of apnoea (0.21 ± 0.04 min) and a significant delay in the righting reflex (3.64 ± 1.63 min in brain-injured relative to 0.19 ± 0.13 min in sham-operated animals; $p < 0.0001$, unpaired *t*-test with Welch's correction). By 7 days post-injury, there were no gross morphological alterations in the brain following a single mild lateral FPI: cortical thickness, as well as the number and somal size of cortical layer 5 YFP+ projection neurons, remained unchanged (**Table 1**, $p > 0.05$ for all comparisons). Moreover, there was no change in axonal number (axons per field of view) in the external and internal capsules, or the length of apical oblique dendrites (total length of dendrite per field of view) of layer 5 pyramidal neurons (**Table 1**). Epothilone D treatment did not significantly ($p > 0.05$ for all comparisons) affect any of these parameters, with cortical thickness, number and size of YFP+ cells, number of YFP+ axons in both the external and internal capsules and length of YFP+ apical oblique dendrites remaining unaltered following peripherally administered epothilone D (**Table 1**).

Epothilone D Treatment Altered Dendritic Spine Length, density, and Morphology

Dendritic spines were analyzed from radially projecting/oblique branches of layer 5 projection neuron apical dendrites at the layer 4/5 boarder (**Figures 1A,B**). All major morphological spine classes (mushroom, stubby, thin) were represented in all mouse groups (**Figure 1C**). Initial analysis segregated the total spine population by length – spines (<2.5 μm) and filopodia (>2.5 μm) (Hering and Sheng, 2001) – and revealed a significant decrease ($p < 0.05$) in average spine length (**Figure 1D**), but not filopodial length (**Figure 1E**), in response to epothilone D treatment relative to vehicle treatment in both brain-injured and sham-operated animals. Furthermore, binning the spines by length showed that epothilone D treatment resulted in a significantly higher proportion ($p < 0.05$) of shorter (<1.5 μm) spines and significantly lower proportion ($p < 0.05$) of longer spines (1.5–2.5 μm) (**Figure 1F**). With respect to density, spine density was significantly increased ($p < 0.05$) in sham-operated, but not brain-injured animals (**Figure 1G**) in response to epothilone D treatment, whereas filopodial density was unaltered in both sham-operated and brain-injured animals (**Figure 1H**). Analysis of morphological sub-class revealed a significant increase ($p < 0.05$) specifically in mushroom spines in both brain-injured and sham-operated animals in response to epothilone D treatment (**Figure 1I**).

TABLE 1 | Histological analyses comparing brain-injured and sham-operated animals following drug treatment.

	Sham veh	FPI veh	Sham Epo	FPI Epo
Cortical thickness (mm)	1.11 ± 0.06	1.07 ± 0.05	1.10 ± 0.05	1.08 ± 0.05
YFP+ cell density (per mm^2)	36.67 ± 8.85	38.50 ± 10.43	35.67 ± 8.31	36.4 ± 4.72
YFP+ cell size (μm^2)	159 ± 14.11	158.5 ± 13.4	159.67 ± 12.03	161.6 ± 6.54
Number axons Ext cap (per fov)	105.17 ± 24.12	101.5 ± 25.49	110.33 ± 26.46	83.83 ± 35.61
Number axons Int cap (per fov)	166.5 ± 20.81	164.33 ± 27.86	167.33 ± 35.24	161 ± 40.33
Dendrite length (μm)	1.27 ± 0.57	1.12 ± 0.51	1.08 ± 0.38	1.10 ± 0.37

Mice were exposed to a lateral fluid percussion injury or sham-operation and treated with epothilone D (2 mg/kg) or vehicle. Histological analyses confirmed there were no significant differences ($p > 0.05$) between groups for any of the parameters assessed. Ext cap, external capsule; int cap, internal capsule; fov, field of view; veh, vehicle; Epo, epothilone D; FPI, lateral fluid percussion injury.

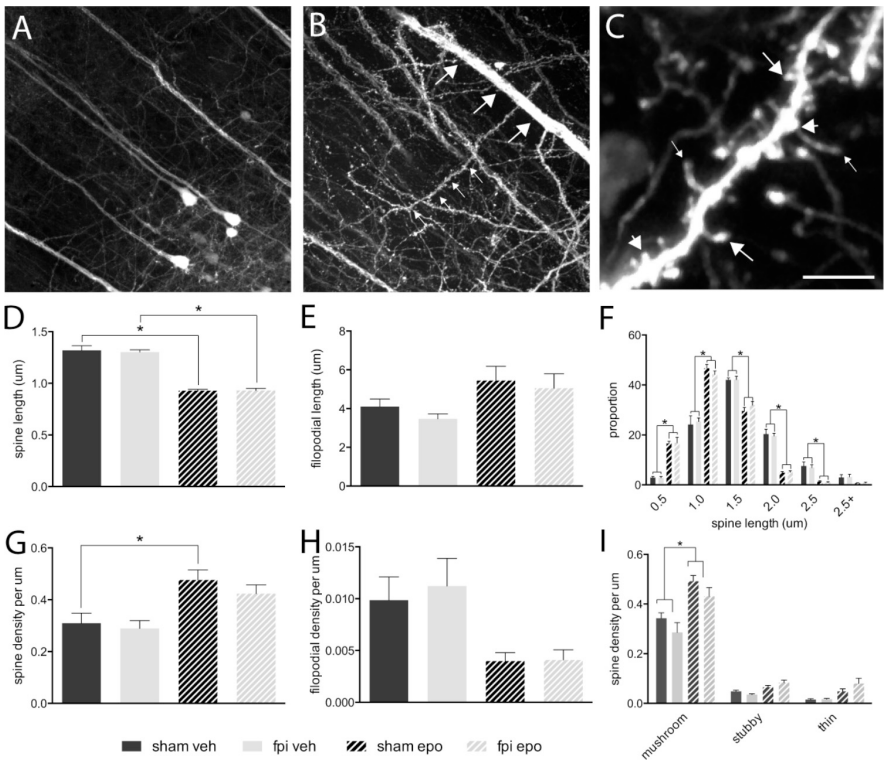

FIGURE 1 | Dendritic spine alterations in layer 5 pyramidal neurons in the adult mouse brain following mild lateral fluid percussion brain injury and epothilone D treatment. Analysis was performed on layer 5 YFP-expressing neuron **(A)** apical oblique dendrites, which are laterally projecting spiney dendrites in layer 4/5 (small arrows, **B**) protruding from layer 5 neuron apical dendrites (large arrows, **B**). For analysis, dendritic protrusions/spines were classified both by length (spines <2.5 μm, **D**,**F**; filopodia > 2.4 μm, **E**,**G**) and morphology (**C**,**I**): either mushroom (large arrows in **C**), stubby (short arrows in **C**), or thin (small arrows in **C**). Epothilone D treatment resulted in a significant decrease in spine length in both brain-injured and sham-operated animals, relative to their vehicle-treated controls **(D)**, whereas filopodial length was unaffected **(E)**. Binning the data by length revealed that epothilone D treatment resulted in a significantly higher proportion of shorter spines (up to 1.5 μm) and significantly lower proportion of longer spines (1.5–2.5 μm) **(F)**. Moreover, epothilone D treatment significantly increased the density of dendritic spines in sham-operated, but not brain-injured animals **(G)**, while filopodial density was unaffected **(H)**. Analysis by morphological sub-class showed that the epothilone D treatment resulted in increased density of mushroom spines in both brain-injured and sham-operated animals relative to their vehicle-treated counterparts, while density of stubby and thin spines was unaffected **(I)**. Data are presented as mean ± SEM and were analyzed by one-way **(D,E,G,H)** or two-way **(F,I)** ANOVA, followed by Tukey's multiple comparison test. A p-value of < 0.05 was considered significant (*). Scale bar **(A)** = 85 μm; **(B)** = 45 μm; **(C)** = 3.5 μm. Yellow fluorescent protein (YFPH); sham-operated, vehicle-treated (sham veh); fluid percussion injury, vehicle-treated (fpi veh), sham-operated, epothilone D-treated (sham epo); fluid percussion injury, epothilone D-treated (fpi epo).

Axonal Degeneration in the External and Internal White Matter Tracts Was a Major Feature of the Injured Brain and Was Not Altered by Epothilone D Treatment

By 7 days post-injury, a single mild lateral FPI had generated a distinct pattern of ipsilateral axonal damage throughout the external (**Figure 2A**) and internal (**Figure 2B**) capsule white matter tracts. Although the majority (85–90%) of YFP expressing axons remained intact, a significant proportion ($p < 0.05$) of axons showed a degenerating, beaded morphology or a disconnected, degenerated and bulbar axonal fragment morphology within the ipsilateral external capsule of brain-injured relative to sham-operated animals (**Figures 2C,D**). These axonal changes after mild FPI did not reach significance in the ipsilateral internal capsule (**Figure 2D**) or contralateral external capsule (not shown). Further analysis of the axonal response to mild FPI revealed that number and size of degenerated/dystrophic bulbar axonal fragments was significantly increased ($p < 0.05$) in the ipsilateral external capsule (**Figures 2E,F**). Moreover, degenerated axonal bulb number, but not size, was significantly increased ($p < 0.05$) in the ipsilateral internal capsule (**Figures 2E,F**) after mild FPI. Interestingly, epothilone D treatment did not alter any aspect of the axonal response to mild FPI (**Figures 2D–F**).

Mild Lateral FPI Evoked a Limited Ipsilateral Astrogliotic Response That Was Not Influenced BY Epothilone D Treatment

Astrocyte activation was quantitated as the area occupied by GFAP immunoreactive profiles at 7 days post-injury. GFAP was significantly increased ($p < 0.05$) in the ipsilateral vs. contralateral cortex of all mice (sham-operated vehicle treated ipsilateral cortex, 6.20 ± 0.68% vs. sham-operated vehicle

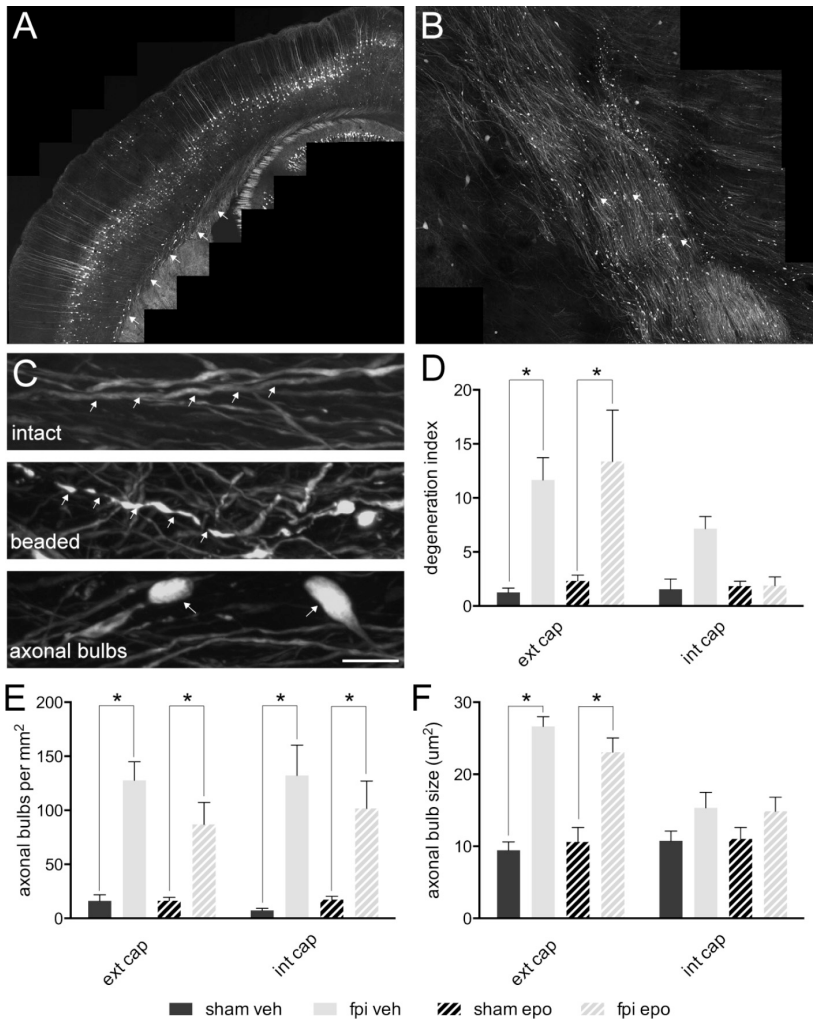

FIGURE 2 | Axonal alterations in major white matter tracts in the adult mouse brain following mild lateral fluid percussion brain injury and epothilone D treatment. Mild lateral fluid percussion injury to the adult mouse brain generated a stereotypical and widespread pattern of axonal damage in the external **(A)** and internal **(B)** capsule white matter tracts. At 7 days post-injury the majority of axons remained intact (arrows, upper panel in **C**), while a proportion showed a degenerating, beaded morphology (arrows, middle panel in **C**) or a degenerated, fragmented and disconnected 'axonal bulb' morphology (arrows, lower panel in **C**). The proportion of beaded axons (out of the total axon population) was significantly increased in the ipsilateral external capsule of brain-injured animals relative to their sham-operated counterparts, but was unaltered in the ipsilateral internal capsule **(D)**. Analysis of axonal bulbs indicated that there were significantly more axonal bulbs in both the external and internal capsules of brain-injured animals relative to their sham-operated counterparts **(E)**. Moreover, axonal bulbs were significantly larger in the external, but not internal, capsule of brain injured animals relative to their sham-operated counterparts **(F)**. Data are presented as mean ± SEM and were analysed by two-way ANOVA **(D–F)** followed by Tukey's multiple comparison test. A p-value < 0.05 was considered significant (*). Scale bar **(A)** = 400 μm; **(B)** = 125 μm; **(C)** = 10 μm. Sham-operated, vehicle-treated (sham veh); fluid percussion injury, vehicle-treated (fpi veh); sham-operated, epothilone D-treated (sham epo); fluid percussion injury, epothilone D-treated (fpi epo); ipsilateral external capsule (ext cap); ipsilateral internal capsule (int cap).

treated contralateral cortex, 2.98 ± 0.37%; brain-injured vehicle treated ipsilateral cortex, 6.13 ± 0.79% vs. brain-injured vehicle treated contralateral cortex, 3.23 ± 0.54%; sham-operated epothilone treated ipsilateral cortex, 5.91 ± 0.64% vs. sham-operated epothilone treated contralateral cortex, 5.61 ± 0.32%; brain-injured epothilone treated ipsilateral cortex, 5.61 ± 0.32% vs. brain-injured epothilone treated contralateral cortex, 2.87 ± 0.25%), indicating that the craniectomy itself generated mild astroglial activation. More interestingly, GFAP immunoreactive profiles (as measured by percentage area occupied by GFAP immunoreactivity) were significantly increased in the external capsule of brain-injured animals (vehicle-treated 5.79 ± 0.49%; epothilone-treated 5.20 ± 0.55%) relative to their sham-operated (vehicle-treated 3.58 ± 0.05%; epothilone-treated 3.63 ± 0.53%) controls; however, this change did not extend to the internal capsule.

DISCUSSION

Despite the absence of overt structural damage and the presence of normal neuroimaging in a majority of mTBI

cases, subtle widespread and progressing damage within neural circuits is thought to underlie the development, and potentially ongoing evolution, of impairments in neurosensory, cognitive, psychosocial, and physical function (Iverson, 2005, 2010; Farkas and Povlishock, 2007; Dean and Sterr, 2013; McMahon et al., 2014; Hill et al., 2016; Shultz et al., 2016; Wang and Li, 2016; Wilde et al., 2016; de Koning et al., 2017). The cellular alterations contributing to pathology in the aftermath of mTBI are not fully understood and there exists no treatment to halt or reverse the damage to neural circuits. Thus, we investigated the discrete subcellular reactions of axonal and somato-dendritic compartments following transient structural brain injury and epothilone D-induced microtubule stabilization. We should note that this study represents a proof-of-concept investigation demonstrating that peripherally administered epothilone D can enter the brain and have an effect on neurons. In accordance with established protocols (Carbonell et al., 1998; Spain et al., 2010; Alder et al., 2011) we showed that a single episode of mild TBI generated significant loss of consciousness, as measured by injury-induced apnoea and delayed righting, in the absence of overt macroscopic change. At the cellular level there was no significant loss of YFP+ neurons, axons or dendrites or dendritic spines and no evidence of neuronal atrophy by 7 days post injury. Moreover, the dose of epothilone D was well tolerated and there were no overt indications of ill health or drug-induced cellular degeneration.

Dendritic spine loss is a characteristic feature of a variety of diseases and injuries of the nervous system (Fiala et al., 2002a; Campbell et al., 2012). Moreover, synapse loss is a likely key candidate for the emergence of functional deficits following TBI. Correct functioning of the neuronal cytoskeleton is crucial for the maintenance of neuronal integrity. Actin has a well-established and integral role in the function of dendritic spines (Matus, 2000; Hotulainen and Hoogenraad, 2010; Lei et al., 2016). More recently, microtubules have been implicated in spine formation and maintenance (Gu et al., 2008; Jaworski et al., 2009; Kapitein et al., 2010; Dent, 2016). To determine the effect of microtubule stabilization at the level of dendritic spines, and to avoid any potential confounding effects of the craniotomy, we examined spines on the radially projecting branches, residing in layer 4/5, of layer 5 YFP+ cortical projection neuron apical dendrites. Interestingly, while filopodia remained unaltered in terms of both length and density, epothilone D had dramatic effects on the spine population, causing an overall reduction in spine length, a shift to a greater proportion of short spines, and an increase in the formation of mushroom spines. The increase in spine density, specifically of mushroom spines, was an unanticipated response to epothilone D treatment and was observed both within the brain-injured and sham-operated cortex. This may indicate a more generalized effect of microtubule stabilization at the subtle level of the dendritic spine, rather than a neuroprotective effect of the drug evoked by injury. It is notable that the increase in spine density occurred specifically in the mushroom spines, which have previously been shown to be a relatively stable population likely to host synapses (Hering and Sheng, 2001; Fiala et al., 2002b). Although we were unable to trace axons to determine innervation interactions between degenerating axons and newly formed spines or determine the functionality of the newly formed spines using the current methodology, future studies quantifying colocalization of synaptic markers, ultrastructural and electorphysiological analysis as well as *in vivo* imaging of synaptic turnover could be used to determine the presense/absence and functionality of synapses on newly formed spines and validate the therapeutic potential of epothilone D.

Although the current study did not directly address the mechanism by which epothilone D increased spine density, it is plausibile that this may be due to a direct effect on the spines themselves, the axons innervating the spines or a more indirect effect. Nonetheless, in terms of therapeutic potential, microtubule stabilization may be useful for preserving spine and synapse integrity following injury. In accordance with this, we revealed a distinct increase in spine density following epothilone treatment. Moreover, spine restoration has been demonstrated following epothilone D treatment in an Alzheimer's disease model (Penazzi et al., 2016). Although further investigations into the mechanisms of spine generation and maintenance by epothilone D are required, we postulate that microtubule stabilization and polymerization with epothilone D may prevent microtubule disassembly and catastrophe within both the dendrite shaft and spines, preserving spine integrity and reducing spine loss. If spine generation continues, this may contribute to an overall increase in spine density. Whether this is a detrimental or beneficial response in the aftermath of mTBI remains to be elucidated. Interestingly, since changes in spine morphology have been linked to alterations in synaptic strength and implicated in learning and memory (Bourne and Harris, 2007; Gu et al., 2008; Jaworski et al., 2009), manipulation of microtubule dynamics could potentially be used to modulate these parameters. As the epothilone D induced increase in spine density was unanticipated, based on previous literature future studies should determine whether these alterations evoke measureable functional responses in terms of electrophysiological and functional output.

Mild TBI has been described as a progressive disorder. Although we did not see a significant loss of axons, dendrites or spines by 7 days post-injury in the current study, there was certainly observable axonal damage throughout the ipsilateral cortex and white matter. Interestingly, the epothilone D treatment regime used in the current study did not have a protective effect on degenerating axons and our previous study using a mouse model of amyotrophic lateral sclerosis showed chronic epothilone D exposure may be detrimental to axons (Clark et al., 2018). However, using an *in vitro* model of structural axonal injury we have previously shown that low dose epothilone D has a protective effect on injured axons by increasing injury-induced axonal sprouting (Brizuela et al., 2015), indicating that microtubule stabilization within damaged axons may be partially responsible for the previously described neuroprotective effect of epothilone D and may have feed forward effects with regard to dendritic spine innervation. If followed to

later post-injury time points, it is possible we may have observed evidence of neuronal atrophy, progressive axonal degeneration and spine loss following mild lateral FPI, as has been shown in other studies of brain injury (Fiala et al., 2002a; Chen et al., 2010; Gao and Chen, 2011; Gao et al., 2011; Greer et al., 2011; Campbell et al., 2012; Johnson et al., 2012b; Winston et al., 2013) and the previously described therapeutic effects of epothilone D may have been revealed. In our hands, and in accordance with previous studies, mild lateral FPI generated widespread traumatic axonal injury, which was particularly evident in the external and internal capsule white matter tracts (Smith and Meaney, 2000; Spain et al., 2010; Wang and Ma, 2010; Ekmark-Lewen et al., 2013; Smith et al., 2013; Hill et al., 2016). This included both beaded, degenerating axons and degenerated, dystrophic axonal fragments/bulbs. Both phenotypes have been reported in the literature and may represent stages of degeneration, differences in vulnerability between different axonal sub-classes or brain regions, or be specific to the mechanical forces sustained during injury (Reeves et al., 2005; Browne et al., 2011; Hånell et al., 2014).

Interestingly, axonal sprouting has been observed in certain classes of damaged axons in experimental models of brain injury (Salin et al., 1995; Batchelor et al., 2002; Deller et al., 2006; Dickson et al., 2007; Blizzard et al., 2011; Greer et al., 2011). Although not observed in the current study, it is possible that epothilone D could be used to modulate this response. Indeed, using an *in vitro* model, we have shown that epothilone D has dose-dependent effects on regenerating cortical neurons (Brizuela et al., 2015). This concept has important implications for dose-dependent modulation of axonal sprouting *in vivo*, for example enhancing adaptive regenerative attempts or dampening maladaptive sprouting, which may underlie the development of epileptic activity in the aftermath of injury (Santhakumar et al., 2001; Kharatishvili et al., 2006; Bolkvadze and Pitkänen, 2012).

In response to FPI we observed mild ipsilateral astroglial activation in the absence of glial scar formation. Contrary to previous studies, astroglial activation was not influenced by microtubule stabilization in the current study (Hellal et al., 2011; Popovich et al., 2014; Ruschel et al., 2015). This may have been due to a range of factors including the type of agent used (a taxane versus an epothilone), the concentration or timing of the epothilone D dose, the mild nature of the glial activation, or the context of the injury (for example, brain versus spinal cord). The absence of an observable injury-induced alteration in dendritic spine density in the current study may have been due to the spine population investigated, the proximity of the spines to the site of impact, the brain region assessed and its proximity to the injury, as well as the time point at which analysis was performed. Therefore, to elucidate the efficacy of microtubule stabilization as a therapeutic intervention for mTBI further investigations will be required to reveal the full repertoire of effects of microtubule stabilization in both the acute and chronic phases of the injury response. Future studies will use a range of dose regimes, including various concentrations and times of administration throughout the post-injury sequalae, to capture the dynamic aspects of injury-induced degeneration and remodeling.

In summary, our findings indicate that peripherally administered microtubule-stabilizing drugs alter synaptic plasticity at the level of the dendritic spine. This has important implications for controlling neuroplasticity in the aftermath of brain injury. More generally, microtubule-stabilizing agents may be useful for manipulating various aspects of the neuro-glial response to injury and disease, as well as providing a modulatory tool for investigating microtubule dynamics *per se*. Due to the ubiquity of microtubules it will be imperative to consider the full repertoire of roles in which they are involved, and take into consideration the interplay between intrinsic factors such as neuronal class and age and extrinsic factors such as the type and severity of injury.

AUTHOR CONTRIBUTIONS

All authors have made a substantial contribution to the work and approved it for publication. Specifically JC, TD, CB conceived and designed the experiments, wrote the manuscript and analyzed and interpreted the data. JC, ZZ, MB, and KL performed the experiments and acquired the data.

FUNDING

This research was supported by the National Health and Medical Research Council of Australia, Select Foundation, Brain Foundation Australia, Motor Accident Insurance Board Tasmania, Flack Foundation, Internal Research Grant Scheme (University of Tasmania), and Tasmanian Masonic Centenary Medical Research Foundation.

ACKNOWLEDGMENTS

We would like to thank Dr. Katherine Lewis for technical editing and proofreading the manuscript.

REFERENCES

Alder, J., Fujioka, W., Lifshitz, J., Crockett, D. P., and Thakker-Varia, S. (2011). Lateral fluid percussion: model of traumatic brain injury in mice. *J. Vis. Exp.* 54:3063. doi: 10.3791/3063

Altmann, K. H., Wartmann, M., and O'Reilly, T. (2000). Epothilones and related structures – a new class of microtubule inhibitors with potent in vivo antitumor activity. *Biochim. Biophys. Acta* 1470, M79–M91. doi: 10.1016/S0304-419X(00)00009-3

Andrieux, A., Salin, P., Schweitzer, A., Bégou, M., Pachoud, B., Brun, P., et al. (2006). Microtubule stabilizer ameliorates synaptic function and behavior in a mouse model for schizophrenia. *Biol. Psychiatry* 60, 1224–1230. doi: 10.1016/j.biopsych.2006.03.048

Baas, P. W., and Ahmad, F. J. (2013). Beyond taxol: microtubule-based treatment of disease and injury of the nervous system. *Brain* 136, 2937–2951. doi: 10.1093/brain/awt153

Barten, D. M., Fanara, P., Andorfer, C., Hoque, N., Wong, P. Y. A., Husted, K. H., et al. (2012). Hyperdynamic microtubules, cognitive deficits, and pathology are

improved in Tau transgenic mice with low doses of the microtubule-stabilizing agent BMS-241027. *J. Neurosci.* 32, 7137–7145. doi: 10.1523/JNEUROSCI.0188-12.2012

Batchelor, P., Porritt, M., Martinello, P., Parish, C., Liberatore, G., Donnan, G., et al. (2002). Macrophages and microglia produce local trophic gradients that stimulate axonal sprouting toward but not beyond the wound edge. *Mol. Cell. Neurosci.* 21, 436–453. doi: 10.1006/mcne.2002.1185

Belanger, H. G., Vanderploeg, R. D., Curtiss, G., and Warden, D. L. (2007). Recent neuroimaging techniques in mild traumatic brain injury. *J. Neuropsychiatry Clin. Neurosci.* 19, 5–20. doi: 10.1176/jnp.2007.19.1.5

Blizzard, C. A., Chuckowree, J. A., King, A. E., Hosie, K. A., Mccormack, G. H., Chapman, J. A., et al. (2011). Focal damage to the adult rat neocortex induces wound healing accompanied by axonal sprouting and dendritic structural plasticity. *Cereb. Cortex* 21, 281–291. doi: 10.1093/cercor/bhq091

Blyth, B. J., and Bazarian, J. J. (2010). traumatic alterations in consciousness: traumatic brain injury. *Emerg. Med. Clin. North Am.* 28, 571–594. doi: 10.1016/j.emc.2010.03.003

Bolkvadze, T., and Pitkänen, A. (2012). Development of post-traumatic epilepsy after controlled cortical impact and lateral fluid-percussion-induced brain injury in the mouse. *J. Neurotrauma* 29, 789–812. doi: 10.1089/neu.2011.1954

Bourne, J., and Harris, K. M. (2007). Do thin spines learn to be mushroom spines that remember? *Curr. Opin. Neurobiol.* 17, 381–386. doi: 10.1016/j.conb.2007.04.009

Brizuela, M., Blizzard, C. A., Chuckowree, J. A., Dawkins, E., Gasperini, R. J., Young, K. M., et al. (2015). The microtubule-stabilizing drug Epothilone D increases axonal sprouting following transection injury in vitro. *Mol. Cell. Neurosci.* 66(Pt B), 129–140. doi: 10.1016/j.mcn.2015.02.006

Browne, K. D., Chen, X.-H., Meaney, D. F., and Smith, D. H. (2011). Mild traumatic brain injury and diffuse axonal injury in swine. *J. Neurotrauma* 28, 1747–1755. doi: 10.1089/neu.2011.1913

Brunden, K. R., Ballatore, C., Lee, V. M., Smith, A. B., and Trojanowski, J. Q. (2012). Brain-penetrant microtubule-stabilizing compounds as potential therapeutic agents for tauopathies. *Biochem. Soc. Trans.* 40, 661–666. doi: 10.1523/JNEUROSCI.0780-09.2009

Brunden, K. R., Yao, Y., Potuzak, J. S., Ferrer, N. I., Ballatore, C., James, M. J., et al. (2011). The characterization of microtubule-stabilizing drugs as possible therapeutic agents for Alzheimer's disease and related tauopathies. *Pharmacol. Res.* 63, 341–351. doi: 10.1016/j.phrs.2010.12.002

Brunden, K. R., Zhang, B., Carroll, J., Yao, Y., Potuzak, J. S., Hogan, A.-M., et al. (2010). Epothilone D improves microtubule density, axonal integrity, and cognition in a transgenic mouse model of tauopathy. *J. Neurosci.* 30, 13861–13866. doi: 10.1523/JNEUROSCI.3059-10.2010

Büki, A., and Povlishock, J. T. (2006). All roads lead to disconnection?–Traumatic axonal injury revisited. *Acta Neurochir.* 148, 181–193; discussion193–184. doi: 10.1007/s00701-005-0674-4

Campbell, J. N., Register, D., and Churn, S. B. (2012). Traumatic brain injury causes an FK506-sensitive loss and an overgrowth of dendritic spines in rat forebrain. *J. Neurotrauma* 29, 201–217. doi: 10.1089/neu.2011.1761

Carbonell, W. S., Maris, D. O., McCall, T., and Grady, M. S. (1998). Adaptation of the fluid percussion injury model to the mouse. *J. Neurotrauma* 15, 217–229. doi: 10.1089/neu.1998.15.217

Cartelli, D., Casagrande, F., Busceti, C. L., Bucci, D., Molinaro, G., Traficante, A., et al. (2013). Microtubule alterations occur early in experimental parkinsonism and the microtubule stabilizer epothilone D is neuroprotective. *Sci. Rep.* 3:1837. doi: 10.1038/srep01837

Chen, J. R., Wang, T. J., Wang, Y. J., and Tseng, G. F. (2010). The immediate large-scale dendritic plasticity of cortical pyramidal neurons subjected to acute epidural compression. *Neuroscience* 167, 414–427. doi: 10.1016/j.neuroscience.2010.02.028

Chen, J.-R., Wang, Y.-J., and Tseng, G.-F. (2003). The effect of epidural compression on cerebral cortex: a rat model. *J. Neurotrauma* 20, 767–780. doi: 10.1089/089771503767869999

Chen, Q. H., Ganesh, T., Brodie, P., Slebodnick, C., Jiang, Y., Banerjee, A., et al. (2008). Design, synthesis and biological evaluation of bridged epothilone D analogues. *Org. Biomol. Chem.* 6, 4542–4552. doi: 10.1039/b814823f

Chuckowree, J. A., and Vickers, J. C. (2003). Cytoskeletal and morphological alterations underlying axonal sprouting after localized transection of cortical neuron axons in vitro. *J. Neurosci.* 23, 3715–3725. doi: 10.1523/JNEUROSCI.23-09-03715.2003

Clark, J. A., Blizzard, C. A., Breslin, M. C., Yeaman, E. J., Lee, K. M., Chuckowree, J. A., et al. (2018). Epothilone D accelerates disease progression in the SOD1G93A mouse model of amyotrophic lateral sclerosis. *Neuropathol. Appl. Neurobiol.* doi: 10.1111/nan.12473 [Epub ahead of print].

Cross, D. J., Garwin, G. G., Cline, M. M., Richards, T. L., Yarnykh, V., Mourad, P. D., et al. (2015). Paclitaxel improves outcome from traumatic brain injury. *Brain Res.* 1618, 299–308. doi: 10.1016/j.brainres.2015.06.006

de Koning, M. E., Scheenen, M. E., van der Horn, H. J., Hageman, G., Roks, G., Spikman, J. M., et al. (2017). Non-hospitalized patients with mild traumatic brain injury: the forgotten minority. *J. Neurotrauma* 34, 257–261. doi: 10.1089/neu.2015.4377

Dean, P. J., and Sterr, A. (2013). Long-term effects of mild traumatic brain injury on cognitive performance. *Front. Hum. Neurosci.* 7:30. doi: 10.3389/fnhum.2013.00030

DeKosky, S. T., and Ikonomovic, M. D. (2010). Traumatic brain injury—football, warfare, and long-term effects. *N. Engl. J. Med.* 363, 1293–1296. doi: 10.1056/NEJMp1007051

Deller, T., Haas, C., Freiman, T., Phinney, A., Jucker, M., and Frotscher, M. (2006). Lesion-induced axonal sprouting in the central nervous system. *Adv. Exp. Med. Biol.* 557, 101–121. doi: 10.1007/0-387-30128-3_6

Dent, E. W. (2016). Of microtubules and memory: implications for microtubule dynamics in dendrites and spines. *Mol. Biol. Cell* 28, 1–8. doi: 10.1091/mbc.E15-11-0769

Dickson, T., Chung, R., McCormack, G., Staal, J., and Vickers, J. (2007). Acute reactive and regenerative changes in mature cortical axons following injury. *Neuroreport* 18, 283. doi: 10.1097/WNR.0b013e3280143cdb

Ekmark-Lewen, S., Flygt, J., Kiwanuka, O., Meyerson, B. J., Lewén, A., Hillered, L., et al. (2013). Traumatic axonal injury in the mouse is accompanied by a dynamic inflammatory response, astroglial reactivity and complex behavioral changes. *J. Neuroinflammation* 10:44. doi: 10.1186/1742-2094-10-44

Ertürk, A., Hellal, F., Enes, J., and Bradke, F. (2007). Disorganized microtubules underlie the formation of retraction bulbs and the failure of axonal regeneration. *J. Neurosci.* 27, 9169–9180. doi: 10.1523/JNEUROSCI.0612-07.2007

Farkas, O., and Povlishock, J. (2007). Cellular and subcellular change evoked by diffuse traumatic brain injury: a complex web of change extending far beyond focal damage. *Prog. Brain Res.* 161, 43–59. doi: 10.1016/S0079-6123(06)61004-2

Feng, G., Mellor, R. H., Bernstein, M., Keller-Peck, C., Nguyen, Q. T., Wallace, M., et al. (2000). Imaging neuronal subsets in transgenic mice expressing multiple spectral variants of GFP. *Neuron* 28, 41–51. doi: 10.1016/S0896-6273(00)00084-2

Fiala, J. C., Allwardt, B., and Harris, K. M. (2002a). Dendritic spines do not split during hippocampal LTP or maturation. *Nat. Neurosci.* 5, 297–298. doi: 10.1038/nn830

Fiala, J. C., Spacek, J., and Harris, K. M. (2002b). Dendritic spine pathology: cause or consequence of neurological disorders? *Brain Res. Brain Res. Rev.* 39, 29–54. doi: 10.1016/S0165-0173(02)00158-3

Gao, X., and Chen, J. (2011). Mild traumatic brain injury results in extensive neuronal degeneration in the cerebral cortex. *J. Neuropathol. Exp. Neurol.* 70, 183–191. doi: 10.1097/NEN.0b013e31820c6878

Gao, X., Deng, P., Xu, Z. C., and Chen, J. (2011). Moderate traumatic brain injury causes acute dendritic and synaptic degeneration in the hippocampal dentate gyrus. *PLoS One* 6:e24566. doi: 10.1371/journal.pone.0024566.s002

Goodin, S. (2004). Epothilones: mechanism of action and biologic activity. *J. Clin. Oncol.* 22, 2015–2025. doi: 10.1200/JCO.2004.12.001

Greer, J. E., Mcginn, M. J., and Povlishock, J. T. (2011). Diffuse traumatic axonal injury in the mouse induces atrophy, c-jun activation, and axonal outgrowth in the axotomized neuronal population. *J. Neurosci.* 31, 5089–5105. doi: 10.1523/JNEUROSCI.5103-10.2011

Gu, J., Firestein, B. L., and Zheng, J. Q. (2008). Microtubules in dendritic spine development. *J. Neurosci.* 28, 12120–12124. doi: 10.1523/JNEUROSCI.2509-08.2008

Hånell, A., Greer, J. E., Mcginn, M. J., and Povlishock, J. T. (2014). Traumatic brain injury-induced axonal phenotypes react differently to treatment. *Acta Neuropathol.* 129, 317–332. doi: 10.1007/s00401-014-1376-x

Hellal, F., Hurtado, A., Ruschel, J., Flynn, K. C., Laskowski, C. J., Umlauf, M., et al. (2011). microtubule stabilization reduces scarring and causes axon regeneration after spinal cord injury. *Science* 331, 928–931. doi: 10.1126/science.1201148

Hering, H., and Sheng, M. (2001). Dendritic spines: structure, dynamics and regulation. *Nat. Rev. Neurosci.* 2, 880–888. doi: 10.1038/35104061

Hill, C. S., Coleman, M. P., and Menon, D. K. (2016). Traumatic axonal injury: mechanisms and translational opportunities. *Trends Neurosci.* 39, 311–324. doi: 10.1016/j.tins.2016.03.002

Hotulainen, P., and Hoogenraad, C. C. (2010). Actin in dendritic spines: connecting dynamics to function. *J. Cell Biol.* 189, 619–629. doi: 10.1038/nn1630

Hur, E.-M., and Lee, B. D. (2014). Microtubule-targeting agents enter the Central Nervous System (CNS): double-edged swords for treating CNS injury and disease. *Int. Neurourol. J.* 18, 171–178. doi: 10.5213/inj.2014.18.4.171

Iverson, G. L. (2005). Outcome from mild traumatic brain injury. *Curr. Opin. Psychiatry* 18, 301–317. doi: 10.1097/01.yco.0000165601.29047.ae

Iverson, G. L. (2010). Clinical and methodological challenges with assessing mild traumatic brain injury in the military. *J. Head Trauma Rehabil.* 25, 313–319. doi: 10.1097/HTR.0b013e3181d6f9bd

Jagoda, A. S., Bazarian, J. J., Bruns, JJ Jr, Cantrill, S. V., Gean, A. D., Howard, P. K., et al. (2009). Clinical policy: neuroimaging and decisionmaking in adult mild traumatic brain injury in the acute setting. *J. Emerg. Nurs.* 35, e5–e40. doi: 10.1016/j.jen.2008.12.010

Jang, E.-H., Sim, A., Im, S.-K., and Hur, E.-M. (2016). Effects of microtubule stabilization by epothilone B depend on the type and age of neurons. *Neural Plast.* 2016:5056418. doi: 10.1155/2016/5056418

Jaworski, J., Kapitein, L. C., Gouveia, S. M., Dortland, B. R., Wulf, P. S., Grigoriev, I., et al. (2009). Dynamic microtubules regulate dendritic spine morphology and synaptic plasticity. *Neuron* 61, 85–100. doi: 10.1016/j.neuron.2008.11.013

Johnson, V. E., Stewart, W., and Smith, D. H. (2012a). Axonal pathology in traumatic brain injury. *Exp. Neurol.* 246, 35–43. doi: 10.1016/j.expneurol.2012.01.013

Johnson, V. E., Stewart, W., and Smith, D. H. (2012b). Widespread tau and amyloid-Beta pathology many years after a single traumatic brain injury in humans. *Brain Pathol.* 22, 142–149. doi: 10.1111/j.1750-3639.2011.00513.x

Kapitein, L. C., Yau, K. W., and Hoogenraad, C. C. (2010). Microtubule dynamics in dendritic spines. *Methods Cell Biol.* 97, 111–132. doi: 10.1016/S0091-679X(10)97007-6

Kharatishvili, I., Nissinen, J. P., McIntosh, T. K., and Pitkänen, A. (2006). A model of posttraumatic epilepsy induced by lateral fluid-percussion brain injury in rats. *Neuroscience* 140, 685–697. doi: 10.1016/j.neuroscience.2006.03.012

Khrapunovich-Baine, M., Menon, V., Yang, C.-P., Northcote, P. T., Miller, J. H., Angeletti, R. H., et al. (2011). Hallmarks of molecular action of microtubule stabilizing agents: effects of epothilone B, ixabepilone, peloruside A, and laulimalide on microtubule conformation. *J. Biol. Chem.* 286, 11765–11778. doi: 10.1074/jbc.M110.162214

Lei, W., Omotade, O. F., Myers, K. R., and Zheng, J. Q. (2016). Actin cytoskeleton in dendritic spine development and plasticity. *Curr. Opin. Neurobiol.* 39, 86–92. doi: 10.1016/j.conb.2016.04.010

Lifshitz, J., Witgen, B., and Grady, M. (2007). Acute cognitive impairment after lateral fluid percussion brain injury recovers by 1 month: evaluation by conditioned fear response. *Behav. Brain Res.* 177, 347–357. doi: 10.1016/j.bbr.2006.11.014

Matus, A. (2000). Actin-based plasticity in dendritic spines. *Science* 290, 754–758. doi: 10.1126/science.290.5492.754

Maxwell, W. L., and Graham, D. I. (1997). Loss of axonal microtubules and neurofilaments after stretch-injury to guinea pig optic nerve fibers. *J. Neurotrauma* 14, 603–614. doi: 10.1089/neu.1997.14.603

McMahon, P. J., Hricik, A., Yue, J. K., Puccio, A. M., Inoue, T., Lingsma, H. F., et al. (2014). Symptomatology and functional outcome in mild traumatic brain injury: results from the prospective TRACK-TBI study. *J. Neurotrauma* 31, 26–33. doi: 10.1089/neu.2013.2984

Meaney, D. F., and Smith, D. H. (2011). Biomechanics of concussion. *Clin. Sports Med.* 30, 19–31. doi: 10.1016/j.csm.2010.08.009

Michaud, L. B. (2009). The epothilones: how pharmacology relates to clinical utility. *Ann. Pharmacother.* 43, 1294–1309. doi: 10.1345/aph.1M005

Moscarello, M. A., Mak, B., Nguyen, T. A., Wood, D. D., Mastronardi, F., and Ludwin, S. K. (2002). Paclitaxel (Taxol) attenuates clinical disease in a spontaneously demyelinating transgenic mouse and induces remyelination. *Mult. Scler.* 8, 130–138. doi: 10.1191/1352458502ms776oa

Penazzi, L., Tackenberg, C., Ghori, A., Golovyashkina, N., Niewidok, B., Selle, K., et al. (2016). A&beta-mediated spine changes in the hippocampus are microtubule-dependent and can be reversed by a subnanomolar concentration of the microtubule-stabilizing agent epothilone D. *Neuropharmacology* 105, 84–95. doi: 10.1016/j.neuropharm.2016.01.002

Popovich, P. G., Tovar, C. A., Lemeshow, S., Yin, Q., and Jakeman, L. B. (2014). Independent evaluation of the anatomical and behavioral effects of Taxol in rat models of spinal cord injury. *Exp. Neurol.* 261, 97–108. doi: 10.1016/j.expneurol.2014.06.020

Reeves, T. M., Phillips, L. L., and Povlishock, J. T. (2005). Myelinated and unmyelinated axons of the corpus callosum differ in vulnerability and functional recovery following traumatic brain injury. *Exp. Neurol.* 196, 126–137. doi: 10.1016/j.expneurol.2005.07.014

Ruschel, J., Hellal, F., Flynn, K. C., Dupraz, S., Elliott, D. A., Tedeschi, A., et al. (2015). Systemic administration of epothilone B promotes axon regeneration after spinal cord injury. *Science* 348, 347–352. doi: 10.1126/science.aaa2958

Salin, P., Tseng, G., Hoffman, S., Parada, I., and Prince, D. (1995). Axonal sprouting in layer V pyramidal neurons of chronically injured cerebral cortex. *J. Neurosci.* 15, 8234–8245. doi: 10.1523/JNEUROSCI.15-12-08234.1995

Santhakumar, V., Ratzliff, A. D., Jeng, J., Toth, Z., and Soltesz, I. (2001). Long-term hyperexcitability in the hippocampus after experimental head trauma. *Ann. Neurol.* 50, 708–717. doi: 10.1002/ana.1230

Schneider, C. A., Rasband, W. S., and Eliceiri, K. W. (2012). NIH Image to ImageJ: 25 years of image analysis. *Nat. Methods* 9, 671–675. doi: 10.1038/nmeth.2089

Sengottuvel, V., Leibinger, M., Pfreimer, M., Andreadaki, A., and Fischer, D. (2011). Taxol facilitates axon regeneration in the mature CNS. *J. Neurosci.* 31, 2688–2699. doi: 10.1523/JNEUROSCI.4885-10.2011

Shultz, S. R., McDonald, S. J., Haar, C. V., Meconi, A., Vink, R., van Donkelaar, P., et al. (2016). The potential for animal models to provide insight into mild traumatic brain injury: translational challenges and strategies. *Neurosci. Biobehav. Rev.* 76(Pt B), 1–19. doi: 10.1016/j.neubiorev.2016.09.014

Smith, D., and Meaney, D. (2000). Axonal damage in traumatic brain injury. *Neuroscientist* 6, 483–495. doi: 10.1177/107385840000600611

Smith, D. H., Hicks, R., and Povlishock, J. T. (2013). Therapy development for diffuse axonal injury. *J. Neurotrauma* 30, 307–323. doi: 10.1089/neu.2012.2825

Spain, A., Daumas, S., Lifshitz, J., Rhodes, J., Andrews, P., Horsburgh, K., et al. (2010). Mild fluid percussion injury in mice produces evolving selective axonal pathology and cognitive deficits relevant to human brain injury. *J. Neurotrauma* 27, 1429–1438. doi: 10.1089/neu.2010.1288

Stone, J., Okonkwo, D., Dialo, A., Rubin, D., Mutlu, L., Povlishock, J., et al. (2004). Impaired axonal transport and altered axolemmal permeability occur in distinct populations of damaged axons following traumatic brain injury. *Exp. Neurol.* 190, 59–69. doi: 10.1016/j.expneurol.2004.05.022

Tang-Schomer, M. D., Johnson, V. E., Baas, P. W., Stewart, W., and Smith, D. H. (2012). Partial interruption of axonal transport due to microtubule breakage accounts for the formation of periodic varicosities after traumatic axonal injury. *Exp. Neurol.* 233, 364–372. doi: 10.1016/j.expneurol.2011.10.030

Thompson, H. J., Lifshitz, J., Marklund, N., Grady, M. S., Graham, D. I., Hovda, D. A., et al. (2005). Lateral fluid percussion brain injury: a 15-year review and evaluation. *J. Neurotrauma* 22, 42–75. doi: 10.1089/neu.2005.22.42

Wang, H.-C., and Ma, Y.-B. (2010). Experimental models of traumatic axonal injury. *J. Clin. Neurosci.* 17, 157–162. doi: 10.1016/j.jocn.2009.07.099

Wang, M. L., and Li, W. B. (2016). Cognitive impairment after traumatic brain injury: the role of MRI and possible pathological basis. *J. Neurol. Sci.* 370, 244–250. doi: 10.1016/j.jns.2016.09.049

Wilde, E. A., Li, X., Hunter, J. V., Narayana, P. A., Hasan, K., Biekman, B., et al. (2016). Loss of consciousness is related to white matter injury in mild traumatic brain injury. *J. Neurotrauma* 33, 2000–2010. doi: 10.1089/neu.2015.4212

Winston, C. N., Chellappa, D., Wilkins, T., Barton, D. J., Washington, P. M., Loane, D. J., et al. (2013). Controlled cortical impact results in an extensive loss of dendritic spines that is not mediated by injury-induced amyloid-beta accumulation. *J. Neurotrauma* 30, 1966–1972. doi: 10.1089/neu.2013.2960

Zhang, B., Maiti, A., Shively, S., Lakhani, F., McDonald-Jones, G., Bruce, J., et al. (2005). Microtubule-binding drugs offset tau sequestration by stabilizing microtubules and reversing fast axonal transport deficits in a tauopathy model. *Proc. Natl. Acad. Sci. U.S.A.* 102, 227–231. doi: 10.1073/pnas.0406361102

Zhao, Y., Fang, W. S., and Pors, K. (2009). Microtubule stabilising agents for cancer chemotherapy. *Expert Opin. Ther. Pat.* 19, 607–622. doi: 10.1517/13543770902775713

Conflict of Interest Statement: The authors declare that the research was conducted in the absence of any commercial or financial relationships that could be construed as a potential conflict of interest.

frontiers in Cellular Neuroscience

ORIGINAL RESEARCH
published: 03 August 2018
doi: 10.3389/fncel.2018.00217

ASD-Associated *De Novo* Mutations in Five Actin Regulators Show Both Shared and Distinct Defects in Dendritic Spines and Inhibitory Synapses in Cultured Hippocampal Neurons

Iryna Hlushchenko[1], *Pushpa Khanal*[1], *Amr Abouelezz*[1,2,3], *Ville O. Paavilainen*[2,4] *and Pirta Hotulainen*[1]*

[1] *Minerva Foundation Institute for Medical Research, Helsinki, Finland,* [2] *HiLIFE, University of Helsinki, Helsinki, Finland,* [3] *Neuroscience Center, University of Helsinki, Helsinki, Finland,* [4] *Institute of Biotechnology, University of Helsinki, Helsinki, Finland*

OPEN ACCESS

Edited by:
Monica Mendes Sousa, i3S, Instituto de Investigação e Inovação em Saúde, Portugal

Reviewed by:
Marco Rust, Philipps University of Marburg, Germany
Jaewon Ko, Daegu Gyeongbuk Institute of Science and Technology (DGIST), South Korea
Maurizio Giustetto, Università degli Studi di Torino, Italy

***Correspondence:**
Pirta Hotulainen
pirta.hotulainen@helsinki.fi

Received: *14 February 2018*
Accepted: *03 July 2018*
Published: *03 August 2018*

Citation:
Hlushchenko I, Khanal P, Abouelezz A, Paavilainen VO and Hotulainen P (2018) ASD-Associated De Novo Mutations in Five Actin Regulators Show Both Shared and Distinct Defects in Dendritic Spines and Inhibitory Synapses in Cultured Hippocampal Neurons. Front. Cell. Neurosci. 12:217. doi: 10.3389/fncel.2018.00217

Many actin cytoskeleton-regulating proteins control dendritic spine morphology and density, which are cellular features often altered in autism spectrum disorder (ASD). Recent studies using animal models show that autism-related behavior can be rescued by either manipulating actin regulators or by reversing dendritic spine density or morphology. Based on these studies, the actin cytoskeleton is a potential target pathway for developing new ASD treatments. Thus, it is important to understand how different ASD-associated actin regulators contribute to the regulation of dendritic spines and how ASD-associated mutations modulate this regulation. For this study, we selected five genes encoding different actin-regulating proteins and induced ASD-associated *de novo* missense mutations in these proteins. We assessed the functionality of the wild-type and mutated proteins by analyzing their subcellular localization, and by analyzing the dendritic spine phenotypes induced by the expression of these proteins. As the imbalance between excitation and inhibition has been suggested to have a central role in ASD, we additionally evaluated the density, size and subcellular localization of inhibitory synapses. Common for all the proteins studied was the enrichment in dendritic spines. ASD-associated mutations induced changes in the localization of α-actinin-4, which localized less to dendritic spines, and for SWAP-70 and SrGAP3, which localized more to dendritic spines. Among the wild-type proteins studied, only α-actinin-4 expression caused a significant change in dendritic spine morphology by increasing the mushroom spine density and decreasing thin spine density. We hypothesized that mutations associated with ASD shift dendritic spine morphology from mushroom to thin spines. An M554V mutation in α-actinin-4 (*ACTN4*) resulted in the expected shift in dendritic spine morphology by increasing the density of thin spines.

In addition, we observed a trend toward higher thin spine density with mutations in myosin IXb and SWAP-70. Myosin IIb and myosin IXb expression increased the proportion of inhibitory synapses in spines. The expression of mutated myosin IIb (Y265C), SrGAP3 (E469K), and SWAP-70 (L544F) induced variable changes in inhibitory synapses.

Keywords: autism spectrum disorder, actin cytoskeleton, dendritic spines, inhibitory synapses, *de novo* point mutations

INTRODUCTION

Autism spectrum disorder (ASD) comprises a range of neurological conditions characterized by social deficits, repetitive behaviors, and accompanying comorbidities, including intellectual disability, epilepsy, hyperactivity, and anxiety. ASD has a strong genetic component and almost 1000 genes are currently associated with ASD (SFARI Gene: https://gene.sfari.org/database/human-gene/). Many ASD-associated mutations are rare protein-disrupting *de novo* mutations that arose in the germline. Mutations can be copy-number variants (CNVs) or single-base-pair mutations. Numerous ASD susceptibility genes are involved in regulating the postsynaptic site of glutamatergic synapses (Peça and Feng, 2012; Bourgeron, 2015), the development and maturation of synaptic contacts (Gilman et al., 2011), or synaptic transmission (Li et al., 2014). Most excitatory glutamatergic synapses are located on small dendritic protrusions known as dendritic spines. The formation, maturation, and elimination of dendritic spines lie at the core of synaptic transmission and memory formation (Yang et al., 2009; Roberts et al., 2010). Studies of postmortem human ASD brains revealed an increased spine density, which is—at least in some cases—the result of defective dendritic spine pruning (Tang et al., 2014).

Numerous studies have demonstrated a pivotal role for the actin cytoskeleton in the formation and elimination, motility and stability, and size and shape of dendritic spines (Hotulainen and Hoogenraad, 2010). Actin filaments are polar structures with one end growing more rapidly (the plus or "barbed" end) than the other (the minus or "pointed" end). Constant removal of the actin subunits from the pointed ends and addition at the barbed ends is called actin treadmilling. Synaptic stimulation rapidly changes the actin treadmilling rate (Star et al., 2002; Okamoto et al., 2004; Hlushchenko et al., 2016). The actin treadmilling rate, as well as the three-dimensional organization of actin filaments, are regulated by actin-binding proteins (Hotulainen and Hoogenraad, 2010). Many actin regulators are associated with ASD and these proteins are often involved in the regulation of the structure and function of excitatory synapses (Joensuu et al., 2017). However, our knowledge of whether ASD-associated mutations in actin regulators affect their functions in dendritic spines or synapses is limited.

Recent studies using different animal models have shown that autistic symptoms can be rescued by either manipulating actin regulators or by rescuing dendritic spine density or morphology (Dolan et al., 2013; Duffney et al., 2015). Although it is not yet clear how aberrant dendritic spines and behavioral consequences are connected, these results suggest that actin regulators controlling dendritic spines may play direct causal roles in ASD-related behavior. The social deficits and NMDA receptor hypofunction displayed by *Shank3*-deficient mice were rescued by inhibiting the activity of the actin filament-depolymerizing protein, cofilin, or by activating Rac1, the actin cytoskeleton master-regulator (Duffney et al., 2015). Remarkably, Dolan and colleagues showed that a single administration of p21-activated kinase inhibitor, small molecule FRAX486, was sufficient to recover the phenotype in adult *Fmr1*-knockout mice, demonstrating that a post-diagnostic therapy could be possible for Fragile-X adults (Dolan et al., 2013). p21-activated kinase is a Rac1 effector, which regulates spines through modulation of actin cytoskeleton dynamics. Based on these results, the actin cytoskeleton has recently emerged as a potential new target for new ASD treatments. Thus, it is important to understand how different ASD-associated actin regulators contribute to the regulation of dendritic spines and how ASD-associated mutations modulate this regulation.

When we started this study, the SFARI Gene Database was not yet available. Therefore, to find ASD-associated missense mutations in actin regulators, we relied on the gene and mutation lists published by (Fromer et al., 2014) , which summarized *de novo* mutations in genes associated with different neuropsychiatric diseases. From this list, we selected ASD-associated genes encoding the known actin-regulating proteins: *SRGAP3*, *TRIO*, *MYO9B*, *MYO7B*, *MYH10*, *MYO15A*, *ACTN4*, *SWAP70*, *NEB*, and *TTN*. Nebulin (*NEB*) and titin (*TTN*) are giant proteins (nebulin 600–900 kDa, titin up to 4.2 MDa), mostly known for their function in muscle sarcomeres. Although they may also play roles in neurons, they were excluded from further studies because of their large size, which makes molecular biology approaches challenging.

Next, the expression patterns of the identified genes were investigated using the Allen Brain Atlas (mouse brain). *MYO7B* was not found in the Allen Brain Atlas, and a literature search indicated that it is not expressed in the brain (Chen et al., 2001). *MYO15A* seemed to show very weak expression in the brain. Thus, these two myosins were excluded from further experiments. Attempts to clone *TRIO* constructs were unsuccessful and therefore the final study was carried out with five genes: *ACTN4*, *MYO9B*, *SWAP70*, *MYH10*, and *SRGAP3*. The mutations we investigated are all unique, one-allele *de novo* mutations leading to mixed expression of wild-type and mutated proteins. The selected genes also have other mutations; currently, the SFARI Gene database reports 3 variants for *ACTN4* (inheritance pattern unknown or *de novo*), 27 variants for *MYO9B* (both familial and *de novo*) and 4 variants for *SRGAP3*

(all *de novo*). *SWAP70* and *MYH10* are not listed in the SFARI Gene database.

Alpha(α)-actinin-4 (*ACTN4*) is expressed in the hippocampus, cortex, and cerebellum in the brain (Kalinowska et al., 2015). The main function of α-actinins is to cross-link actin filaments into bundles (Otey and Carpen, 2004). Cross-linking actin filaments provides the rigidity and stability for filaments. In neurons, α-actinin-4 is enriched at excitatory synapses and co-localizes with group 1 metabotropic glutamate receptors (mGluRs) (Kalinowska et al., 2015). α-actinin-4 supports the transition of thin spines to mushroom spines and is required for the mGluR-induced dynamic remodeling of dendritic protrusions (Kalinowska et al., 2015).

Non-muscle myosin IIb (*MYH10*), or non-muscle myosin heavy chain IIb (NMMHCIIb) (referred to here as myosin IIb) is important for the normal development and function of dendritic spines (Zhang, 2005; Ryu et al., 2006; Rex et al., 2010; Hodges et al., 2011) and is re-located into dendritic spines during neuronal maturation (Ryu et al., 2006). Myosin IIb localizes to the base of mushroom spine heads (Korobova and Svitkina, 2010; Rubio et al., 2011) where it facilitates the stabilization of spines through actin cross-linking (Koskinen et al., 2014). Simultaneously, myosin IIb-induced contractility enhances the dynamics of actin filaments on the spine surface, thus facilitating the fast fine-tuning of spine shape (Koskinen et al., 2014). The *MYH10* gene is associated with various neurological diseases, such as schizophrenia and autism (Fromer et al., 2014).

The human myosin IXb (*MYO9B*) protein is mostly studied in cancer cell lines, where it localizes to sites of actin polymerization (van den Boom et al., 2007). However, myosin IXb is also expressed in the central nervous system. In cortical neurons, it controls RhoA activity, thereby regulating the growth and branching of dendritic processes (Long et al., 2013). Knockdown of myosin IXb in cultured cortical neurons or in the developing cortex results in decreased dendrite length and number (Long et al., 2013).

SWAP-70 (*SWAP70*) takes part in DNA recombination in the nucleus (Borggrefe et al., 1998) and regulates the actin cytoskeleton in the cytosol (Hilpelä et al., 2003; Chacón-Martínez et al., 2013). SWAP-70 binds the plasma membrane through the binding of its plecstrin homology domain to phosphoinositide PI(3,4)P2 (Hilpelä et al., 2003). SWAP-70 was identified as an interaction partner of myosin IXb in a two-hybrid screening (Hilpelä et al., 2003), but this putative interaction remains to be confirmed. Although SWAP-70 is expressed in the brain (Hilpelä et al., 2003), its function has not been studied in neurons.

SLIT-ROBO Rho GTPase-activating protein 3 (SrGAP3, Gene: *SRGAP3*) is ubiquitously expressed in the developing nervous system (Bacon et al., 2009, 2013). SrGAP3 supports the initiation of spines and inhibits the transition of thin spines to mushroom spines. Knocking out *SrGAP3* decreases the number of dendritic filopodia during early mouse development (Carlson et al., 2011).

The most commonly observed dendritic spine phenotype associated with ASD is an increased density of thin spines (Comery et al., 1997). Thus, our main hypothesis was that genetic mutations associated with ASD shift dendritic spine morphology from mushroom spines to thin spines. To test this hypothesis, we studied how ASD-associated single base-pair *de novo* mutations in five selected genes affect the localization and function of the encoded proteins, and whether these mutations change the proteins' overexpression effects on dendritic spine density and morphology in primary rat hippocampal neurons.

As the imbalance between excitation and inhibition has been suggested to have a central role in ASD (Rubenstein and Merzenich, 2003; Südhof, 2008; Uzunova et al., 2016; Lee et al., 2017), we analyzed the density and size of inhibitory synapses. Postmortem neuropathological studies of people with ASD have demonstrated a decreased density of GABA receptors in the cortex (Blatt and Fatemi, 2011). In mouse models, both upregulation and suppression in inhibitory synaptic transmission have been detected (Isshiki et al., 2014). Thus, we did not have clear expectations regarding the kind of changes we should see. Therefore, we hypothesized that there are alterations in the size and density of inhibitory synapses in neurons expressing proteins with ASD-linked mutations. We further hypothesized that the localization of inhibitory synapses in spines vs. dendritic shafts affects the efficiency or modality of inhibition. Thus, we also analyzed the ratio of inhibitory synapses in spines vs. dendritic shaft. None of the proteins studied was found to be part of the inhibitory synapse complex (Uezu et al., 2016) so we did not expect them to directly regulate inhibitory synapses. However, these proteins could affect inhibitory synapse dynamics and thus their localization, size and density through the regulation of actin dynamics (Wierenga, 2017).

MATERIALS AND METHODS

Plasmid Construction

pEGFP-N1 and mCherry-C1 plasmids were purchased from Clontech Laboratories Inc. Wild-type mCherry-tagged α-actinin 4 (ACTN4) and Slit-Robo GAP3 (SRGAP3) were generated at the Genome Biology Unit cloning service (Biocenter Finland, University of Helsinki). Briefly, entry clones [clone-IDs: 100011237 (ACTN4) and 100069053 (SrGAP3)] from the human ORFeome collaboration library were transferred into mCherry-tagged mammalian expression destination vectors using standard LR Gateway cloning. mCherry-tagged SWAP-70, myosin IXb, and myosin IIb constructs were kind gifts from Martin Bähler (SWAP-70 and Myosin IXb, WestfalianWilhelms-University, Münster, Germany) and Alan Rick Horwitz (MHCIIb, University of Virginia, USA). Mutant constructs were generated through PCR-mediated site-directed mutagenesis (Zheng et al., 2004). Purified PCR products were treated for 2 h using DpnI (New England Biolabs) and 5 μl were used to transform competent DH5-α cells. Transformants were inoculated on LB plates containing appropriate antibiotics for selection and 5 colonies were selected for mini-prep. All wild-type and mutated constructs were verified by DNA sequencing. The primers used for each mutation are listed in **Table 1**. Mutagenized bases are listed in lower-case.

TABLE 1 | The primers used for each mutation.

Construct	Mutation	Primers	
ACTN4	M554V	*forward*:	CAGGACgTGTTCATCGTCC ATACCATCGAGGAG
		reverse:	GTATGGACGATGAACAcGT CCTGGAGGTCCTCC
MYO9B	K1872R	*forward*:	GATGCTCATCcgGGAACAG ATGAGGAAATACAAGG
		reverse:	CTGTTCCcgGATGAGCATCT CCACACACG
SRGAP3	E469K	*forward*:	CTGGGCaAAGGGGAAAGA GCAGAATGCG
		reverse:	CTTTCCCCTTtGCCCAGGG TCTGCTTGAG
SWAP70	L544F	*forward*:	CCATCATGAAGGATTcATTC GACTGATAGAACCAGG
		reverse:	GTCGAATgAATCCTTCATGA TGGGCCACTTTG
MYH10	Y265C	*forward*:	GATGTAACTGGCTgTATCGT TGGGGCCAACATTG
		reverse:	CCCAACGATAcAGCCAGTT ACATCAAAGTTGATCCG

Plasmids were first tested in U2OS cells to confirm that they were expressed and localized as expected (data not shown).

Neuronal Cultures, Transfections, Immunofluorescence, and Fixed Sample Preparation

Hippocampal neuronal cultures were prepared as described previously (Bertling et al., 2012). Animals were handled in accordance with Finnish laws and ethics under the EU directive 2010/63/EU (licenses: ESAVI-4943-04.10.07-2016 and GMO 3/S/12). Briefly, the hippocampi of embryonal day 17 Wistar rat fetuses of either sex were dissected and brains obtained. The meninges were then removed and hippocampi isolated. Cells were dissociated with 0.05% papain and mechanical trituration. The cells were plated on coverslips (diameter 13 mm) coated with 0.1 mg/ml Poly-L-Lysine (Sigma) at a density of 150,000 cells per coverslip and cultured in Neurobasal medium (Gibco) supplemented with B-27 (Invitrogen), L-glutamine (Invitrogen) and penicillin–streptomycin (Lonza). Transient transfections were performed, as described earlier (Hotulainen et al., 2009), on DIV13-14 using Lipofectamine 2000 (Invitrogen). The neurons were then fixed on DIV 15-16 with 4% PFA for 20 min, then washed 3 times with PBS. For inhibitory synapse labeling, the cells were then permeabilized with 0.2% TritonX-100 in PBS for 10 min and then blocked with 3% normal donkey serum and 0.5% BSA in PBS for 30 min. Antibodies were diluted separately in blocking solution at 1:500 for primary anti-gephyrin antibody (rabbit, Synaptic Systems) and 1:400 for secondary Alexa-488 (anti-rabbit, Molecular probes), and subsequently 25 µl was dropped onto a parafilm that was then covered by the coverslip. Each antibody was incubated for 1 h at room temperature. The coverslips were washed 3 times for 10 min with 0.2% BSA in PBS after each incubation, then mounted on microscope slides using Shandon Immu-Mount (Thermo Scientific).

Confocal Imaging and Protein Localization Analysis

Imaging was performed on either a Zeiss LSM780 or LSM880 inverted confocal microscope. A 63× 1.4 NA oil immersion objective lens and Immersol 518F (Zeiss) immersion oil were used to image the fixed samples. For each neuron, a *z*-stack of 20–30 optical sections was obtained with 0.2–0.3 µm steps in the *z* axis and a pixel size of 0.066 × 0.066 µm for 1–2 dendritic segments. Image files were processed with Zeiss ZEN and Fiji software (Schindelin et al., 2012, 2015). Fiji software was used to calculate spine–to-dendrite intensity ratios. First, 3D image data was converted to 2D using Z-projection based on maximum intensity. To measure the ratio, the average intensity of fluorescence for the protein of interest was measured from a circular region of interest (ROI) in the spine head and compared to the average fluorescence intensity of the equal-sized ROI in the adjacent dendrite. The result was normalized to the intensity distribution of GFP in the same ROIs. For each neuron 9–10 spines were analyzed and the median value was then taken as representative for the cell. Therefore, for each group we analyzed at least 140 spines. Box plots were then created using a BoxPlotR web-tool (http://shiny.chemgrid.org/boxplotr/).

Dendritic Spine Morphology and Density Analysis

For the analysis of spine density and morphology, tiff image files comprising *z*-stacks of 20–30 optical sections per dendritic segment were directly processed with NeuronStudio, a software package specifically designed for spine detection and analysis (Rodriguez et al., 2008). The voxel size of the images was 0.066 × 0.066 × 0.2–0.3 µm. The EGFP signal was used to analyze dendritic morphology. After modeling the dendrite surface, the spines were auto-detected and classified as "mushroom," "thin," or "stubby" by the software. The model was then corrected manually: the protrusions missed by the algorithm were added and classified, the false labeling of other structures as spines was removed. Protrusions with a length between 0.1 and 5 µm, and width between 0.1 and 3 µm were retained as spines. Measurements obtained by NeuronStudio were further processed in MATLAB R2015a to extract spine number, lengths, head widths, and the total length of dendritic segments, and summarized in a spreadsheet application (MS Excel).

Density and Size Analysis of Inhibitory Synapses

Fiji software was used for the analysis of the density and size of inhibitory synapses. 3D images were opened in Fiji and used to create maximum intensity projections. The "straight line" tool was used to measure the length of the selected portion of the image. Lines were drawn, and the length was measured along the length of a dendrite. The data was then copied to an excel file and the sum of all the lines obtained gave

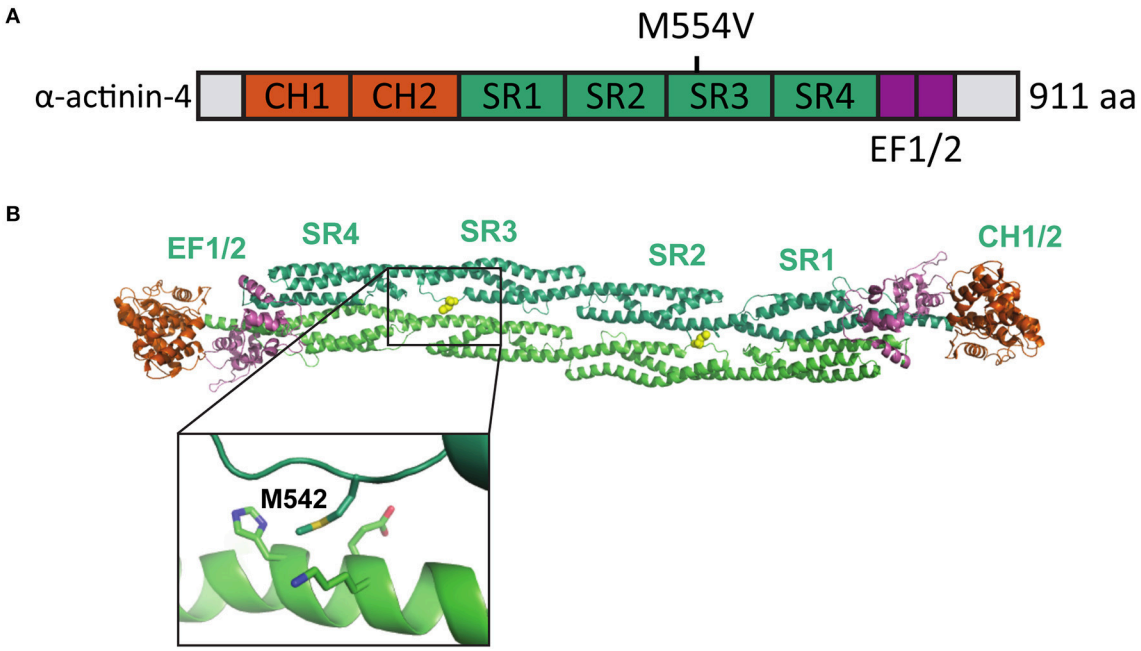

FIGURE 1 | Location of the mutated amino acid in the α-actinin structure. **(A)** Primary structure of human α-actinin-4 with the M554V mutation indicated. **(B)** Structure of human α-actinin-2 (PDB ID 4D1E) with methionine corresponding to the α-actinin-4 M554 and surrounding residues highlighted (close-up).

the total length of the dendrite/s. The number of individual inhibitory synapses along the dendrite and the dendritic spines, indicated by bright green dots, was determined. Dots smaller than 0.1 μm were disregarded. The same "straight line" tool was used to measure the diameter of each synapse. The density, percentage of synapses on spines, and average diameter of synapses for inhibitory synapses was then calculated from the data obtained.

Statistics

Statistical analysis was performed with the SPSS Statistics software package. To examine group differences, one-way ANOVA was used with Bonferroni *post-hoc* test when the compared groups' variances were equal and Games-Howell *post-hoc* test when the variances were unequal. To examine the difference in spine length, width, and width-to-length ratio distributions between the groups, we used the 2-sample Kolmogorov-Smirnov nonparametric test.

Figures and Molecular Modeling

All structural figures were generated with PyMol software (The PyMOL Molecular Graphics System, Version 2.0 Schrödinger, LLC). Images were prepared for the publication using standard tools of Fiji software (Schindelin et al., 2012, 2015). The bar charts were created in MS Excel and the cumulative distribution curves in MATLAB R2015a. The final figure layouts were generated with Inkscape: Open Source Scalable Vector Graphics Editor.

Availability of Materials and Data

All material and data (pictures, plasmids, analyses) are available upon request.

RESULTS

α-Actinin-4 Point Mutation M554V Alters Localization and Overexpression-Induced Dendritic Spine Phenotype

Iossifov et al. (2012) identified a missense A to G change in the *ACTN4* gene in a child exhibiting ASD symptoms. This base change leads to an amino acid substitution [methionine (M) 554 to valine (V)] in the spectrin repeat-3 of the α-actinin-4 protein (**Figure 1A**). The formation of homodimers is required for efficient α-actinin actin filament cross-linking activity. As the M554V mutation localizes to the known binding interface of the α-actinin homodimer (Ylänne et al., 2001) (**Figure 1B**), we hypothesized that this mutation may prevent or interfere with the correct assembly of cellular actin filament bundles.

To analyze the effects of M554V on α-actinin-4 subcellular localization, we transfected primary rat hippocampal neurons at days-*in-vitro* (DIV) 13 and analyzed the ratio of spine to dendritic localization of mCherry, human wild-type α-actinin-4 linked to mCherry, or mCherry-M554V-α-actinin-4 at DIV15. Fluorescence intensity was normalized to co-expressed EGFP (**Figure 2A**). Both α-actinin-4 constructs were expressed at similar levels in the cells analyzed. Wild-type α-actinin-4 was highly enriched in dendritic spines at a ratio of 6.64 ± 0.50 compared to diffuse GFP with a ratio

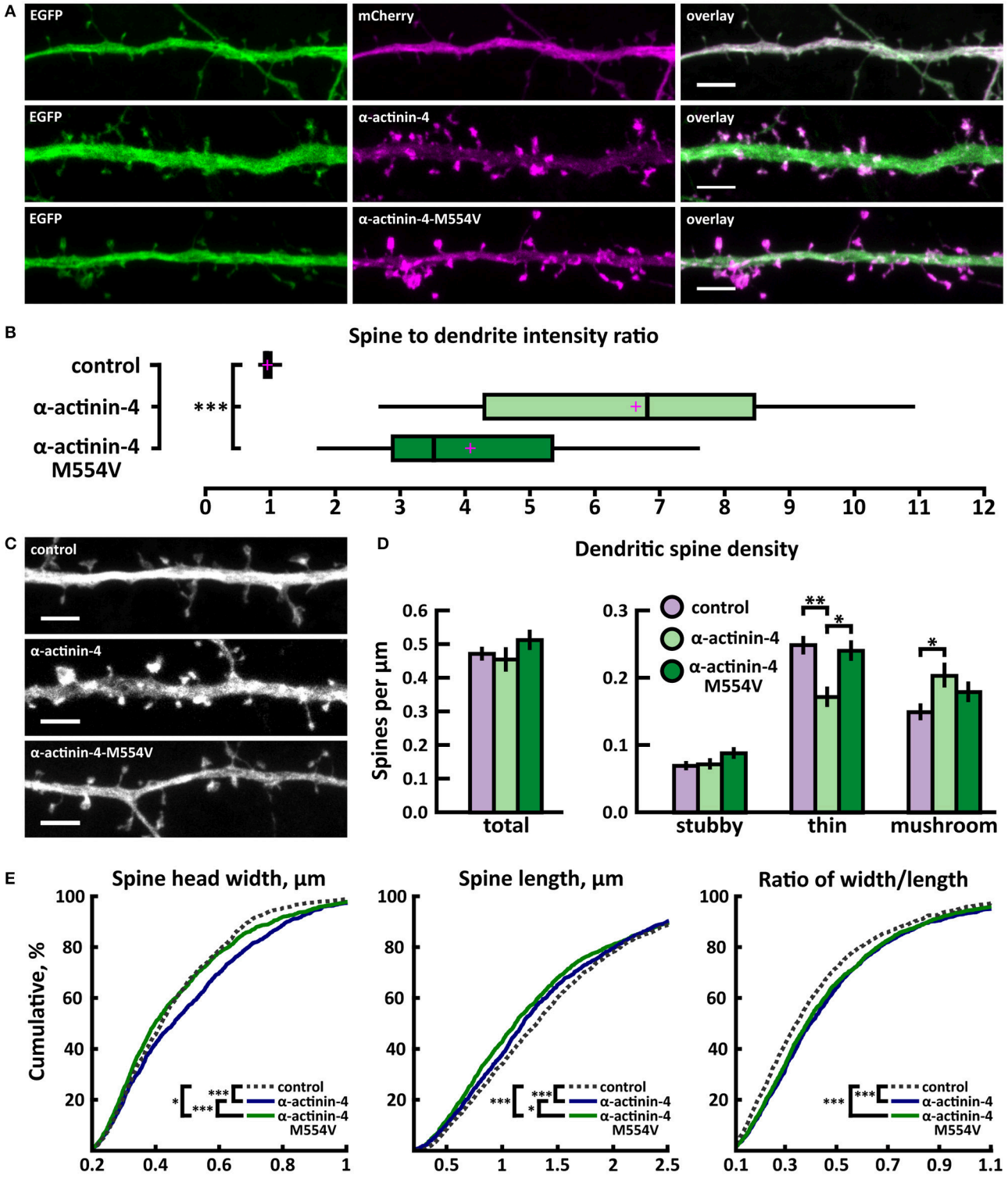

FIGURE 2 | Characterization of protein localization, dendritic spine density and morphology in DIV14-15 hippocampal neurons expressing EGFP and mCherry (control), wild-type α-actinin-4-mCherry or mutated α-actinin-4-M554V-mCherry. **(A)** Representative maximum projections of confocal Z-stacks for EGFP, mCherry, and wild-type and mutated α-actinin-4 localization. Scale bars, 4 µm. **(B)** The quantification of protein localization revealed enrichment of wt α-actinin-4 to dendritic spines and the decrease in accumulation for α-actinin-4-M554V. Spine-to-dendrite fluorescence intensity ratios: control: 0.98 ($n = 34$ cells, 339 spines), α-actinin-4: 6.64 ($n = 26$ cells, 260 spines), α-actinin-4-M554V: 4.1 ($n = 30$ cells, 299 spines). Center lines show the medians; box limits indicate the 25th and 75th percentiles

(Continued)

FIGURE 2 | as determined by R software; whiskers extend 1.5 times the interquartile range from the 25th and 75th percentiles, outliers are represented by dots; crosses represent sample means. ***$p < 0.001$ as determined by one-way ANOVA test with Games-Howell *post-hoc* test. **(C)** Maximum projections of confocal Z-stacks of dendrites from neurons overexpressing EGFP along with either mCherry, α-actinin-4-mCherry or α-actinin-4-M554V-mCherry. Only EGFP channel is shown and was used to assess spine density and morphology. Scale bar, 4 μm. **(D)** Quantification of dendritic spine density calculated as number of spines per 1 μm of dendrite. The first left cluster of bars represents total spine density. Densities of thin, mushroom, stubby, and total spines were as follows: wt: thin = 0.25, mushroom = 0.15, stubby = 0.07, total = 0.48 spines/μm ($n = 34$ neurons, 1,937 spines, 4,091 μm dendrite); α-actinin-4: thin = 0.18, mushroom = 0.21, stubby = 0.08, total = 0.46 spines/μm ($n = 26$ neurons, 1,229 spines, 2,816 μm dendrite); α-actinin-4-M554V: thin = 0.24, mushroom = 0.18, stubby = 0.09, total = 0.51 spines/μm ($n = 30$ neurons, 1,750 spines, 3,573 μm dendrite). Data is pooled from 4 experiments and represented as mean ± SEM. *$p < 0.05$, **$p < 0.01$ as determined by one-way ANOVA test with Bonferroni *post-hoc* test. **(E)** Cumulative distributions of the width, length and the ratio of width to length of dendritic spines for neurons expressing either mCherry (control), α-actinin-4-mCherry or α-actinin-4-M554V-mCherry. Curves are a combination of data points each representing an individual spine. Matching tail regions of the curves are not shown. *$p < 0.05$, ***$p < 0.001$ as determined by pairwise two-sample Kolmogorov-Smirnov test.

of 0.98 ± 0.01 (**Figures 2A,B**, **Table 2**). M554V-α-actinin-4 also localized to dendritic spines—albeit to a much lesser extent than wild-type α-actinin-4 at a ratio of 4.10 ± 0.29 (**Figures 2A,B**).

To assess possible changes in dendritic spines, we analyzed dendritic spine morphology and density in neurons co-transfected with EGFP and wild-type or mutated α-actinin-4-mCherry. Dendritic spine density and morphology were analyzed using the NeuronStudio software (Rodriguez et al., 2008) using EGFP intensity. The overexpression of wild-type α-actinin-4 resulted in an increase in mushroom spine density, while mutated α-actinin-4 failed to induce such an increase when compared to control cells expressing mCherry (**Figures 2C,D**). Thin spine density was decreased in wild-type α-actinin-4 expressing cells compared to control cells, whereas in mutant α-actinin-4 expressing cells the thin spine density was significantly increased compared to wild-type expressing cells (**Figures 2C,D**, **Table 2**). The cumulative distributions of spine head width, length, and width-to-length ratios showed some significant differences. Wild-type—but not mutant—overexpressing cells had a higher proportion of spines with wider heads in the range of 0.2–0.8 μm, whereas both wild-type and mutant overexpressing cells had slightly higher proportions of shorter spines in the range of 0.5–2.5 μm (**Figure 2E**). From the distributions of width-to-length ratios of spines we can see that in cells overexpressing wild-type or mutant α-actinin-4, more spines possessed mature morphology (i.e., wide head, short neck) compared to controls. This suggests that changes in spine widths and lengths occur proportionally in the same spines. Taken together, these results show that mutated α-actinin-4 is less concentrated in dendritic spines and fails to mimic the effect of the wild-type protein on dendritic spine morphology.

Next, we analyzed the density and size of inhibitory synapses, as well as the proportion of inhibitory synapses in spines, by visualizing inhibitory synapses using gephyrin antibody staining. To check the specificity of gephyrin staining, we co-stained cells with the pre-synaptic VGAT antibody (**Figure 3**). This co-staining showed co-localization between gephyrin puncta and the presynaptic VGAT marker, ruling out the possibility of unspecific gephyrin staining (**Figure 3**). Analysis of gephyrin puncta revealed that the overexpression of wild-type α-actinin-4 reduced the density of inhibitory synapses (**Figure 4**, **Table 2**). However, the change varied between experiments and, therefore, this result did not reach statistical significance. Mutated α-actinin-4 enhanced this effect of wild-type protein and the difference between mutant α-actinin-4 and control cells was significant (**Figure 4B**). The changes in synapse size or the proportion of synapses on dendritic spines were not significant (**Figure 4B**).

In summary, we found that M554V point mutation in α-actinin-4 reduces the localization of α-actinin-4 to dendritic spines. The expression of α-actinin-4-M554V in hippocampal neurons resulted in an increased thin spine density compared to the expression of wild-type α-actinin-4. The mutation in α-actinin-4 enhanced the effect of wild-type protein in decreasing the inhibitory synapse density, and the difference in density between control and mutant α-actinin-4 expressing neurons was significant. These results suggest that the ASD-associated M554V mutation leads to a loss-of–function or reduced-function effect in α-actinin-4 in the regulation of dendritic spines. However, this mutation enhances the effect of wild-type α-actinin-4 in inhibitory synapses (**Table 2**).

Myosin IIb Mutation Y265C Expression Reduces Inhibitory Synapse Size and the Proportion of Inhibitory Synapses in Spines

A *de novo* missense mutation T to C in the *MYH10* gene was found by whole exome sequencing of parent–child trios exhibiting sporadic ASD (O'Roak et al., 2012) (**Figures 5A,B**). This base change leads to the substitution of tyrosine-265 (Y265) to cysteine (C) in the myosin IIb protein. Y265 is located in the center of the myosin IIb motor domain and participates in a potentially stabilizing hydrogen bond interaction with the neighboring glutamate-263. These residues are distal from the motor domain ATP binding site but could contribute to the ATPase activity by affecting the stability and overall folding of this domain (**Figures 5A,B**).

As expected from earlier work (Korobova and Svitkina, 2010; Rubio et al., 2011), wild-type myosin IIb localized to the base of the spine head, showing enrichment in spines vs. dendrites (**Figures 6A,B**). The mutated myosin IIb exhibited similar localization (**Figures 6A,B**). Spine analysis did not reveal any differences in spine density between control, myosin IIb wild-type, and myosin IIb-Y265C (**Figures 6C,D**). Cumulative distribution analysis showed slight changes in spine morphology (**Figure 6E**). Neurons overexpressing wild-type myosin IIb exhibited a smaller proportion of wider spines compared to controls and neurons overexpressing myosin-IIb-Y265C. Mutant-expressing neurons showed an increased fraction of wider spines and a decreased proportion of long spines compared

TABLE 2 | Result summary table.

Comparison of wild-type (wt) protein phenotypes to control phenotype and mutant expression phenotype to wild-type phenotype					
	α-actinin-4	**Myosin IIb**	**Myosin IXb**	**SWAP-70**	**SrGAP3**
Localization to spines (ratio spine/shaft)					
Ctrl vs. wt	0.98 vs. 6.64	0.93 vs. 1.73	0.92 vs. 1.65	0.98 vs. 1.15	0.99 vs. 1.32
Ctrl vs. mut	0.98 vs. 4.1	0.93 vs. 1.79	0.92 vs. 1.61	0.98 vs. 1.78	0.99 vs. 1.42
wt vs. mut	6.64 vs. 4.1	1.73 vs. 1.79	1.65 vs. 1.61	1.15 vs. 1.78	1.32 vs. 1.42
Total spine density (spines/μm)					
Ctrl vs. wt	0.48 vs. 0.46	0.55 vs. 0.57	0.48 vs. 0.44	0.39 vs. 0.46	0.45 vs. 0.54
Ctrl vs. mut	0.48 vs. 0.51	0.55 vs. 0.61	0.48 vs. 0.49	0.39 vs. 0.54	0.45 vs. 0.54
wt vs. mut	0.46 vs. 0.51	0.57 vs. 0.61	0.44 vs. 0.49	0.46 vs. 0.54	0.54 vs. 0.54
Thin spine density (spines/μm)					
Ctrl vs. wt	0.25 vs. 0.18	0.25 vs. 0.27	0.24 vs. 0.24	0.19 vs. 0.25	0.23 vs. 0.29
Ctrl vs. mut	0.25 vs. 0.24	0.25 vs. 0.27	0.24 vs. 0.27	0.19 vs. 0.31	0.23 vs. 0.28
wt vs. mut	0.18 vs. 0.24	0.27 vs. 0.27	0.24 vs. 0.27	0.25 vs. 0.31	0.29 vs. 0.28
Mushroom spine density (spines/μm)					
Ctrl vs. wt	0.15 vs. 0.21	0.20 vs. 0.21	0.18 vs. 0.15	0.16 vs. 0.18	0.16 vs. 0.18
Ctrl vs. mut	0.15 vs. 0.18	0.20 vs. 0.22	0.18 vs. 0.15	0.16 vs. 0.18	0.16 vs. 0.19
wt vs. mut	0.21 vs. 0.18	0.21 vs. 0.22	0.15 vs. 0.15	0.18 vs. 0.18	0.18 vs. 0.19
Total spine head size (μm)					
Ctrl vs. wt	0.46 vs. 0.46	0.49 vs. 0.43	0.46 vs. 0.42	0.44 vs. 0.44	0.44 vs. 0.45
Ctrl vs. mut	0.46 vs. 0.46	0.49 vs. 0.49	0.46 vs. 0.43	0.44 vs. 0.40	0.44 vs. 0.45
wt vs. mut	0.46 vs. 0.46	0.43 vs. 0.49	0.42 vs. 0.43	0.44 vs. 0.40	0.45 vs. 0.45
Inhibitory synapse density (synapses/μm)					
Ctrl vs. wt	0.40 vs. 0.31	0.37 vs. 0.45	0.37 vs. 0.37	0.38 vs. 0.38	0.37 vs. 0.41
Ctrl vs. mut	0.40 vs. 0.25	0.37 vs. 0.39	0.37 vs. 0.40	0.38 vs. 0.28	0.37 vs. 0.51
wt vs. mut	0.31 vs. 0.25	0.45 vs. 0.39	0.37 vs. 0.40	0.38 vs. 0.28	0.41 vs. 0.51
Inhibitory synapse size (μm)					
Ctrl vs. wt	0.43 vs. 0.44	0.44 vs. 0.46	0.44 vs. 0.48	0.42 vs. 0.38	0.44 vs. 0.38
Ctrl vs. mut	0.43 vs. 0.44	0.44 vs. 0.42	0.44 vs. 0.44	0.42 vs. 0.40	0.44 vs. 0.39
wt vs. mut	0.44 vs. 0.44	0.46 vs. 0.42	0.48 vs. 0.44	0.38 vs. 0.40	0.38 vs. 0.39
Proportion of inhibitory synapses in spines vs. shaft					
Ctrl vs. wt	0.38 vs. 0.37	0.33 vs. 0.43	0.33 vs. 0.41	0.34 vs. 0.37	0.33 vs. 0.33
Ctrl vs. mut	0.38 vs. 0.31	0.33 vs. 0.34	0.33 vs. 0.39	0.34 vs. 0.34	0.33 vs. 0.42
wt vs. mut	0.37 vs. 0.31	0.43 vs. 0.34	0.41 vs. 0.39	0.37 vs. 0.34	0.33 vs. 0.42
Main changes for wt vs. control	Decreased thin spine density and increased mushroom spine density	Increased proportion of inhibitory synapses in spines	Increased proportion of inhibitory synapses in spines	No significant changes in spines or inhibitory synapses	Reduced inhibitory synapse size
Main changes for mutant vs. wt	Reduced localization to spines and increased thin spines density	Reduced size of inhibitory synapses and reduced proportion of inhibitory synapses in spines	No significant changes	Enhanced spine localization, reduced spine head size and reduced inhibitory synapse density	Increased localization to spines, increased proportion of inhibitory synapses in spines

Values obtained from wild-type (ctrl vs. wt) or mutated protein (ctrl vs. mut) expressing cells are compared to control cells, and values obtained from cells expressing wild-type proteins are compared to values of mutant protein expressing cells (wt vs. mut). A statistically significant ($p < 0.05$) increase is highlighted with green and decrease with blue.

to wild-type myosin IIb-expressing neurons. In summary, only minor changes in dendritic spines were observed upon myosin IIb-Y265C over-expression.

The analysis of inhibitory synapses showed that wild-type myosin IIb expression increased the proportion of inhibitory synapses in spines compared to control cells

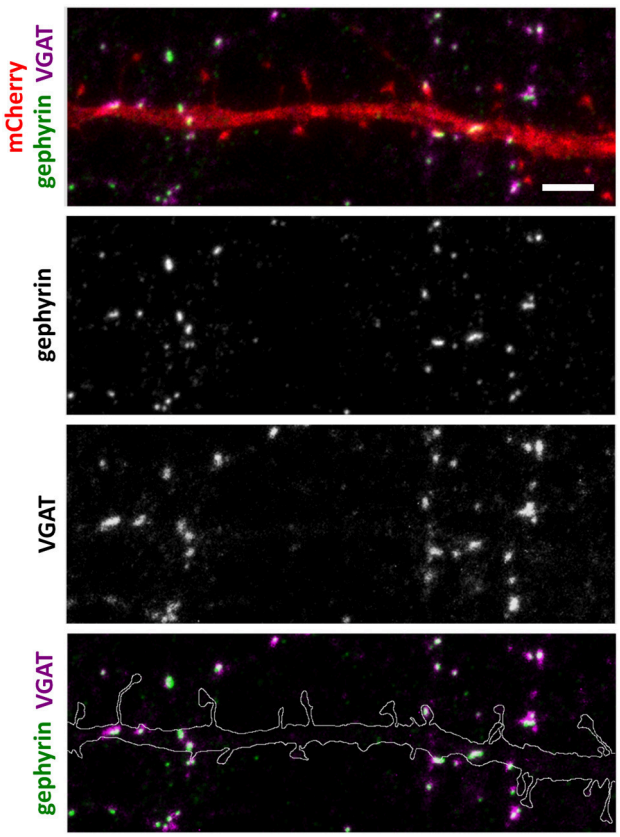

FIGURE 3 | Inhibitory synapse localization in a DIV15 hippocampal neuron expressing mCherry and stained with postsynaptic anti-gephyrin (Alexa-488) and presynaptic anti-VGAT (Alexa-594) antibodies. In overlay, mCherry is shown in red, anti-gephyrin antibody staining in green, and anti-VGAT antibody staining in magenta. The line indicates the contour of dendrites (from mCherry). Scale bar, 5 μm.

(**Figures 7A,B**, **Table 2**). In contrast, mutant-expressing cells had fewer inhibitory synapses located on dendritic spines compared to wild-type overexpressing neurons (**Figures 7A,B**, **Table 2**). Moreover, the size of inhibitory synapses was smaller in neurons overexpressing myosin IIb-Y265C compared to neurons expressing wild-type myosin IIb.

In summary, the Y265C-mutation induced slight changes in the morphology and size of dendritic spines compared to neurons expressing wild-type myosin IIb. The expression of the mutant reduced the size of inhibitory synapses and the proportion of inhibitory synapses located on spines, compared to wild-type expression.

Myosin IXB Increases the Proportion of Inhibitory Synapses in Spines

Whole exome sequencing applied to families with an ASD child revealed A/G *de novo* missense mutations in the *MYO9B* gene leading to an amino acid change [lysine (K) 1872 to arginine (R)] in the RhoGAP domain of the myosin IXb protein (Iossifov et al., 2014) (**Figure 8A**). K1872 is involved in a stabilizing salt-bridge interaction with E1796 within the RhoGAP domain. However, it is not likely that the conservative lysine to arginine mutation would result in significant domain destabilization or functional change (**Figures 8A,B**).

Over-expression of wild-type and myosin IXb-K1872R-mCherry constructs revealed enrichment in spine heads 1.6 times that of mCherry (**Figures 9A,B**). Spine analysis revealed no significant changes in spine density in neurons expressing either wild-type or myosin IXb-K1872R-mCherry constructs (**Figures 9C,D**, **Table 2**). Thin spine density was slightly increased in neurons expressing mutated myosin IXb, but this change did not reach statistical significance. Examination of the cumulative distribution of spine morphological aspects such as width, length, and width-to-length ratio showed only minor differences (**Figure 9E**). Neurons expressing wild-type or myosin IXb-K1872R had a marginally higher proportion of thinner spines in the range of 0.3–0.7 μm. The lengths and width-to-length ratios of spines had very comparable distributions for all three groups (**Figure 9E**).

Wild-type myosin IXb expression increased the proportion of inhibitory synapses compared to control cells (**Figures 10A,B**, **Table 2**). The K1872R mutation did not cause any significant changes in inhibitory synapses when compared to wild-type expression.

SWAP-70 Mutant L544F Expression Enhances Localization to Spines and Reduces the Spine Width and Inhibitory Synapse Density

Whole exome sequencing of families with an ASD child revealed a *de novo* missense mutation A/T in *SWAP70*, leading to an amino acid change of leucine (L) 544 to phenylalanine (F) in the C-terminus of SWAP-70 (**Figure 11A**). The C-terminus of SWAP-70 (amino acids 525–585) is known to be critical for actin binding (Ihara et al., 2006), so a mutation in this region could putatively affect the protein's actin binding properties.

Wild-type SWAP-70 was slightly enriched in dendritic spines when expressed as an mCherry fusion protein in neurons (**Figures 11B,C**). SWAP-70 L544F-mutation significantly enhanced the spine localization (**Figures 11B,C**, **Table 2**). Spine analysis showed increased total and thin spine density for SWAP-70 expressing neurons. The L544F-mutation enhanced these effects, and the difference between cells expressing mutated SWAP-70 and cells expressing mCherry was statistically significant (**Figures 11D,E**). On average, spine protrusion lengths or head widths in SWAP-70-overexpressing cells were not different from control. However, with the introduction of the mutant SWAP-70-L544F, dendritic spines became thinner (average head width of 0.40 ± 0.01 μm for the mutant vs. 0.44 ± 0.01 μm for wild-type, $p < 0.05$) compared to wild-type SWAP-70. In addition, the distribution of spine morphology parameters showed a similar change toward an increased proportion of thin and short spines (**Figure 11F**). The density of inhibitory synapses was significantly decreased in mutant-overexpressing neurons compared to both control and wild type-overexpressing neurons (**Figures 12A,B**, **Table 2**).

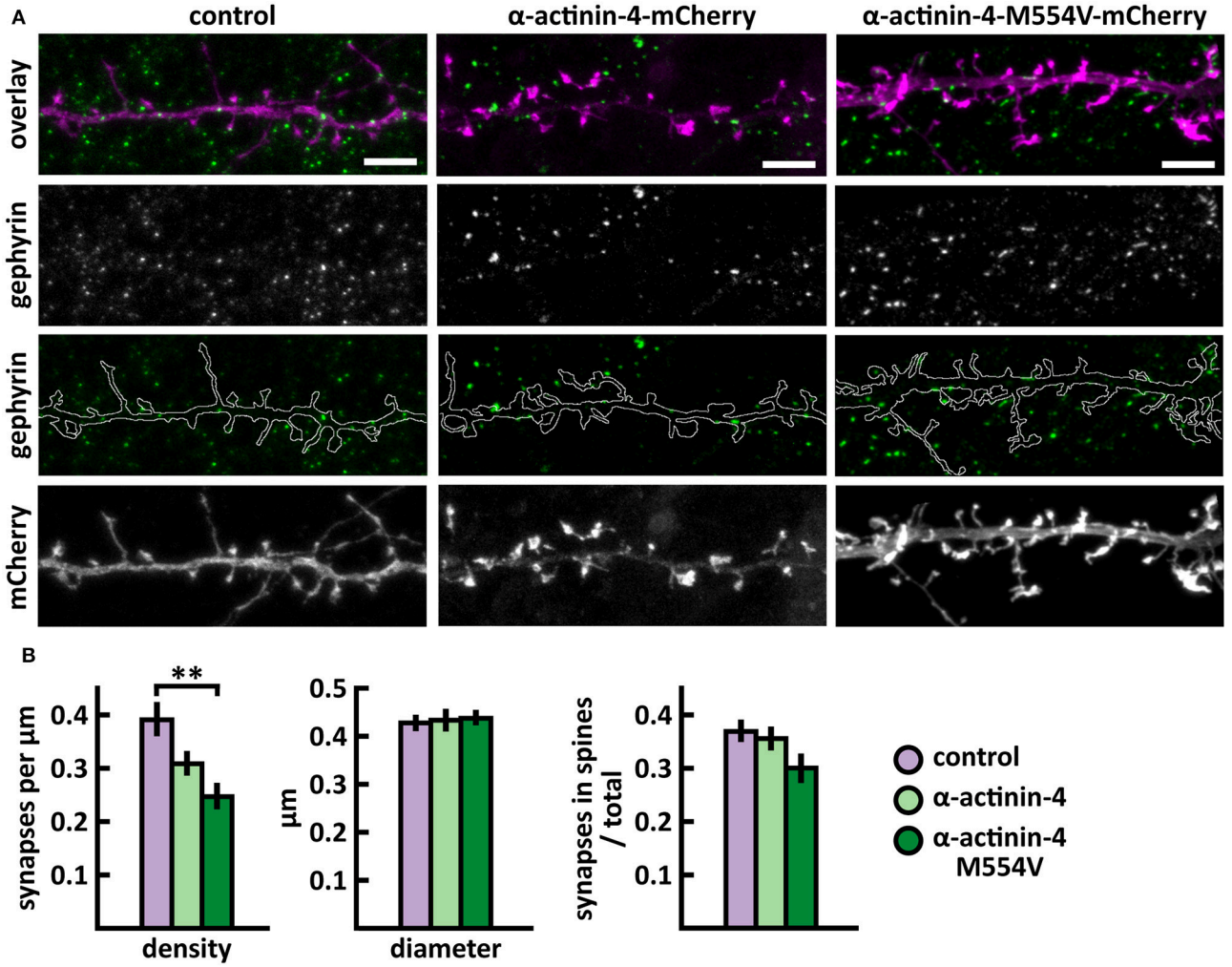

FIGURE 4 | Characterization of the inhibitory synapses in DIV15 hippocampal neurons expressing either mCherry (control), wild-type α-actinin-4-mCherry or α-actinin-4-M554V-mCherry and stained with anti-gephyrin antibody. **(A)** In overlay, mCherry is shown in magenta and anti-gephyrin antibody staining in green. The line indicates the contour of dendrites (from mCherry). Scale bars, 5 µm. **(B)** Quantification of inhibitory synapse properties. From left to right: (1) Mean density of synapses calculated as the number of gephyrin puncta per µm of the dendrite: control = 0.40; α-actinin-4 = 0.31; α-actinin-4-M554V = 0.25. (2) Mean diameter of individual gephyrin puncta in µm: control = 0.43; α-actinin-4 = 0.44; α-actinin-4-M554V = 0.44. (3) Proportion of the gephyrin puncta located on dendritic spines as a fraction of the total number of puncta: control = 0.38; α-actinin-4 = 0.37; α-actinin-4-M554V = 0.31. Data in **(B)** represent n(control) = 19 cells, n(α-actinin-4) = 21 cells, n(α-actinin-4-M554V) = 20 cells, pooled from 3 experiments. $^{**}p < 0.01$ as determined by one-way ANOVA with Bonferroni's *post-hoc* test. Data is represented as mean ± SEM.

Taken together, wild-type SWAP-70 was neither enriched in dendritic spines, nor did its overexpression alter dendritic spine density or morphology. Wild-type SWAP-70 overexpression did not affect inhibitory synapses either. In contrast, mutated SWAP-70 was enriched in dendritic spines and its overexpression changed the morphology of spines, making them narrower. It also reduced the density of inhibitory synapses by almost 30% compared to wild-type expressing cells (**Figure 12B**). We conclude that the SWAP-70-L544F mutation changes its function from a non-synaptic regulator to a regulator of dendritic spines and inhibitory synapses.

SrGAP3 Mutant E469K Expression Enhances Localization to Spines and Increases the Proportion of Inhibitory Synapses in Spines

A *de novo* C/T missense variant in the *SRGAP3* gene was identified in an ASD proband (Sanders et al., 2012). In the SrGAP3 protein, this mutation changes glutamic acid-469 to lysine (E469K), thus changing the charge of the amino acid (**Figure 13A**).

The mutated SrGAP3 construct enhanced the dendritic spine localization of SrGAP3 (**Figures 13B,C**). Spine analysis showed

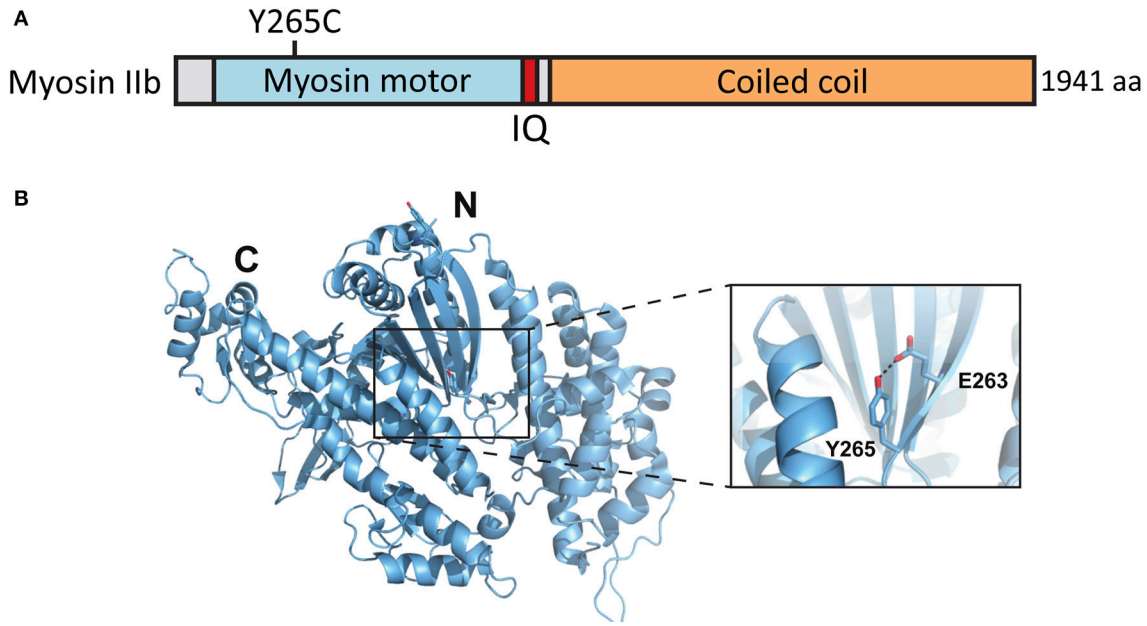

FIGURE 5 | Location of the mutated amino acid in the myosin IIb structure. **(A)** Primary structure of human myosin IIb with the Y265C mutation indicated. **(B)** Structure of human myosin IIb (PDB ID 4PD3) with residue Y265 and surrounding residues highlighted (close-up).

a significant increase in the density of total and thin spines in neurons that overexpressed SrGAP3-E469K compared to control neurons (**Figures 13D,E**). We did not observe any difference in the distribution of head widths, lengths, or width-to-length ratios between all 3 groups (**Figure 13F**). SrGAP3 wild-type expression decreased the size of inhibitory synapses, whereas the expression of mutated SrGAP3 increased the proportion of inhibitory synapses in spines compared to wild-type SrGAP3 expression (**Figures 14A,B**).

These results show that the E469K mutation enhances the localization of SrGAP3 to dendritic spines. Both wild-type and mutated SrGAP3 increased the density of total and thin spines, and the change between the control and mutated-SrGAP3 groups was statistically significant. The mutation also changed the location of inhibitory synapses by increasing their ratio in dendritic spines.

DISCUSSION

Both genetic and anatomical studies suggest an important role for defective synapse or spine regulation in ASD. Many actin-modulating proteins known to regulate dendritic spine morphology and density are associated with ASD (Joensuu et al., 2017). However, current knowledge about the mutational effects of these proteins is poor. This has hampered the ability to deduce the prevalence of common defects or cellular phenotypes across different genes and mutations. Based on current literature, we concluded that dendritic spines and inhibitory synapses are good parameters to test the functional consequences of mutations. Dendritic spines are especially suitable because three of the proteins studied (α-actinin-4, myosin IIb, and SrGAP3) have known functions in regulating dendritic spine density and morphology (Zhang, 2005; Ryu et al., 2006; Rex et al., 2010; Carlson et al., 2011; Hodges et al., 2011; Kalinowska et al., 2015). The selection of these parameters was also favored by the fact that both dendritic spines and inhibitory synapses are relatively easy to analyze and could therefore be used for high-throughput screening in future studies. Synaptic transmission would have been another parameter to evaluate, but because the depletion and overexpression of α-actinin-4 resulted in no change in basal synaptic transmission (Kalinowska et al., 2015), we estimated that it is more plausible to detect changes in dendritic spine morphology.

The proper localization of proteins is critical for their correct functioning. Thus, we first analyzed the localization of wild-type and mutated proteins (results summarized in **Table 2**). Common for all the proteins studied was the enrichment in dendritic spines, suggesting that they can have a role in the regulation of dendritic spine number or morphology. Localization analysis confirmed earlier published results for α-actinin-4 (Kalinowska et al., 2015), myosin IIb (Korobova and Svitkina, 2010; Rubio et al., 2011), and SrGAP3 (Carlson et al., 2011). The mutations induced changes in the localization of α-actinin-4, which localized less to dendritic spines, and for SWAP-70 and SrGAP3, which localized more to dendritic spines. These results show that single amino acid changes can affect the subcellular localization of proteins and a mutation can either reduce (loss-of-function) or induce (gain-of-function) a specific localization.

Next, we studied whether these mutations affect the proteins' overexpression effects on dendritic spine density and morphology in primary hippocampal neurons. Among the wild-type proteins studied, only α-actinin-4 overexpression

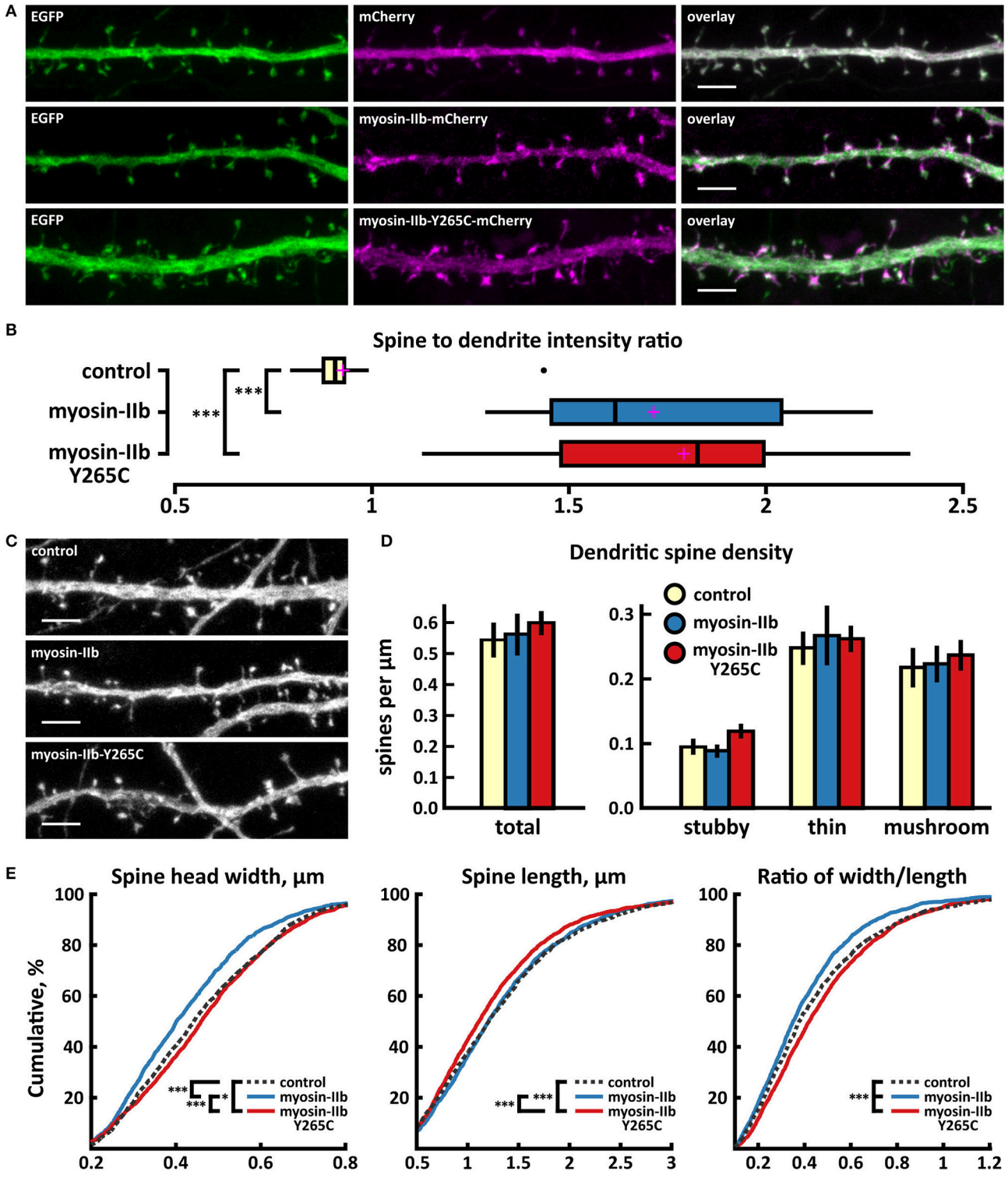

FIGURE 6 | Characterization of protein localization, dendritic spine density and morphology in DIV14-15 hippocampal neurons expressing EGFP and mCherry (control), myosin-IIb-mCherry or mutated myosin-IIb-Y265C-mCherry. **(A)** Representative maximum projections of confocal Z-stacks for EGFP, mCherry, and wild-type and mutated myosin-IIb localization. Scale bars 4 µm. **(B)** The quantification of protein localization revealed similar enrichment for both wt and mutated myosin-IIb to dendritic spines. Spine-to-dendrite fluorescence intensity ratios: control: 0.93 (n = 17 cells, 170 spines), myosin-IIb: 1.73 (n = 17 cells, 170 spines), myosin-IIb-Y265C 1.79 (n = 18 cells, 180 spines). Center lines show the medians; box limits indicate the 25th and 75th percentiles as determined by R software; whiskers extend 1.5

(Continued)

FIGURE 6 | times the interquartile range from the 25th and 75th percentiles, outliers are represented by dots; crosses represent sample means. ***$p < 0.001$ as determined by one-way ANOVA test with Games-Howell *post-hoc* test. **(C)** Maximum projections of confocal Z-stacks of dendrites from neurons overexpressing EGFP along with either mCherry, myosin-IIb-mCherry, or myosin-IIb-Y265C-mCherry. Only EGFP channel is shown and was used to assess spine density and morphology. Scale bar, 4 μm. **(D)** Quantification of dendritic spine density calculated as number of spines per 1 μm of dendrite. The first left cluster of bars represents total spine density. Densities of thin, mushroom, stubby, and total spines were as follows: wt: thin = 0.25, mushroom = 0.2, stubby = 0.1, total = 0.55 spines/μm ($n = 17$ neurons, 1,825 spines, 3,354 μm dendrite); myosin-IIb: thin = 0.27, mushroom = 0.2, stubby = 0.09, total = 0.57 spines/μm ($n = 17$ neurons, 1,718 spines, 3,459 μm dendrite); myosin-IIb-Y265C: thin = 0.27, mushroom = 0.22, stubby = 0.12, total = 0.61 spines/μm ($n = 18$ neurons, 2,253 spines, 3,877 μm dendrite). Data is pooled from 2 experiments and represented as mean ±SEM. Significant differences were not detected by one-way ANOVA test with Games-Howell or Bonferroni *post-hoc* test. **(E)** Cumulative distributions of the width, length, and the ratio of width to length of dendritic spines for neurons expressing either mCherry (control), myosin-IIb-mCherry or myosin-IIb-Y265C-mCherry. Curves are a combination of data points each representing an individual spine. Matching tail regions of the curves are not shown. *$p < 0.05$, ***$p < 0.001$ as determined by pairwise two-sample Kolmogorov-Smirnov test.

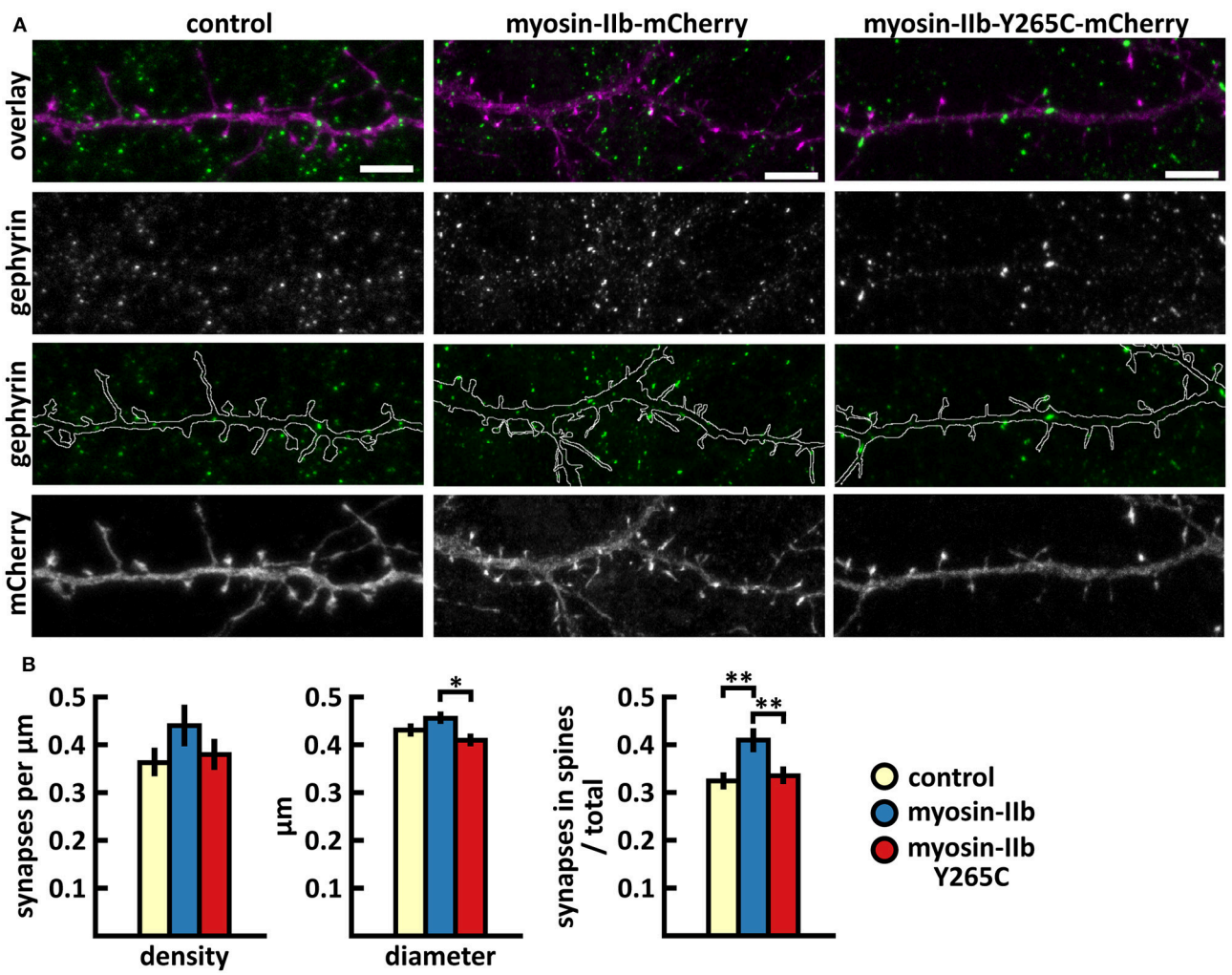

FIGURE 7 | Characterization of the inhibitory synapses in DIV15 hippocampal neurons expressing either mCherry (control), wild-type myosin IIb-mCherry or myosin IIb-Y265C-mCherry and stained with anti-gephyrin antibody. **(A)** In overlay, mCherry is shown in magenta and anti-gephyrin antibody staining in green. The line indicates the contour of dendrites (from mCherry). Scale bars, 5 μm. **(B)** Quantification of inhibitory synapse properties. From left to right: (1) Mean density of synapses calculated as the number of gephyrin puncta per μm of the dendrite: control = 0.37; myosin IIb = 0.45; myosin IIb-Y265C = 0.39. (2) Mean diameter of individual gephyrin puncta in μm: control = 0.44; myosin IIb = 0.46; myosin IIb-Y265C = 0.42 3. Proportion of the gephyrin puncta located on dendritic spines as a fraction of the total number of puncta: control=0.33; myosin IIb = 0.43; myosin IIb-Y265C = 0.34. Data in **(B)** represent n(control) = 17 cells, n(myosin IIb) = 20 cells, n(myosin IIb-Y265C) = 19 cells, pooled from 3 experiments. *$p < 0.05$ and **$p < 0.01$ as determined by one-way ANOVA with Bonferroni's *post-hoc* test. Data is represented as mean ±SEM.

caused a significant change in dendritic spine morphology. This result confirms the earlier reported spine phenotype (Kalinowska et al., 2015). The spine phenotypes of autism-linked proteins have been variable, but, for example, Shank3 overexpression results in an increase in mushroom spines and in spine head width, similar to α-actinin-4 (Durand et al., 2012). Based on the results

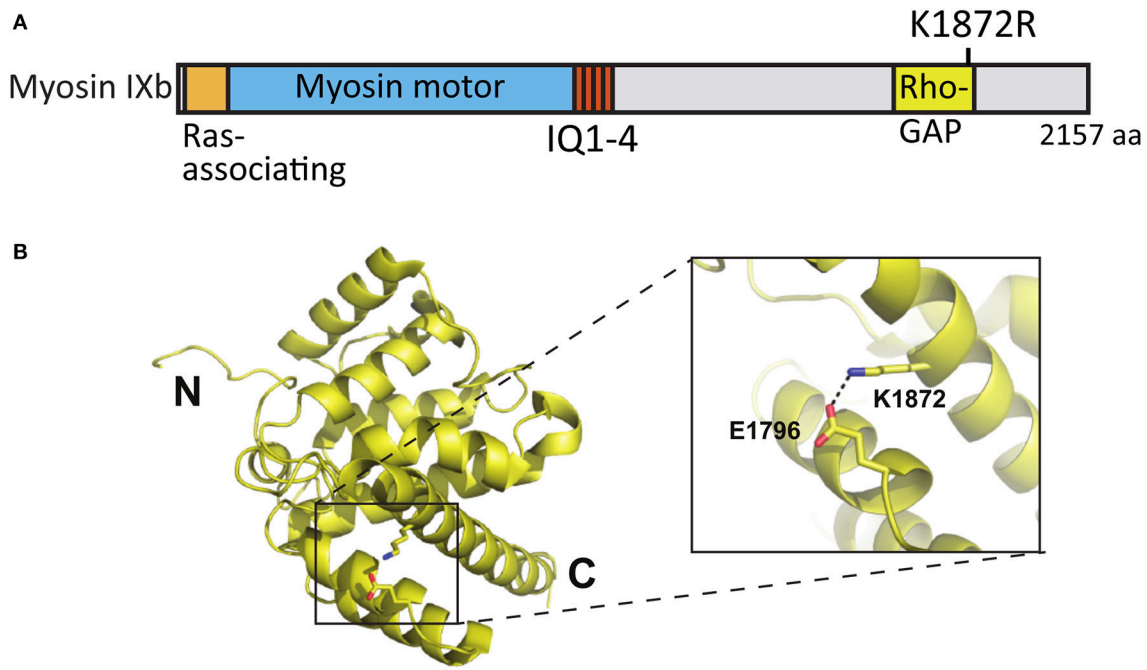

FIGURE 8 | Location of the mutated amino acid in the myosin IXb structure. **(A)** Primary structure of human myosin IXb with the K1872R mutation indicated. **(B)** Structure of human myosin IXb (PDB ID 5C5S) with residue K1872 and surrounding residues highlighted (close-up).

of spine analysis, together with published results, we conclude that wild-type α-actinin-4 (Kalinowska et al., 2015), myosin IIb (Zhang, 2005; Ryu et al., 2006; Rex et al., 2010; Hodges et al., 2011), and SrGAP3 (Carlson et al., 2011) have a clear function in regulating dendritic spine density and morphology (summarized in **Table 2**). Although wild-type myosin IXb and SWAP-70 seem to not have a big impact on spines, this is the first report testing their possible roles in dendritic spines.

We hypothesized that mutations associated with ASD shift dendritic spine morphology from mushroom spines to thin spines. α-actinin-4-M554V mutation resulted in the expected shift in dendritic spine morphology by increasing the thin spine density. This change is similar to what was observed upon the overexpression of ASD-associated Shank3 mutants, which resulted in mostly thinner spines (Durand et al., 2012). In addition to significant changes with the ACTN4 mutation, we saw a trend toward more thin spines with mutations in myosin IXb and SWAP-70 when compared to wild-type proteins. SWAP-70-L544F enhanced the induced increase in thin spine density by the wild-type protein, and the difference between controls and mutation constructs was statistically significant. The increase in thin spines is well supported by the fact that SWAP-70-L544F also increased total spine density and decreased total spine head size, compared to controls. Total spine head size was significantly decreased even when the results were compared to wild-type SWAP-70. Taken together, although most of the changes were mild and the differences between wild-type and mutated proteins were not always significant, we observed a trend toward an increased proportion of thin spines.

Current literature suggests that, compared to bigger mushroom spines, thin spines are structurally more dynamic and transient (Kasai et al., 2003; Holtmaat et al., 2005). Thin spines have weaker synapses than mushroom spines, but they are more susceptible to potentiation (Matsuzaki et al., 2004). Mushroom spines with large heads exhibit more AMPA receptors and stronger excitatory postsynaptic responses (Matsuzaki et al., 2001), and are stable *in vivo* over months (Grutzendler et al., 2002; Trachtenberg et al., 2002; Holtmaat et al., 2005). These correlations have led to the proposal that the small dynamic spines are preferentially involved in learning, whereas larger stable spines mediate long-term memory storage (Kasai et al., 2003). Thus, it is probable that the most frequently observed effect of the mutations—the increased density of thin spines—also affects neuronal function and behavior. Accordingly, studies on Fragile-X syndrome (FXS) and *Shank1* ASD-mouse models have shown a correlation between spine morphology, neuron functionality, and behavior, supporting the importance of proper dendritic spine morphology and density for normal synaptic plasticity and behavior. In the *Fmr1*-deficient FXS mouse model, dendritic spines are thin and elongated and the density is increased (Comery et al., 1997). Neurons of *Fmr1* KO mice exhibit altered synaptic plasticity (Huber et al., 2002; Zhao et al., 2005; Nosyreva and Huber, 2006). In the *Fmr1* KO synapses, a lower ratio of AMPA to NMDA receptors was detected early in development compared to wildtype controls (Pilpel et al., 2009). These data demonstrate that the lack of Fmr1 produces alterations in normal synaptic activity, which likely contributes to the FXS

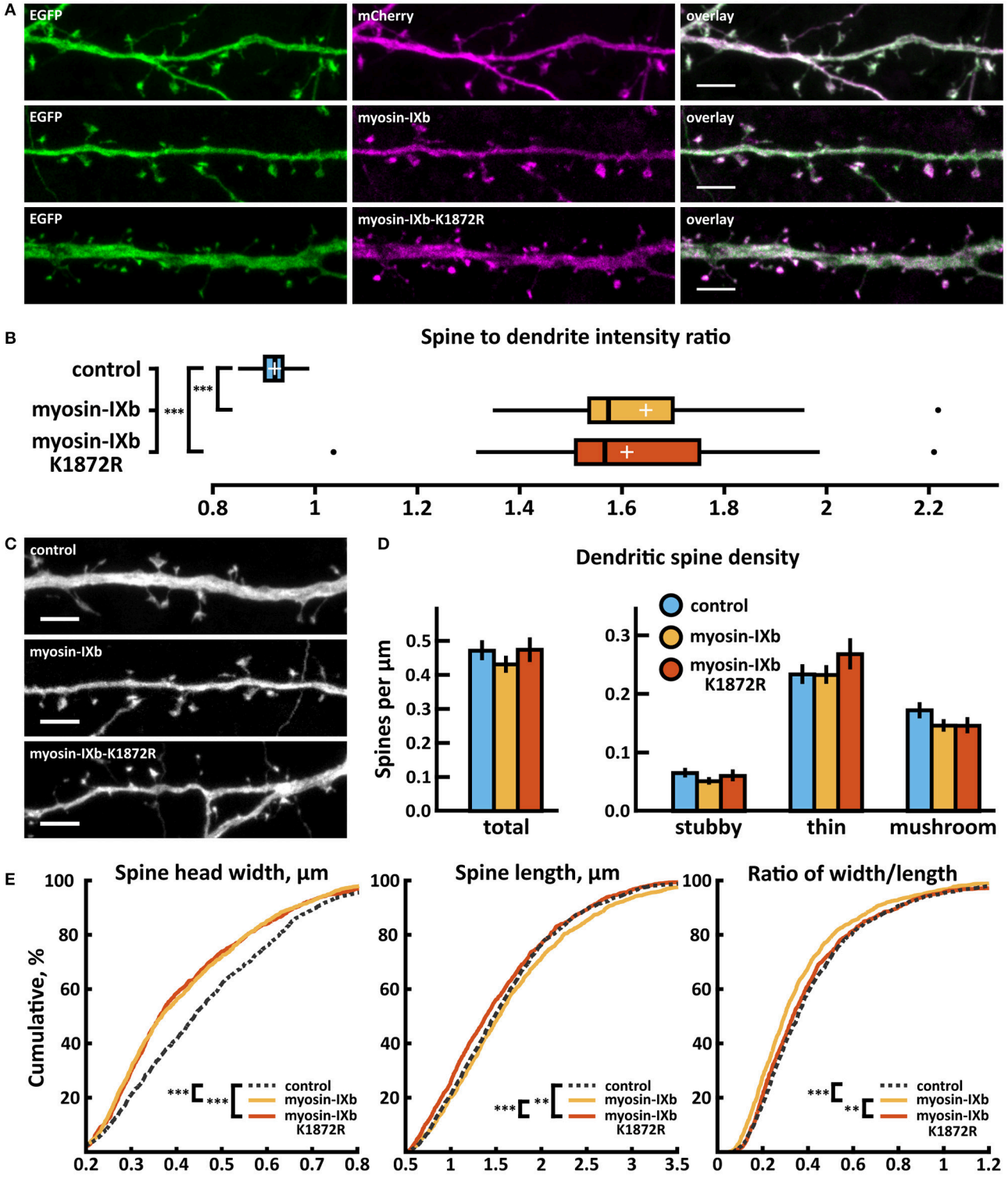

FIGURE 9 | Characterization of protein localization, dendritic spine density and morphology in DIV14-15 hippocampal neurons expressing EGFP and mCherry (control), wild-type myosin-IXb-mCherry or mutated myosin-IXb-K1872R-mCherry. **(A)** Representative maximum projections of confocal Z-stacks for EGFP, mCherry, and wild-type and mutated myosin IXb localization. Scale bars, 4 µm. **(B)** The quantification of protein localization revealed revealed similar enrichment for both wt and mutated myosin-IXb to dendritic spines. Spine-to-dendrite fluorescence intensity ratios: control: 0.92 ($n = 21$ cells, 210 spines), myosin-IXb: 1.65 ($n = 18$ cells, 180 spines), myosin-IXb-K1872R: 1.61 ($n = 14$ cells, 140 spines). Center lines show the medians; box limits indicate the 25th and 75th percentiles as determined by R

(Continued)

FIGURE 9 | software; whiskers extend 1.5 times the interquartile range from the 25th and 75th percentiles, outliers are represented by dots; crosses represent sample means. ***$p < 0.001$ as determined by one-way ANOVA test with Games-Howell *post-hoc* test. **(C)** Maximum projections of confocal Z-stacks of dendrites from neurons overexpressing EGFP along with either mCherry, myosin-IXb-mCherry or myosin-IXb-K1872R-mCherry. Only EGFP channel is shown and was used to assess spine density and morphology. Scale bar, 4 μm. **(D)** Quantification of dendritic spine density calculated as number of spines per 1 μm of dendrite. The first left cluster of bars represents total spine density. Densities of thin, mushroom, stubby, and total spines were as follows: wt: thin = 0.24, mushroom = 0.18, stubby = 0.07, total = 0.48 spines/μm ($n = 21$ neurons, 1,567 spines, 3,321 μm dendrite); myosin-IXb: thin = 0.24, mushroom = 0.15, stubby = 0.06, total = 0.44 spines/μm ($n = 18$ neurons, 1,059 spines, 2,475 μm dendrite); myosin-IXb-K1872R: thin = 0.27, mushroom = 0.15, stubby = 0.06, total = 0.49 spines/μm ($n = 14$ neurons, 1,006 spines, 2,120 μm dendrite). Data is pooled from 3 experiments and represented as mean ±SEM. Significant differences were not detected by one-way ANOVA test with Bonferroni *post-hoc* test. **(E)** Cumulative distributions of the width, length, and the ratio of width to length of dendritic spines for neurons expressing either mCherry (control), myosin-IXb-mCherry or myosin-IXb-K1872R-mCherry. Curves are a combination of data points each representing an individual spine. Matching tail regions of the curves are not shown. **$p < 0.01$, ***$p < 0.001$ as determined by pairwise two-sample Kolmogorov-Smirnov test.

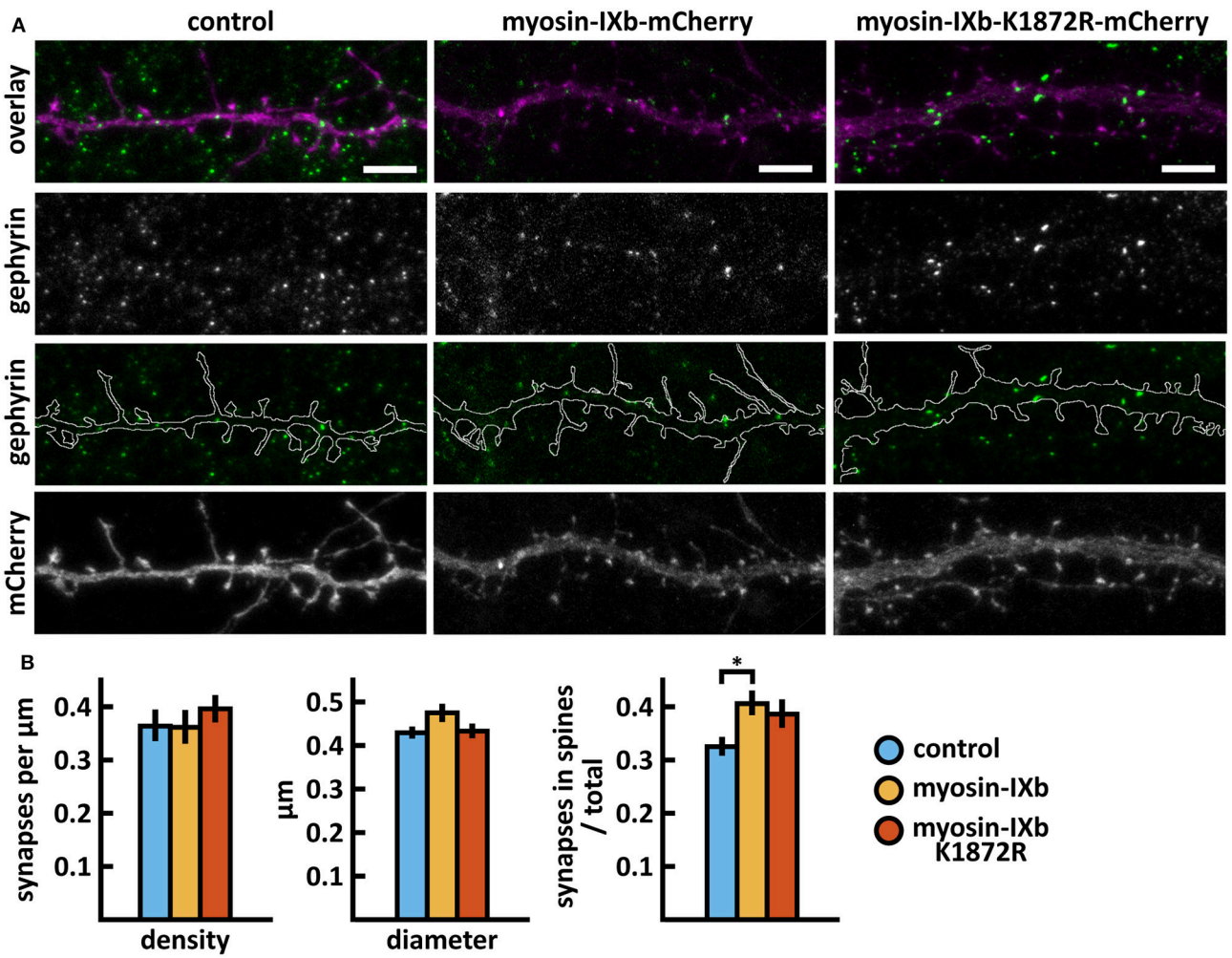

FIGURE 10 | Characterization of the inhibitory synapses in DIV15 hippocampal neurons expressing either mCherry (control), wild-type myosin IXb-mCherry or myosin IXb-K1872R-mCherry and stained with anti-gephyrin antibody. **(A)** In overlay, mCherry is shown in magenta and anti-gephyrin antibody staining in green. The line indicates the contour of dendrites (from mCherry). Scale bars, 5 μm. **(B)** Quantification of inhibitory synapse properties. From left to right: (1) Mean density of synapses calculated as the number of gephyrin puncta per μm of the dendrite: control = 0.37; myosin IXb = 0.37; myosin IXb-K1872R = 0.40. (2) Mean diameter of individual gephyrin puncta in μm: control = 0.44; myosin IXb = 0.48; myosin IXb-K1872R = 0.44 3. Proportion of the gephyrin puncta located on dendritic spines as a fraction of the total number of puncta: control = 0.33; myosin IXb = 0.41; myosin IXb-K1872R = 0.39. Data in **(B)** represent n(control) = 17 cells, n(myosin IXb) = 24 cells, n(myosin IXb-K1872R) = 24 cells, pooled from 2 experiments. *$p < 0.05$ as determined by one-way ANOVA with Bonferroni's *post-hoc* test. Data is represented as mean ± SEM.

phenotype. Behavioral analyses have revealed autism-related behavior, such as hyperactivity, repetitive behaviors, and seizures (reviewed in Kazdoba et al., 2014). By rescuing the spine density or morphology, autism-related behavior was rescued (Dolan et al., 2013; Pyronneau et al., 2017). *Shank1*-KO mice showed thinner dendritic spines, smaller excitatory synapses,

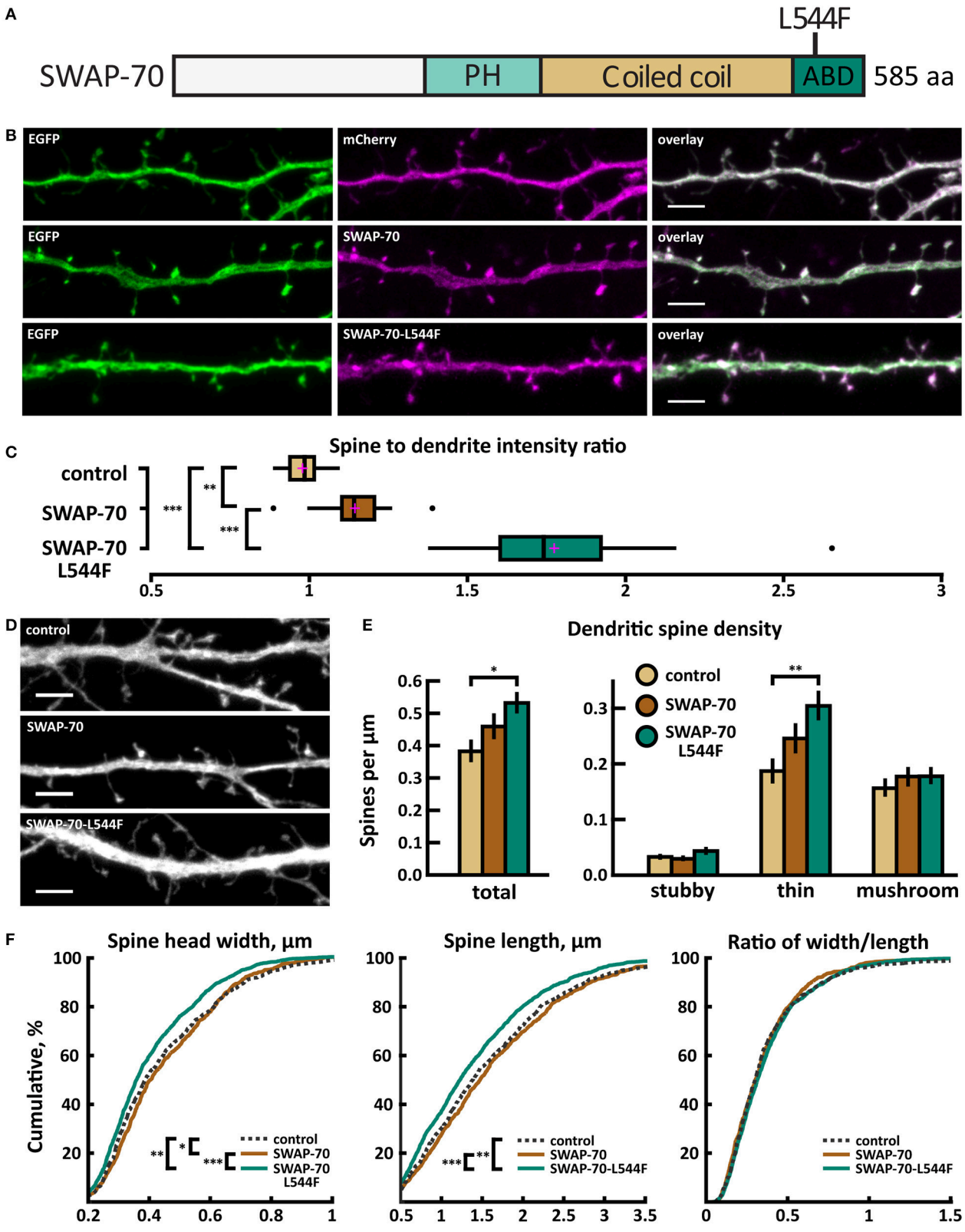

FIGURE 11 | Characterization of protein localization, dendritic spine density and morphology in DIV14-15 hippocampal neurons expressing EGFP and mCherry (control), wild-type SWAP-70-mCherry or mutated SWAP-70-L544F-mCherry. **(A)** Primary structure of human SWAP-70 with mutation L544F indicated. **(B)** Representative maximum projections of confocal Z-stacks for EGFP, mCherry, and wild-type and mutated SWAP-70 localization. Scale bars 4 µm. **(C)** The

(Continued)

FIGURE 11 | quantification of protein localization revealed slightly enriched localization of wt SWAP-70 and the clear accumulation of SWAP-70-L544F in dendritic spines. Spine-to-dendrite fluorescence intensity ratios: control: 0.98 ($n = 15$ cells, 147 spines), SWAP-70: 1.15 ($n = 15$ cells, 173 spines), SWAP-70-L544F: 1.78 ($n = 18$ cells, 180 spines). Center lines show the medians; box limits indicate the 25th and 75th percentiles as determined by R software; whiskers extend 1.5 times the interquartile range from the 25th and 75th percentiles, outliers are represented by dots; crosses represent sample means. $^{**}p < 0.01$, $^{***}p < 0.001$ as determined by one-way ANOVA test with Bonferroni *post-hoc* test. **(D)** Maximum projections of confocal Z-stacks of dendrites from neurons overexpressing EGFP along with either mCherry, SWAP-70-mCherry or SWAP-70-L544F-mCherry. Only EGFP channel is shown and was used to assess spine density and morphology. Control image is re-used from **Figure 2C**. Scale bar, 4 μm. **(E)** Quantification of dendritic spine density calculated as number of spines per 1 μm of dendrite. The first left cluster of bars represents total spine density. Densities of thin, mushroom, stubby, and total spines were as follows: wt: thin = 0.19, mushroom = 0.16, stubby = 0.04, total = 0.39 spines/μm ($n = 15$ neurons, 753 spines, 1,994 μm dendrite); SWAP-70: thin = 0.25, mushroom = 0.18, stubby = 0.03, total = 0.46 spines/μm ($n = 16$ neurons, 762 spines, 1,780 μm dendrite); SWAP-70-L544F: thin = 0.31, mushroom = 0.18, stubby = 0.05, total = 0.54 spines/μm ($n = 20$ neurons, 1,403 spines, 2,672 μm dendrite). Data is pooled from 2 experiments and represented as mean ±SEM. $^{*}p < 0.05$, $^{**}p < 0.01$ as determined by one-way ANOVA test with Bonferroni *post-hoc* test. **(F)** Cumulative distributions of the width, length and the ratio of width to length of dendritic spines for neurons expressing either mCherry (control), SWAP-70-mCherry or SWAP-70-L544F-mCherry. Curves are a combination of data points each representing an individual spine. Matching tail regions of the curves are not shown. $^{*}p < 0.05$, $^{**}p < 0.01$, $^{***}p < 0.001$ as determined by pairwise two-sample Kolmogorov-Smirnov test.

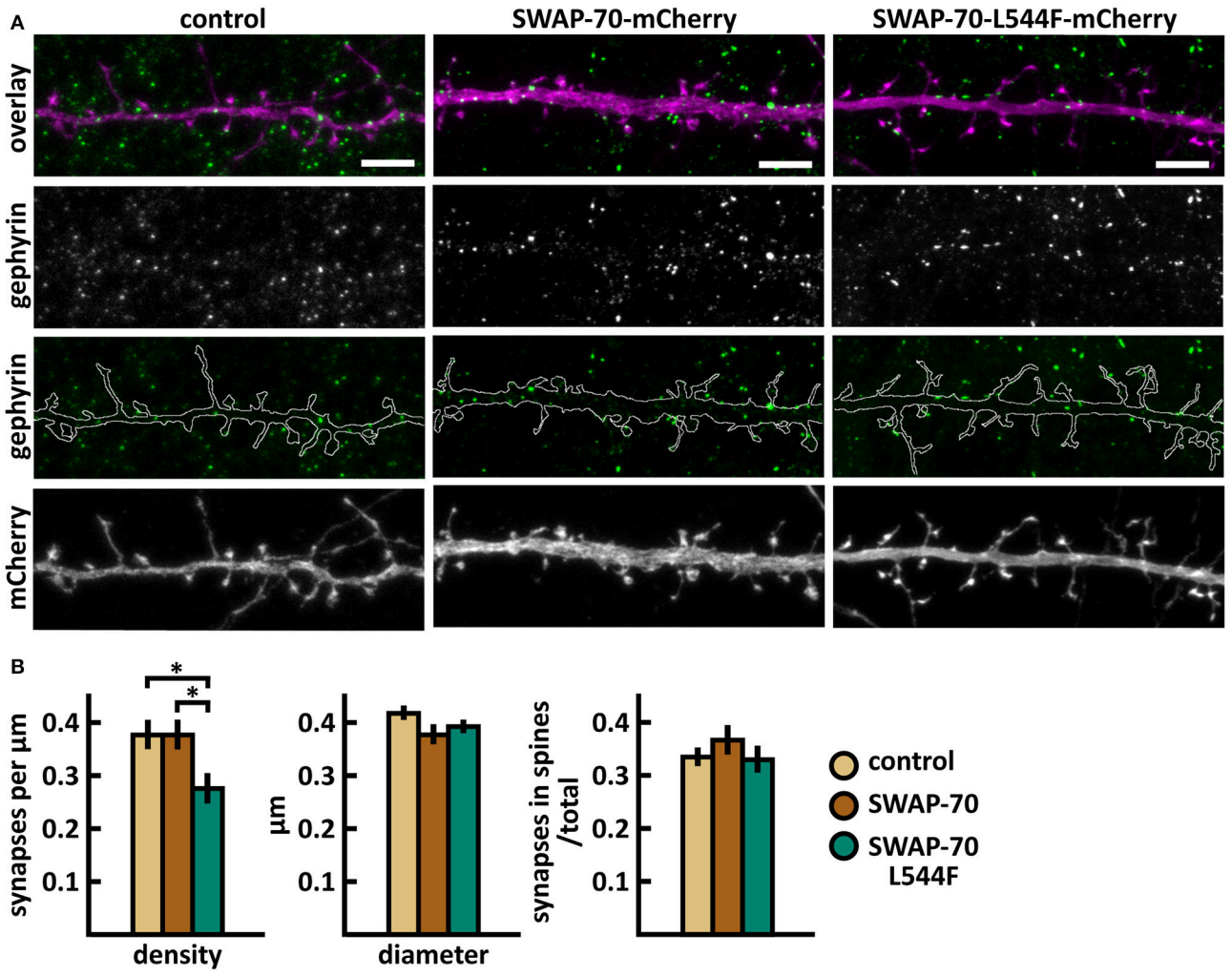

FIGURE 12 | Characterization of the inhibitory synapses in DIV15 hippocampal neurons expressing either mCherry (control), wild-type SWAP-70-mCherry or SWAP-70-L544F-mCherry and stained with anti-gephyrin antibody. **(A)** In overlay, mCherry is shown in magenta and anti-gephyrin antibody staining in green. The line indicates the contour of dendrites (from mCherry). Scale bars, 5 μm. **(B)** Quantification of inhibitory synapse properties. From left to right: (1) Mean density of synapses calculated as the number of gephyrin puncta per μm of the dendrite: control = 0.38; SWAP-70 = 0.38; SWAP-70-L544F = 0.28. (2) Mean diameter of individual gephyrin puncta in μm: control = 0.42; SWAP-70 = 0.38; SWAP-70-L544F = 0.40 3. Proportion of the gephyrin puncta located on dendritic spines as a fraction of the total number of puncta: control = 0.34; SWAP-70 = 0.37; SWAP-70-L544F = 0.34. Data in B represent n(control) = 21 cells, n(SWAP-70) = 23 cells, n(SWAP-70-L544F) = 26 cells, pooled from 4 experiments. $^{*}p < 0.05$ as determined by one-way ANOVA with Bonferroni's *post-hoc* test. Data is represented as mean ±SEM.

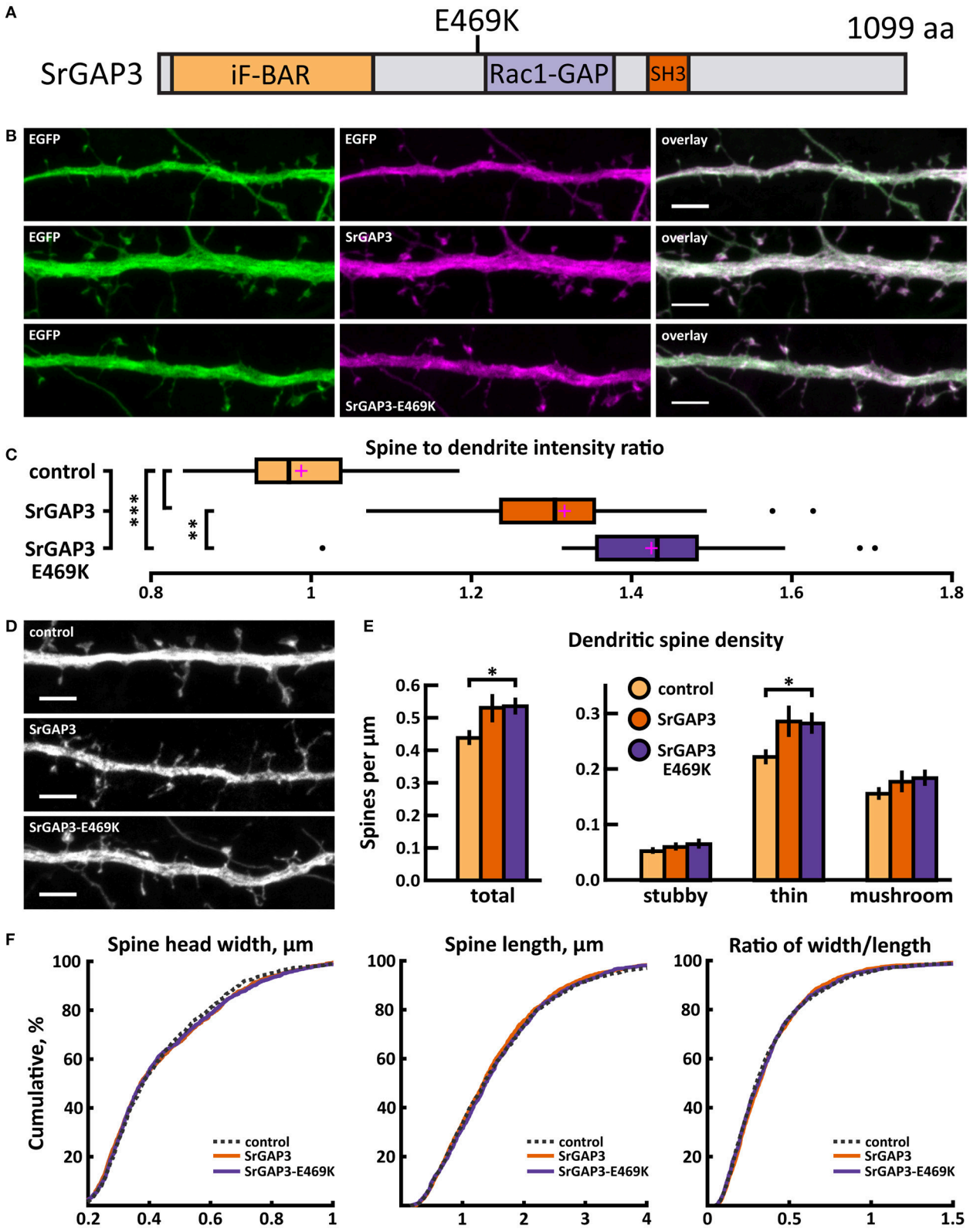

FIGURE 13 | Characterization of protein localization, dendritic spine density and morphology in DIV14-15 hippocampal neurons expressing EGFP and mCherry (control), wild-type SrGAP3-mCherry or mutated SrGAP3-E469K-mCherry. **(A)** Primary structure of human SrGAP3 with mutation E469K indicated. **(B)** Representative maximum projections of confocal Z-stacks for EGFP, mCherry, and wild-type and mutated SrGAP3 localization. Scale bars 4 µm. **(C)** The quantification of protein

(Continued)

FIGURE 13 | localization revealed similar localization of both wt and mutated SrGAP3 to dendritic spines. Spine-to-dendrite fluorescence intensity ratios: control: 0.99 ($n = 34$ neurons, 337 spines), SrGAP3: 1.32 ($n = 25$ neurons, 257 spines), SrGAP3-E469K: 1.42 ($n = 23$ neurons, 229 spines). Center lines show the medians; box limits indicate the 25th and 75th percentiles as determined by R software; whiskers extend 1.5 times the interquartile range from the 25th and 75th percentiles, outliers are represented by dots; crosses represent sample means. $^{**}p < 0.01$, $^{***}p < 0.001$ as determined by one-way ANOVA test with Games-Howell *post-hoc* test. **(D)** Maximum projections of confocal Z-stacks of dendrites from neurons overexpressing EGFP along with either mCherry, SrGAP3-mCherry or SrGAP3-E469K-mCherry. Only EGFP channel is shown and was used to assess spine density and morphology. Scale bar, 4 μm. **(E)** Quantification of dendritic spine density calculated as number of spines per 1 μm of dendrite. The first left cluster of bars represents total spine density. Densities of thin, mushroom, stubby, and total spines were as follows: wt: thin = 0.23, mushroom = 0.16, stubby = 0.06, total = 0.45 spines/μm ($n = 34$ neurons, 1,459 spines, 3,401 μm dendrite); SrGAP3: thin = 0.29, mushroom = 0.19, stubby = 0.07, total = 0.54 spines/μm ($n = 25$ neurons, 1,431 spines, 2,792 μm dendrite); SrGAP3-E469K: thin = 0.28, mushroom = 0.19, stubby = 0.07, total = 0.54 spines/μm ($n = 23$ neurons, 1,087 spines, 2,025 μm dendrite). Data is pooled from 3 experiments and represented as mean ±SEM. $^{*}p < 0.05$ as determined by one-way ANOVA test with Games-Howell *post-hoc* test. **(F)** Cumulative distributions of the width, length and the ratio of width to length of dendritic spines for neurons expressing either mCherry (control), SrGAP3-mCherry or SrGAP3-E469K-mCherry. Curves are a combination of data points each representing an individual spine. Matching tail regions of the curves are not shown. Significant differences were not detected by pairwise two-sample Kolmogorov-Smirnov test.

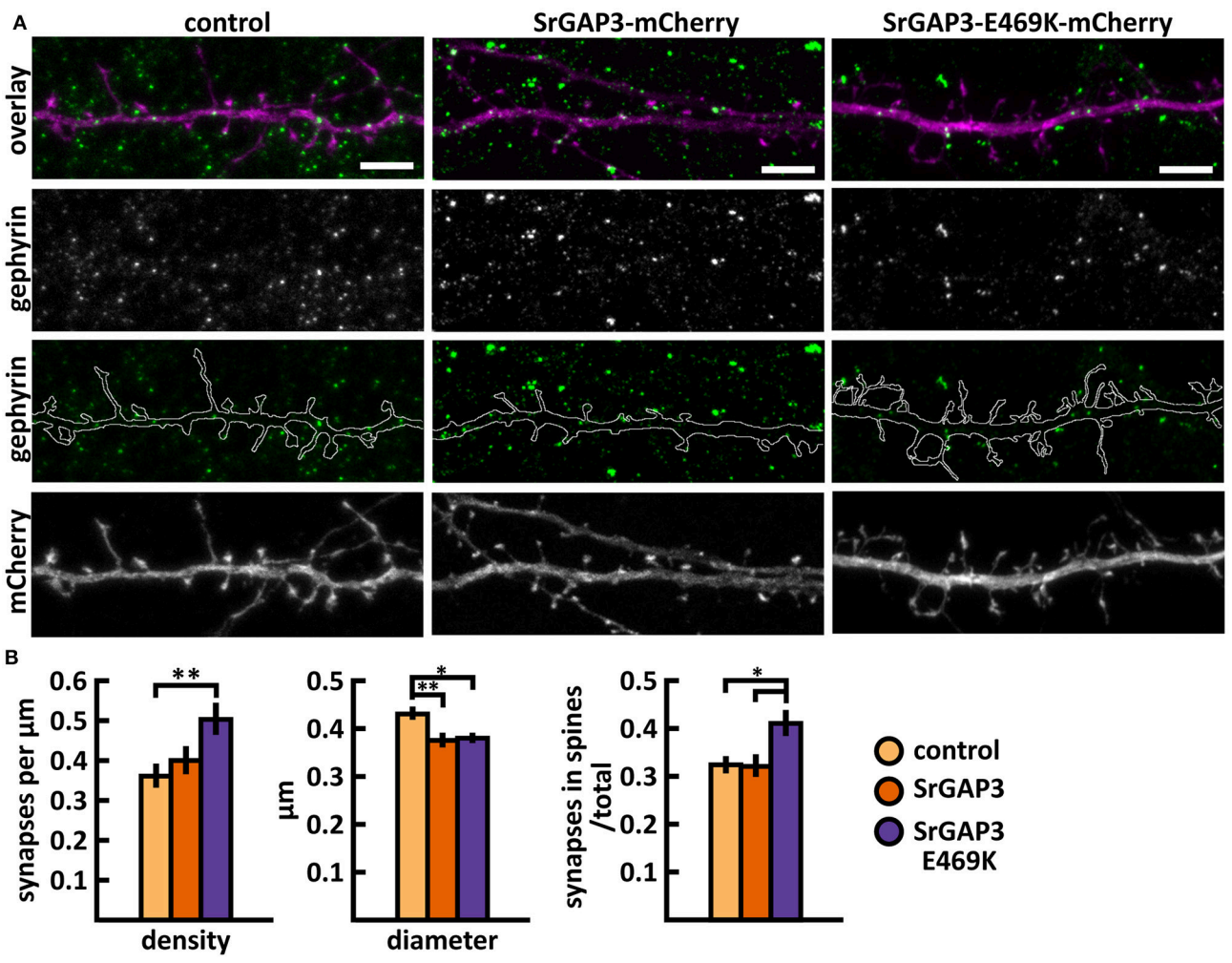

FIGURE 14 | Characterization of the inhibitory synapses in DIV15 hippocampal neurons expressing either mCherry (control), wild-type SrGAP3-mCherry or SrGAP3-E469K-mCherry and stained with anti-gephyrin antibody. **(A)** In overlay, mCherry is shown in magenta and anti-gephyrin antibody staining in green. The line indicates the contour of dendrites (from mCherry). Scale bars, 5 μm. **(B)** Quantification of inhibitory synapse properties. From left to right: (1) Mean density of synapses calculated as the number of gephyrin puncta per μm of the dendrite: control = 0.37; SrGAP3 = 0.41; SrGAP3-E469K = 0.51. (2) Mean diameter of individual gephyrin puncta in μm: control = 0.44; SrGAP3 = 0.38; SrGAP3-E469K = 0.39. 3. Proportion of the gephyrin puncta located on dendritic spines as a fraction of the total number of puncta: control = 0.33; SrGAP3 = 0.33; SrGAP3-E469K = 0.42. Data in B represent n(control) = 17 cells, n(SrGAP3) = 19 cells, n(SrGAP3-E469K) = 18 cells, pooled from 3 experiments. $^{*}p < 0.05$ and $^{**}p < 0.01$ as determined by one-way ANOVA with Bonferroni's *post-hoc* test. Data is represented as mean ±SEM.

and weaker basal synaptic transmission (Hung et al., 2008). In contrast to FXS mice, synaptic plasticity was normal in these mice. Behaviorally, they had increased anxiety-related behavior and impaired contextual fear memory (Hung et al., 2008). In line with the idea that small dynamic spines are preferentially involved in learning, whereas larger stable spines mediate long-term memory storage (Kasai et al., 2003), *Shank1*-deficient mice displayed enhanced performance in a spatial learning task but their long-term memory was impaired (Hung et al., 2008).

Finally, we analyzed the size, density, and localization of inhibitory synapses. In addition to increasing our knowledge of the effects of ASD-mutations, we provide here new information for whether actin binding proteins in general affect inhibitory synapses. This is still a very poorly characterized field and these results may open new avenues for actin regulation of inhibitory synapses. Changes in inhibitory synapses varied between the proteins studied. Myosin IIb and myosin IXb increased the proportion of inhibitory synapses in spines, whereas SrGAP3 decreased the size of inhibitory synapses. Thus, it seems that actin-binding proteins can affect various parameters in inhibitory synapses but the detailed molecular mechanisms are still open. In the future, it will also be interesting to see whether the spiny localization of inhibitory synapses will affect the inhibition efficiency or modality of the synapses. Currently, it seems that positions of shaft inhibitory synapses determine the hotspots of synapse remodeling, where both new spines and new inhibitory synapses are more likely to be formed (Chen et al., 2012; Isshiki et al., 2014). Furthermore, inhibitory synapses in spines seem to stabilize spines (Isshiki et al., 2014). In line with this result, the loss of inhibitory synapses from spines could indicate an increased turnover rate of spines. This is interesting in the context of ASD as an increased turnover of spines was found to be a common parameter for two tested ASD-mouse models (Isshiki et al., 2014). Here, the expression of mutated myosin IIb (Y265C) reduced, but mutated SrGAP3 (E469K) increased, the proportion of inhibitory synapses in spines (**Table 2**). In addition, α-actinin-4, myosin IXb, and SWAP-70 mutations showed a trend toward a reduced proportion of spiny inhibitory synapses. Furthermore, the expression of myosin IIb-Y265C decreased the inhibitory synapse size and SWAP-70-L544F expression decreased the density of inhibitory synapses.

It is important to note that although we did not observe changes in dendritic spines or inhibitory synapses for all mutations, it is possible that the mutations do affect synaptic transmission and behavior. The effects of the mutations are obviously not restricted to synapses, but mutations can affect other cellular processes in the brain, from dendrite growth to the various functions of glial cells. Functional defects of glial cells are implicated in ASD (Petrelli et al., 2016) and, in fact, all genes studied here are expressed in higher levels in human astrocytes than in neurons (Zhang et al., 2014).

With overexpression analysis in cultured neurons we can only determine whether a mutation changes the protein's function. Proper evaluation of the contribution of a mutation to the development of autism requires knock-in animal studies. A very nice example of this is a thorough evaluation of *SHANK3* ASD and schizophrenia mutations in mouse models showing both shared and distinct defects in synaptic transmission, behavior, and spine density (Zhou et al., 2016). However, these type of studies are time-consuming and require plenty of resources. Therefore, the pre-screening of mutations is necessary to pre-select mutations for detailed studies. Furthermore, our screening-type experiments give a broader view on the impact of *de novo* missense mutations and which cellular parameters should and could be used as readouts for protein functionality. From these five genes, only the α-actinin-4 mutation showed a substantial effect on dendritic spines and should be taken to further animal studies. The effects of all the other mutations were relatively mild, but it is possible that under suitable circumstances, possibly enhanced by other mutations or risk-variants, these mutations can contribute to the development of autism.

AUTHOR CONTRIBUTIONS

IH carried out the experiments and analyses for **Figures 2**, **6**, **9**, **11**, **13**; PK was responsible for inhibitory synapse experiments and analyses presented in **Figures 3**, **4**, **7**, **10**, **12**, **14**. AA designed and cloned all mutation constructs. VP generated the protein structures for **Figures 1**, **5**, **8** and placed the hypotheses of the functional consequences of different mutations. PH conceived the theoretical ideas in this work, drew final conclusions and led the writing of the manuscript. IH, PK, AA, and VP wrote sections of the manuscript. All authors contributed to writing and editing of the manuscript. IH was responsible for the final layout of the Figures.

FUNDING

This work has been supported by the Instrumentarium Foundation senior researcher fellowship (PH, IH), Kordelin's foundation (grant 170192) (IH) and Minerva Foundation (PH, PK). VP is supported by the Academy of Finland (grant 289737), and the Sigrid Juselius Foundation.

ACKNOWLEDGMENTS

We are grateful to Martin Bähler for kindly providing mCherry-SWAP-70 and mCherry-myosin IXb plasmids and to Rick Horwitz for mCherry-MHCIIB plasmid. We thank Rimante Minkeviciene for hippocampal neuron dissociation and David Micinski for English proofreading. Imaging was performed at the Biomedicum Imaging Unit (BIU) of University of Helsinki.

REFERENCES

Bacon, C., Endris, V., and Rappold, G. (2009). Dynamic expression of the Slit-Robo GTPase activating protein genes during development of the murine nervous system. *J. Comp. Neurol.* 513, 224–236. doi: 10.1002/cne.21955

Bacon, C., Endris, V., and Rappold, G. A. (2013). The cellular function of srGAP3 and its role in neuronal morphogenesis. *Mech. Dev.* 130, 391–395. doi: 10.1016/j.mod.2012.10.005

Bertling, E., Ludwig, A., Koskinen, M., and Hotulainen, P. (2012). Methods for three-dimensional analysis of dendritic spine dynamics. *Methods Enzymol.* 506, 391–406. doi: 10.1016/B978-0-12-391856-7.00043-3

Blatt, G. J., and Fatemi, S. H. (2011). Alterations in GABAergic biomarkers in the autism brain: research findings and clinical implications. *Anat. Rec. Adv. Integr. Anat. Evol. Biol.* 294, 1646–1652. doi: 10.1002/ar.21252

Borggrefe, T., Wabl, M., Akhmedov, A. T., and Jessberger, R. (1998). A B-cell-specific DNA recombination complex. *J. Biol. Chem.* 273, 17025–17035. doi: 10.1074/jbc.273.27.17025

Bourgeron, T. (2015). From the genetic architecture to synaptic plasticity in autism spectrum disorder. *Nat. Rev. Neurosci.* 16, 551–563. doi: 10.1038/nrn3992

Carlson, B. R., Lloyd, K. E., Kruszewski, A., Kim, I.-H., Rodriguiz, R. M., Heindel, C., et al. (2011). WRP/srGAP3 facilitates the initiation of spine development by an inverse F-BAR domain, and its loss impairs long-term memory. *J. Neurosci.* 31, 2447–2460. doi: 10.1523/JNEUROSCI.4433-10.2011

Chacón-Martínez, C. A., Kiessling, N., Winterhoff, M., Faix, J., Müller-Reichert, T., and Jessberger, R. (2013). The switch-associated protein 70 (SWAP-70) bundles actin filaments and contributes to the regulation of F-actin dynamics. *J. Biol. Chem.* 288, 28687–28703. doi: 10.1074/jbc.M113.461277

Chen, J. L., Villa, K. L., Cha, J. W., So, P. T. C., Kubota, Y., and Nedivi, E. (2012). Clustered dynamics of inhibitory synapses and dendritic spines in the adult neocortex. *Neuron* 74, 361–373. doi: 10.1016/j.neuron.2012.02.030

Chen, Z.-Y., Hasson, T., Zhang, D.-S., Schwender, B. J., Derfler, B. H., Mooseker, M. S., et al. (2001). Myosin-VIIb, a novel unconventional myosin, is a constituent of microvilli in transporting epithelia. *Genomics* 72, 285–296. doi: 10.1006/geno.2000.6456

Comery, T. A., Harris, J. B., Willems, P. J., Oostra, B. A., Irwin, S. A., Weiler, I. J., et al. (1997). Abnormal dendritic spines in fragile X knockout mice: maturation and pruning deficits. *Proc. Natl. Acad. Sci. U.S.A.* 94, 5401–5404. doi: 10.1073/pnas.94.10.5401

Dolan, B. M., Duron, S. G., Campbell, D. A., Vollrath, B., Shankaranarayana Rao, B. S., Ko, H.-Y., et al. (2013). Rescue of fragile X syndrome phenotypes in Fmr1 KO mice by the small-molecule PAK inhibitor FRAX486. *Proc. Natl. Acad. Sci. U.S.A.* 110, 5671–5676. doi: 10.1073/pnas.1219383110

Duffney, L. J., Zhong, P., Wei, J., Matas, E., Cheng, J., Qin, L., et al. (2015). Autism-like deficits in shank3-deficient mice are rescued by targeting actin regulators. *Cell Rep.* 11, 1400–1413. doi: 10.1016/j.celrep.2015.04.064

Durand, C. M., Perroy, J., Loll, F., Perrais, D., Fagni, L., Bourgeron, T., et al. (2012). SHANK3 mutations identified in autism lead to modification of dendritic spine morphology via an actin-dependent mechanism. *Mol. Psychiatry* 17, 71–84. doi: 10.1038/mp.2011.57

Fromer, M., Pocklington, A. J., Kavanagh, D. H., Williams, H. J., Dwyer, S., Gormley, P., et al. (2014). De novo mutations in schizophrenia implicate synaptic networks. *Nature* 506, 179–184. doi: 10.1038/nature12929

Gilman, S. R., Iossifov, I., Levy, D., Ronemus, M., Wigler, M., and Vitkup, D. (2011). Rare de novo variants associated with autism implicate a large functional network of genes involved in formation and function of synapses. *Neuron* 70, 898–907. doi: 10.1016/j.neuron.2011.05.021

Grutzendler, J., Kasthuri, N., and Gan, W.-B. (2002). Long-term dendritic spine stability in the adult cortex. *Nature* 420, 812–816. doi: 10.1038/nature01276

Hilpelä, P., Oberbanscheidt, P., Hahne, P., Hund, M., Kalhammer, G., Small, J. V., et al. (2003). SWAP-70 identifies a transitional subset of actin filaments in motile cells. *Mol. Biol. Cell* 14, 3242–3253. doi: 10.1091/mbc.e03-01-0043

Hlushchenko, I., Koskinen, M., and Hotulainen, P. (2016). Dendritic spine actin dynamics in neuronal maturation and synaptic plasticity. *Cytoskeleton* 73, 435–441. doi: 10.1002/cm.21280

Hodges, J. L., Newell-Litwa, K., Asmussen, H., Vicente-Manzanares, M., and Horwitz, A. R. (2011). Myosin IIB activity and phosphorylation status determines dendritic spine and post-synaptic density morphology. *PLoS ONE* 6:e24149. doi: 10.1371/journal.pone.0024149

Holtmaat, A. J., Trachtenberg, J. T., Wilbrecht, L., Shepherd, G. M., Zhang, X., Knott, G. W., et al. (2005). Transient and persistent dendritic spines in the neocortex *in vivo*. *Neuron* 45, 279–291. doi: 10.1016/j.neuron.2005.01.003

Hotulainen, P., and Hoogenraad, C. C. (2010). Actin in dendritic spines: connecting dynamics to function. *J. Cell Biol.* 189, 619–629. doi: 10.1083/jcb.201003008

Hotulainen, P., Llano, O., Smirnov, S., Tanhuanpää, K., Faix, J., Rivera, C., et al. (2009). Defining mechanisms of actin polymerization and depolymerization during dendritic spine morphogenesis. *J. Cell Biol.* 185, 323–339. doi: 10.1083/jcb.200809046

Huber, K. M., Gallagher, S. M., Warren, S. T., and Bear, M. F. (2002). Altered synaptic plasticity in a mouse model of fragile X mental retardation. *Proc. Natl. Acad. Sci.U.S.A.* 99, 7746–7750. doi: 10.1073/pnas.122205699

Hung, A. Y., Futai, K., Sala, C., Valtschanoff, J. G., Ryu, J., Woodworth, M. A., et al. (2008). Smaller dendritic spines, weaker synaptic transmission, but enhanced spatial learning in mice lacking shank1. *J. Neurosci.* 28, 1697–1708. doi: 10.1523/JNEUROSCI.3032-07.2008

Ihara, S., Oka, T., and Fukui, Y. (2006). Direct binding of SWAP-70 to non-muscle actin is required for membrane ruffling. *J. Cell Sci.* 119, 500–507. doi: 10.1242/jcs.02767

Iossifov, I., O'Roak, B. J., Sanders, S. J., Ronemus, M., Krumm, N., Levy, D., et al. (2014). The contribution of de novo coding mutations to autism spectrum disorder. *Nature* 515, 216–221. doi: 10.1038/nature13908

Iossifov, I., Ronemus, M., Levy, D., Wang, Z., Hakker, I., Rosenbaum, J., et al. (2012). De novo gene disruptions in children on the autistic spectrum. *Neuron* 74, 285–299. doi: 10.1016/j.neuron.2012.04.009

Isshiki, M., Tanaka, S., Kuriu, T., Tabuchi, K., Takumi, T., and Okabe, S. (2014). Enhanced synapse remodelling as a common phenotype in mouse models of autism. *Nat. Commun.* 5:4742. doi: 10.1038/ncomms5742

Joensuu, M., Lanoue, V., and Hotulainen, P. (2017). Dendritic spine actin cytoskeleton in autism spectrum disorder. *Prog. Neuropsychopharmacol. Biol. Psychiatry*. 84, 362–381. doi: 10.1016/j.pnpbp.2017.08.023

Kalinowska, M., Chávez, A. E., Lutzu, S., Castillo, P. E., Bukauskas, F. F., and Francesconi, A. (2015). Actinin-4 governs dendritic spine dynamics and promotes their remodeling by metabotropic glutamate receptors. *J. Biol. Chem.* 290, 15909–15920. doi: 10.1074/jbc.M115.640136

Kasai, H., Matsuzaki, M., Noguchi, J., Yasumatsu, N., and Nakahara, H. (2003). Structure–stability–function relationships of dendritic spines. *Trends Neurosci.* 26, 360–368. doi: 10.1016/S0166-2236(03)00162-0

Kazdoba, T. M., Leach, P. T., Silverman, J. L., and Crawley, J. N. (2014). Modeling fragile X syndrome in the Fmr1 knockout mouse. *Intractable Rare Dis. Res.* 3, 118–133. doi: 10.5582/irdr.2014.01024

Korobova, F., and Svitkina, T. (2010). Molecular architecture of synaptic actin cytoskeleton in hippocampal neurons reveals a mechanism of dendritic spine morphogenesis. *Mol. Biol. Cell* 21, 165–176. doi: 10.1091/mbc.e09-07-0596

Koskinen, M., Bertling, E., Hotulainen, R., Tanhuanpää, K., and Hotulainen, P. (2014). Myosin IIb controls actin dynamics underlying the dendritic spine maturation. *Mol. Cell. Neurosci.* 61, 56–64. doi: 10.1016/j.mcn.2014.05.008

Lee, E., Lee, J., and Kim, E. (2017). Excitation/inhibition imbalance in animal models of autism spectrum disorders. *Biol. Psychiatry* 81, 838–847. doi: 10.1016/j.biopsych.2016.05.011

Li, J., Shi, M., Ma, Z., Zhao, S., Euskirchen, G., Ziskin, J., et al. (2014). Integrated systems analysis reveals a molecular network underlying autism spectrum disorders. *Mol. Syst. Biol.* 10, 774–774. doi: 10.15252/msb.20145487

Long, H., Zhu, X., Yang, P., Gao, Q., Chen, Y., and Ma, L. (2013). Myo9b and RICS modulate dendritic morphology of cortical neurons. *Cereb. Cortex* 23, 71–79. doi: 10.1093/cercor/bhr378

Matsuzaki, M., Ellis-Davies, G. C. R., Nemoto, T., Miyashita, Y., Iino, M., and Kasai, H. (2001). Dendritic spine geometry is critical for AMPA receptor expression in hippocampal CA1 pyramidal neurons. *Nat. Neurosci.* 4, 1086–1092. doi: 10.1038/nn736

Matsuzaki, M., Honkura, N., Ellis-Davies, G. C. R., and Kasai, H. (2004). Structural basis of long-term potentiation in single dendritic spines. *Nature* 429, 761–766. doi: 10.1038/nature02617

Nosyreva, E. D., and Huber, K. M. (2006). Metabotropic receptor-dependent long-term depression persists in the absence of protein synthesis in the mouse model of fragile X syndrome. *J. Neurophysiol.* 95, 3291–3295. doi: 10.1152/jn.01316.2005

O'Roak, B. J., Vives, L., Girirajan, S., Karakoc, E., Krumm, N., Coe, B. P., et al. (2012). Sporadic autism exomes reveal a highly interconnected protein network of de novo mutations. *Nature* 485, 246–250. doi: 10.1038/nature10989

Okamoto, K., Nagai, T., Miyawaki, A., and Hayashi, Y. (2004). Rapid and persistent modulation of actin dynamics regulates postsynaptic reorganization underlying bidirectional plasticity. *Nat. Neurosci.* 7, 1104–1112. doi: 10.1038/nn1311

Otey, C. A., and Carpen, O. (2004). Alpha-actinin revisited: a fresh look at an old player. *Cell Motil. Cytoskeleton* 58, 104–111. doi: 10.1002/cm.20007

Peça, J., and Feng, G. (2012). Cellular and synaptic network defects in autism. *Curr. Opin. Neurobiol.* 22, 866–872. doi: 10.1016/j.conb.2012.02.015

Petrelli, F., Pucci, L., and Bezzi, P. (2016). Astrocytes and microglia and their potential link with autism spectrum disorders. *Front. Cell. Neurosci.* 10:21. doi: 10.3389/fncel.2016.00021

Pilpel, Y., Kolleker, A., Berberich, S., Ginger, M., Frick, A., Mientjes, E., et al. (2009). Synaptic ionotropic glutamate receptors and plasticity are developmentally altered in the CA1 field of *Fmr1* knockout mice. *J. Physiol. (Lond).* 587, 787–804. doi: 10.1113/jphysiol.2008.160929

Pyronneau, A., He, Q., Hwang, J.-Y., Porch, M., Contractor, A., and Zukin, R. S. (2017). Aberrant Rac1-cofilin signaling mediates defects in dendritic spines, synaptic function, and sensory perception in fragile X syndrome. *Sci. Signal.* 10:eaan0852. doi: 10.1126/scisignal.aan0852

Rex, C. S., Gavin, C. F., Rubio, M. D., Kramar, E. A., Chen, L. Y., Jia, Y., et al. (2010). Myosin IIb regulates actin dynamics during synaptic plasticity and memory formation. *Neuron* 67, 603–617. doi: 10.1016/j.neuron.2010.07.016

Roberts, T. F., Tschida, K. A., Klein, M. E., and Mooney, R. (2010). Rapid spine stabilization and synaptic enhancement at the onset of behavioural learning. *Nature* 463, 948–952. doi: 10.1038/nature08759

Rodriguez, A., Ehlenberger, D. B., Dickstein, D. L., Hof, P. R., and Wearne, S. L. (2008). Automated three-dimensional detection and shape classification of dendritic spines from fluorescence microscopy images. *PLoS ONE* 3:e1997.doi: 10.1371/journal.pone.0001997

Rubenstein, J. L., and Merzenich, M. M. (2003). Model of autism: increased ratio of excitation/inhibition in key neural systems. *Genes. Brain. Behav.* 2, 255–67. doi: 10.1034/j.1601-183X.2003.00037.x

Rubio, M. D., Johnson, R., Miller, C. A., Huganir, R. L., and Rumbaugh, G. (2011). Regulation of synapse structure and function by distinct myosin II motors. *J. Neurosci.* 31, 1448–1460. doi: 10.1523/JNEUROSCI.3294-10.2011

Ryu, J., Liu, L., Wong, T. P., Wu, D. C., Burette, A., Weinberg, R., et al. (2006). A critical role for myosin IIb in dendritic spine morphology and synaptic function. *Neuron* 49, 175–182. doi: 10.1016/j.neuron.2005.12.017

Sanders, S. J., Murtha, M. T., Gupta, A. R., Murdoch, J. D., Raubeson, M. J., Willsey, A. J., et al. (2012). De novo mutations revealed by whole-exome sequencing are strongly associated with autism. *Nature* 485, 237–241. doi: 10.1038/nature10945

Schindelin, J., Arganda-Carreras, I., Frise, E., Kaynig, V., Longair, M., Pietzsch, T., et al. (2012). Fiji: an open-source platform for biological-image analysis. *Nat. Methods* 9, 676–682. doi: 10.1038/nmeth.2019

Schindelin, J., Rueden, C. T., Hiner, M. C., and Eliceiri, K. W. (2015). The Image j ecosystem: an open platform for biomedical image analysis. *Mol. Reprod. Dev.* 82, 518–529. doi: 10.1002/mrd.22489

Star, E. N., Kwiatkowski, D. J., and Murthy, V. N. (2002). Rapid turnover of actin in dendritic spines and its regulation by activity. *Nat. Neurosci.* 5, 239–246. doi: 10.1038/nn811

Südhof, T. C. (2008). Neuroligins and neurexins link synaptic function to cognitive disease. *Nature* 455, 903–911. doi: 10.1038/nature07456

Tang, G., Gudsnuk, K., Kuo, S. H., Cotrina, M. L., Rosoklija, G., Sosunov, A., et al. (2014). Loss of mTOR-Dependent macroautophagy causes autistic-like synaptic pruning deficits. *Neuron* 83, 1131–1143. doi: 10.1016/j.neuron.2014.07.040

Trachtenberg, J. T., Chen, B. E., Knott, G. W., Feng, G., Sanes, J. R., Welker, E., et al. (2002). Long-term *in vivo* imaging of experience-dependent synaptic plasticity in adult cortex. *Nature* 420, 788–794. doi: 10.1038/nature01273

Uezu, A., Kanak, D. J., Bradshaw, T. W. A., Soderblom, E. J., Catavero, C. M., Burette, A. C., et al. (2016). Identification of an elaborate complex mediating postsynaptic inhibition. *Science* 353, 1123–1129. doi: 10.1126/science.aag0821

Uzunova, G., Pallanti, S., and Hollander, E. (2016). Excitatory/inhibitory imbalance in autism spectrum disorders: implications for interventions and therapeutics. *World J. Biol. Psychiatry* 17, 174–186. doi: 10.3109/15622975.2015.1085597

van den Boom, F., Düssmann, H., Uhlenbrock, K., Abouhamed, M., and Bähler, M. (2007). The Myosin IXb motor activity targets the myosin IXb RhoGAP domain as cargo to sites of actin polymerization. *Mol. Biol. Cell* 18, 1507–1518. doi: 10.1091/mbc.e06-08-0771

Wierenga, C. J. (2017). Live imaging of inhibitory axons: synapse formation as a dynamic trial-and-error process. *Brain Res. Bull.* 129, 43–49. doi: 10.1016/j.brainresbull.2016.09.018

Yang, G., Pan, F., and Gan, W.-B. (2009). Stably maintained dendritic spines are associated with lifelong memories. *Nature* 462, 920–924. doi: 10.1038/nature08577

Ylänne, J., Scheffzek, K., Young, P., and Saraste, M. (2001). Crystal structure of the alpha-actinin rod: four spectrin repeats forming a thight dimer. *Cell. Mol. Biol. Lett.* 6:234.

Zhang, H. (2005). A GIT1/PIX/Rac/PAK signaling module regulates spine morphogenesis and synapse formation through MLC. *J. Neurosci.* 25, 3379–3388. doi: 10.1523/JNEUROSCI.3553-04.2005

Zhang, Y., Chen, K., Sloan, S. A., Bennett, M. L., Scholze, A. R., O'Keeffe, S., et al. (2014). An RNA-sequencing transcriptome and splicing database of glia, neurons, and vascular cells of the cerebral cortex. *J. Neurosci.* 34, 11929–11947. doi: 10.1523%2FJNEUROSCI.1860-14.2014

Zhao, M.-G., Toyoda, H., Ko, S. W., Ding, H.-K., Wu, L.-J., and Zhuo, M. (2005). Deficits in trace fear memory and long-term potentiation in a mouse model for fragile X syndrome. *J. Neurosci.* 25, 7385–7392. doi: 10.1523/JNEUROSCI.1520-05.2005

Zheng, L., Baumann, U., and Reymond, J.-L. (2004). An efficient one-step site-directed and site-saturation mutagenesis protocol. *Nucleic Acids Res.* 32:e115. doi: 10.1093/nar/gnh110

Zhou, Y., Kaiser, T., Monteiro, P., Zhang, X., Van der Goes, M. S., Wang, D., et al. (2016). Mice with shank3 mutations associated with asd and schizophrenia display both shared and distinct defects. *Neuron* 89, 147–162. doi: 10.1016/j.neuron.2015.11.023

Conflict of Interest Statement: The authors declare that the research was conducted in the absence of any commercial or financial relationships that could be construed as a potential conflict of interest.

frontiers in Cellular Neuroscience

REVIEW
published: 08 August 2018
doi: 10.3389/fncel.2018.00226

Repositioning Microtubule Stabilizing Drugs for Brain Disorders

*Artemis Varidaki, Ye Hong and Eleanor T. Coffey**

Turku Centre for Biotechnology, Åbo Akademi University and University of Turku, Biocity, Tykistokatu, Turku, Finland

Microtubule stabilizing agents are among the most clinically useful chemotherapeutic drugs. Mostly, they act to stabilize microtubules and inhibit cell division. While not without side effects, new generations of these compounds display improved pharmacokinetic properties and brain penetrance. Neurological disorders are intrinsically associated with microtubule defects, and efforts to reposition microtubule-targeting chemotherapeutic agents for treatment of neurodegenerative and psychiatric illnesses are underway. Here we catalog microtubule regulators that are associated with Alzheimer's and Parkinson's disease, amyotrophic lateral sclerosis, schizophrenia and mood disorders. We outline the classes of microtubule stabilizing agents used for cancer treatment, their brain penetrance properties and neuropathy side effects, and describe efforts to apply these agents for treatment of brain disorders. Finally, we summarize the current state of clinical trials for microtubule stabilizing agents under evaluation for central nervous system disorders.

Keywords: microtubules, cytoskeleton, kinase, psychiatric disorder, schizophrenia, depression, neurodegenerative disease, cancer

OPEN ACCESS

Edited by:
C. Laura Sayas,
Universidad de La Laguna, Spain

Reviewed by:
Illana Gozes,
Tel Aviv University, Israel
Charles Harrington,
University of Aberdeen, United Kingdom
Laura Anne Lowery,
Boston College, United States

****Correspondence:***
Eleanor T. Coffey
ecoffey@btk.fi

Received: *15 May 2018*
Accepted: *12 July 2018*
Published: *08 August 2018*

Citation:
Varidaki A, Hong Y and Coffey ET (2018) Repositioning Microtubule Stabilizing Drugs for Brain Disorders. Front. Cell. Neurosci. 12:226. doi: 10.3389/fncel.2018.00226

NEURONS ARE HIGHLY SPECIALIZED CELLS THAT SHOW UNIQUE DEPENDENCIES ON MICROTUBULES

Neuronal cells are highly compartmentalized consisting of a soma, axon(s), dendrites, and synapses. These compartments develop because of particular cytoskeletal arrangements that are specific to neurons (Witte and Bradke, 2008). Axons convey long distance electrical signals leading to neurotransmitter release from nerve terminal active zones. They vary in length from around 1 mm in hippocampal neurons, to 1 m in certain motor neurons; posing a long distance transport challenge. To overcome this, neurons develop a highly specialized transport system constructed from microtubule polymers and microtubule binding proteins (Matamoros and Baas, 2016; Zahavi et al., 2017). Polymers form from alpha/beta tubulin dimers for which several isoforms exist in brain (Cleveland et al., 1978; Gozes and Littauer, 1978). Microtubules display alternating shrinkage and growth controlled by GTP hydrolysis, a process that is inhibited by binding of microtubule-associated protein (MAPs). Several classes of MAPs exist in the nervous system that confer rigidity to microtubule tracks and enable motor proteins to travel long distances carrying cargo (e.g., mitochondria, proteins, and RNA granules) from soma to dendrites, synapses and axonal terminals. Microtubules themselves undergo post-translational modifications, phosphorylation, acetylation, tyrosination, and polyglutamylation (Marchisella et al., 2016), that mark them for binding by specific proteins, in particular motor proteins (Verhey and Gaertig, 2007). Cargo transport in neurons is directional, kinesin motors transport cargo toward axon terminals (anterograde) and dynein motors carry cargo away from axon tips (retrograde) (Vale, 2003).

Microtubules play fundamental roles in diverse cellular processes, including polarization, migration, cell division, and perhaps most crucially in mature neurons, microtubules facilitate cargo transport. It is therefore not surprising that a large number of genetic variants have been identified that influence healthy functioning of the microtubule cytoskeleton, beyond tubulin isoforms themselves or MAPs. Such microtubule regulators include protein kinases and other post-translational modifying enzymes and signaling proteins, motor proteins, adaptors, ligases, chaperones, scaffolds, and adhesion molecules. Genetic disruption of many of these regulators is associated with pathological disturbance of the neuronal cytoskeleton (summarized in **Table 1**).

Neurons are particularly susceptible to microtubule defects and deregulation of the microtubule cytoskeleton occurs in a range of neurodegenerative disorders (Matamoros and Baas, 2016). These include Parkinson's and Alzheimer's disease, amyotrophic lateral sclerosis (ALS) and Parkinsonian disorders e.g., progressive supranuclear palsy, all of which have been linked to polymorphisms in the microtubule stabilizing protein *TAU* (*MAPT*) (Zhang et al., 2017). Neurofibrillary lesions consisting of insoluble Tau (MAPT) filaments form in brains from patients with Alzheimer's, Parkinson's, Pick's disease and in Purkinje cell degeneration and ALS (Goedert et al., 2017). Not only neurodegenerative diseases, but also migration disorders can result from microtubule anomalies. Lissencephaly is one such condition which is linked to genetic aberrations in genes encoding tubulin isoforms and tubulin stabilizing proteins, for example doublecortin (Liu, 2011). It results in cortical lamination defects that produce severe intellectual disability and reduced lifespan (Reiner and Sapir, 2013). Crucially also, genetic mutations in tubulins, MAPs, microtubule regulatory proteins and microtubule motor proteins are among the risk genes for schizophrenia spectrum disorders and depression (Marchisella et al., 2016).

BRAIN DISORDERS ARE ENRICHED FOR DEFECTS IN GENES ENCODING MICROTUBULE REGULATORS

To realize the extent to which microtubule dysregulation is involved in brain disorders, we utilized. Thomson Reuter's MetaCore gene enrichment tool and database that sources disease associations from clinical studies and animal disease models. MetaCore classification of microtubule regulators incorporates a broad range of genes that regulate or associate with microtubules, including non-classical regulators. Two such examples are BRCA1, which regulates γ-tubulin, leading to impaired microtubule nucleation (Sankaran et al., 2007), and KIF26B which lacks the ATPase activity of its motor homologs, but associates with microtubules. Searching for the term "microtubule regulation and disease," several brain diseases emerged with significant enrichment for genes in this category.

ALS showed the highest enrichment for "microtubule regulation and disease" genes, among brain diseases. ALS-associated genes encoded five protein kinases, three microtubule motors and Tau (MAPT) as well as chaperones and scaffolds. The diseases that showed the next highest level of enrichment were schizophrenia and psychotic disorders. Schizophrenia is a heritable disorder where several gene variants combine to confer disease risk. It is interesting that schizophrenia showed the highest percent of genetic associations for tubulin isoforms and MAPs, among brain diseases, while protein kinases and other signaling proteins were also highly represented. Of particular interest, sixty percent of the "microtubule regulation and disease" genes that associated with bipolar disorder corresponded with schizophrenia spectrum disorders, suggesting that these genes may contribute to overlapping negative symptoms. Finally, the disease that associated with the largest overall number of known "microtubule regulation and disease" genes was Alzheimer's disease, which was associated with 82 genes fitting this search term.

It is worth noting that the genetic landscape of Alzheimer's and Parkinson's disease have not been studied as extensively by GWAS as has the classical polygenic disorder, schizophrenia. Instead, Alzheimer's investigations have focused more on a small number of high penetrance gene mutations that cause autosomal dominant Alzheimer's disease. Yet as this accounts for under 10% of cases, disease-spectrum approaches to study Alzheimer's are relevant, and improved technologies increase feasibility (Van Cauwenberghe et al., 2016). Nonetheless, with current information and straightforward bioinformatics analysis, a higher proportional association of microtubule proteins and MAPs is found for psychiatric disorders (schizophrenia and bipolar, 17 and 7.4% respectively) than for Alzheimer's disease (2.4%). Overall, this enrichment for microtubule regulator genes among major brain disorders emphasizes the importance of proper microtubule regulation for brain health.

MICROTUBULE STABILIZING AGENTS IN THE CLINICS

The realization that microtubule dysfunction is associated with neuronal disorders, has fuelled efforts to reapply knowledge gained from cancer therapies, where tubulin polymerisation inhibitors have been used for over 50 years. These drugs are under investigation for the treatment of neurodegenerative and psychiatric disorders, as can be seen from the flurry of clinical trial activity in this area (**Figure 1**; **Table 2**). The story begins with taxol, one of the earliest recognized microtubule stabilizing agents.

PACLITAXEL (TAXOL)

Paclitaxel commonly known as "Taxol" is a member of the taxane family. It is a natural compound, antineoplastic drug that was isolated from the bark of the Pacific yew tree (*Taxus brevifolia)* by the botanist Arthur Barclay in 1962, as part of a National Cancer Institute plant-screening program carried out in collaboration with the U.S. Department of Agriculture from

TABLE 1 | Disease enrichment for "*microtubule regulation and disease*".

Diseases	*P*-value	FDR	Gene Names
Amyotrophic Lateral Sclerosis	6.63E−14	1.88E−12	DCTN1, GSK3B, PRKCZ, KIF3A, MAPK14, DISC1, RNF19A, KIFAP3, APP, GRID2, TRIM63, PRKCA, AKT1, MAPT, ALS2, S100A10, HSPB1, APEX1, CYFIP1, YWHAE
Schizophrenia	1.61E−12	3.17E−11	ATF4, GAPDH, GSK3B, SPTAN1, TUBB, MAP2K1, SLC1A4
Schizophrenia Spectrum and Other Psychotic Disorders	2.47E−12	4.75E−11	BCL2L1, DISC1, CTNNB1, GNAI1, PKP4, APP, CHP1, YWHAE, TUBB2B, MAP1A, DNM1, MED12, SLC9A3R1, GRID2, PRKCA, DPYSL2, GNAI3, AKT1, KIF2A, PLA2G6, NDE1, HTT, TUBA1A, MAP6, SMC3, MAP1B, TPPP3, DAB1, SORBS1, CALM1, MAPK1, PDE4D, KIF21A, FEZ1, CNP, TUBA8, PLA2G3, NR3C1, CAMK2B, HSPA1A, PDE4B, SLC6A4, PRKACA, S100A10, FGR, TFAP2A, BIRC2, PCM1, CCT3, DVL1, CCT2, HSPB1, HDAC2, MAPK3, NDEL1, GNAI2, MDH1, APC, ATP6V0D1, ERCC2, MAP2, ATM, RPS6KA2, SPTA1, TBCB, SNAP29, MAP2K2, AHI1, TCP1
Alzheimer's Disease, Early Onset	4.44E−11	7.40E−10	APP, MAPT, PSEN2, ABCA2, PSEN1
Alzheimer's Disease	1.22E−09	1.77E−08	ATF4, GAPDH, CRYAB, GSK3B, APPBP2, CASP8,MAP2K1, TIAM1, FNTA, HSPA2, DISC1, PRKAR2A, CTNNB1, SIRT2, APP, SLC8A1, DAAM1, SVIL,CSNK1A1, GRID2, PRKCA, AXIN1, FLOT1, KLK6, KIF11, CSNK1D, AKT1, MAPKAPK2,MAPT, ACTR1A, TRIOBP, BRCA1, LCK, HTT, KIF26B, RELB, ZFYVE19, POLB, NEDD9, MAPK1, BCAS3, PCGF5, SNCG, SNX10, DNM1,KIF13B, AGBL4, PLA2G3, KLC1, NME1, HOOK3, PRKAR2B, HSPA1A, NDRG2, F11R, PDE4B, DNM2, SLC6A4, PRKACA, LRP8 (APOER2), DYNC1I1, S100A10, FGR, MYH1, DVL1, PSEN2,MAPK3, CLIC5, APEX1,GNAI1, ABCA2, MARK1, PSEN1, KLK1, STMN1, CEP164, KCNAB2, TPPP,MAP2K2, CDK1, DAXX, B9D2
Bipolar Disorder	4.40E−09	5.74E−08	ATF4, GAPDH, GSK3B, PRKCZ, MAP2K1, SLC1A4, BCL2L1, PCNT, DISC1, CTNNB1, GNAI1, SIRT2, CSNK1A1, MED12, GRID2, PRKCA, CRHBP, CSNK1D, DPYSL2, VAPA, GNAI3,MAPT, TIMELESS,NDE1, MARCKS, SMC3, MAP1B, DAB1, MAPK1,PDE4D, PLA2G3, NR3C1, HSPA1A, SYNJ1, PDE4B, SLC6A4, PRKACA, PAFAH1B1, S100A10, TFAP2A, DVL1, NEIL1, HSPB1, CDC25B, MAPK3, NDEL1, GNAI2, MAP2, RPS6KA2, TRIM55, ATF5, GJA1, MAP2K2, OR2A4
Alzheimer's Disease, Late Onset	9.42E−06	7.12E−05	GSK3B, FNTA, DISC1, APP, SLC8A1, DAAM1, SVIL, GRID2, PRKCA, AXIN1, MAPT, ACTR1A, TRIOBP, KIF26B, RELB, NEDD9, BCAS3, SNX10, KIF13B, AGBL4, HOOK3, PDE4B, DYNC1I1, MYH1, PSEN2, CLIC5, PSEN1, KCNAB2, B9D2
Intellectual Disability	1.39E−05	0.000102	PCNA, DCX, CENPJ, MAP2K1, APP, CSNK1A1, MED12, CDC42, GRID2, BBS4, CSNK1D, DPYSL2, HINT1, SMC3, OFD1, SPAST, PDE4D, FGF13, PLA2G3, NME1, PQBP1, HDAC4, PDE4B, STK26, S100A10, RAB3D, CCT2, HDAC2, MBD1, RPS6KA2, BBS2, PSEN1, STMN1, UPF3B, MAP2K2, STIL, NDN, TCP1, CC2D1A, YWHAE
Parkinsonian Disorders	0.000161	0.000984	GSK3B, BCL2L1, RNF19A, APP, CSNK1A1, ROCK1, GRID2, CSNK1D, RB1, MAPT, ATF4, NEDD9, SNCG, KLC1, HSPA1A, SLC6A4, S100A10, APEX1, KLC3, ERCC2, PSEN1, YWHAE
Schizophrenia, Disorganized	0.000402	0.002275	GSK3B
Schizophrenia, Paranoid	0.00781	0.032133	GSK3B, SLC6A4, YWHAE
Parkinson Disease	0.166085	0.365388	GSK3B, BCL2L1, RNF19A, CSNK1A1, ROCK1, CSNK1D, RB1, MAPT, ATF4, NEDD9, SNCG, KLC1, HSPA1A, SLC6A4, S100A10, APEX1, KLC3, ERCC2, YWHAE
Depression	0.239557	0.470752	PRKCA, SLC6A4
Attention Deficit Disorder with Hyperactivity	0.946547	0.999994	KIF6, SLC6A4
Mental Retardation, Xlinked	0.91368	0.999994	PQBP1, STK26, HDAC2, MBD1, RPS6KA2, UPF3B

Using the MetaCore database, we performed a disease enrichment analysis for the term "microtubule regulation and disease". Enrichment scores (p-value) and false discovery rates (FDR) are shown for nervous system disorders. Colors mark gene groups as follows: tubulin isoforms and microtubule binding proteins (blue1), microtubule motor proteins (red1), protein kinases (purple), other signaling proteins (green1). The literature references for these associations are as follows; for Amyotrophic lateral sclerosis: (Hand et al., 2003; Hu et al., 2003; Maddalena et al., 2003; Süssmuth et al., 2003; Ackerley et al., 2004; Ryoo et al., 2008) schizophrenia and schizophrenia spectrum and other psychotic disorders (Beasley et al., 2002; Callicott et al., 2005; Torrey et al., 2005; Noori–Daloii et al., 2010; Yuan et al., 2010), Alzheimer's disease (Mullan et al., 1992; Cheon et al., 2001; Engidawork et al., 2001; Russ et al., 2001; Figueroa et al., 2002; Howell and Brookes, 2002; Link et al., 2003; Maddalena et al., 2003; Ogawa et al., 2003; Zhu et al., 2003; Verdile et al., 2004; Derkinderen et al., 2005; Evans et al., 2007; Liang et al., 2007, 2009; Ryoo et al., 2008; Potkin et al., 2009; Naj et al., 2010; Engmann et al., 2011; Wijsman et al., 2011) Parkinson's and Parkinsonian disorders (Krüger et al., 1998; Ito et al., 2003; Jordan–Sciutto et al., 2003; Beyer et al., 2004; Kwok et al., 2005; Stichel et al., 2005; Gencer et al., 2012) and bipolar and mood disorders (Wang and Friedman, 1996; Lesort et al., 1999; Beasley et al., 2002; Torrey et al., 2005; Yuan et al., 2010; Bernard et al., 2011).

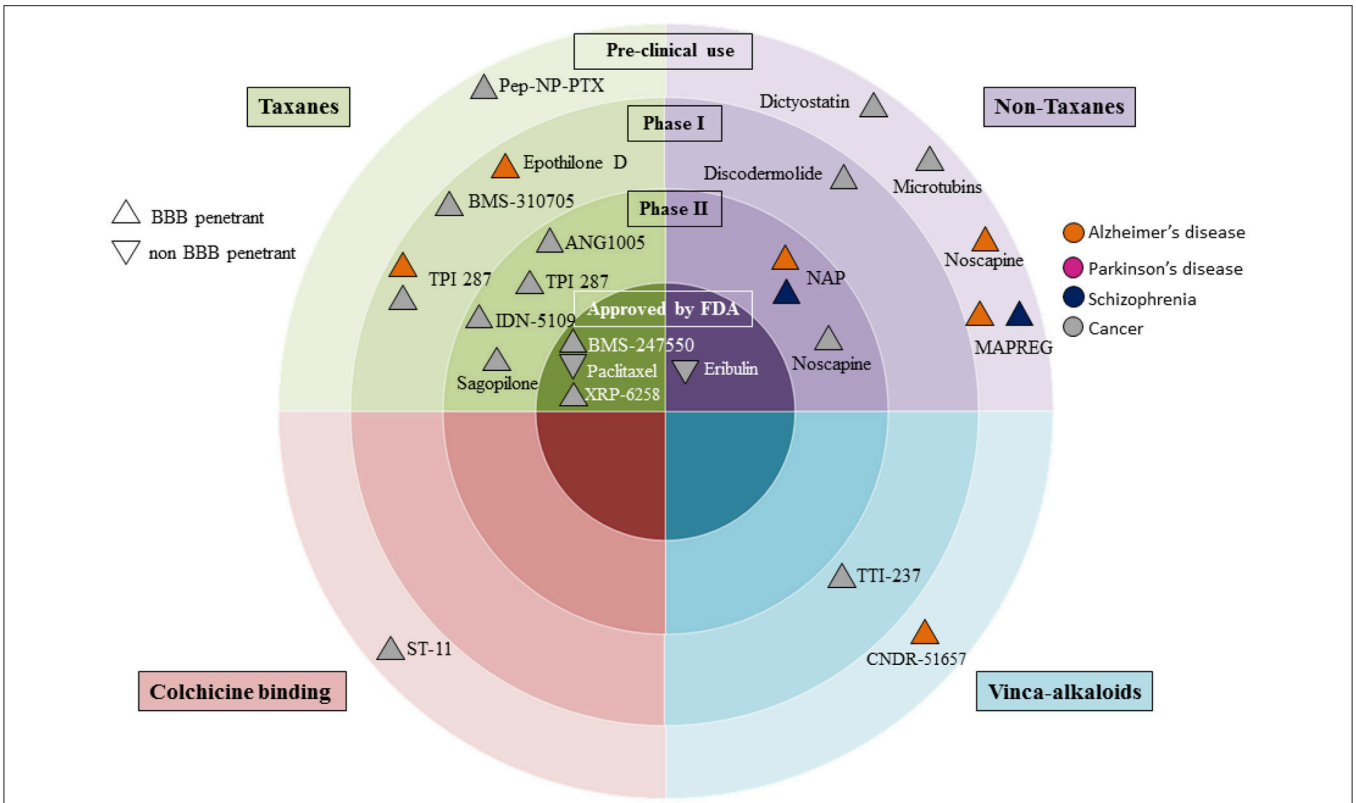

FIGURE 1 | Clinical development of microtubule stabilizing agents for Alzheimer's and Parkinson's disease, schizophrenia and cancer. Microtubule stabilizing agent grouping is according to pre-clinical, or clinical phases. Drugs developed for cancer are in gray; those for Alzheimer's and Parkinson's diseases are coded orange and pink respectively, and those under development for treatment of schizophrenia are in dark purple. We denote blood brain barrier (BBB) penetrance with upright triangles and non-penetrant drugs with an upside down triangle.

1960 to 1980. Taxol was shown to have cytotoxic activity in 1964 and its structure was resolved in 1971 (Wani et al., 1971). Extensive cancer cell anti-mitotic properties were characterized before taxol entered the clinics, 30 years after its discovery (Kingston, 1991). Nowadays, it is a first-line chemotherapy anti-cancer agent for treatment of breast and ovarian cancers (Wani et al., 1971). It exerts a broad-spectrum anti-tumor activity that is effective in both solid and dissociated tumors. Paclitaxel promotes microtubule assembly *in vitro* (Schiff and Horwitz, 1980) and reduces microtubule dynamics. To do this, it binds a single site on the β-tubulin subunit, on the inner surface near to the lateral protofilament interaction sites (Nogales et al., 1995, 1998). Taxol binding prevents compaction at the tubulin dimer interface and results in more stable lateral interactions. This reduces stochastic switching of microtubules between growth and shrinkage, a classical behavior known as "dynamic instability," which is essential for normal functioning of the microtubule cytoskeleton (Alushin et al., 2014).

BLOOD BRAIN BARRIER PENETRANCE

One major drawback for the potential use of paclitaxel in the treatment of neurological and neuropsychiatric diseases is the limited bioavailability of this compound in brain. Taxol does not cross the blood brain barrier. Moreover, taxane family compounds are good substrates for P-glycoprotein transporters or multidrug resistance proteins, which are highly expressed in capillary endothelial cells that form the blood brain barrier (Schinkel et al., 1994; Fellner et al., 2002). P-glycoprotein transporters rapidly export taxanes out from cells into the bloodstream, reducing brain bioavailability and contributing to drug resistance. Smart delivery of paclitaxel in the brain has been investigated. For example, taxol conjugation to the brain delivery peptide Angiopep-2 was tested in efforts to improve its blood brain barrier permeability (Régina et al., 2008; Kurzrock et al., 2012). Angiopep-2 is a 19-mer peptide that binds to the lipoprotein related protein-1 receptor and triggers transcytosis. This approach can facilitate targeting of non-blood brain barrier penetrant drugs to the brain, as it provides a mechanism for the conjugated drug to cross the capillary epithelial cell layer. It may also assist selective targeting of cancer cells that exhibit high expression levels of the lipoprotein-related protein receptor (US patent: WO2004060403 A2). ANG1005 (also known as GRN1005; US patent: US7557182 B2), is a conjugate of Angiopep-2 with paclitaxel. It underwent phase II clinical trials to determine its efficacy against breast cancer and non-small cell lung cancer primary tumors, and in patients suffering

TABLE 2 | Clinical trials describing brain penetrance and nervous system side effects for microtubule stabilizing agents.

Name(s)	Cytoskeletal target	Diseases	Clinicaltrials.gov identifier (Status-study completion date)	BBB penetrance/side effects
Epothilone D (KOS-862, NSC-703147, desoxyepothilone B BMS-241027)	Tubulin	Alzheimer's Disease	NCT01492374 (C) (October 2013)	Brain penetrant/Neurotoxicity severe diarrhea
		Lung cancer	NCT00080509 (T) (November 2004) NCT00081107(C) (December 2004)	
		Colorectal cancer	NCT00077259 (C) (September 2004)	
		Breast cancer	NCT00337649 (C) (April 2008)	
		Prostate cancer	NCT00104130 (T) (February 2005)	
BMS-247550 (ixabepilone)	Tubulin	Breast Cancer	NCT00082433 (C) (March 2008) NCT00789581 (C) (October 2013)	Brain penetrant/CIN, neutropenia, nausea, fatigue, arthralgia, alopecia
BMS-310705	Tubulin	Solid tumors	Phase I (Sessa et al., 2007) (C)	Brain penetrant/neurotoxicity, severe diarrhea
NAP (AL-108, AL-208, davunetide NAPVSIPQ)	EB1/EB3	Schizophrenia	NCT00505765 (C) (April 2009)	Brain penetrant/One patient reported palpitations
		Taupathies	NCT01056965 (A) (July 2017)	
		Mild cognitive impairment in Alzheimer's disease	NCT00422981 (C) (January 2008) NCT00404014 (C) (June 2008)	
		PSP	NCT01110720 (C) (December 2012) NCT01049399 (C) (November 2011)	
TPI 287 (ARC-100)	Unknown	Alzheimer's Disease	NCT01966666 (A) (Est. completion: March 2019)	Brain penetrant/ Seizures, Grade III CIN
		Corticobasal Syndrome, PSP	NCT02133846 (A) (Est. completion: March 2019)	
		Neuroblastoma	NCT00867568 (C) (February 2016) NCT01483820 (T) (December 2014)	
		Metastatic melanoma	NCT01067066 (T) (July, 2016)	
Paclitaxel	Taxol-binding domain	Approved for ovarian, breast and non-small cell lung carcinomas, AIDS-related Kaposi's Sarcoma	Numerous clinical trials	Non-brain penetrant/CIN, neutropenia
ANG1005 (GRN1005)	Taxol-binding domain	Brain metastasis	NCT01497665 (T) (February 2013) NCT02048059 (C) (September 2017) NCT01967810 (C) (September 2017) NCT01480583 (C) (October 2015)	Brain penetrant/neutropenia
Sagopilone (ZK-EPO, ZK 219477)	Tubulin	Brain metastasis	NCT00496379 (T) (January 2012	Brain penetrant/fatigue, CIN, nausea,diarrhea, leucopenia hepatobiliary disorder
		Recurrent Glioblastoma	NCT00424060 (C) (August 2007)	
		Metastatic melanoma	NCT00598507 (C) (January 2013)	
Triazolopyrimidines, Cevipabulin	Vinca site	Advanced malignant solid tumors	NCT00195247 (T) (Not mentioned) NCT00195325 (T) (Not mentioned)	Non brain penetrant/Not reported
IDN-5109 (BAY 59-8862, Ortataxel)	Tubulin	Recurrent glioblastoma	NCT01989884 (S) (December 2016	Brain penetrant/Not reported
		Taxane-refractory NSCLC	NCT00054314 (C)(April 2003) NCT00044538 (C) (June 2004)	
		Metastatic breast cancer	NCT00044525 (C) (February 2004)	
		Refractory Non-Hodgkin's Lymphoma	NCT00044551 (C) (July 2003)	
		Renal cell carcinoma	NCT00044564 (C) (January 2003)	
Cabazitaxel (Jevtana, XRP-6258)	Tubulin	Prostate cancer	NCT00417079 (C) (September 2009)	Brain penetrant/ hypotension, bronchospasm, generalized rash/erythema, severe diarrhea, neutropenia, neurotoxicity fatigue, alopecia, Grade 1 neurotoxicity

(Continued)

TABLE 2 | Continued

Name(s)	Cytoskeletal target	Diseases	Clinicaltrials.gov identifier (Status-Study Completion Date)	BBB penetrant/side effects
		Head and neck cancer	NCT01620242 (C) (April 2015)	
		Breast cancer	NCT01934894 (T) (April 2017) NCT03048942 (A) (Est. completion: August 2022)	
		NSCLC	NCT01438307 (C) (September 2015) NCT01852578 (C) (August 2013)	
		Refractory Glioblastoma Multiforme	NCT01866449 (C) (August 2017)	

from high-grade gliomas (NCT 01497665, NCT 02048059, NCT 01967810, and NCT 01480583). In patients with non-small lung cancer with brain metastasis, the prevailing side effect of this drug was peripheral neuropathy, observed in 37.50% of patients, and neutropenia, which affected 18.75% of patients (**Table 2**).

Another experimental delivery approach is paclitaxel-loaded nanoparticles conjugated to the Pep-1 peptide (Pep-NP-PTX). This delivery system introduced taxol to the brain *via* endocytosis of the interleukin-13 receptor subunit alpha-2 (IL-13RA2), which showed elevated expression in gliomas (Patent application: CN103655517 A). In mice, Pep-NP-PTX showed increased uptake to brain and increased cytostatic effect in glioma cells with no overt toxicity, suggesting that it could represent a viable delivery option (Wang et al., 2015). Yet as discussed below, peripheral neuropathy remains an expected side effect with paclitaxel.

CHEMOTHERAPY-INDUCED PERIPHERAL NEUROPATHY

Chemotherapy-induced peripheral neuropathy (CIPN) is one of the most common adverse side effects of paclitaxel treatment. 30–80% of patients will most likely develop CIPN, depending on the dose and duration of the treatment. Most often, these patients will continue to have CIPN symptoms even after discontinuing the treatment (Cavaletti and Marmiroli, 2010). Paclitaxel can induce acute signs of CIPN as early as 24 h after a single high dose treatment. In order to eliminate this side effect, researchers have studied the benefit of using albumin-coated paclitaxel (ABI-007-Abraxane, also known as nab-paclitaxel), a Food and Drug Administration (FDA)-approved medicine for breast, lung and pancreatic cancer (Ibrahim et al., 2005; Nyman et al., 2005). Albumin-bound paclitaxel produced fewer >grade-3 neuropathies, neutropenia and myalgia in non-small cell lung carcinoma patients than did soluble paclitaxel in a phase III trial (Socinski et al., 2012). However meta-analysis of Abraxane use for treatment of breast cancer (including 2357 patients) concluded that the complete response rate was increased but CIPN side effects were aggravated compared to classical taxanes (Zong et al., 2017). Also, in a phase III study of metastatic breast cancer (NCT 00046527), grade-3 sensory neuropathy was increased in patients receiving Abraxane compared to paclitaxel, although this could be attributed to the higher dose of Abraxane used (Gradishar et al., 2005).

Understanding the mechanism whereby paclitaxel induces CIPN may be beneficial in developing strategies to avoid or ameliorate symptoms of neuropathic pain in patients treated with microtubule stabilizing agents. To this end, it was recently shown that microtubule stabilization by paclitaxel decreases axonal transport and downregulates translation of *bclw* mRNA in axons. This in turn leads to activation of a degenerative cascade triggered by mitochondrial dysfunction and activation of the proteolytic enzyme calpain and subsequent axonal degradation (Pease–Raissi et al., 2017). Cognitive deficit is a more recently recognized side effect of chemotherapy, especially in elderly patients (Mandilaras et al., 2013). It will be interesting to see whether drugs with reduced CIPN will also show less cognitive side effects.

CABAZITAXEL

Cabazitaxel (Jevtana, XRP-6258) is a second-generation microtubule-binding drug from the taxane family. It received approval by the FDA in 2010 for the treatment of refractory metastatic prostate cancer (Abidi, 2013). A phase III study (NCT 00417079) of patients with metastatic prostate cancer showed that Cabazitaxel prolonged the survival rate of the patients, with only 1% of patients suffering from grade-3 peripheral neuropathy (de Bono et al., 2010). Cabazitaxel is an attractive anticancer compound compared to paclitaxel as it displays poor affinity for the P-glycoprotein receptor multi-drug resistance pump and as a consequence is blood-brain penetrant (Cisternino et al., 2003). As such, phase II trial (NCT 01866449) used it for treatment of refractory glioblastoma multiforme. Cabazitaxel underwent evaluation for its efficacy in ameliorating pediatric brain tumors such as atypical teratoid rhabdoid tumors, medulloblastomas, and central nervous system primitive neuroectodermal tumors (Girard et al., 2015). Like classical taxanes, cabazitaxel exerts anti-proliferative and pro-apoptotic effects in glioma while disrupting cell cycle by its effects on the microtubule cytoskeleton. Remarkably, it does this at a dose that is non-toxic to surrounding primary neurons and astrocytes (Ghoochani et al., 2016), suggesting that low levels could be viable for treatment of microtubule disorders in brain, in addition to tumors.

DISCODERMOLIDE AND ITS ANALOG DICTYOSTATIN

Discodermolide is a polyhydroxylated lactone that was isolated from the marine sponge *Discodermia dissolute* (Gunasekera et al., 1990). This compound stabilizes microtubules more potently than paclitaxel and retains anti-tumor activity in cell lines that express high levels of P-glycoprotein and are normally resistant to taxanes (Kowalski et al., 1997). Discodermolide binds with higher affinity to tubulin dimers compared to paclitaxel. X-ray crystallography has shown that discodermolide binds the taxane pocket of β-tubulin, but it does this differently to paclitaxel (Sáez-Calvo et al., 2017). More specifically, while paclitaxel binds to the M-loop of tubulin, discodermolide binds preferentially to the N-terminal H1S2 loop, helping to promote a synergistic effect of these two drugs (Martello et al., 2000; Khrapunovich–Baine et al., 2009). Discodermolide has been in phase I clinical trials for treatment of advanced solid malignancies, where patients did not display any severe neuropathy or neutropenia but did show signs of pulmonary toxicity (Mita et al., 2004). The discodermolide analog dictyostatin has comparable properties to discodermolide in terms of tubulin binding and polymerization (Madiraju et al., 2005). However, dictyostatin shows improved brain bioavailability, 55-times higher than that of discodermolide. Dictyostatin increases levels of acetylated tubulin in brains of mice, indicating that it increases microtubule stability *in vivo*, as expected. Indeed, dictyostatin is a more potent microtubule-stabilizing agent when compared to discodermolide (Brunden et al., 2013). This together with its improved pharmacodynamic properties suggest that dictyostatin could be suitable for treating central nervous system disorders.

EPOTHILONES

The Epothilones are pharmacological agents comprising 16-membered macrocyclic lactones isolated from the soil dwelling bacteria *Sorangium cellulosum* (Hoefle et al., 1993) (Patent number: DE4138042 A1). Like taxol, they bind and stabilize microtubule polymers, promoting stabilization at sub-micromolar concentrations and inducing cytotoxicity through cell cycle arrest (Bollag et al., 1995; Giannakakou et al., 2000; Nettles et al., 2004). Epothilones have additional advantages that confer increased potency compared to other anti-neoplastic agents. They are water-soluble and amenable to large-scale production through bacterial fermentation. Most importantly however, epothilones are also poor substrates for the P-glycoprotein transport pump, thereby increasing brain bioavailability (Bollag et al., 1995; Aller et al., 2009).

EPOTHILONE ANALOGS AND CLINICAL TRIALS

Since its first identification, several epothilone analogs underwent synthesis resulting in higher anti-tumor efficacy compared to paclitaxel (EPO906) and the original natural compound epothilones A and B (Hoefle et al., 1993). Among these, epothilone B shows the highest potency. Analogs of epothilone B, such as epothilone D (BMS-241027) display a maximum tolerated dose of 25 mg/kg compared to 0.3 mg/kg for epothilone B (Chou et al., 1998). Moreover, the activity of BMS-247550 (also known as ixabepilone), a lactam analog of epothilone B, is twice as high as paclitaxel (Lee et al., 2001). Another epothilone B analog, BMS-310705, was developed to improve compound solubility, however clinical development was discontinued due to associated severe toxic side-effects and because ixabepilone received FDA approval for treatment of breast cancer (Overmoyer et al., 2005; Sessa et al., 2007; Brogdon et al., 2014).

Additionally, sagopilone (ZK-EPO, ZK-Epothilone, ZK 219477) was developed as the first synthetic epothilone designed for cancer treatment (Klar et al., 2006). It shows good brain bioavailability (Hoffmann et al., 2009), and entered phase II trial for breast cancer metastasis (NCT 00496379). However, the trial terminated; side effects of this compound included fatigue, nausea, diarrhea, leucopenia, CIPN and hepatobiliary disorders (Freedman et al., 2011).

EPOTHILONES IN ANIMAL MODELS OF NEURODEGENERATION AND SPINAL CORD INJURY

In experimental studies, epothilones underwent testing against several brain diseases, including tauopathies and Parkinson's disease (Brunden et al., 2011; Ruschel et al., 2015). More specifically systemic injection of a low dose (0.75 mg/mg body weight) of epothilone B to rats following spinal cord injury promoted axonal recovery (Ruschel et al., 2015). Interestingly, in the same experiments, epotheline B also reduced fibrotic scaring. The microtubule-stabilizing drug at once reduced microtubule polarization in fibroblasts, while promoting microtubule polarization in neurons. By this means, it facilitated axon regrowth into the injured area. This ground breaking study suggested that epotheline B could be useful for clinical treatment of CNS injury. A later study addressed the effect of epotheline B on physiological pruning of axonal branches and synapses. Studying the neuromuscular junction, the authors identified that disassembly of synapses was elicited locally by microtubule disassembly and that a single injection with epothilone B slowed this synapse elimination (Brill et al., 2016). The effect attributed to stabilization of microtubules because EB3 comet density reduced and tubulin content increased. Together these studies provided impetus to harness microtubule-stabilizing drugs such as epothilone B for therapy. More recently, epothilone D was shown to facilitate recovery of hind limb function after spinal cord injury in rats (Sandner et al., 2018), yet in the $SOD1^{G93A}$ mouse model of ALS, epothilone D accelerated disease progression (Clark et al., 2018), indicating that more work is needed in a variety of models.

POTENTIAL BENEFITS OF EPOTHILONES FOR TAUOPATHIES

Study of paclitaxel binding to microtubules revealed that it displaced Tau from microtubules, suggesting that paclitaxel and tau share a common binding site and microtubule stabilization mechanism (Kar et al., 2003). Tauopathies represent a class of neurodegenerative diseases where there is pathological aggregation of Tau. Hyper-phosphorylated Tau, a pathological hallmark of tauopathies, binds more poorly to microtubules and forms filamentous or amorphous aggregates (Iqbal et al., 2010). Epothilones provide a potential means to recover microtubule stability in the absence of this endogenous stabilizer.

Epothilone D has proven beneficial for amelioration of Tau-related pathologies in experimental animal models, where Tau mis-folding leads to impaired microtubule stability. The widely utilized MAPT (Tau)-PS19 transgenic mice are one such example. These mice harbor the disease-associated P301S mutation that gives rise to "4T" Tau, which harbors four microtubule-binding domains. The expression of Tau in PS19 mice is five-fold higher than endogenous levels, and they develop hallmarks of Alzheimer's disease including neuronal loss in the hippocampus, spreading the neocortex and entorhinal cortex. They also develop neurofibrillary-like inclusions accompanied by micro-gliosis, astrocytosis, although notably they do not develop amyloid plaques (Yoshiyama et al., 2007). Low doses of epothilone D (lower than those used in phase II clinical trials), increased microtubule density in MAPT(Tau)-PS19 mice. The drug also reduced axonal dystrophy and enhanced cognitive performance (Brunden et al., 2010). Furthermore, in neuronal cultures from amyloid precursor protein-mice, epothilone D treatment increased dendritic spine density (Penazzi et al., 2016). Because of such findings, epothilone D underwent clinical trial investigation in patients with mild Alzheimer's disease. In these studies, Tau provided a biomarker readout from cerebrospinal fluid; while cognitive performance and functional magnetic resonance imaging were additional outcome measures (NCT 01492374). This trial ended and further investigation of epothilone D discontinued. No results are posted so far (**Tables 1**, **2**; **Figure 1**).

In the rTg4510 Alzheimer's mouse model, where P301L is conditionally expressed, stochastic microtubule dynamics decrease. Injection with epothilone D recovered baseline dynamics and improved cognitive function in these mice (Barten et al., 2012). A follow up study showed that epothilone D treatment reversed several other features such as microtubule density, axonal dystrophy, and insoluble Tau. Thus, pathological Tau-related hallmarks reduced without any notable side effects in Tau transgenic mice (Zhang et al., 2012). An important finding from these experiments was that epothilone D, by stabilizing microtubule polymers, restored microtubule dynamics. Counter intuitively perhaps, drug-induced stabilization of microtubules did not immobilize them in a way that perturbed normal physiological regulation. This finding increased expectation that this molecule, or its analogs, could provide a beneficial treatment for Alzheimer's disease. However, following a phase I trial that used epothilone D for Alzheimer's disease discontinued, a new trial commenced and results are awaited (NCT 01966666).

POTENTIAL BENEFIT OF EPOTHILONES FOR PARKINSON'S DISEASE

Epothilone D treatment ameliorates hallmarks of Parkinson's disease in animal models. Degeneration of nigrostriatal dopaminergic neurons in the substantia nigra pars compacta is the disease-defining hallmark of Parkinson's disease in patients. In recent years, there is emerging evidence that microtubule instability may contribute to the disease etiology. For example MAPT(Tau)-containing neurofibrillary tangles are observed in both Parkinson's and Alzheimer's patients (Bancher et al., 1987; Joachim et al., 1987). Moreover, MAPT(Tau) variants confer genetic risk for Parkinson's disease (Simón–Sánchez et al., 2009). Furthermore, the environmental toxin rotenone, exposure to which is associated with increased risk to develop Parkinson's disease, destabilizes microtubules leading to cell-specific toxicity of midbrain dopaminergic neurons. Microtubule stabilizing drugs such as taxol rescued viability in these neurons (Ren et al., 2005). Similarly, in the 1-methyl-4-phenyl-1,2,3,6-tetrahydropyridine (MPTP) model of Parkinson's disease, epothilone D treatment prevented the loss of dopaminergic neurons in the substantia nigra pars compacta. These effects were attributed to the rescue of microtubule instability induced by MPTP (Cartelli et al., 2013; Killinger and Moszczynska, 2016).

POTENTIAL BENEFIT OF EPOTHILONES FOR PSYCHIATRIC DISORDERS

The effect of epothilone D was tested in mice lacking the gene for microtubule-associated protein-6 (MAP6)/stable tubule only polypeptide (STOP). These mice are used as a model for psychiatric disorders because they exhibit anatomical and behavioral hallmarks associated with schizophrenia that are reversible by treatment with anti-psychotic drugs. For example they display depressed and anxious behavior, altered serotonergic tone and impaired cognitive function (Fournet et al., 2012; Marchisella et al., 2016), while diffusion tensor imaging of MAP6 knockout mice revealed several neuronal tract deficits (Gimenez et al., 2017). In addition, they show impaired sensorimotor gating in the pre-pulse inhibition paradigm, and hyperactivity in a locomotor test, compared to their wild-type littermates (Volle et al., 2013). Promising results were obtained with epothilone D in these mice, where treatment induced an increase in synapse density and improved synaptic function measured by long-term potentiation (Andrieux et al., 2006). While preliminary, the association of anomalies in genes encoding microtubule-stabilizing proteins with psychiatric disorders (Marchisella et al., 2016), suggests that more widespread testing of epothilone and other microtubule stabilizing drugs in similar models is warranted.

TPI-287—ANTI-TUMOR AGENT IN CLINICAL TRIALS FOR TREATMENT OF NEURODEGENERATIVE DISEASES

TPI-287 is a third generation taxane (US patents: US7879904 and US7745650). It is a semisynthetic derivative of abeo-taxane and is widely used in cancer therapy. Like other taxanes, TPI-287 binds to tubulin and promotes microtubule stabilization and as a small molecule, it has the ability to cross the blood brain barrier. Experimentally it was investigated as a drug to treat breast cancer that had metastasised to brain. It effectively reduced tumor size after intravenous administration, however unpublished data indicated that there was loss of body weight as a side effect of treatment (Fitzgerald et al., 2012). TPI-287 is in Phase I clinical trial for treatment of mild to moderate symptoms of Alzheimer's disease (NCT 01966666). In this trial, three arms of patients receive different doses of TPI-287, following which patients are monitored for improvement in cognitive function. In addition, Aβ and Tau biomarker expression is measured from cerebrospinal fluid biopsies. The primary goal is to determine the maximum tolerated dose. TPI-287 is also in phase I (NCT 02133846) for treatment of primary 4-repeat tauopathies (4RT), corticobasal syndrome (CBS; or corticobasal degeneration) and progressive supranuclear palsy. Even though both clinical trials are active, and no side effects were reported so far. A completed phase I trial for treatment of neuroblastoma used higher TPI-287 doses (NCT 00867568 and NCT 01483820). These reported that 16.67% of patients showed serious side effects, such as seizures. Also, phase I clinical trial for metastatic melanoma (NCT 01067066) showed that 24% of the patients exhibited grade-3 peripheral neuropathy (McQuade et al., 2016).

IDN-5109

IDN-5109 (BAY 59-8862, Ortataxel) also belongs to the third generation of taxanes. It is possible to administer orally and it is more active than paclitaxel, displaying also greater solubility (Polizzi et al., 1999; Nicoletti et al., 2000; Jordan et al., 2002). It is a blood-brain barrier penetrant taxane analog, exhibiting a 15-fold higher brain to plasma ratio (Laccabue et al., 2001). Currently, IDN-5109 is in phase II for recurrent glioblastoma (NCT 01989884), taxane-refractory non-small-lung cell carcinoma (NCT 00054314 and NCT 00044538) and metastatic breast cancer (NCT 00044525), refractory NonHodgkin's lymphoma (NCT 00044551) and renal cell carcinoma (NCT 00044564). Clearly, it will be of interest to establish whether neuropathy side effects diminish with this compound. Testing in models of brain disorders is still awaiting.

NON-TAXANE GROUP MICROTUBULE STABILIZERS: NAP AND D-SAL

NAP, also known as davunetide, is an intranasal neuropeptide (NAPVSIPQ) derived from the activity-dependent neuroprotective protein (ADNP). The minimal 8 amino acid peptide NAP is neuroprotective (Gozes et al., 2005). ADNP mRNA levels have been shown to be dysregulated in Alzheimer's disease and in schizophrenia (Matsuoka et al., 2008; Dresner et al., 2011; Merenlender–Wagner et al., 2015; Ivashko–Pachima et al., 2017; Sragovich et al., 2017), and mutations in the ADNP gene have been found in patients with autism spectrum disorder (Helsmoortel et al., 2014). Clinical symptoms in patients carrying the ADNP mutation, so called Helsmoortel-Van der Aa syndrome or ADNP syndrome, have been well characterized (Van Dijck et al., 2018). The mechanism of action of NAP is believed to involve microtubules. NAP decorates microtubules in cultured cells, although in a purified system, increasing concentrations of NAP failed to induce tubulin polymerization (Yenjerla et al., 2010). More recently however, NAP was shown to interact with microtubule end-binding proteins EB1 and EB3, leading to increased dendritic spine density (Oz et al., 2014). Furthermore, NAP increases Tau binding to EB1/EB3 as part of its cyto-protective mechanism (Gozes et al., 2017, 2018; Ivashko–Pachima et al., 2017). ADNP also participates in the mammalian SWI/SNF complex, which is a multiprotein chromatin-remodeling complex (Mandel and Gozes, 2007).

POTENTIAL BENEFIT OF NAP FOR TREATMENT OF PSYCHIATRIC AND NEURODEGENERATIVE DISORDERS

Interestingly, NAP is brain penetrant when administered either by intranasal delivery (AL-108) (Gozes et al., 2000), intravenously (AL-208) (Leker et al., 2002) or intraperitoneally (Spong et al., 2001). NAP can exert its neuroprotective effects at very low concentrations, improving short-term memory in Apo-E mice, a mouse model for Alzheimer's disease (Bassan et al., 1999). Like the L-isomer, the D-amino acid analog of NAP (D-NAP) is also neuroprotective and D-NAP also improves cognitive deficits in Apo-E mice (Brenneman et al., 2004). In the Thy-α-Syn mouse model of Parkinson's disease, where human α-synuclein expression is under the control of the Thy-1 promoter, NAP treatment reduces both phosphorylated tau and α-synuclein aggregates in the substantia nigra (Fleming et al., 2011; Magen et al., 2014). This decrease in hyper-phosphorylated Tau is also evident in a mouse model of Alzheimer's disease, where NAP enhances axonal transport and improves cognitive performance in the Morris water maze (Matsuoka et al., 2008; Jouroukhin et al., 2013). Additionally, NAP promotes microtubule invasion into neuronal growth cones (Oz et al., 2012). Thus, NAP appears to promote microtubule stability by increasing the affinity of microtubules for Tau binding. Notably, NAP blocks phosphorylation of Tau on Ser-262 (Magen et al., 2014), a residue required for EB1/EB3 interaction (Ramirez–Rios et al., 2016). It is therefore likely that reduction of hyper-phosphorylated Tau by NAP is central for its mechanism (Quraishe et al., 2013; Ivashko–Pachima et al., 2017). Moreover, ADNP itself shows potential as a blood biomarker for Alzheimer's disease (Malishkevich et al., 2016).

Significantly, in the context of psychiatric disorders, NAP reverses the hyperactivity of MAP6/STOP null mice, a mouse model for schizophrenia (Merenlender–Wagner et al., 2010).

Moreover, NAP treatment prevents neuronal death often seen with clozapine, a commonly used anti-psychotic drug for treatment of schizophrenia (Merenlender–Wagner et al., 2014). Moreover, NAP reduces depressive-like behavior in mice following social isolation, exemplified by reduced immobility in the forced swim test and reduced anhedonic phenotype (Liu et al., 2017). NAP administration in DISC1 knockout mice, a model for schizophrenia, reduces anxiety levels in the elevated plus maze. On the other hand, combined treatment with the antipsychotic drug risperidone, failed to induce the same anxiolytic response. The authors attributed this to occlusion of the NAP binding site on microtubules by risperidone (Vaisburd et al., 2015). This indicates once more that the mode of action of NAP involves microtubules.

NAP is currently in phase II trial (NCT 00505765) for treatment of schizophrenia where the effect of intranasal NAP (AL-108) administration at two different doses is assessed. This derives from positive results in an earlier study using the UCSD performance based skills assessment (UPSA). While there was no significant improvement in cognitive scoring, the UPSA score showed significant improvement in functional capacity among patients (Javitt et al., 2012). A follow-up, double-blind study demonstrated no effect of a high dose of NAP (davunetide) in elevating N-acetylaspartate (Jarskog et al., 2013), a metabolite that is proposed to be slightly reduced in schizophrenia patients, although this is controversial (Steen et al., 2005). Moreover, NAP is in phase II trial (NCT 01056965) to assess its effects on mild cognitive impairment in Alzheimer's disease. Earlier analysis showed that NAP was well tolerated by Alzheimer's patients with no obvious side effects, and there was some improvement in individual memory tasks but not for composite memory score (Gozes et al., 2009; Morimoto et al., 2013). As an extension of the NAP studies, a shorter 4-amino acid peptide termed "SKIP" which is binds the EB binding site of ADNP is being studied in animal models for potential applications in psychiatric disorders (Amram et al., 2016).

TRIAZOLOPYRIMIDINES

Triazolopyrimidines are non-naturally occurring microtubule stabilizing compounds. Rather than acting like other microtubule stabilizing drugs, to stabilize the lateral edges, they bind in the vinca-site, normally targeted by agents such as vinblastine, acting to stabilize the longitudinal contacts between tubulin subunits (Sáez-Calvo et al., 2017). Triazolopyrimidines display similar properties to other microtubule stabilizing agents in promoting microtubule polymerization. Some of these compounds CNDR-51549 and CNDR51555 (US patent: US20170173016 A1) are capable of crossing the blood-brain barrier and increase the acetylated form of tubulin which reflects the stable pool (Lou et al., 2014; Cornec et al., 2015). Moreover, CNDR-51657 is capable of reducing hyperphosphorylated Tau induced by okadaic acid treatment (Kovalevich et al., 2016). Cevipabulin (TTI-237) (Beyer et al., 2008), another compound from this family which is not brain penetrant, has undergone phase I clinical trials for treatment of advanced malignant solid tumors (NCT 00195247 and NCT 00195325).

CONCLUSIONS

Finding new treatments for neurological disorders has proven to be an extremely challenging task. The realization that microtubule disruption plays a central role in brain disease opens up the possibility to benefit from knowledge gained from existing cancer therapeutics. Starting with the discovery of taxol in a National Cancer Institute-funded screening program in 1962, an array of brain penetrant microtubule stabilizers were developed with the goal of treating gliomas. Now, microtubule-stabilizing agents are under investigation for treatment of a variety of brain disorders. While this endeavor has not been without hurdles, we can expect that the high demand for therapeutic breakthroughs in this area will drive progress toward successful clinical outcome. In a field where receptor drugs dominate, this represents a completely new departure that looks promising.

AUTHOR CONTRIBUTIONS

AV, YH, and EC contributed to the conception and writing of the manuscript.

FUNDING

This work was funded by Åbo Akademi University, the Academy of Finland, MATTI, and Mol Bio Doctoral Programmes, Marie Curie r'BIRTH ITN.

ACKNOWLEDGMENTS

We are grateful to Peter James, Lund University for assistance with MetaCore^{TR}.

REFERENCES

Abidi, A. (2013). Cabazitaxel:a novel taxane for metastatic castration–resistant prostate cancer–current implications and future prospects. *J. Pharmacol. Pharmacother.* 4, 230–237. doi: 10.4103/0976–500X.119704

Ackerley, S. A. J., Grierson, B. S., Perkinton, M. S., Brownlees, J., Byers, H. L., Miller, C. C. et al. (2004). p38alpha stress–activated protein kinase phosphorylates neurofilaments and is associated with neurofilament pathology in amyotrophic lateral sclerosis. *Mol. Cell. Neurosci.* 26, 354–364. doi: 10.1016/j.mcn.2004.02.009

Aller, S. G., Yu, J., Ward, A., Weng, Y., Chittaboina, S., Zhuo, R., et al. (2009). Structure of P–glycoprotein reveals a molecular basis for poly–specific drug binding. *Science* 323, 1718–1722. doi: 10.1126/science.1168750

Alushin, G. M., Lander, G. C., Kellogg, E. H., Zhang, R., Baker, D., and Nogales, E. (2014). High–resolution microtubule structures reveal the structural transitions in αβ–tubulin upon GTP hydrolysis. *Cell* 157, 1117–1129. doi: 10.1016/j.cell.2014.03.053

Amram, N., Hacohen–Kleiman, G., Sragovich, S., Malishkevich, A., Katz, J., Touloumi, O., et al. (2016). Sexual divergence in microtubule function, the

novel intranasal microtubule targeting SKIP normalizes axonal transport and enhances memory. *Mol. Psychiatry* 21, 1467–1476. doi: 10.1038/mp.2015.208

Andrieux, A., Salin, P., Schweitzer, A., Begou, M., Pachoud, B., Brun, P., et al. (2006). Microtubule stabilizer ameliorates synaptic function and behavior in a mouse model for schizophrenia. *Biol. Psychiatry* 60, 1224–1230. doi: 10.1016/j.biopsych.2006.03.048

Bancher, C., Lassmann, H., Budka, H., Grundke–Iqbal, I., Iqbal, K., Wiche, G., et al. (1987). Neurofibrillary tangles in Alzheimer's disease and progressive supranuclear palsy, antigenic similarities and differences. Microtubule–associated protein tau antigenicity is prominent in all types of tangles. *Acta Neuropathol.* 74, 39–46. doi: 10.1007/BF00688336

Barten, D. M., Fanara, P., Andorfer, C., Hoque, N., Wong, P. Y., Husted, K. H., et al. (2012). Hyperdynamic microtubules, cognitive deficits, and pathology are improved in tau transgenic mice with low doses of the microtubule–stabilizing agent BMS−241027. *J. Neurosci.* 32, 7137–7145. doi: 10.1523/JNEUROSCI.0188–12.2012

Bassan, M., Zamostiano, R., Davidson, A., Pinhasov, A., Giladi, E., Perl, O., et al. (1999). Complete sequence of a novel protein containing a femtomolar–activity–dependent neuroprotective peptide. *J. Neurochem.* 72, 1283–1293. doi: 10.1046/j.1471–4159.1999.0721283.x

Beasley, C., Cotter, D., and Everall, I. (2002). An investigation of the Wnt–signalling pathway in the prefrontal cortex in schizophrenia, bipolar disorder and major depressive disorder. *Schizophr. Res.* 58, 63–67. doi: 10.1016/S0920-9964(01)00376-0

Bernard, R., Kerman, I. A., Thompson, R. C., Jones, E. G., Bunney, W. E., Barchas, J. D., et al. (2011). Altered expression of glutamate signaling, growth factor, and glia genes in the locus coeruleus of patients with major depression. *Mol. Psychiatry* 16, 634–646. doi: 10.1038/mp.2010.44

Beyer, C. F., Zhang, N., Hernandez, R., Vitale, D., Lucas, J., Nguyen, T., et al. (2008). TTI−237, a novel microtubule–active compound with *in vivo* antitumor activity. *Cancer Res.* 68, 2292–2300. doi: 10.1158/0008-5472.CAN-07-1420

Beyer, K., Lao, J. I., Carrato, C., Mate, J. L., Lopez, D., Ferrer, I., et al. (2004). Differential expression of alpha–synuclein isoforms in dementia with lewy bodies. *Neuropathol. Appl. Neurobiol.* 30, 601–607. doi: 10.1111/j.1365–2990.2004.00572.x

Bollag, D. M., McQueney, P. A., Zhu, J., Hensens, O., Koupal, L., Liesch, J., et al. (1995). Epothilones, a new class of microtubule–stabilizing agents with a taxol–like mechanism of action. *Cancer Res.* 55, 2325–2333.

Brenneman, D. E., Spong, C. Y., Hauser, J. M., Abebe, D., Pinhasov, A., Golian, T., et al. (2004). Protective peptides that are orally active and mechanistically nonchiral. *J. Pharmacol. Exp. Ther.* 309, 1190–1197. doi: 10.1124/jpet.103.063891

Brill, M. S., Kleele, T., Ruschkies, L., Wang, M., Marahori, N. A., Reuter, M. S., et al. (2016). Branch–Specific microtubule destabilization mediates axon branch loss during neuromuscular synapse elimination. *Neuron* 92, 845–856. doi: 10.1016/j.neuron.2016.09.049

Brogdon, C. F., Lee, F. Y., and Canetta, R. M. (2014). Development of other microtubule–stabilizer families, the epothilones and their derivatives. *Anticancer Drugs* 25, 599–609. doi: 10.1097/CAD.0000000000000071

Brunden, K. R., Gardner, N. M., James, M. J., Yao, Y., Trojanowski, J. Q., Lee, V. M., et al. (2013). MT–Stabilizer, dictyostatin, exhibits prolonged brain retention and activity, potential therapeutic implications. *ACS Med. Chem. Lett.* 4, 886–889. doi: 10.1021/ml400233e

Brunden, K. R., Yao, Y., Potuzak, J. S., Ferrer, N. I., Ballatore, C., James, M. J., et al. (2011). The characterization of microtubule–stabilizing drugs as possible therapeutic agents for Alzheimer's disease and related tauopathies. *Pharmacol. Res.* 63, 341–351. doi: 10.1016/j.phrs.2010.12.002

Brunden, K. R., Zhang, B., Carroll, J., Yao, Y., Potuzak, J. S., Hogan, A. M., et al. (2010). Epothilone D improves microtubule density, axonal integrity, and cognition in a transgenic mouse model of tauopathy. *J. Neurosci.* 30, 13861–13866. doi: 10.1523/JNEUROSCI.3059–10.2010

Callicott, J. H., Straub, R. E., Pezawas, L., Egan, M. F., Mattay, V. S., Hariri, A. R., et al. (2005). Variation in DISC1 affects hippocampal structure and function and increases risk for schizophrenia. *Proc. Natl. Acad. Sci. U.S.A.* 102, 8627–8632. doi: 10.1073/pnas.0500515102

Cartelli, D., Casagrande, F., Busceti, C. L., Bucci, D., Molinaro, G., Traficante, A., et al. (2013). Microtubule alterations occur early in experimental parkinsonism and the microtubule stabilizer epothilone D is neuroprotective. *Sci. Rep.* 3:1837. doi: 10.1038/srep01837

Cavaletti, G., and Marmiroli, P. (2010). Chemotherapy–induced peripheral neurotoxicity. *Nat. Rev. Neurol.* 6, 657–666. doi: 10.1038/nrneurol.2010.160

Cheon, M. S., Fountoulakis, M., Cairns, N. J., Dierssen, M., Herkner, K., and Lubec, G. (2001). Decreased protein levels of stathmin in adult brains with Down syndrome and Alzheimer's disease. *J. Neural Transm. Suppl.* 61, 281–288. doi: 10.1007/78-3-7091-6262-0_23

Chou, T. C., Zhang, X. G., Balog, A., Su, D. S., Meng, D., Savin, K., et al. (1998). Desoxyepothilone B, an efficacious microtubule–targeted antitumor agent with a promising *in vivo* profile relative to epothilone B. *Proc. Natl. Acad. Sci. U.S.A.* 95, 9642–9647. doi: 10.1073/pnas.95.16.9642

Cisternino, S., Bourasset, F., Archimbaud, Y., Semiond, D., Sanderink, G., and Scherrmann, J. M. (2003). Nonlinear accumulation in the brain of the new taxoid TXD258 following saturation of P–glycoprotein at the blood–brain barrier in mice and rats. *Br. J. Pharmacol.* 138, 1367–1375. doi: 10.1038/sj.bjp.0705150

Clark, J. A., Blizzard, C. A., Breslin, M. C., Yeaman, E. J., Lee, K. M., Chuckowree, J. A., et al. (2018). Epothilone D accelerates disease progression in the SOD1^{G93A}. *Neuropathol. Appl. Neurobiol.* doi: 10.1111/nan.12473. [Epub ahead of print].

Cleveland, D. W., Kirschner, M. W., and Cowan, N. J. (1978). Isolation of separate mRNAs for alpha– and beta–tubulin and characterization of the corresponding *in vivo* translation products. *Cell* 15, 1021–1031. doi: 10.1016/0092-8674(78)90286-6

Cornec, A. S., James, M. J., Kovalevich, J., Trojanowski, J. Q., Lee, V. M., Smith, A. B. III, et al. (2015). Pharmacokinetic, pharmacodynamic and metabolic characterization of a brain retentive microtubule (MT)–stabilizing triazolopyrimidine. *Bioorg. Med. Chem. Lett.* 25, 4980–4982. doi: 10.1016/j.bmcl.2015.03.002

de Bono, J. S., Oudard, S., Ozguroglu, M., Hansen, S., Machiels, J. P., Kocak, I., et al. (2010). Prednisone plus cabazitaxel or mitoxantrone for metastatic castration–resistant prostate cancer progressing after docetaxel treatment, a randomised open–label trial. *Lancet* 376, 1147–1154. doi: 10.1016/S0140–6736(10)61389–X

Derkinderen, P., Scales, T. M., Hanger, D. P., Leung, K. Y., Byers, H. L., Ward, M. A., et al. (2005). Tyrosine 394 is phosphorylated in Alzheimer's paired helical filament tau and in fetal tau with c–Abl as the candidate tyrosine kinase. *J. Neurosci.* 25, 6584–6593. doi: 10.1523/JNEUROSCI.1487–05.2005

Dresner, E., Agam, G., and Gozes, I. (2011). Activity–dependent neuroprotective protein (ADNP) expression level is correlated with the expression of the sister protein ADNP2, deregulation in schizophrenia. *Eur. Neuropsychopharmacol.* 21, 355–361. doi: 10.1016/j.euroneuro.2010.06.004

Engidawork, E., Gulesserian, T., Yoo, B. C., Cairns, N., and Lubec, G. (2001). Alteration of caspases and apoptosis–related proteins in brains of patients with Alzheimer's disease. *Biochem. Biophys. Res. Commun.* 281, 84–93. doi: 10.1006/bbrc.2001.4306

Engmann, O., Hortobagyi, T., Thompson, A. J., Guadagno, J., Troakes, C., Soriano, S., et al. (2011). Cyclin–dependent kinase 5 activator p25 is generated during memory formation and is reduced at an early stage in Alzheimer's disease. *Biol. Psychiatry* 70, 159–168. doi: 10.1016/j.biopsych.2011.04.011

Evans, T. A., Raina, A. K., Delacourte, A., Aprelikova, O., Lee, H. G., Zhu, X., et al. (2007). BRCA1 may modulate neuronal cell cycle re–entry in Alzheimer disease. *Int. J. Med. Sci.* 4, 140–145. doi: 10.7150/ijms.4.140

Fellner, S., Bauer, B., Miller, D. S., Schaffrik, M., Fankhanel, M., Spruss, T., et al. (2002). Transport of paclitaxel (Taxol) across the blood–brain barrier *in vivo* and *in vivo*. *J. Clin. Invest.* 110, 1309–1318. doi: 10.1172/JCI0215451

Figueroa, D. J., Morris, J. A., Ma, L., Kandpal, G., Chen, E., Li, Y. M., et al. (2002). Presenilin–dependent gamma–secretase activity modulates neurite outgrowth. *Neurobiol. Dis.* 9, 49–60. doi: 10.1006/nbdi.2001.0447

Fitzgerald, D. P., Emerson, D. L., Qian, Y., Anwar, T., Liewehr, D. J., Steinberg, S. M., et al. (2012). TPI−287, a new taxane family member, reduces the brain metastatic colonization of breast cancer cells. *Mol. Cancer Ther.* 11, 1959–1967. doi: 10.1158/1535-7163.MCT-12-0061

Fleming, S. M., Mulligan, C. K., Richter, F., Mortazavi, F., Lemesre, V., Frias, C., et al. (2011). A pilot trial of the microtubule–interacting peptide (NAP) in mice overexpressing alpha–synuclein shows improvement in motor function and reduction of alpha–synuclein inclusions. *Mol. Cell Neurosci.* 46, 597–606. doi: 10.1016/j.mcn.2010.12.011

Fournet, V., Schweitzer, A., Chevarin, C., Deloulme, J. C., Hamon, M., Giros, B., et al. (2012). The deletion of STOP/MAP6 protein in mice triggers highly altered mood and impaired cognitive performances. *J. Neurochem*. 121, 99–114. doi: 10.1111/j.1471-4159.2011.07615.x

Freedman, R. A., Bullitt, E., Sun, L., Gelman, R., Harris, G., Ligibel, J. A., et al. (2011). A phase II study of sagopilone (ZK 219477; ZK–EPO) in patients with breast cancer and brain metastases. *Clin. Breast Cancer* 11, 376–383. doi: 10.1016/j.clbc.2011.03.024

Gencer, M., Dasdemir, S., Cakmakoglu, B., Cetinkaya, Y., Varlibas, F., Tireli, H., et al. (2012). DNA repair genes in Parkinson's disease. *Genet. Test. Mol. Biomarkers* 16, 504–507. doi: 10.1089/gtmb.2011.0252

Ghoochani, A., Hatipoglu Majernik, G., Sehm, T., Wach, S., Buchfelder, M., Taubert, H., et al. (2016). Cabazitaxel operates anti–metastatic and cytotoxic via apoptosis induction and stalls brain tumor angiogenesis. *Oncotarget* 7, 38306–38318. doi: 10.18632/oncotarget.9439

Giannakakou, P., Gussio, R., Nogales, E., Downing, K. H., Zaharevitz, D., Bollbuck, B., et al. (2000). A common pharmacophore for epothilone and taxanes, molecular basis for drug resistance conferred by tubulin mutations in human cancer cells. *Proc. Natl. Acad. Sci. U.S.A*. 97, 2904–2909. doi: 10.1073/pnas.040546297

Gimenez, U., Boulan, B., Mauconduit, F., Taurel, F., Leclercq, M., Denarier, E., et al. (2017). 3D imaging of the brain morphology and connectivity defects in a model of psychiatric disorders, MAP6–KO mice. *Sci. Rep*. 7:10308. doi: 10.1038/s41598-017-10544-2

Girard, E., Ditzler, S., Lee, D., Richards, A., Yagle, K., Park, J., et al. (2015). Efficacy of cabazitaxel in mouse models of pediatric brain tumors. *Neuro Oncol*. 17, 107–115. doi: 10.1093/neuonc/nou163

Goedert, M., Eisenberg, D. S., and Crowther, R. A. (2017). Propagation of tau aggregates and neurodegeneration. *Ann. Rev. Neurosci*. 40, 189–210. doi: 10.1146/annurev-neuro-072116-031153

Gozes, I., Giladi, E., Pinhasov, A., Bardea, A., and Brenneman, D. E. (2000). Activity–dependent neurotrophic factor, intranasal administration of femtomolar–acting peptides improve performance in a water maze. *J. Pharmacol. Exp. Ther*. 293, 1091–1098.

Gozes, I., Ivashko–Pachima, Y., and Sayas, C. L. (2018). ADNP, a Microtubule interacting protein, provides neuroprotection through end binding proteins and tau, an amplifier effect. *Front. Mol. Neurosci*. 11:151. doi: 10.3389/fnmol.2018.00151

Gozes, I., and Littauer, U. Z. (1978). Tubulin microheterogeneity increases with rat brain maturation. *Nature* 276, 411–413. doi: 10.1038/276411a0

Gozes, I., Morimoto, B. H., Tiong, J., Fox, A., Sutherland, K., Dangoor, D., et al. (2005). NAP, research and development of a peptide derived from activity–dependent neuroprotective protein (ADNP). *CNS Drug Rev*. 11, 353–368. doi: 10.1111/j.1527-3458.2005.tb00053.x

Gozes, I., Stewart, A., Morimoto, B., Fox, A., Sutherland, K., and Schmeche, D. (2009). Addressing Alzheimer's disease tangles, from NAP to AL−108. *Curr. Alzheimer Res*. 6, 455–460. doi: 10.2174/156720509789207895

Gozes, I., Van Dijck, A., Hacohen–Kleiman, G., Grigg, I., Karmon, G., Giladi, E., et al. Bedrosian–Sermone (2017). Premature primary tooth eruption in cognitive/motor–delayed ADNP–mutated children. *Transl. Psychiatry* 7:e1043. doi: 10.1038/tp.2017.27

Gradishar, W. J., Tjulandin, S., Davidson, N., Shaw, H., Desai, N., Bhar, P., et al. (2005). Phase III trial of nanoparticle albumin–bound paclitaxel compared with polyethylated castor oil–based paclitaxel in women with breast cancer. *J. Clin. Oncol*. 23, 7794–7803. doi: 10.1200/JCO.2005.04.937

Gunasekera, S. P., Gunasekera, M., Longley, R. E., and Schulte, G. K. (1990). Discodermolide, a new bioactive polyhydroxylated lactone from the marine sponge *Discodermia dissoluta*. *J. Organ. Chem*. 55, 4912–4915. doi: 10.1021/jo00303a029

Hand, C. K., Devon, R. S., Gros–Louis, F., Rochefort, D., Khoris, J., Meininger, V., et al. (2003). Mutation screening of the ALS2 gene in sporadic and familial amyotrophic lateral sclerosis. *Arch. Neurol*. 60, 1768–1771. doi: 10.1001/archneur.60.12.1768

Helsmoortel, C., Vulto–van Silfhout, A. T., Coe, B. P., Vandeweyer, G., Rooms, L., Van der Aa, J., et al. (2014). A SWI/SNF–related autism syndrome caused by de novo mutations in ADNP. *Nat. Genet*. 46, 380–384. doi: 10.1038/ng.2899

Hoefle, G. P. D., Bedorf, N. D., Gerth, K. D., and Reichenbach, H. P. D. (1993). *Epothilone, Deren Herstellungsverfahren Sowie Sie Enthaltende Mittel Epothilones, their Manufacturing Processes as Well as Medium Containing them*. Google Patents, PCT/EP1997006442. Braunschweig: WIPO.

Hoffmann, J., Fichtner, I., Lemm, M., Lienau, P., Hess–Stumpp, H., Rotgeri, A., et al. (2009). Sagopilone crosses the blood–brain barrier *in vivo* to inhibit brain tumor growth and metastases. *Neuro Oncol*. 11, 158–166. doi: 10.1215/15228517-2008-072

Howell, W. M., and Brookes, A. J. (2002). Evaluation of multiple presenilin 2 SNPs for association with early–onset sporadic Alzheimer disease. *Am. J. Med. Genet*. 111, 157–163. doi: 10.1002/ajmg.10533

Hu, J. H., Zhang, H., Wagey, R., Krieger, C., and Pelech, S. L. (2003). Protein kinase and protein phosphatase expression in amyotrophic lateral sclerosis spinal cord. *J. Neurochem*. 85, 432–442. doi: 10.1046/j.1471-4159.2003.01670.x

Ibrahim, N. K., Samuels, B., Page, R., Doval, D., Patel, K. M., Rao, S. C., et al. (2005). Multicenter phase II trial of ABI-007, an albumin-bound paclitaxel, in women with metastatic breast cancer. *J. Clin. Oncol*. 23, 6019–6026. doi: 10.1200/jco.2005.11.013

Iqbal, K., Liu, F., Gong, C. X., and Grundke–Iqbal, I. (2010). Tau in Alzheimer disease and related tauopathies. *Curr. Alzheimer Res*. 7, 656–664. doi: 10.2174/156720510793611592

Ito, T., Niwa, J., Hishikawa, N., Ishigaki, S., Doyu, M., and Sobue, G. (2003). Dorfin localizes to Lewy bodies and ubiquitylates synphilin−1. *J. Biol. Chem*. 278, 29106–29114. doi: 10.1074/jbc.M302763200

Ivashko–Pachima, Y., Sayas, C. L., Malishkevich, A., and Gozes, I. (2017). ADNP/NAP dramatically increase microtubule end–binding protein–Tau interaction, a novel avenue for protection against tauopathy. *Mol. Psychiatry* 22, 1335–1344. doi: 10.1038/mp.2016.255

Jarskog, L. F., Dong, Z., Kangarlu, A., Colibazzi, T., Girgis, R. R., Kegeles, L. S., et al. (2013). Effects of davunetide on N–acetylaspartate and choline in dorsolateral prefrontal cortex in patients with schizophrenia. *Neuropsychopharmacology* 38, 1245–1252. doi: 10.1038/npp.2013.23

Javitt, D. C., Buchanan, R. W., Keefe, R. S., Kern, R., McMahon, R. P., Green, M. F., et al. (2012). Effect of the neuroprotective peptide davunetide (AL−108) on cognition and functional capacity in schizophrenia. *Schizophr. Res*. 136, 25–31. doi: 10.1016/j.schres.2011.11.001

Joachim, C. L., Morris, J. H., Kosik, K. S., and Selkoe, D. J. (1987). Tau antisera recognize neurofibrillary tangles in a range of neurodegenerative disorders. *Ann. Neurol*. 22, 514–520. doi: 10.1002/ana.410220411

Jordan, M. A., Ojima, I., Rosas, F., Distefano, M., Wilson, L., Scambia, G., et al. (2002). Effects of novel taxanes SB–T−1213 and IDN5109 on tubulin polymerization and mitosis. *Chem. Biol*. 9, 93–101. doi: 10.1016/S1074-5521(01)00097-7

Jordan–Sciutto, K. L., Dorsey, R., Chalovich, E. M., Hammond, R. R., and Achim, C. L. (2003). Expression patterns of retinoblastoma protein in Parkinson disease. *J. Neuropathol. Exp. Neurol*. 62, 68–74. doi: 10.1093/jnen/62.1.68

Jouroukhin, Y., Ostritsky, R., Assaf, Y., Pelled, G., Giladi, E., and Gozes, I. (2013). NAP (davunetide) modifies disease progression in a mouse model of severe neurodegeneration, protection against impairments in axonal transport. *Neurobiol. Dis*. 56, 79–94. doi: 10.1016/j.nbd.2013.04.012

Kar, S., Fan, J., Smith, M. J., Goedert, M., and Amos, L. A. (2003). Repeat motifs of tau bind to the insides of microtubules in the absence of taxol. *EMBO J*. 22, 70–77. doi: 10.1093/emboj/cdg001

Khrapunovich–Baine, M., Menon, V., Verdier–Pinard, P., Smith, A. B. III, Angeletti, R. H., Fiser, A., et al. (2009). Distinct pose of discodermolide in taxol binding pocket drives a complementary mode of microtubule stabilization. *Biochemistry* 48, 11664–11677. doi: 10.1021/bi901351q

Killinger, B. A., and Moszczynska, A. (2016). Epothilone D prevents binge methamphetamine–mediated loss of striatal dopaminergic markers. *J. Neurochem*. 136, 510–525. doi: 10.1111/jnc.13391

Kingston, D. G. (1991). The chemistry of taxol. *Pharmacol. Ther*. 52, 1–34. doi: 10.1016/0163-7258(91)90085-Z

Klar, U., Buchmann, B., Schwede, W., Skuballa, W., Hoffmann, J., and Lichtner, R. B. (2006). Total synthesis and antitumor activity of ZK–EPO, the first fully synthetic epothilone in clinical development. *Angew. Chem. Int. Ed. Engl*. 45, 7942–7948. doi: 10.1002/anie.200602785

Kovalevich, J., Cornec, A. S., Yao, Y., James, M., Crowe, A., Lee, V. M., et al. (2016). Characterization of brain–penetrant pyrimidine–containing

molecules with differential microtubule–stabilizing activities developed as potential therapeutic agents for Alzheimer's disease and related tauopathies. *J. Pharmacol. Exp. Ther*. 357, 432–450. doi: 10.1124/jpet.115.231175

Kowalski, R. J., Giannakakou, P., Gunasekera, S. P., Longley, R. E., Day, B. W., and Hamel, E. (1997). The microtubule–stabilizing agent discodermolide competitively inhibits the binding of paclitaxel (Taxol) to tubulin polymers, enhances tubulin nucleation reactions more potently than paclitaxel, and inhibits the growth of paclitaxel–resistant cells. *Mol. Pharmacol*. 52, 613–622. doi: 10.1124/mol.52.4.613

Krüger, R., Kuhn, W., Muller, T., Woitalla, D., Graeber, M., Kosel, S., et al. (1998). Ala30Pro mutation in the gene encoding alpha–synuclein in Parkinson's disease. *Nat. Genet*. 18, 106–108. doi: 10.1038/ng0298-106

Kurzrock, R., Gabrail, N., Chandhasin, C., Moulder, S., Smith, C., Brenner, A., et al. (2012). Safety, pharmacokinetics, and activity of GRN1005, a novel conjugate of angiopep−2, a peptide facilitating brain penetration, and paclitaxel, in patients with advanced solid tumors. *Mol. Cancer Ther*. 11, 308–316. doi: 10.1158/1535-7163.MCT-11-0566

Kwok, J. B., Hallupp, M., Loy, C. T., Chan, D. K., Woo, J., Mellick, G. D., et al. (2005). GSK3B polymorphisms alter transcription and splicing in Parkinson's disease. *Ann. Neurol*. 58, 829–839. doi: 10.1002/ana.20691

Laccabue, D., Tortoreto, M., Veneroni, S., Perego, P., Scanziani, E., Zucchetti, M., et al. (2001). A novel taxane active against an orthotopically growing human glioma xenograft. *Cancer* 92, 3085–3092. doi: 10.1002/1097-0142(20011215)92:12<3085::AID-CNCR10150>3.0.CO;2-S

Lee, F. Y., Borzilleri, R., Fairchild, C. R., Kim, S. H., Long, B. H., Reventos–Suarez, C., et al. (2001). BMS−247550, a novel epothilone analog with a mode of action similar to paclitaxel but possessing superior antitumor efficacy. *Clin. Cancer Res*. 7, 1429–1437.

Leker, R. R., Teichner, A., Grigoriadis, N., Ovadia, H., Brenneman, D. E., Fridkin, M., et al. (2002). NAP, a femtomolar–acting peptide, protects the brain against ischemic injury by reducing apoptotic death. *Stroke* 33, 1085–1092. doi: 10.1161/01.STR.0000014207.05597.D7

Lesort, M., Greendorfer, A., Stockmeier, C., Johnson, G. V., and Jope, R. S. (1999). Glycogen synthase kinase−3β, β–catenin, and tau in postmortem bipolar brain. *J. Neural Transm*. 106, 1217–1222.

Liang, X., Slifer, M., Martin, E. R., Schnetz–Boutaud, N., Bartlett, J., Anderson, B., et al. (2009). Genomic convergence to identify candidate genes for Alzheimer disease on chromosome 10. *Hum Mutat*. 30, 463–471. doi: 10.1002/humu.20953

Liang, Z., Liu, F., Grundke–Iqbal, I., Iqbal, K., and Gong, C. X. (2007). Down–regulation of cAMP–dependent protein kinase by over–activated calpain in Alzheimer disease brain. *J. Neurochem*. 103, 2462–2470. doi: 10.1111/j.1471–4159.2007.04942.x

Link, C. D., Taft, A., Kapulkin, V., Duke, K., Kim, S., Fei, Q., et al. (2003). Gene expression analysis in a transgenic caenorhabditis elegans alzheimer's disease model. *Neurobiol. Aging* 24, 397–413. doi: 10.1016/S0197-4580(02)00224-5

Liu, F., Liu, Y. P., Lei, G., Liu, P., Chu, Z., Gao, C. G., et al. (2017). Antidepressant effect of recombinant NT4–NAP/AAV on social isolated mice through intranasal route. *Oncotarget* 8, 10103–10113. doi: 10.18632/oncotarget.14356

Liu, J. S. (2011). Molecular genetics of neuronal migration disorders. *Curr. Neurol. Neurosci. Rep*. 11, 171–178. doi: 10.1007/s11910-010-0176-5

Lou, K., Yao, Y., Hoye, A. T., James, M. J., Cornec, A. S., Hyde, E., et al. (2014). Brain–penetrant, orally bioavailable microtubule–stabilizing small molecules are potential candidate therapeutics for Alzheimer's disease and related tauopathies. *J. Med. Chem*. 57, 6116–6127. doi: 10.1021/jm5005623

Maddalena, A., Papassotiropoulos, A., Muller–Tillmanns, B., Jung, H. H., Hegi, T., Nitsch, R. M., et al. (2003). Biochemical diagnosis of Alzheimer disease by measuring the cerebrospinal fluid ratio of phosphorylated tau protein to beta–amyloid peptide42. *Arch. Neurol*. 60, 1202–1206. doi: 10.1001/archneur.60.9.1202

Madiraju, C., Edler, M. C., Hamel, E., Raccor, B. S., Balachandran, R., Zhu, G., et al. (2005). Tubulin assembly, taxoid site binding, and cellular effects of the microtubule–stabilizing agent dictyostatin. *Biochemistry* 44, 15053–15063. doi: 10.1021/bi050685l

Magen, I., Ostritsky, R., Richter, F., Zhu, C., Fleming, S. M., Lemesre, V., et al. (2014). Intranasal NAP (davunetide) decreases tau hyperphosphorylation and moderately improves behavioral deficits in mice overexpressing alpha–synuclein. *Pharmacol. Res. Perspect*. 2:e00065. doi: 10.1002/prp2.65

Malishkevich, A., Marshall, G. A., Schultz, A. P., Sperling, R. A., Aharon–Peretz, J., and Gozes, I. (2016). Blood–Borne activity–dependent neuroprotective protein (ADNP) is correlated with premorbid intelligence, clinical stage, and alzheimer's disease biomarkers. *J. Alzheimers Dis*. 50, 249–260. doi: 10.3233/JAD-150799

Mandel, S., and Gozes, I. (2007). Activity–dependent neuroprotective protein constitutes a novel element in the SWI/SNF chromatin remodeling complex. *J. Biol. Chem*. 282, 34448–34456. doi: 10.1074/jbc.M704756200

Mandilaras, V., Wan–Chow–Wah, D., Monette, J., Gaba, F., Monette, M., and Alfonso, L. (2013). The impact of cancer therapy on cognition in the elderly. *Front. Pharmacol*. 4:48. doi: 10.3389/fphar.2013.00048

Marchisella, F., Coffey, E. T., and Hollos, P. (2016). Microtubule and microtubule associated protein anomalies in psychiatric disease. *Cytoskeleton (Hoboken)* 73, 596–611. doi: 10.1002/cm.21300

Martello, L. A., McDaid, H. M., Regl, D. L., Yang, C. P., Meng, D., Pettus, T. R., et al. (2000). Taxol and discodermolide represent a synergistic drug combination in human carcinoma cell lines. *Clin. Cancer Res*. 6, 1978–1987.

Matamoros, A. J., and Baas, P. W. (2016). Microtubules in health and degenerative disease of the nervous system. *Brain Res. Bull*. 126, 217–225. doi: 10.1016/j.brainresbull.2016.06.016

Matsuoka, Y., Jouroukhin, Y., Gray, A. J., Ma, L., Hirata–Fukae, C., Li, H. F., et al. (2008). A neuronal microtubule–interacting agent, NAPVSIPQ, reduces tau pathology and enhances cognitive function in a mouse model of Alzheimer's disease. *J. Pharmacol. Exp. Ther*. 325, 146–153. doi: 10.1124/jpet.107.130526

McQuade, J. L., Posada, L. P., Lecagoonporn, S., Cain, S., Bassett Jr. R. L, Patel, S. P., et al. (2016). A phase I study of TPI 287 in combination with temozolomide for patients with metastatic melanoma. *Melanoma Res*. 26, 604–608. doi: 10.1097/CMR.0000000000000296

Merenlender–Wagner, A., Malishkevich, A., Shemer, Z., Udawela, M., Gibbons, A., Scarr, E., et al. (2015). Autophagy has a key role in the pathophysiology of schizophrenia. *Mol. Psychiatry* 20, 126–132. doi: 10.1038/mp.2013.174

Merenlender–Wagner, A., Pikman, R., Giladi, E., Andrieux, A., and Gozes, I. (2010). NAP (davunetide) enhances cognitive behavior in the STOP heterozygous mouse-a microtubule–deficient model of schizophrenia. *Peptides* 31, 1368–1373. doi: 10.1016/j.peptides.2010.04.011

Merenlender–Wagner, A., Shemer, Z., Touloumi, O., Lagoudaki, R., Giladi, E., Andrieux, A., et al. (2014). New horizons in schizophrenia treatment, autophagy protection is coupled with behavioral improvements in a mouse model of schizophrenia. *Autophagy* 10, 2324–2332. doi: 10.4161/15548627.2014.984274

Mita, A., Lockhart, A. C., Chen, T. L., Bochinski, K., Curtright, J., Cooper, W., et al. (2004). A phase I pharmacokinetic (PK) trial of XAA296A (Discodermolide) administered every 3 wks to adult patients with advanced solid malignancies. *J. Clin. Oncol*. 22, 2025–2025. doi: 10.1200/jco.2004.22.14_suppl.2025

Morimoto, B. H., Schmechel, D., Hirman, J., Blackwell, A., Keith, J., and Gold, M. (2013). A double–blind, placebo–controlled, ascending–dose, randomized study to evaluate the safety, tolerability and effects on cognition of AL−108 after 12 weeks of intranasal administration in subjects with mild cognitive impairment. *Dement. Geriatr. Cogn. Disord*. 35, 325–336. doi: 10.1159/000348347

Mullan, M., Crawford, F., Axelman, K., Houlden, H., Lilius, L., Winblad, B., et al. (1992). A pathogenic mutation for probable Alzheimer's disease in the APP gene at the N–terminus of beta–amyloid. *Nat. Genet*. 1, 345–347. doi: 10.1038/ng0892-345

Naj, A. C., Beecham, G. W., Martin, E. R., Gallins, P. J., Powell, E. H., Konidari, I., et al. (2010). Dementia revealed, novel chromosome 6 locus for late–onset Alzheimer disease provides genetic evidence for folate–pathway abnormalities. *PLoS Genet*. 6:e1001130. doi: 10.1371/journal.pgen.1001130

Nettles, J. H., Li, H., Cornett, B., Krahn, J. M., Snyder, J. P., and Downing, K. H. (2004). The binding mode of epothilone A on alpha,beta–tubulin by electron crystallography. *Science* 305, 866–869. doi: 10.1126/science.1099190

Nicoletti, M. I., Colombo, T., Rossi, C., Monardo, C., Stura, S., Zucchetti, M., et al. (2000). IDN5109, a taxane with oral bioavailability and potent antitumor activity. *Cancer Res*. 60, 842–846.

Nogales, E., Wolf, S. G., and Downing, K. H. (1998). Structure of the alpha beta tubulin dimer by electron crystallography. *Nature* 391, 199–203. doi: 10.1038/34465

Nogales, E., Wolf, S. G., Khan, I. A., Ludue–a, R. F., and Downing, K. H. (1995). Structure of tubulin at 6.5 A and location of the taxol–binding site. *Nature* 375, 424–427. doi: 10.1038/375424a0

Noori–Daloii, M. R., Kheirollahi, M., Mahbod, P., Mohammadi, F., Astaneh, A. N., Zarindast, M. R., et al. (2010). Alpha– and beta–synucleins mRNA expression in lymphocytes of schizophrenia patients. *Genet. Test. Mol. Biomarkers* 14, 725–729. doi: 10.1089/gtmb.2010.0050

Nyman, D. W., Campbell, K. J., Hersh, E., Long, K., Richardson, K., Trieu, V., et al. (2005). Phase I and pharmacokinetics trial of ABI-007, a novel nanoparticle formulation of paclitaxel in patients with advanced nonhematologic malignancies. *J. Clin. Oncol.* 23, 7785–7793. doi: 10.1200/jco.2004.00.6148

Ogawa, O., Lee, H. G., Zhu, X., Raina, A., Harris, P. L., Castellani, R. J., et al. (2003). Increased p27, an essential component of cell cycle control, in Alzheimer's disease. *Aging Cell* 2, 105–110. doi: 10.1046/j.1474-9728.2003.00042.x

Overmoyer, B., Waintraub, S., Kaufman, P. A., Doyle, T., Moore, H., Modiano, M., et al. (2005). Phase II trial of KOS−862 (epothilone D) in anthracycline and taxane pretreated metastatic breast cancer. *J. Clin. Oncol.* 23, 778–778. doi: 10.1200/jco.2005.23.16_suppl.778

Oz, S., Ivashko–Pachima, Y., and Gozes, I. (2012). The ADNP derived peptide, NAP modulates the tubulin pool, implication for neurotrophic and neuroprotective activities. *PloS ONE* 7:e51458. doi: 10.1371/journal.pone.0051458

Oz, S., Kapitansky, O., Ivashco–Pachima, Y., Malishkevich, A., Giladi, E., Skalka, N., et al. (2014). The NAP motif of activity–dependent neuroprotective protein (ADNP) regulates dendritic spines through microtubule end binding proteins. *Mol. Psychiatry* 19, 1115–1124. doi: 10.1038/mp.2014.97

Pease–Raissi, S. E., Pazyra–Murphy, M. F., Li, Y., Wachter, F., Fukuda, Y., Fenstermacher, S. J., et al. (2017). Paclitaxel reduces axonal bclw to initiate IP3R1–dependent axon degeneration. *Neuron* 96, 373.e6–386.e6. doi: 10.1016/j.neuron.2017.09.034

Penazzi, L., Tackenberg, C., Ghori, A., Golovyashkina, N., Niewidok, B., Selle, K., et al. (2016). Abeta–mediated spine changes in the hippocampus are microtubule–dependent and can be reversed by a subnanomolar concentration of the microtubule–stabilizing agent epothilone D. *Neuropharmacology* 105, 84–95. doi: 10.1016/j.neuropharm.2016.01.002

Polizzi, D., Pratesi, G., Tortoreto, M., Supino, R., Riva, A., Bombardelli, E., et al. (1999). A novel taxane with improved tolerability and therapeutic activity in a panel of human tumor xenografts. *Cancer Res.* 59, 1036–1040.

Potkin, S.G., Guffanti, G., Lakatos, A., Turner, J. A., Kruggel, F., Fallon, J. H., et al., (2009). Hippocampal atrophy as a quantitative trait in a genome–wide association study identifying novel susceptibility genes for Alzheimer's disease. *PLoS ONE* 4:e6501. doi: 10.1371/journal.pone.0006501

Quraishe, S., Cowan, C. M., and Mudher, A. (2013). NAP (davunetide) rescues neuronal dysfunction in a Drosophila model of tauopathy. *Mol. Psychiatry* 18, 834–842. doi: 10.1038/mp.2013.32

Ramirez–Rios, S., Denarier, E., Prezel, E., Vinit, A., Stoppin–Mellet, V., Devred, F., et al. (2016). Tau antagonizes end–binding protein tracking at microtubule ends through a phosphorylation–dependent mechanism. *Mol. Biol. Cell* 27, 2924–2934. doi: 10.1091/mbc.e16-01-0029

Régina, A., Demeule, M., Che, C., Lavallee, I., Poirier, J., Gabathuler, R., et al. (2008). Antitumour activity of ANG1005, a conjugate between paclitaxel and the new brain delivery vector Angiopep−2. *Br. J. Pharmacol.* 155, 185–197. doi: 10.1038/bjp.2008.260

Reiner, O., and Sapir, T. (2013). LIS1 functions in normal development and disease. *Curr. Opin. Neurobiol.* 23, 951–956. doi: 10.1016/j.conb.2013.08.001

Ren, Y., Liu, W., Jiang, H., Jiang, Q., and Feng, J. (2005). Selective vulnerability of dopaminergic neurons to microtubule depolymerization. *J. Biol. Chem.* 280, 34105–34112. doi: 10.1074/jbc.M503483200

Ruschel, J., Hellal, F., Flynn, K. C., Dupraz, S., Elliott, D. A., Tedeschi, A., et al. (2015). Axonal regeneration. Systemic administration of epothilone B promotes axon regeneration after spinal cord injury. *Science* 348, 347–352. doi: 10.1126/science.aaa2958

Russ, C., Lovestone, S., and Powell, J. F. (2001). Identification of sequence variants and analysis of the role of the glycogen synthase kinase 3 beta gene and promoter in late onset Alzheimer's disease. *Mol. Psychiatry* 6, 320–324. doi: 10.1038/sj.mp.4000852

Ryoo, S. R., Cho, H. J., Lee, H. W., Jeong, H. K., Radnaabazar, C., Kim, Y. S., et al. (2008). Dual–specificity tyrosine(Y)–phosphorylation regulated kinase 1A–mediated phosphorylation of amyloid precursor protein, evidence for a functional link between Down syndrome and Alzheimer's disease. *J. Neurochemistry* 104, 1333–1344. doi: 10.1111/j.1471-4159.2007.05075.x

Sáez-Calvo, G., Sharma, A., Balaguer, F. A., Barasoain, I., Rodriguez–Salarichs, J., Olieric, N., et al. (2017). Triazolopyrimidines are microtubule–stabilizing agents that bind the vinca inhibitor site of tubulin. *Cell Chem. Biol.* 24, 737.e6–750.e6. doi: 10.1016/j.chembiol.2017.05.016

Sandner, B., Puttagunta, R., Motsch, M., Bradke, F., Ruschel, J., Blesch, A., et al. (2018). Systemic epothilone D improves hindlimb function after spinal cord contusion injury in rats. *Exp. Neurol.* 306, 250–259. doi: 10.1016/j.expneurol.2018.01.018

Sankaran, S., Crone, D. E., Palazzo, R. E., and Parvin, J. D. (2007). BRCA1 regulates gamma–tubulin binding to centrosomes. *Cancer Biol. Ther.* 6, 1853–1857. doi: 10.4161/cbt.6.12.5164

Schiff, P. B., and Horwitz, S. B. (1980). Taxol stabilizes microtubules in mouse fibroblast cells. *Proc. Natl. Acad. Sci. U.S.A.* 77, 1561–1565. doi: 10.1073/pnas.77.3.1561

Schinkel, A. H., Smit, J. J., van Tellingen, O., Beijnen, J. H., Wagenaar, E., van Deemter, L., et al. (1994). Disruption of the mouse mdr1a P–glycoprotein gene leads to a deficiency in the blood–brain barrier and to increased sensitivity to drugs. *Cell* 77, 491–502. doi: 10.1016/0092-8674(94)90212-7

Sessa, C., Perotti, A., Llado, A., Cresta, S., Capri, G., Voi, M., et al. (2007). Phase I clinical study of the novel epothilone B analogue BMS−310705 given on a weekly schedule. *Ann. Oncol.* 18, 1548–1553. doi: 10.1093/annonc/mdm198

Simón–Sánchez, J., Schulte, C., Bras, J. M., Sharma, M., Gibbs, J. R., Berg, D., et al. (2009). Genome–wide association study reveals genetic risk underlying Parkinson's disease. *Nat. Genet.* 41, 1308–1312. doi: 10.1038/ng.487

Socinski, M. A., Bondarenko, I., Karaseva, N. A., Makhson, A. M., Vynnychenko, I., Okamoto, I., et al. (2012). Weekly nab–paclitaxel in combination with carboplatin versus solvent–based paclitaxel plus carboplatin as first–line therapy in patients with advanced non–small–cell lung cancer, final results of a phase III trial. *J. Clin. Oncol.* 30, 2055–2062. doi: 10.1200/JCO.2011.39.5848

Spong, C. Y., Abebe, D. T., Gozes, I., Brenneman, D. E., and Hill, J. M. (2001). Prevention of fetal demise and growth restriction in a mouse model of fetal alcohol syndrome. *J. Pharmacol. Exp. Ther.* 297, 774–779.

Sragovich, S., Merenlender–Wagner, A., and Gozes, I. (2017). ADNP plays a key role in autophagy: from autism to schizophrenia and alzheimer's disease. *Bioessays* 39:1700054. doi: 10.1002/bies.201700054

Steen, R. G., Hamer, R. M., and Lieberman, J. A. (2005). Measurement of brain metabolites by 1H magnetic resonance spectroscopy in patients with schizophrenia, a systematic review and meta–analysis. *Neuropsychopharmacology* 30, 1949–1962. doi: 10.1038/sj.npp.1300850

Stichel, C. C., Schoenebeck, B., Foguet, M., Siebertz, B., Bader, V., Zhu, X. R., et al. (2005). sgk1, a member of an RNA cluster associated with cell death in a model of Parkinson's disease. *Eur. J. Neurosci.* 21, 301–316. doi: 10.1111/j.1460-9568.2005.03859.x

Süssmuth, S. D., Tumani, H., Ecker, D., and Ludolph, A. C. (2003). Amyotrophic lateral sclerosis, disease stage related changes of tau protein and S100 beta in cerebrospinal fluid and creatine kinase in serum. *Neurosci. Lett.* 353, 57–60. doi: 10.1016/j.neulet.2003.09.018

Torrey, E. F., Barci, B. M., Webster, M. J., Bartko, J. J., Meador–Woodruff, J. H., and Knable, M. B. (2005). Neurochemical markers for schizophrenia, bipolar disorder, and major depression in postmortem brains. *Biol. Psychiatry* 57, 252–260. doi: 10.1016/j.biopsych.2004.10.019

Vaisburd, S., Shemer, Z., Yeheskel, A., Giladi, E., and Gozes, I. (2015). Risperidone and NAP protect cognition and normalize gene expression in a schizophrenia mouse model. *Sci Rep.* 5:16300. doi: 10.1038/srep16300

Vale, R. D. (2003). The molecular motor toolbox for intracellular transport. *Cell* 112, 467–480. doi: 10.1016/S0092-8674(03)00111-9

Van Cauwenberghe, C., Van Broeckhoven, C., and Sleegers, K. (2016). The genetic landscape of Alzheimer disease, clinical implications and perspectives. *Genet. Med.* 18, 421–430. doi: 10.1038/gim.2015.117

Van Dijck, A., Vulto–van Silfhout, A. T, Cappuyns, E. I. M., van der Werf Mancini, G. M., Tzschach, A., Kooy, R. F. et al. (2018). Clinical presentation of a complex neurodevelopmental disorder caused by mutations in ADNP. *Biol. Psychiatry* doi: 10.1016/j.biopsych.2018.02.1173. [Epub ahead of print].

Verdile, G., Gnjec, A., Miklossy, J., Fonte, J., Veurink, G., Bates, K., et al. (2004). Protein markers for Alzheimer disease in the frontal cortex and cerebellum. *Neurology* 63, 1385–1392. doi: 10.1212/01.WNL.0000141848.45315.A6

Verhey, K. J., and Gaertig, J. (2007). The tubulin code. *Cell Cycle* 6, 2152–2160. doi: 10.4161/cc.6.17.4633

Volle, J., Brocard, J., Saoud, M., Gory–Faure, S., Brunelin, J., Andrieux, A., et al. Suaud–Chagny (2013). Reduced expression of STOP/MAP6 in mice leads to cognitive deficits. *Schizophr. Bull.* 39, 969–978. doi: 10.1093/schbul/sbs113

Wang, B., Lv, L., Wang, Z., Jiang, Y., Lv, W., Liu, X., et al. (2015). Improved anti–glioblastoma efficacy by IL−13Ralpha2 mediated copolymer nanoparticles loaded with paclitaxel. *Sci. Rep.* 5:16589. doi: 10.1038/srep16589

Wang, H. Y., and Friedman, E. (1996). Enhanced protein kinase C activity and translocation in bipolar affective disorder brains. *Biol. Psychiatry* 40, 568–575. doi: 10.1016/0006-3223(95)00611-7

Wani, M. C., Taylor, H. L., Wall, M. E., Coggon, P., and McPhail, A. T. (1971). Plant antitumor agents. VI. The isolation and structure of taxol, a novel antileukemic and antitumor agent from *Taxus brevifolia*. *J. Am. Chem. Soc.* 93, 2325–2327. doi: 10.1021/ja00738a045

Wijsman, E. M., Pankratz, N. D., Choi, Y., Rothstein, J. H., Faber, K. M., Cheng, R., et al. (2011). Genome–wide association of familial late–onset Alzheimer's disease replicates BIN1 and CLU and nominates CUGBP2 in interaction with APOE. *PLoS Genet.* 7:e1001308. doi: 10.1371/journal.pgen.1001308

Witte, H., and Bradke, F. (2008). The role of the cytoskeleton during neuronal polarization. *Curr. Opin. Neurobiol.* 18, 479–487. doi: 10.1016/j.conb.2008.09.019

Yenjerla, M., LaPointe, N. E., Lopus, M., Cox, C., Jordan, M. A., Feinstein, S. C., et al. (2010). The neuroprotective peptide NAP does not directly affect polymerization or dynamics of reconstituted neural microtubules. *J. Alzheimers Dis.* 19, 1377–1386. doi: 10.3233/JAD-2010-1335

Yoshiyama, Y., Higuchi, M., Zhang, B., Huang, S. M., Iwata, N., Saido, T. C., et al. (2007). Synapse loss and microglial activation precede tangles in a P301S tauopathy mouse model. *Neuron* 53, 337–351. doi: 10.1016/j.neuron.2007.01.010

Yuan, P., Zhou, R., Wang, Y., Li, X., Li, J., Chen, G., et al. (2010). Altered levels of extracellular signal–regulated kinase signaling proteins in postmortem frontal cortex of individuals with mood disorders and schizophrenia. *J. Affect. Disord.* 124, 164–169. doi: 10.1016/j.jad.2009.10.017

Zahavi, E. E., Maimon, R., and Perlson, E. (2017). Spatial–specific functions in retrograde neuronal signalling. *Traffic* 18, 415–424. doi: 10.1111/tra.12487

Zhang, B., Carroll, J., Trojanowski, J. Q., Yao, Y., Iba, M., Potuzak, J. S., et al. (2012). The microtubule–stabilizing agent, epothilone D, reduces axonal dysfunction, neurotoxicity, cognitive deficits, and Alzheimer–like pathology in an interventional study with aged tau transgenic mice. *J. Neurosci.* 32, 3601–3611. doi: 10.1523/JNEUROSCI.4922-11.2012

Zhang, C. C., Zhu, J. X., Wan, Y., Tan, L., Wang, H. F., and Yu, J. T. (2017). Meta–analysis of the association between variants in MAPT and neurodegenerative diseases. *Oncotarget* 8, 44994–45007. doi: 10.18632/oncotarget.16690

Zhu, X., Sun, Z., Lee, H. G., Siedlak, S. L., Perry, G., and Smith, M. A. (2003). Distribution, levels, and activation of MEK1 in Alzheimer's disease. *J. Neurochem.* 86, 136–142. doi: 10.1046/j.1471-4159.2003.01820.x

Zong, Y., Wu, J., and Shen, K. (2017). Nanoparticle albumin–bound paclitaxel as neoadjuvant chemotherapy of breast cancer, a systematic review and meta–analysis. *Oncotarget* 8, 17360–17372. doi: 10.18632/oncotarget.14477

Conflict of Interest Statement: The authors declare that the research was conducted in the absence of any commercial or financial relationships that could be construed as a potential conflict of interest.

frontiers in Cellular Neuroscience

REVIEW
published: 21 August 2018
doi: 10.3389/fncel.2018.00261

Important Shapeshifter: Mechanisms Allowing Astrocytes to Respond to the Changing Nervous System During Development, Injury and Disease

Juliane Schiweck, Britta J. Eickholt and Kai Murk**

Institute for Biochemistry, Charité Universitätsmedizin Berlin, Berlin, Germany

Astrocytes are the most prevalent glial cells in the brain. Historically considered as "merely supporting" neurons, recent research has shown that astrocytes actively participate in a large variety of central nervous system (CNS) functions including synaptogenesis, neuronal transmission and synaptic plasticity. During disease and injury, astrocytes efficiently protect neurons by various means, notably by sealing them off from neurotoxic factors and repairing the blood-brain barrier. Their ramified morphology allows them to perform diverse tasks by interacting with synapses, blood vessels and other glial cells. In this review article, we provide an overview of how astrocytes acquire their complex morphology during development. We then move from the developing to the mature brain, and review current research on perisynaptic astrocytic processes, with a particular focus on how astrocytes engage synapses and modulate their formation and activity. Comprehensive changes have been reported in astrocyte cell shape in many CNS pathologies. Factors influencing these morphological changes are summarized in the context of brain pathologies, such as traumatic injury and degenerative conditions. We provide insight into the molecular, cellular and cytoskeletal machinery behind these shape changes which drive the dynamic remodeling in astrocyte morphology during injury and the development of pathologies.

Keywords: astrocytes, morphology, CNS, pathology, cytoskeleton, astrogliosis, brain trauma, synapse

OPEN ACCESS

Edited by:
C. Laura Sayas, Universidad de La Laguna, Spain

Reviewed by:
Matteo Bergami, Universitätsklinikum Köln, Germany
Reno Cervo Reyes, Department of Psychiatry, University of California San Francisco, United States

****Correspondence:***
Kai Murk
kai.murk@charite.de
Britta J. Eickholt
britta.eickholt@charite.de

Received: *02 May 2018*
Accepted: *31 July 2018*
Published: *21 August 2018*

Citation:
Schiweck J, Eickholt BJ and Murk K (2018) Important Shapeshifter: Mechanisms Allowing Astrocytes to Respond to the Changing Nervous System During Development, Injury and Disease. Front. Cell. Neurosci. 12:261. doi: 10.3389/fncel.2018.00261

INTRODUCTION

Astrocytes have classically been depicted as star-like cells (Ramón y Cajal, 1913), however advanced visualization techniques have instead revealed astrocytes as bush- or sponge-like cells, each of which covers a distinct territory in the central nervous system (CNS; Bushong et al., 2004; Benediktsson et al., 2005). One of the most intriguing features of mature astrocytes is their extraordinary complexity: at high resolution, the ramification of the spongiform astrocytic processes into myriads of nanoscopic protrusions can be observed, frequently of sizes below the diffraction limit of light, and associated with synapses (Witcher et al., 2007; Medvedev et al., 2014). Their morphological complexity correlates with the plethora of functions astrocytes execute in the healthy CNS, including maintaining homeostasis, providing metabolic and neurotrophic support, promoting synaptogenesis, neurotransmitter uptake and recycling, modulating the plasticity and density of synapses. All of these tasks require close contacts between astrocytes and their targets, where the interactions are particularly plastic and can change depending on the individual

physiological conditions. Moreover, astrocytes respond to pathologies in a process known as reactive astrogliosis, when they undergo substantial morphological changes to protect the CNS from inflammation, infection and neurodegeneration. In this review article, we summarize current knowledge of how astrocytes acquire, maintain and change their elaborate morphology through their molecular machinery and, in particular, via the cytoskeleton. We begin by describing the developmental process of astrogenesis and then focus on how astrocytes associate with and influence synapses in the mature CNS via their smallest processes, the perisynaptic astrocytic processes (PAPs). Finally, we discuss reactive astrogliosis and concentrate on the pathologies leading to the most profound shifts in astrocyte shape.

DEVELOPMENT: HOW TO BECOME A STAR

Like neurons, astrocytes originate from radial glial cells, which, despite their uniform appearance, form different progenitor domains within the ventricles of the developing brain, and generate cell subtypes with distinct morphological, functional and positional identities. Neurogenesis and gliogenesis from radial glial cells follow a step-like arrangement during development (Hirabayashi and Gotoh, 2005). In the mouse brain, neurogenesis starts at day E11 of prenatal development. The first cells exhibiting astrocyte characteristics appear between E16–E18, when neurogenesis decreases in favor of gliogenesis (Costa et al., 2009; Gao et al., 2014). However, the vast majority of astrocytes will only become detectable during the first 3 weeks after birth. Astrogenesis requires the early commitment of glial cell precursors to the astrocyte lineage, and the subsequent colonization of the CNS by differentiating astrocytes.

Early and intermediate astrocyte progenitors are difficult to trace and manipulate. To our knowledge, unique factors which actively instruct precursors to differentiate into astrocytes have not to date been identified. Rather, it appears that astrogenesis relies on the repression of neurogenic genes through numerous signaling pathways (Kanski et al., 2014; Nagao et al., 2016). However, the pro-gliogenic transcription factors involved are not restricted to astrocyte differentiation as they are also required for the generation of oligodendrocytes (Stolt et al., 2003). To acquire their positional identity, differentiating astrocytes "re-use" molecular mechanisms, such as the homeodomain code, which neurons follow earlier in development (Hochstim et al., 2008). Subsequent to the principal commitment of precursor cells to the astrocyte lineage, astrocyte progenitors leave their cradles and populate the entire CNS (Bandeira et al., 2009). Region-specific fate mapping in the spinal cord and cortex revealed that the migration of astrocyte progenitors occurs along radial glial cell processes (**Figure 1A**; Tsai et al., 2012). However these processes disappear early in postnatal development, raising the question as to how later-appearing astrocytes reach their specific locations throughout the CNS (Rakic, 2003). One possible explanation is that early emerging astrocytic precursors migrate along the radial glial cells and pioneer unhabituated brain regions. After reaching their final positions, these pioneer astrocytes expand by symmetric cell division and colonize defined brain areas. Tracing experiments in the postnatal cortex demonstrated the capability of astrocytes to generate up to 50% of the total astrocyte numbers via symmetric cell division (Ge et al., 2012). Another 10% of cortical astrocytes

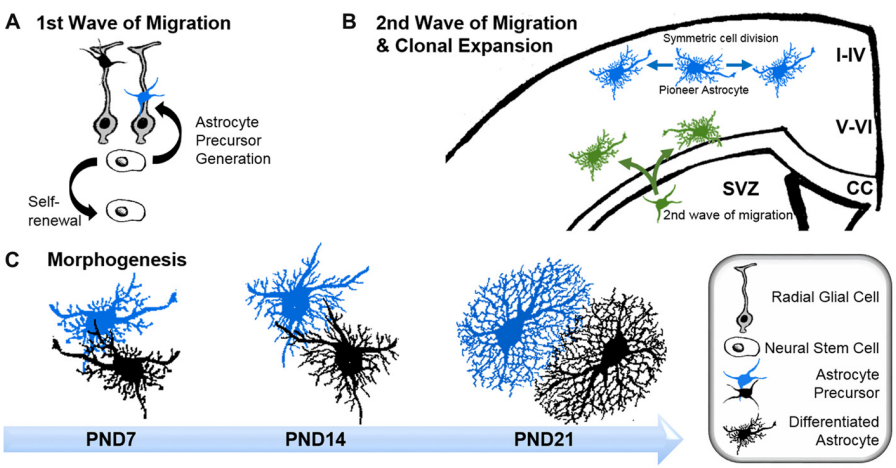

FIGURE 1 | Astrogenesis and morphogenesis of astrocytes during development. **(A)** First wave of progenitor migration: asymmetric division of neural stem cells within the ventricular zones creates the first wave of astrocyte precursor cells (black and blue), which migrate along the processes of radial glial cells (gray) towards their final location in the central nervous system (CNS). **(B)** Clonal expansion of pioneering astrocytes and second wave of migrating astrocyte progenitor during late development: pioneering astrocytes of the first migration wave (blue) undergo symmetric cell division in the upper cortical layers, while a second wave of astrocyte progenitors emerges from the subventricular zone (SVZ; green), predominantly colonizing the lower cortical layers. Corpus callosum (CC). **(C)** Time course of astrocyte morphogenesis during postnatal development, demonstrated by two neighboring astrocytes (blue and black). Differentiating astrocytes possess long main processes at postnatal day (PND) 7, which invade the domains of neighboring astrocytes. At PND14, ramification into smaller processes has increased, whilst the extent of invasion into domains of neighboring astrocytes is reduced. Three weeks after birth, at PND21, astrocytes have acquired their complex morphologies within their distinct domains. At this stage, only very limited intermingling with neighboring astrocytes occurs.

are generated directly from radial glial cells during their final cell division (Masahira et al., 2006). The remaining 40% of the total astrocyte population are derived from progenitor cells originating from the subventricular zone (SVZ). Despite the absence of the guiding processes of radial glial cells, this astrocyte population nonetheless continues to migrate along the tracks of pioneering cells (Jacobsen and Miller, 2003; Rakic, 2003). It is currently unknown how these "latecomers" move along formerly beaten tracks, nor how they find their precise destination in the developing brain. These "second wave" astrocytes typically cover shorter distances compared to the pioneering astrocytes, and populate the cortical layers adjacent to the SVZs (**Figure 1B**; Ge et al., 2012).

After arriving at their designated position, astrocytes begin to express their canonical markers, such as glial fibrillary acidic protein (GFAP), S100β, Aldh1L1, Sox9, AldoC, Glt1 and glutamine synthase (for a review see Molofsky et al., 2012). During this period, astrocytes also initiate the formation of their stellate morphology (**Figure 1C**). The time course in forming the uniquely ramified morphology of astrocytes has been documented in rats by Bushong et al. (2004) using immunolabeling and dye filling. In brief, during the first week of postnatal development, protoplasmic astrocytes display considerable diversity in morphology. S100ß and GFAP-positive cells extend between three and six long main processes and develop a ramification of fine, stringy or filamentous processes. At this stage, astrocytes are not yet restricted to the defined domains typically observed for mature astrocytes, and can extend their long main processes beyond any rudimentary boundaries. By postnatal week 2, astrocytes have adopted a more uniform morphology, with complex ramification patterns of their processes. However, the astrocytic processes are still stringy or filiform and have not yet matured into the characteristic spongiform shapes. During this period, the well-documented astrocytic territorial domains are recognizable for the first time, although overlap of processes is still present. By postnatal week 3–4, astrocytes have matured into their terminally differentiated state through the establishment of dense spongiform processes within their individual domains. However, the morphological and functional identity of astrocytes is not entirely hardwired but rather depends on the individual environment, particularly on the input of surrounding neurons throughout their lifetime.

Scientists are only now beginning to comprehend the molecular signals and their downstream mechanisms involved in establishing astrocyte morphology. Genetic studies in *Drosophila* identified neuron-secreted FGFs as critical for the elaboration of astrocyte morphology (Stork et al., 2014). Recent work in the optical lobe of *Drosophila* showed a role for the transmembrane leucine-rich repeat protein Lapsyn in regulating the morphogenesis of the astrocyte-like medulla neuropil glia, which also cooperates with FGF to promote astrocyte branch formation and survival (Richier et al., 2017). Moreover, a comprehensive study in the rodent cerebellum indicated that the acquired identity of astrocytes could be overwritten by surrounding neurons (Farmer et al., 2016). In this study, the authors demonstrate that the morphogen sonic hedgehog secreted from the adult Purkinje cells sustains the functional identity of adjacent Bergmann glia. Manipulating sonic hedgehog in the mature cerebellum induces another astrocyte subpopulation, so-called velate astrocytes, to acquire the transcriptome and electrophysiological characteristics of Bergmann glia. Taken together, these studies show that astrocytes represent a population of particularly plastic and heterogeneous cells, which are responsive to their neuronal neighbors.

WHAT STARS ARE MADE OF AND WHAT KEEPS THEM IN SHAPE

The development of the stunning complexity of astrocytes from the thin precursor cylindrical radial glial cells necessarily involves extensive remodeling of the cytoskeleton. However very little is known about the molecular machinery behind these comprehensive shapeshifts. A key reason contributing to this limited insight is that the commonly-used cell culture astrocyte models do not accurately recapitulate astrocytes *in situ* or during normal morphogenesis. While neurons develop spontaneously from apolar progenitors and form mature cells with elaborate axon and dendrite morphologies in culture, astrocytes in serum-enriched cultures acquire a polygonal morphology analogous to non-neuronal cells (McCarthy and de Velllis, 1980). More importantly, transcriptome analysis revealed that cultured polygonal astrocytes have different genetic profiles compared to astrocytes *in situ*, but share similar profiles with immature and reactive astrocytes (Foo et al., 2012). Changes in culture conditions and pharmacological treatments, such as artificially increasing intracellular cAMP levels, can convert polygonal astrocytes into stellate astrocytes within a matter of minutes (Shapiro, 1973). However, this process does not resemble *in vivo* differentiation of progenitor cells into ramified astrocytes. Instead, this so-called process of "stellation" is a model used to identify the cellular architecture necessary to maintain the typical astrocyte morphology. Keeping these limitations in mind, we review here what is known about the cytoskeletal organization of stellate astrocytes in culture and *in vivo*.

Microtubules

The function of microtubules has rarely been addressed in stellate astrocytes in general, and during astrogenesis in particular. An early electron microscopy study demonstrated dense microtubule networks in mature astrocytes, compared to immature astrocytes that exhibit more loosely packed microtubules (Peters and Vaughn, 1967). Only recently, microtubules were visualized for the first time in radial glia and their astroglia progeny in living brain tissue (Eom et al., 2011). Short-term live imaging revealed the restriction of microtubules to the main processes, where they appear to be relatively stable. In cell culture, the *in vivo* distribution of microtubules is analogously present in stellating astrocytes, where microtubules co-extend with intermediate filaments in forming the processes. Pharmacological inhibition of microtubule polymerization during stellation prevents the transition of astrocytes into the star-like cells (Goetschy et al., 1986). Nonetheless comprehensive

analyses of the changes and functions of microtubules in astrocytes during stellation are not currently available and further studies are needed.

Intermediate Filaments

Intermediate filaments have been studied extensively in astrocytes thanks to the availability of knockout mouse models. Like microtubules, intermediate filaments are restricted to the main processes of astrocytes *in vivo* (**Figure 2A**; Bushong et al., 2002). The interconnected scaffold-like network in astrocytes is a composite of different intermediate filament proteins which change during development and maturation. Astrocyte progenitors express the intermediate filament proteins of vimentin, nestin and synemin, whereas maturing and differentiated astrocytes express only GFAP and vimentin (Sultana et al., 2000). During adulthood, GFAP expression in astrocytes varies largely depending on the brain region. In the cortex, 85% of astrocytes are negative for GFAP but upregulate this intermediate filament protein again during aging (Kimelberg, 2004). GFAP or vimentin are the essential subunits for polymerizing intermediate filaments. In immature astrocytes deficient in both GFAP and vimentin, nestin itself is unable to polymerize into filaments (Pekny et al., 1999). Intermediate filaments also play a scaffolding role in organizing the cytoplasm and organelles, and modulate directed vesicle transport (Potokar et al., 2007). However, deficiencies in GFAP and/or vimentin have no obvious effect on the outgrowth of astrocytic processes in mixed neuronal cultures or on the development and maturation of astrocytes *in vivo*, despite impaired intermediate filament formation (Pekny et al., 1995, 1998).

The Actin Cytoskeleton

Studies that induced drastic shapeshifting between polygonal and stellate morphologies of astrocytes in cell culture have increased our understanding of the actin cytoskeleton in this process. In their polygonal shape, astrocytes possess prominent actin fibers that depend on a high activation state of myosin-II (John, 2004). In contrast, when astrocytes adopt stellate shapes *in vitro*, they exhibit a lack of actin fibers and instead establish Arp2/3-dependent actin networks (Murk et al., 2013). Branched Arp2/3-based actin arrays and the machinery for linear actin filaments act in direct opposition to each other, and rely on distinct signaling pathways (Rotty et al., 2015). Signaling through receptors such as beta-adrenergic receptors activates PKA and/or PKCepsilon and inhibits the ROCK-RhoA-axis. Concurrently, an increase in Rac1 activity drives the remodeling of contractile actin fibers into branched actin arrays (Moonen et al., 1976; Ramakers and Moolenaar, 1998; Burgos et al., 2007; Racchetti et al., 2012; Kobayashi et al., 2013; Murk et al., 2013). In addition to experiments using polygonal astrocytes, improved cell culture models based on defined culture media (Scholze et al., 2014; Wolfes and Dean, 2018), immunopanning (Foo et al., 2012), 3D scaffolds and matrices (Lau et al., 2014; Woo et al., 2017), and organoids (Renner et al., 2017) will facilitate functional studies of the underlying molecular machinery controlling astrocyte morphogenesis.

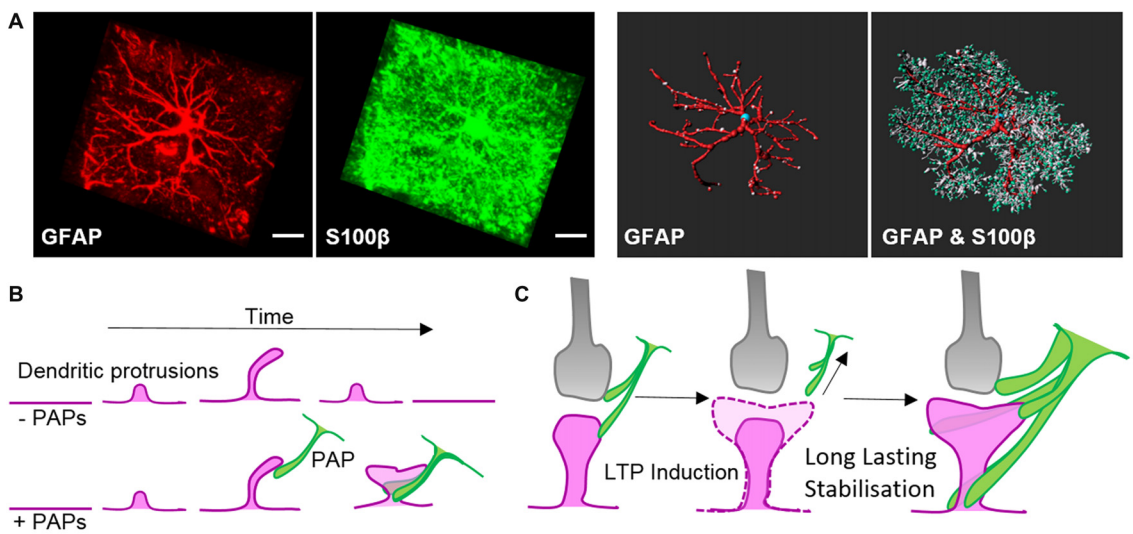

FIGURE 2 | Morphology of astrocytes *in vivo* and their dynamic association with synapses. **(A)** *Z*-projection of a cortical rat astrocyte (P14), stained for glial fibrillary acidic protein (GFAP; red) and S100β (green), by confocal microscopy after tissue clearance (left). Scale bars: 10 μm. 3D rendering and morphometric analyses show the restriction of the intermediate filament protein GFAP to main processes, which are decorated with myriads of fine S100β-positive processes (right; with permission from Murk et al., 2013). **(B)** Schematic of dendritic filopodia, with the precursors of dendritic spines, emerging from dendrites (magenta) in the absence (top) or presence of perisynaptic astrocytic processes (PAPs; green, bottom). Without the support of astrocytic processes, sprouting dendritic filopodia have a short lifespan and are likely to retract. Astrocytic processes contact filopodia-like protrusions, which then exhibit an increased stability and higher tendency to develop into mature dendritic spines. **(C)** Schematic of a mature tripartite synapse consisting of the pre-synapse (gray), post-synapse (magenta) and PAPs (green), which respond to long-term potentiation (LTP) with structural changes. Induction of LTP transiently enhances the motility and retraction of PAPs allowing growth of the postsynaptic dendritic spine to occur. Subsequent to dendritic spine remodeling, PAPs intensify their coverage of synapses.

A STARRING ROLE FOR ASTROCYTES AT SYNAPSES

The main processes of astrocytes form the basis of their star-like shape, while their true spongiform morphology relies on myriads of small protrusions. After birth, the sophisticated ramification into nanoscopic astroglial protrusions occurs in parallel with synaptogenesis, when astrocytes begin to associate with developing neuronal connections via PAPs and establish "tripartite synapses." The frequency of establishing tripartite synapses depends on the brain area and local neuronal activity (Araque et al., 1999). Studies in different organisms from *Drosophila* to humans indicate PAPs as conserved structures that are essential for brain function. Consistently, the number of PAP-associated synapses covered by astrocytes is increasing from fly to human (Oberheim et al., 2009; Stork et al., 2014). For instance, a single rodent astrocyte can associate with up to 120,000 synapses (Bushong et al., 2002), whereas a human astrocyte, according to a several-fold larger cell size and a 10-fold increase in the number of main processes, contacts up to two million synapses (Oberheim et al., 2006, 2009). These hominid-specific characteristics in astrocyte morphology are fundamental for sophisticated learning and memory, as shown in chimeric mice harboring human induced pluripotent stem cells (iPSC)-derived astrocytes. The transplanted human astrocytes replace the host's astroglia and develop the characteristic larger ramification of normal human astrocytes. Moreover, the chimeric mice show substantially enhanced synaptic plasticity and learning, compared to control animals (Han et al., 2013). Although further experimental evidence is needed to directly test for the link of PAPs in moderating synaptic responses in tripartite synapses, the correlation of enhanced learning and memory with increasing ramification and astrocyte-synapse interactions is impressive. It implies PAPs are key structures that astrocytes require to actively partake in synaptic activity.

Astrocytes control the ionic homeostasis of the CNS (Simard and Nedergaard, 2004) where they modulate synaptic plasticity by active buffering of potassium ions (Pannasch et al., 2011). In addition, astrocytes clear neurotransmitters and recycle their inactive derivatives back to the presynaptic terminal (Schousboe et al., 2013). Gliotransmitters such as d-serine, glutamate, ATP, taurine and TNFα are secreted by astrocytes and regulate synaptic activity (Panatier et al., 2006; Stellwagen and Malenka, 2006; Cao et al., 2013; Martin-Fernandez et al., 2017; Tan et al., 2017; Van Horn et al., 2017). During postnatal development, astrocytes sequentially secrete a range of factors, such as thrombospondins and hevin, that are involved in initiating the formation of silent synapses (Christopherson et al., 2005; Kucukdereli et al., 2011; Singh et al., 2016). Subsequently, other astrocyte-secreted factors, such as glypicans 4 and 6, turn the established silent synapses into active connections (Allen et al., 2012). To establish and maintain a neuronal network with individually controllable synapses through diffusible molecules require a tight spatial-temporal control of signaling in vicinity of synapses. The molecular equipment required for these tasks, including metabotropic glutamate receptors (mGluRs), glutamate transporters and ion channels, is enriched in PAPs and is thus in immediate proximity to synapses (Chaudhry et al., 1995; Higashi et al., 2001; Lavialle et al., 2011).

Along with locally secreted factors, PAPs influence synapses through direct contact mediated by cell adhesion molecules. Filopodial precursors of dendritic spines are endowed with a substantially enhanced lifespan and develop into mature dendritic spines with greater frequency in direct association with PAPs (**Figure 2B**, Nishida and Okabe, 2007). Immunohistochemical and electron microscopy studies showed several cell adhesion molecules that appear to link PAPs to synapses. Several molecules, such as SynCAM1, NCAM and $\alpha_v\beta_3$-integrins, form connections between PAPs and synapses (Theodosis et al., 2004; Hermosilla et al., 2008; Sandau et al., 2011), but their true nature regarding astrocyte-neuron interactions still needs to be demonstrated in functional approaches. One striking example of a shapeshifter transmembrane protein on astrocytes that affects neuronal functions is neuroligin 2. Neuroligin 2 localizes to astrocyte processes and its specific deletion in astrocytes affects astrocyte morphogenesis and substantially imbalances neuronal circuits by impairing the formation of excitatory synapses (Stogsdill et al., 2017). The γ-protocadherins (γ-Pcdhs) are another candidate for cell adhesion molecules that can functionally connect astrocytes and neurons (Keeler et al., 2015). γ-Pcdhs are present on PAPs and directly drive synaptogenesis in neuron-astrocyte co-culture models (Garrett and Weiner, 2009). However, γ-Pcdhs also directly link neuronal pre- and post-synapses (Rubinstein et al., 2015; Molumby et al., 2016, 2017). Accordingly, the modulation of synapses via γ-Pcdhs likely only relies on PAPs to some extent.

Several studies indicate a supportive role for astrocytes on synapses, whereas others discovered an essential function in reducing the total number and structural plasticity of synapses. One of the first pairs of cell adhesion molecules analyzed in a functional approach is the receptor tyrosine kinase EphA4 and its ligand ephrin-A3 that exhibit a negative regulative effect on excitatory synapses. In the adult hippocampus, EphA4 is restricted to dendritic spines, whereas ephrin-A3 is enriched on adjacent PAPs. The interaction of neuronal EphA4 with astrocytic ephrin-A3 evokes spine retraction, a process which is distorted in EphA4-deficient mice (Murai et al., 2003). Reverse signaling from neuronal EphA4 towards astrocytic ephrin-A3 evokes decreased levels of the glutamate transporters Glt1 and GLAST in PAPs, which correlates with shrinking dendritic spines (Carmona et al., 2009; Filosa et al., 2014). EphA4-ephrin-A3 signaling thus represents a means of how cell-cell contact-based neuron-glial communication can induce negative structural plasticity in neurons. In addition, astrocytic processes contain the phagocytic receptors MERKT and MEGF10 that have both been identified in mediating synapse elimination through active engulfment (Chung et al., 2013).

The Dynamic Cytoskeleton in PAPs

The interplay of PAPs with synapses alters depending on the organism's physiological condition, such as parturition, lactation, chronic dehydration, starvation, voluntary exercise

or sleep deprivation (Theodosis, 2002; Procko et al., 2011; Tatsumi et al., 2016; Bellesi et al., 2017). Recently, quantitative measurements in the sensory-visual cortex during eye occlusion demonstrated the plasticity of PAPs covering synapses. These experiments demonstrated clearly that PAPs are particularly dynamic during development as well as during activity of synaptic circuits (Stogsdill et al., 2017). Overall morphological changes in PAPs in response to environmental cues seem to occur slowly over hours to days, whereas live imaging experiments *ex* and *in vivo* revealed extensive structural plasticity PAPs within much shorter time-frames—of only minutes (**Figure 2C**; Bernardinelli et al., 2014; Perez-Alvarez et al., 2014). Activation of synapses through stimulating metabotropic glutamate receptors or glutamate uncaging triggered transiently increased PAP motility which ultimately evoked a more stable interaction of PAPs with dendritic spines (**Figure 2C**; Bernardinelli et al., 2014).

Rapid changes in PAPs highlight a prominent role for a dynamic cytoskeleton during structural remodeling of astrocytes (Bernardinelli et al., 2014). In view of the fact that PAPs are devoid of microtubules and intermediate filaments, all structural changes in PAPs are likely to involve the reorganization of the actin cytoskeleton. Dynamic PAPs present as miniature versions of lamellipodia and filopodia, the F-actin-rich subcellular compartments of migrating non-neuronal cells (Hirrlinger et al., 2004). Analogous to typical lamellipodia, extensions of PAPs are severely impaired upon inactivating the small GTPase Rac1 (Nishida and Okabe, 2007), and likely depend on inhibition of Rac1 downstream targets, such as actin regulators forming Arp2/3-dependent branched actin arrays (Rottner et al., 2017). Accordingly, direct inhibition of the Arp2/3 complex in brain tissue or knockdown of its upstream regulators N-WASP, WAVE2 and PICK1 in cell culture induces profound alterations in the morphological complexity of astrocytes. On the one hand, Arp2/3 inactivation *in situ* has been associated with the loss of fine astrocytic processes (Murk et al., 2013). On the other hand, small G-actin binding proteins called profilins, which charge actin monomers with ATP and mainly enhance actin polymerization (Jockusch et al., 2007), modulate the overall complexity of astrocytes and actin turnover in PAPs. Isoform-specific knockdowns of either ubiquitous profilin 1 or CNS-specific profilin 2a which is involved in neurons in presynaptic membrane trafficking and dendritic spine remodeling (Pilo Boyl et al., 2007; Michaelsen et al., 2010), reduce the total volume of astrocytes in organotypic slices. However, selective inhibition of profilin 1 affects the number and movement of filopodia processes by slowing the reorganization of filamentous actin (Molotkov et al., 2013; Schweinhuber et al., 2015).

Another actin binding protein prominently localized to PAPs is ezrin, a linker protein connecting the actin cytoskeleton directly to the plasma membrane (Derouiche and Frotscher, 2001; Haseleu et al., 2013). Active ezrin is exclusively located in PAPs and is required for motility of astrocytic filopodia induced by glutamate-activating mGluR3 and 5 (Lavialle et al., 2011). In addition to the typical actin regulators, connexin30 has also been shown to regulate synaptic strength by controlling the synaptic location of astroglial processes (Pannasch et al., 2014). Deletion of connexin30 evokes increased ramification and process length, with PAPs invading the synaptic cleft and causing elevated uptake of glutamate at excitatory synapses. The molecular details that underlie connexin30 regulation of PAPs are currently unclear, but appear to involve its intracellular C-terminus, which is likely to be a hub for interactions with as-yet unidentified actin regulators. A potential candidate might be drebrin, an actin regulator binding sidewise to filaments, which has been shown to interact with connexin43 in cultured astrocytes (Butkevich et al., 2004). However, whether drebrin does indeed bind and control connexin30 function in astrocytes is not known.

STARS WITH SENSITIVE FEET

While astrocytes use PAPs to register, support and modulate neuronal activity at synapses, they also almost entirely encompass the vasculature of the CNS with processes known as endfeet. In conjunction with specialized endothelial cells, pericytes and an elaborate basal lamina, astrocytic endfeet create the blood brain barrier to facilitate the brain's selective uptake of required nutrients and metabolites, the exclusion of toxic substances and immune cells as well as the efflux of waste products (Daneman and Prat, 2015). Perivascular endfeet possess prominent orthogonal arrays of intramembranous particles at their plasma membrane, where aquaporins and potassium channels accumulate (Rash et al., 1998; Warth et al., 2005). Accordingly, astrocytic endfeet act as major hubs to regulate the ion and water homeostasis in the CNS (Min and van der Knaap, 2018). Endfeet and PAPs emplace astrocytes as cellular interface between synapses and vasculature, where they enable the appropriate supply of oxygen and energy to neurons according to their activity-dependent demands. Intensive research showed the ability of astrocytes to regulate the local cerebral blood flow by sensing and relaying neuronal signals to the vasculature. The currently discussed mechanisms of astrocyte-mediated blood flow control comprise potassium siphoning, metabolic neurovascular coupling and intracellular calcium waves, which evoke the synthesis of vasoactive metabolites (see for review MacVicar and Newman, 2015). Despite the relevance of endfeet for astrocyte functions, very little information is available on their intracellular structures. Microtubules have been visualized in endfeet of perivascular astrocytes in a single *in vivo* study but their role in this subcellular compartment is unknown (Eom et al., 2011). Immunohistochemical analyses revealed prominent GFAP-positive intermediate filaments in endfeet. Endfeet differ distinctively in their fine structures between rodents and humans. Perivascular GFAP appears in rats as rosettes around blood vessels and creates the impression of an incomplete coverage of the vasculature by the astrocyte endfeet (Rungger-Brändle et al., 1993). In contrast, in humans GFAP in endfeet exhibits a densely packed, tile-like pattern entirely encompassing the blood vessels (Oberheim et al., 2009). More recent electron microscopy 3D reconstructions demonstrated the complete coverage of blood vessels in the rat brain by astrocyte endfeet despite the rosette-like GFAP localization

(Mathiisen et al., 2010). Under normal conditions, blood vessels in the brain and spinal cord from GFAP- and vimentin-deficient mice frequently show increased dilatation (Pekny et al., 1999). To our knowledge, the microanatomy of actin filaments in astrocyte endfeet is unknown. Indications for a putative role of actin in astrocytes are indirect, reported from loss-of-function studies and cell culture experiments. Astrocyte endfeet have enriched protein complexes composed of the transmembrane protein dystroglycan and its associated ligands syntrophin and dystrophin, and in other cell types this complex bridges the actin cytoskeleton with laminins in the extracellular matrix (Higginson and Winder, 2005). Moreover, the defined localization of potassium channels and aquaporin-4 in the plasma membrane of endfeet partially depends on tethered dystroglycan protein complexes. In cell culture, the actin cytoskeleton directly governs the localization of aquaporin-4 (Nicchia et al., 2008). Deleting the focal adhesion adapter protein vinculin in Bergmann glia disturbs the GFAP distribution in endfeet but has no obvious effect on neurovascular functions (Winkler et al., 2013).

FROM STARS TO SCARS

Dealing With Insults

Under normal conditions, the majority of astroglia occupy a distinct territory in the brain parenchyma, with the most distant processes of neighboring astrocytes exhibiting very limited intermingling (Bushong et al., 2002). In terms of morphological plasticity, microscopic observations at low magnification give the impression that astrocytes are rather quiescent under normal conditions. Only the smallest astrocyte protrusions—such as PAPs—are motile and alter their shape upon neuronal activity. However, in response to injury and other pathological conditions, astrocytes undergo astrogliosis and become "reactive." This process is accompanied by dramatic changes in morphology, including prominent hypertrophy, altered ramification and outgrowth of particularly long processes (**Figure 3**). Astrogliosis is recognized as a defense mechanism that controls inflammation and the blood-brain barrier integrity. An important contribution of astrogliosis is the isolation of non-injured tissue from damaged areas, and the support of neuronal circuit and tissue regeneration (Burda et al., 2016). The molecular triggers and specific signaling mechanisms of reactive astrogliosis have been reviewed in detail (Sofroniew, 2009; Ben Haim et al., 2015); here we discuss known morphological changes that occur during reactive astrogliosis and present the scope of their physiological function.

Shapeshifting of reactive astrocytes depends on the nature and severity of the CNS insult. Acute and diffuse trauma without tissue damage evoke a transient upregulation of GFAP and other intermediate filament proteins in conjunction with minor and reversible hypertrophy of both astrocyte cell bodies and main processes (Wilhelmsson et al., 2006). Reactive astrocytes thereby uphold their local domains and do not proliferate. Longer lasting and more severe injuries provoke higher GFAP levels in astrocytes and lead to more prominent cell body hypertrophy associated with the interpenetrative extension of distant processes into adjacent astrocyte domains and occasional

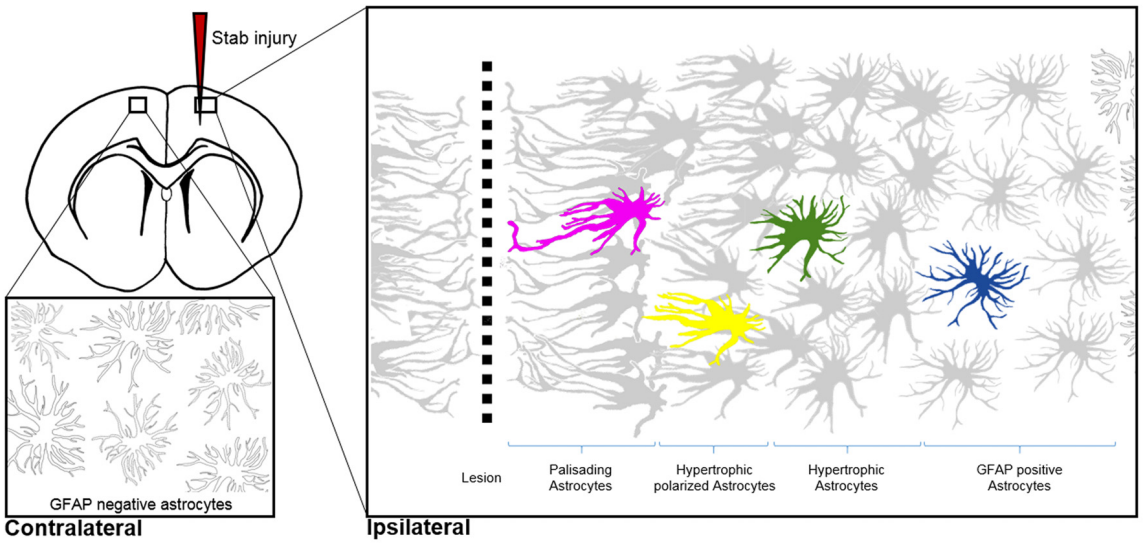

FIGURE 3 | Morphological hallmarks of reactive astrocytes in traumatic brain injury. Typical distribution of reactive astrocytes after a cortical stab wound in the mouse cortex 7 days after injury. Schematic drawings show the main processes of astrocytes, which contain high levels of GFAP (gray) upon injury. GFAP-positive astrocytes exhibit different morphologies depending on their distance from the lesion site: in the immediate vicinity (magenta), astrocytes polarize and extend long "palisading" processes. In the second row, multiple processes of the hypertrophic astrocytes (yellow) are orientated towards the injury site; with increased distance, astrocytes possess hypertrophic cell bodies and primarily main processes (green). Finally, reactive astrocytes at the border of the unaffected parenchyma upregulate GFAP but show no signs of hypertrophy (blue). Note that cortical astrocytes in the uninjured contralateral hemisphere sparsely express GFAP, as indicated with silhouettes (bottom left image).

hot spots of cell proliferation (Myer et al., 2006). Reverting hypertrophy and downregulating GFAP levels in highly reactive astrocytes is possible, but correlates negatively with the duration and severity of the diffuse brain injury (Petito et al., 1990). Traumatic brain injuries with severe tissue penetration and profound lesions create the most prominent response of reactive astrocytes by collectively forming a glial scar to protect the surrounding parenchyma from spreading inflammation, infection and neurodegeneration (**Figure 3**). Astrocytes that are in the vicinity of focal lesions resemble "palisades," bordering, orienting and extending long processes towards the injury site. Live imaging experiments in mice with cortical stab wounds revealed that 45% of reactive astrocytes are polarized. Polarized and elongated cells originate from mature astrocytes through their transient de-differentiation and proliferation (Bardehle et al., 2013; Wanner et al., 2013). Astrocytes behind the palisades manifest prominent hypertrophy and a tendency to orientate most processes towards the lesion (Kanemaru et al., 2013). With increasing distance from the injury, the hallmarks of astrogliosis—such as hypertrophy and elevated GFAP levels—tend to decrease, and appear to be analogous to mild diffuse CNS injuries (**Figure 3**). Live imaging and ablation experiments demonstrated the local occurrence of reactive astrogliosis at the insult site without any active migration of additional astrocytes from neighboring brain areas (Bardehle et al., 2013; Tsai et al., 2012).

In comparison to microglia that respond to CNS insults within minutes, the time course of morphological changes for astrocytes is relatively slow (Nimmerjahn et al., 2005). Hypertrophy and GFAP upregulation appear after 2–3 days post-injury, with palisading astrocytes observed approximately 1 week after injury (Robel et al., 2011). Nevertheless, astrogliosis and glial scarring are essential for the early phase of tissue protection after traumatic injuries, as reactive astrocytes protect against spreading cell death and inflammation after spinal cord injuries (Faulkner et al., 2004). In close proximity to lesion sites, palisading and hypertrophic astrocytes sustain their reactivity permanently, whereas astrocytes at greater distances from the injury return to their normal state (Bardehle et al., 2013). Persistent glial scars have been considered a crucial part of the failure of regenerative treatments of traumatic brain and spinal cord injuries (Cregg et al., 2014). Whether reactive astrocytes represent a major hurdle or a benefit for regenerative treatments remains a topic of intensive debate (Anderson et al., 2016).

Stars in Disease

Scar-forming astrocytes have been reported in a number of pathological conditions such as Alzheimer's disease (AD) and brain tumors, but follow a more complex response pattern during the progression of these diseases. During the later phases of AD, reactive astrocytes form prominent glial scar-like barriers around amyloid plaques and disrupt the anthropoid-specific architecture of non-reactive astrocytes in the neocortex (Colombo et al., 2002). Whether astrocyte reactivity also occurs in earlier phases of AD is currently under debate. PET scans in patients and some mouse models indicate astrogliosis as an early component of AD development (Heneka et al., 2005; Carter et al., 2012). In contrast, the triple transgenic mouse model of AD exhibits comprehensive cytoskeletal atrophy of astrocytes prior to amyloid plaque-associated astrogliosis (Kulijewicz-Nawrot et al., 2012). The precise role of astrocytes in AD needs to be further investigated as both astrocyte atrophy and astrogliosis may indicate the participation of astrocytes in the neuropathology of this disease.

Gliomas are also surrounded by activated astrocytes initially with prominent palisades (**Figure 4**; Le et al., 2003). However in this disease, the astrogliosis response is unable to isolate the tumor from the intact tissue. Gliomas exploit reactive astrocytes together with other cell types to create a favorable

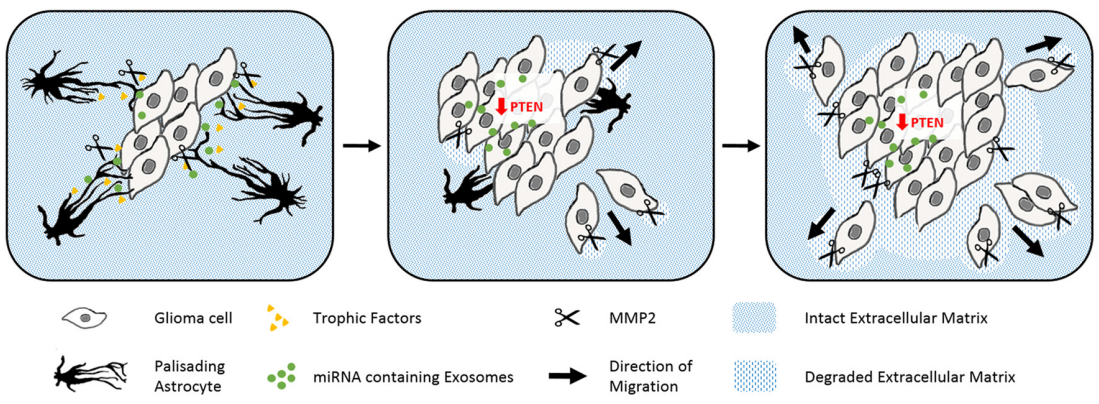

FIGURE 4 | The abuse of scarring astrocytes by glioma. Schematic drawings of how reactive astrocytes turn from initially tumor containing to cancer promoting cells. Astrocytes (black) form prominent palisading processes in response to growing glioma masses (gray rhomboid cells). Glioma derived signals force the reactive astrocytes to secret trophic factors (yellow), pro matrix metalloproteinase-2 (scissors) and microRNA containing exosomes (green, left). The uptake of microRNA containing exosomes evokes the epigenetical downregulation of tumor suppressing PTEN in glioma. PTEN depletion and astrocyte-derived trophic signals enhance the cell proliferation of the glioma cells. Expanding tumor cells use matrix metalloproteinases to degrade the surrounding extracellular matrix (blue stripped pattern) and begin to penetrate the glial scar (center). In the late phase, glioma have comprehensively degraded their adjacent extracellular matrix and seemingly consumed the originally tumor encompassing astrocytes (right).

microenvironment. Neurotrophic factors and pro-matrix metalloproteinase-2 (MMP2) secreted from astrocytes promote tumor growth (Hoelzinger et al., 2007; Lee et al., 2009). Interestingly, gliomas enhance cell proliferation and invasive migration via an astrocyte-induced knockdown of the key tumor suppressor PTEN. The epigenetic downregulation of PTEN in the cancer cells relies on the uptake of microRNAs, which are packaged in exosomes and secreted from neighboring astrocytes upon tumor-derived signals (Zhang et al., 2015). Brain tumors then consume the bordering reactive astrocytes over time, before they invade and disrupt the surrounding tissue as well as the blood-brain barrier (Watkins et al., 2014).

Profound changes in astrocyte cell morphology and function are induced by external signals and computed from pathological and physiological cues. Non-reactive astrocytes persistently survey their environment for abnormalities such as pathogenic, aggregated and serum proteins, as well as cytokines and chemokines. Contact with these cues activates multiple receptors and signaling pathways, which then trigger astrocyte reactivity programs (Burda et al., 2016). Besides pathological signals, astrocytes constantly receive instructions from healthy neurons, which actively suppress astrocyte reactivity. Key molecules within these signaling pathways include neuron-derived FGF-2 and astrocytic β1-integrin. Interestingly, loss-of-function of both factors causes astrocyte reactivity in the absence of any pathological condition (Robel et al., 2009; Kang et al., 2014). One important signal mediator involved in various signaling pathways, is the aforementioned lipid and protein phosphatase PTEN, a key molecule in antagonizing the PI3K signaling pathways (Kreis et al., 2014). PTEN is involved in the regulation of cell size and proliferation of astrocytes as well as the formation of glial scars (Fraser et al., 2004; Dey et al., 2008; Renault-Mihara et al., 2017). Mechanistic details from the nestin-STAT3$^{+/-}$ mouse model which has impaired astrogliosis show that the affected astrocytes upregulate PTEN. The intrinsic defects in glial scarring comprising process orientation and elongation as well as leukocyte seclusion are rescued through PTEN inhibition, which evokes substantial cytoskeletal remodeling by changing the activation state of the small GTPases RhoA and its downstream effectors (**Table 1**; Renault-Mihara et al., 2017).

In contrast to the wealth of knowledge on stimuli, receptors and signaling pathways evoking astrogliosis, we know very little about the downstream machinery exerting the functional and morphological changes in reactive astrocytes. One factor

TABLE 1 | Mouse disease models targeting or affecting cytoskeletal regulators *in vivo*.

Mouse models	Effects in disease models	Open questions and remarks
Cdc42 Tamoxifen-induced *GLAST/eGFP Cdc42*$^{loxP/loxP}$ mice Traumatic brain injury (Robel et al., 2011; Bardehle et al., 2013)	Impairment of pathology-induced proliferation of astrocytes but increased numbers in microglia upon traumatic brain injury. No obvious defects in microtubule organization and dynamics.	No process outgrowth related-phenotype in contrast to previously reported microtubule dependent defects in cultured astrocytes (Etienne-Manneville and Hall, 2001). Unclear, whether diverging outcomes rely on differences between cultured and astrocytes *in vivo*, or mosaic pattern of scattered Cdc42-deficient astrocytes *in vivo*.
GFAP and Vimentin *GFAP*$^{-/-}$*Vim*$^{-/-}$ mice 1. Brain and spinal cord injuries (Pekny et al., 1999) 2. Sciatic nerve lesion (Berg et al., 2013) 3. Entorhinal cortex lesion (Wilhelmsson et al., 2004) 4. Photothrombosis model for stroke (Liu et al., 2014) *GFAP*$^{-/-}$*Vimentin*$^{-/-}$*PPT1* $^{-/-}$ mice 5. Batten disease (Macauley et al., 2011) *GFAP*$^{-/-}$*Vimentin*$^{-/-}$ *in APPswe/PS1dE9 AD background* 6. Alzheimers disease (Kamphuis et al., 2014)	1. Impaired hypertrophy of cell bodies and main processes, less dense glial scars, frequent bleedings into lesion sites. 2. Complete axon regeneration. 3. Enhanced Synaptic regeneration. 4. Enhanced axonal remodeling and improved motor recovery. 5. Rapid onset and progression of disease through impaired blood-brain-barrier and profound neuroinflammatory response. 6. Less interaction of astrocytes with Aβ plaques. No effect on Aβ plaque load.	Wide range in beneficial and detrimental phenotypes by GFAP/Vimentin deficient mice among the different disease models.
STAT3 Nestin-Stat3$^{-/-}$ Mice Spinal cord injury (Renault-Mihara et al., 2017)	Attenuated up-regulation of GFAP, failure of astrocyte hypertrophy, and pronounced disruption of astroglial scar. Reactive astrocytes fail to elongate and show no preferential orientation towards the lesion. Reduced activation of RhoA. Rescuable by reduction in PTEN.	Study indicates a predominant role of the actin cytoskeleton in reactive astrocytes in contrast to previous findings (Etienne-Manneville and Hall, 2001).
Palladin Adult rats Cerebral cortex injury (Boukhelifa et al., 2003)	Upregulation of Palladin.	Role in modulation of actin cytoskeleton upon injury not explored.
a-Actinin Adult mice Cortical stab wound injury (Abd-El-Basset and Fedoroff, 1997)	Upregulation of a-actinin.	Role in modulation of actin cytoskeleton upon injury not explored.

Summary of in vivo studies with mouse disease models, which, either directly addressed or reported phenotypes associated with the cytoskeleton.

partially responsible for the swelling of astrocytes is simply water, which is increasingly taken up through aquaporin-4, and which reactive astrocytes upregulate and redistribute from their perivascular endfeet over the entire plasma membrane (Saadoun et al., 2005; Ren et al., 2013). Aquaporin-4-dependent water uptake contributes to the defense response of astrocytes, as shown in loss of function experiments, where deleting this water channel perturbs the ability of astrocytes to migrate in cell culture and to form glial scars *in vivo* (Saadoun et al., 2005). Furthermore, loss of aquaporin-4 impairs astrocyte secretion of proinflammatory cytokines in autoimmune encephalitis (Liu et al., 2014). However, the effective impact of aquaporin-4-dependent water uptake in reactive astrocytes in pathological conditions is currently under debate. Depending on the individual nature of the pathological condition, changes in astrocytic aquaporin-4 can either facilitate or counteract the formation of cerebral edema (for a review see Stokum et al., 2015).

Another major driving force in hypertrophy and process outgrowth in scar-forming astrocytes is the cytoskeleton. Below we discuss in depth the individual filament systems of the cytoskeleton in reactive astrocytes and their shape changes under pathological changes, and review *in vivo* analyses and studies using cultured astrocytes.

Microtubule Activity in Scar-Forming Astrocytes

Cell biology experiments provide substantial insights into the function of the microtubule network during palisading of scar-forming astrocytes. One of the most frequently used cell culture models is the scratch injury model of polygonal astrocytes grown in a 2D monolayer (Etienne-Manneville, 2006). This assay provokes the coordinated orientation, polarization and extension of astrocytes into the wound area, analogous to palisading astroglia during traumatic brain injury (**Figures 5**, **6**), although it should be noted that cultured cells migrate unlike their counterparts *in vivo* (Bardehle et al., 2013). Astrocyte polarization begins with the microtubule-dependent reorientation of both the microtubule-organizing center and the Golgi apparatus (Etienne-Manneville and Hall, 2001). The reorientation of the Golgi in astrocytes by microtubules is distinct from that in other cells, as Golgi alignment relies solely on the actin cytoskeleton during migration of most other cell types (Magdalena et al., 2003). Microtubules are particularly enriched in long astrocytic processes (up to 150 μm; **Figure 6**). Moreover, microtubules reach the extreme tip of these astrocyte protrusions in contrast to other cell types, where only a minority of microtubules selectively enter the actin-enriched leading edge (Schober et al., 2007; Dent et al., 2011; Sakamoto et al., 2013). Treatment with the tubulin depolymerizing agent nocodazole demonstrated the integral function of microtubules for the directed outgrowth of palisade-like processes.

A key molecule in the directed elongation of astrocyte processes is the small GTPase Cdc42, which regulates the alignment of the microtubule-organizing center and Golgi through an mPar6-PKCzeta signaling complex (Etienne-Manneville and Hall, 2001). Downstream targets of Cdc42-mPar6-PKCzeta are dynein motor proteins and inactive GSK3-beta, which induces the steering interaction of the tumor suppressor protein, adenomatous polyposis coli (APC) with the microtubule plus-ends (**Figure 5**; Etienne-Manneville and

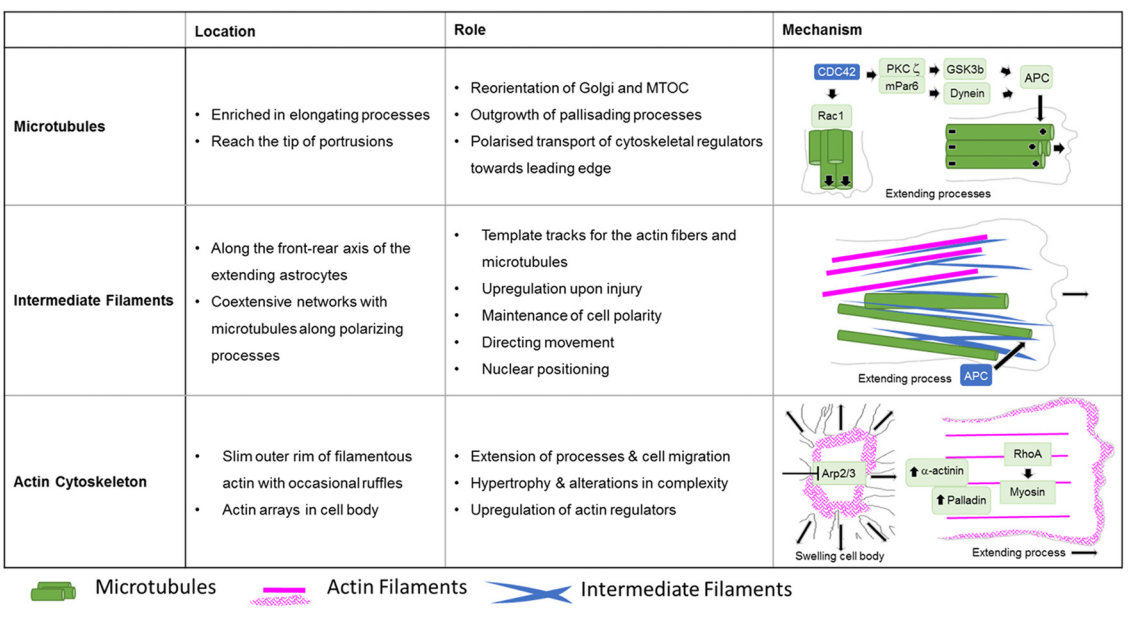

FIGURE 5 | Roles of cytoskeletal systems during the Injury response of astrocytes *in vitro*. Summary in view of the localization and roles of microtubules, intermediate and actin filaments in cultured astrocytes upon injury. The schematic drawings depict the cytoskeletal systems and their major regulators involved in extension of astrocyte processes and cell body hypertrophy.

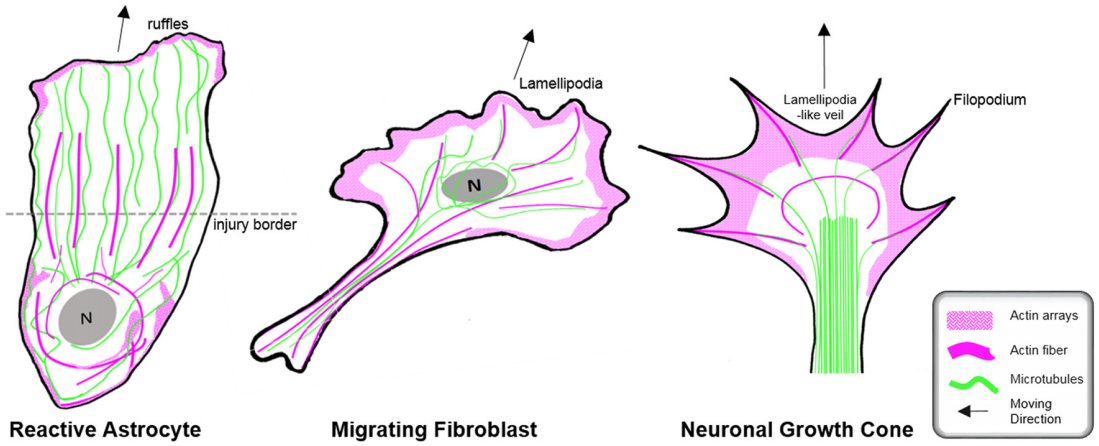

FIGURE 6 | Organization of the cytoskeleton in reactive astrocytes in comparison to fibroblasts and neurons *in vitro*. Schematic drawings of microtubules (green) and F-actin arrays and fibers (magenta) in cultured mouse astrocytes after injury (left), migrating fibroblasts (center) and in extending axonal growth cones of developing neurons (right). The dashed line indicates the injury border and the nucleus is shown in gray (N). Elongated polygonal astrocytes at the wound edge extend into the cell-free space and have actin filaments (magenta) that are organized around the cell body and in bundles reaching into the center of the processes, while the leading edge possesses only a narrow outer rim of filamentous actin within sparse ruffles (left). Microtubules are enriched throughout the processes and reach into the extreme tip. In contrast, both fibroblasts and neuronal growth cones exhibit prominent actin arrays and fibers in the periphery of their leading edge forming filopodia, lamellipodia or lamellipodia-like veils. Most of their microtubules are present behind the actin-rich periphery, where microtubules form dense parallel bundles in growth cones. Microtubules extending into the actin-rich periphery frequently associate with actin fibers of filopodia.

Hall, 2003). Cdc42 is actively delivered towards the leading edge through anterograde transport by Arf6-positive vesicles (Osmani et al., 2010). Moreover, Cdc42 controls microtubule-dependent outgrowth of astrocyte processes through Rac1 (**Figure 5**; Etienne-Manneville and Hall, 2001). However, inducible genetic deletion of Cdc42 *in vivo* does not affect the orientation of palisading astrocytes but impairs their pathology-induced proliferation in traumatic brain injuries (**Table 1**; Robel et al., 2011; Bardehle et al., 2013). Whether this *in vivo* phenotype relies on differences in microtubule regulation between genuine and cultured astrocytes or the mosaic pattern of scattered Cdc42 deficient astrocytes influenced by the majority of surrounding wildtype cells, is currently unknown. Future work will need to further study the significance of microtubules in reactive astrocytes through comprehensive studies *in vivo* and additional cell culture models.

Intermediate Filaments in Glial Scarring

Because of the prominent upregulation of intermediate proteins in reactive astrocytes, this filament network is traditionally seen as the most relevant cytoskeletal system in astrogliosis (Sultana et al., 2000). In contrast to during development, intermediate filaments substantially participate in astrogliosis and glial scarring, with their impact dependent on the CNS region and the type of pathology. Of note, GFAP and vimentin deficiency impairs the hypertrophy of cell bodies and main processes in reactive astrocytes. Moreover, glial scars that occur as a consequence of brain or spinal cord injuries are less dense and are frequently accompanied by significant bleeding in the central lesion sites (**Table 1**; Pekny et al., 1999). Deleting both intermediate proteins affects axon remodeling and motor behavioral recovery in mice after stroke and correlates with increased sensitivity of astrocytes to oxidative stress during hypoxia and subsequent reperfusion (de Pablo et al., 2013; Liu et al., 2014). Furthermore, the loss of GFAP and vimentin in a mouse model for chronic neurodegenerative Batten disease impairs the blood-brain barrier and accelerates the onset and progression of the pathology (Macauley et al., 2011). The absence of intermediate filaments also affects the interaction of astrocytes with amyloid plaques in AD mouse models, albeit without significant effect on the AD plaque load (**Table 1**; Kamphuis et al., 2014). However, deficiency in GFAP and vimentin may also have beneficial effects, as shown in GFAP- and vimentin-deficient mice exhibiting complete axon regeneration after induction of a sciatic nerve lesion (**Table 1**; Berg et al., 2013). In addition, a lack of GFAP and vimentin induces remarkable synaptic regeneration after entorhinal cortex lesions (**Table 1**; Wilhelmsson et al., 2004).

The fine structure of the intermediate filament network was mainly studied in culture after scratch induced-injuries, where intermediate filaments run along the cells' front-rear polarity axis in elongating astrocytes (Sakamoto et al., 2013). Intermediate filaments play an important role in establishing and maintaining cell polarity, directing movement and control of nuclear positioning, and interacting and coordinating with other filament systems of the cytoskeleton (Dupin et al., 2011; Sakamoto et al., 2013; Leduc and Etienne-Manneville, 2017). Intermediate filaments and microtubules create coextensive networks along the elongated processes of astrocytes (**Figure 5**) and the arrangement of both filament types is coordinated through APC (Sakamoto et al., 2013). On the one hand, a major role of intermediate filaments may involve the creation of template tracks for microtubules to enhance persistence of cell polarity and directed movement (**Figure 5**; Gan et al., 2016). Alternatively, microtubules may

be required to establish stabilizing intermediate filaments according to increased anterograde and reduced retrograde transport of intermediate filament subunits along microtubules in extending astrocytes (Leduc and Etienne-Manneville, 2017). Along with microtubules, intermediate filaments associate with actin filaments and control the assembly of actin fibers and orientate traction forces for direct cell movement (**Figure 5**; Costigliola et al., 2017; Jiu et al., 2017).

The Actin Cytoskeleton During Astrogliosis

In contrast to the comprehensive knowledge on the actin cytoskeleton in non-neuronal cells and neurons, little is currently known regarding the nature and function of the actin filament cytoskeleton in astrocytes in general (as described above) and, in particular, during astrogliosis. Available data indicate distinct differences in the actin organization of polarizing astrocytes after injury, compared to other extending or migrating cells (**Figure 6**; Dent et al., 2011; Steffen et al., 2017). In cell culture, protruding processes of polygonal astrocytes exhibit a slim outer rim of filamentous actin with occasional ruffles, where other growing or migrating cells such as fibroblasts and neurons possess prominent actin meshworks and fibers in their periphery and form lamellipodia and filopodia (**Figure 6**; Etienne-Manneville and Hall, 2001). In scar-forming astrocytes, most actin filaments are instead concentrated around the cell body. Depolymerizing actin filaments with the toxin cytochalasin D seems to have little effect on the formation of long processes in polygonal astrocytes but blocks their artificial migration in scratch wound assays (Etienne-Manneville and Hall, 2001). In contrast, astrocytes with STAT3-dependent defects in reactivity and process elongation also present defects in actin-dependent focal adhesion disassembly and have substantially enhanced actomyosin tonus, while the organization of microtubules is unaffected (**Table 1**; Renault-Mihara et al., 2017). Moreover, astrocytes do respond to injury *in vitro* and *in vivo* by a drastic upregulation of the actin regulators α-actinin and its ligand palladin, which are known to reorganize actin filaments through crosslinking and bundling (**Table 1**; Abd-El-Basset and Fedoroff, 1997; Boukhelifa et al., 2003). The particular injury-specific increase and accumulation of actin regulators in scar-forming astrocytes imply a currently unknown contribution of the actin cytoskeleton to glial scarring.

Although the relevance of actin dynamics in palisading astrocytes is not clear, studies in astrocytes in culture and in tissues indicate a role of the actin cytoskeleton in controlling hypertrophy and alterations in astrocyte complexity. Acute inhibition of the Arp2/3 complex in brain slices increases the astrocyte cell body size and abundance of large processes analogous to reactive astrocytes in diffuse trauma. Moreover, inactivating the Arp2/3 complex accelerates the hypertrophy of stellate astrocytes in the oxygen/glucose-deprivation model of stroke, whereas overactivating Arp2/3 by depleting its endogenous inhibitor PICK1 or overexpressing the activator N-WASP suppresses cell body expansion (**Figure 5**; Murk et al., 2013). This is in line with other studies indicating a switch from Rac1 and Arp2/3-dependent networks towards actin organization in reactive astrocytes relying on RhoA and linear actin filaments in association with myosin (John, 2004; Renault-Mihara et al., 2017). However, the expansion of astrocyte cell bodies and main processes upon Arp2/3 inhibition is another indication of distinct actin organization in astrocytes compared to other cells, where the Arp2/3 inactivation instead leads to shrinkage, collapse or inhibited outgrowth (**Figure 6**; Korobova and Svitkina, 2008; Wu et al., 2012).

CONCLUDING REMARKS

The morphological features of astrocytes are integral to the normal shape and functioning of the CNS from late embryonic development throughout all stages of an organism's life. Despite their critical relevance in both normal and disease states, the molecular mechanisms behind the plastic morphology of astrocytes are poorly understood. Nonetheless, improvements in cell culture methods and the development of new tools and elaboration of sophisticated microscopy techniques will allow observation and manipulation of more authentic astrocyte settings. In this context, nanoscopic PAP-synapse interactions are becoming increasingly accessible with super-resolution light microscopy, and as such, provide an appealing experimental alternative to sophisticated electron microscopy (Heller et al., 2017). Recently introduced astrocyte-specific and inducible gene targeting models will allow the functional characterization of astrocytes throughout the entire CNS without undesired collateral damage in neurogenic radial glia cells (Srinivasan et al., 2016; Winchenbach et al., 2016). Finally, human-specific and disease-relevant characteristics of astrocytes, which are associated with abnormal morphologies and functions (Windrem et al., 2017) can now be studied *in vivo*. The substitution of murine astrocytes through the implantation of glial progenitors derived from human-iPSC makes it possible to investigate the specific role and contribution of abnormal astrocytes in diverse pathologies. A better understanding of the plasticity of astrocyte morphology and function will help us to gain insight into the fundamental properties of this profound shapeshifter in both normal cells and diverse human pathologies.

AUTHOR CONTRIBUTIONS

JS, BJE and KM wrote the manuscript. JS and KM created the figures.

FUNDING

We acknowledge support from the German Research Foundation (DFG) and the Open Access Publication Fund of Charité—Universitätsmedizin Berlin.

ACKNOWLEDGMENTS

This article relies on a wealth of data from many different laboratories. We have cited the appropriate original publications wherever possible, and we apologize to all researchers whose work on astrocytes was not included in this article.

REFERENCES

Abd-El-Basset, E. M., and Fedoroff, S. (1997). Upregulation of F-actin and α-actinin in reactive astrocytes. *J. Neurosci. Res.* 49, 608–616. doi: 10.1002/(sici)1097-4547(19970901)49:5<608::aid-jnr11>3.0.co;2-r

Allen, N. J., Bennett, M. L., Foo, L. C., Wang, G. X., Smith, S. J., and Barres, B. A. (2012). Astrocyte glypicans 4 and 6 promote formation of excitatory synapses via GluA1 AMPA receptors. *Nature* 486, 410–414. doi: 10.1038/nature11059

Anderson, M. A., Burda, J. E., Ren, Y., Ao, Y., O'Shea, T. M., Kawaguchi, R., et al. (2016). Astrocyte scar formation aids central nervous system axon regeneration. *Nature* 532, 195–200. doi: 10.1038/nature17623

Araque, A., Parpura, V., Sanzgir, R. P., and Haydon, P. G. (1999). Tripartite synapses: glia, the unacknowledged partner. *Trends Neurosci.* 22, 208–215. doi: 10.1016/s0166-2236(98)01349-6

Bandeira, F., Lent, R., and Herculano-Houzel, S. (2009). Changing numbers of neuronal and non-neuronal cells underlie postnatal brain growth in the rat. *Proc. Natl. Acad. Sci. U S A* 106, 14108–14113. doi: 10.1073/pnas.0804650106

Bardehle, S., Krüger, M., Buggenthin, F., Schwausch, J., Ninkovic, J., Clevers, H., et al. (2013). Live imaging of astrocyte responses to acute injury reveals selective juxtavascular proliferation. *Nat. Neurosci.* 16, 580–586. doi: 10.1038/nn.3371

Bellesi, M., de Vivo, L., Chini, M., Gilli, F., Tononi, G., and Cirelli, C. (2017). Sleep loss promotes astrocytic phagocytosis and microglial activation in mouse cerebral cortex. *J. Neurosci.* 37, 5263–5273. doi: 10.1523/JNEUROSCI.3981-16.2017

Ben Haim, L., Carrillo-de Sauvage, M.-A., Ceyzériat riat, K., and Escartin, C. (2015). Elusive roles for reactive astrocytes in neurodegenerative diseases. *Front. Cell. Neurosci.* 9:278. doi: 10.3389/fncel.2015.00278

Benediktsson, A. M., Schachtele, S. J., Green, S. H., and Dailey, M. E. (2005). Ballistic labeling and dynamic imaging of astrocytes in organotypic hippocampal slice cultures. *J. Neurosci. Methods* 141, 41–53. doi: 10.1016/j.jneumeth.2004.05.013

Berg, A., Zelano, J., Pekna, M., Wilhelmsson, U., Pekny, M., and Cullheim, S. (2013). Axonal regeneration after sciatic nerve lesion is delayed but complete in GFAP- and vimentin-deficient mice. *PLoS One* 8:e79395. doi: 10.1371/journal.pone.0079395

Bernardinelli, Y., Randall, J., Janett, E., Nikonenko, I., König, S., Jones, E. V., et al. (2014). Activity-dependent structural plasticity of perisynaptic astrocytic domains promotes excitatory synapse stability. *Curr. Biol.* 24, 1679–1688. doi: 10.1016/j.cub.2014.06.025

Boukhelifa, M., Hwang, S. J., Valtschanoff, J. G., Meeker, R. B., Rustioni, A., and Otey, C. A. (2003). A critical role for palladin in astrocyte morphology and response to injury. *Mol. Cell. Neurosci.* 23, 661–668. doi: 10.1016/s1044-7431(03)00127-1

Burda, J. E., Bernstein, A. M., and Sofroniew, M. V. (2016). Astrocyte roles in traumatic brain injury. *Exp. Neurol.* 275, 305–315. doi: 10.1016/j.expneurol.2015.03.020

Burgos, M., Calvo, S., Molina, F., Vaquero, C. F., Samarel, A., Llopis, J., et al. (2007). PKCε induces astrocyte stellation by modulating multiple cytoskeletal proteins and interacting with Rho a signalling pathways: implications for neuroinflammation. *Eur. J. Neurosci.* 25, 1069–1078. doi: 10.1111/j.1460-9568.2007.05364.x

Bushong, E. A., Martone, M. E., and Ellisman, M. H. (2004). Maturation of astrocyte morphology and the establishment of astrocyte domains during postnatal hippocampal development. *Int. J. Dev. Neurosci.* 22, 73–86. doi: 10.1016/j.ijdevneu.2003.12.008

Bushong, E. A., Martone, M. E., Jones, Y. Z., and Ellisman, M. H. (2002). Protoplasmic astrocytes in CA1 stratum radiatum occupy separate anatomical domains. *J. Neurosci.* 22, 183–192. doi: 10.1523/JNEUROSCI.22-01-00183.2002

Butkevich, E., Hülsmann, S., Wenzel, D., Shirao, T., Duden, R., and Majoul, I. (2004). Drebrin is a novel connexin-43 binding partner that links gap junctions to the submembrane cytoskeleton. *Curr. Biol.* 14, 650–658. doi: 10.1016/j.cub.2004.03.063

Cao, X., Li, L. P., Wang, Q., Wu, Q., Hu, H. H., Zhang, M., et al. (2013). Astrocyte-derived ATP modulates depressive-like behaviors. *Nat. Med.* 19, 773–777. doi: 10.1038/nm.3162

Carmona, M. A., Murai, K. K., Wang, L., Roberts, A. J., and Pasquale, E. B. (2009). Glial ephrin-A3 regulates hippocampal dendritic spine morphology and glutamate transport. *Proc. Natl. Acad. Sci. U S A* 106, 12524–12529. doi: 10.1073/pnas.0903328106

Carter, S. F., Scholl, M., Almkvist, O., Wall, A., Engler, H., Langstrom, B., et al. (2012). Evidence for astrocytosis in prodromal Alzheimer disease provided by ^{11}c-deuterium-l-deprenyl: a multitracer PET paradigm combining ^{11}C-pittsburgh compound B and ^{18}F-FDG. *J. Nucl. Med.* 53, 37–46. doi: 10.2967/jnumed.110.087031

Chaudhry, F. A., Lehre, K. P., van Lookeren Campagne, M., Ottersen, O. P., Danbolt, N. C., and Storm-Mathisen, J. (1995). Glutamate transporters in glial plasma membranes: highly differentiated localizations revealed by quantitative ultrastructural immunocytochemistry. *Neuron* 15, 711–720. doi: 10.1016/0896-6273(95)90158-2

Christopherson, K. S., Ullian, E. M., Stokes, C. C. A., Mullowney, C. E., Hell, J. W., Agah, A., et al. (2005). Thrombospondins are astrocyte-secreted proteins that promote CNS synaptogenesis. *Cell* 120, 421–433. doi: 10.1016/j.cell.2004.12.020

Chung, W. S., Clarke, L. E., Wang, G. X., Stafford, B. K., Sher, A., Chakraborty, C., et al. (2013). Astrocytes mediate synapse elimination through MEGF10 and MERTK pathways. *Nature* 504, 394–400. doi: 10.1038/nature12776

Colombo, J. A., Quinn, B., and Puissant, V. (2002). Disruption of astroglial interlaminar processes in Alzheimer's disease. *Brain Res. Bull.* 58, 235–242. doi: 10.1016/s0361-9230(02)00785-2

Costa, M. R., Bucholz, O., Schroeder, T., and Götz, M. (2009). Late origin of glia-restricted progenitors in the developing mouse cerebral cortex. *Cereb. Cortex* 19, i135–i143. doi: 10.1093/cercor/bhp046

Costigliola, N., Ding, L., Burckhardt, C. J., Han, S. J., Gutierrez, E., Mota, A., et al. (2017). Vimentin fibers orient traction stress. *Proc. Natl. Acad. Sci. U S A* 114, 5195–5200. doi: 10.1073/pnas.1614610114

Cregg, J. M., DePaul, M. A., Filous, A. R., Lang, B. T., Tran, A., and Silver, J. (2014). Functional regeneration beyond the glial scar. *Exp. Neurol.* 253, 197–207. doi: 10.1016/j.expneurol.2013.12.024

Daneman, R., and Prat, A. (2015). The blood-brain barrier. *Cold Spring Harb. Perspect. Biol.* 7:a020412. doi: 10.1101/cshperspect.a020412

de Pablo, Y., Nilsson, M., Pekna, M., and Pekny, M. (2013). Intermediate filaments are important for astrocyte response to oxidative stress induced by oxygen-glucose deprivation and reperfusion. *Histochem. Cell Biol.* 140, 81–91. doi: 10.1007/s00418-013-1110-0

Dent, E. W., Gupton, S. L., and Gertler, F. B. (2011). The growth cone cytoskeleton in axon outgrowth and guidance. *Cold Spring Harb. Perspect. Biol.* 3:a001800. doi: 10.1101/cshperspect.a001800

Derouiche, A., and Frotscher, M. (2001). Peripheral astrocyte processes: monitoring by selective immunostaining for the actin-binding ERM proteins. *Glia* 36, 330–341. doi: 10.1002/glia.1120

Dey, N., Crosswell, H. E., Pradip, D., Parsons, R., Peng, Q., Jing, D. S., et al. (2008). The protein phosphatase activity of PTEN regulates Src family kinases and controls glioma migration. *Cancer Res.* 68, 1862–1871. doi: 10.1158/0008-5472.can-07-1182

Dupin, I., Sakamoto, Y., and Etienne-Manneville, S. (2011). Cytoplasmic intermediate filaments mediate actin-driven positioning of the nucleus. *J. Cell Sci.* 124, 865–872. doi: 10.1242/jcs.076356

Eom, T. Y., Stanco, A., Weimer, J., Stabingas, K., Sibrack, E., Gukassyan, V., et al. (2011). Direct visualization of microtubules using a genetic tool to analyse radial progenitor-astrocyte continuum in brain. *Nat. Commun.* 2:446. doi: 10.1038/ncomms1460

Etienne-Manneville, S. (2006). *In vitro* assay of primary astrocyte migration as a tool to study Rho GTPase function in cell polarization. *Methods Enzymol.* 406, 565–578. doi: 10.1016/s0076-6879(06)06044-7

Etienne-Manneville, S., and Hall, A. (2001). Integrin-mediated activation of Cdc42 controls cell polarity in migrating astrocytes through PKCζ. *Cell* 106, 489–498. doi: 10.1016/s0092-8674(01)00471-8

Etienne-Manneville, S., and Hall, A. (2003). Cdc42 regulates GSK-3β and adenomatous polyposis coli to control cell polarity. *Nature* 421, 753–756. doi: 10.1038/nature01423

Farmer, W. T., Abrahamsson, T., Chierzi, S., Lui, C., Zaelzer, C., Jones, E. V., et al. (2016). Neurons diversify astrocytes in the adult brain through sonic hedgehog signaling. *Science* 351, 849–854. doi: 10.1126/science.aab3103

Faulkner, J. R., Herrmann, J. E., Woo, M. J., Tansey, K. E., Doan, N. B., and Sofroniew, M. V. (2004). Reactive astrocytes protect tissue and

preserve function after spinal cord injury. *J. Neurosci.* 24, 2143–2155. doi: 10.1523/JNEUROSCI.3547-03.2004

Filosa, A., Paixão, S., Honsek, S. D., Carmona, M. A., Becker, L., Feddersen, B., et al. (2014). Neuron-glia communication via EphA4/ephrinA3 modulates LTP through glial glutamate transport. *Nat. Neurosci.* 12, 1285–1292. doi: 10.1038/nn.2394

Foo, L. C., Allen, N. J., Bushong, E. A., Ventura, P. B., Chung, W., Zhou, L., et al. (2012). Development of a novel method for the purification and culture of rodent astrocytes. *Neuron* 71, 799–811. doi: 10.1016/j.neuron.2011.07.022

Fraser, M. M., Zhu, X., Kwon, C. H., Uhlmann, E. J., Gutmann, D. H., and Baker, S. J. (2004). Pten loss causes hypertrophy and increased proliferation of astrocytes *in vivo*. *Cancer Res.* 64, 7773–7779. doi: 10.1158/0008-5472.can-04-2487

Gan, Z., Ding, L., Burckhardt, C. J., Lowery, J., Zaritsky, A., Sitterley, K., et al. (2016). Vimentin intermediate filaments template microtubule networks to enhance persistence in cell polarity and directed migration. *Cell Syst.* 3, 252.e8–263.e8. doi: 10.1016/j.cels.2016.08.007

Gao, P., Postiglione, M. P., Krieger, T. G., Hernandez, L., Wang, C., Han, Z., et al. (2014). Deterministic progenitor behavior and unitary production of neurons in the neocortex. *Cell* 159, 775–788. doi: 10.1016/j.cell.2014.10.027

Garrett, A. M., and Weiner, J. A. (2009). Control of CNS synapse development by γ-protocadherin-mediated astrocyte-neuron contact. *J. Neurosci.* 29, 11723–11731. doi: 10.1523/JNEUROSCI.2818-09.2009

Ge, W. P., Miyawaki, A., Gage, F. H., Jan, Y. N., and Jan, L. Y. (2012). Local generation of glia is a major astrocyte source in postnatal cortex. *Nature* 484, 376–380. doi: 10.1038/nature10959

Goetschy, J. F., Ulrich, G., Aunis, D., and Ciesielski-Treska, J. (1986). The organization and solubility properties of intermediate filaments and microtubules of cortical astrocytes in culture. *J. Neurocytol.* 15, 375–387. doi: 10.1007/bf01611439

Han, X., Chen, M., Wang, F., Windrem, M., and Wang, S. (2013). Forebrain engraftment by human glial progenitor cells enhances synaptic plasticity and learning in adult mice. *Cell Stem Cell* 12, 342–353. doi: 10.1016/j.stem.2012.12.015

Haseleu, J., Anlauf, E., Blaess, S., Endl, E., and Derouiche, A. (2013). Studying subcellular detail in fixed astrocytes: dissociation of morphologically intact glial cells (DIMIGs). *Front. Cell. Neurosci.* 7:54. doi: 10.3389/fncel.2013.00054

Heller, J. P., Michaluk, P., Sugao, K., and Rusakov, D. A. (2017). Probing nano-organization of astroglia with multi-color super-resolution microscopy. *J. Neurosci. Res.* 95, 2159–2171. doi: 10.1002/jnr.24026

Heneka, M. T., Sastre, M., Dumitrescu-Ozimek, L., Dewachter, I., Walter, J., Klockgether, T., et al. (2005). Focal glial activation coincides with increased BACE1 activation and precedes amyloid plaque deposition in APP[V717I] transgenic mice. *J. Neuroinflammation* 2:22. doi: 10.1186/1742-2094-2-22

Hermosilla, T., Muñoz, D., Herrera-molina, R., Valdivia, A., Muñoz, N., Nham, S., et al. (2008). Direct Thy-1/αVβ3 integrin interaction mediates neuron to astrocyte communication. *Biochim. Biophys. Acta* 1783, 1111–1120. doi: 10.1016/j.bbamcr.2008.01.034

Higashi, K., Fujita, A., Inanobe, A., Tanemoto, M., Doi, K., Kubo, T., et al. (2001). An inwardly rectifying K^+ channel, Kir4.1, expressed in astrocytes surrounds synapses and blood vessels in brain. *Am. J. Physiol. Physiol.* 281, C922–C931. doi: 10.1152/ajpcell.2001.281.3.c922

Higginson, J. R., and Winder, S. J. (2005). Dystroglycan: a multifunctional adaptor protein. *Biochem. Soc. Trans.* 33, 1254–1255. doi: 10.1042/BST20051254

Hirabayashi, Y., and Gotoh, Y. (2005). Stage-dependent fate determination of neural precursor cells in mouse forebrain. *Neurosci. Res.* 51, 331–336. doi: 10.1016/j.neures.2005.01.004

Hirrlinger, J., Hülsmann, S., and Kirchhoff, F. (2004). Astroglial processes show spontaneous motility at active synaptic terminals *in situ*. *Eur. J. Neurosci.* 20, 2235–2239. doi: 10.1111/j.1460-9568.2004.03689.x

Hochstim, C., Deneen, B., Lukaszewicz, A., Zhou, Q., and Anderson, D. J. (2008). Identification of positionally distinct astrocyte subtypes whose identities are specified by a homeodomain code. *Cell* 133, 510–522. doi: 10.1016/j.cell.2008.02.046

Hoelzinger, D. B., Demuth, T., and Berens, M. E. (2007). Autocrine factors that sustain glioma invasion and paracrine biology in the brain microenvironment. *J. Natl. Cancer Inst.* 99, 1583–1593. doi: 10.1093/jnci/djm187

Jacobsen, C. T., and Miller, R. H. (2003). Control of astrocyte migration in the developing cerebral cortex. *Dev. Neurosci.* 25, 207–216. doi: 10.1159/000072269

Jiu, Y., Peränen, J., Schaible, N., Cheng, F., Eriksson, J. E., Krishnan, R., et al. (2017). Vimentin intermediate filaments control actin stress fiber assembly through GEF-H1 and RhoA. *J. Cell Sci.* 130, 892–902. doi: 10.1242/jcs.196881

Jockusch, B. M., Murk, K., and Rothkegel, M. (2007). The profile of profilins. *Rev. Physiol. Biochem. Pharmacol.* 159, 131–149. doi: 10.1007/112_2007_704

John, G. R. (2004). Interleukin-1 induces a reactive astroglial phenotype via deactivation of the Rho GTPase-rock axis. *J. Neurosci.* 24, 2837–2845. doi: 10.1523/JNEUROSCI.4789-03.2004

Kamphuis, W., Middeldorp, J., Kooijman, L., Sluijs, J. A., Kooi, E. J., Moeton, M., et al. (2014). Glial fibrillary acidic protein isoform expression in plaque related astrogliosis in Alzheimer's disease. *Neurobiol. Aging* 35, 492–510. doi: 10.1016/j.neurobiolaging.2013.09.035

Kanemaru, K., Kubota, J., Sekiya, H., Hirose, K., Okubo, Y., and Iino, M. (2013). Calcium-dependent N-cadherin up-regulation mediates reactive astrogliosis and neuroprotection after brain injury. *Proc. Natl. Acad. Sci. U S A* 110, 11612–11617. doi: 10.1073/pnas.1300378110

Kang, W., Balordi, F., Su, N., Chen, L., Fishell, G., and Hebert, J. M. (2014). Astrocyte activation is suppressed in both normal and injured brain by FGF signaling. *Proc. Natl. Acad. Sci. U S A* 111, E2987–E2995. doi: 10.1073/pnas.1320401111

Kanski, R., van Strien, M. E., van Tijn, P., and Hol, E. M. (2014). A star is born: new insights into the mechanism of astrogenesis. *Cell. Mol. Life Sci.* 71, 433–447. doi: 10.1007/s00018-013-1435-9

Keeler, A. B., Molumby, M. J., and Weiner, J. A. (2015). Protocadherins branch out: multiple roles in dendrite development. *Cell Adhes. Migr.* 9, 214–226. doi: 10.1080/19336918.2014.1000069

Kimelberg, H. K. (2004). The problem of astrocyte identity. *Neurochem. Int.* 45, 191–202. doi: 10.1016/s0197-0186(03)00286-9

Kobayashi, M., Debold, E. P., Turner, M. A., and Kobayashi, T. (2013). Cardiac muscle activation blunted by a mutation to the regulatory component, troponin T. *J. Biol. Chem.* 288, 26335–26349. doi: 10.1074/jbc.M113.494096

Korobova, F., and Svitkina, T. (2008). Arp2/3 complex is important for filopodia formation, growth cone motility, and neuritogenesis in neuronal cells. *Mol. Biol. Cell* 19, 1561–1574. doi: 10.1091/mbc.E07-09-0964

Kreis, P., Leondaritis, G., Lieberam, I., and Eickholt, B. J. (2014). Subcellular targeting and dynamic regulation of PTEN: implications for neuronal cells and neurological disorders. *Front. Mol. Neurosci.* 7:23. doi: 10.3389/fnmol.2014.00023

Kucukdereli, H., Allen, N. J., Lee, A. T., Feng, A., Ozlu, M. I., Conatser, L. M., et al. (2011). Control of excitatory CNS synaptogenesis by astrocyte-secreted proteins Hevin and SPARC. *Proc. Natl. Acad. Sci. U S A* 108, E440–E449. doi: 10.1073/pnas.1104977108

Kulijewicz-Nawrot, M., Verkhratsky, A., Chvátal, A., Syková, E., and Rodríguez, J. J. (2012). Astrocytic cytoskeletal atrophy in the medial prefrontal cortex of a triple transgenic mouse model of Alzheimer's disease. *J. Anat.* 221, 252–262. doi: 10.1111/j.1469-7580.2012.01536.x

Lau, C. L., Kovacevic, M., Tingleff, T. S., Forsythe, J. S., Cate, H. S., Merlo, D., et al. (2014). 3D Electrospun scaffolds promote a cytotrophic phenotype of cultured primary astrocytes. *J. Neurochem.* 130, 215–226. doi: 10.1111/jnc.12702

Lavialle, M., Aumann, G., Anlauf, E., Pröls, F., Arpin, M., and Derouiche, A. (2011). Structural plasticity of perisynaptic astrocyte processes involves ezrin and metabotropic glutamate receptors. *Proc. Natl. Acad. Sci. U S A* 108, 12915–12919. doi: 10.1073/pnas.1100957108

Le, D. M., Besson, A., Fogg, D. K., Choi, K. S., Waisman, D. M., Goodyer, C. G., et al. (2003). Exploitation of astrocytes by glioma cells to facilitate invasiveness: a mechanism involving matrix metalloproteinase-2 and the urokinase-type plasminogen activator-plasmin cascade. *J. Neurosci.* 23, 4034–4043. doi: 10.1523/JNEUROSCI.23-10-04034.2003

Leduc, C., and Etienne-Manneville, S. (2017). Regulation of microtubule-associated motors drives intermediate filament network polarization. *J. Cell Biol.* 216, 1689–1703. doi: 10.1083/jcb.201607045

Lee, J., Lund-Smith, C., Borboa, A., Gonzalez, A. M., Baird, A., and Eliceiri, B. P. (2009). Glioma-induced remodeling of the neurovascular unit. *Brain Res.* 1288, 125–134. doi: 10.1016/j.brainres.2009.06.095

Liu, Z., Li, Y., Cui, Y., Roberts, C., Lu, M., Wilhelmsson, U., et al. (2014). Beneficial effects of gfap/vimentin reactive astrocytes for axonal remodeling and motor

behavioral recovery in mice after stroke. *Glia* 62, 2022–2033. doi: 10.1002/glia.22723

Macauley, S. L., Pekny, M., and Sands, M. S. (2011). The role of attenuated astrocyte activation in infantile neuronal ceroid lipofuscinosis. *J. Neurosci.* 31, 15575–15585. doi: 10.1523/JNEUROSCI.3579-11.2011

MacVicar, B. A., and Newman, E. A. (2015). Astrocyte regulation of blood flow in the brain. *Cold Spring Harb. Perspect. Biol.* 7:a020388. doi: 10.1101/cshperspect.a020388

Magdalena, J., Millard, T. H., and Machesky, L. M. (2003). Microtubule involvement in NIH 3T3 Golgi and MTOC polarity establishment. *J. Cell Sci.* 116, 743–756. doi: 10.1242/jcs.00288

Martin-Fernandez, M., Jamison, S., Robin, L. M., Zhao, Z., Martin, E. D., Aguilar, J., et al. (2017). Synapse-specific astrocyte gating of amygdala-related behavior. *Nat. Neurosci.* 20, 1540–1548. doi: 10.1038/nn.4649

Masahira, N., Takebayashi, H., Ono, K., Watanabe, K., Ding, L., Furusho, M., et al. (2006). Olig2-positive progenitors in the embryonic spinal cord give rise not only to motoneurons and oligodendrocytes, but also to a subset of astrocytes and ependymal cells. *Dev. Biol.* 293, 358–369. doi: 10.1016/j.ydbio.2006.02.029

Mathiisen, T. M., Lehre, K. P., Danbolt, N. C., and Ottersen, O. P. (2010). The perivascular astroglial sheath provides a complete covering of the brain microvessels: an electron microscopic 3D reconstruction. *Glia* 58, 1094–1103. doi: 10.1002/glia.20990

McCarthy, K. D., and de Velllis, J. (1980). Preparation of separate astroglial and oligodendroglial cell cultures from rat cerebral tissue. *J. Cell Biol.* 85, 890–902. doi: 10.1083/jcb.85.3.890

Medvedev, N., Popov, V., Henneberger, C., Kraev, I., Rusakov, D. A., and Stewart, M. G. (2014). Glia selectively approach synapses on thin dendritic spines. *Philos. Trans. R. Soc. Lond. B Biol. Sci.* 369:20140047. doi: 10.1098/rstb.2014.0047

Michaelsen, K., Murk, K., Zagrebelsky, M., Dreznjak, A., Jockusch, B. M., Rothkegel, M., et al. (2010). Fine-tuning of neuronal architecture requires two profilin isoforms. *Proc. Natl. Acad. Sci. U S A* 107, 15780–15785. doi: 10.1073/pnas.1004406107

Min, R., and van der Knaap, M. S. (2018). Genetic defects disrupting glial ion and water homeostasis in the brain. *Brain Pathol.* 28, 372–387. doi: 10.1111/bpa.12602

Molofsky, A. V., Krenick, R., Ullian, E., Tsai, H. H., Deneen, B., Richardson, W. D., et al. (2012). Astrocytes and disease: a neurodevelopmental perspective. *Genes Dev.* 26, 891–907. doi: 10.1101/gad.188326.112

Molotkov, D., Zobova, S., Arcas, J. M., and Khiroug, L. (2013). Calcium-induced outgrowth of astrocytic peripheral processes requires actin binding by Profilin-1. *Cell Calcium* 53, 338–348. doi: 10.1016/j.ceca.2013.03.001

Molumby, M. J., Anderson, R. M., Newbold, D. J., Koblesky, N. K., Garrett, A. M., Schreiner, D., et al. (2017). γ-protocadherins interact with neuroligin-1 and negatively regulate dendritic spine morphogenesis. *Cell Rep.* 18, 2702–2714. doi: 10.1016/j.celrep.2017.02.060

Molumby, M. J., Keeler, A. B., and Weiner, J. A. (2016). Homophilic protocadherin cell-cell interactions promote dendrite complexity. *Cell Rep.* 15, 1037–1050. doi: 10.1016/j.celrep.2016.03.093

Moonen, G., Heinen, E., and Goessens, G. (1976). Comparative ultrastructural study of the effects of serum-free medium and dibutyryl-cyclic AMP on newborn rat astroblasts. *Cell Tissue Res.* 167, 221–227. doi: 10.1007/bf00224329

Murai, K. K., Nguyen, L. N., Irie, F., Yamaguchi, Y., and Pasquale, E. B. (2003). Control of hippocampal dendritic spine morphology through ephrin-A3/EphA4 signaling. *Nat. Neurosci.* 6, 153–160. doi: 10.1038/nn994

Murk, K., Blanco Suarez, E. M., Cockbill, L. M. R., Banks, P., and Hanley, J. G. (2013). The antagonistic modulation of Arp2/3 activity by N-WASP, WAVE2 and PICK1 defines dynamic changes in astrocyte morphology. *J. Cell Sci.* 126, 3873–3883. doi: 10.1242/jcs.125146

Myer, D. J., Gurkoff, G. G., Lee, S. M., Hovda, D. A., and Sofroniew, M. V. (2006). Essential protective roles of reactive astrocytes in traumatic brain injury. *Brain* 129, 2761–2772. doi: 10.1093/brain/awl165

Nagao, M., Ogata, T., Sawada, Y., and Gotoh, Y. (2016). Zbtb20 promotes astrocytogenesis during neocortical development. *Nat. Commun.* 7:11102. doi: 10.1038/ncomms11102

Nicchia, G. P., Rossi, A., Mola, M. G., Procino, G., Frigeri, A., and Svelto, M. (2008). Actin cytoskeleton remodeling governs aquaporin-4 localization in astrocytes. *Glia* 56, 1755–1766. doi: 10.1002/glia.20724

Nimmerjahn, A., Kirchhoff, F., and Helmchen, F. (2005). Neuroscience: resting microglial cells are highly dynamic surveillants of brain parenchyma *in vivo*. *Science* 308, 1314–1318. doi: 10.1126/science.1110647

Nishida, H., and Okabe, S. (2007). Direct astrocytic contacts regulate local maturation of dendritic spines. *J. Neurosci.* 27, 331–340. doi: 10.1523/JNEUROSCI.4466-06.2007

Oberheim, N. A., Takano, T., Han, X., He, W., Lin, J. H. C., Wang, F., et al. (2009). Uniquely hominid features of adult human astrocytes. *J. Neurosci.* 29, 3276–3287. doi: 10.1523/JNEUROSCI.4707-08.2009

Oberheim, N. A., Wang, X., Goldman, S., and Nedergaard, M. (2006). Astrocytic complexity distinguishes the human brain. *Trends Neurosci.* 29, 547–553. doi: 10.1016/j.tins.2006.08.004

Osmani, N., Peglion, F., Chavrier, P., and Etienne-Manneville, S. (2010). Cdc42 localization and cell polarity depend on membrane traffic. *J. Cell Biol.* 191, 1261–1269. doi: 10.1083/jcb.201003091

Panatier, A., Theodosis, D. T., Mothet, J. P., Touquet, B., Pollegioni, L., Poulain, D. A., et al. (2006). Glia-derived D-serine controls NMDA receptor activity and synaptic memory. *Cell* 125, 775–784. doi: 10.1016/j.cell.2006.02.051

Pannasch, U., Freche, D., Dallérac, G., Ghézali, G., Escartin, C., Ezan, P., et al. (2014). Connexin 30 sets synaptic strength by controlling astroglial synapse invasion. *Nat. Neurosci.* 17, 549–558. doi: 10.1038/nn.3662

Pannasch, U., Vargová, L., Reingruber, J., Ezan, P., Holcman, D., Giaume, C., et al. (2011). Astroglial networks scale synaptic activity and plasticity. *Proc. Natl. Acad. Sci. U S A* 108, 8467–8472. doi: 10.1073/pnas.1016650108

Pekny, M., Eliasson, C., Chien, C. L., Kindblom, L. G., Liem, R., Hamberger, A., et al. (1998). GFAP-deficient astrocytes are capable of stellation *in vitro* when cocultured with neurons and exhibit a reduced amount of intermediate filaments and an increased cell saturation density. *Exp. Cell Res.* 239, 332–343. doi: 10.1006/excr.1997.3922

Pekny, M., Johansson, C. B., Eliasson, C., Stakeberg, J., Wallén, A., Perlmann, T., et al. (1999). Abnormal reaction to central nervous system injury in mice lacking glial fibrillary acidic protein and vimentin. *J. Cell Biol.* 145, 503–514. doi: 10.1083/jcb.145.3.503

Pekny, M., Leveen, P., Pekna, M., Eliasson, C., Berthold, C., Westermark, B., et al. (1995). Mice lacking glial fibrillary acidic protein display astrocytes devoid of intermediate filaments but develop and reproduce normally. *EMBO J.* 14, 1590–1598.

Perez-Alvarez, A., Navarrete, M., Covelo, A., Martin, E. D., and Araque, A. (2014). Structural and functional plasticity of astrocyte processes and dendritic spine interactions. *J. Neurosci.* 34, 12738–12744. doi: 10.1523/JNEUROSCI.2401-14.2014

Peters, A., and Vaughn, J. E. (1967). Microtubules and filaments in the axons and astrocytes of early postnatal rat optic nerves. *J. Cell Biol.* 32, 113–119. doi: 10.1083/jcb.32.1.113

Petito, C. K., Morgello, S., Felix, J. C., and Lesser, M. L. (1990). The two patterns of reactive astrocytosis in postischemic rat brain. *J. Cereb. Blood Flow Metab.* 10, 850–859. doi: 10.1038/jcbfm.1990.141

Pilo Boyl, P., Di Nardo, A., Mulle, C., Sassoè-Pognetto, M., Panzanelli, P., Mele, A., et al. (2007). Profilin2 contributes to synaptic vesicle exocytosis, neuronal excitability, and novelty-seeking behavior. *EMBO J.* 26, 2991–3002. doi: 10.1038/sj.emboj.7601737

Potokar, M., Kreft, M., Li, L., Daniel Andersson, J., Pangršič, T., Chowdhury, H. H., et al. (2007). Cytoskeleton and vesicle mobility in astrocytes. *Traffic* 8, 12–20. doi: 10.1111/j.1600-0854.2006.00509.x

Procko, C., Lu, Y., and Shaham, S. (2011). Glia delimit shape changes of sensory neuron receptive endings in *C. elegans*. *Development* 138, 1371–1381. doi: 10.1242/dev.058305

Racchetti, G., D'Alessandro, R., and Meldolesi, J. (2012). Astrocyte stellation, a process dependent on Rac1 is sustained by the regulated exocytosis of enlargeosomes. *Glia* 60, 465–475. doi: 10.1002/glia.22280

Rakic, P. (2003). Developmental and evolutionary adaptations of cortical radial glia. *Cereb. Cortex* 13, 541–549. doi: 10.1093/cercor/13.6.541

Ramakers, G. J. A., and Moolenaar, W. H. (1998). Regulation of astrocyte morphology by RhoA and lysophosphatidic acid. *Exp. Cell Res.* 245, 252–262. doi: 10.1006/excr.1998.4224

Ramón y Cajal, S. (1913). Un nuevo proceder para la impregnación de la neuroglía. *Bol. Soc. Esp. Bio.* 2, 104–108.

Rash, J. E., Yasumura, T., Hudson, C. S., Agre, P., and Nielsen, S. (1998). Direct immunogold labeling of aquaporin-4 in square arrays of astrocyte and ependymocyte plasma membranes in rat brain and spinal cord. *Proc. Natl. Acad. Sci. U S A* 95, 11981–11986. doi: 10.1073/pnas.95.20.11981

Ren, Z., Iliff, J. J., Yang, L., Yang, J., Chen, X., Chen, M. J., et al. (2013). 'Hit & Run' model of closed-skull traumatic brain injury (TBI) reveals complex patterns of post-traumatic AQP4 dysregulation. *J. Cereb. Blood Flow Metab.* 33, 834–845. doi: 10.1038/jcbfm.2013.30

Renault-Mihara, F., Mukaino, M., Shinozaki, M., Kumamaru, H., Kawase, S., Baudoux, M., et al. (2017). Regulation of RhoA by STAT3 coordinates glial scar formation. *J. Cell Biol.* 216, 2533–2550. doi: 10.1083/jcb.201610102

Renner, M., Lancaster, M. A., Bian, S., Choi, H., Ku, T., Peer, A., et al. (2017). Self-organized developmental patterning and differentiation in cerebral organoids. *EMBO J.* 36, 1316–1329. doi: 10.15252/embj.201694700

Richier, B., Vijandi, C. D. M., Mackensen, S., and Salecker, I. (2017). Lapsyn controls branch extension and positioning of astrocyte-like glia in the *Drosophila* optic lobe. *Nat. Commun.* 8:317. doi: 10.1038/s41467-017-00384-z

Robel, S., Bardehle, S., Lepier, A., Brakebusch, C., and Götz, M. (2011). Genetic deletion of cdc42 reveals a crucial role for astrocyte recruitment to the injury site *in vitro* and *in vivo*. *J. Neurosci.* 31, 12471–12482. doi: 10.1523/JNEUROSCI.2696-11.2011

Robel, S., Mori, T., Zoubaa, S., Schlegel, J., Sirko, S., Faissner, A., et al. (2009). Conditional deletion of ß1-integrin in astroglia causes partial reactive gliosis. *Glia* 57, 1630–1647. doi: 10.1002/glia.20876

Rottner, K., Faix, J., Bogdan, S., Linder, S., and Kerkhoff, E. (2017). Actin assembly mechanisms at a glance. *J. Cell Sci.* 130, 3427–3435. doi: 10.1242/jcs.206433

Rotty, J. D., Wu, C., Haynes, E. M., Suarez, C., Winkelman, J. D., Johnson, H. E., et al. (2015). Profilin-1 serves as a gatekeeper for actin assembly by Arp2/3-dependent and—independent pathways. *Dev. Cell* 32, 54–67. doi: 10.1016/j.devcel.2014.10.026

Rubinstein, R., Thu, C. A., Goodman, K. M., Wolcott, H. N., Bahna, F., Mannepalli, S., et al. (2015). Molecular logic of neuronal self-recognition through protocadherin domain interactions. *Cell* 163, 629–642. doi: 10.1016/j.cell.2015.09.026

Rungger-Brändle, E., Messerli, J. M., Niemeyer, G., and Eppenberger, H. M. (1993). Confocal microscopy and computer-assisted image reconstruction of astrocytes in the mammalian retina. *Eur. J. Neurosci.* 5, 1093–1106. doi: 10.1111/j.1460-9568.1993.tb00963.x

Saadoun, S., Papadopoulos, M. C., Watanabe, H., Yan, D., Manley, G. T., and Verkman, A. S. (2005). Involvement of aquaporin-4 in astroglial cell migration and glial scar formation. *J. Cell Sci.* 118, 5691–5698. doi: 10.1242/jcs.02680

Sakamoto, Y., Boëda, B., and Etienne-Manneville, S. (2013). APC binds intermediate filaments and is required for their reorganization during cell migration. *J. Cell Biol.* 200, 249–258. doi: 10.1083/jcb.201206010

Sandau, U. S., Mungenast, A. E., Alderman, Z., Sardi, S. P., Fogel, A. I., Taylor, B., et al. (2011). SynCAM1, a synaptic adhesion molecule, is expressed in astrocytes and contributes to erbB4 receptor-mediated control of female sexual development. *Endocrinology* 152, 2364–2376. doi: 10.1210/en.2010-1435

Schober, J. M., Komarova, Y. A., Chaga, O. Y., Akhmanova, A., and Borisy, G. G. (2007). Microtubule-targeting-dependent reorganization of filopodia. *J. Cell Sci.* 120, 1235–1244. doi: 10.1242/jcs.003913

Scholze, A. R., Foo, L. C., Mulinyawe, S., and Barres, B. A. (2014). BMP signaling in astrocytes downregulates EGFR to modulate survival and maturation. *PLoS One* 9:e110668. doi: 10.1371/journal.pone.0110668

Schousboe, A., Bak, L. K., and Waagepetersen, H. S. (2013). Astrocytic control of biosynthesis and turnover of the neurotransmitters glutamate and GABA. *Front. Endocrinol.* 4:102. doi: 10.3389/fendo.2013.00102

Schweinhuber, S. K., Meßerschmidt, T., Hänsch, R., Korte, M., and Rothkegel, M. (2015). Profilin isoforms modulate astrocytic morphology and the motility of astrocytic processes. *PLoS One* 10:e0117244. doi: 10.1371/journal.pone.0117244

Shapiro, D. L. (1973). Morphological and biochemical alterations in foetal rat brain cells cultured in the presence of monobutyryl cyclic AMP. *Nature* 241, 203–204. doi: 10.1038/241203a0

Simard, M., and Nedergaard, M. (2004). The neurobiology of glia in the context of water and ion homeostasis. *Neuroscience* 129, 877–896. doi: 10.1016/j.neuroscience.2004.09.053

Singh, S. K., Fiorelli, R., Kupp, R., Rajan, S., Szeto, E., Lo Cascio, C., et al. (2016). Post-translational modifications of OLIG2 regulate glioma invasion through the TGF-β pathway. *Cell Rep.* 16, 950–966. doi: 10.1016/j.celrep.2016.06.045

Sofroniew, M. V. (2009). Molecular dissection of reactive astrogliosis and glial scar formation. *Trends Neurosci.* 32, 638–647. doi: 10.1016/j.tins.2009.08.002

Srinivasan, R., Lu, T. Y., Chai, H., Xu, J., Huang, B. S., Golshani, P., et al. (2016). New transgenic mouse lines for selectively targeting astrocytes and studying calcium signals in astrocyte processes *in situ* and *in vivo*. *Neuron* 92, 1181–1195. doi: 10.1016/j.neuron.2016.11.030

Steffen, A., Stradal, T. E. B., and Rottner, K. (2017). Signalling pathways controlling cellular actin organization. *Handb. Exp. Pharmacol.* 233, 321–353. doi: 10.1007/164_2016_35

Stellwagen, D., and Malenka, R. C. (2006). Synaptic scaling mediated by glial TNF-α. *Nature* 440, 1054–1059. doi: 10.1038/nature04671

Stogsdill, J. A., Ramirez, J., Liu, D., Kim, Y. H., Baldwin, K. T., Enustun, E., et al. (2017). Astrocytic neuroligins control astrocyte morphogenesis and synaptogenesis. *Nature* 551, 192–197. doi: 10.1038/nature24638

Stokum, J. A., Kurland, D. B., Gerzanich, V., and Simard, J. M. (2015). Mechanisms of astrocyte-mediated cerebral edema. *Neurochem. Res.* 40, 317–328. doi: 10.1007/s11064-014-1374-3

Stolt, C. C., Lommes, P., Sock, E., Chaboissier, M. C., Schedl, A., and Wegner, M. (2003). The Sox9 transcription factor determines glial fate choice in the developing spinal cord. *Genes Dev.* 17, 1677–1689. doi: 10.1101/gad.259003

Stork, T., Sheehan, A., Tasdemir-Yilmaz, O. E., and Freeman, M. R. (2014). Neuron-Glia interactions through the heartless fgf receptor signaling pathway mediate morphogenesis of *Drosophila* astrocytes. *Neuron* 83, 388–403. doi: 10.1016/j.neuron.2014.06.026

Sultana, S., Sernett, S. W., Bellin, R. M., Robson, R. M., and Skalli, O. (2000). Intermediate filament protein synemin is transiently expressed in a subset of astrocytes during development. *Glia* 30, 143–153. doi: 10.1002/(sici)1098-1136(200004)30:2<143::aid-glia4>3.0.co;2-z

Tan, Z., Liu, Y., Xi, W., Lou, H. F., Zhu, L., Guo, Z., et al. (2017). Glia-derived ATP inversely regulates excitability of pyramidal and CCK-positive neurons. *Nat. Commun.* 8:13772. doi: 10.1038/ncomms13772

Tatsumi, K., Okuda, H., Morita-Takemura, S., Tanaka, T., Isonishi, A., Shinjo, T., et al. (2016). Voluntary exercise induces astrocytic structural plasticity in the globus pallidus. *Front. Cell. Neurosci.* 10:165. doi: 10.3389/fncel.2016.00165

Theodosis, D. T. (2002). Oxytocin-secreting neurons: a physiological model of morphological neuronal and glial plasticity in the adult hypothalamus. *Front. Neuroendocrinol.* 23, 101–135. doi: 10.1006/frne.2001.0226

Theodosis, D. T., Piet, R., Poulain, D. A., and Oliet, S. H. R. (2004). Neuronal, glial and synaptic remodeling in the adult hypothalamus: functional consequences and role of cell surface and extracellular matrix adhesion molecules. *Neurochem. Int.* 45, 491–501. doi: 10.1016/j.neuint.2003.11.003

Tsai, H., Li, H., Fuentealba, L. C., Molofsky, A. V., Taveira-Marques, R., Zhuang, H., et al. (2012). Regional astrocyte allocation regulates CNS synaptogenesis and repair. *Science* 337, 358–362. doi: 10.1126/science.1222381

Van Horn, M. R., Strasser, A., Miraucourt, L. S., Pollegioni, L., and Ruthazer, E. S. (2017). The gliotransmitter d-serine promotes synapse maturation and axonal stabilization *in vivo*. *J. Neurosci.* 37, 6277–6288. doi: 10.1523/JNEUROSCI.3158-16.2017

Wanner, I. B., Anderson, M. A., Song, B., Levine, J., Fernandez, A., Gray-Thompson, Z., et al. (2013). Glial scar borders are formed by newly proliferated, elongated astrocytes that interact to corral inflammatory and fibrotic cells via STAT3-dependent mechanisms after spinal cord injury. *J. Neurosci.* 33, 12870–12886. doi: 10.1523/JNEUROSCI.2121-13.2013.

Warth, A., Mittelbronn, M., and Wolburg, H. (2005). Redistribution of the water channel protein aquaporin-4 and the K^+ channel protein Kir4.1 differs in low- and high-grade human brain tumors. *Acta Neuropathol.* 109, 418–426. doi: 10.1007/s00401-005-0984-x

Watkins, S., Robel, S., Kimbrough, I. F., Robert, S. M., Ellis-Davies, G., and Sontheimer, H. (2014). Disruption of astrocyte-vascular coupling and the blood-brain barrier by invading glioma cells. *Nat. Commun.* 5:4196. doi: 10.1038/ncomms5196

Wilhelmsson, U., Bushong, E. A., Price, D. L., Smarr, B. L., Phung, V., Terada, M., et al. (2006). Redefining the concept of reactive astrocytes as cells that remain within their unique domains upon reaction to injury. *Proc. Natl. Acad. Sci. U S A* 103, 17513–17518. doi: 10.1073/pnas.0602841103

Wilhelmsson, U., Li, L., Pekna, M., Berthold, C. H., Blom, S., and Eliasson, C. (2004). Absence of glial fibrillary acidic protein and vimentin prevents hypertrophy of astrocytic processes and improves post-traumatic regeneration. *J. Neurosci.* 24, 5016–5021. doi: 10.1523/JNEUROSCI.0820-04.2004

Winchenbach, J., Düking, T., Berghoff, S. A., Stumpf, S. K., Hülsmann, S., Nave, K.-A., et al. (2016). Inducible targeting of CNS astrocytes in Aldh1l1-CreERT2 BAC transgenic mice. *F1000Res.* 5:2934. doi: 10.12688/f1000research.10509.1

Windrem, M. S., Osipovitch, M., Liu, Z., Bates, J., Chandler-Militello, D., Zou, L., et al. (2017). Human iPSC glial mouse chimeras reveal glial contributions to schizophrenia. *Cell Stem Cell* 21, 195.e6–208.e6. doi: 10.1016/j.stem.2017.06.012

Winkler, U., Hirrlinger, P. G., Sestu, M., Wilhelm, F., Besser, S., Zemljic-Harpf, A. E., et al. (2013). Deletion of the cell adhesion adaptor protein vinculin disturbs the localization of GFAP in Bergmann glial cells. *Glia* 61, 1067–1083. doi: 10.1002/glia.22495

Witcher, M. R., Kirov, S. A., and Harris, K. M. (2007). Plasticity of perisynaptic astroglia during synaptogenesis in the mature rat hippocampus. *Glia* 55, 13–23. doi: 10.1002/glia.20415

Wolfes, A. C., and Dean, C. (2018). Culturing *in vivo*-like murine astrocytes using the fast, simple, and inexpensive AWESAM protocol. *J. Vis. Exp.* 131:e56092. doi: 10.3791/56092

Woo, J., Im, S.-K., Chun, H., Jung, S.-Y., Oh, S.-J., Choi, N., et al. (2017). Functional characterization of resting and adenovirus-induced reactive astrocytes in three-dimensional culture. *Exp. Neurobiol.* 26, 158–167. doi: 10.5607/en.2017.26.3.158

Wu, C., Asokan, S. B., Berginski, M. E., Haynes, E. M., Sharpless, N. E., Griffith, J. D., et al. (2012). Arp2/3 is critical for lamellipodia and response to extracellular matrix cues but is dispensable for chemotaxis. *Cell* 148, 973–987. doi: 10.1016/j.cell.2011.12.034

Zhang, L., Zhang, S., Yao, J., Lowery, F. J., Zhang, Q., Huang, W. C., et al. (2015). Microenvironment-induced PTEN loss by exosomal microRNA primes brain metastasis outgrowth. *Nature* 527, 100–104. doi: 10.1038/nature15376

Conflict of Interest Statement: The authors declare that the research was conducted in the absence of any commercial or financial relationships that could be construed as a potential conflict of interest.

frontiers in Molecular Neuroscience

MINI REVIEW
published: 04 September 2018
doi: 10.3389/fnmol.2018.00319

The Regulation of Axon Diameter: From Axonal Circumferential Contractility to Activity-Dependent Axon Swelling

Ana Rita Costa[1†], *Rita Pinto-Costa*[1,2†], *Sara Castro Sousa*[1] *and Mónica Mendes Sousa*[1*]

[1]*Nerve Regeneration Group, Instituto de Biologia Molecular e Celular (IBMC) and Instituto de Inovação e Investigação em Saúde, University of Porto, Porto, Portugal,* [2]*Instituto de Ciências Biomédicas Abel Salazar (ICBAS), University of Porto, Porto, Portugal*

In the adult nervous system axon caliber varies widely amongst different tracts. When considering a given axon, its diameter can further fluctuate in space and time, according to processes including the distribution of organelles and activity-dependent mechanisms. In addition, evidence is emerging supporting that in axons circumferential tension/contractility is present. Axonal diameter is generically regarded as being regulated by neurofilaments. When neurofilaments are absent or low, microtubule-dependent mechanisms can also contribute to the regulation of axon caliber. Despite this knowledge, the fine-tune mechanisms controlling diameter and circumferential tension throughout the lifetime of an axon, remain largely elusive. Recent data supports the role of the actin-spectrin-based membrane periodic skeleton and of non-muscle myosin II in the control of axon diameter. However, the cytoskeletal arrangement that underlies circumferential axonal contraction and expansion is still to be discovered. Here, we discuss in a critical viewpoint the existing knowledge on the regulation of axon diameter, with a specific focus on the possible role played by the axonal actin cytoskeleton.

Keywords: axon diameter, axonal contractility, axonal tension, axonal cytoskeleton, membrane periodic skeleton

OPEN ACCESS

Edited by:
Christian Gonzalez-Billault, Universidad de Chile, Chile

Reviewed by:
Annie Andrieux, CEA Grenoble, France
Archan Ganguly, University of California, San Diego, United States

***Correspondence:**
Mónica Mendes Sousa
msousa@ibmc.up.pt

[†]*These authors have contributed equally to this work*

Received: *14 May 2018*
Accepted: *17 August 2018*
Published: *04 September 2018*

Citation:
Costa AR, Pinto-Costa R, Sousa SC and Sousa MM (2018) The Regulation of Axon Diameter: From Axonal Circumferential Contractility to Activity-Dependent Axon Swelling. Front. Mol. Neurosci. 11:319. doi: 10.3389/fnmol.2018.00319

INTRODUCTION

During development, after reaching their synaptic targets, axons increase their caliber several fold to achieve the large diameters needed for the rapid conduction of action potentials. In the adult nervous system the diameter of axons belonging to different tracts varies by nearly 100-fold (∼0.1–10 μm), in accordance with a wide variation in conduction velocity (Perge et al., 2012). When considering a single axon, its diameter can fluctuate in space and time depending on several variables including the distribution of organelles (which is particularly relevant in unmyelinated axons; Greenberg et al., 1990), and activity-dependent mechanisms (Fields, 2011). Mature axons do probably need to further fine-tune their caliber to additional conditions such as deformations imposed by movement (specially in the case of the peripheral nervous system) or induced by axonal degeneration. However, the molecular mechanisms regulating diameter throughout the lifetime of an axon, remain largely elusive.

The axonal cytoskeleton has three major components: microtubules, neurofilaments and actin (Leterrier et al., 2017). Axonal diameter is traditionally regarded as being under the control of the expression and phosphorylation of neurofilaments, the neuron-specific intermediate filaments.

Loss of all axonal neurofilaments results in smaller caliber myelinated axons with slower conduction velocities (Ohara et al., 1993; Sakaguchi et al., 1993; Zhu et al., 1997; Kriz et al., 2000). C-terminal domain neurofilament phosphorylation is a key component of radial growth (de Waegh et al., 1992) as it aligns and bundles neurofilaments and extends their sidearms (Leterrier et al., 1996) promoting the crosslinking among neurofilaments and other cytoskeletal components (Gotow et al., 1994). This sequence of events leads to an increase in inter-filament spacing and thereby to the increase of axon diameter (Nixon et al., 1994). Assembly of compact myelin is a key driver in the initiation of radial axonal growth as signaling from myelinating glia triggers the above events (de Waegh et al., 1992). Accordingly, unmyelinated regions of a given axon have smaller diameters, containing less phosphorylated, and more compact neurofilaments (Hsieh et al., 1994).

In small caliber axons that express low levels of neurofilaments, microtubule organization contributes to the regulation of axon diameter (Friede and Samorajs, 1970; Alfei et al., 1991). In arthropods, that totally lack neurofilaments (Benshalom and Reese, 1985; Goldstein and Gunawardena, 2000) axon diameter is also controlled by microtubule-dependent mechanisms. In *Drosophila*, two giant Ankyrin2 isoforms (Ank2-L and Ank2-XL) and the microtubule-associated protein 1B (MAP1B) homolog Futsch form an evenly spaced, grid-like membrane-associated microtubule-organizing complex that determines axon diameter in the absence of neurofilaments (Stephan et al., 2015). Interestingly, a similar grid-like microtubule organization has been observed in mammalian retinal axons, where microtubule tract number correlates with axon diameter (Hsu et al., 1998; Perge et al., 2012). On a different note, and further supporting the significant role of microtubules in the control of axon shape and diameter, axon degeneration is often accompanied by focal axonal enlargements—axonal swellings—that have been mainly related to the disorganization of the microtubule cytoskeleton (Saxena and Caroni, 2007).

Although it has long been known that axons are contractile along their longitudinal axis (Dennerll et al., 1988; George et al., 1988; Rajagopalan et al., 2010) only recent emerging evidence support that axons may also exert contractility/tension along their circumferential axis (Fan et al., 2017). The role of the axonal cytoskeleton, namely of actin microfilament organization and dynamics in the regulation of axonal tension, is beginning to come to light. This has been made possible by the development of novel actin probes, super-resolution microscopy and state-of-the-art live imaging that allowed unveiling previously undiscovered axonal actin structures (Leterrier et al., 2017).

REGULATION OF AXON DIAMETER BY THE MEMBRANE PERIODIC SKELETON: THE ROLE OF ADDUCIN

It is now recognized that the mature axon shaft has two distinct actin cytoskeletal arrangements: (i) a submembranous stable actin-spectrin network (the membrane periodic skeleton), composed of actin rings regularly spaced by spectrin tetramers approximately every 190 nm (Xu et al., 2013; **Figure 1**), and (ii) deep dynamic actin trails, consisting of focal actin hot spots and elongating actin polymers along the shaft (Ganguly et al., 2015; Roy, 2016). Work from our group and others demonstrated that the membrane periodic skeleton is present in every neuron type, ranging from central to peripheral nervous system neurons (D'Este et al., 2015; He et al., 2016; Leite et al., 2016), including both excitatory and inhibitory neurons (D'Este et al., 2016; He et al., 2016), being observed in fixed and live cells, and in brain tissue sections, without substantial differences between unmyelinated and myelinated axons (Xu et al., 2013; Lukinavičius et al., 2014; Zhong et al., 2014). In hippocampal neuron cultures, the membrane periodic skeleton emerges early during axon development, after axon specification, and propagates from proximal regions to distal ends of axons, spanning almost the complete axon shaft of mature neurons (Han et al., 2017). Once matured, the structure is thought to be highly stable, with slow turnover of its components (Zhong et al., 2014). Recent data obtained using hippocampal neuron cultures support that the subcortical neuronal cytoskeleton is differentially regulated in the different neuronal compartments (Han et al., 2017; **Figure 1**). In mature neurons, a 1D membrane periodic skeleton is present not only in axons but also in a substantial fraction of dendrites. However, in dendrites, this structure develops slower and forms with a lower propensity than in axons (Han et al., 2017). In contrast, in the somatodendritic compartment, an actin-spectrin based 2D polygonal lattice is slowly formed, resembling the expanded erythrocyte membrane skeleton (Han et al., 2017). *In vitro*, in hippocampal neurons, the average dendritic diameter is higher than that of axons, which led to the hypothesis that the lower propensity of 1D lattice formation in dendrites could stem from their larger diameter (Han et al., 2017). Yet, further analyses showed little dependence between dendrite diameter and formation of the membrane periodic skeleton. The authors did however not exclude the hypothesis that in very wide neurites, in which the membrane is locally nearly flat, the actin-spectrin network may adopt a different structural form (Han et al., 2017).

The discovery of the membrane periodic skeleton opened new perspectives on how the actin cytoskeleton might support the neuronal architecture and function. Although its assembly mechanism and function remain largely elusive, the actin-spectrin network may provide mechanical support for the long and thin structure of axons which can be particularly vulnerable to tissue pressure. Supporting this notion, in *C. elegans*, deletion of beta spectrin leads to axon breakage upon movement of the worm (Hammarlund et al., 2007).

In axonal actin rings, the actin-binding protein adducin caps the barbed end of actin filaments (Xu et al., 2013). Hence, in the initial model of the organization of the membrane periodic skeleton, actin rings were proposed to be made of short filaments (Xu et al., 2013), likely assisted by additional actin-binding proteins (**Figure 1**). Work from our group has further demonstrated that *in vitro*, in the absence of adducin, actin rings present an increased diameter which *in vivo* results in progressive axon enlargement, followed by axon degeneration

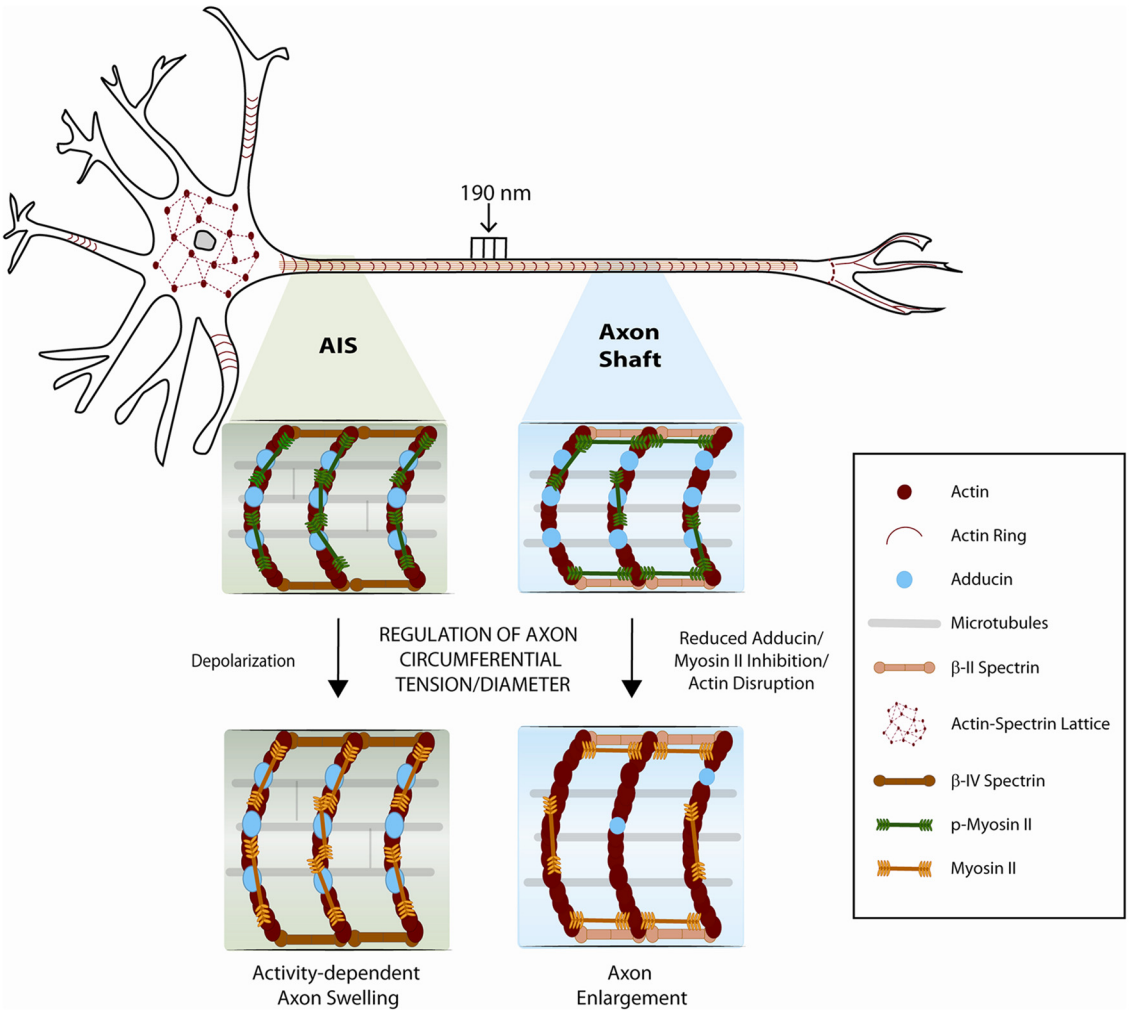

FIGURE 1 | Schematic representation of the neuronal cytoskeleton. The role of the membrane periodic cytoskeleton and of myosin-II in the control of the axonal circumferential contractility is emphasized. In mature neurons, a 1D membrane periodic skeleton is present not only in axons but also in a fraction of dendrites. In contrast, in the somatodendritic compartment, an actin-spectrin based 2D polygonal lattice is formed, resembling the expanded erythrocyte membrane skeleton. Phosphorylated myosin light chain is highly enriched at the axon initial segment, where it may participate in the regulation of axon diameter during action potential firing. In the axon shaft, circumferential and longitudinal axon tension may also result from the regulation of an actomyosin network that remains to be solved at the structural level. Adducin, and additional actin-binding proteins that might be associated to axonal actin rings, may further contribute to fine-tune axon diameter.

and loss (Leite et al., 2016; **Figure 1**). These findings support that the capping activity of adducin is required to maintain axon diameter. Of note, *in vitro*, the actin ring diameter of both WT and α-adducin KO neurons narrowed over time. This supports that actin filaments that compose the axonal actin rings are more dynamic than initially suggested, being able to adapt to variations in axon diameter. Analysis throughout time of F-actin content in actin rings supported that axon constriction occurs with bundling and condensation of actin filaments within rings (Leite et al., 2016). Since both WT and α-adducin KO neurons decrease actin ring diameter over time in culture, the dynamics of the submembranous actin-spectrin network is probably regulated by additional actin-binding proteins. Variations in axon diameter also raise exciting questions on the arrangement of spectrin tetramers within the membrane periodic skeleton. Future experiments should address how spectrin density i.e., its lateral spacing within axons is adjusted when variations of axon caliber occur.

There are several resemblances between the actin-spectrin lattice in neurons and erythrocytes. In red blood cells, spectrin, actin and associated proteins form a cortical cytoskeleton that confers strength and elasticity (Mohandas and Gallagher, 2008). The lack of adducin results in misshaped erythrocytes that are less resistant to mechanical stress, including osmotic pressure (Gilligan et al., 1999; Robledo et al., 2008). Recently, using super-resolution microscopy, it has been demonstrated that red blood cells contain bipolar filaments of non-muscle myosin II associated to the membrane skeleton (Smith et al., 2018). Non-muscle myosin II-mediated contractility is a highly

conserved mechanism for generating mechanical forces and translocation of the actin cytoskeleton in non-muscle cells (Vicente-Manzanares et al., 2009). Myosin II is a hexameric molecule consisting of a dimer of heavy chains, two regulatory light chains and two essential light chains (Vicente-Manzanares et al., 2009). Similarly to smooth muscle myosin, non-muscle myosin II is activated by phosphorylation of myosin light chain, either by an initial single phosphorylation at Ser19 or by sequential phosphorylation of Thr18 and Ser19 (Vicente-Manzanares et al., 2009). Myosin light chain phosphorylation activates both the contractile ATPase activity of non-muscle myosin II and the assembly of myosin filaments needed to coordinate force generation (Vicente-Manzanares et al., 2009). In red blood cells, the non-muscle myosin II light chain is phosphorylated, indicating active regulation of its motor activity and filament assembly. Inhibition of non-muscle myosin II with blebbistatin, an inhibitor of its motor activity (Kovács et al., 2004), enhances membrane deformability and decreases membrane tension. This supports a role for myosin II-mediated contractility in promoting membrane stiffness and maintaining red blood cell shape. Similarly to erythrocytes and to actin rings that exist in other biological contexts, the membrane periodic skeleton may have a more dynamic nature than initially anticipated, fine-tuning the circumferential contractility/tension of the axon shaft (Leite and Sousa, 2016). One can also not exclude the participation of the deep axonal actin cytoskeleton i.e., the actin hot spots and actin trails in the regulation of the axonal circumferential and/or longitudinal tension.

MECHANISMS REGULATING AXONAL LONGITUDINAL AND CIRCUMFERENTIAL CONTRACTILITY

Unperturbed neurons maintain an intrinsic longitudinal rest tension along their axons both *in vitro* (Heidemann and Buxbaum, 1990) and *in vivo* (Siechen et al., 2009). *In vitro*, when tension is increased, a rapid axon elongation takes place (Bray, 1984; Pfister et al., 2004) in a process known as "axon stretch growth" (reviewed in Smith (2009)). In the case of embryonic rat dorsal root ganglia neurons, exposure to mechanical tension enables elongation at a rate of 8 mm/day resulting in axons a thousand times their original length (Pfister et al., 2004). Evidence of severe axon stretch growth is found *in vivo* in nature and is well pictured by the rapid expansion in the blue whale's spine axons that grow at a rate higher than 30 mm/day (Smith, 2009). In contrast, in response to loss of tension, axons contract as is the case after resection or surgical incision (Shaw and Bray, 1977; Joshi et al., 1985; George et al., 1988; Gallo, 2004). This longitudinal contraction eventually leads to the re-establishment of the axonal rest tension. The actomyosin network has emerged as a central regulator of the intrinsic axial tension (i.e., axonal contractility along the longitudinal direction) both *in vitro* (Dennerll et al., 1988; Lamoureux et al., 1989) and *in vivo* (Siechen et al., 2009; Xu et al., 2010; Tofangchi et al., 2016; **Figure 1**).

In vivo, in embryonic *Drosophila*, when motor neuron axons are slackened mechanically, axons shorten within 2–4 min and restore their straight configuration (Tofangchi et al., 2016). This longitudinal contractility decreases dramatically after myosin II knockdown and inhibition, namely by using ML-7, an inhibitor of myosin light chain kinase (Saitoh et al., 1987), and Y-27,632 (Uehata et al., 1997), an inhibitor of Rho-associated protein kinase (ROCK). Further supporting the involvement of myosin II in longitudinal axonal contractility, disruption of actin filaments in embryos treated with cytochalasin D and latrunculin A (Spector et al., 1989), significantly impaired axonal contraction. Interestingly, the rate of contraction is faster when microtubules are disrupted by either nocodazole or colchicine (Tofangchi et al., 2016). Using trypsin-mediated detachment in chick embryo DRG neuron cultures, as an alternative model to evaluate axonal longitudinal contraction (Mutalik et al., 2018), blebbistatin inhibits axon straightening upon trypsin-induced de-adhesion. In contrast to the *Drosophila* model, in chick DRG neurons nocodazole reduces axonal contraction (Mutalik et al., 2018). As such, the role of microtubules in longitudinal axonal contraction awaits further clarification.

In addition to longitudinal contractility, using confocal microscopy and spatial light interference microscopy, it has been recently shown that *Drosophila* axons also actively maintain contractility/tension along the circumferential axis (Fan et al., 2017). Similarly to axial tension, circumferential tension is also regulated by myosin-II (**Figure 1**). Increased axonal diameter is generated by disruption of actin filaments or by myosin II inhibition using either ML-7 or the ROCK inhibitor 27632 (Fan et al., 2017). These results suggest that the actomyosin machinery is contractile along the circumferential direction of axons such that the relaxation of tension results in increased axonal diameter. The authors also raised the hypothesis that circumferential tension applies a compressive force on microtubules, and that the force balance between cortical actin and microtubule results in an equilibrium diameter of the axon. Accordingly, a decrease in axon diameter was observed when microtubules were disrupted with nocodazole or colchicine. In this context, it is interesting to note that the membrane periodic skeleton is thought to interact with axonal microtubules (Zhong et al., 2014; Qu et al., 2017). Additionally, in *Drosophila* neurons, formins (actin nucleators that crosslink actin and microtubules) were shown to contribute to the actin-spectrin network (Qu et al., 2017). As such, one cannot exclude that cytoskeleton crosslinkers may also be involved in modulating axon diameter. An additional layer of regulation may be provided by Ca^{2+} levels. Given that Ca^{2+}-calmodulin controls adducin (Gardner and Bennett, 1987; Kuhlman et al., 1996) and non-muscle myosin II activity (Somlyo and Somlyo, 2003), it is plausible that changes in axon diameter might be regulated by Ca^{2+} influx.

Overall, a mechanism in which longitudinal and circumferential axonal tension are coupled, is supported by recent data (Fan et al., 2017), as they share similar time constants of evolution; i.e., the times to generate longitudinal tension and to contract the diameter to their respective steady values are similar. However, the cytoskeletal arrangement that underlies

axial and circumferential axonal contractility, and their coupling, remains to be resolved.

ACTIVITY-DEPENDENT CHANGES OF AXON DIAMETER: AXONAL SWELLING DURING ACTION POTENTIAL GENERATION

Several data support that axon diameter is dynamic and regulated by activity-dependent mechanisms. In fact, nerves and axons from different species including giant axons of squid (Iwasa and Tasaki, 1980; Tasaki and Iwasa, 1982), crayfish (Hill et al., 1977) and cuttlefish (Hill, 1950), the garfish olfactory nerve (Tasaki et al., 1989; Tasaki and Byrne, 1990), the bullfrog olfactory bulb (Tasaki and Byrne, 1988), dorsal root ganglia and spinal cord (Tasaki and Byrne, 1983), are known to swell during the production of an action potential (reviewed in Fields (2011)). In the squid giant axon, swelling starts nearly at the onset of the action potential and the peak of swelling during excitation coincides accurately with the peak of the action potential recorded intracellularly (Iwasa and Tasaki, 1980). Of note, concurrently with axon swelling, longitudinal shortening of nerve fibers occurs (Tasaki and Iwasa, 1982; Tasaki et al., 1989). This observation points towards the similarities between the mechanical changes that occur in the muscle and those that take place in the nerve (Tasaki and Byrne, 1990).

Recently, the inability of conventional light microscopy to resolve thin unmyelinated axons, which can have diameters well below 200 nm i.e., below the limit of resolution of an optical microscope, has been overcome by the development of super-resolution microscopy. In agreement with the above seminal studies, using time-lapse STED microscopy in mouse brain slices, axons were shown to swell after high-frequency action potential firing (Chéreau et al., 2017). In these settings, whereas synaptic boutons underwent a rapid transient enlargement that decayed, the axon shaft showed a more delayed and progressive increase in diameter, swelling gradually over the duration of the experiment (approximately 1 h). Electrophysiological experiments revealed a short phase of slowed down action potential conduction linked to the transient enlargement of the synaptic boutons (Chéreau et al., 2017). This initial phase was followed by a sustained increase in conduction speed when the axon shaft widened. In summary, increasing axon diameters accelerated action potential conduction along the axons. This finding is in line with cable theory (Goldstein and Rall, 1974) as axons of increased diameter have less internal electrical resistance, which facilitates the spread of action potential. This study shows that activity-dependent changes in the nanoscale axon morphology modify the speed of action potentials along hippocampal unmyelinated axons, revealing a new layer of complexity for the regulation of axon physiology. The authors raised the hypothesis that rapid redistribution and/or *de novo* synthesis of membrane might be the source of the activity-dependent net enlargement of axons.

Lately, new insights have been provided for the physical mechanisms that may account for the increase in axon diameter during action potential firing (Berger et al., 2018). The axon initial segment, located in the proximal axon of multipolar neurons, is the region where action potentials are generated (Ogawa and Rasband, 2008). This region is crucial for fine-tuning neuronal excitability as its structural properties, including length and/or location relative to the soma, change in an activity-dependent manner (Yamada and Kuba, 2016). The mechanisms that underlie the assembly of the axon initial segment in the proximal axon and its plasticity are still poorly understood. Recently, it has been demonstrated that phosphorylated myosin light chain is highly enriched in the axon initial segment (Berger et al., 2018) where its contractile activity may function as the molecular mechanism regulating activity-dependent changes of axon diameter (**Figure 1**). Interestingly, myosin light chain was shown to be rapidly lost during depolarization, via Ca^{2+}-dependent mechanisms, destabilizing actin and thereby providing a mechanism for activity-dependent structural plasticity of the axon initial segment (Berger et al., 2018). Using STORM nanoscopy, the authors proposed that activated phospho-myosin light chain associates with the periodic actin cytoskeleton forming actomyosin rings at the axon initial segment, and raised the hypothesis that myosin II filaments are oriented parallel to the actin rings. It is however interesting to speculate the possible existence of an alternative model, in which myosin filaments might not be exclusively oriented in parallel to actin rings, thus providing the additional control of longitudinal axonal contractility (**Figure 1**).

CONCLUSION AND PERSPECTIVES

The cytoskeletal arrangement that regulates circumferential axonal contraction and expansion is just starting to be unveiled. Understanding its structure is likely to be a challenging enterprise as it will most probably rely on the simultaneous detection of multiple axonal components by super-resolution microscopy. Additionally, although axons are generally depicted as straight regular structures, even *in vitro* their courses can be tortuous with complex twisting that may hamper withdrawing straightforward conclusions. If, as suggested by an emergent body of literature, an actomyosin network participates in the fine control of axon diameter, a possible interplay between the axonal subcortical cytoskeleton and the deep axonal actin filaments, as putative anchors of myosin filaments, may need to be explored. This is certainly a very exciting field of research that will further the notion that the cytoskeleton in the axon shaft is likely to be much more dynamic than initially expected.

AUTHOR CONTRIBUTIONS

MS, AC, RP-C and SS wrote the manuscript.

FUNDING

This work from the authors' group was supported by Prémio Melo e Castro—Santa Casa da Misericórdia de Lisboa; by the Infrastructure for NMR, EM and X-rays for Translational

Research (iNEXT); and by FEDER—Fundo Europeu de Desenvolvimento Regional funds through the Norte Portugal Regional Operational Programme (NORTE 2020), Portugal 2020, and by Portuguese funds through FCT—Fundação para a Ciência e a Tecnologia/Ministério da Ciência, Tecnologia e Ensino Superior in the framework of the project NORTE-01-0145-FEDER-028623. AC and RP-C are funded by Fundação para a Ciência e Tecnologia—FCT (fellowships SFRH/BPD/114912/2016 and SFRH/BD/112112/2015, respectively).

ACKNOWLEDGMENTS

We are indebted to Dr. Marco Lampe (EMBL, Heidelberg), for all the enthusiastic technical and conceptual support provided to our analysis of the axonal cytoskeleton.

REFERENCES

Alfei, L., Albani, L. M., Mosetti, A. R., Scarfo, C., and Stefanelli, A. (1991). Cytoskeletal components and calibers in developing fish mauthner axon (Salmo-Gairdneri Rich). *J. Comp. Neurol.* 314, 164–170. doi: 10.1002/cne.903140115

Benshalom, G., and Reese, T. S. (1985). Ultrastructural observations on the cytoarchitecture of axons processed by rapid-freezing and freeze-substitution. *J. Neurocytol.* 14, 943–960. doi: 10.1007/bf01224806

Berger, S. L., Leo-Macias, A., Yuen, S., Khatri, L., Pfennig, S., Zhang, Y. Q., et al. (2018). Localized myosin II activity regulates assembly and plasticity of the axon initial segment. *Neuron* 97, 555.e6–570.e6. doi: 10.1016/j.neuron.2017.12.039

Bray, D. (1984). Axonal growth in response to experimentally applied mechanical tension. *Dev. Biol.* 102, 379–389. doi: 10.1016/0012-1606(84)90202-1

Chéreau, R., Saraceno, G. E., Angibaud, J., Cattaert, D., and Nägerl, U. V. (2017). Superresolution imaging reveals activity-dependent plasticity of axon morphology linked to changes in action potential conduction velocity. *Proc. Natl. Acad. Sci. U S A* 114, 1401–1406. doi: 10.1073/pnas.1607541114

Dennerll, T. J., Joshi, H. C., Steel, V. L., Buxbaum, R. E., and Heidemann, S. R. (1988). Tension and compression in the cytoskeleton of Pc-12 neurites II: quantitative measurements. *J. Cell Biol.* 107, 665–674. doi: 10.1083/jcb.107.2.665

D'Este, E., Kamin, D., Göttfert, F., El-Hady, A., and Hell, S. W. (2015). STED nanoscopy reveals the ubiquity of subcortical cytoskeleton periodicity in living neurons. *Cell Rep.* 10, 1246–1251. doi: 10.1016/j.celrep.2015.02.007

D'Este, E., Kamin, D., Velte, C., Göttfert, F., Simons, M., and Hell, S. W. (2016). Subcortical cytoskeleton periodicity throughout the nervous system. *Sci. Rep.* 6:22741. doi: 10.1038/srep22741

de Waegh, S. M., Lee, V. M. Y., and Brady, S. T. (1992). Local modulation of neurofilament phosphorylation, axonal caliber and slow axonal-transport by myelinating schwann-cells. *Cell* 68, 451–463. doi: 10.1016/0092-8674(92)90183-d

Fan, A., Tofangchi, A., Kandel, M., Popescu, G., and Saif, T. (2017). Coupled circumferential and axial tension driven by actin and myosin influences *in vivo* axon diameter. *Sci. Rep.* 7:14188. doi: 10.1038/s41598-017-13830-1

Fields, R. D. (2011). Signaling by neuronal swelling. *Sci. Signal.* 4:tr1. doi: 10.1126/scisignal.4155tr1

Friede, R. L., and Samorajs, T. (1970). Axon caliber related to neurofilaments and microtubules in sciatic nerve fibers of rats and mice. *Anat. Rec.* 167, 379–387. doi: 10.1002/ar.1091670402

Gallo, G. (2004). Myosin II activity is required for severing-induced axon retraction *in vitro*. *Exp. Neurol.* 189, 112–121. doi: 10.1016/j.expneurol.2004.05.019

Ganguly, A., Tang, Y., Wang, L. N., Ladt, K., Loi, J., Dargent, B., et al. (2015). A dynamic formin-dependent deep F-actin network in axons. *J. Cell Biol.* 210, 401–417. doi: 10.1083/jcb.201506110

Gardner, K., and Bennett, V. (1987). Modulation of spectrin actin assembly by erythrocyte adducin. *Nature* 328, 359–362. doi: 10.1038/328359a0

George, E. B., Schneider, B. F., Lasek, R. J., and Katz, M. J. (1988). Axonal shortening and the mechanisms of axonal motility. *Cell Motil. Cytoskeleton* 9, 48–59. doi: 10.1002/cm.970090106

Gilligan, D. M., Lozovatsky, L., Gwynn, B., Brugnara, C., Mohandas, N., and Peters, L. L. (1999). Targeted disruption of the β adducin gene (*Add2*) causes red blood cell spherocytosis in mice. *Proc. Natl. Acad. Sci. U S A* 96, 10717–10722. doi: 10.1073/pnas.96.19.10717

Goldstein, L. S. B., and Gunawardena, S. (2000). Flying through the *Drosophila* cytoskeletal genome. *J. Cell Biol.* 150, F63–F68. doi: 10.1083/jcb.150.2.F63

Goldstein, S. S., and Rall, W. (1974). Changes of action potential shape and velocity for changing core conductor geometry. *Biophys. J.* 14, 731–757. doi: 10.1016/s0006-3495(74)85947-3

Gotow, T., Tanaka, T., Nakamura, Y., and Takeda, M. (1994). Dephosphorylation of the largest neurofilament subunit protein influences the structure of crossbridges in reassembled neurofilaments. *J. Cell Sci.* 107, 1949–1957.

Greenberg, M. M., Leitao, C., Trogadis, J., and Stevens, J. K. (1990). Irregular geometries in normal unmyelinated axons: a 3D serial EM analysis. *J. Neurocytol.* 19, 978–988. doi: 10.1007/bf01186825

Hammarlund, M., Jorgensen, E. M., and Bastiani, M. J. (2007). Axons break in animals lacking β-spectrin. *J. Cell Biol.* 176, 269–275. doi: 10.1083/jcb.200611117

Han, B. R., Zhou, R. B., Xia, C. L., and Zhuang, X. W. (2017). Structural organization of the actin-spectrin-based membrane skeleton in dendrites and soma of neurons. *Proc. Natl. Acad. Sci. U S A* 114, E6678–E6685. doi: 10.1073/pnas.1705043114

He, J., Zhou, R. B., Wu, Z. H., Carrasco, M. A., Kurshan, P. T., Farley, J. E., et al. (2016). Prevalent presence of periodic actin-spectrin-based membrane skeleton in a broad range of neuronal cell types and animal species. *Proc. Natl. Acad. Sci. U S A* 113, 6029–6034. doi: 10.1073/pnas.1605707113

Heidemann, S. R., and Buxbaum, R. E. (1990). Tension as a regulator and integrator of axonal growth. *Cell Motil. Cytoskeleton* 17, 6–10. doi: 10.1002/cm.970170103

Hill, D. K. (1950). The volume change resulting from stimulation of a giant nerve fibre. *J. Physiol.* 111, 304–327. doi: 10.1113/jphysiol.1950.sp004481

Hill, B. C., Schubert, E. D., Nokes, M. A., and Michelson, R. P. (1977). Laser interferometer measurement of changes in crayfish axon diameter concurrent with action potential. *Science* 196, 426–428. doi: 10.1126/science.850785

Hsieh, S. T., Kidd, G. J., Crawford, T. O., Xu, Z. S., Lin, W. M., Trapp, B. D., et al. (1994). Regional modulation of neurofilament organization by myelination in normal axons. *J. Neurosci.* 14, 6392–6401. doi: 10.1523/JNEUROSCI.14-11-06392.1994

Hsu, A., Tsukamoto, Y., Smith, R. G., and Sterling, P. (1998). Functional architecture of primate cone and rod axons. *Vision Res.* 38, 2539–2549. doi: 10.1016/s0042-6989(97)00370-2

Iwasa, K., and Tasaki, I. (1980). Mechanical changes in squid giant-axons associated with production of action-potentials. *Biochem. Biophys. Res. Commun.* 95, 1328–1331. doi: 10.1016/0006-291x(80)91619-8

Joshi, H. C., Chu, D., Buxbaum, R. E., and Heidemann, S. R. (1985). Tension and compression in the cytoskeleton of Pc-12 neurites. *J. Cell Biol.* 101, 697–705. doi: 10.1083/jcb.101.3.697

Kovács, M., Tóth, J., Hetényi, C., Málnási-Csizmadia, A., and Sellers, J. R. (2004). Mechanism of blebbistatin inhibition of myosin II. *J. Biol. Chem.* 279, 35557–35563. doi: 10.1074/jbc.M405319200

Kriz, J., Zhu, Q. Z., Julien, J. P., and Padjen, A. L. (2000). Electrophysiological properties of axons in mice lacking neurofilament subunit genes: disparity between conduction velocity and axon diameter in absence of NF-H. *Brain Res.* 885, 32–44. doi: 10.1016/s0006-8993(00)02899-7

Kuhlman, P. A., Hughes, C. A., Bennett, V., and Fowler, V. M. (1996). A new function for adducin. Calicium calmodulin-regulated capping of the barbed ends of actin filaments. *J. Biol. Chem.* 271, 7986–7991. doi: 10.1074/jbc.271.14.7986

Lamoureux, P., Buxbaum, R. E., and Heidemann, S. R. (1989). Direct evidence that growth cones pull. *Nature* 340, 156–162. doi: 10.1038/340159a0

Leite, S. C., Sampaio, P., Sousa, V. F., Nogueira-Rodrigues, J., Pinto-Costa, R., Peters, L. L., et al. (2016). The actin-binding protein α-adducin is required for maintaining axon diameter. *Cell Rep.* 15, 490–498. doi: 10.1016/j.celrep.2016.03.047

Leite, S. C., and Sousa, M. M. (2016). The neuronal and actin commitment: why do neurons need rings? *Cytoskeleton* 73, 424–434. doi: 10.1002/cm.21273

Leterrier, C., Dubey, P., and Roy, S. (2017). The nano-architecture of the axonal cytoskeleton. *Nat. Rev. Neurosci.* 18, 713–726. doi: 10.1038/nrn.2017.129

Leterrier, J. F., Käs, J., Hartwig, J., Vegners, R., and Janmey, P. A. (1996). Mechanical effects of neurofilament cross-bridges. Modulation by phosphorylation, lipids and interactions with F-actin. *J. Biol. Chem.* 271, 15687–15694. doi: 10.1074/jbc.271.26.15687

Lukinavičius, G., Reymond, L., D'Este, E., Masharina, A., Göttfert, F., Ta, H., et al. (2014). Fluorogenic probes for live-cell imaging of the cytoskeleton. *Nat. Methods* 11, 731–733. doi: 10.1038/nmeth.2972

Mohandas, N., and Gallagher, P. G. (2008). Red cell membrane: past, present and future. *Blood* 112, 3939–3948. doi: 10.1182/blood-2008-07-161166

Mutalik, S. P., Joseph, J., Pullarkat, P. A., and Ghose, A. (2018). Cytoskeletal mechanisms of axonal contractility. *Biophys. J.* 115, 713–724. doi: 10.1016/j.bpj.2018.07.007 [Epub ahead of print].

Nixon, R. A., Paskevich, P. A., Sihag, R. K., and Thayer, C. Y. (1994). Phosphorylation on carboxyl-terminus domains of neurofilament proteins in retinal ganglion-cell neurons *in-vivo*: influences on regional neurofilament accumulation, interneurofilament spacing, and axon caliber. *J. Cell Biol.* 126, 1031–1046. doi: 10.1083/jcb.126.4.1031

Ogawa, Y., and Rasband, M. N. (2008). The functional organization and assembly of the axon initial segment. *Curr. Opin. Neurobiol.* 18, 307–313. doi: 10.1016/j.conb.2008.08.008

Ohara, O., Gahara, Y., Miyake, T., Teraoka, H., and Kitamura, T. (1993). Neurofilament deficiency in quail caused by nonsense mutation in neurofilament-L gene. *J. Cell Biol.* 121, 387–395. doi: 10.1083/jcb.121.2.387

Perge, J. A., Niven, J. E., Mugnaini, E., Balasubramanian, V., and Sterling, P. (2012). Why do axons differ in caliber? *J. Neurosci.* 32, 626–638. doi: 10.1523/JNEUROSCI.4254-11.2012

Pfister, B. J., Iwata, A., Meaney, D. F., and Smith, D. H. (2004). Extreme stretch growth of integrated axons. *J. Neurosci.* 24, 7978–7983. doi: 10.1523/JNEUROSCI.1974-04.2004

Qu, Y., Hahn, I., Webb, S. E. D., Pearce, S. P., and Prokop, A. (2017). Periodic actin structures in neuronal axons are required to maintain microtubules. *Mol. Biol. Cell* 28, 296–308. doi: 10.1091/mbc.E16-10-0727

Rajagopalan, J., Tofangchi, A., and Saif, M. T. A. (2010). *Drosophila* neurons actively regulate axonal tension *in vivo*. *Biophys. J.* 99, 3208–3215. doi: 10.1016/j.bpj.2010.09.029

Robledo, R. F., Ciciotte, S. L., Gwynn, B., Sahr, K. E., Gilligan, D. M., Mohandas, N., et al. (2008). Targeted deletion of α-adducin results in absent β- and γ-adducin, compensated hemolytic anemia and lethal hydrocephalus in mice. *Blood* 112, 4298–4307. doi: 10.1182/blood-2008-05-156000

Roy, S. (2016). Waves, rings, and trails: the scenic landscape of axonal actin. *J. Cell Biol.* 212, 131–134. doi: 10.1083/jcb.201511016

Saitoh, M., Ishikawa, T., Matsushima, S., Naka, M., and Hidaka, H. (1987). Selective-inhibition of catalytic activity of smooth-muscle myosin light chain kinase. *J. Biol. Chem.* 262, 7796–7801.

Sakaguchi, T., Okada, M., Kitamura, T., and Kawasaki, K. (1993). Reduced diameter and conduction-velocity of myelinated fibers in the sciatic-nerve of a neurofilament-deficient mutant quail. *Neurosci. Lett.* 153, 65–68. doi: 10.1016/0304-3940(93)90078-y

Saxena, S., and Caroni, P. (2007). Mechanisms of axon degeneration: from development to disease. *Prog. Neurobiol.* 83, 174–191. doi: 10.1016/j.pneurobio.2007.07.007

Shaw, G., and Bray, D. (1977). Movement and extension of isolated growth cones. *Exp. Cell Res.* 104, 55–62. doi: 10.1016/0014-4827(77)90068-4

Siechen, S., Yang, S. Y., Chiba, A., and Saif, T. (2009). Mechanical tension contributes to clustering of neurotransmitter vesicles at presynaptic terminals. *Proc. Natl. Acad. Sci. U S A* 106, 12611–12616. doi: 10.1073/pnas.0901867106

Smith, D. H. (2009). Stretch growth of integrated axon tracts: extremes and exploitations. *Prog. Neurobiol.* 89, 231–239. doi: 10.1016/j.pneurobio.2009.07.006

Smith, A. S., Nowak, R. B., Zhou, S., Giannetto, M., Gokhin, D. S., Papoin, J., et al. (2018). Myosin IIA interacts with the spectrin-actin membrane skeleton to control red blood cell membrane curvature and deformability. *Proc. Natl. Acad. Sci. U S A* 115, E4377–E4385. doi: 10.1073/pnas.1718285115

Somlyo, A. P., and Somlyo, A. V. (2003). Ca^{2+} sensitivity of smooth muscle and nonmuscle myosin II: modulated by G proteins, kinases and myosin phosphatase. *Physiol. Rev.* 83, 1325–1358. doi: 10.1152/physrev.00023.2003

Spector, I., Shochet, N. R., Blasberger, D., and Kashman, Y. (1989). Latrunculins—novel marine macrolides that disrupt microfilament organization and affect cell-growth: I. Comparison with cytochalasin D. *Cell Motil. Cytoskeleton* 13, 127–144. doi: 10.1002/cm.970130302

Stephan, R., Goellner, B., Moreno, E., Frank, C. A., Hugenschmidt, T., Genoud, C., et al. (2015). Hierarchical microtubule organization controls axon caliber and transport and determines synaptic structure and stability. *Dev. Cell* 33, 5–21. doi: 10.1016/j.devcel.2015.02.003

Tasaki, I., and Byrne, P. M. (1983). Swelling of frog dorsal-root ganglion and spinal-cord produced by afferent volley of impulses. *Brain Res.* 272, 360–363. doi: 10.1016/0006-8993(83)90584-x

Tasaki, I., and Byrne, P. M. (1988). Large mechanical changes in the bullfrog olfactory-bulb evoked by afferent fiber stimulation. *Brain Res.* 475, 173–176. doi: 10.1016/0006-8993(88)90214-4

Tasaki, I., and Byrne, P. M. (1990). Volume expansion of nonmyelinated nerve-fibers during impulse conduction. *Biophys. J.* 57, 633–635. doi: 10.1016/s0006-3495(90)82580-7

Tasaki, I., and Iwasa, K. (1982). Rapid pressure changes and surface displacements in the squid giant-axon associated with production of action-potentials. *Jpn. J. Physiol.* 32, 69–81. doi: 10.2170/jjphysiol.32.69

Tasaki, I., Kusano, K., and Byrne, P. M. (1989). Rapid mechanical and thermal-changes in the garfish olfactory nerve associated with a propagated impulse. *Biophys. J.* 55, 1033–1040. doi: 10.1016/s0006-3495(89)82902-9

Tofangchi, A., Fan, A., and Saif, M. T. A. (2016). Mechanism of axonal contractility in embryonic *drosophila* motor neurons *in vivo*. *Biophys. J.* 111, 1519–1527. doi: 10.1016/j.bpj.2016.08.024

Uehata, M., Ishizaki, T., Satoh, H., Ono, T., Kawahara, T., Morishita, T., et al. (1997). Calcium sensitization of smooth muscle mediated by a Rho-associated protein kinase in hypertension. *Nature* 389, 990–994. doi: 10.1038/40187

Vicente-Manzanares, M., Ma, X. F., Adelstein, R. S., and Horwitz, A. R. (2009). Non-muscle myosin II takes centre stage in cell adhesion and migration. *Nat. Rev. Mol. Cell Biol.* 10, 778–790. doi: 10.1038/nrm2786

Xu, G., Knutsen, A. K., Dikranian, K., Kroenke, C. D., Bayly, P. V., and Taber, L. A. (2010). Axons pull on the brain, but tension does not drive cortical folding. *J. Biomech. Eng.* 132:071013. doi: 10.1115/1.4001683

Xu, K., Zhong, G. S., and Zhuang, X. W. (2013). Actin, spectrin and associated proteins form a periodic cytoskeletal structure in axons. *Science* 339, 452–456. doi: 10.1126/science.1232251

Yamada, R., and Kuba, H. (2016). Structural and functional plasticity at the axon initial segment. *Front. Cell. Neurosci.* 10:250. doi: 10.3389/fncel.2016.00250

Zhong, G. S., He, J., Zhou, R. B., Lorenzo, D., Babcock, H. P., Bennett, V., et al. (2014). Developmental mechanism of the periodic membrane skeleton in axons. *Elife* 3:e04581. doi: 10.7554/eLife.04581

Zhu, Q. Z., Couillarddesprés, S., and Julien, J. P. (1997). Delayed maturation of regenerating myelinated axons in mice lacking neurofilaments. *Exp. Neurol.* 148, 299–316. doi: 10.1006/exnr.1997.6654

Conflict of Interest Statement: The authors declare that the research was conducted in the absence of any commercial or financial relationships that could be construed as a potential conflict of interest.

frontiers in Cellular Neuroscience

REVIEW
published: 09 October 2018
doi: 10.3389/fncel.2018.00338

Hyperphosphorylation of Tau Associates With Changes in Its Function Beyond Microtubule Stability

Alejandra D. Alonso[1,2,3], Leah S. Cohen[1], Christopher Corbo[4], Viktoriya Morozova[1,2], Abdeslem Elldrissi[1,2], Greg Phillips[1,2] and Frida E. Kleiman[3,5]*

[1]Department of Biology and Center for Developmental Neuroscience, College of Staten Island, The City University of New York, Staten Island, NY, United States, [2]Biology Program, The Graduate Center, The City University of New York, New York, NY, United States, [3]Biochemistry Program, The Graduate Center, The City University of New York, New York, NY, United States, [4]Department of Biology, Wagner College, Staten Island, NY, United States, [5]Department of Chemistry, Hunter College, The City University of New York, New York, NY, United States

Tau is a neuronal microtubule associated protein whose main biological functions are to promote microtubule self-assembly by tubulin and to stabilize those already formed. Tau also plays an important role as an axonal microtubule protein. Tau is an amazing protein that plays a key role in cognitive processes, however, deposits of abnormal forms of tau are associated with several neurodegenerative diseases, including Alzheimer disease (AD), the most prevalent, and Chronic Traumatic Encephalopathy (CTE) and Traumatic Brain Injury (TBI), the most recently associated to abnormal tau. Tau post-translational modifications (PTMs) are responsible for its gain of toxic function. Alonso et al. (1996) were the first to show that the pathological tau isolated from AD brains has prion-like properties and can transfer its toxic function to the normal molecule. Furthermore, we reported that the pathological changes are associated with tau phosphorylation at Ser199 and 262 and Thr212 and 231. This pathological version of tau induces subcellular mislocalization in cultured cells and neurons, and translocates into the nucleus or accumulated in the perinuclear region of cells. We have generated a transgenic mouse model that expresses pathological human tau (PH-Tau) in neurons at two different concentrations (4% and 14% of the total endogenous tau). In this model, PH-Tau causes cognitive decline by at least two different mechanisms: one that involves the cytoskeleton with axonal disruption (at high concentration), and another in which the apparent neuronal morphology is not grossly affected, but the synaptic terminals are altered (at lower concentration). We will discuss the putative involvement of tau in proteostasis under these conditions. Understanding tau's biological activity on and off the microtubules will help shed light to the mechanism of neurodegeneration and of normal neuronal function.

Keywords: tau, PH-tau, hyperphosphorylation, propagation, microtubules, neurodegeneration

OPEN ACCESS

Edited by:
Jesus Avila, Universidad Autonoma de Madrid, Spain

Reviewed by:
Michal Novak, Slovak Academy of Sciences (SAS), Slovakia
Ruben Vidal, Indiana University, Purdue University Indianapolis, United States

****Correspondence:***
Alejandra D. Alonso
alejandra.alonso@csi.cuny.edu

Received: *15 May 2018*
Accepted: *13 September 2018*
Published: *09 October 2018*

Citation:
Alonso AD, Cohen LS, Corbo C, Morozova V, Elldrissi A, Phillips G and Kleiman FE (2018) Hyperphosphorylation of Tau Associates With Changes in Its Function Beyond Microtubule Stability. Front. Cell. Neurosci. 12:338. doi: 10.3389/fncel.2018.00338

INTRODUCTION

Tauopathies are a group of dementias that have in common the formation of intracellular filamentous deposits seeded by the microtubule-associated protein tau, in abnormally hyperphosphorylated form(s). These disorders share a common disease mechanism and includes Alzheimer disease (AD), fronto-temporal dementia with Parkinsonism linked to chromosome 17 (FTDP-17), amyotrophic lateral sclerosis, cortical basal degeneration, dementia pugilistica, Pick's disease, progressive supranuclear palsy, tangle-only dementia, Chronic Traumatic Encephalopathy (CTE) and Traumatic Brain Injury (TBI). Tau inclusions are common among all of these tauopathies leading to diverse phenotypic manifestations, brain dysfunction, and degeneration. These diseases all implicate abnormal tau, with the absence of other disease-specific abnormalities (except in AD), in the onset and/or progression of disease.

Microtubule assembly is promoted and stabilized by the predominantly neuronal protein tau (Weingarten et al., 1975). In the central nervous system, tau has six isoforms derived from a single gene by alternative pro-mRNA splicing (Goedert et al., 1989; Himmler et al., 1989). In the human brain, tau isoforms range in size from 352 to 441 amino acids, with differences in the number of tubulin-binding domain repeats (R), three or four consisting of 31 or 32 amino acids near the C-terminus, or two, one, or no inserts of 29 amino acids near the N-terminus. Under normal conditions, tau is a phosphoprotein, in which isoform expression and degree of phosphorylation are developmentally regulated. However, in the disease state, tau has been found to be abnormally hyperphosphorylated and contains significantly higher phosphate content than the normal tau resulting from the phosphorylation at new sites on the protein (Kopke et al., 1993).

Axonal transport is essential to the growth and survival of a neuron throughout its life. Disruption of microtubules, as are observed in patients with AD, interrupts axonal transport which prevents vesicles and organelles from reaching the synapses. These result in the slow and steady deterioration of the synapses and retrograde degeneration. Mutations of *MAPT*, the tau gene, were discovered in 1998 and co-segregate with the disease in FTDP-17, providing unequivocal evidence that abnormalities in tau alone are enough to cause neurodegenerative disease (Hutton et al., 1998; Poorkaj et al., 1998; Spillantini et al., 1998). We have shown that hyperphosphorylation of tau can result in inhibition of microtubule assembly and can disrupt the preassembled microtubules *in vitro* (Alonso et al., 1994, 1997, 2001b). Though the majority of evidence thus far supports the relationship of tau toxicity with disruption of the microtubule system, emerging evidence suggest that tau biological functions are not restricted to the cytoskeletal system: tau is present in the nuclei (Brady et al., 1995; Greenwood and Johnson, 1995; Frost et al., 2014; Multhaup et al., 2015; Bukar Maina et al., 2016) though this physiological function remains elusive; tau self-acetylation activity has been described but physiological consequences of this modification remains uncertain (Cohen et al., 2013); tau has also been shown to be present in the dendrites under pathological conditions and impair synaptic function (Hoover et al., 2010). More recently, the idea of tau transmitting the disease as a prion-like protein is becoming more attractive. As tau is found in the extracellular space and can be uptaken by neighbor neurons, this tau-mediated pathway might represent an attractive model of therapeutical target to halt neurodegeneration. In this review article, we will discuss the putative mechanisms of tau-induced neurodegeneration in light of the current knowledge and our own experience with tau models.

TAU: PATHOLOGICAL GAIN OF FUNCTION

Tau Isoforms and Post-translational Modifications

The gene for tau, *MAPT*, is located on chromosome 17q21.1. It is a single copy gene which undergoes alternative splicing to generate six isoforms found in the human brain (as reviewed in Andreadis, 2005). The number of N-terminal inserts can vary (0N, 1N, or 2N) as well as the number of C-terminal repeats (3R or 4R). These repeats are located in the microtubule binding domain (MTBD), which can lead to differential polymerization rates when mixed with tubulin. When analyzed in microtubule polymerization reactions, recombinant proteins representing each of these six tau isoforms and the 3R proteins had slower rates of polymerization than 4R proteins independently of the N-terminal composition (Goedert and Jakes, 1990). The 4R and 3R isoforms of tau can be found in an approximately 1:1 ratio in normal adult brains with the 1N form at the highest level (50%), 0N (40%) and 2N (10%; Higuchi et al., 2002). Each of the six isoforms have been found in the brains of AD and other tauopathies (including Downs Syndrome, amyotrophic lateral sclerosis, Niemann-Pick disease Type C and some FTDP-17 mutations) at similar ratios as normal brains (Higuchi et al., 2002; Connell et al., 2005). Other tauopathies, including cortical basil degeneration, progressive supranuclear palsy, and other FTDP-17 mutations, appear to express more 4R proteins than 3R proteins at both the mRNA and protein levels (Higuchi et al., 2002; Connell et al., 2005). Brains from Pick's Disease patients show higher 3R levels than 4R in the sarkosyl insoluble fractions, and this change in the ratio appears to occur post-transcriptionally (Higuchi et al., 2002; Connell et al., 2005).

Tau function is modulated by many post-translational modifications (PTMs) including, but not limited to, phosphorylation, acetylation, ubiquitination and protein fragmentation (as reviewed in Beharry et al., 2014; Alonso et al., 2016). As the review of all of tau PTMs is extremely challenging due to the large number of modified sites and by the coexistence of multiple types of modifications, this review article will focus on how tau changes due to phosphorylation can affect microtubule stability and regulate not fully elucidated tau functions. Many of the PTMs lead to changes in the interaction of tau with other molecules by changing the charge of an amino acid, or by removing a section of the protein as occurs in fragmentation. The cleavage of tau by calpains and/or caspases

can result in molecules that are aggregate-prone which can cause other full-length tau molecules to aggregate with it (Chung et al., 2001; Gamblin et al., 2003; Guillozet-Bongaarts et al., 2005; Mondragón-Rodríguez et al., 2008a,b).

Microtubules and Tau in Alzheimer's Disease

In neurons from patients with AD, there is a decrease in microtubules and a several-fold increase in the concentration of tau (Kopke et al., 1993). There are three different pools of tau in the brains of AD patients: AD tau is most similar to normal tau and is not hyperphosphorylated; AD Phosphorylated tau (AD P-tau) is soluble hyperphosphorylated tau; and paired helical filaments (PHFs)-tau is insoluble and hyperphosphorylated. AD tau in AD brains is decreased by about 60% compared to tau found in normal brain. AD P-tau, as well as normally phosphorylated tau, can be isolated from AD brain in solution (Kopke et al., 1993). Analyzing microtubule-promoting activity of tau from AD brains, we found that AD tau has normal activity in *in vitro* assembly of microtubules assays. Conversely, AD P-tau did not promote microtubule assembly but this activity was recovered upon dephosphorylation with alkaline phosphatase treatment (Alonso et al., 1994; **Figure 1**). Interestingly, we found that AD P-tau inhibited the microtubule assembly promoted by normal tau, MAP1 and MAP2 (Alonso et al., 1997). Pre-incubation of AD P-tau with normal tau prior to the addition to tubulin inhibited not only the normal tau-microtubule–promoting activity but also destroyed microtubules already present. This was probably due to interactions between tau and AD P-tau resulting in the sequestering of normal tau from the tubulin, and suggesting that AD P-tau has prion-like activity.

AD P-Tau Has Prion-Like Properties

The ability of AD P-tau to bind normal tau was verified using a solid phase binding assay (Alonso et al., 1996). Quantitation of this binding was performed using an *in vitro* assay in solution and we observed that the binding of AD P-tau to normal tau was non-saturable (Alonso et al., 1996). Furthermore, analysis by electron microscopy indicated that the products of these reactions were bundles of filaments (Alonso et al., 1996). Based on these results, we hypothesized that the hyperphosphorylation of tau changed its conformation in such a way that this change could be transferred to the normal protein, acting as a prion-like molecule to seed pathological tau self-assembly. The ability of hyperphosphorylated tau to bind normal tau was also observed in yeast, a less complex cellular model (Vandebroek et al., 2005). Expression in yeast of the human four-repeat and three-repeat isoforms demonstrated that these isoforms became phosphorylated at pathological sites and assumed a pathological conformation resulting in aggregate formation. The phosphorylation was modulated by yeast kinases Mds1 and Pho85, orthologs of GSK-3β and cdk5. The Van Leuven group observed many biochemical characteristics similar to those we had already observed with human tau including a positive correlation between tau aggregation and phosphorylation; slower mobility in SDS-PAGE with increased phosphorylation; increase in the formation of filaments with isolated hyperphosphorylated tau, and induction of nucleation, or seeding, of normal-non-P-tau assembly by this hyperphosphorylated tau (Vandebroek et al., 2005). The prion-like properties of hyperphosphorylated tau are due to its biochemical stability, which promotes the aggregation of tau, and are consistent with our observations using hyperphosphorylated tau isolated from Alzheimer brain (Alonso et al., 1996). The conformational change transfer by AD P-tau to normal tau is similar to a property of a prion protein. We were the first to link hyperphosphorylation of tau to these nucleation properties of tau (Alonso et al., 1994, 1997, 2001a).

Hyperphosphorylation Induces Prion-Like Tau Self-Assembly

In AD progression, tau becomes hyperphosphorylated prior to the appearance of neurofibrillary tangles (Bancher et al., 1989). Hyperphosphorylated tau shows a 2-3-fold increase in the number of moles of phosphate per mole of protein

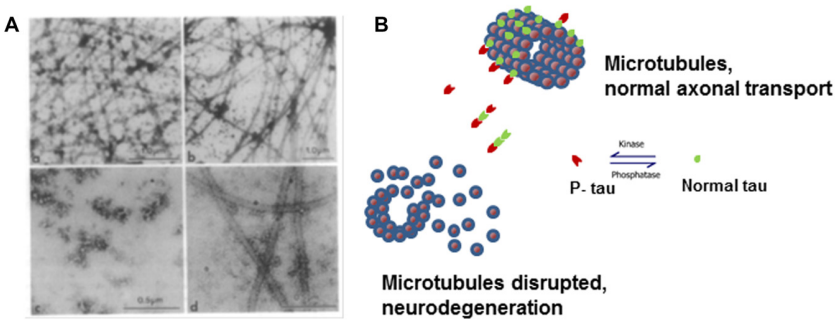

FIGURE 1 | Microtubule disruption can be caused by hyperphosphorylation of tau. **(A)** Electron micrographs showing the products of microtubule assembly. The microtubules were negatively stained with phosphotungstic acid. Rat brain tubulin was placed in an *in vitro* reaction in the presence of **(a)** control acid-soluble tau, **(b)** Alzheimer disease (AD) acid-soluble tau, **(c)** AD Phosphorylated tau (AD P-tau) and **(d)** AD P-tau after dephosphorylation. Very few microtubules were observed in the presence of AD P-tau and dephosphorylation appears to slightly rescue microtubule disruption (Alonso et al., 1994). **(B)** Cartoon model of microtubule disruption due to P-tau sequestration of normal tau away from the tubulin resulting in instability and loss of cytoskeletal structure. Image reproduced as authorized by the editors of Alonso et al. (2016).

(Kopke et al., 1993) which results from the appearance of new phosphorylated sites. The increase in phosphorylation can lead to neuronal degeneration triggered by tau self-assembly into tangles composed of PHFs and straight filaments (SFs). In *in vitro* assays at varying pHs, AD P-tau self-assembled into tangles of PHFs mixed with SFs (Alonso et al., 2001b). The PHFs generated were ∼20 nm wide which narrowed to ∼10 nm at approximately every 80 nm similar to those of AD PHFs. Within the PHFs, protofilaments (4 nm) and SFs (∼15 nm) were observed, also similar to those found in AD. Dephosphorylation of AD P-tau inhibited the self-assembly of tau (Alonso et al., 1994), suggesting that hyperphosphorylation was required for filament formation.

Tau intermolecular association leading to self-assembly appears to occur through the MTBD, whereas the flanking regions can inhibit these interactions (von Bergen et al., 2000; Pérez et al., 2001; Alonso et al., 2004). These tau regions have concentrated positively charged residues, and we postulate that these patches might be responsible for the inhibition of tau self-assembly. Supporting this idea, when two N-terminal inserts of tau, which are highly negative, are present, tau self-assembly is induced (Alonso et al., 2001b). Phosphorylation of tau, which introduces negative charges in these regions, results in tau molecules that acquire the ability to bind normal tau. Tau-tau interactions begin to form when there are ∼4 moles of phosphate per mole of protein, polymerization of tau leading to fibril formation begins when there are ∼10 moles of phosphate per mole of protein (Alonso et al., 2001b, 2004). From these results, we understand that there are at least two different conformational states of tau induced by differential phosphorylation. Similar results are observed by the oxidation of tau by carbonyl addition to Lys residues, which changes positively charged residues to negatively charged ones under oxidative-stress conditions (Santa-María et al., 2005). Consistent with this model, tau molecules modified by truncation, which eliminates the positive fragment, can also induce tau self-assembly (Zhou et al., 2018). In this context, when polyanions are used to induce aggregation, such as RNA, polyGlu, or heparin, it would not be surprising that certain phosphorylation sites appeared to be inhibitory of tau aggregation (Schneider et al., 1999).

To further understand these structural characteristics of tau, six isoforms of tau were expressed heterologously, phosphorylated by treatment with normal brain extract which contains the kinases and we followed their ability to bind normal tau and to inhibit microtubule-promoting activity (Alonso et al., 2001a,b). Proteins treated with rat brain extract became hyperphosphorylated, ∼12 moles phosphate per mole of protein (P-tau), which is similar in phospho-level to AD P-tau. These hyperphosphorylated recombinant proteins were able to self-assemble into tangles of PHFs/SFs (Alonso et al., 2001a,b) and inhibit microtubule assembly activity (Alonso et al., 2001b). Interestingly, the presence of FTDP-17 mutations on tau also induced conformational changes (Jicha et al., 1999), decreased the formation of microtubules (Bunker et al., 2006), and/or increased the ability of tau to self-assemble (Goedert et al., 1999). To analyze why these mutations may alter tau activity in a similar manner as phosphorylation, we generated recombinant tau proteins containing FTDP-17 mutations (R406W, P301L, V337M, or G272V) and incubated in brain extract as above (Alonso et al., 2004). The results showed that the presence of these mutations increased the rate and extent of phosphorylation (∼16–18 moles of phosphate per mole of protein), suggesting that the mutations induced the conformational changes described above (Alonso et al., 2004). These results indicate that the mutated tau molecules are better substrates for kinases than wild-type tau. This effect was observed by another group that reported higher phosphorylation at Ser202 in FTDP-17 mutant tau (Han et al., 2009). Furthermore, these tau mutants showed filament at lower mole amounts of phosphate per mole of protein (Alonso et al., 2004).

Together, our studies indicate that hyperphosphorylation confers upon tau a toxic property, due to its ability to bind normal tau and MAPs. However, we have previously shown that tau filaments do not inhibit microtubule assembly and do not bind other MAPs potentially due to the neutralization of the tau peptide involved in tau self-assembly (Ganguly et al., 2015) by intermolecular interactions (Alonso et al., 2006). Consistent with this, morphometric study of brain biopsy specimen shows that the decrease in microtubule density in AD patients was unrelated to PHF accumulation (Cash et al., 2003). In aged tau transgenic mice from Takashima's group, synapse loss was found in the same brain region as hyperphosphorylated tau (Kimura et al., 2007). Based on these findings, we hypothesize that once tau becomes hyperphosphorylated it can bind normal MAPs and disrupt microtubules, resulting in the interruption of axoplasmic transport and in synaptic degeneration. However, upon tau self-assembly, there will be no contact region for normal MAPs thereby no disruption of the microtubule network and axonal transport. This model is in agreement with the results of the European Tau meeting held last year that has determined that in tauopathies, tau in aggregates is always hyperphosphorylated (Mudher et al., 2017).

What Is Hyperphosphorylated Tau? How Can We Study the Gain of Toxic Function?

Though the defect in tau that leads to aggregation and neurodegeneration is commonly referred to as hyperphosphorylated tau, its definition is still unclear. The debate is whether tau toxic effect is due to a general increase in moles of phosphate per mole of protein regardless as to where these modifications are or whether there is a need for phosphorylation at specific sites within a molecule. Long-range interaction in tau, and other intrinsically disordered proteins (IDPs), are modulated by intra- and inter-molecular interactions and by PTMs, such as phosphorylation, acetylation and others (Bibow et al., 2011). As an IDP, the secondary structure of tau is not defined, however, tau structural information is very important in the formation of PHF/SF in AD brains (Fitzpatrick et al., 2017). This indicates that our observations on tau self-assembly using the whole molecule hold more weight than those using different fragments of tau. The regions

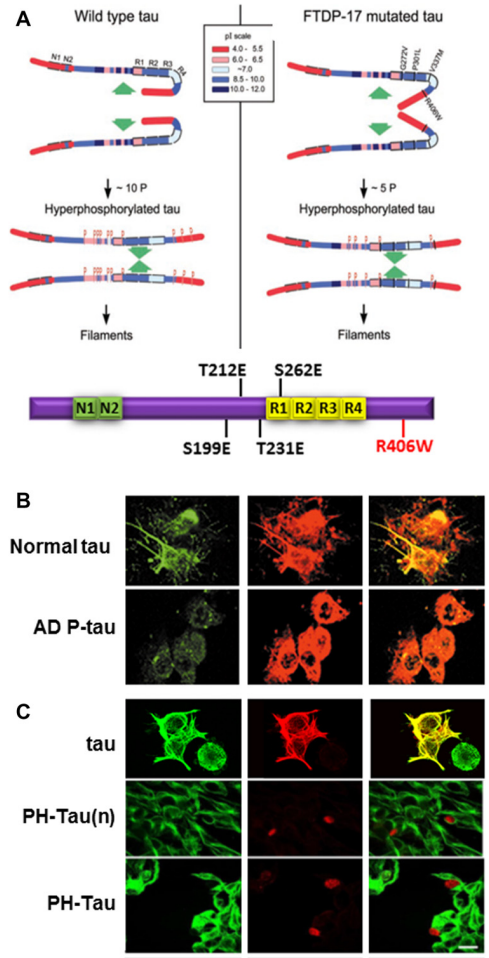

FIGURE 2 | Pathological human tau (PH-Tau) mimics AD P-tau. **(A)** A hypothetical scheme of the phosphorylation-induced self-assembly of wild-type (left) and fronto-temporal dementia with Parkinsonism linked to chromosome 17 (FTDP-17) mutated tau proteins (right). Tau self-assembles mainly through the microtubule binding domain (MTBD)/repeat R2 and R3. The β-structure of R2 and R3 is depicted at the cartoon on the bottom. Regions of tau molecule both N-terminal and C-terminal to the repeats are inhibitory of self-assembly. Hyperphosphorylation of tau neutralizes these basic inhibitory domains, enabling tau-tau interaction. The C-terminal region beyond Pro397 (398–441) is a highly acidic segment masks the repeats. Phosphorylation of tau at Ser396 and/or Ser404 opens this segment, allowing tau-tau interaction through the repeats. FTDP-17 mutations make tau a more favorable substrate for phosphorylation than the wild-type tau. The mutated tau proteins achieve the conformation required to self-assemble at a lower level of incorporated phosphate. Although the FTDP-17 mutant tau proteins have conformations that are more prone to polymerize, in the absence of hyperphosphorylation, the highly basic segments and the C-terminus interfere with polymerization. Phosphorylation sites are indicated by *red P*s at Ser/Thr positions in tau (left panel): 199, 202, 205, 212, 231, 235, 262, 396, 404 and 422; and in FTDP-17 mutant tau (right panel): 199, 212, 231, 262 and 396, respectively. Image taken from Alonso et al. (2004). The Tau cartoon at the bottom indicates the pseudophosphorylated version of tau that is used in our studies, PH-Tau (Di et al., 2016). **(B)** AD P-tau inhibits regeneration of microtubules. To induce microtubule assembly 3T3 cells expressing AD P-tau were incubated with 15% fresh rat brain cytosol in buffer containing 1 mM GTP for 1 h at 37°C. Cells were processed for immunofluorescence staining by using DM1-A Ab against tubulin (green) and 134d rabbit polyclonal Ab

(*Continued*)

FIGURE 2 | Continued

against tau (red). AD P-tau, but not normal tau, inhibited microtubule assembly (Alonso et al., 2006). **(C)** PH-Tau, as AD P-tau, inhibits microtubule assembly when expressed in cells. CHO cells were transfected with either tau, PH-Tau on the normal tau background (PH-Tau(n)), or PH-Tau on the R406W background. After 48 h, the cells were permeabilized with 0.1% Nonidet P-40 before fixing and then processed for immunocytochemistry as described in **(B)**. Merge is shown in yellow. Bar, 25 μm (Alonso et al., 2010). This research was originally published by Alonso et al. (2010).

N-terminal to the MTBD are very basic with a pI of more than nine and are separated from other parts of the protein by Pro residues which are known to introduce kinks in protein structure (**Figure 2A**). The positive charges in this region can mask the negative charges in the MTBD to limit intermolecular interactions. At the start of tau polymerization, three residues in this basic region (Thr212, Thr231 and Ser262) have been shown to be at least 50% phosphorylated, decreasing the pI of the region (Alonso et al., 2004). On the C-terminal side of the MTBD, there is a second basic region and phosphorylation of Ser396 and/or Ser404 may also change the pI, increasing the potential for intermolecular interactions leading to tau self-assembly.

Cells treated with AD P-tau showed decreased microtubule stability (Alonso et al., 2006; **Figure 2B**). Based on our knowledge of phosphorylation events in AD brains, we used phosphomimetics, with and without the FTDP-17 mutation R406W, to determine whether hyperphosphorylation was site-specific. Residues that were determined to have about five moles of phosphate incorporated per mole of protein when self-assembly occurred were changed to Glu to mimic the negative charge of phosphorylation or to Ala as a non-phosphorylatable control. During the initial analysis, nine sites were found to fit the criteria described above Ser199, Ser202, Ser205, Thr212, Thr231, Ser235, Ser262, Ser396 and Ser404. Vectors were generated by site-directed mutagenesis and then transfected into mammalian cells. Tau proteins containing the Ala mutations expressed in cell lines acted similarly to wild-type tau. Conversely, for most of the Glu mutations some tau dissociation from tubulin was observed, but none exhibited complete microtubule disruption (Alonso et al., 2010). Therefore, single phosphorylation events did not appear to change the charge of the molecule enough to convert tau into an AD P-tau like toxic molecule. To try to mimic the toxic nature of tau, double and triple mutant proteins were expressed in cells, and the triple combination of T212E/S235E/S262E was observed to bind weakly to microtubules with a concomitant decrease in tubulin staining. Furthermore, the triple mutant protein aggregated in the cytoplasm and nuclear space and sequestered normal tau similarly to AD P-tau *in vitro* (Alonso et al., 2010; **Figure 2C** compared to **Figure 2B**). A fourth residue, Ser199, was found to be highly phosphorylated in the pseudophosphorylated tau compared to wild-type, suggesting that phosphorylation at this fourth site was able to convert tau into a molecule that had gained toxic function. This toxicity was enhanced by the FTDP-17 mutation R406W (**Figure 2C**). For our future work, we have focused on a molecule called Pathological

Human tau (PH-Tau) containing the phosphomimetics of tau at these four sites (S199, T212, T231 and S262) with the R406W mutation.

Models Used to Study the Role of Tau in AD and Other Neurodegenerative Disorders

Human tau has been overexpressed in many mouse models which have been shown to reproduce the cognitive impairment found in AD (Berger et al., 2007; Eckermann et al., 2007; Lasagna-Reeves et al., 2011; Roberson et al., 2011; Sydow et al., 2011; Webster et al., 2014) and neuronal death[1]. The level of heterologous tau expression in many of these models is very high compared to levels of endogenous tau which could lead to mechanistic differences in the analysis of the neurons. Furthermore, the analysis gets more complicated since tau has six isoforms, many of these models express variations of human tau, with or without mouse tau, and with or without FTDP-17 mutations (Lewis et al., 2000, 2001; Tanemura et al., 2001, 2002; Tatebayashi et al., 2002; Santacruz et al., 2005; Schindowski et al., 2006; Yoshiyama et al., 2007; Hundelt et al., 2011; Flunkert et al., 2013). Neurodegeneration is observed in most of these models, but these mice also have phenotypes not commonly found in AD, i.e., motor deficiencies due to tau accumulation in the spinal cord (Lewis et al., 2000; Yoshiyama et al., 2007). Many groups have switched to the TetOff system to better regulate tau expression levels and localization. This system utilizes the Calmodulin Cam kinase II promoter which leads to expression in the neurons and can be regulated using doxycycline in the diet (Tatebayashi et al., 2002; Hundelt et al., 2011). Tau expressed in most of these model systems become phosphorylated at common Ser/Thr residues that can be linked to pathogenic phosphorylation sites found in AD as compiled by the Hanger group[2].

A top priority in the research of neurodegenerative disease is the development of therapeutics. The mouse models that are generated to express tau phosphomimetics may be a useful tool in developing and analyzing new treatments for dementia related to the hyperphosphorylation of tau. However, as described above, one must be careful to use pseudophosphorylation patterns that induce similar conformational changes in tau to those observed in AD P-tau. For example, a mouse model of hyperphosphorylation which studied a tau molecule containing 10 different pseudophosphorylated residues was generated with no cognitive impairment or neurodegeneration observed (Hundelt et al., 2011). Conversely, our studies, including cell and neuronal culture, *Drosophila*, and a mouse model, which target four specific sites (S199, T212, T231 and S262) on tau resulted in cell death in culture and neurodegeneration and learning deficiencies in *Drosophila* and mice (Alonso et al., 2010; Beharry et al., 2013; Di et al., 2016). Furthermore, we showed that the toxic effect was stronger when the sites chosen for pseudophosphorylation were paired with the FTDP-17 mutation R406W (Alonso et al., 2010; Beharry et al., 2013). In our mouse model that uses the TetOff system, we found that PH-Tau was expressed in the forebrain of the mouse and resulted in the formation of aggregates, synaptic disruption, neurodegeneration, astrocytosis and cognitive decline (Di et al., 2016; **Figure 3**). In this model, PH-tau expression is regulated by the addition (suppressed) or removal (induced) of doxycycline to/from the food and/or water of these animals. When expression was induced, levels of PH-Tau increased up to 14% of total tau protein (i.e., 14 molecules of PH-Tau per 100 molecules of murine tau) and aggregates were detected. When expression was suppressed, there were baseline levels of PH-Tau observed. At this low level, PH-Tau was detected biochemically as oligomers and triggered early cognitive deficits (**Figure 3A**), and loss of synapses in the hippocampus as determined by decreases in synaptic protein levels and quantitation of electron micrographs (**Figures 3B,C**). While PH-Tau was barely detectable by immunohistochemistry in tissue sections from these animals, some PH-Tau was observable and appeared to have translocated in the nucleus. Dramatic neuronal loss was not observed in those animals (**Figure 3D**), but the synaptic changes suggest that at low levels the effect of abnormal tau expression might not be related to changes in the cytoskeleton but to its presence in the nucleus and regulation of protein expression. Interestingly, when PH-Tau expression was induced, cognitive decline was somewhat rescued (**Figure 3A**), the oligomeric forms of PH-Tau decreased but the sarkosyl-insoluble tau increased, and the decrease of synaptic proteins and synaptic terminals appeared to be reversed (**Figures 3B,C**). We can speculate that at higher levels, PH-Tau begins to seed a larger amount of self-aggregation as observed by the formation of sarkosyl-insoluble tau and that this may prevent the toxic protein from entering the nucleus. In fact, tau localization was observed in the perinuclear region of the neurons compared to the nuclear localization in the low expressing brains (data not shown). Neuronal death increased in both the CA1 and CA3 regions of the hippocampus from the mice in which PH-Tau expression was induced (**Figure 3D**). By increasing the expression of PH-Tau, which resulted in the increase of its aggregation propensity into sarkosyl insoluble aggregates, the impairment of cytoskeletal function begins potentially by the sequestering of normal tau from the microtubules, thereby increasing their instability (Di et al., 2016). These results are comparable to the effects of hyperphosphorylated tau in the brains of AD patients. Based on these different observations, it appears that the specific sites that are phosphorylated or modified, rather than the number of sites, may be an important factor in tau toxicity.

CONCLUSIONS AND FUTURE DIRECTIONS

It is apparent that tau hyperphosphorylation is an early event in the disease progression for AD and other tauopathies, though there are other modifications that can also affect the protein. From all that we have learnt through our research and those of our fellow scientists, we can propose that these

[1] Alzforum.Org

[2] https://docs.google.com/spreadsheets/d/1hGYs1ZcupmTnbB7n6qs1r_WVTXHt1O7NBLyKBN7EOUQ/edit#gid=0

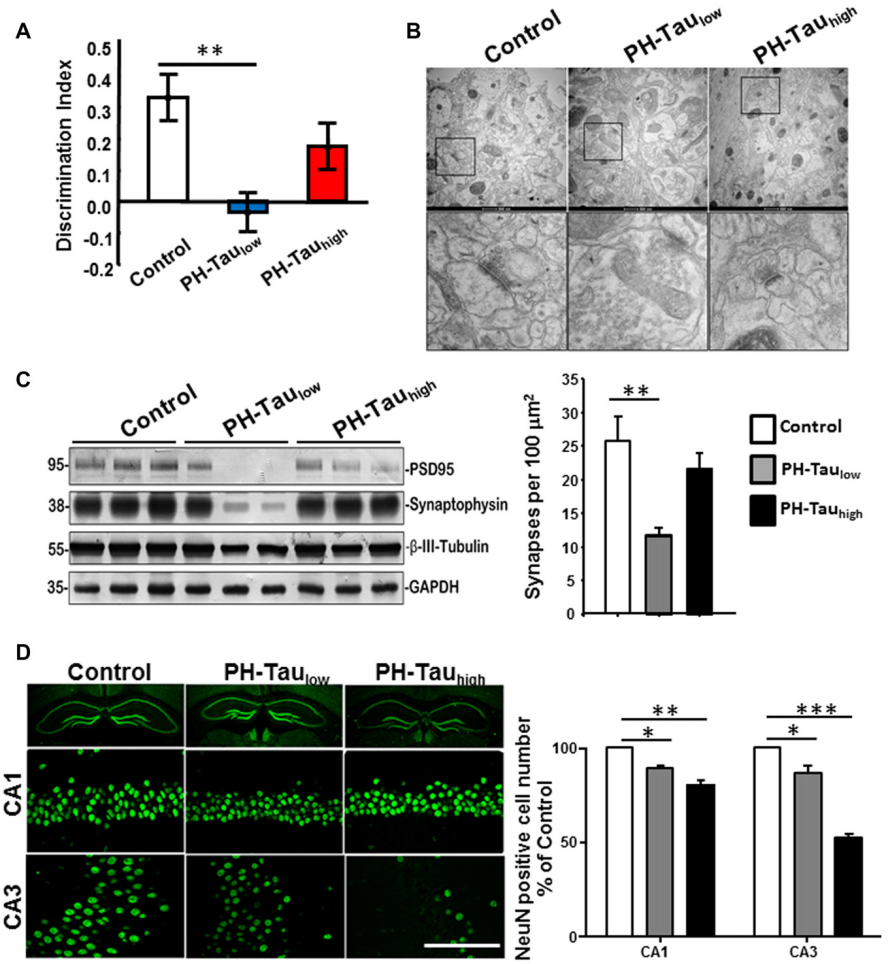

FIGURE 3 | Characterization of PH-Tau mouse model. **(A)** Bigenic mice (12-month old) were tested for behavior deficits in the Novel Object Recognition task. Significant decreases in spatial memory and memory storage were observed. **(B)** PH-Tau$_{low}$ mice shows significant loss of synapses, decreased post-synaptic density and enlarged pre-synaptic portion. Decrease in the length of the post-synaptic density was observed in both PH-Tau$_{low}$ and PH-Tau$_{high}$ mice. Synapses in CA1 stratum radiatum area are shown in the magnified images of square boxes. Quantitation of the number of synapses in the CA1 stratum radiatum area is shown in the bottom of the figure. **(C)** Representative Western blot of mouse hippocampus homogenate. The levels of synaptophysin, PSD95 and β-III-tubulin were measured. Loss of synaptic proteins was observed in PH-Tau$_{low}$ mice. **(D)** Coronal slices of hippocampus stained with antibody NeuN recognizing nucleus of neurons (Left). Scale bar = 50 µm. Counts of the NeuN positive cells in both the CA1 and CA3 regions. $^{*}p < 0.05$, $^{**}p < 0.01$, $^{***}p < 0.001$; right; Di et al. (2016).

modifications of tau can modulate different events at the cellular levels with important consequences for its physiology (**Figure 4**), including converting the protein from a microtubule stabilizer to a microtubule disrupter inducing a pathological state. Changes in the cytoskeleton might not be the only effect of these mdifications on tau. In our lab, tau has been observed to translocate into the cell nucleus (Alonso et al., 2010; Di et al., 2016). Though tau has been shown to interact with nuclear DNA, hyperphosphorylation can alter this interaction with potential changes at the chromatin and transcriptional level, thereby changing its physiological role (Hua and He, 2003; Wei et al., 2008; Padmaraju et al., 2010; Sultan et al., 2011; Qi et al., 2015). Our preliminary studies suggest that tau in the nucleus may also be involved in the regulation of mRNA stability, which would result in potential changes at the transcriptome and proteome by regulating gene expression, thus affecting cellular function during the progression of neurodegeneration. We have recently found that tau can associate with factors involved in mRNA 3′ processing, such as the tumor suppressor p53 (Devany et al., 2013) and PARN deadenylase (Cevher et al., 2010), and that the formation of tau/p53/PARN complex(es) in the nucleus can regulate mRNA 3′ end processing. Interestingly, these interactions are regulated by tau phosphorylation state (Baquero et al., 2015). These changes might happen at very early stages of disease progression.

We have described above how hyperphosphorylated tau can destabilize the microtubules but it can also interact with actin causing a destabilization of these microfilaments (Elie et al., 2015). Disruption of the microfilaments can lead to zeiosis of the cell membrane due to their important role in membrane stability. We have observed that as membrane pinches off

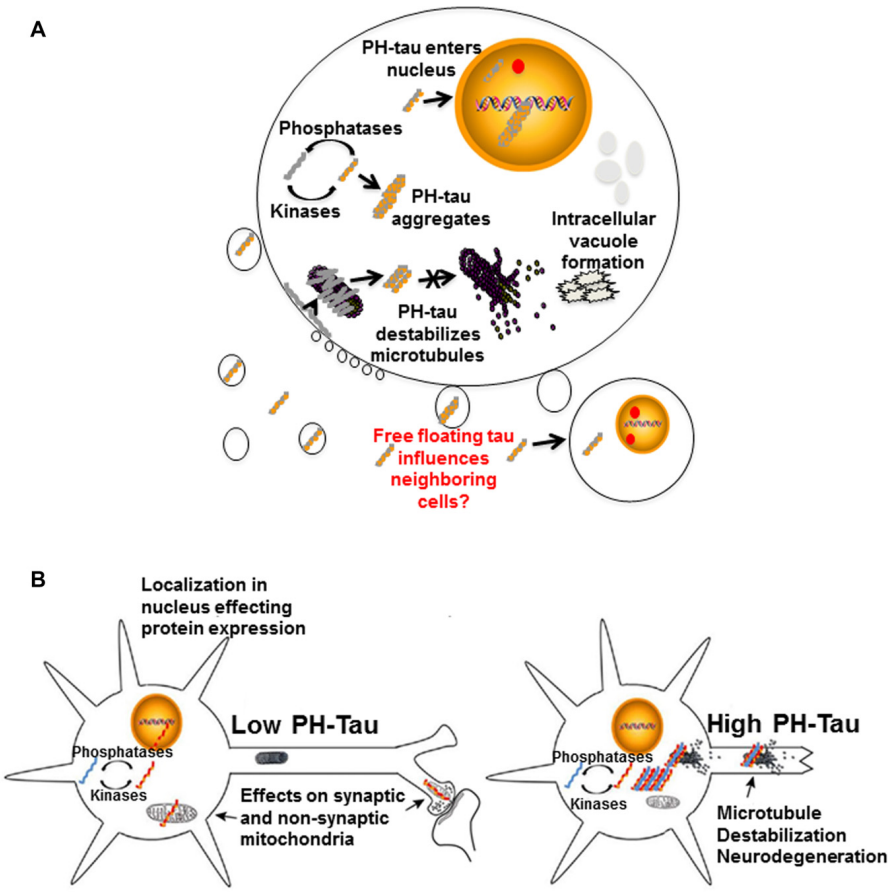

FIGURE 4 | Proposed mechanisms of neurodegeneration. **(A)** Hyperphosphorylation of tau affects multiple cellular processes. PH-tau aggregates are formed when the balance between kinases and phosphorylases is disrupted. The aggregates can begin to disrupt the stability of the microtubules. This toxic molecule has also been shown to translocate into the nucleus, cause intracellular degeneration, protein aggregation and vacuole formation. The presence of tau in the nucleus might be involved in alterations of protein expression. Disruption of the actin cytoskeleton can lead to membrane zeiosis and tau can be released from the cells, potentially propagating the disease to neighboring cells. Image reproduced from Alonso et al. (2016). Permissions were obtained through RightsLink License Number: 4358781157689. **(B)** Left panel: low level of PH-tau expression results in translocation to the nucleus, synaptic dysfunction and mitochondrial disruption. The presence of tau in the nucleus might be involved in alterations of protein expression. Right panel: high levels of PH-Tau expression results in protein aggregation, microtubule disruption and loss of synapses. Loss of cytoskeletal stability leads to neurodegeneration (Alonso et al., 2017). Permission granted to reproduce figure from Alonso et al. (2017).

during exocytosis, there is a release of hyperphosphorylated tau within the vesicles. These tau-containing vesicles have the potential to be taken up through endocytosis, or some other mechanism, into neighboring cells. We were the first to show that hyperphosphorylated tau sequesters healthy tau protein causing it to take on the toxic function of the pathological protein (Alonso et al., 1996). These findings support the prion-like nature of hyperphosphorylated tau which can spread its pathology to surrounding cells by moving from cell to cell and sequestering healthy tau which causes a disruption of all cytoskeleton components, destabilization of the organelles, disruption of protein synthesis and eventually zeiosis induction.

Zeiosis of the cell membrane is expected to release hyperphosphorylated tau-containing membrane vesicles. While we do not know the physiological role, if any, of tau in the extracellular space, it is possible that soluble hyperphosphorylated tau is uptaken by non-affected neurons through its interaction with the muscarinic receptor triggering the signal transduction pathway (Gómez-Ramos et al., 2006, 2008). Supporting this model, our preliminary results indicate that the muscarinic receptors are involved in tau's uptake (Morozova et al., 2017). It is also possible that hyperphosphorylated tau-containing membrane vesicles are taken up by endocytosis by surrounding cells. This model of tau transmission might be therefore addressed with immunotherapy (Iqbal et al., 2018).

Different scenarios can be considered where the levels of hyperphosphorylated tau begin increasing to toxic levels due to kinase overactivity, phosphatase deficiency, failure in the clearance system or a combination of these and others. Early in disease progression, modified tau may translocate into the

nucleus, move to synapses, or interfere with mitochondrial homeostasis (**Figure 4B**, left). Any or all of these physiological changes could lead to cognitive impairment without significant structural changes, as observed in our mouse model under conditions of low PH-Tau expression (Di et al., 2016). As disease progression continues, the levels of pathological tau tend to increase in the neurons to levels that begin to disrupt microtubule stability and other cytoskeletal components which can trigger retrograde neurodegeneration (**Figure 4B**, right). Despite these different mechanisms, it appears that therapeutics to reduce the levels of hyperphosphorylated tau as well as therapeutics aimed at preventing cytoskeleton disruption remain as key targets for tauopathies (Corbo and Alonso, 2011). The development of combination therapies that address the multiple physiological changes induced by hyperphosphorylated tau may help to unravel the process of neurodegeneration and reduce the number of patients affected.

AUTHOR CONTRIBUTIONS

AA is the lead principal investigator (PI) and has contributed in all the experiments and overseen the writing process. LC contributed actively with the writing along with AE (contributor in the behavioral studies), GP (studies of tissue electron microscopy), CC and VM (contributed with cell experiments). All contributed to the writing of the manuscript. FK collaborated with AA in the studies of mRNA processing and tau involvement in the cleavage of the polyA tail. FK wrote the entire manuscript and contributed particularly in the tau-DNA interactions.

FUNDING

The support for this work was provided in part with an National Institutes of Health (NIH) grant R15AG034524-01, 1R15AG058197-01, Alzheimer's Association (Chicago, IL, USA) IIRG-09-133206 and PSC-CUNY.

REFERENCES

Alonso, A. D., Beharry, C., Corbo, C. P., and Cohen, L. S. (2016). Molecular mechanism of prion-like tau-induced neurodegeneration. *Alzheimers Dement.* 12, 1090–1097. doi: 10.1016/j.jalz.2015.12.014

Alonso, A. D., Cohen, L. S., and Morozova, V. (2017). "The tau misfolding pathway to dementia," in *Protein Folding Disorders in the Central Nervous System*, eds J. Ghiso and A. Rostagno (New York, NY: World Scientific Publishing), 83–107.

Alonso, A. D., Di Clerico, J., Li, B., Corbo, C. P., Alaniz, M. E., Grundke-Iqbal, I., et al. (2010). Phosphorylation of tau at Thr212, Thr231, and Ser262 combined causes neurodegeneration. *J. Biol. Chem.* 285, 30851–30860. doi: 10.1074/jbc.M110.110957

Alonso, A. D., Grundke-Iqbal, I., and Iqbal, K. (1996). Alzheimer's disease hyperphosphorylated tau sequesters normal tau into tangles of filaments and disassembles microtubules. *Nat. Med.* 2, 783–787. doi: 10.1038/nm0796-783

Alonso, A. D., Grundke-Iqbal, I., Barra, H. S., and Iqbal, K. (1997). Abnormal phosphorylation of tau and the mechanism of Alzheimer neurofibrillary degeneration: sequestration of microtubule-associated proteins 1 and 2 and the disassembly of microtubules by the abnormal tau. *Proc. Natl. Acad. Sci. U S A* 94, 298–303. doi: 10.1073/pnas.94.1.298

Alonso, A. D., Li, B., Grundke-Iqbal, I., and Iqbal, K. (2006). Polymerization of hyperphosphorylated tau into filaments eliminates its inhibitory activity. *Proc. Natl. Acad. Sci. U S A* 103, 8864–8869. doi: 10.1073/pnas.0603214103

Alonso, A. D., Mederlyova, A., Novak, M., Grundke-Iqbal, I., and Iqbal, K. (2004). Promotion of hyperphosphorylation by frontotemporal dementia tau mutations. *J. Biol. Chem.* 279, 34873–34881. doi: 10.1074/jbc.M405131200

Alonso, A. D., Zaidi, T., Grundke-Iqbal, I., and Iqbal, K. (1994). Role of abnormally phosphorylated tau in the breakdown of microtubules in Alzheimer disease. *Proc. Natl. Acad. Sci. U S A* 91, 5562–5566. doi: 10.1073/pnas.91.12.5562

Alonso, A. D., Zaidi, T., Novak, M., Barra, H. S., Grundke-Iqbal, I., and Iqbal, K. (2001a). Interaction of tau isoforms with Alzheimer's disease abnormally hyperphosphorylated tau and *in vitro* phosphorylation into the disease-like protein. *J. Biol. Chem.* 276, 37967–37973. doi: 10.1074/jbc.M105365200

Alonso, A. D., Zaidi, T., Novak, M., Grundke-Iqbal, I., and Iqbal, K. (2001b). Hyperphosphorylation induces self-assembly of tau into tangles of paired helical filaments/straight filaments. *Proc. Natl. Acad. Sci. U S A* 98, 6923–6928. doi: 10.1073/pnas.121119298

Andreadis, A. (2005). Tau gene alternative splicing: expression patterns, regulation and modulation of function in normal brain and neurodegenerative diseases. *Biochim. Biophys. Acta* 1739, 91–103. doi: 10.1016/j.bbadis.2004.08.010

Bancher, C., Brunner, C., Lassmann, H., Budka, H., Jellinger, K., Wiche, G., et al. (1989). Accumulation of abnormally phosphorylated tau precedes the formation of neurofibrillary tangles in Alzheimer's disease. *Brain Res.* 477, 90–99. doi: 10.1016/0006-8993(89)91396-6

Baquero, J., Ordonez, M., Alonso, A. D., and Kleinman, F. E. (2015). "Tau phosphorylation plays a role in mRNA 3′ end processing," in *Proceedings of the 4th Metabolism in Neurological Disease and 11th Brain Research Conference, Society for Neuroscience*, New York, NY.

Beharry, C., Alaniz, M. E., and Alonso, A. D. (2013). Expression of Alzheimer-like pathological human tau induces a behavioral motor and olfactory learning deficit in *Drosophila melanogaster*. *J. Alzheimers Dis.* 37, 539–550. doi: 10.3233/jad-130617

Beharry, C., Cohen, L. S., Di, J., Ibrahim, K., Briffa-Mirabella, S., and Alonso, A. D. (2014). Tau-induced neurodegeneration: mechanisms and targets. *Neurosci. Bull.* 30, 346–358. doi: 10.1007/s12264-013-1414-z

Berger, Z., Roder, H., Hanna, A., Carlson, A., Rangachari, V., Yue, M., et al. (2007). Accumulation of pathological tau species and memory loss in a conditional model of tauopathy. *J. Neurosci.* 27, 3650–3662. doi: 10.1523/JNEUROSCI.0587-07.2007

Bibow, S., Ozenne, V., Biernat, J., Blackledge, M., Mandelkow, E., and Zweckstetter, M. (2011). Structural impact of proline-directed pseudophosphorylation at AT8, AT100, and PHF1 epitopes on 441-residue tau. *J. Am. Chem. Soc.* 133, 15842–15845. doi: 10.1021/ja205836j

Brady, R. M., Zinkowski, R. P., and Binder, L. I. (1995). Presence of tau in isolated nuclei from human brain. *Neurobiol. Aging* 16, 479–486. doi: 10.1016/0197-4580(95)00023-8

Bukar Maina, M., Al-Hilaly, Y. K., and Serpell, L. C. (2016). Nuclear tau and its potential role in Alzheimer's disease. *Biomolecules* 6:9. doi: 10.3390/biom6010009

Bunker, J. M., Kamath, K., Wilson, L., Jordan, M. A., and Feinstein, S. C. (2006). FTDP-17 mutations compromise the ability of tau to regulate microtubule dynamics in cells. *J. Biol. Chem.* 281, 11856–11863. doi: 10.1074/jbc.M509420200

Cash, A. D., Aliev, G., Siedlak, S. L., Nunomura, A., Fujioka, H., Zhu, X., et al. (2003). Microtubule reduction in Alzheimer's disease and aging is independent of tau filament formation. *Am. J. Pathol.* 162, 1623–1627. doi: 10.1016/S0002-9440(10)64296-4

Cevher, M. A., Zhang, X., Fernandez, S., Kim, S., Baquero, J., Nilsson, P., et al. (2010). Nuclear deadenylation/polyadenylation factors regulate 3′ processing in response to DNA damage. *EMBO J.* 29, 1674–1687. doi: 10.1038/emboj.2010.59

Chung, C. W., Song, Y. H., Kim, I. K., Yoon, W. J., Ryu, B. R., Jo, D. G., et al. (2001). Proapoptotic effects of tau cleavage product generated by caspase-3. *Neurobiol. Dis.* 8, 162–172. doi: 10.1006/nbdi.2000.0335

Cohen, T. J., Friedmann, D., Hwang, A. W., Marmorstein, R., and Lee, V. M. (2013). The microtubule-associated tau protein has intrinsic

acetyltransferase activity. *Nat. Struct. Mol. Biol.* 20, 756–762. doi: 10.1038/nsmb.2555

Connell, J. W., Rodriguez-Martin, T., Gibb, G. M., Kahn, N. M., Grierson, A. J., Hanger, D. P., et al. (2005). Quantitative analysis of tau isoform transcripts in sporadic tauopathies. *Mol. Brain Res.* 137, 104–109. doi: 10.1016/j.molbrainres.2005.02.014

Corbo, C. P., and Alonso, A. D. (2011). Therapeutic targets in Alzheimer's disease and related tauopathies. *Prog. Mol. Biol. Transl. Sci.* 98, 47–83. doi: 10.1016/B978-0-12-385506-0.00002-8

Devany, E., Zhang, X., Park, J. Y., Tian, B., and Kleiman, F. E. (2013). Positive and negative feedback loops in the p53 and mRNA 3′ processing pathways. *Proc. Natl. Acad. Sci. U S A* 110, 3351–3356. doi: 10.1073/pnas.1212533110

Di, J., Cohen, L. S., Corbo, C. P., Phillips, G. R., El Idrissi, A., and Alonso, A. D. (2016). Abnormal tau induces cognitive impairment through two different mechanisms: synaptic dysfunction and neuronal loss. *Sci. Rep.* 6:20833. doi: 10.1038/srep20833

Eckermann, K., Mocanu, M. M., Khlistunova, I., Biernat, J., Nissen, A., Hofmann, A., et al. (2007). The β-propensity of Tau determines aggregation and synaptic loss in inducible mouse models of tauopathy. *J. Biol. Chem.* 282, 31755–31765. doi: 10.1074/jbc.M705282200

Elie, A., Prezel, E., Guérin, C., Denarier, E., Ramirez-Rios, S., Serre, L., et al. (2015). Tau co-organizes dynamic microtubule and actin networks. *Sci. Rep.* 5:9964. doi: 10.1038/srep09964

Fitzpatrick, A. W. P., Falcon, B., He, S., Murzin, A. G., Murshudov, G., Garringer, H. J., et al. (2017). Cryo-EM structures of tau filaments from Alzheimer's disease. *Nature* 547, 185–190. doi: 10.1038/nature23002

Flunkert, S., Hierzer, M., Löffler, T., Rabl, R., Neddens, J., Duller, S., et al. (2013). Elevated levels of soluble total and hyperphosphorylated tau result in early behavioral deficits and distinct changes in brain pathology in a new tau transgenic mouse model. *Neurodegener. Dis.* 11, 194–205. doi: 10.1159/000338152

Frost, B., Hemberg, M., Lewis, J., and Feany, M. B. (2014). Tau promotes neurodegeneration through global chromatin relaxation. *Nat. Neurosci.* 17, 357–366. doi: 10.1038/nn.3639

Gamblin, T. C., Chen, F., Zambrano, A., Abraha, A., Lagalwar, S., Guillozet, A. L., et al. (2003). Caspase cleavage of tau: linking amyloid and neurofibrillary tangles in Alzheimer's disease. *Proc. Natl. Acad. Sci. U S A* 100, 10032–10037. doi: 10.1073/pnas.1630428100

Ganguly, P., Do, T. D., Larini, L., LaPointe, N. E., Sercel, A. J., Shade, M. F., et al. (2015). Tau assembly: the dominant role of PHF6 (VQIVYK) in microtubule binding region repeat R3. *J. Phys. Chem. B* 119, 4582–4593. doi: 10.1021/acs.jpcb.5b00175

Goedert, M., and Jakes, R. (1990). Expression of separate isoforms of human tau protein: correlation with the tau pattern in brain and effects on tubulin polymerization. *EMBO J.* 9, 4225–4230. doi: 10.1002/j.1460-2075.1990.tb07870.x

Goedert, M., Jakes, R., and Crowther, R. A. (1999). Effects of frontotemporal dementia FTDP-17 mutations on heparin-induced assembly of tau filaments. *FEBS Lett.* 450, 306–311. doi: 10.1016/s0014-5793(99)00508-6

Goedert, M., Spillantini, M. G., Jakes, R., Rutherford, D., and Crowther, R. A. (1989). Multiple isoforms of human microtubule-associated protein tau: sequences and localization in neurofibrillary tangles of Alzheimer's disease. *Neuron* 3, 519–526. doi: 10.1016/0896-6273(89)90210-9

Gómez-Ramos, A., Díaz-Hernández, M., Cuadros, R., Hernández, F., and Avila, J. (2006). Extracellular tau is toxic to neuronal cells. *FEBS Lett.* 580, 4842–4850. doi: 10.1016/j.febslet.2006.07.078

Gómez-Ramos, A., Díaz-Hernández, M., Rubio, A., Miras-Portugal, M. T., and Avila, J. (2008). Extracellular tau promotes intracellular calcium increase through M1 and M3 muscarinic receptors in neuronal cells. *Mol. Cell. Neurosci.* 37, 673–681. doi: 10.1016/j.mcn.2007.12.010

Greenwood, J. A., and Johnson, G. V. (1995). Localization and *in situ* phosphorylation state of nuclear tau. *Exp. Cell Res.* 220, 332–337. doi: 10.1006/excr.1995.1323

Guillozet-Bongaarts, A. L., Garcia-Sierra, F., Reynolds, M. R., Horowitz, P. M., Fu, Y., Wang, T., et al. (2005). Tau truncation during neurofibrillary tangle evolution in Alzheimer's disease. *Neurobiol. Aging* 26, 1015–1022. doi: 10.1016/j.neurobiolaging.2004.09.019

Han, D., Qureshi, H. Y., Lu, Y., and Paudel, H. K. (2009). Familial FTDP-17 missense mutations inhibit microtubule assembly-promoting activity of tau by increasing phosphorylation at Ser202 *in vitro*. *J. Biol. Chem.* 284, 13422–13433. doi: 10.1074/jbc.M901095200

Higuchi, M., Trojanowski, J., and Lee, V. M. (2002). "Tau protein and tauopathy," in *Neuropsychopharmacology: The Fifth Generation of Progress*, eds K. L. Davis, D. Charney, J. T. Coyle and C. Nemeroff (Philadelphia, PA: Lippincott, Williams and Wilkins), 1339–1354.

Himmler, A., Drechsel, D., Kirschner, M. W., and Martin, D. W. Jr. (1989). Tau consists of a set of proteins with repeated C-terminal microtubule-binding domains and variable N-terminal domains. *Mol. Cell. Biol.* 9, 1381–1388. doi: 10.1128/mcb.9.4.1381

Hoover, B. R., Reed, M. N., Su, J., Penrod, R. D., Kotilinek, L. A., Grant, M. K., et al. (2010). Tau mislocalization to dendritic spines mediates synaptic dysfunction independently of neurodegeneration. *Neuron* 68, 1067–1081. doi: 10.1016/j.neuron.2010.11.030

Hua, Q., and He, R. Q. (2003). Tau could protect DNA double helix structure. *Biochim. Biophys. Acta* 1645, 205–211. doi: 10.1016/s1570-9639(02)00538-1

Hundelt, M., Fath, T., Selle, K., Oesterwind, K., Jordan, J., Schultz, C., et al. (2011). Altered phosphorylation but no neurodegeneration in a mouse model of tau hyperphosphorylation. *Neurobiol. Aging* 32, 991–1006. doi: 10.1016/j.neurobiolaging.2009.06.007

Hutton, M., Lendon, C. L., Rizzu, P., Baker, M., Froelich, S., Houlden, H., et al. (1998). Association of missense and 5′-splice-site mutations in tau with the inherited dementia FTDP-17. *Nature* 393, 702–705. doi: 10.1038/31508

Iqbal, K., Liu, F., and Gong, C. X. (2018). Recent developments with tau-based drug discovery. *Expert Opin. Drug Discov.* 13, 399–410. doi: 10.1080/17460441.2018.1445084

Jicha, G. A., Rockwood, J. M., Berenfeld, B., Hutton, M., and Davies, P. (1999). Altered conformation of recombinant frontotemporal dementia-17 mutant tau proteins. *Neurosci. Lett.* 260, 153–156. doi: 10.1016/s0304-3940(98)00980-x

Kimura, T., Yamashita, S., Fukuda, T., Park, J. M., Murayama, M., Mizoroki, T., et al. (2007). Hyperphosphorylated tau in parahippocampal cortex impairs place learning in aged mice expressing wild-type human tau. *EMBO J.* 26, 5143–5152. doi: 10.1038/sj.emboj.7601917

Kopke, E., Tung, Y. C., Shaikh, S., Alonso, A. D., Iqbal, K., and Grundke-Iqbal, I. (1993). Microtubule-associated protein tau. Abnormal phosphorylation of a non-paired helical filament pool in Alzheimer disease. *J. Biol. Chem.* 268, 24374–24384.

Lasagna-Reeves, C. A., Castillo-Carranza, D. L., Sengupta, U., Clos, A. L., Jackson, G. R., and Kayed, R. (2011). Tau oligomers impair memory and induce synaptic and mitochondrial dysfunction in wild-type mice. *Mol. Neurodegener.* 6:39. doi: 10.1186/1750-1326-6-39

Lewis, J., Dickson, D. W., Lin, W. L., Chisholm, L., Corral, A., Jones, G., et al. (2001). Enhanced neurofibrillary degeneration in transgenic mice expressing mutant tau and APP. *Science* 293, 1487–1491. doi: 10.1126/science.1058189

Lewis, J., McGowan, E., Rockwood, J., Melrose, H., Nacharaju, P., Van Slegtenhorst, M., et al. (2000). Neurofibrillary tangles, amyotrophy and progressive motor disturbance in mice expressing mutant (P301L) tau protein. *Nat. Genet.* 25, 402–405. doi: 10.1038/78078

Mondragón-Rodríguez, S., Basurto-Islas, G., Santa-Maria, I., Mena, R., Binder, L. I., Avila, J., et al. (2008a). Cleavage and conformational changes of tau protein follow phosphorylation during Alzheimer's disease. *Int. J. Exp. Pathol.* 89, 81–90. doi: 10.1111/j.1365-2613.2007.00568.x

Mondragón-Rodríguez, S., Mena, R., Binder, L. I., Smith, M. A., Perry, G., and Garcia-Sierra, F. (2008b). Conformational changes and cleavage of tau in Pick bodies parallel the early processing of tau found in Alzheimer pathology. *Neuropathol. Appl. Neurobiol.* 34, 62–75. doi: 10.1111/j.1365-2990.2007.00853.x

Morozova, V., Cohen, L. S., and Alonso, A. D. (2017). *Receptor Mediated Prion-Like Propagation of PH-Tau*. Washington, DC: Society for Neuroscience Meeting.

Mudher, A., Colin, M., Dujardin, S., Medina, M., Dewachter, I., Alavi Naini, S. M., et al. (2017). What is the evidence that tau pathology spreads through prion-like propagation? *Acta Neuropathol. Commun.* 5:99. doi: 10.1186/s40478-017-0488-7

Multhaup, G., Huber, O., Buée, L., and Galas, M. C. (2015). Amyloid precursor protein (APP) metabolites APP intracellular fragment (AICD), Aβ42, and Tau in nuclear roles. *J. Biol. Chem.* 290, 23515–23522. doi: 10.1074/jbc.r115.677211

Padmaraju, V., Indi, S. S., and Rao, K. S. (2010). New evidences on Tau-DNA interactions and relevance to neurodegeneration. *Neurochem. Int.* 57, 51–57. doi: 10.1016/j.neuint.2010.04.013

Pérez, M., Arrasate, M., Montejo De Garcini, E., Muñoz, V., and Avila, J. (2001). *In vitro* assembly of tau protein: mapping the regions involved in filament formation. *Biochemistry* 40, 5983–5991. doi: 10.1021/bi002961w

Poorkaj, P., Bird, T. D., Wijsman, E., Nemens, E., Garruto, R. M., Anderson, L., et al. (1998). Tau is a candidate gene for chromosome 17 frontotemporal dementia. *Ann. Neurol.* 43, 815–825. doi: 10.1002/ana.410430617

Qi, H., Cantrelle, F.-X., Benhelli-Mokrani, H., Smet-Nocca, C., Buée, L., Lippens, G., et al. (2015). Nuclear magnetic resonance spectroscopy characterization of interaction of Tau with DNA and its regulation by phosphorylation. *Biochemistry* 54, 1525–1533. doi: 10.1021/bi5014613

Roberson, E. D., Halabisky, B., Yoo, J. W., Yao, J., Chin, J., Yan, F., et al. (2011). Amyloid-β/Fyn-induced synaptic, network and cognitive impairments depend on tau levels in multiple mouse models of Alzheimer's disease. *J. Neurosci.* 31, 700–711. doi: 10.1523/JNEUROSCI.4152-10.2011

Santacruz, K., Lewis, J., Spires, T., Paulson, J., Kotilinek, L., Ingelsson, M., et al. (2005). Tau suppression in a neurodegenerative mouse model improves memory function. *Science* 309, 476–481. doi: 10.1126/science.1113694

Santa-María, I., Smith, M. A., Perry, G., Hernández, F., Avila, J., and Moreno, F. J. (2005). Effect of quinones on microtubule polymerization: a link between oxidative stress and cytoskeletal alterations in Alzheimer's disease. *Biochim. Biophys. Acta* 1740, 472–480. doi: 10.1016/j.bbadis.2004.11.024

Schindowski, K., Bretteville, A., Leroy, K., Bégard, S., Brion, J. P., Hamdane, M., et al. (2006). Alzheimer's disease-like tau neuropathology leads to memory deficits and loss of functional synapses in a novel mutated tau transgenic mouse without any motor deficits. *Am. J. Pathol.* 169, 599–616. doi: 10.2353/ajpath.2006.060002

Schneider, A., Biernat, J., von Bergen, M., Mandelkow, E., and Mandelkow, E. M. (1999). Phosphorylation that detaches tau protein from microtubules (Ser262, Ser214) also protects it against aggregation into Alzheimer paired helical filaments. *Biochemistry* 38, 3549–3558. doi: 10.1021/bi981874p

Spillantini, M. G., Murrell, J. R., Goedert, M., Farlow, M. R., Klug, A., and Ghetti, B. (1998). Mutation in the tau gene in familial multiple system tauopathy with presenile dementia. *Proc. Natl. Acad. Sci. U S A* 95, 7737–7741. doi: 10.1073/pnas.95.13.7737

Sultan, A., Nesslany, F., Violet, M., Bégard, S., Loyens, A., Talahari, S., et al. (2011). Nuclear tau, a key player in neuronal DNA protection. *J. Biol. Chem.* 286, 4566–4575. doi: 10.1074/jbc.M110.199976

Sydow, A., Van der Jeugd, A., Zheng, F., Ahmed, T., Balschun, D., Petrova, O., et al. (2011). Tau-induced defects in synaptic plasticity, learning and memory are reversible in transgenic mice after switching off the toxic Tau mutant. *J. Neurosci.* 31, 2511–2525. doi: 10.1523/JNEUROSCI.5245-10.2011

Tanemura, K., Akagi, T., Murayama, M., Kikuchi, N., Murayama, O., Hashikawa, T., et al. (2001). Formation of filamentous tau aggregations in transgenic mice expressing V337M human tau. *Neurobiol. Dis.* 8, 1036–1045. doi: 10.1006/nbdi.2001.0439

Tanemura, K., Murayama, M., Akagi, T., Hashikawa, T., Tominaga, T., Ichikawa, M., et al. (2002). Neurodegeneration with tau accumulation in a transgenic mouse expressing V337M human tau. *J. Neurosci.* 22, 133–141. doi: 10.1523/JNEUROSCI.22-01-00133.2002

Tatebayashi, Y., Miyasaka, T., Chui, D. H., Akagi, T., Mishima, K., Iwasaki, K., et al. (2002). Tau filament formation and associative memory deficit in aged mice expressing mutant (R406W) human tau. *Proc. Natl. Acad. Sci. U S A* 99, 13896–13901. doi: 10.1073/pnas.202205599

Vandebroek, T., Vanhelmont, T., Terwel, D., Borghgraef, P., Lemaire, K., Snauwaert, J., et al. (2005). Identification and isolation of a hyperphosphorylated, conformationally changed intermediate of human protein tau expressed in yeast. *Biochemistry* 44, 11466–11475. doi: 10.1021/bi0506775

von Bergen, M., Friedhoff, P., Biernat, J., Heberle, J., Mandelkow, E. M., and Mandelkow, E. (2000). Assembly of tau protein into Alzheimer paired helical filaments depends on a local sequence motif (^{306}VQIVYK^{311}) forming β structure. *Proc. Natl. Acad. Sci. U S A* 97, 5129–5134. doi: 10.1073/pnas.97.10.5129

Webster, S. J., Bachstetter, A. D., Nelson, P. T., Schmitt, F. A., and Van Eldik, L. J. (2014). Using mice to model Alzheimer's dementia: an overview of the clinical disease and the preclinical behavioral changes in 10 mouse models. *Front. Genet.* 5:88. doi: 10.3389/fgene.2014.00088

Wei, Y., Qu, M. H., Wang, X. S., Chen, L., Wang, D. L., Liu, Y., et al. (2008). Binding to the minor groove of the double-strand, tau protein prevents DNA from damage by peroxidation. *PLoS One* 3:e2600. doi: 10.1371/journal.pone.0002600

Weingarten, M. D., Lockwood, A. H., Hwo, S. Y., and Kirschner, M. W. (1975). A protein factor essential for microtubule assembly. *Proc. Natl. Acad. Sci. U S A* 72, 1858–1862. doi: 10.1073/pnas.72.5.1858

Yoshiyama, Y., Higuchi, M., Zhang, B., Huang, S. M., Iwata, N., Saido, T. C., et al. (2007). Synapse loss and microglial activation precede tangles in a P301S tauopathy mouse model. *Neuron* 53, 337–351. doi: 10.1016/j.neuron.2007.01.010

Zhou, Y., Shi, J., Chu, D., Hu, W., Guan, Z., Gong, C. X., et al. (2018). Relevance of phosphorylation and truncation of tau to the etiopathogenesis of Alzheimer's disease. *Front. Aging Neurosci.* 10:27. doi: 10.3389/fnagi.2018.00027

Conflict of Interest Statement: The authors declare that the research was conducted in the absence of any commercial or financial relationships that could be construed as a potential conflict of interest.

frontiers in Cellular Neuroscience

ORIGINAL RESEARCH
published: 29 January 2019
doi: 10.3389/fncel.2019.00005

Distinct Functions for Mammalian CLASP1 and -2 During Neurite and Axon Elongation

Carmen Laura Sayas[1,2,3], Sreya Basu[1], Michael van der Reijden[1], Eugenio Bustos-Morán[2†], Marcia Liz[4], Monica Sousa[4], Wilfred F. J. van IJcken[5], Jesus Avila[2,6] and Niels Galjart[1]**

[1]Department of Cell Biology, Erasmus Medical Center, University Medical Center Rotterdam, Rotterdam, Netherlands, [2]Centro de Biología Molecular Severo Ochoa (CSIC-Universidad Autónoma de Madrid (UAM)), Madrid, Spain, [3]Instituto de Tecnologías Biomédicas (ITB), Universidad de La Laguna (ULL), Tenerife, Spain, [4]Instituto de Biologia Molecular e Celular—IBMC and Instituto de Inovação e Investigação em Saúde, University of Porto, Porto, Portugal, [5]Center for Biomics, Erasmus Medical Center, University Medical Center Rotterdam, Rotterdam, Netherlands, [6]Centro Investigación Biomédica en Red Enfermedades Neurodegenerativas (CIBERNED), Madrid, Spain

OPEN ACCESS

Edited by:
Claudio Rivera,
Aix-Marseille Université, France

Reviewed by:
Irina Kaverina,
Vanderbilt University, United States
Orly Reiner,
Weizmann Institute of Science, Israel

***Correspondence:**
Carmen Laura Sayas
csayasca@ull.edu.es
Niels Galjart
n.galjart@erasmusmc.nl

†Present address:
Eugenio Bustos-Morán,
Servicio de Inmunología,Instituto Investigación Sanitaria Princesa (IIS-IP), Hospital Universitario de la Princesa, Universidad Autónoma de Madrid, Madrid, Spain

Received: *22 July 2018*
Accepted: *08 January 2019*
Published: *29 January 2019*

Citation:
Sayas CL, Basu S, van der Reijden M, Bustos-Morán E, Liz M, Sousa M, van IJcken WFJ, Avila J and Galjart N (2019) Distinct Functions for Mammalian CLASP1 and -2 During Neurite and Axon Elongation. Front. Cell. Neurosci. 13:5. doi: 10.3389/fncel.2019.00005

Mammalian cytoplasmic linker associated protein 1 and -2 (CLASP1 and -2) are microtubule (MT) plus-end tracking proteins that selectively stabilize MTs at the edge of cells and that promote MT nucleation and growth at the Golgi, thereby sustaining cell polarity. *In vitro* analysis has shown that CLASPs are MT growth promoting factors. To date, a single CLASP1 isoform (called CLASP1α) has been described, whereas three CLASP2 isoforms are known (CLASP2α, -β, and -γ). Although CLASP2β/γ are enriched in neurons, suggesting isoform-specific functions, it has been proposed that during neurite outgrowth CLASP1 and -2 act in a redundant fashion by modulating MT dynamics downstream of glycogen synthase kinase 3 (GSK3). Here, we show that in differentiating N1E-115 neuroblastoma cells CLASP1 and CLASP2 differ in their accumulation at MT plus-ends and display different sensitivity to GSK3-mediated phosphorylation, and hence regulation. More specifically, western blot (WB) analysis suggests that pharmacological inhibition of GSK3 affects CLASP2 but not CLASP1 phosphorylation and fluorescence-based microscopy data show that GSK3 inhibition leads to an increase in the number of CLASP2-decorated MT ends, as well as to increased CLASP2 staining of individual MT ends, whereas a reduction in the number of CLASP1-decorated ends is observed. Thus, in N1E-115 cells CLASP2 appears to be a prominent target of GSK3 while CLASP1 is less sensitive. Surprisingly, knockdown of either CLASP causes phosphorylation of GSK3, pointing to the existence of feedback loops between CLASPs and GSK3. In addition, CLASP2 depletion also leads to the activation of protein kinase C (PKC). We found that these differences correlate with opposite functions of CLASP1 and CLASP2 during neuronal differentiation, i.e., CLASP1 stimulates neurite extension, whereas CLASP2 inhibits it. Consistent with knockdown results in N1E-115 cells, primary *Clasp2* knockout (KO) neurons exhibit early accelerated neurite and axon outgrowth, showing longer axons than control neurons. We propose a model in which neurite outgrowth is fine-tuned by differentially posttranslationally modified isoforms of CLASPs

acting at distinct intracellular locations, thereby targeting MT stabilizing activities of the CLASPs and controlling feedback signaling towards upstream kinases. In summary, our findings provide new insight into the roles of neuronal CLASPs, which emerge as regulators acting in different signaling pathways and locally modulating MT behavior during neurite/axon outgrowth.

Keywords: cytoskeleton, microtubules, microtubule plus-end tracking proteins, cytoplasmic linker associated proteins (CLASPs), neuronal differentiation, axon outgrowth

INTRODUCTION

Neurons are highly polarized cells, with two biochemically and functionally distinct compartments emerging from the cell body: a long and thin axon that transmits signals, and multiple shorter dendrites that receive signals. This high degree of polarization is crucial for neurons to reach their proper targets and establish synaptic contacts that lead to the formation of a functional nervous system. Neuronal polarization and axon extension are largely controlled by the actin and microtubule (MT) cytoskeletons, and their associated proteins, which transduce extracellular signals into the necessary morphological changes. It is generally assumed that neurite elongation is promoted by MT stabilization (Zhou et al., 2004; Witte et al., 2008; Neukirchen and Bradke, 2011).

The dynamic behavior of the MT network is regulated by different types of MT associated proteins (MAPs), among which are the MT plus-end tracking proteins (+TIPs), a heterogeneous MAP sub-group whose members specifically associate with the ends of growing MTs (Akhmanova and Steinmetz, 2015). Most +TIPs require End Binding (EB) proteins (in particular EB1 or -3) for MT-end binding. By contrast, EB proteins themselves track MT ends autonomously (Bieling et al., 2007, 2008) and they have therefore been termed the "core" +TIPs.

Mammalian cytoplasmic linker associated protein 1 and -2 (CLASP1 and -2) are homologous +TIPs that are encoded by different genes (Akhmanova et al., 2001). Both CLASPs contain a serine/arginine-rich domain in which two short SxIP motifs are embedded, with which CLASPs interact with EB-proteins and bind MT ends (Mimori-Kiyosue et al., 2005; Honnappa et al., 2009). Interestingly, this domain is also responsible for the interaction with the scaffolding protein IQGAP1 (Watanabe et al., 2009), the cell polarity factor PAR3 (Matsui et al., 2015) and the adaptor protein Dab1 (Dillon et al., 2017). CLASPs are further characterized by a C-terminal protein-protein interaction domain, that binds partners like CLIP-115 and -170 (Akhmanova et al., 2001), LL5α and -β (Lansbergen et al., 2006), and GCC185 (Efimov et al., 2007). CLASPs also have so-called TOGL motifs, which are structurally similar to the TOG domains in XMAP215 (Al-Bassam and Chang, 2011), and which are distributed throughout the proteins. Whereas only a single CLASP1 isoform (called CLASP1α) has been described to date, three CLASP2 isoforms are known, termed CLASP2α, -β, and -γ (Akhmanova et al., 2001). The α-isoforms contain three TOGL domains of which the first is located at the N-terminus of the proteins. CLASP2β/γ lack TOGL1 and hence these isoforms only contain two TOGL domains. *In vitro* experiments suggest that CLASPs promote MT growth (Yu et al., 2016; Aher et al., 2018; Lawrence et al., 2018), and that TOGL1 might confer additional properties to CLASP-α isoforms (Yu et al., 2016).

Some of the +TIPs, including CLASPs (Akhmanova et al., 2001), Adenomatous Polyposis Coli (APC; Zhou et al., 2004), and Actin Crosslinking Family 7 (ACF7; Wu et al., 2011) can selectively stabilize MTs in specific regions of the cell upon reception of signaling cues. It is noteworthy that all these +TIPs are regulated by glycogen synthase kinase 3 (GSK3), a constitutively active kinase with a central role in neurite and axon outgrowth (Beurel et al., 2015). GSK3 inactivation results in an increased affinity of CLASP2 for MT ends (Akhmanova et al., 2001; Wittmann and Waterman-Storer, 2005) due to dephosphorylation of CLASP2 in the domain that binds EB-proteins and MTs (Kumar et al., 2009, 2012; Watanabe et al., 2009). Conversely, CLASP2 phosphorylation by GSK3 greatly impairs the ability of CLASP2 to bind MT ends. GSK3, in turn, is controlled by a number of upstream signaling molecules, for example atypical protein kinase C (aPKC), a kinase that induces neurite extension when activated (Shi et al., 2003, 2004). Most models depict a pathway in which an upstream signal leads to the inactivation of GSK3 by phosphorylation on serine 9 (for GSK3β) or 21 (for GSK3α), which in turn results in the dephosphorylation of a GSK3 target, for example a +TIP like APC (Zhou et al., 2004), allowing MT stabilization and neurite elongation.

CLASPs selectively stabilize MTs at the cell cortex in migrating fibroblasts (Akhmanova et al., 2001). They do this by forming complexes with membrane-anchored proteins such as LL5β, thereby attaching MTs to the cell cortex and promoting local MT rescue (Mimori-Kiyosue et al., 2005; Lansbergen et al., 2006). In addition, CLASPs were shown to enhance MT nucleation at the Golgi, in conjunction with GCC185 (Efimov et al., 2007). CLASP function has also been studied during neurite, axon and dendrite outgrowth; however, different results were obtained depending on the organism or neuronal cell type studied and the approach used. This has led to a somewhat confusing view in the field about the precise role of CLASPs in these processes. For example, mutations that inactivate Orbit/MAST, the single *Drosophila melanogaster* ortholog of CLASPs, caused axon guidance defects *in vivo* and led to ectopic crossing of the midline in the central nervous system (Lee et al., 2004), whereas a knockdown of Orbit/MAST in cultured *Drosophila* primary neurons revealed only a small effect on neurite outgrowth (Beaven et al., 2015). *Xenopus laevis* contains a single *CLASP* gene which encodes a protein (XCLASP1) that mostly resembles human CLASP1. The

depletion of XCLASP1 was shown to hamper axon extension (Marx et al., 2013). By contrast, in mammalian neurons, knockdown of CLASP2 in cortical neurons resulted in longer axons (Hur et al., 2011), whereas in hippocampal neurons (HNs) it resulted in shorter axons (Beffert et al., 2012; Dillon et al., 2017). In addition, in dorsal root ganglia (DRG) neurons, the single knockdown of CLASP2 was less effective, but that of CLASP1 or the combined depletion of CLASP1 and -2 impeded neurite outgrowth (Hur et al., 2011).

We have studied the functions of CLASP1 and -2 in differentiating N1E-115 neuroblastoma cells, and in *Clasp2* mouse knockout (KO) neurons. We show that CLASPs have distinct localizations and roles in N1E-115 cells during neurite outgrowth, and that CLASP1 stimulates extension and CLASP2 impairs it. We also demonstrate that *Clasp2* KO HNs undergo significantly faster neurite and axon outgrowth at early stages, suggesting a role for CLASP2 as a negative regulator of neurite/axon extension. We similarly observed enhanced neurite extension in CLASP2-deficient DRG neurons, indicating that CLASP2 acts as a brake in neurite extension in different neuronal types. We attribute the opposing functions of the CLASPs to a different expression and distribution of isoforms in neurons, and a different sensitivity for GSK3. Furthermore, distinct feedback signaling towards upstream kinases, such as GSK3 and PKC, may also distinguish the CLASPs. Our data suggest that the mammalian *Clasp1* and *-2* genes have evolved to couple distinct MT behaviors to specific signaling cascades.

MATERIALS AND METHODS

Antibodies

We used the following commercial primary antibodies (Abs): mouse anti-α-tubulin, mouse anti-β-tubulin, mouse anti-α-Tyrosinated-tubulin, mouse anti-α-Acetylated tubulin, mouse anti-β-actin, and rabbit anti-GAPDH (all from Sigma-Aldrich); mouse anti-βIII tubulin (Promega), mouse anti-α-detyrosinated (Glu)-tubulin (Abcam); mouse anti-GFP (Roche); rabbit anti-Akt-phosphoSer (Ser 473), rabbit anti-GSK3-α/β-phosphoSer (Ser 21/Ser9), rabbit anti-GSK3-α/β (Cell Signaling), rat anti-CLASP1 (#1A6) and -CLASP2 (#12H2, Absea antibodies). We also used previously described primary rabbit anti-CLASP1 [#402, for immunofluorescence (IF), and #2292 for western blot (WB)], and rabbit anti-CLASP2 (#2358, both for IF and WB; Akhmanova et al., 2001). In IF studies, anti-mouse, anti-rabbit or anti-rat secondary antibodies conjugated with either 488, 555 or 594 Alexa fluorochrome, were used (Molecular Probes). HRP-conjugated secondary antibodies used in WB assays (anti-mouse-HRP, and anti-rabbit-HRP) were purchased from Jackson ImmunoResearch.

Cell Culture and Mice

N1E-115 mouse neuroblastoma cells (ATCC) were cultured in Dulbecco's Modified Eagle's Medium (DMEM) containing 10% fetal bovine serum (FBS), 2 mM of L-glutamine, 100 U/ml penicillin and 100 mg/ml streptomycin at 37°C in a 5% CO_2 atmosphere incubator. Cell differentiation was triggered either by overnight serum starvation leading mostly to cell flattening or to neurite extension in some cells, or by culturing the cells for 6–7 days in DMEM containing 2% FBS and 1.25% dimethyl sulfoxide (DMSO), to induce a neuron-like phenotype with long and thin neurites.

Cultures of dissociated hippocampal pyramidal cells from wild-type (WT) and *Clasp2* KO mice were prepared as described (Banker and Cowan, 1977). Upon hippocampi dissection and treatment with papain and DNase (Worthington Biochemical Corporation), 10,000 cells were plated on 12 mm glass-coverslips coated with 100 μg/ml poly-L-lysine and 10 μg/ml laminin in Neurobasal medium containing 10% horse serum. Three hours after plating, medium was replaced with Neurobasal medium supplemented with 2 mM L-glutamine, 2 mM D-pyruvate, 2% B27, 100 U/ml penicillin and 100 mg/ml streptomycin. All culturing media and supplements were purchased from Gibco Invitrogen Corporation. Neuronal cultures were maintained for 1 day *in vitro* (DIV) or 2DIV in a humidified 37°C incubator with 5% CO_2.

Primary sensory DRG neurons were isolated from 4-week-old mice as described (Fleming et al., 2009). Briefly, DRG were digested with 0.125% collagenase IV-S (Sigma-Aldrich) for 1.5 h at 37°C and centrifuged over a 15% albumin cushion for 10 min at 200 *g*. Dissociated neurons were seeded on poly-L-lysine/laminin-coated coverslips in 24-well plates at 5,000 cells per well and cultured for 12 h.

This study was carried out in accordance with European, national and local animal legislation. Protocols were approved by the Erasmus MC animal ethical committee (DEC), the IBMC Ethical Committee, and the Portuguese Veterinarian Board.

Plasmids and Transfection

Previously described expression plasmids were used: GFP-CLASP1α, GFP-CLASP2α, and GFP-CLASP2γ (Akhmanova et al., 2001), mutant constructs GFP-CLASP2-9SA, GFP-CLASP2-8SD, and their WT control (which are slightly shorter versions of GFP-CLASP2γ; Kumar et al., 2009) and EB3-GFP (Stepanova et al., 2003). Different GFP-bearing shRNA plasmids against mouse CLASP1 or CLASP2 and a non-targeting one were purchased from Dharmacon and used in transient transfection experiments. N1E-115 cells were transfected using Lipofectamine TM 2000 (Invitrogen, Carlsbad, CA, USA), following the manufacturer's protocol, for 48 h or 72 h, respectively.

shRNA Constructs, Lentiviral Transduction and Generation of Stable Cell Lines

Five different mouse CLASP1 and mouse CLASP2 shRNA lentiviral constructs (Mission, Sigma-Aldrich) were used in this study. A scramble shRNA construct was used as a control. Constructs were first validated in transient transfection in N1E-115 cells and the two that were most effective in downregulating the endogenous CLASP proteins were used in each case for the lentiviral transduction. For CLASP1 we used TRCN0000253373 (5′CCGGAGATTGGAACCAGACTTATA TCTCGAGATATAAGTCTGGTTCCAATCTTTTTTG3′) and TRCN0000265397 (5′CCGGTTGGGTGAACTCTAGCAATT ACTCGAGTAATTGCTAGAGTTCACCCAATTTTTG3′). For CLASP2 we used TRCN0000183632 (5′ CCGGGAACTTGAAG

AGACGTTAAATCTCGAGATTTAACGTCTCTTCAAGTTC TTTTTTG3′).

Subconfluent HEK-293T cells were cotransfected with each of the selected shRNA constructs along with both pCMVdR8.74 (Addgene) and pMD2G (Addgene) plasmids, using Lipofectamine TM 2000 (Invitrogen) following the manufacturer's protocol. Viruses were collected 48 h post-transfection and used in each case to infect N1E-115 cells for 24 h. Stable cell lines were obtained upon puromycin selection (Sigma-Aldrich) for 2–3 weeks.

Chemicals and Treatments

N1E-115 cells were treated with different chemicals to study their effects on CLASP localization. Three structurally different compounds were used to inhibit GSK3: lithium chloride (LiCl) along with myo-Inositol (as lithium also inhibits Inositol-monophosphatases; sodium chloride was used as a control), SB-216763 (Tocris), or CHIR99021 (abbreviated as CHIR, Tocris Biochemicals). The growth factors insulin (Sigma-Aldrich) and insulin-like growth factor-1 (IGF-1; Millipore) were used to study GSK3-mediated CLASP relocalization at MT plus-ends. Specific inhibitors were used to block the activity of different kinases: Wortmannin, a PI3-K inhibitor; Triciribine, an Akt inhibitor; U0126, a MEK1/2 inhibitor; and R0-318220, a PKC inhibitor. These inhibitors were all purchased from Calbiochem.

Western Blotting and Immunoprecipitation

N1E-115 cells were washed three times with phosphate-buffered saline (PBS) and harvested in cold lysis buffer containing 1% SDS, 1 mM EDTA, 1 mM EGTA, and 25 mM Tris (pH 7.5). Cell extracts were boiled for 10 min, centrifuged for 15 min at 13,000 rpm and sonicated for 15 s. Proteins (25–50 μg) were separated by SDS-PAGE and either transferred to nitrocellulose filters or to PVDF membranes. Filters were blocked with 10% non-fat powder milk or 5% bovine serum albumin (BSA) in Tris-buffered saline (TBS)-0.1% Tween 20 (TBS-T) and incubated with primary antibodies overnight (4°C). After three washes with TBS-T, filters were incubated with the corresponding peroxidase-conjugated secondary antibody (Jackson Immunoresearch) for 1 h, and then washed again with TBS-T three times. Immunoreactivity was visualized by enhanced chemiluminescence detection (ECL, Amersham).

To immunoprecipitate proteins from transfected HEK293 cells a 15 cm plate of HEK293 cells was transfected with 10 μg of construct. After 24 h cells were harvested by centrifugation and dounced in ice-cold lysis buffer [20 mM Tris pH7.5, 150 mM NaCl, 20 mM glycerophosphate, 5 mM MgCl2, 0.1% NP-40, 5% glycerol and IX protease inhibitors (cOmplete, Roche)]. Lysate was cleared by centrifugation at 13,000 rpm for 20 min at 4°C, and the cleared extract was loaded on 100 μL of Protein-A Affi-prep beads (Bio-Rad) cross-linked to 10 μg of rabbit polyclonal GFP antibody (a kind gift of Dr. Kerstin Wendt). The extract was incubated for 2 h at 4°C, washed three times with ice-cold TBS plus 0.01% Tween 20 (TBS-T), and proteins were eluted in 100 mM Glycine, pH 2.0. Rabbit IgG (Santa Cruz, sc-2027) was used as a control.

For cross-linking antibody to beads: 100 μL of Protein-A beads were incubated with 10 μg antibody in 1 mL TBS-T for 2 h at 4°C. Beads were washed three times with 0.2 M Sodium borate (pH 9.0). Then, 1mL of 20 mM DMP (Sigma, D8388) in 0.2 M Sodium borate was added to the beads for 30 min at room temperature. Beads were washed three times in 250 mM Tris pH 8.0 and then three times with TBS-T before binding to extract.

Immunofluorescence, Confocal Microscopy and Image Processing

N1E-115 cells or primary neurons were subject to 100% methanol-1 mM EGTA fixation for 10 min at −20°C, in some instances (depending on the primary antibody used) followed by 4% paraformaldehyde fixation for 15 min at room temperature. Cells were then permeabilized/blocked for 1 h with PBS/0.1% Triton X-100/3% (w/v) BSA. Next, cells were incubated overnight at 4° with primary antibodies (see Antibodies subheading above). After three washes with PBS, cells were incubated for 1 h with secondary antibodies (Molecular Probes). Double or triple-stained cells were analyzed with a DMRBE fluorescence microscope equipped with a Hamamatsu CCD camera or with a Zeiss LSM 510 Meta confocal microscope. ImageJ software (Schneider et al., 2012) was used to quantify CLASP comet density and length. CLASP-comet density was defined as the number of CLASP-highlighted comets counted in delimited cell areas of 100 μm^2. Comet lengths were defined as the distances from the peak fluorescence intensity (FI) at the MT tip to the baseline lattice intensity. A number of MT-comets (specified in the Figure legends in each case) were counted in 5–10 cells per condition in each experiment. ImageJ software was also used to quantify MT stability by measuring FI of α-tyrosinated tubulin (dynamic MTs) and α-acetylated tubulin (stable MTs). For measuring neurite outgrowth in DRGs, immunocytochemistry for βIII-tubulin was performed. All neurites with a length greater than the cell body diameter were measured using ImageJ/NeuronJ (Schneider et al., 2012). Measurements were done with the observer blinded to genotypes in over 100 neurons per condition. Two independent experiments with duplicates were performed.

Live Cell Imaging and Quantification of MT Dynamics

EB3-GFP was transfected into N1E-115 cells, and cells were filmed 24 h after transfection. Cells were either treated with insulin (5 μg/ml) for 15 min or not treated. Cells were observed at 37°C with a LSM 510 confocal laser scanning microscope (Zeiss), as described previously (Stepanova et al., 2003). The optical slice (z-dimension) was set to 1 μm in most experiments. Laser intensity and gain values were adapted to obtain optimal signal-to-noise ratios. Time-lapse series were acquired every 1 or 2 s for 60 or 30 frames, respectively. Images were recorded by using LSM 510 software. To analyze EB3-GFP comet displacements and MT growth speed, the Manual tracking plug-in of ImageJ software was used.

RT-PCR

For RNA isolation, cells were washed with PBS and then collected in TRI Reagent (Sigma). RNA was isolated using the RNeasy Mini Kit (Qiagen). For qRT-PCR, cDNA was generated using Random Primers (Invitrogen) and Superscript IV reverse transcriptase (Thermo Fisher) according to the manufacturer's instructions. PCR reactions were run on a C1000 Thermal Cycler (Bio-Rad) using SyBR-Green (Sigma).

RNA-Sequencing

Purity and quality of isolated RNA was assessed by the RNA 6000 Nano assay on a 2100 Bioanalyzer (Agilent Technologies). One microgram total RNA was used as starting material for Illumina Truseq sequencing. Poly-A tail containing mRNA was purified with oligo-dT attached to magnetic beads. Subsequently, mRNA was fragmented into ∼200 bp fragments followed by first-strand cDNA synthesis using reverse transcriptase and random primers. Next, second-strand synthesis was performed using DNA polymerase I and RNaseH treatment. End-repair, phosphorylation and A-tailing were carried out followed by adapter ligation, size selection on gel and PCR amplification. PCR products were purified by Qiaquick PCR purification. Samples were sequenced on HiSeq 2000 to generate 36 bp reads and a 7 bp index read. Samples were de-multiplexed and aligned to mouse build mm9 reference genome using Tophat alignment software (Trapnell et al., 2009). RNA was further analyzed using Cufflinks (Trapnell et al., 2010).

Statistical Analysis

In each case, sets of 3–5 experiments were performed. All graphing and statistical tests were done using SPSS17 and R software. Statistical analyses were performed using parametric (Student *t*-test or ANOVA, depending on the case) and non-parametric (Mann-Whitney test) tests depending on normality of the data sets (assessed by Shapiro-Wilk). *P*-values are indicated in the graphs and $p < 0.05$ was considered to indicate a statistically significant difference ($^{*}p < 0.05$; $^{**}p < 0.005$; $^{***}p < 0.0005$ and ns, not significant, as stated in bar graphs). All data were expressed as the mean ± standard error of the mean (SEM), or standard deviation (SD), as stated in each case.

RESULTS

Different Distribution of CLASPs in Differentiating Neuronal Cells

To address CLASP1 and CLASP2 function and behavior in neuronal cells, we used the N1E-115 mouse neuroblastoma cell line. Upon serum starvation, most of these cells flatten down; this resembles the first stages of neuronal differentiation, making N1E-115 cells a useful model in which to study the localization, function and regulation of proteins during neuronal development. Surprisingly, the localization of endogenous CLASP1 and CLASP2 at MT growing ends diverged in these early differentiating N1E-115 cells. Whereas CLASP1 was detected in a typical "comet-like" pattern on MT-plus ends throughout the cell (**Figure 1A**, upper panel), CLASP2 was diffuse in the cytosol and was hardly detected at MT plus-ends (**Figure 1A**, lower panel). We quantified CLASP staining at MT plus-ends by measuring both the length of the fluorescence intensity (FI) distribution on individual comets (expressed as comet length in μm) as well as the density of comets in cells (expressed as comet number per 100 μm^2) using EB1 signal as a reference (see "Materials and Methods" section for an explanation on how measurements were done). We found slightly but significantly longer comets for CLASP1 (0.77 ± 0.12 μm) compared to EB1-stained comets (0.69 ± 0.005 μm), and slightly but significantly shorter ones for CLASP2 (0.58 ± 0.009 μm; **Figure 1B**, CLASP1 vs. EB1, $p < 0.005$; CLASP2 vs. EB1, $p < 0.0005$; CLASP1 vs. CLASP2, $p < 0.0005$). However, CLASP1 comet density was higher than that of CLASP2 (CLASP1: 13.95 ± 1.64 comets/100 μm^2; CLASP2: 2.31 ± 0.4 comets/100 μm^2), and almost equaled that of EB1 (19.46 ± 1.23 comets/100 μm^2; **Figure 1C**, CLASP1 vs. CLASP2, $p < 0.0005$; CLASP1 vs. EB1, $p > 0.05$, and CLASP1 vs. CLASP2, $p < 0.0005$). Thus, in flat differentiating cells, CLASP1 accumulates at the distal ends of growing MTs in the cell whereas CLASP2 does not.

To examine the localization of CLASP1 and -2 during neuronal differentiation, we analyzed N1E-115 cells bearing neurites. Notably, whereas CLASP1 staining was prominent in MT plus-ends in the cell body and the proximal part of the neurite, declining progressively in intensity in the growth cone, CLASP2 localized at the ends of growing MTs along the neurite and was enriched in the growth cone (**Figures 1D,E**). The localization of CLASPs was also analyzed in 1DIV mouse primary HNs, a well-established system to study neuronal polarization and differentiation (Dotti et al., 1988). These neurons follow a predictable temporal sequence of morphological changes that involves initial spreading of a lamellipodium around the cell body (stage 1), which is later replaced by 3–4 minor neurites (stage 2), one of which becomes the axon (stage 3). In stage 2 neurons, CLASP2 showed a prominent localization in the distal tips of elongating neurites where CLASP1 was less abundant (**Figure 1F**, left panel). Stage 3 HNs showed CLASP2 enrichment in the growth cones of extending axons, while CLASP1 staining intensity was highest in the cell body and declined along the axon length (**Figure 1F**, right panel). Taken together these data indicate that the localization of CLASP1 and -2 proteins differs during neuronal differentiation, both in neuroblastoma cell lines and in primary neurons.

CLASP1 and CLASP2 Are Differentially Regulated by GSK3

CLASP2 binding to MTs was shown to be regulated by GSK3 (Akhmanova et al., 2001; Wittmann and Waterman-Storer, 2005; Kumar et al., 2009; Watanabe et al., 2009). Because of the similarity of the two proteins in the region that is phosphorylated by GSK3 (Kumar et al., 2012), CLASP1 was assumed to react similarly to this kinase during neurite outgrowth (Hur et al., 2011). However, when we treated N1E-115 cells with LiCl (**Figure 2A**) or SB-216763 (**Supplementary Figure S1A**), two different inhibitors of GSK3, the responses of CLASPs

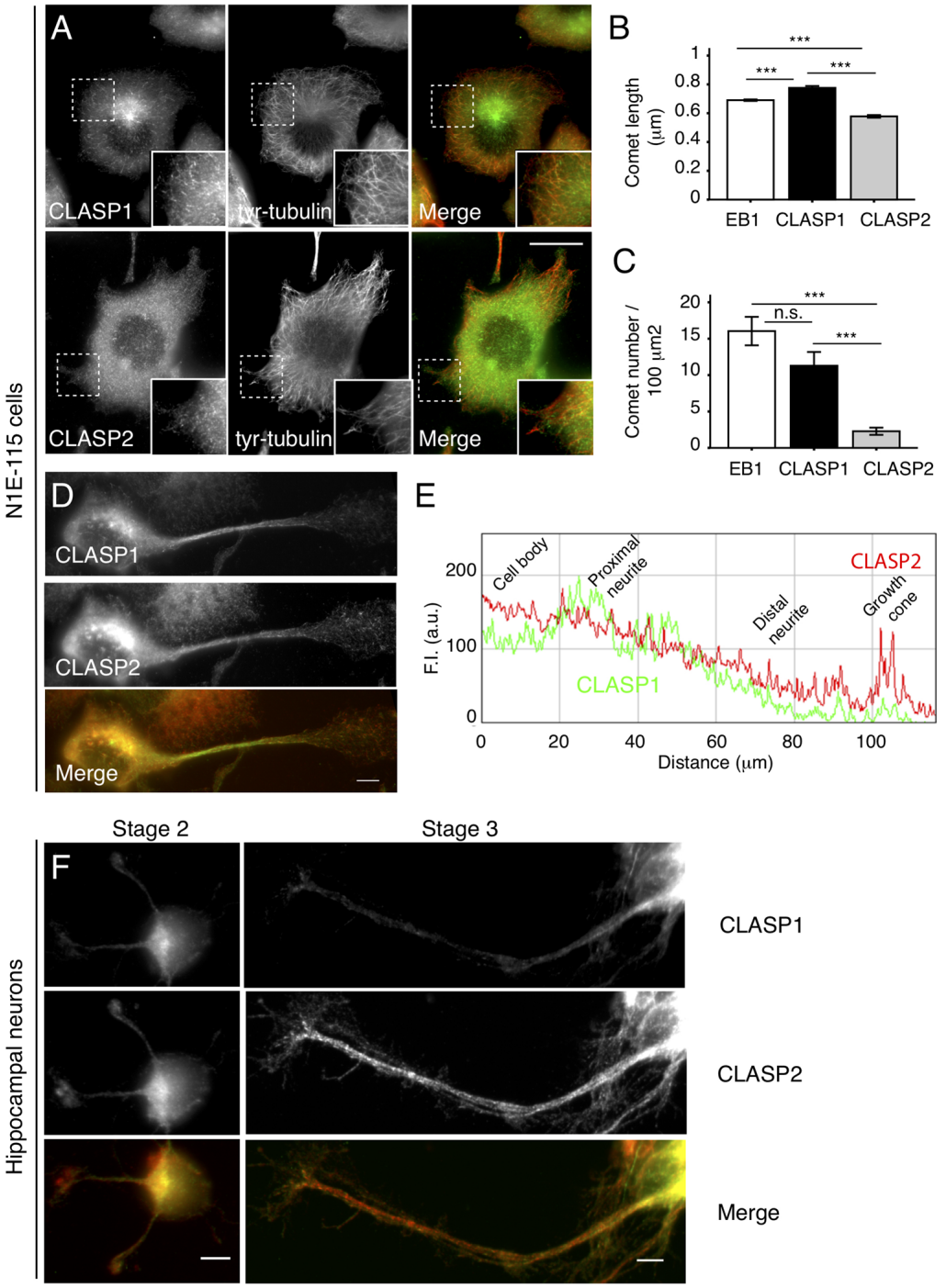

FIGURE 1 | Intracellular distribution of cytoplasmic linker associated protein 1 and -2 (CLASP1 and -2) in differentiating N1E-115 cells and young primary hippocampal neurons (HNs). **(A)** CLASP1 and CLASP2 distribution in flattened N1E-115 cells. Fluorescence images of cells that were serum-deprived overnight, fixed and stained with antibodies against CLASP1 (upper left panel, green in the merged image) or CLASP2 (lower left panel, green in the merged image) and tyrosinated-tubulin (middle panel, red in the merged images). Scale bar = 20 μm. Insets show protein localization in more detail. **(B,C)** Quantification of microtubule (MT) plus-end staining (comets). Comet length **(B)** and density **(C)** of MT plus ends stained with end binding 1 (EB1), CLASP1 or CLASP2 antibodies, were measured in immunofluorescence (IF) images such as depicted in panel **(A)**. Comets were counted in 3–4 squares of 100 μm^2 per cell. EB1: n = 3566 comets/24 cells; CLASP1: n = 699 comets/19 cells; CLASP2: n = 962 comets/48 cells. ANOVA tests were performed in **(B,C)**. Standard error of the mean (SEM) is depicted in each bar graph. **(D)** Localization of CLASP1 and -2 in neurite-bearing N1E-115 cells. Cells were fixed and stained with antibodies against CLASP1 (green in merge) and -2 (red in merge). In **(E)** a plot is shown with the fluorescence intensity (FI) distribution of CLASP1 (green) vs. CLASP2 (red) in process-bearing cells, from the cell body to the growth cone. **(F)** Localization of CLASP1 (green in merge) and -2 (red in merge) in mouse primary 1 days *in vitro* (DIV) HNs, at differentiation stages 2 and 3. Scale bars = 50 μm.

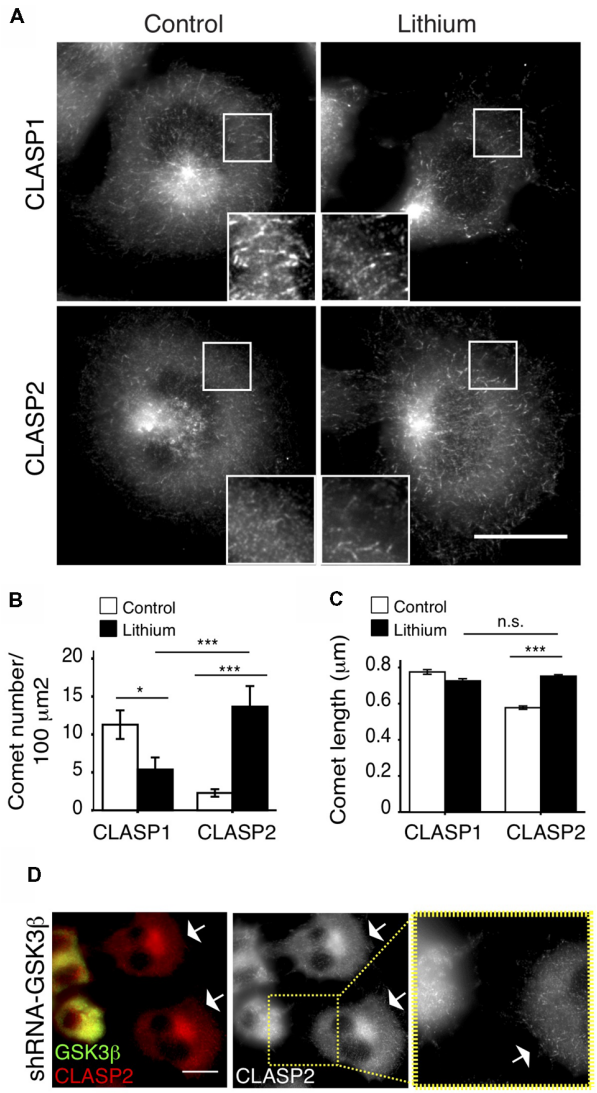

FIGURE 2 | Differential regulation of CLASP1 and -2 by glycogen synthase kinase 3 (GSK3). **(A)** CLASP distribution in control N1E-115 cells and cells treated with lithium chloride (LiCl; Lithium), a well-known GSK3 inhibitor. Serum-starved N1E-115 cells were treated with Lithium (20 mM), along with myo-inositol (10 mM), for 4 h, fixed and stained with antibodies against CLASP1 (upper panels) or CLASP2 (lower panels). The control cells shown were treated with sodium chloride (20 mM) and myo-inositol (10 mM) for 4 h. Scale bar = 20 μm. **(B)** Quantification of CLASP1 and -2 comet density (number of comets/100 μm^2) and **(C)** comet length (in μm). Comets were counted in 3–4 squares of 100 μm^2 per cell. CLASP1: Control: 699; Lithium: 869. CLASP2: Control: 962; Lithium: 1610. Control vs. Lithium treatment was compared for each CLASP. Also, CLASP1 and CLASP2 comet density and lengths were compared after Lithium treatment in **(B,C)**. ANOVA tests were performed. SEM was depicted in each bar graph. **(D)** CLASP2 localization in N1E-115 cells upon GSK3β knockdown by shRNA, in comparison with control (non-transfected) cells. Cells were transfected with shRNA-GSK3β, fixed 72 h later and stained with antibodies against GSK3 (green in merge) and CLASP2 (red in merge). White arrows point to non-transfected cells. Scale bar = 20 μm. Inset shows detailed CLASP2 pattern in control and GSK3 knockdown cell.

in their localization clearly differed. CLASP2, which was mostly diffuse in the cytosol before treatment, became clearly detectable at MT plus-ends upon GSK3 inhibition, while CLASP1 remained accumulated at MT ends (**Figure 2A** and **Supplementary Figure S1A**). Quantification revealed a dramatic increase in the number of CLASP2-stained comets per 100 μm^2 upon LiCl treatment (Control: 2.5 ± 0.8 comets/100 μm^2; LiCl: 13.7 ± 2.5 comets/100 μm^2, $p < 0.0005$), yet a decrease in the number of CLASP1-stained comets (Control: 11.25 ± 2 comets/100 μm^2; LiCl: 5.02 ± 1.8 comets/100 μm^2, $p < 0.05$; **Figure 2B**). Moreover, CLASP2 comets were slightly but significantly longer upon GSK3 inhibition (Control = 0.578 ± 0.09 μm; LiCl = 0.752 ± 0.08 μm, $p < 0.0005$), while CLASP1 comet length did not change (Control = 0.776 ± 0.01 μm; LiCl = 0.726 ± 0.01 μm, $p > 0.05$; **Figure 2C**). Of note, after LiCl treatment, the density of CLASP2 comets was higher than that of CLASP1 ($p < 0.05$; **Figure 2B**), whereas comet length was equal for CLASP1 and CLASP2 ($p > 0.05$; **Figure 2C**). Consistent with these results, the knockdown of GSK3β led to an increased accumulation of CLASP2 at MT ends (**Figure 2D**).

The differential GSK3-mediated phosphorylation of CLASP1 and CLASP2 was further analyzed by western blot. For this experiment N1E-115 cells were first serum-starved overnight and subsequently either treated for 3 h with the GSK3 inhibitor CHIR99021, or not treated (control cells). Cell lysates were then examined for the presence of posttranslationally modified forms of CLASP1 and -2 using specific antibodies. In control cells we detected two CLASP2 bands, which we assume to represent phosphorylated and non-phosphorylated forms of CLASP2α (**Supplementary Figure S1B**, left panel). In cells treated with CHIR99021 only a lower band was detected, i.e., non-phosphorylated CLASP2. We only detected one CLASP1 protein, irrespective of whether cells were treated with CHIR99021 or not (**Supplementary Figure S1B**, right panel). These data are consistent with the immunofluorescent staining patterns of CLASP1 and -2, and suggest that in N1E-115 cells CLASP2 is a GSK3 target, whereas CLASP1 is not.

Ensembl database searches revealed *Clasp1* mRNAs which either contain or lack an internal small exon encoding 36 aminoacids. Interestingly, this exon covers the second SxIP domain of CLASPs with surrounding conserved multiple GSK3 phosphorylation consensus sites described in CLASP2 (Kumar et al., 2009). Using RT-PCR on mRNA derived from N1E-115 cells we examined possible alternative splicing of this exon in the *Clasp1* gene. Results indeed suggest that in N1E-115 cells the SxIP-containing *Clasp1* exon is mostly missing (**Supplementary Figure S1C**). Lack of this small region in CLASP1 might explain why this protein is not sensitive to GSK3 in N1E-115 cells.

We next investigated the localization of GFP-tagged CLASP1 and -2 isoforms. We examined N1E-115 cells expressing GFP-CLASPs at low levels because at high expression levels the GFP-CLASPs started to bind along the MT lattice and even bundled them (data not shown). Importantly, the patterns of the different GFP-tagged isoforms resembled those of the endogenous proteins, i.e., in control cells GFP-CLASP1α localized to MT plus ends, whereas GFP-CLASP2α and -γ were largely diffuse in the cytosol (**Supplementary Figure S2A**

Control-left panels, and **Supplementary Figures S2B,C**). Upon LiCl treatment, the localization of GFP-CLASP1α did not change much compared to the control situation; by contrast GFP-tagged CLASP2α and 2γ changed localization, from diffuse cytosolic to MT plus-ends (**Supplementary Figure S2A**, Lithium-medium panels and **Supplementary Figures S2B,C**). Thus, the distribution of GFP-tagged CLASPs mimics that of the endogenous proteins, both in the control situation and upon GSK3 inhibition. Taken together, our results suggest that in neuroblastoma cells CLASPs are differentially regulated by GSK3.

Regulation of CLASP Distribution by Insulin and IGF-1

CLASP2 plays a role in the stabilization of a subset of MTs oriented towards the leading edge of migrating fibroblasts (Akhmanova et al., 2001; Drabek et al., 2006), and accumulates at MT ends upon GSK3 inhibition in N1E-115 cells. These cells have been shown to form extensive lamellipodia and membrane ruffles in response to insulin (van Rossum et al., 2003), a well-known physiological inducer of GSK3 inhibition (Welsh and Proud, 1993). Therefore, insulin seemed a good candidate regulator of CLASP function by GSK3 in our cell model. After confirming the lamellipodia-forming effect of short insulin treatments (2 μg/ml for 10 min, data not shown), the distribution of each CLASP was analyzed and compared in control vs. insulin-treated cells. Insulin addition induced CLASP2 binding to MT plus-ends throughout the cytoplasm (**Figures 3A,D**), with a prominent localization of long CLASP2-positive comet dashes on cortical regions proximal to cell edges. Interestingly, CLASP2 comets were longer after insulin addition (Control: 0.58 ± 0.009 μm; Insulin: 0.75 ± 0.006 μm, $p < 0.0005$), whereas CLASP1 comets became shorter (Control: 0.77 ± 0.01 μm; Insulin: 0.54 ± 0.02 μm, $p < 0.0005$; **Figure 3B**). CLASP2 comet density was significantly and dramatically enhanced in response to insulin (Control: 2.31 ± 0.4 comets/100 μm^2; insulin: 12.74 ± 1.3 comets/100 μm^2, $p < 0.0005$), while the density of CLASP1-positive dashes was also augmented, but to a lesser extent (Control: 13.95 ± 1.64 comets/100 μm^2; insulin: 21 ± 4.2 comets/100 μm^2, $p < 0.005$; **Figure 3C**). Comparison between CLASP1 vs. CLASP2 comets after treatment revealed that CLASP2 comets were slightly but significantly longer than CLASP1 comets ($p < 0.0005$) whereas the density of CLASP1 comets was higher than that of CLASP2 ($p < 0.05$). Insulin exerted similar effects on GFP-tagged CLASP1 and CLASP2, leading to a clear relocalization of GFP-CLASP2 isoforms α and γ at cortical MT plus-ends (**Supplementary Figure S2A**, insulin right panel, and **Supplementary Figures S2B,C**). In addition, whereas CLASP2 was clearly detected in nascent growth cones and neurite tips in insulin-treated N1E-115 cells, CLASP1 accumulated less prominently in these regions (**Figure 3D**).

IGF-1 evokes similar signaling cascades as insulin (Laurino et al., 2005) and has similar effects on CLASP2 localization in N1E-115 cells (data not shown). Since IGF-1 has been shown to stimulate neuronal polarity, axon extension and membrane expansion in primary neurons (Feldman et al., 1997; Pfenninger et al., 2003), we checked the effect of adding IGF-1 to 1DIV mouse HNs on CLASP localization. As described (Pfenninger et al., 2003), IGF-1 induced an expansion of the growth cone area, and we observed a concomitant redistribution of CLASP2 (**Figure 3E**). Therefore, CLASP2 distribution in growth cones can be regulated by extracellular signals involved in neuronal polarity and neurite extension. In summary, our data show that insulin provokes an overall accumulation of CLASP2 at MT-plus

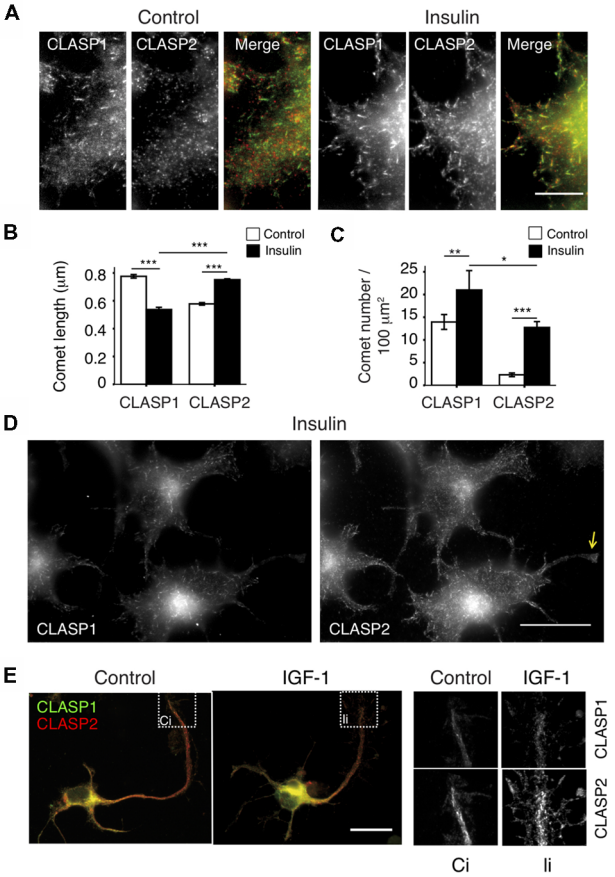

FIGURE 3 | Differential regulation of CLASP1 and -2 by Insulin and insulin-like growth factor-1 (IGF-1). **(A)** Insulin regulates CLASP1 and -2 distribution differently. Serum-starved N1E-115 cells were either treated with vehicle (Control) or insulin (2 μg/ml for 10 min), and subsequently fixed and stained with antibodies against CLASP1 (green in merge) and CLASP2 (red in merge). Double IF confocal images of endogenous CLASP1 and CLASP2 at edges of control and insulin-treated cells are shown. Scale bar = 20 μm. **(B,C)** Quantification of MT plus-ends. Average CLASP comet lengths **(B)** or MT density (number of MT plus-ends stained by CLASPs per 100 μm^2, **C**) before and after insulin addition are depicted ± SEM. Comets were compared in Control cells vs. Insulin-treated cells for each CLASP. CLASP1 and CLASP2 comet lengths and density were also compared post-treatment. ANOVA tests were performed. **(D)** CLASP2, but not CLASP1, localizes prominently in neurite tips and growth cones in insulin-treated N1E-115 cells, as shown in serum starved cells, fixed and stained with anti-CLASP1 and CLASP2. Yellow arrow points to a neurite tip. Scale bar = 20 μm. **(E)** IGF-1 induces CLASP2 relocalization to enlarged growth cones in 1DIV mouse HNs. Neurons were fixed and stained with anti-CLASP1 (green in merge) and anti-CLASP2 (red in merge). Insets show details of CLASPs localization in growth cones in control (Ci) and IGF-1-treated (Ii) neurons. Scale bar = 20 μm.

ends, with more and longer comets. This effect is different for CLASP1, with increased number but shorter CLASP1-stained comets, pointing to insulin as a differential regulator of CLASP function in neuronal cells. IGF-1 resembles insulin in its actions on CLASP localization in 1DIV hippocampal primary neurons.

Acetylation is a posttranslational modification (PTM) on tubulin that is often used as indicator of MT stability (Cambray-Deakin and Burgoyne, 1987). In control N1E-115 cells, only a few acetylated MTs were present, localized in the perinuclear region together with CLASP2 (**Supplementary Figure S3A**, upper panel). After insulin addition, cells showed a dense array of acetylated MTs oriented toward the lamellipodia cell edge, which correlated with CLASP2 comets (**Supplementary Figure S3A**, lower panel), similar to what occurs in polarized migrating cells (Akhmanova et al., 2001). Insulin also induced a net increase in acetylated tubulin in these cells (**Supplementary Figure S3B**). We counted the total number of growing MTs per μm^2 before and after insulin addition, using an antibody against EB1, and found that insulin did not significantly alter the amount of growing MTs; however, the length of EB1 comets was reduced after insulin treatment (data not shown). In confocal time-lapse experiments we confirmed that EB1-GFP comets were shortened in response to insulin (data not shown), and that MT growth speed, as measured by tracking EB1-GFP comets, was reduced ($p < 0.05$; **Supplementary Figure S3C**). Taken together these results indicate that in serum-starved N1E-115 cells insulin induces the stabilization of a subset of MTs that are oriented towards the lamellipodial cell edge and that become acetylated. The accumulation of CLASP2 at the ends of growing MTs in insulin-treated cells correlates with a reduced MT growth rate, suggesting an important role for CLASP2 in the dampening of MT polymerization speed. These data are consistent with *in vitro* properties reported for CLASPs, which have been shown to reduce MT growth rate and cause persistent MT growth (Yu et al., 2016; Aher et al., 2018; Lawrence et al., 2018).

Feedback Signaling by the CLASPs

Since the effect of insulin on CLASP2 binding to MT plus ends was more pronounced than on CLASP1 in N1E-115 cells, we focused on CLASP2 for our subsequent signaling analysis. N1E-115 cells were pretreated with inhibitors of either PI3-K (Wortmannin or LY-294002) or Akt (Triciribine) in order to assess their role on insulin-mediated CLASP2 relocalization to MT plus-ends. Both Wortmannin and LY-294002 abolished insulin-induced CLASP2 accumulation at MT plus tips (**Figure 4A**, upper panel, and data not shown), concomitant with an inhibition of lamellipodia formation as previously reported (van Weering et al., 1998). However, Akt inhibition did not abolish but enhanced the insulin-induced increase in CLASP2 comet density (**Figure 4A**, lower panel, compare with **Figures 3A,D**). WB analysis revealed the correct action of the respective inhibitors on PI3K and Akt in N1E-115 cells (**Figure 4B**). Of note, while Wortmannin blocked GSK3 serine phosphorylation and its concomitant inhibition, Triciribine did not abolish the increase in GSK3-PS levels, suggesting first that Akt is not involved in insulin-mediated GSK3 inhibition in N1E-115 cells and second that GSK3 inhibition is crucial for CLASP2 relocalization after insulin treatment. To confirm the latter point, a constitutively active mutant of GSK3β (Ser9 replaced by Ala, and therefore non-phosphorylatable) was expressed in N1E-115 cells and the effect of insulin on CLASP2 was tested. In insulin-treated and GSK3β-S9A-HA transfected cells, CLASP2 was mainly diffuse in the cytoplasm as compared with the surrounding non-transfected cells in which CLASP2 accumulated at MT growing ends (**Figure 4C**). These results indicate that insulin-induced GSK3 phosphorylation and inhibition leads to CLASP2 relocalization downstream of PI3-K, but these processes are not mediated by Akt.

The observations that insulin treatment gives rise to lamellipodia and stable MTs, that insulin-mediated CLASP2 relocalization to MT plus-ends involves inactivation of GSK3, and that CLASP2 is a direct substrate of GSK3 (Kumar et al., 2009) are all consistent with CLASP2 acting downstream of GSK3. However, the possibility that CLASP2 might crosstalk with GSK3 has never been tested. For that purpose, we examined whether knockdown of CLASP2 caused GSK3 serine phosphorylation. We transiently depleted CLASP2 in N1E-115 cells using four independent shRNAs. Strikingly, in each case we found a significant increase in the phosphorylation state of GSK3α/β (**Figure 4D**). We extended these studies to N1E-115 cells that were stably depleted of either CLASP1 or CLASP2. Depletion of either CLASP induced an increase in the level of phosphorylated GSK3α/β (**Figure 4E**). We next tested the effect of inhibitors of three important GSK3 regulators (i.e., MEK1/2, PKC, and AKT). Inhibition of MEK1/2 or AKT did not affect the increased phosphorylation of GSK3 after CLASP depletion (**Figure 4F**). By contrast, inhibition of PKC significantly impaired this effect both after CLASP1 and CLASP2 knockdown (**Figure 4F**). Finally, we observed that knockdown of CLASP2—but not of CLASP1—caused the phosphorylation, and thus activation, of PKC (**Figure 4G**).

CLASP2 has been shown to interact with the cell polarity factor PAR3; this interaction is required for association with, and phosphorylation by, aPKC (Matsui et al., 2015). It is noteworthy that the interaction with PAR3 is in the GSK3-sensitive S/R-rich domain of CLASP2 that is also responsible for the interaction with EB-proteins. Mutant forms of CLASP2 have been made, in which all GSK3 phosphorylation sites were either mutated to alanine (9SA, phosphorylation-resistant) or aspartic acid (8SD, phosphorylation-mimic); the association of these mutants with MT ends was shown to be enhanced or reduced, respectively, as compared to WT protein (Kumar et al., 2009). We tested whether the interaction between CLASP2 and aPKC was influenced by these mutations by performing immunoprecipitations in cells expressing WT GFP-CLASP2, GFP-CLASP2-9SA, or -8SD, and examining co-precipitation of active (i.e., phosphorylated) aPKC. Interestingly, we only detected an interaction between WT GFP-CLASP2 and phospho-aPKC, but not with either of the mutant GFP-CLASP2 proteins (**Figure 4H**). These data suggest that modification of the GSK3 sites in the S/R domain of CLASP2 abrogates the interaction with active aPKC.

Our combined data suggest that the shRNA-mediated depletion of either CLASP1 or CLASP2 causes serine phosphorylation of GSK3; in addition, CLASP2 depletion

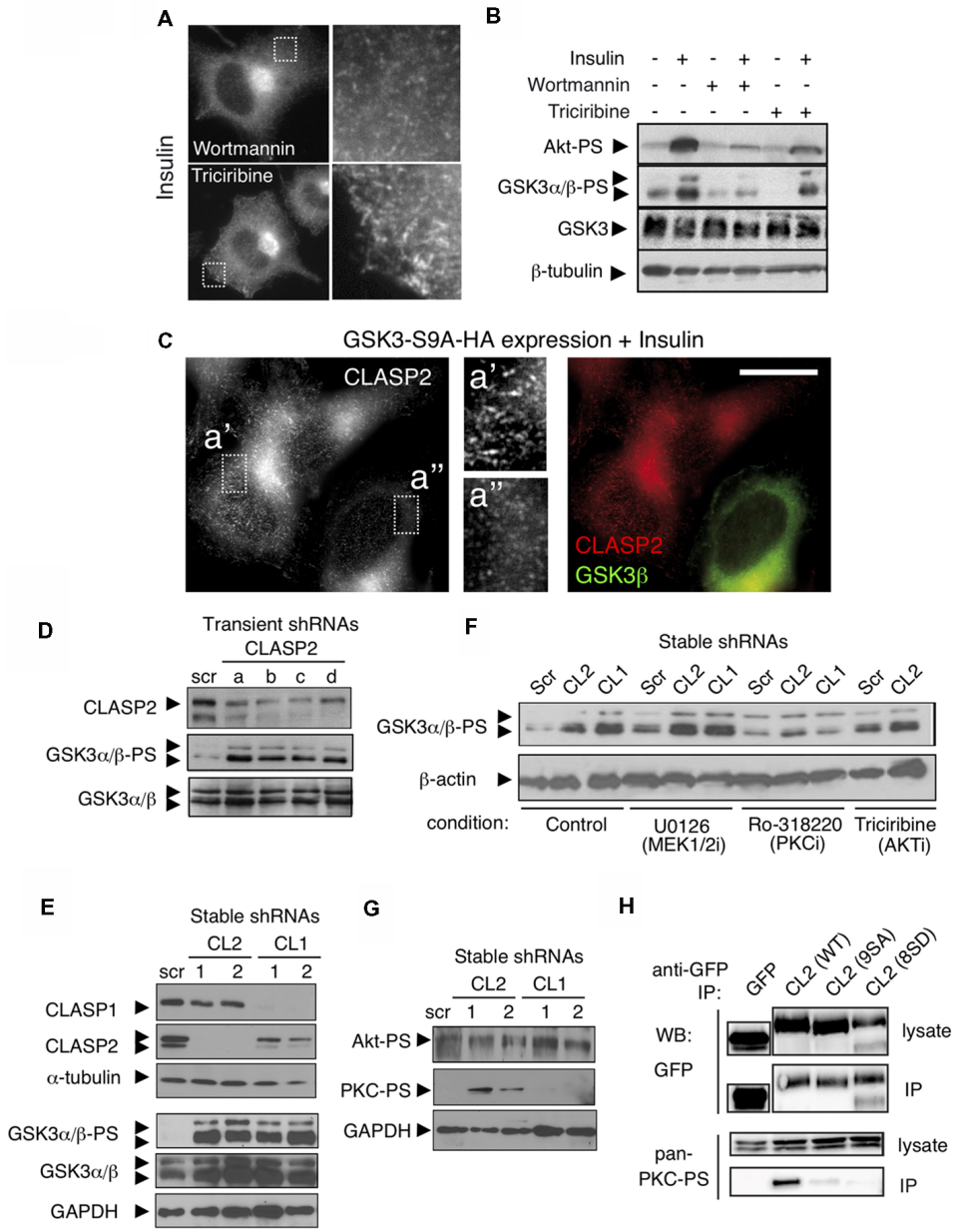

FIGURE 4 | Knockdown of the CLASPs reveals a role in feedback loop signaling. **(A)** Inhibition of PI3K but not of Akt, blocks Insulin-induced binding of CLASP2 to MT plus-ends. CLASP localization was assessed by IF in serum starved insulin-treated (2 μg/ml for 10 min) N1E-115 cells, pretreated with Wortmannin (PI3K inhibitor, 100 nM, 30 min) or Triciribine (Akt inhibitor, 10 μM, 30 min). **(B)** Insulin induces an increase in serine phosphorylation of GSK3α/β, downstream of PI3K but not of Akt, in N1E-115 cells. Western blots (WBs) show Insulin-mediated signaling in serum starved N1E-115 cells, pretreated with PI3K or Akt inhibitors. We used antibodies against Akt-PS (Ser473), GSK3α/β-PS (Ser9/Ser21), total GSK3 and β-tubulin. **(C)** Active GSK3β abolishes CLASP2 relocalization to MT plus-ends induced by Insulin. N1E-115 cells were transfected with constitutively active GSK3β (GSK3β-S9A-HA), treated with Insulin as above, fixed 48 h post-transfection, and double stained with anti-HA (green in merge, to stain active GSK3β) and anti-CLASP2 (red in merge). **(D)** Transient knockdown of CLASP2 increases GSK3 serine phosphorylation. N1E-115 cells were transfected with the indicated shRNA constructs. After 72 h, cells were lysed and the levels of the indicated proteins examined by WB. **(E)** Stable depletion of CLASP1 and -2 enhances GSK3 serine-phosphorylation. N1E-115 cells were transfected with the indicated shRNA constructs and selected with puromycin. Resistant clones were picked and examined for CLASP1 or -2 knockdown. In two of each, we next examined the levels of phosphorylated and total GSK3 by WB. **(F)** Inhibition of protein kinase C (PKC) alleviates CLASP-depletion-mediated GSK3 phosphorylation. Stable N1E-115 clones expressing the indicated shRNAs were treated with inhibitors (i) against MEK1/2 (U0126, 1 μM, 30 min), PKC (Ro318220, 0.5 μM, 30 min), or Akt (Triciribine, 10 μM, 30 min). Cells were subsequently lysed and the levels of the indicated proteins examined by WB. **(G)** Depletion of CLASP2—but not of CLASP1—leads to increased phosphorylation of atypical PKC (aPKC) but not of Akt. N1E-115 clones stably-depleted in CLASP1 or CLASP2 were lysed and the levels of the indicated phospho-proteins (Akt-PS and PKC-PS) were examined by WB **(H)** Interaction of CLASP2 with phosphorylated aPKC. N1E-115 cells were transiently transfected with wild type (WT) GFP-CLASP2 [CL2 (WT)], GFP-CLASP2-9SA, or with GFP-CLASP2-8SD. After 1 day, cells were lysed and the GFP-tagged forms of CLASP2 were pulled-down with anti-GFP antibodies. Lysates and co-IPs were examined by WB using antibodies against the indicated proteins.

also results in the phosphorylation and activation of PKC, another kinase with which CLASP2 appears to interact. Thus, CLASP1 and CLASP2 are not only substrates of different kinases (e.g., GSK3 and PKC) but they also act upstream of these kinases in distinct feedback loops that regulate kinase activities.

Distinct Roles for CLASP1 and -2 in Neurite Outgrowth in N1E-115 Cells

Our findings show that, in differentiating neuronal cells, CLASP1 and CLASP2 display different MT binding behavior and subcellular localization, are differently regulated by GSK3, and activate distinct signaling pathways and feedback loops, when knocked-down. All these data suggest that CLASP1 and -2 play distinct roles during neurite outgrowth and are non-redundant. To address this issue, we first examined the expression of CLASP isoforms (**Figure 5A**) in N1E-115 cells. We found that under basal (i.e., non-differentiating) conditions, N1E-115 cells expressed CLASP1α, CLASP2α, and CLASP2β/γ (**Figure 5B**, note that CLASP2β/γ cannot be distinguished by WB). An RT-PCR-based analysis suggested approximately equal levels of the *Clasp* mRNAs (**Supplementary Figure S4**). Neuronal differentiation induction [either by overnight serum starvation (SF) or by DMSO-containing medium for 1, 3, and 5 days] led to an increase in the level of CLASP2β/γ compared to CLASP2α (**Figure 5B**), which is consistent with whole brain extract results (Drabek et al., 2012), and indicates a specific role for the shorter isoforms of CLASP2 during neurite extension in N1E-115 cells.

We next transiently depleted CLASP1 and -2 using two different GFP-bearing shRNA constructs for each protein (**Figure 5C** and **Supplementary Figure S5A**). Interestingly, in cells cultured under basal conditions, the knockdown of CLASP1 resulted in an increase in the amount of round (undifferentiated) cells and a decrease in the percentage of flat cells and cells with neurites (in differentiation), whereas depletion of CLASP2 caused a reduction in cell rounding with a concomitant cell flattening, and increase in the number of cells with neurites (**Figures 5D,E**, and **Supplementary Figures S5A,B**). Overexpression of GFP-tagged CLASP1 in non-differentiating cells led to an increase in the number of cells with neurites, whereas overexpression of CLASP2 only caused a moderate increase (**Figure 5F**). Co-expression of CLASP1 and 2 induced a huge rise in the percentage of flat cells and disappearance of round cells (**Figure 5F**).

Since an increase in MT stabilization (and hence acetylated tubulin levels) has been associated with neurite/axon outgrowth during neuronal differentiation (Witte et al., 2008) and CLASPs have been shown to locally regulate MT stability (Drabek et al., 2006), we checked whether the differences exerted by CLASP1 and -2 on neurite outgrowth correlated with a distinct action of CLASPs on tubulin acetylation. Both transient (**Supplementary Figure S5B**) and stable knockdown of CLASP1 caused a decrease in the level of acetylated α-tubulin (**Figures 5G,H** and **Supplementary Figures S5C,D**), whereas overexpression increased the amount of this marker of stable MTs (**Figures 5I,J**). By contrast, knockdown of CLASP2 did not change the level of acetylated tubulin (**Figures 5G,H**), and CLASP2 overexpression only mildly increased it (**Figures 5I,J**). Taken together these data indicate that mammalian CLASPs have opposing roles during neurite outgrowth of N1E-115 cells, with CLASP1 stimulating extension and CLASP2 hampering it. Thus, even though mammalian CLASPs are highly similar proteins their function in neurite elongation and effects on MTs appear to differ.

Neurite and Axon Extension Are Accelerated in *Clasp2* Knockout Neurons

To analyze the role of CLASP2 in primary neurons we cultured embryonic HNs (**Supplementary Figure S6**), derived from WT and *Clasp2* KO mice (Drabek et al., 2012). HNs were first analyzed after 1DIV, using antibodies against βIII tubulin and Tau1 to monitor neurite extension and axon formation, respectively (**Figure 6A**), and phalloidin to examine the actin network (**Figure 6B**). This analysis revealed that neurite extension was enhanced and axon formation was accelerated in *Clasp2* KO neurons (**Figures 6A,D,F**). In addition, actin protrusions were diminished in *Clasp2* KO neurons (**Figure 6**). Quantifications revealed that the average number of neurites present in CLASP2-deficient neurons remained unchanged but their length was enhanced (**Figures 6C,D**), as compared with WT neurons. The lack of CLASP2 did not seem to affect neuronal polarity, as *Clasp2* KO neurons had one axon per neuron, like control cells (**Figure 6E**). However, we found a significant increase in the number of CLASP2-deficient neurons that had reached stage 3 of differentiation after 1DIV (**Figures 6F,G**) and 2 DIV (**Figure 6F**), and more neurons with longer axons (**Figure 6H**). Hence, 1DIV and 2DIV *Clasp2* KO neurons show an accelerated initiation of axon extension and present longer neurites and axons.

Since we observed an enriched localization of CLASP2 in WT neurite tips, and axonal growth cones (see **Figure 1F**), we analyzed MT and actin cytoskeletons in distal axons and growth cones of 2 DIV hippocampal WT and KO neurons. In WT neurons, MT bundles were located in the center of the growth cone, with some individual MTs entering the peripheral domain (**Figure 6I**). In *Clasp2* KO neurons, both dynamic and stable MTs (stained with antibodies recognizing tyrosinated or detyrosinated tubulin, respectively) entered more extensively into the actin-rich domain of the growth cone, with more overlap between tyrosinated and detyrosinated MTs, and actin filaments (**Figure 6I**). Significant effects were found in growth cones of *Clasp2* KO neurons, i.e., growth cones were smaller, and not only less well spread and simpler and with fewer filopodia than WT growth cones, but they also contained reduced amounts of polymerized actin (**Figures 6I,J**). These results indicate that both actin and MT dynamics are locally altered in growth cones of *Clasp2* KO neurons.

We next examined DRG neurons after 4 DIV and found that CLASP2 depletion did not affect neurite formation, as the percentage of cells bearing neurites was similar to WT DRG neurons (data not shown) and total neurite length remained unchanged (**Supplementary Figure S7A**). However, *Clasp2* KO DRG neurons displayed an increase, both of the length of the longest neurite and in the mean neurite length

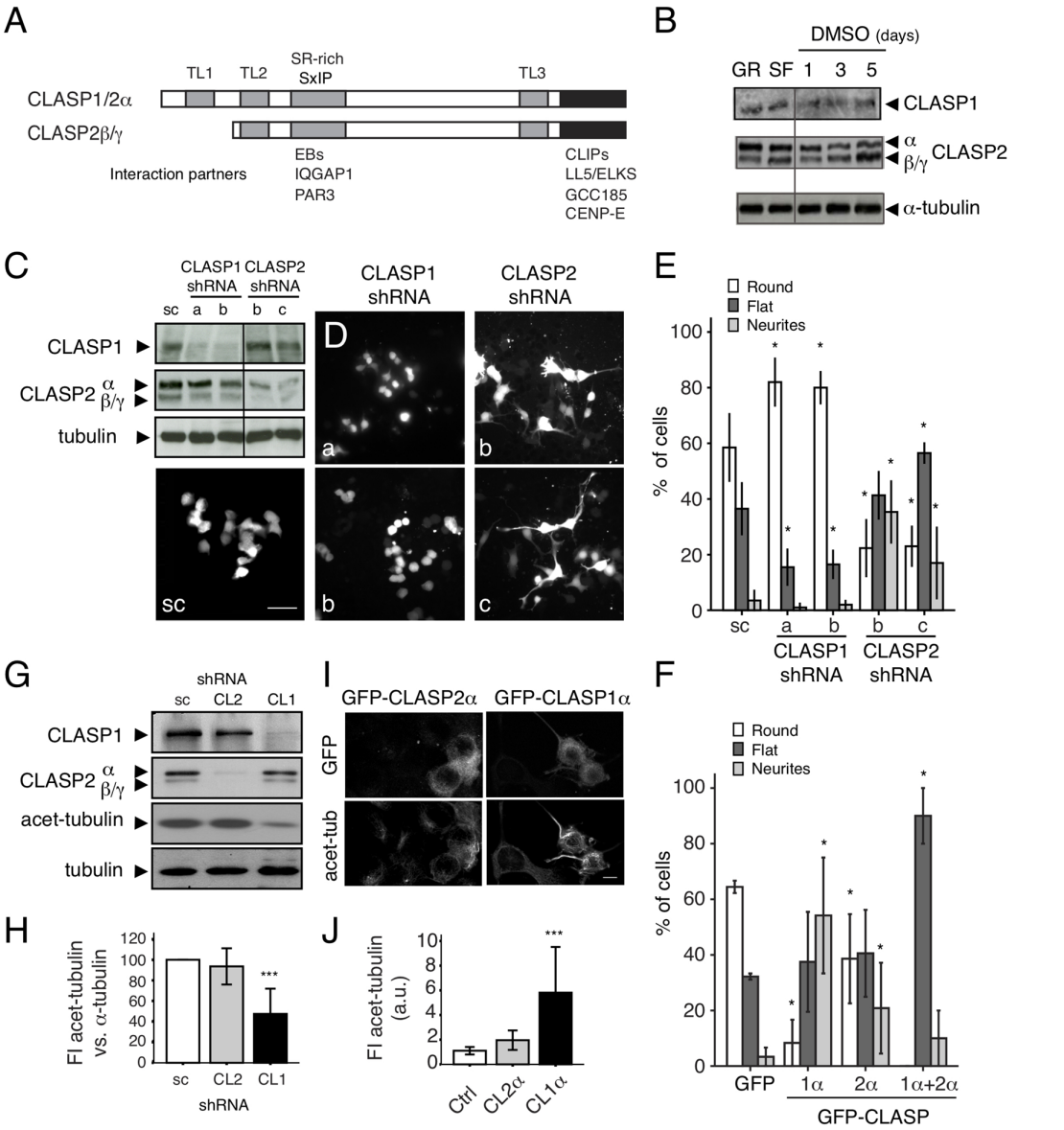

FIGURE 5 | Opposing roles of CLASP1 and CLASP2 in N1E-115 cells. **(A)** Schematic representation of CLASP domains and isoforms. The position of the TOGL (TL) and serine/arginine-rich (SR-rich) motifs is indicated by gray bars. Interaction partners and the regions in CLASPs with which they interact, are shown underneath. **(B)** CLASP1 and -2 expression (WB) in N1E-115 cells before and after differentiation, by overnight serum deprivation (SF for Serum Free) or with dimethyl sulfoxide (DMSO) for 1, 3, and 5 days. **(C,D)** Transient knockdown of CLASP1 and -2 in N1E-115 cells. WBs of lysates **(C)** and IF staining in N1E-115 cells **(D)** transfected with a scrambled shRNA construct or with different shRNA constructs targeting CLASP1 or CLASP2 (a and b for CLASP1 and b and c for CLASP2). Cells were either lysed for WB or fixed for IF, 72 h post-transfection. Cells were not serum-starved but were maintained in 10% fetal bovine serum (FBS)-containing medium. In **(C)** we used anti-α-tubulin as a loading control. In **(D)**, Scale bar = 50 μm. shRNA constructs bear GFP as a reporter. **(D,E)** In the IF experiments, GFP-expressing CLASP1-depleted cells present mostly round morphology, whereas CLASP2-depleted cells show a differentiated morphology (flat or with neurites). This was quantified in E. Number of cells with each different morphology (round, flat or neurite-bearing cells) was compared in cells transfected with either CLASP1-or CLASP2-shRNAs vs. the scramble shRNAs (scramble/control). Student *T*-tests were performed. The effects had different extents depending on the shRNA used. **(F)** Overexpression of GFP-CLASP1α induced dramatic neurite outgrowth and GFP-CLASP2α only moderate neurite extension in N1E-115 cells. Transfected N1E-115 cells were counted for the presence of round, flat and neurite-bearing cells. Comparisons for statistical analyses were done between control cells (transfected with GFP) and cells transfected with either CLASP1α, CLASP2α, or CLASP1α+CLASP2α. Student *T*-tests were performed. Standard deviation (SD) is depicted in the bar graphs in **(E,F)**. **(G–J)** MT stability in CLASP knockdowns. **(G)** Lysates of N1E-115 cells stably depleted of either CLASP1 or CLASP2 were examined by WB, using antibodies against CLASP1, -2 and acetylated-tubulin (stable MTs). Total α-tubulin and GAPDH were used as loading controls. **(H)** Densitometric quantification of acetylated-tubulin vs. α-tubulin in representative WBs of control stable cells (scr) or cells deficient in CLASP1 or -2. **(I)** IF confocal images show N1E-115 cells transfected with GFP-CLASP1α or GFP-CLASP2α and stained for acetylated tubulin. **(J)** Quantification of FI in arbitrary units (a.u.) of acetylated tubulin in control (non-transfected) cells and cells ectopically expressing GFP-CLASP2α or GFP-CLASP1α from representative fluorescent images. SD is depicted in bar graphs of **(H,J)**.

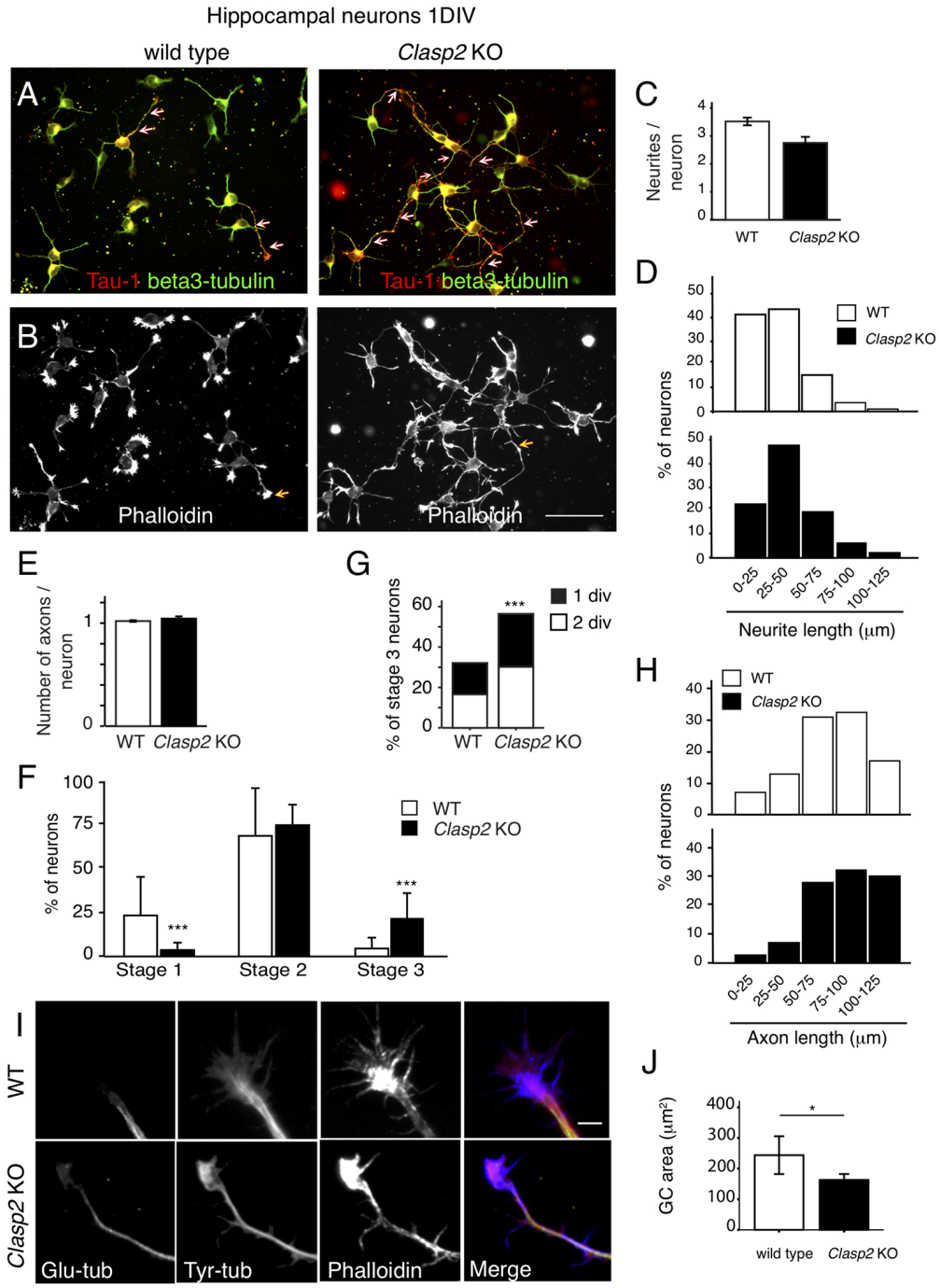

FIGURE 6 | *Clasp2* knockout (KO) neurons develop longer neurites and show accelerated axon outgrowth. **(A,B)** WT and *Clasp2* KO HNs were cultured for 1 day *in vitro* (1DIV), fixed and stained with antibodies against Tau1 (an axonal marker, red in merge), βIII-tubulin (a neuronal marker, green in merge; **A**) and phalloidin (F-actin; **B**). **(C)** Quantification of the mean number of primary neurites/neuron in WT and *Clasp2* KO neurons. No differences were found. Student *T*-test was performed. SD is depicted. **(D)** Histograms showing the distribution of primary neurite length in WT and *Clasp2* KO neurons. The latter present the same number of primary neurites, but these are longer. **(E)** Quantification of the number of axons/neuron reveals no differences between WT and *Clasp2* KO neurons. **(F–H)** *Clasp2* KO neurons develop premature and longer axons. In **(F)** the percentage of neurons in stage 1, 2 or 3 (at 1DIV) was quantified and represented in histograms. In **(G)**, the percentage of stage 3 neurons was quantified in 1 and 2DIV WT vs. *Clasp2* KO neurons. In **(H)** the histograms represent the distribution of axon lengths of WT and *Clasp2* KO neurons. **(I,J)** Growth cone morphology in the absence of CLASP2. The actin and MT cytoskeleton were visualized in 2DIV WT and *Clasp2* KO neurons using anti-α-detyrosinated-tubulin (Glu-tub, green in merge) and anti-α-tyrosinated-tubulin (Tyr-tub, red in merge) antibodies, in combination with phalloidin (F-actin, blue in merge). Scale bar = 10 μm. In **(J)** a quantification of growth cone area is shown using phalloidin staining. WT neurons have wider growth cones with more polymerized actin than *Clasp2* KO neurons. Student *T*-test was performed. SD is depicted in bar graph.

(**Supplementary Figures S7B,C**), and a decreased segment number (**Supplementary Figure S7D**), suggesting that in normal DRG neurons CLASP2 restricts axonal elongation in favor of axonal branching. Overall, our data suggest that deficiency in CLASP2 leads to longer neurites, and axons tipped by smaller growth cones, in correlation with alterations in MT and actin growth cone networks. These results point to CLASP2 as a brake for neurite and axon extension in different types of neurons.

We have shown previously that CLASP2 is most abundantly expressed in the brain (Akhmanova et al., 2001), and that CLASP2β/γ are the major isoforms present in brain protein extracts (Drabek et al., 2012). Next generation sequencing of RNA (RNA-Seq) from 3DIV HNs suggested increased *Clasp2*β/γ levels compared to *Clasp2*α-mRNA (**Supplementary Figures S8A,B**). Moreover, RNA-Seq showed that both in hippocampal and in DRG neurons *Clasp2* mRNA levels are higher than *Clasp1* (**Supplementary Figure S8C**). Given the relative enrichment of CLASP2 in growth cones, as shown by immunofluorescent staining experiments (**Figures 1F**, **3E**), these data suggest that the amounts of CLASP2β /γ in this neuronal compartment might exceed the level of CLASP1α.

DISCUSSION

Mammalian CLASPs are homologous proteins that are often similarly localized and have overlapping functions in non-neuronal cells (e.g., Mimori-Kiyosue et al., 2005). It has been proposed that CLASP1 and CLASP2 are also redundant in neurons (Hur et al., 2011). Here, we reveal distinct functions for the CLASPs in N1E-115 neuroblastoma cells with CLASP1 stimulating neurite outgrowth and CLASP2 acting as a break. Results in primary *Clasp2* hippocampal and DRG KO neurons support a role for CLASP2 as an antagonist of neurite and axon outgrowth.

CLASP2 has been shown to be phosphorylated by GSK3 on different serine residues in the S/R-rich region surrounding two SxIP motifs (Kumar et al., 2009, 2012; Watanabe et al., 2009). Since CLASP1 is quite similar to CLASP2 it is generally thought that CLASP1 and -2 are regulated in the same manner by GSK3. However, our data suggest that CLASP2 is a major target of GSK3β in N1E-115 cells and neurons, while CLASP1 is not. For example, in serum-starved N1E-115 cells CLASP2 was hardly localized at MT plus ends indicating high GSK3 activity (which is confirmed by low GSK3-serine phosphorylation in these cells), and globally relocalized to MT-plus ends throughout the cell after GSK3 inhibition or knockdown. By contrast, GSK3 inhibition induced a modest reduction in CLASP1 binding to MT-growing ends. Moreover, WB analyses also indicated that in neuroblastoma cells CLASP2 is phosphorylated by GSK3 but CLASP1 is not. Thus, in N1E-115 cells CLASP1 and -2 display different sensitivity towards GSK3. One reason for this different behavior could be that in N1E-115 cells the majority of *Clasp1* mRNAs lack an internal small exon encoding the second SxIP domain of CLASP1 with many of the GSK3 phosphorylation consensus sites.

We also observed CLASP2 relocalization to MT plus-ends upon insulin or IGF-1 treatment in neuroblastoma cells or neurons, respectively. Both growth factors induce GSK3 inhibition corroborating that CLASP2 binding to MTs in neuronal cells is modulated by different signaling pathways that converge at the GSK3 level. Remarkably, in L6 myotubes, CLASP2 has been shown to be phosphorylated and to participate in the activation of MT-based glucose transport in response to insulin (Langlais et al., 2012), supporting a role for CLASP2 in insulin signaling in different cell types. Moreover, while CLASP2 behavior downstream of insulin mimics that after GSK3 inhibition in our cell system, CLASP1 does not respond equally to both stimuli. This suggests that CLASP1 localization might be modulated by different kinases and/or phosphatases regulated by insulin.

In our experiments GFP-tagged CLASP1 and -2 localized and behaved like endogenous proteins. This reinforces our antibody-based results, and also suggests that GSK3 phosphorylation interferes with GFP-tagged CLASP2—but not GFP-CLASP1—interaction with MT plus-ends. Mild overexpression of GFP-CLASP2 in differentiating cells will therefore initially yield phosphorylated protein, and this form of GFP-CLASP2 is not able to stabilize MTs. By contrast, mild overexpression of GFP-CLASP1 yields molecules that are not phosphorylated and that can increase the amount of stable (acetylated) MTs. These observations explain results shown in **Figures 5I,J**. It should be noted that GFP-CLASP1 does contain the small exon encoding the second SxIP motif, and hence resembles CLASP2 in this area of the protein. Thus, besides alternative splicing, other mechanisms can also underlie differential sensitivity of CLASP1 and -2 to GSK3. As GSK3 requires a "priming" kinase to function optimally, one possibility is that priming sites in CLASP1 and -2 differ.

Another surprising finding of our work is that knockdown of either CLASP1 or CLASP2 leads to the serine phosphorylation of GSK3. We have previously shown that the RNAi-mediated depletion of 4.1R, a CLASP2 interaction partner, also results in enhanced GSK3 phosphorylation (Ruiz-Saenz et al., 2013). CLASPs seem to act as regulators of GSK3 by modulating the activity of upstream factors, such as serine/threonine kinases or phosphatases. In line with this, we show that inhibition of PKC -but not of ERK or Akt-blocks GSK3 phosphorylation induced by CLASP depletion. This suggests that CLASP downregulation induces GSK3 phosphorylation by PKC. Interestingly, we observe that knockdown of CLASP2—but not of CLASP1- results in the phosphorylation and activation of aPKC. CLASP2 has been shown to be phosphorylated by—and interact with—active forms of PKC (Lanza et al., 2010). Moreover, a crosstalk between CLASP2 and the polarity complex PAR3/PAR6/aPKC has been reported: CLASP2 interacts directly with PAR3 and this interaction is required for CLASP2 phosphorylation by aPKC (Matsui et al., 2015). We here show a GSK3-dependent CLASP2/aPKC interaction, since only WT CLASP2 binds active aPKC while CLASP2 mutants in the GSK3 phosphorylation sites do not, neither the phosphomimetic nor the non-phosphorylatable forms. A possible explanation for this is that the non-phosphorylatable

form of CLASP2 interacts more strongly with GSK3, as the kinase makes a vain attempt to phosphorylate CLASP2; GSK3 binding in turn inhibits PAR3 interaction and hence the association between CLASP2 and aPKC. Of note, GSK3 has been reported to interact with, and be regulated by, Par6/aPKC, leading to the recruitment of APC, another +TIP, to MT plus-ends during centrosome reorientation (Etienne-Manneville and Hall, 2003). Thus, a complex interplay between CLASP2, GSK3 and aPKC seems to exist, in which CLASP2 acts both as substrate and upstream regulator of both kinases. The fact that CLASPs appear to be part of a network involved in feedback loop signaling to GSK3 and other upstream kinases such as PKC indicates that CLASPs play a complex regulatory role in signal transduction. Part of CLASP function may be to facilitate the formation of signaling complexes. These findings have consequences for the interpretation of results of other studies in which CLASPs were depleted using RNAi. It will be interesting to examine whether other +TIPs (e.g., APC and ACF7) control upstream kinases and if so, which cascades are involved.

We describe here that CLASP proteins display opposite functions during neuronal development, with CLASP1 promoting neurite extension and CLASP2 acting as a negative regulator of neuritogenesis/axonogenesis. A model incorporating our results, including feedback loop signaling mediated by CLASPs, is schematized in **Supplementary Figure S9**. In neurite-bearing N1E-115 cells as well as in primary HNs, CLASP2 accumulates at MT plus-ends along the neurite/axon shaft and in the growth cone, whereas CLASP1 is enriched at MT growing ends present in soma and proximal region of neurites/axon. The levels of CLASP2β/γ increase during neurite extension whereas CLASP2α levels diminish; since CLASP2β appears to be membrane-bound (Akhmanova et al., 2001), we propose that in growth cones CLASP1α and CLASP2γ are the main CLASP proteins present, with CLASP2 being more prominent than CLASP1 (**Supplementary Figure S9**). This is interesting in view of a recent report, which suggests that the N-terminal TOGL1 domain of CLASP2α exerts an auto-regulatory effect, releasing the inhibitory action of the C-terminal region on the TOGL2 domain, which is proposed to be responsible for the MT catastrophe suppressor function of CLASP2 (Aher et al., 2018). Thus, CLASP2γ, which lacks the TOGL1 domain, would only be able to suppress catastrophes when the C-terminal domain interacts with other proteins, for example when CLASP2γ is bound to the cell cortex *via* interaction partners like LL5β (Lansbergen et al., 2006). During neurite/axon extension, different growth factors engage to growth cone receptors triggering diverse signaling pathways that converge at GSK3 phosphorylation and inactivation in the growth cone. Switching GSK3 from an active to an inactive form affects CLASP2 but not CLASP1 function, and it may even increase local CLASP2 concentration, as the protein attaches both to MT ends and the cell cortex and becomes less diffusive. Competition of CLASP2γ with CLASP1α at MT ends may lead to local MT stabilization in growth cone regions where GSK3 is inactive, whereas persistent MT growth, mediated by CLASP1α, is observed in growth cone regions where GSK3 is active, and in proximal neurite/axon shafts where it is enriched (**Supplementary Figure S9**). An extra layer of complexity arises when taking into account that CLASP2 is a direct GSK3 target in neuronal cells and a binding partner and modulator of aPKC, and that both CLASPs are upstream regulators of GSK3. Since several MT-interacting proteins, both classical MAPs and +TIPs, are direct GSK3 targets, the indirect output of CLASP actions on MT dynamics becomes even more complex. Thus, the final outcome of CLASP actions in neuronal development will most likely depend on a finely tuned balance between their expression levels, subcellular localization, as well as their involvement in signaling feedback loops.

Our *Clasp2* knockdown data in N1E-115 cells as well as the *Clasp2* KO results in primary HNs are consistent with a previous study that showed increased axon outgrowth in cortical neurons in which CLASP2 was depleted by shRNA and RNAi-mediated approaches (Hur et al., 2011). However, these authors did not observe any effect on axon extension upon CLASP1 downregulation. Moreover, they showed that in DRG neurons the single knockdown of CLASP2 was less effective, but that of CLASP1 or the combined depletion of CLASP1 and -2 impeded neurite outgrowth (Hur et al., 2011), contrary to the increase in neurite length that we show in DRG neurons obtained from our *Clasp2* KO mice. Our data do not concur with other reports in which knockdown of CLASP2 was shown to impede, rather than enhance, neurite extension in HNs (Beffert et al., 2012; Dillon et al., 2017). One reason for the different outcomes in RNAi/shRNA-mediated knockdown studies involving the CLASPs may be a varying interference with feedback loop signaling networks, which may produce different outcomes in terms of the cytoskeletal organization involved in neurite/axon extension. For example, we show here that CLASP2 depletion affects GSK3 and aPKC. The latter is known to promote axon elongation (Shi et al., 2003, 2004). Inhibition of GSK3 has also been reported to induce axon outgrowth (Kim et al., 2006); this was shown to partly be due to the enhanced binding of some of its substrates, such as APC or CRMP2, to MTs, thereby controlling MT dynamics and stability in the axon and growth cone (Zhou et al., 2004; Yoshimura et al., 2005).

Clasp2 KO neurons present longer axons tipped by smaller growth cones, with altered MT and actin cytoskeletons. This suggests that CLASP2 deficiency might lead to local changes in MT and actin dynamics in the growth cone. Absence of CLASP2 would allow CLASP1 to occupy MT ends, and promote sustained MT growth in peripheral regions of the growth cone. This would explain our observation that in *Clasp2* KO neurons dynamic (tyrosinated) MTs appear to penetrate the peripheral regions of the growth cone more often, probably contributing to the enhanced extension of the axon. We also find a reduction in the amount of filopodia and polymerized actin in *Clasp2* KO growth cones, as compared to control neurons. This is in agreement with a previous report showing that depletion of CLASP in spinal cord neurons of *Xenopus* (which only express one CLASP) leads to a reduction in F-actin in growth cones (Marx et al., 2013). Also in *Xenopus* growth cones, CLASP2 has been reported to modulate the distribution of F-actin structures downstream of Abl (Engel et al., 2014), a

tyrosine kinase that binds actin and phosphorylates regulators of the actin cytoskeleton (Colicelli, 2010). CLASP2 also interacts with IQGAP1, a regulator of the actin cytoskeleton (Watanabe et al., 2009). In addition, a number of actin-associated proteins as well as actin-MT crosslinking proteins have been described to be part of the genetic interactome of the *Drosophila* CLASP homolog (Lowery et al., 2010). Thus, in the absence of CLASP2, the disruption of the interactions between CLASP2 and IQGAP1 and other actin regulators, might contribute to actin cytoskeleton defects found in growth cones of *Clasp2* KO neurons.

In summary, we present evidence of opposing functions of CLASP1 and CLASP2 in developing neuronal cells, and we relate them to differential CLASP1 and -2 MT plus-end binding and subcellular localization, as well as their distinct involvement in signaling cascades, both as substrates and upstream regulators. Focusing on CLASP2, we shed light into its role as a negative regulator of neurite and axon extension.

AUTHOR CONTRIBUTIONS

CS performed the majority of the experiments, interpreted results, and wrote the manuscript. SB, MR, EB-M, ML, MS, and WI performed experiments and interpreted results. JA interpreted results. NG performed some of the experiments, interpreted results, and wrote the manuscript. All authors helped to complete the manuscript.

FUNDING

This work was funded by a European Reintegration Grant (ERG) from the European Commission (FP6-2002-MOBILITY-11, grant agreement: ID: 517582) granted to CS and NG.

ACKNOWLEDGMENTS

We thank Umut Akinci for performing the RT-PCR experiments in N1E-115 cells, and Liu Zhe for isolating RNA from hippocampal neuronal cultures for RNA-Seq. We thank Dr. Kerstin Wendt for the anti-GFP antibodies.

SUPPLEMENTARY MATERIAL

The Supplementary Material for this article can be found online at: https://www.frontiersin.org/articles/10.3389/fncel.2019.00005/full#supplementary-material

REFERENCES

Aher, A., Kok, M., Sharma, A., Rai, A., Olieric, N., Rodriguez-Garcia, R., et al. (2018). CLASP suppresses microtubule catastrophes through a single TOG domain. *Dev. Cell* 46, 40.e8–58.e8. doi: 10.1016/j.devcel.2018.05.032

Akhmanova, A., Hoogenraad, C. C., Drabek, K., Stepanova, T., Dortland, B., Verkerk, T., et al. (2001). Clasps are CLIP-115 and -170 associating proteins involved in the regional regulation of microtubule dynamics in motile fibroblasts. *Cell* 104, 923–935. doi: 10.1016/s0092-8674(01)00288-4

Akhmanova, A., and Steinmetz, M. O. (2015). Control of microtubule organization and dynamics: two ends in the limelight. *Nat. Rev. Mol. Cell Biol.* 16, 711–726. doi: 10.1038/nrm4084

Al-Bassam, J., and Chang, F. (2011). Regulation of microtubule dynamics by TOG-domain proteins XMAP215/Dis1 and CLASP. *Trends Cell Biol.* 21, 604–614. doi: 10.1016/j.tcb.2011.06.007

Banker, G. A., and Cowan, W. M. (1977). Rat hippocampal neurons in dispersed cell culture. *Brain Res.* 126, 397–425. doi: 10.1016/0006-8993(77)90594-7

Beaven, R., Dzhindzhev, N. S., Qu, Y., Hahn, I., Dajas-Bailador, F., Ohkura, H., et al. (2015). *Drosophila* CLIP-190 and mammalian CLIP-170 display reduced microtubule plus end association in the nervous system. *Mol. Biol. Cell* 26, 1491–1508. doi: 10.1091/mbc.e14-06-1083

Beffert, U., Dillon, G. M., Sullivan, J. M., Stuart, C. E., Gilbert, J. P., Kambouris, J. A., et al. (2012). Microtubule plus-end tracking protein CLASP2 regulates neuronal polarity and synaptic function. *J. Neurosci.* 32, 13906–13916. doi: 10.1523/JNEUROSCI.2108-12.2012

Beurel, E., Grieco, S. F., and Jope, R. S. (2015). Glycogen synthase kinase-3 (GSK3): regulation, actions, and diseases. *Pharmacol. Ther.* 148, 114–131. doi: 10.1016/j.pharmthera.2014.11.016

Bieling, P., Kandels-Lewis, S., Telley, I. A., van Dijk, J., Janke, C., and Surrey, T. (2008). CLIP-170 tracks growing microtubule ends by dynamically recognizing composite EB1/tubulin-binding sites. *J. Cell Biol.* 183, 1223–1233. doi: 10.1083/jcb.200809190

Bieling, P., Laan, L., Schek, H., Munteanu, E. L., Sandblad, L., Dogterom, M., et al. (2007). Reconstitution of a microtubule plus-end tracking system *in vitro*. *Nature* 450, 1100–1105. doi: 10.1038/nature06386

Cambray-Deakin, M. A., and Burgoyne, R. D. (1987). Acetylated and detyrosinated α-tubulins are co-localized in stable microtubules in rat meningeal fibroblasts. *Cell Motil. Cytoskeleton* 8, 284–291. doi: 10.1002/cm.970080309

Colicelli, J. (2010). ABL tyrosine kinases: evolution of function, regulation, and specificity. *Sci. Signal.* 3:re6. doi: 10.1126/scisignal.3139re6

Dillon, G. M., Tyler, W. A., Omuro, K. C., Kambouris, J., Tyminski, C., Henry, S., et al. (2017). CLASP2 links reelin to the cytoskeleton during neocortical development. *Neuron* 93, 1344.e5–1358.e5. doi: 10.1016/j.neuron.2017.02.039

Dotti, C. G., Sullivan, C. A., and Banker, G. A. (1988). The establishment of polarity by hippocampal neurons in culture. *J. Neurosci.* 8, 1454–1468. doi: 10.1523/JNEUROSCI.08-04-01454.1988

Drabek, K., Gutiérrez, L., Vermeij, M., Clapes, T., Patel, S. R., Boisset, J. C., et al. (2012). The microtubule plus-end tracking protein CLASP2 is required for hematopoiesis and hematopoietic stem cell maintenance. *Cell Rep.* 2, 781–788. doi: 10.1016/j.celrep.2012.08.040

Drabek, K., van Ham, M., Stepanova, T., Draegestein, K., van Horssen, R., Sayas, C. L., et al. (2006). Role of CLASP2 in microtubule stabilization and the regulation of persistent motility. *Curr. Biol.* 16, 2259–2264. doi: 10.1016/j.cub.2006.09.065

Efimov, A., Kharitonov, A., Efimova, N., Loncarek, J., Miller, P. M., Andreyeva, N., et al. (2007). Asymmetric CLASP-dependent nucleation of noncentrosomal microtubules at the trans-Golgi network. *Dev. Cell* 12, 917–930. doi: 10.1016/j.devcel.2007.04.002

Engel, U., Zhan, Y., Long, J. B., Boyle, S. N., Ballif, B. A., Dorey, K., et al. (2014). Abelson phosphorylation of CLASP2 modulates its association with microtubules and actin. *Cytoskeleton* 71, 195–209. doi: 10.1002/cm.21164

Etienne-Manneville, S., and Hall, A. (2003). Cdc42 regulates GSK-3β and adenomatous polyposis coli to control cell polarity. *Nature* 421, 753–756. doi: 10.1038/nature01423

Feldman, E. L., Sullivan, K. A., Kim, B., and Russell, J. W. (1997). Insulin-like growth factors regulate neuronal differentiation and survival. *Neurobiol. Dis.* 4, 201–214. doi: 10.1006/nbdi.1997.0156

Fleming, C. E., Mar, F. M., Franquinho, F., Saraiva, M. J., and Sousa, M. M. (2009). Transthyretin internalization by sensory neurons is megalin mediated and necessary for its neuritogenic activity. *J. Neurosci.* 29, 3220–3232. doi: 10.1523/JNEUROSCI.6012-08.2009

Honnappa, S., Gouveia, S. M., Weisbrich, A., Damberger, F. F., Bhavesh, N. S., Jawhari, H., et al. (2009). An EB1-binding motif acts as a microtubule tip localization signal. *Cell* 138, 366–376. doi: 10.1016/j.cell.2009.04.065

Hur, E. M., Saijilafu, Lee, B. D., Kim, S. J., Xu, W. L., and Zhou, F. Q. (2011). GSK3 controls axon growth via CLASP-mediated regulation of growth cone microtubules. *Genes Dev.* 25, 1968–1981. doi: 10.1101/gad.17015911

Kim, W. Y., Zhou, F. Q., Zhou, J., Yokota, Y., Wang, Y. M., Yoshimura, T., et al. (2006). Essential roles for GSK-3s and GSK-3-primed substrates in neurotrophin-induced and hippocampal axon growth. *Neuron* 52, 981–996. doi: 10.1016/j.neuron.2006.10.031

Kumar, P., Chimenti, M. S., Pemble, H., Schönichen, A., Thompson, O., Jacobson, M. P., et al. (2012). Multisite phosphorylation disrupts arginine-glutamate salt bridge networks required for binding of cytoplasmic linker-associated protein 2 (CLASP2) to end-binding protein 1 (EB1). *J. Biol. Chem.* 287, 17050–17064. doi: 10.1074/jbc.M111.316661

Kumar, P., Lyle, K. S., Gierke, S., Matov, A., Danuser, G., and Wittmann, T. (2009). GSK3β phosphorylation modulates CLASP-microtubule association and lamella microtubule attachment. *J. Cell Biol.* 184, 895–908. doi: 10.1083/jcb.200901042

Langlais, P., Dillon, J. L., Mengos, A., Baluch, D. P., Ardebili, R., Miranda, D. N., et al. (2012). Identification of a role for CLASP2 in insulin action. *J. Biol. Chem.* 287, 39245–39253. doi: 10.1074/jbc.m112.394148

Lansbergen, G., Grigoriev, I., Mimori-Kiyosue, Y., Ohtsuka, T., Higa, S., Kitajima, I., et al. (2006). CLASPs attach microtubule plus ends to the cell cortex through a complex with LL5β. *Dev. Cell* 11, 21–32. doi: 10.1016/j.devcel.2006.05.012

Lanza, D. C., Meirelles, G. V., Alborghetti, M. R., Abrile, C. H., Lenz, G., and Kobarg, J. (2010). FEZ1 interacts with CLASP2 and NEK1 through coiled-coil regions and their cellular colocalization suggests centrosomal functions and regulation by PKC. *Mol. Cell. Biochem.* 338, 35–45. doi: 10.1007/s11010-009-0317-9

Laurino, L., Wang, X. X., de la Houssaye, B. A., Sosa, L., Dupraz, S., Cáceres, A., et al. (2005). PI3K activation by IGF-1 is essential for the regulation of membrane expansion at the nerve growth cone. *J. Cell Sci.* 118, 3653–3662. doi: 10.1242/jcs.02490

Lawrence, E. J., Arpag, G., Norris, S. R., and Zanic, M. (2018). Human CLASP2 specifically regulates microtubule catastrophe and rescue. *Mol. Biol. Cell* 29, 1168–1177. doi: 10.1091/mbc.E18-01-0016

Lee, H., Engel, U., Rusch, J., Scherrer, S., Sheard, K., and Van Vactor, D. (2004). The microtubule plus end tracking protein Orbit/MAST/CLASP acts downstream of the tyrosine kinase Abl in mediating axon guidance. *Neuron* 42, 913–926. doi: 10.1016/j.neuron.2004.05.020

Lowery, L. A., Lee, H., Lu, C., Murphy, R., Obar, R. A., Zhai, B., et al. (2010). Parallel genetic and proteomic screens identify Msps as a CLASP-Abl pathway interactor in *Drosophila*. *Genetics* 185, 1311–1325. doi: 10.1534/genetics.110.115626

Marx, A., Godinez, W. J., Tsimashchuk, V., Bankhead, P., Rohr, K., and Engel, U. (2013). *Xenopus* cytoplasmic linker-associated protein 1 (XCLASP1) promotes axon elongation and advance of pioneer microtubules. *Mol. Biol. Cell* 24, 1544–1558. doi: 10.1091/mbc.E12-08-0573

Matsui, T., Watanabe, T., Matsuzawa, K., Kakeno, M., Okumura, N., Sugiyama, I., et al. (2015). PAR3 and aPKC regulate Golgi organization through CLASP2 phosphorylation to generate cell polarity. *Mol. Biol. Cell* 26, 751–761. doi: 10.1091/mbc.E14-09-1382

Mimori-Kiyosue, Y., Grigoriev, I., Lansbergen, G., Sasaki, H., Matsui, C., Severin, F., et al. (2005). CLASP1 and CLASP2 bind to EB1 and regulate microtubule plus-end dynamics at the cell cortex. *J. Cell Biol.* 168, 141–153. doi: 10.1083/jcb.200405094

Neukirchen, D., and Bradke, F. (2011). Cytoplasmic linker proteins regulate neuronal polarization through microtubule and growth cone dynamics. *J. Neurosci.* 31, 1528–1538. doi: 10.1523/JNEUROSCI.3983-10.2011

Pfenninger, K. H., Laurino, L., Peretti, D., Wang, X., Rosso, S., Morfini, G., et al. (2003). Regulation of membrane expansion at the nerve growth cone. *J. Cell Sci.* 116, 1209–1217. doi: 10.1242/jcs.00285

Ruiz-Saenz, A., van Haren, J., Sayas, C. L., Rangel, L., Demmers, J., Millán, J., et al. (2013). Protein 4.1R binds to CLASP2 and regulates dynamics, organization and attachment of microtubules to the cell cortex. *J. Cell Sci.* 126, 4589–4601. doi: 10.1242/jcs.120840

Schneider, C. A., Rasband, W. S., and Eliceiri, K. W. (2012). NIH Image to ImageJ: 25 years of image analysis. *Nat. Methods* 9, 671–675. doi: 10.1038/nmeth.2089

Shi, S. H., Cheng, T., Jan, L. Y., and Jan, Y. N. (2004). APC and GSK-3β are involved in mPar3 targeting to the nascent axon and establishment of neuronal polarity. *Curr. Biol.* 14, 2025–2032. doi: 10.1016/j.cub.2004.11.009

Shi, S. H., Jan, L. Y., and Jan, Y. N. (2003). Hippocampal neuronal polarity specified by spatially localized mPar3/mPar6 and PI 3-kinase activity. *Cell* 112, 63–75. doi: 10.1016/s0092-8674(02)01249-7

Stepanova, T., Slemmer, J., Hoogenraad, C. C., Lansbergen, G., Dortland, B., De Zeeuw, C. I., et al. (2003). Visualization of microtubule growth in cultured neurons via the use of EB3-GFP (end-binding protein 3-green fluorescent protein). *J. Neurosci.* 23, 2655–2664. doi: 10.1523/JNEUROSCI.23-07-02655.2003

Trapnell, C., Pachter, L., and Salzberg, S. L. (2009). TopHat: discovering splice junctions with RNA-Seq. *Bioinformatics* 25, 1105–1111. doi: 10.1093/bioinformatics/btp120

Trapnell, C., Williams, B. A., Pertea, G., Mortazavi, A., Kwan, G., van Baren, M. J., et al. (2010). Transcript assembly and quantification by RNA-Seq reveals unannotated transcripts and isoform switching during cell differentiation. *Nat. Biotechnol.* 28, 511–515. doi: 10.1038/nbt.1621

van Rossum, A. G., de Graaf, J. H., Schuuring-Scholtes, E., Kluin, P. M., Fan, Y. X., Zhan, X., et al. (2003). Alternative splicing of the actin binding domain of human cortactin affects cell migration. *J. Biol. Chem.* 278, 45672–45679. doi: 10.1074/jbc.M306688200

van Weering, D. H., de Rooij, J., Marte, B., Downward, J., Bos, J. L., and Burgering, B. M. (1998). Protein kinase B activation and lamellipodium formation are independent phosphoinositide 3-kinase-mediated events differentially regulated by endogenous Ras. *Mol. Cell. Biol.* 18, 1802–1811. doi: 10.1128/mcb.18.4.1802

Watanabe, T., Noritake, J., Kakeno, M., Matsui, T., Harada, T., Wang, S., et al. (2009). Phosphorylation of CLASP2 by GSK-3β regulates its interaction with IQGAP1, EB1 and microtubules. *J. Cell Sci.* 122, 2969–2979. doi: 10.1242/jcs.046649

Welsh, G. I., and Proud, C. G. (1993). Glycogen synthase kinase-3 is rapidly inactivated in response to insulin and phosphorylates eukaryotic initiation factor eIF-2B. *Biochem. J.* 294, 625–629. doi: 10.1042/bj2940625

Witte, H., Neukirchen, D., and Bradke, F. (2008). Microtubule stabilization specifies initial neuronal polarization. *J. Cell Biol.* 180, 619–632. doi: 10.1083/jcb.200707042

Wittmann, T., and Waterman-Storer, C. M. (2005). Spatial regulation of CLASP affinity for microtubules by Rac1 and GSK3β in migrating epithelial cells. *J. Cell Biol.* 169, 929–939. doi: 10.1083/jcb.200412114

Wu, X., Shen, Q. T., Oristian, D. S., Lu, C. P., Zheng, Q., Wang, H. W., et al. (2011). Skin stem cells orchestrate directional migration by regulating microtubule-ACF7 connections through GSK3β. *Cell* 144, 341–352. doi: 10.1016/j.cell.2010.12.033

Yoshimura, T., Kawano, Y., Arimura, N., Kawabata, S., Kikuchi, A., and Kaibuchi, K. (2005). GSK-3β regulates phosphorylation of CRMP-2 and neuronal polarity. *Cell* 120, 137–149. doi: 10.1016/j.cell.2004.11.012

Yu, N., Signorile, L., Basu, S., Ottema, S., Lebbink, J. H. G., Leslie, K., et al. (2016). Isolation of functional tubulin dimers and of tubulin-associated proteins from mammalian cells. *Curr. Biol.* 26, 1728–1736. doi: 10.1016/j.cub.2016.04.069

Zhou, F. Q., Zhou, J., Dedhar, S., Wu, Y. H., and Snider, W. D. (2004). NGF-induced axon growth is mediated by localized inactivation of GSK-3β and functions of the microtubule plus end binding protein APC. *Neuron* 42, 897–912. doi: 10.1016/j.neuron.2004.05.011

Conflict of Interest Statement: The authors declare that the research was conducted in the absence of any commercial or financial relationships that could be construed as a potential conflict of interest.

frontiers in Cellular Neuroscience

ORIGINAL RESEARCH
published: 12 June 2019
doi: 10.3389/fncel.2019.00239

Activated PPARγ Abrogates Misprocessing of Amyloid Precursor Protein, Tau Missorting and Synaptotoxicity

Susanne Moosecker[1], Patrícia Gomes[2,3], Chrysoula Dioli[2,3], Shuang Yu[1], Ioannis Sotiropoulos[2,3] and Osborne F. X. Almeida[1]**

[1] Department Stress Neurobiology and Neurogenetics, Max Planck Institute of Psychiatry, Munich, Germany, [2] Life and Health Sciences Research Institute (ICVS), Medical School, University of Minho, Braga, Portugal, [3] ICVS/3B's – PT Government Associate Laboratory, Guimarães, Portugal

OPEN ACCESS

Edited by:
C. Laura Sayas,
Universidad de La Laguna, Spain

Reviewed by:
Marcella Reale,
Università degli Studi G. d'Annunzio Chieti e Pescara, Italy
Gunnar Keppler Gouras,
Lund University, Sweden

***Correspondence:**
Ioannis Sotiropoulos
ioannis@med.uminho.pt
Osborne F. X. Almeida
osa@psych.mpg.de

Specialty section:
This article was submitted to Cellular Neuropathology, a section of the journal Frontiers in Cellular Neuroscience

Received: 07 January 2019
Accepted: 13 May 2019
Published: 12 June 2019

Citation:
Moosecker S, Gomes P, Dioli C, Yu S, Sotiropoulos I and Almeida OFX (2019) Activated PPARγ Abrogates Misprocessing of Amyloid Precursor Protein, Tau Missorting and Synaptotoxicity. Front. Cell. Neurosci. 13:239. doi: 10.3389/fncel.2019.00239

Type 2 diabetes increases the risk for dementia, including Alzheimer's disease (AD). Pioglitazone (Pio), a pharmacological agonist of the peroxisome proliferator-activated receptor γ (PPARγ), improves insulin sensitivity and has been suggested to have potential in the management of AD symptoms, albeit through mostly unknown mechanisms. We here investigated the potential of Pio to counter synaptic malfunction and loss, a characteristic of AD pathology and its accompanying cognitive deficits. Results from experiments on primary mouse neuronal cultures and a human neural cell line (SH-SY5Y) show that Pio treatment attenuates amyloid β (Aβ)-triggered the pathological (mis-) processing of amyloid precursor protein (APP) and inhibits Aβ-induced accumulation and hyperphosphorylation of Tau. These events are accompanied by increased glutamatergic receptor 2B subunit (GluN2B) levels that are causally linked with neuronal death. Further, Pio treatment blocks Aβ-triggered missorting of hyperphosphorylated Tau to synapses and the subsequent loss of PSD95-positive synapses. These latter effects of Pio are PPARγ-mediated since they are blocked in the presence of GW9662, a selective PPARγ inhibitor. Collectively, these data show that activated PPARγ buffer neurons against APP misprocessing, Tau hyperphosphorylation and its missorting to synapses and subsequently, synaptic loss. These first insights into the mechanisms through which PPARγ influences synaptic loss make a case for further exploration of the potential usefulness of PPARγ agonists in the prevention and treatment of synaptic pathology in AD.

Keywords: Alzheimer's disease, amyloid beta, pioglitazone, PPARγ, neurons, Tau missorting, synaptic degradation

Abbreviations: Aβ, amyloid β; ABCA1, ATP-binding cassette transporter ABCA1; AD, Alzheimer's disease; APP, amyloid precursor protein; BACE1, β-secretase 1; DIV, days *in vitro*; FCS, fetal calf serum; GFAP, glial acidic fibrillary protein [GFAP]; GluN2B, glutamatergic receptor 2B subunit; GSK-3β, glycogen synthase kinase 3β; PGC-1α, peroxisome proliferator-activated receptor gamma coactivator 1α; Pio, pioglitazone; PPARγ, peroxisome proliferator-activated receptor γ; PSD-95, postsynaptic density-95; p-Tau, phosphorylated tau; T2D, type 2 diabetes; TZD, thiazolidinediones.

INTRODUCTION

While age represents the greatest risk for developing AD, modern lifestyle which frequently leads to obesity and T2D also appears to increase risk for developing AD (Biessel and Despa, 2018). While the link between T2D and AD may be equivocal (see Vemuri et al., 2017) and awaits longitudinal studies in humans that use new imaging technologies such as positron emission tomography (PET; see Arnold et al., 2018), evidence exists for an association between perturbed insulin signaling and AD histopathology, namely, Aβ aggregates and Tau protein-containing neurofibrillary tangles (NFT) (de la Monte and Tong, 2014; Mullins et al., 2017; Arnold et al., 2018). The latter, complement reports that animal models of diabetes exhibit cognitive impairments and features of AD neuropathology (Clodfelder-Miller et al., 2006). Together, these data make it plausible that AD may be amenable to antidiabetic treatments (for review, see Govindarajulu et al., 2018).

Insulin insensitivity, a mainstay of T2D, can be treated by activating PPARγ with TZD such as Pio (Ahmadian et al., 2013). Various TZD have also been shown to improve cognition in AD patients and mouse models of the disease (Risner et al., 2006; Hanyu et al., 2010; Mandrekar-Colucci et al., 2012; Searcy et al., 2012; Ahmadian et al., 2013). However, mechanisms through which TZD exert their effects in the brain remain elusive. In support of previous reports (Moreno et al., 2004; Lu et al., 2011; Warden et al., 2016), we recently mapped the expression of functional PPARγ in the rodent brain (Pissioti, 2016; Moosecker, 2018) and demonstrated the presence of TZD-responsive substrate(s) in the brain. Among other brain areas, PPARγ were localized in the frontal cortex and hippocampus, two cognitive centers that are particularly susceptible to neurodegeneration in AD.

In contrast to earlier views that aggregated Aβ and Tau are responsible for cognitive dysfunction in AD, recent work implicates soluble Aβ and hyperphosphorylated Tau protein as triggers of synaptic dysfunction and loss. Since synaptic malfunction and loss correlates strongly with cognitive deficits in AD patients (Wang and Mandelkow, 2016; Müller et al., 2017), a better understanding of the pathophysiology of soluble Aβ and hyperphosphorylated Tau is imperative. While our own early studies showed that soluble Aβ causes synaptic degradation (Roselli et al., 2005, 2011; Liu et al., 2010; Chang et al., 2016), the role of Tau and its abnormal hyperphosphorylation in synaptic dysfunction is gaining increasing attention (Kimura et al., 2007; Ittner et al., 2010; Lopes et al., 2016). An important impetus for this shift in focus was the demonstration that Tau, usually considered to be an axonal protein (Kubo et al., 2018), is localized in dendrites (Hoover et al., 2010; Ittner et al., 2010) and that, in fact, Tau can be *de novo* synthesized and hyperphosphorylated in dendrites and spines (Frandemiche et al., 2014; Pinheiro et al., 2016; Kobayashi et al., 2017).

The *in vitro* studies reported here focused on whether, and how, activation of PPARγ can influence the synaptotoxic effects of Aβ and/or Tau. Our experiments show that Pio-activated neuronal PPARγ inhibits APP misprocessing and protects against Aβ-induced synaptic degradation. In addition, the PPARγ agonist attenuated Tau missorting and hyperphosphorylation in Aβ-exposed neurons.

MATERIALS AND METHODS

Drugs

Soluble $A\beta_{1-42}$ was prepared from peptide obtained from American Peptide Co. (Sunnyvale, CA, United States; Cat. #62-0-80), according to Roselli et al. (2005) and Stine et al. (2011) and used at a concentration of 1 μM. Pio (Pio, 10 μM) and GW9662 (1 μM), both purchased from Sigma-Aldrich (Taufkirchen, Germany) were used after solution in dimethylsulfoxide (DMSO; final DMSO concentration 0.01%). Doses of Pio were chosen on the basis of previous cell culture studies (Inestrosa et al., 2004; Chang et al., 2015).

Cell Culture

The human neuroblastoma cell line, SH-SY5Y [American Tissue Culture Collection (ATCC®), CRL-2266™, Germany] was cultured in Minimum Essential Medium with Glutamax®, supplemented with 10% FCS, 1% penicillin-streptomycin, and 2 mM L-glutamine. When ∼ 20% confluent (6×5^{10} cells/well of a 6-well plate), cells were differentiated with 50 μM retinoic acid (Sigma-Aldrich) in 1% FCS medium for 5 days, followed by 20 ng/ml nerve growth factor (NGF; Bio-Techne, Wiesbaden, Germany) for a further 5 days. Cells were maintained at 37°C in an incubator with 5% CO_2 and 95% relative humidity.

Primary Neural Cell Cultures

Primary frontocortical and hippocampal cultures were prepared from brains of CD1 mice aged 5 days, according to previously described protocols (Lu et al., 2005; Roselli et al., 2005). For molecular/biochemical analyses, cells were plated on gelatine/poly-D-lysine-coated plates and maintained in Neurobasal/B27 medium supplemented with basic fibroblast growth factor (10 ng/ml; Life Technologies (Eggenstein, Germany) and kanamycin (100 μg/ml; Life Technologies). For immunocytochemical analyses, cells were plated at a density of 400–500 cells/mm^2 on poly-D-lysine-coated glass coverslips (Yu et al., 2010), and grown in Neurobasal/B27 before use after 14 days *in vitro* (14 DIV). Cultures were comprised of 15–20% of mature [microtubule-associated protein 2 (MAP2)-positive] neurons, 20–25% of astrocytes [glial acidic fibrillary acidic protein (GFAP)-positive], and ∼1% of O4-positive oligodendrocytes; microglia (anti-CD68, -CD1b and -Iba1 labeled) were undetectable. Experiments adhered to European Union Council Directive (2010/63/EU) and local regulations on use of animals.

Cell Viability Assay

The MTS assay kit (CellTiter 96® AQueous One Solution Cell Proliferation Assay (Promega, Mannheim, Germany) was used to monitor cell viability, following the manufacturer's instructions. Briefly, after exposure to MTS solution (3 h in dark), the optical

density (490 nm) of the supernatant was measured in an ELISA reader (BioTek Instruments, Winooski, VT, United States).

Immunofluorescence Staining and Image Analysis

Cells were stained as described by Roselli et al. (2005). Briefly, cells were fixed in ice-cold 4% paraformaldehyde for 15 min, washed in PBS (3 × 5 min) before permeabilization with 0.1% Triton X-100 (30 min), and blocked in 10% FCS (30 min, RT). Primary and secondary antibody solutions were prepared in 0.01 M PBS containing 0.1% Triton X-100 and 10% FCS. Cells were incubated (16 h; 4°C), with primary antibodies against postsynaptic density-95 (PSD-95; 1:1000; Neuromab, Davis, CA, United States; #75-028), synapsin 1,2 (1:1500; Synaptic Systems, Göttingen, Germany; #16002), and/or pTau (pS396-Tau) (1:1000; abcam, Cambridge, United Kingdom; ab109390) in PBST (0.01 M PBS + 0.03% Triton X100). After washing (3 × 30min in 0.01 M PBS), cells were incubated with one of the following secondary antibodies, as appropriate: goat-anti-rabbit Alexa Fluor 488 (1:1000; Invitrogen, Eggenstein, Germany; # A110374) or goat-anti- mouse Alexa Fuor 594 (1:1000; Invitrogen; # A110029)] for 1 h at RT; nuclei were counterstained with followed by Hoechst dye 33341 (Sigma; 1:50000; 10 min, RT). Images were obtained using a laser scanning confocal microscope (Olympus Fluoview 1000, Hamburg, Germany). For image quantification, 100 cells in 5 separate fields on each coverslip (3–6 coverslips per condition) were analyzed. The number of stained puncta on a defined dendritic length (100 μm) were quantified using SynPAnal software to monitor synaptic density (Danielson and Lee, 2014).

Immunoblotting

Cells were homogenized in lysis buffer [10 mM HEPES pH 7.9, 150 mM NaCl, 1 mM EGTA, 10% glycerol, 1% NP-40, Complete Protease Inhibitor (Roche, Mannheim, Germany), Phosphatase Inhibitor Cocktails II and III (Sigma)] using a sonifier (5 pulses, 20 kHz). After centrifugation (14,000 × *g*; 20 min), the protein content of the lysates (supernatants) were determined by the Lowry assay (Lowry et al., 1951); spectroscopic measurements (absorption wavelength: 750 nM) were made with a Synergy-HT plate reader (BioTek Instruments, Winooski, VT, United States). Sodium dodecyl sulfate-polyacrylamide gel (10%) electrophoresis (SDS-PAGE) was used to resolve heat-denatured (95°C; 10 min) protein lysates (30 μg). After electrophoresis, proteins were transferred onto 0.2 μm nitrocellulose membranes (BioRad, Hercules, CA, United States) by Turbo Transfer (BioRad). Transfer quality was assessed by incubating with Ponceau-S solution. Membranes were subsequently blocked in 5% non-fat milk or 5% BSA in TBS-T (1 h, RT), before overnight incubation (4°C) with one of the following primary antisera: APP A4 (1:500; Millipore, Burlington, MA, United States; #MAB348), BACE (D105E5) (1:1000; Cell Signaling; #5606), nicastrin (1:1000; Sigma; #N16660), pS202-Tau (1:1500; Abcam; ab108387); pT205-Tau (1:1500; Abcam; ab4841), pT231-Tau (1:1500; Abcam; ab151559), pS356-Tau (1:1500; Abcam; ab92682), PHF1 (p396/404-Tau; 1:1000; kind gift form Dr. Peter Davies, New York, NY, United States), Tau5 (1:1500; Abcam; ab 80579), GluN2B (1:1000, Abcam 65783), pSer9-GSK3β and total GSK3β (1:1000, Cell Signaling) and either actin (1:2500; Chemicon/Fischer Scientific, Munich, Germany; #MAB1501R) or GAPDH (1:1500, Abcam; ab8245). After thorough washing, membranes were incubated with a corresponding horseradish peroxidase (HRP)-conjugated secondary antibody [goat anti-rabbit (1:1000; Fischer Scientific; #31460) or goat anti-mouse (1:2000; BioRad; 170-6516)] for 1 h (RT). Clarity™ Western ECL reagent (Biorad) was used to visualize (ChemiDoc MP Imaging System; BioRad) and quantify (ImageLab 5.1 Software from BioRad) proteins.

PCR Analysis

Total RNA was isolated from cell lysates using the NucleoSpin (RNA) kit (Macherey-Nagel, Duren, Germany) and RNA concentrations were determined with a NanoPhotometer (SmartSpec™ Plus, Biorad).

Reverse Transcription

Complementary DNA (cDNA) was prepared from 1 μg RNA using a RevertAid RT Reverse Transcription kit (Thermo Scientific) with an oligo deoxythymine (dT) primer. Polymerase chain reactions (PCR) were performed using Taq DNA Polymerase kits (Fermentas/ThermoFisher) and the following primers:

ABCA1: fwd 5′-GACATCCTGAAGCCAATCC-3′
rev 5′-GTAGTTGTTGTCCTCATACC-3′
PGC-1α: fwd 5′-CGTGTCGAGACTCAGTGTC-3′
rev 5′-GTGTCTGTAGTGGCTTGATTC-3′
GAPDH: fwd 5′-CCATCACCATCTTCCAGG-3′
rev 5′-GTTGAAGTCGCAGGAGACAAC-3′

The PCR products were quantified using a Roche LightCycler 96. Relative expression levels of target genes were computed according to Pfaffl (2001).

Statistical Analysis

Statistical analysis and graphic representations were performed using GraphPad Prism software (GraphPad, San Diego, United States). Numerical data were analyzed by 1-way ANOVA or Kruskall-Wallis tests, and *post hoc* tests, as appropriate. Values were considered significant when $p < 0.05$.

RESULTS

Activation of PPARγ Attenuates APP Misprocessing, Tau Accumulation and Aβ-Induced Neurotoxicity in Differentiated SHSY5Y Cells

Initially, we examined whether differentiated human SH-SY5Y cells express functional PPARγ. For that purpose, we monitored the expression of two PPARγ target genes, *peroxisome proliferator-activated receptor gamma coactivator 1-α (PGC-1α)* and *ABCA1* (Strum et al., 2007; Kang and Rivest, 2012) after

treating cells with the potent PPARγ agonist, Pio (10 μM; 24 h). As shown in **Supplementary Figure 1**, Pio induced the expression of the mRNA levels of *PGC-1α* and *ABCA1*. These effects were abolished when cells were co-treated with Pio and the PPARγ antagonist GW9662, indicating that the actions of Pio were mediated by endogenous PPARγ (**Supplementary Figure 1**).

The neurodegenerative cascade leading to AD is initiated by Aβ. Here, to examine the role of PPARγ in modulating neuropathological markers of AD, we exploited our previously described model in which Aβ was shown to increase misprocessing of APP (Catania et al., 2009). Western blot analysis revealed that treatment of cells with Aβ (1 μM; 24 h) upregulated APP levels (**Figures 1A,E**) as well as those of β-secretase (BACE1) (**Figures 1B,E**) and nicastrin (**Figures 1C,E**) which sequentially contribute to the generation of Aβ. It may be extrapolated from these observations that exogenous Aβ stimulates the misprocessing of APP into Aβ. Importantly, concomitant exposure with Pio abolished the ability of Aβ to increase the expression of APP, BACE1 and nicastrin protein (**Figures 1A–C,E**).

Growing appreciation of the neurotoxic role of Tau protein (Takashima et al., 1998; Rapoport et al., 2002; Ittner et al., 2016) prompted an examination of how Aβ, in the presence or absence of Pio (10 μM), influences Tau metabolism in differentiated SH-SY5Y cells. As shown in **Figures 1D,E**, immunoblot analysis revealed that incubation of cells with Aβ results in increased levels of total Tau, an effect blocked when cells were co-treated with Pio. Further, Aβ treatment increased Tau phosphorylation (pS396/404-Tau) (**Figure 1F**) while decreasing the amount of inactive (pSer9) GSK-3β (**Figure 1G**); the effects of Aβ on pTau were also reversed by Pio (**Figures 1E–G**). In addition, we monitored the levels of NR2B subunit of the glutamate (NMDA) receptor (GluN2B) which is strongly implicated in neurotoxicity. Consistent with previous evidence that GluN2B largely mediate the neurotoxic actions of Aβ and Tau (Ittner et al., 2010), we observed that Aβ elevate GluN2B levels (**Figures 1H,E**) and, at the same time, compromises cell viability (**Figure 1I**). Both of these Aβ-induced phenomena were blocked when cells were co-treated with Pio, although Pio *per se* did not have any effect, i.e., Pio did not exert any effect in the absence of Aβ (**Supplementary Figure 2**).

Synaptic Degradation Induced by Aβ in Primary Neuronal Cultures Is Blocked by Pio Treatment

Since both Aβ and hyperphosphorylated Tau are known to disrupt synaptic function, we next examined the potential of Pio to prevent Aβ-driven synaptotoxicity in differentiated cultures derived from mouse frontal cortex and hippocampus; cultures were used at DIV 14, when 15–20% of the cells are MAP2-positive (mature neurons) bearing synapsin 1,2-immunoreactive mature synapses. Both frontocortical and hippocampal cultures express transcriptionally active PPARγ and display similar responses to Aβ (Moosecker, 2018). As shown previously (Roselli et al., 2005; Liu et al., 2010), synaptic loss was assessed by counting (SynPal software) apposed postsynaptic PSD-95- and presynaptic synapsin 1, 2- immunoreactive elements in confocal images (**Figure 2A**).

Neurons exposed to Aβ showed fewer synapses (reduced PSD-95 and synapsin puncta density (**Figures 2A–D**). This result is consistent with previous findings by Roselli et al., (2005) and Liu et al. (2010). Interestingly, the synaptic loss caused by Aβ was blocked in the presence of the PPARγ agonist Pio (**Figures 2A–D**), suggesting that Pio protects against Aβ synaptotoxicity.

Pioglitazone Counteracts Aβ-Driven Tau Hyperphosphorylation in Primary Cultures

In light of the fact that (i) Aβ induces Tau hyperphosphorylation (Takashima et al., 1998; Sotiropoulos et al., 2011), (ii) Tau hyperphosphorylation is causally linked to synaptic dysfunction and loss (Kimura et al., 2007), and (iii) Pio reduces the cytotoxic actions of Aβ (cf. **Figure 1J**), we also examined whether Pio can interfere with Aβ-triggered Tau hyperphosphorylation by monitoring drug effects on different phospho-epitopes of Tau (around and within its microtubule-binding domain) (see **Figure 3A**).

Our analysis revealed that exposure of primary neurons to Aβ leads to increased levels of various forms of pTau (pSer202-Tau, pThr205-Tau, pThr231-Tau, pSer356 and pSer396/Ser404), as shown in **Figure 3F** (representative immunoblots) and **Figures 3B–G** (semi-quantitative data). Notably, although Pio alone did not exert any effect on Tau protein (**Supplementary Figure 2**), the PPARγ agonist blocked Aβ-upregulated levels of pSer202-Tau, pThr205-Tau, pThr231-Tau, pSer356 and pSer396/Ser404-Tau (**Figures 3A–G**).

Prevention of Aβ-Induced Synaptic Missorting of Tau by Pio

Whereas Tau protein expression is confined to axons under normal conditions (Kubo et al., 2018), increased levels of Aβ have been shown to re-direct Tau into dendrites and dendritic spines, via a process termed "missorting" which triggers synaptic loss (Ittner et al., 2010; Zempel et al., 2010). Having observed that Pio exhibits a protective effect against Tau hyperphosphorylation (see **Figure 3**), we next monitored the effect of Pio on the localization of pTau (specifically, pSer396-Tau) in dendrites and synapses.

As shown in **Figure 4**, treatment of neuronal cultures with Aβ was found to increase p-Tau immunoreactivity in dendritic puncta (**Figures 4A,B**). The latter was abrogated when cultures were simultaneously exposed to Pio (**Figures 4A,B**). More detailed analysis of the data, in which the number of PSD-95/synapsin-positive synapses labeled with pTau were quantified, confirmed that Pio can effectively prevent the Aβ-induced mislocalization of pTau in PSD-95/synapsin-positive puncta (**Figure 4C**). Note that, Pio itself did not display activity on any of the synaptic parameters monitored (**Supplementary Figure 3**).

Since the results described in **Figures 1–4** clearly indicate involvement of PPARγ in regulating APP and Tau metabolism, as well as neuronal survival, we considered it important to

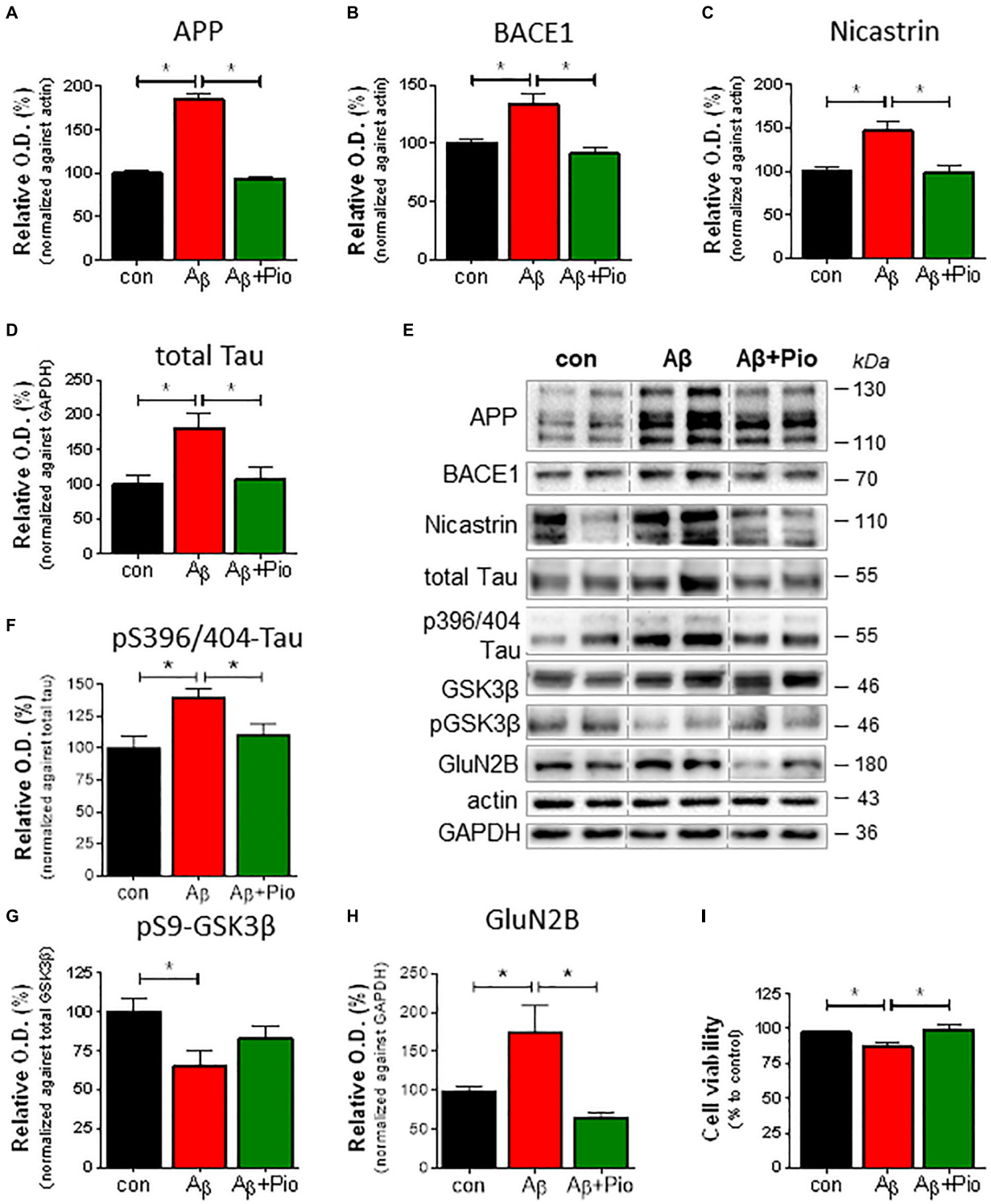

FIGURE 1 | Pioglitazone (Pio) attenuates APP misprocessing, Tau accumulation and Aβ-induced neurotoxicity in differentiated SHSY5Y cells.Exposure to Aβ (1 μM, 24 h) upregulated the levels of APP ($p < 0.0001$) **(A,E)**, BACE-1 ($p = 0.002$) **(B,E)**, and nicastrin ($p = 0.003$) **(C,E)**; co-treatment with the PPARγ agonist, Pio (Pio; 10 μM) abolished these effects of Aβ ($p_{APP} < 0.0001$; $p_{BACE} = 0.001$; $p_{nicastrin} = 0.038$). Exposure to Aβ increased total Tau levels ($p = 0.002$) in a Pio-reversible manner ($p = 0.006$) [1-way ANOVA $F = 7.745$; $p = 0.001$] **(D,E)**. Treatment of cells with Aβ resulted in elevated levels of pS396/404-Tau ($p = 0.015$) in a Pio-reversible manner ($p = 0.029$) [1-way ANOVA $F = 5.551$; $p = 0.015$] **(F,E)**; Aβ also reduced levels of pSer9-GSK3β (inactive GSK3β; ($p = 0.029$) **(G,E)**. Co-treatment of cells with Aβ and Pio failed to show Aβ-driven elevation of GluN2B protein levels ($p = 0.023$) [1-way ANOVA $F = 7.553$; $p = 0.0027$] **(H)** and Aβ-stimulated cell death ($p = 0.008$) [1-way ANOVA $F = 6.113$; $p = 0.007$] **(I)**; $N = 3$-5/condition; different cell cultures. All numeric data represent means ± S.E.M.

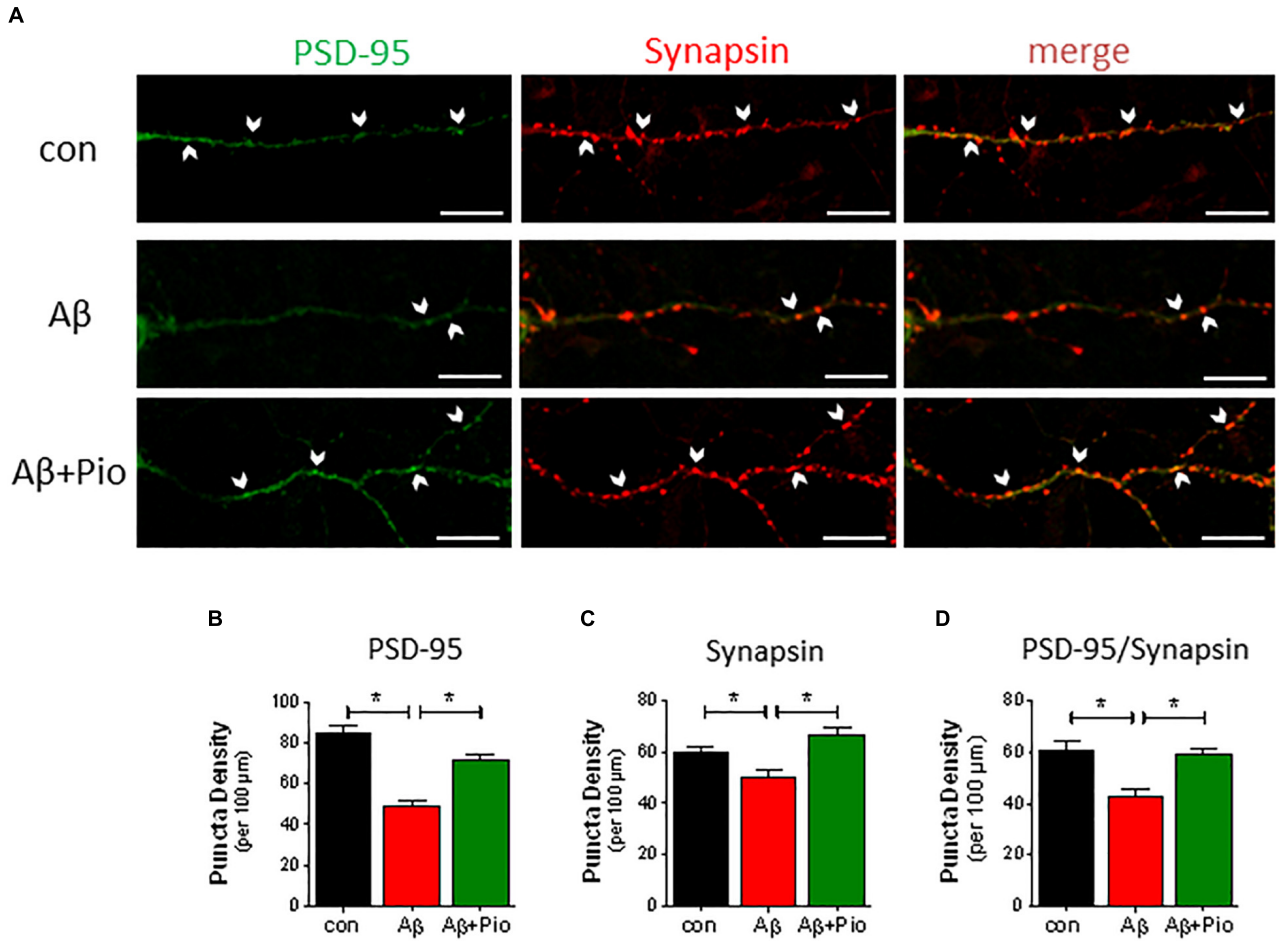

FIGURE 2 | Aβ-induced synaptic loss is rescued by Pio treatment. **(A)** Representative confocal images of synapses (identified by apposed PSD-95-, *green*, and synapsin-, *red*, immunoreactive elements) in mouse primary neuronal cultures under control conditions and exposure to Aβ (1 μM, 24 h) alone Aβ + Pio (Pio, PPARγ agonist). Examples of apposed PSD-95- and synapsin-positive staining are marked with white arrows. **(B)** Puncta analysis of dendrites revealed that Aβ decreases the density of PSD-95 puncta ($p < 0.0001$ vs. control) and that Pio reverts the effects of Aβ ($p < 0.0001$) [1-way ANOVA, $F_{2,63} = 35.01$; $p < 0.0001$]. **(C)** The reduced number of synapsin-positive puncta after Aβ treatment were restored to control levels when cells were co-exposed to Pio ($p = 0.001$) [1-way ANOVA, $F_{2,63} = 10,68$; $p < 0.0001$]. **(D)** Synapses, doubled-labeled for PSD-95 and synapsin immunoreactivity, were reduced after treatment with Aβ ($p = 0.0003$), indicating synaptic degradation and loss. The latter was absent in cells exposed to both Aβ and Pio ($p = 0.0012$) [1-way ANOVA, $F_{2,63} = 10.32$; $p < 0.0001$]; $N = 15$ non-overlapping fields/condition; different cultures, Means ± S.E.M are shown. Scale bar: 10 μm.

investigate whether the interruption of Aβ-induced synaptic loss and mislocalization of pTau by Pio depends on PPARγ. To this end, primary neurons were pre-treated with the PPARγ antagonist GW9662 before exposure to Pio + Aβ. Indeed, as shown in **Figures 5A–C**, PPARγ were demonstrated to mediate the reversal of Aβ-induced missorting of Tau to dendritic spines by Pio: the protective potency of Pio was lost in GW9662-treated cells. Briefly, the percentage of pTau-labeled synapses was greater in Pio + Aβ-treated cells than in cells receiving the combination of GW9662, Pio and Aβ (**Figure 5B**). Similarly, on the basis of PSD-95 puncta density measurements, GW9662 was found to neutralize the rescuing effect of Pio on Aβ-driven synaptic loss (**Figure 5C**). Together, this set of data demonstrates that PPARγ mediate the rescuing actions of Pio against Aβ-triggered synaptotoxity by preventing the missorting of Tau to synapses.

DISCUSSION

Pioglitazone, a pharmacological agonist of the nuclear receptor PPARγ, acts as an insulin sensitizer and is used to treat T2D, a risk factor for AD (Ahmadian et al., 2013; Arnold et al., 2018; Biessel and Despa, 2018). Reports that Pio and other TZD improve cognitive performance in AD patients and in mouse models of the disease (Risner et al., 2006; Hanyu et al., 2010; Mandrekar-Colucci et al., 2012; Searcy et al., 2012; Ahmadian et al., 2013) suggest that PPARγ may be potential therapeutic targets in AD (Zolezzi et al., 2017). A central question in the present work was whether the pro-cognitive and anti-neurodegenerative effects of Pio reflect direct actions in the brain or if they represent a collateral benefit of improved insulin sensitivity. Notably, some authors have also attributed the neuroprotective effects of TZD to

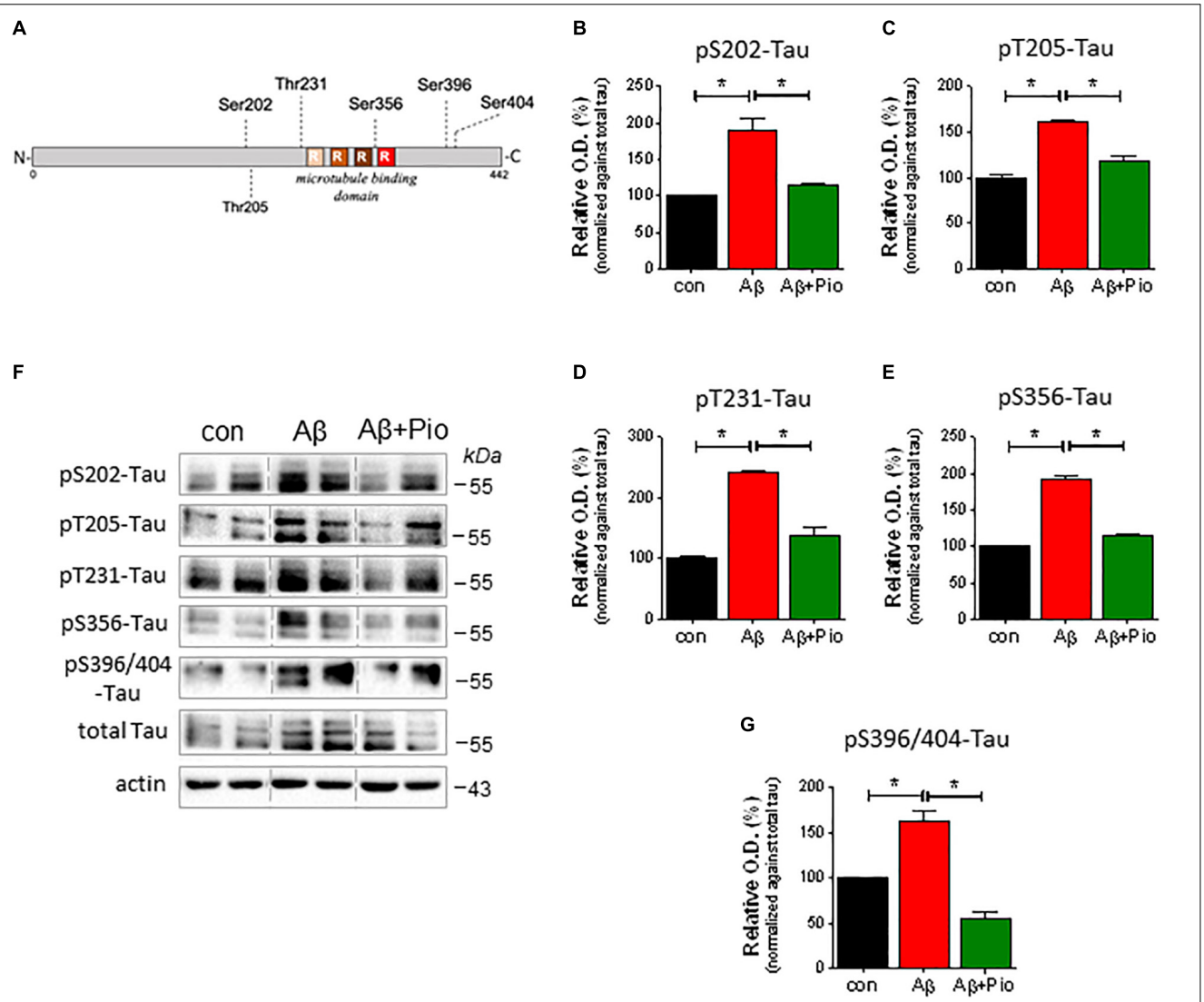

FIGURE 3 | Pioglitazone (Pio) counteracts Aβ-driven Tau hyperphosphorylation. **(A)** Schematic representation of Tau protein and the different phosphorylation epitopes analyzed in this study. **(B–G)** Effects of Aβ (1 μM, 24 h), in presence and absence of Pio (Pio; 10 μM), on the expression of different forms of pTau in 14 DIV primary neurons. Representative immunoblots are shown in **(F)**. Semi-quantitative analysis reveals that, as compared to vehicle treatment, Aβ induces higher levels of pS202-Tau **(B)**, pT205-Tau **(C)**, pT231-Tau **(D)**, pS356-Tau **(E)** and pS396/404-Tau **(G)** ($p < 0.05$ in all cases); all of these effects were attenuated ($p < 0.05$) when cells were co-treated with Pio **(B–G)** [Kruskal-Wallis test $H_2 = 9.881$, $p = 0.0002$]; $N = 3$-5/condition; different cell cultures. Semi-quantitative data are shown as means ± S.E.M.

their anti-inflammatory and/or -oxidative properties (Heneka et al., 2005, 2015; Wang X.K. et al., 2017; Zhang et al., 2017), phenomena that could help explain the purported role of activated PPARγ in a spectrum of neurological diseases (Zolezzi et al., 2017).

Complementing data reported by Xu et al. (2014), we here show that Pio counteracts the detrimental effects of Aβ on neural cell viability. In addition, we found that Pio dampens Aβ-stimulated misprocessing of endogenous APP into Aβ through the mediation of β-secretase 1 (BACE1) and γ-secretase (see Catania et al., 2009). These observations are consistent with previous reports that TZD can reduce APP misprocessing as well as Aβ deposition in transgenic mouse models of AD (Escribano et al., 2010; Mandrekar-Colucci et al., 2012; Skerrett et al., 2015) as well as in primary neural cultures (Mandrekar-Colucci et al., 2012; Skerrett et al., 2015) and in neural cell lines overexpressing APP (Camacho et al., 2004). The inhibitory effect of Pio on APP misprocessing likely reflects transcriptional regulation of BACE1 by PPARγ: the *BACE1* promoter harbors a PPARγ response element (PPRE) (Heneka et al., 2005; Sastre et al., 2006; Chen et al., 2009; Wang X. et al., 2017) and genetic deletion of related PPAR isoforms (PPAR β/δ) leads to increased BACE1 expression in mice (Barroso et al., 2013).

We also report here that Pio prevents the ability of exogenous Aβ to increase the expression of Tau and several phospho-Tau

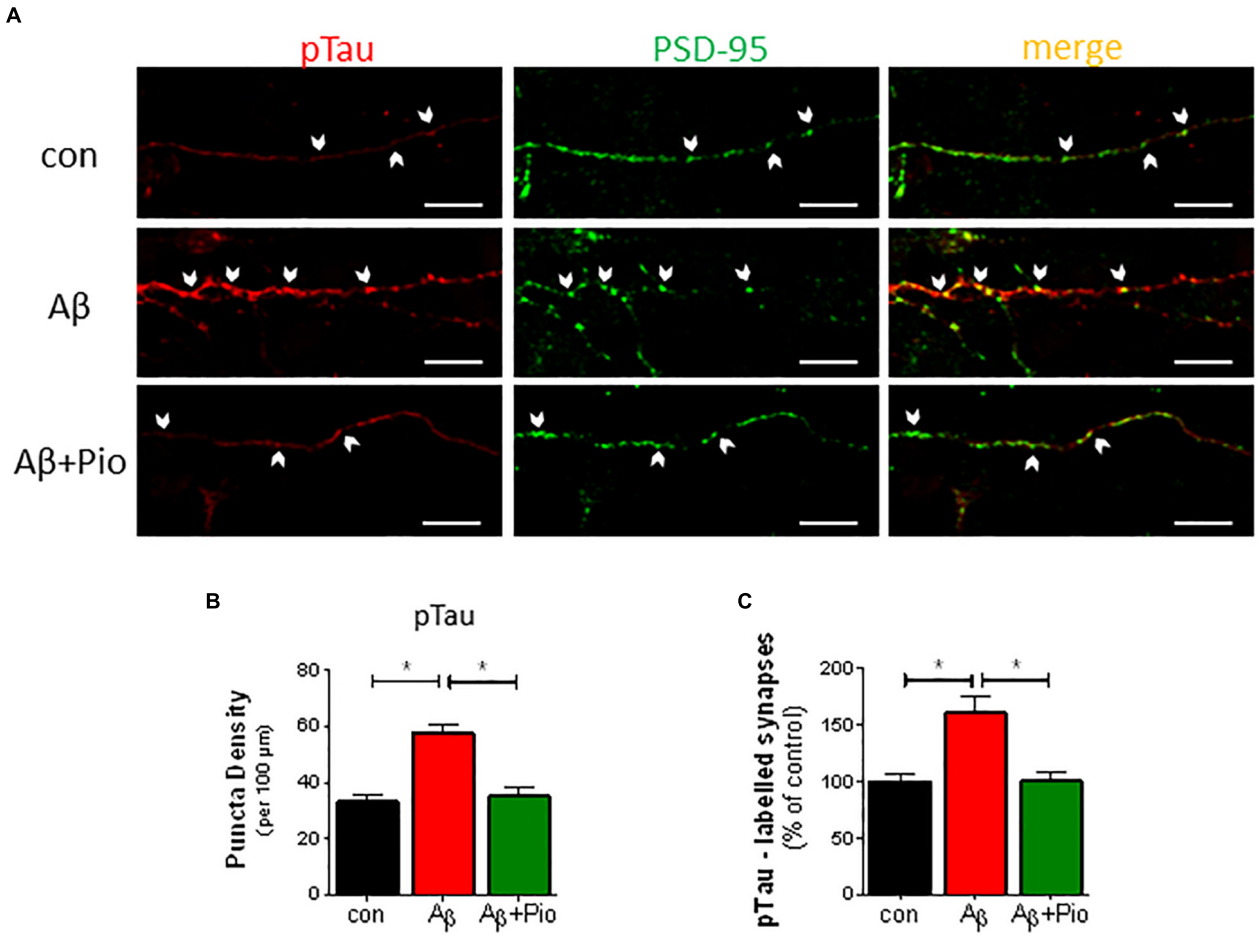

FIGURE 4 | Prevention of Aβ-driven synaptic missorting of phospho-Tau by Pio. **(A)** Representative immunofluorescent images of 14 DIV neurons stained with antibodies against pTau (pSer396-Tau, *red*) and PSD-95 (*green*) after treatment with Aβ (1 μM, 24 h) and/or Pio (10 μM). Examples of apposed PSD-95- and pTau-positive staining are marked with white arrows. **(B)** Density of pTau-positive puncta in dendrites increases after exposure to Aβ ($p < 0.0001$ vs. control) in a Pio-reversible fashion ($p = 0.0002$ vs. Aβ alone) [1-way ANOVA, $F_{2,44} = 18.02$; $p < 0.0001$]. **(C)** The percentage of PSD-95-labeled synaptic puncta that are pTau-positive is higher in Aβ- vs. vehicle-treated cells ($p = 0.0002$), indicating missorting of pTau to synapses. In the presence of Pio, Aβ exhibited a weaker effect on pTau missorting ($p = 0.002$) [1-way ANOVA, $F_{2,76} = 11.79$; $p < 0.0001$]; $N = 15$ non-overlapping fields/condition; different cultures. Means ± S.E.M. are depicted. Scale bar: 10 μm.

epitopes that are found in the brains of AD patients (see Iqbal et al., 2016). The latter observation, which is consistent with a previous report that TZD reduce Tau hyperphosphorylation in a 3 × Tg mouse model of AD (Yu et al., 2015), is important since Tau is now recognized as a critical mediator of the synaptotoxic effects of Aβ (Kimura et al., 2007; Roberson et al., 2007; Ittner et al., 2010; Lopes et al., 2016). Together, this and the previous set of data suggest that activation of PPARγ breaks the link between Aβ-induced neurotoxicity and tau pathology.

The present work also examined the possibility that PPARγ may be involved in synaptic dysfunction and loss, two events that appear to underpin memory loss in AD patients (Xu et al., 2014; Chen et al., 2015; Canter et al., 2016). In line with our previous findings in frontocortical (Roselli et al., 2005) and hippocampal (Liu et al., 2010) neurons, Aβ was here found to induce a loss of synapses, seen as a reduction in the number of apposed synapsin- and PSD-95-immunoreactive puncta. Further, and in confirmation of results reported by Xu et al. (2014), we show that Aβ-induced degradation of synapses can be blocked by co-treating neurons with Pio. Interestingly, earlier studies reported that TZD-activated PPARγ promote synaptic plasticity (Nenov et al., 2015). Notwithstanding a role for neurotrophins in mediating the neuroplastic effects of activated PPARγ (Kariharan et al., 2015), analysis of the data presented in this paper suggest, for the first time, that PPARγ-mediated inhibition of Tau mislocalization (missorting) to the dendritic compartment represents an important mechanism through which TZD impede progression of the neurodegenerative cascade initiated by Aβ. In agreement with earlier reports (Hoover et al., 2010; Zempel et al., 2010), we observed that Aβ leads to an accumulation of hyperphosphorylated Tau in dendritic spines; the latter event is believed to activate a pathway that upregulates GluN2B receptor expression which, in turn, culminates in synaptic dysfunction and

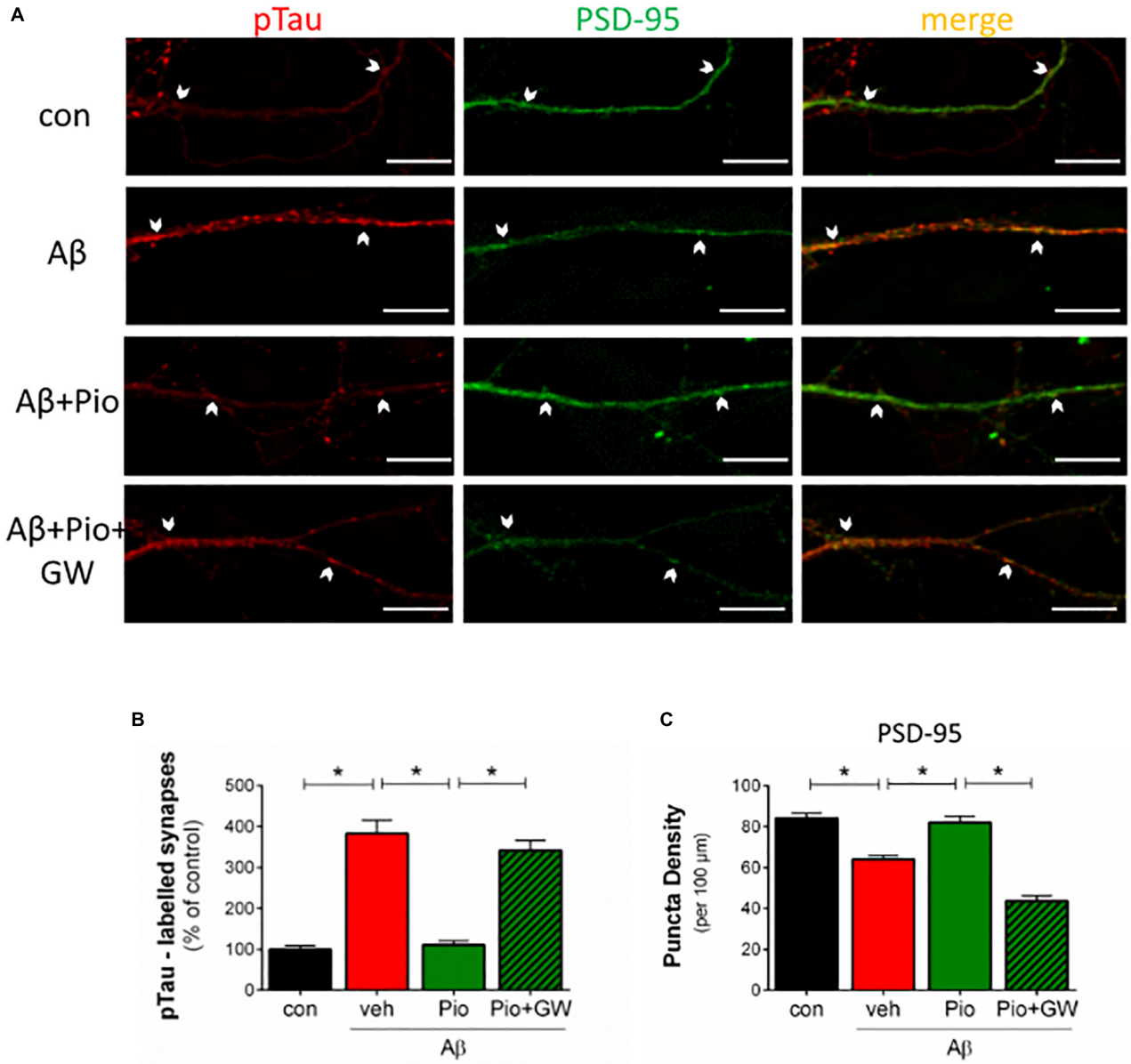

FIGURE 5 | Protective actions of Pio against Aβ-induced missorting of Tau and synaptic loss are PPARγ-mediated. **(A)** Primary cultures were pre-treated with the specific PPARγ antagonist GW9662 (GW) before exposure to Aβ alone, or Aβ + Pio (PPARγ agonist). Cells were immunostained for PSD-95 (*green*) and pTau (pSer396-Tau; *red*) and examined by confocal microscopy. Examples of apposed PSD-95- and pTau-positive staining are marked with white arrows. **(B)** Shows that Aβ leads to an increase ($p < 0.0001$) in the percentage of pTau-positive synaptic puncta (PSD-labeled), an effect blocked when Pio is also present. Importantly, Pio failed to counter the effects of Aβ when cells were pre-exposed to GW9662 ($p < 0.0001$ in all cases) [1-way ANOVA, $F_{3,37} = 62.40$; $p < 0.0001$]. **(C)** Shows that GW9662 also blocks the protective effects of Pio ($p < 0.0001$) against the loss of PSD-95-positive puncta in neurons treated with Aβ ($p = 0.0002$) [1-way ANOVA, $F_{3,48} = 45.44$; $p < 0.0001$]; $N = 15$ non-overlapping fields/condition. Numerical data shown represent means ± S.E.M. Scale bar: 10 μm.

elimination (Hoover et al., 2010; Ittner et al., 2010; Lopes et al., 2016). Briefly, our results indicate that Pio prevents Aβ-driven hyperphosphorylation and intraneuronal trafficking of Tau. It is important to note here that Hoover et al. (2010) demonstrated that hyperphosphorylation of Tau is necessary for the missorting and accumulation of Tau at synapses.

In summary, the current experiments provide new insights into the mechanisms through which activated PPARγ can provide neuroprotection by acting directly on neural substrates, independently of their insulin-sensitizing properties in the periphery. Interestingly, the protective actions of Pio only became manifest when neurons were challenged with an insult, namely, elevated Aβ levels. Lastly, this work introduces the notion that prevention of the mislocalization of Tau to dendrites is a key mechanism underlying the neuroprotective actions of PPARγ agonists.

AUTHOR CONTRIBUTIONS

SM performed experiments, analyzed, and interpreted data, wrote the first drafts of the manuscript. PG and CD contributed to immunoblotting assays and analysis, and graphic presentation. SY helped with primary cultures and immunocytochemistry. SM, IS, and OA conceptualized the study. IS and OA supervised the work and finalized the manuscript. Parts of this work are adapted from a Ph.D. thesis by SM, submitted to Technical University, Munich (Ph.D. awarded: February 2019).

FUNDING

This work was supported by the SwitchBox Project, funded by the European Union (FP7-Health, Contract 259772) to OA, and by grants from the Portuguese North Regional Operational Program (ON.2) under the National Strategic Reference Framework (QREN), through the European Regional Development Fund (FEDER), Project Estratégico co-funded by FCT (PEst-C/SAU/LA0026/2013), the European Regional Development Fund COMPETE (FCOMP-01-0124- FEDER-037298), Project NORTE-01-0145-FEDER-000013 (Portugal 2020 Partnership Agreement, European Regional Development Fund), FEDER funds from Competitiveness Factors Operational Programme (COMPETE), and grants from the Portuguese Foundation for Science and Technology (FCT) to IS (POCI-01-0145-FEDER-007038) and to PG (PD/BD/135271/2017). The funding agencies played no role in the design, execution or interpretation of the findings reported herein. SM was partly supported by a pre-doctoral fellowship from the Max Planck Society and received a Short-Term Scientific Mission bursary from COST Action MouseAge (BM1402).

ACKNOWLEDGMENTS

We thank Professor Hans Hauner (Technical University of Munich) for encouragement and critical suggestions during this work, Albin Varga and his team for help with animal breeding and care, Oliver Kattner for help with analysis of confocal images and Dr. Ulrike Schmidt for sharing lab and office space.

SUPPLEMENTARY MATERIAL

The Supplementary Material for this article can be found online at: https://www.frontiersin.org/articles/10.3389/fncel.2019.00239/full#supplementary-material

REFERENCES

Ahmadian, M., Suh, J. M., Hah, N., Liddle, C., Atkins, A. R., Downes, M., et al. (2013). PPARγ signaling and metabolism: the good, the bad and the future. *Nat. Med.* 19, 557–566. doi: 10.1038/nm.3159

Arnold, S. E., Arvanitakis, Z., Macauley-Rambach, S. L., Koenig, A. M., Wang, H. Y., Ahima, R. S., et al. (2018). Brain insulin resistance in type 2 diabetes and Alzheimer disease: concepts and conundrums. *Nat. Rev. Neurol.* 14, 168–181. doi: 10.1038/nrneurol.2017.185

Barroso, E., del Valle, J., Porquet, D., Vieira Santos, A. M., Salvadó, L., and Rodríguez-Rodríguez, R. (2013). Tau hyperphosphorylation and increased BACE1 and RAGE levels in the cortex of PPARβ/δ-null mice. *Biochim. Biophys. Acta* 1832, 1241–1248. doi: 10.1016/j.bbadis.2013.03.006

Biessel, G. J., and Despa, F. (2018). Cognitive decline and dementia in diabetes mellitus: mechanisms and clinical implications. *Nat. Rev. Endocrinol.* 14, 591–604. doi: 10.1038/s41574-018-0048-7

Camacho, I. E., Serneels, L., Spittaels, K., Merchiers, P., Dominguez, D., and De Strooper, B. (2004). Peroxisome-proliferator-activated receptor gamma induces a clearance mechanism for the amyloid-beta peptide. *J. Neurosci.* 24, 10908–10917. doi: 10.1523/jneurosci.3987-04.2004

Canter, R. G., Penny, J., and Tsai, L.-H. (2016). The road to restoring neural circuits for the treatment of Alzheimer's disease. *Nature* 539, 187–196. doi: 10.1038/nature20412

Catania, C., Sotiropoulos, I., Silva, R., Onofri, C., Breen, K. C., Sousa, N., et al. (2009). The amyloidogenic potential and behavioral correlates of stress. *Mol. Psychiatry* 14, 95–105. doi: 10.1038/sj.mp.4002101

Chang, K. L., Pee, H. N., Tan, W. P., Dawe, G. S., Holmes, E., Nicholson, J. K., et al. (2015). Metabolic profiling of CHO-AβPP695 cells revealed mitochondrial dysfunction prior to amyloid-β pathology and potential therapeutic effects of both PPARγ and PPARα Agonisms for Alzheimer's disease. *J. Alzheimers Dis.* 44, 215–231. doi: 10.3233/jad-140429

Chang, L., Zhang, Y., Liu, J., Song, Y., Lv, A., Li, Y., et al. (2016). Differential regulation of N-Methyl.D-aspartate receptor subunits is an early event in the actions of soluble amyloid β (1-40) oligomers on hippocampal neurons. *J. Alzheimers Dis.* 51, 197–212. doi: 10.3233/JAD-150942

Chen, J., Li, S., Sun, W., and Li, J. (2015). Anti-diabetes drug pioglitazone ameliorates synaptic defects in AD transgenic mice by inhibiting cyclin-dependent kinase 5 activity. *PLoS One* 10:e0123864. doi: 10.1371/journal.pone.0123864

Chen, Y., Zhou, K., Wang, R., Liu, Y., Kwak, Y. D., Ma, T., et al. (2009). Antidiabetic drug metformin (GlucophageR) increases biogenesis of Alzheimer's amyloid peptides via up-regulating BACE1 transcription. *Proc. Natl. Acad. Sci. U.S.A.* 106, 3907–3912. doi: 10.1073/pnas.0807991106

Clodfelder-Miller, B. J., Zmijewska, A. A., Johnson, G. V., and Jope, R. S. (2006). Tau is hyperphosphorylated at multiple sites in mouse brain in vivo after streptozotocin-induced insulin deficiency. *Diabetes* 55, 3320–3325. doi: 10.2337/db06-0485

Danielson, E., and Lee, S. H. (2014). SynPAnal: software for rapid quantification of the density and intensity of protein puncta from fluorescence microscopy images of neurons. *PLoS One* 9:e115298. doi: 10.1371/journal.pone.0115298

de la Monte, S. M., and Tong, M. (2014). Brain metabolic dysfunction at the core of Alzheimer's disease. *Biochem. Pharmacol.* 88, 548–559. doi: 10.1016/j.bcp.2013.12.012

Escribano, L., Simón, A. M., Gimeno, E., Cuadrado-Tejedor, M., López de Maturana, R., García-Osta, A., et al. (2010). Rosiglitazone rescues memory impairment in Alzheimer's transgenic mice: mechanisms involving a reduced amyloid and tau pathology. *Neuropsychopharmacology* 35, 1593–1604. doi: 10.1038/npp.2010.32

Frandemiche, M. L., De, Seranno S, Rush, T., Borel, E., Elie, A., Arnal, I., et al. (2014). Activity-dependent tau protein translocation to excitatory synapse is disrupted by exposure to amyloid-beta oligomers. *J. Neurosci.* 34, 6084–6097. doi: 10.1523/JNEUROSCI.4261-13.2014

Govindarajulu, M., Pinky, P. D., Bloemer, J., Ghanei, N., Suppiramaniam, V., and Amin, R. (2018). Signaling Mechanisms of Selective PPARγ Modulators in Alzheimer's Disease. *PPAR Res.* 2018:2010675. doi: 10.1155/2018/2010675

Hanyu, H., Sato, T., Sakurai, H., and Iwamoto, T. (2010). The role of tumour necrosis factor-alpha in cognitive improvement after peroxisome proliferator-activator receptor gamma agonist pioglitazone treatment in Alzheimer's disease. *J. Am. Geriatr. Soc.* 58, 1000–1001. doi: 10.1111/j.1532-5415.2010.02841.x

Heneka, M. T., Carson, M. J., El Khoury, J., Landreth, G. E., Brosseron, F., Feinstein, D. L., et al. (2015). Neuroinflammation in Alzheimer's disease. *Lancet Neurol.* 14, 388–405. doi: 10.1016/S1474-4422(15)70016-5

Heneka, M. T., Sastre, M., Dumitrescu-Ozimek, L., Hanke, A., Dewachter, I., Kuiperi, C., et al. (2005). Acute treatment with the PPARgamma agonist pioglitazone and ibuprofen reduces glial inflammation and Abeta1-42 levels in APPV717I transgenic mice. *Brain* 128, 1442–1453. doi: 10.1093/brain/awh452

Hoover, B. R., Reed, M. N., Su, J., Penrod, R. D., Kotilinek, L. A., Grant, M. K., et al. (2010). Tau mislocalization to dendritic spines mediates synaptic dysfunction independently of neurodegeneration. *Neuron* 68, 1067–1081. doi: 10.1016/j.neuron.2010.11.030

Inestrosa, N. C., Godoy, J. A., Quintanilla, R. A., Koenig, C. S., and Bronfman, M. (2004). Peroxisome proliferator-activated receptor gamma is expressed in hippocampal neurons and its activation prevents beta-amyloid neurodegeneration: role of Wnt signaling. *Exp. Cell Res.* 304, 91–104. doi: 10.1016/j.yexcr.2004.09.032

Iqbal, K., Liu, F., and Gong, C.-X. (2016). Tau and neurodegenerative disease: the story so far. *Nat. Rev. Neurol.* 12, 15–27. doi: 10.1038/nrneurol.2015.225

Ittner, A., Chua, S. W., Bertz, J., Volkerling, A., van der Hoven, J., Gladbach, A., et al. (2016). Site specific phosphorylation of tau inhibits amyloid-b toxicity in AD mice. *Science* 354, 904–908. doi: 10.1126/science.aah6205

Ittner, L. M., Ke, Y. D., Delerue, F., Bi, M., Gladbach, A., van Eersel, J., et al. (2010). Dendritic function of tau mediates amyloid-beta toxicity in Alzheimer's disease mouse models. *Cell* 142, 387–397. doi: 10.1016/j.cell.2010.06.036

Kang, J., and Rivest, S. (2012). Lipid metabolism and neuroinflammation in Alzheimer's disease: a role for liver X receptors. *Endocr. Rev.* 33, 715–746. doi: 10.1210/er.2011-1049

Kariharan, T., Nanayakkara, G., Parameshwaran, K., Bagasrawala, I., Ahuja, M., Abdel-Rahman, E., et al. (2015). Central activation of PPAR-gamma ameliorates diabetes induced cognitive dysfunction and improves BDNF expression. *Neurobiol. Aging* 36, 1451–1461. doi: 10.1016/j.neurobiolaging.2014.09.028

Kimura, T., Yamashita, S., Fukuda, T., Park, J. M., Murayama, M., Mizoroki, T., et al. (2007). Hyperphosphorylated tau in parahippocampal cortex impairs place learning in aged mice expressing wild-type human tau. *EMBO J.* 26, 5143–5152. doi: 10.1038/sj.emboj.7601917

Kobayashi, S., Tanaka, T., Soeda, Y., Almeida, O. F. X., and Takashima, A. (2017). Local somatodendritic translation and hyperphosphorylation of tau protein triggered by ampa and nmda receptor stimulation. *EBioMedicine* 20, 120–126. doi: 10.1016/j.ebiom.2017.05.012

Kubo, A., Misonou, H., Matsuyama, M., Nomori, A., Wada-Kakuda, S., Takashima, A., et al. (2018). Distribution of endogenous normal tau in the mouse brain. *J. Comp. Neurol.* 527, 985–998. doi: 10.1002/cne.24577

Liu, J., Chang, L., Roselli, F., Almeida, O. F., Gao, X., Wang, X., et al. (2010). Amyloid-β induces caspase-dependent loss of PSD-95 and synaptophysin through NMDA receptors. *J. Alzheimers Dis.* 22, 541–556. doi: 10.3233/JAD-2010-100948

Lopes, S., Vaz-Silva, J., Pinto, V., Dalla, C., Kokras, N., Bedenk, B., et al. (2016). Tau protein is essential for stress-induced brain pathology. *Proc. Natl. Acad. Sci. U.S.A.* 113, E3755–E3763. doi: 10.1073/pnas.1600953113

Lowry, O. H., Rosebrough, N. J., Farr, A. L., and Randall, R. J. (1951). Protein measurement with the Folin phenol reagent. *J. Biol. Chem.* 193, 265–275.

Lu, J., Wu, Y., Sousa, N., and Almeida, O. F. (2005). SMAD pathway mediation of BDNF and TGFβ2 regulation of proliferation and differentiation of hippocampal granule neurons. *Development* 132, 3231–3242. doi: 10.1242/dev.01893

Lu, M., Sarruf, D. A., Talukdar, S., Sharma, S., Li, P., Bandyopadhyay, G., et al. (2011). Brain PPAR-γ promotes obesity and is required for the insulin-sensitizing effect of thiazolidinediones. *Nat. Med.* 17, 618–622. doi: 10.1038/nm.2332

Mandrekar-Colucci, S., Karlo, J. C., and Landreth, G. E. (2012). Mechanisms underlying the rapid peroxisome proliferator-activated receptor-γ-mediated amyloid clearance and reversal of cognitive deficits in a murine model of Alzheimer's disease. *J. Neurosci.* 32, 10117–10128. doi: 10.1523/JNEUROSCI.5268-11.2012

Moosecker, S. (2018). *Identification of Functional Peroxisome Proliferated-Activated Receptor γ (PPARγ) in Mouse Brain and its Implication in Alzheimer Disease*. Ph.D. thesis, Technical University of Munich, Munich.

Moreno, S., Farioli-Vecchioli, S., and Cerù, M. P. (2004). Immunolocalization of peroxisome proliferator-activated receptors and retinoid X receptors in the adult rat CNS. *Neuroscience* 123, 131–145. doi: 10.1016/j.neuroscience.2003.08.064

Müller, U. C., Deller, T., and Korte, M. (2017). Not just amyloid: physiological functions of the amyloid precursor protein family. *Nat. Rev. Neurosci.* 18, 281–298. doi: 10.1038/nrn.2017.29

Mullins, R. J., Diehl, T. C., Chia, C. W., and Kapogiannis, D. (2017). Insulin resistance as a link between amyloid-beta and tau pathologies in alzheimer's Disease. *Front. Aging Neurosci.* 9:118. doi: 10.3389/fnagi.2017.00118

Nenov, M. N., Tempia, F., Denner, L., Dineley, K. T., and Laezza, F. (2015). Impaired firing properties of dentate granule neurons in an Alzheimer's disease animal model are rescued by PPARγ agonism. *J. Neurophysiol.* 113, 1712–1726. doi: 10.1152/jn.00419.2014

Pinheiro, S., Silva, J., Mota, C., Vaz-Silva, J., Veloso, A., Pinto, V., et al. (2016). Tau mislocation in glucocorticoid-triggered hippocampal pathology. *Mol. Neurobiol.* 53, 4745–4753. doi: 10.1007/s12035-015-9356-2

Pissioti, A. (2016). *Peroxisome Proliferator-Activated Receptor Gamma (PPARγ): Linking Peripheral Metabolism With Stress-Related Anomalies in the Mouse Brain*. Ph.D. thesis, Technical University of Munich, Munich.

Rapoport, M., Dawson, H. N., Binder, L. I., Vitek, M. P., and Ferreira, A. (2002). Tau is essential to beta -amyloid-induced neurotoxicity. *Proc. Natl. Acad. Sci. U.S.A.* 99, 6364–6369.

Risner, M. E., Saunders, A. M., Altman, J. F., Ormandy, G. C., Craft, S., Foley, I. M., et al. (2006). Efficacy of rosiglitazone in a genetically defined population with mild-to-moderate Alzheimer's disease. *Pharmacogenomics J.* 6, 246–254. doi: 10.1038/sj.tpj.6500369

Roberson, E. D., Scearce-Levie, K., Palop, J. J., Yan, F., Cheng, I. H., Wu, T., et al. (2007). Reducing endogenous tau ameliorates amyloid beta-induced deficits in an Alzheimer's disease mouse model. *Science* 316, 750–754. doi: 10.1126/science.1141736

Roselli, F., Livrea, P., and Almeida, O. F. (2011). CDK5 is essential for soluble amyloid β-induced degradation of GKAP and remodeling of the synaptic actin cytoskeleton. *PLoS One* 6:e23097. doi: 10.1371/journal.pone.0023097

Roselli, F., Tirard, M., Lu, J., Hutzler, P., Lamberti, P., Livrea, P., et al. (2005). Soluble beta-amyloid1-40 induces NMDA-dependent degradation of postsynaptic density-95 at glutamatergic synapses. *J. Neurosci.* 25, 11061–11070. doi: 10.1523/jneurosci.3034-05.2005

Sastre, M., Klockgether, T., and Heneka, M. (2006). Contribution of inflammatory processes to Alzheimer's disease: molecular mechanisms. *Int. J. Dev. Neurosci.* 24, 167–176. doi: 10.1016/j.ijdevneu.2005.11.014

Searcy, J. L., Phelps, J. T., Pancani, T., Kadish, I., Popovic, J., Anderson, K. L., et al. (2012). Long-term pioglitazone treatment improves learning and attenuates pathological markers in a mouse model of Alzheimer's disease. *J. Alzheimers Dis.* 30, 943–961. doi: 10.3233/JAD-2012-111661

Skerrett, R., Pellegrino, M. P., Casali, B. T., Taraboanta, L., and Landreth, G. E. (2015). Combined liver X receptor/peroxisome proliferator-activated receptor γ agonist treatment reduces amyloid β levels and improves behavior in amyloid precursor protein/presenilin 1 Mice. *J. Biol. Chem.* 290, 21591–21602. doi: 10.1074/jbc.M115.652008

Sotiropoulos, I., Catania, C., Pinto, L. G., Silva, R., Pollerberg, G. E., Takashima, A., et al. (2011). Stress acts cumulatively to precipitate Alzheimer's disease-like tau pathology and cognitive deficits. *J. Neurosci.* 31, 7840–7847. doi: 10.1523/JNEUROSCI.0730-11.2011

Stine, W. B., Jungbauer, L., Yu, C., and LaDu, M. J. (2011). Preparing synthetic Aβ in different aggregation states. *Methods Mol. Biol.* 670, 13–32. doi: 10.1007/978-1-60761-744-0_2

Strum, J. C., Shehee, R., Virley, D., Richardson, J., Mattie, M., Selley, P., et al. (2007). Rosiglitazone induces mitochondrial biogenesis in mouse brain. *J. Alzheimers Dis.* 11, 45–51. doi: 10.3233/jad-2007-11108

Takashima, A., Honda, T., Yasutake, K., Michel, G., Murayama, O., Murayama, M., et al. (1998). Activation of tau protein kinase I/glycogen synthase kinase-3beta by amyloid beta peptide (25-35) enhances phosphorylation of tau in hippocampal neurons. *Neurosci. Res.* 31, 317–323. doi: 10.1016/s0168-0102(98)00061-3

Vemuri, P., Knopman, D. S., Lesnick, T. G., Przybelski, S. A., Mielke, M. M., Graff-Radford, J., et al. (2017). Evaluation of amyloid protective factors and alzheimer disease neurodegeneration protective factors in elderly individuals. *JAMA Neurol.* 74, 718–726. doi: 10.1001/jamaneurol.2017.0244

Wang, X. K., Sun, T., Li, Y. J., Wang, Y. H., Li, Y. J., Yang, L. D., et al. (2017). A novel thiazolidinediones ATZD2 rescues memory deficits in a rat model of type 2 diabetes through antioxidant and antiinflammation. *Oncotarget* 18, 107409–107422. doi: 10.18632/oncotarget.22467

Wang, X., Wang, Y., Hu, J. P., Yu, S., Li, B. K., Cui, Y., et al. (2017). Astragaloside IV, a natural PPARγ agonist, reduces Aβ production in alzheimer's disease through inhibition of BACE1. *Mol. Neurobiol.* 54, 2939–2949. doi: 10.1007/s12035-016-9874-6

Wang, Y., and Mandelkow, E. (2016). Tau in physiology and pathology. *Nat. Rev. Neurosci.* 17, 5–21. doi: 10.1038/nrn.2015.1

Warden, A., Truitt, J., Merriman, M., Ponomareva, O., Jameson, K., Ferguson, L., et al. (2016). Localization of PPAR isotypes in the adult mouse and human brain. *Sci. Rep.* 6:27618. doi: 10.1038/srep27618

Xu, S., Liu, G., Bao, X., Wu, J., Li, S., Zheng, B., et al. (2014). Rosiglitazone prevents amyloid-β oligomer-induced impairment of synapse formation and plasticity via increasing dendrite and spine mitochondrial number. *J. Alzheimers Dis.* 39, 239–251. doi: 10.3233/JAD-130680

Yu, S., Patchev, A. V., Wu, Y., Lu, J., Holsboer, F., Zhang, J. Z., et al. (2010). Depletion of the neural precursor cell pool by glucocorticoids. *Ann. Neurol.* 67, 21–30. doi: 10.1002/ana.21812

Yu, Y., Li, X., Blanchard, J., Li, Y., Iqbal, K., Liu, F., et al. (2015). Insulin sensitizers improve learning and attenuate tau hyperphosphorylation and neuroinflammation in 3xTg-AD mice. *J. Neural Transm. (Vienna)* 122, 593–606. doi: 10.1007/s00702-014-1294-z

Zempel, H., Thies, E., Mandelkow, E., and Mandelkow, E. M. (2010). Abeta oligomers cause localized Ca(2+) elevation, missorting of endogenous Tau into dendrites, Tau phosphorylation, and destruction of microtubules and spines. *J. Neurosci.* 30, 11938–11950. doi: 10.1523/JNEUROSCI.2357-10.2010

Zhang, Y., Chen, C., Jiang, Y., Wang, S., Wu, X., and Wang, K. (2017). PPARγ coactivator-1α (PGC-1α) protects neuroblastoma cells against amyloid-beta (Aβ) induced cell death and neuroinflammation via NF-κB pathway. *BMC Neurosci.* 18:69. doi: 10.1186/s12868-017-0387-7

Zolezzi, J. M., Santos, M. J., Bastías-Candia, S., Pinto, C., Godoy, J. A., and Inestrosa, N. C. (2017). PPARs in the central nervous system: roles in neurodegeneration and neuroinflammation. *Biol. Rev. Camb. Philos. Soc.* 92, 2046–2069. doi: 10.1111/brv.12320

Conflict of Interest Statement: The authors declare that the research was conducted in the absence of any commercial or financial relationships that could be construed as a potential conflict of interest.

Advantages of publishing in Frontiers

OPEN ACCESS
Articles are free to read for greatest visibility and readership

FAST PUBLICATION
Around 90 days from submission to decision

HIGH QUALITY PEER-REVIEW
Rigorous, collaborative, and constructive peer-review

TRANSPARENT PEER-REVIEW
Editors and reviewers acknowledged by name on published articles

Frontiers
Avenue du Tribunal-Fédéral 34
1005 Lausanne | Switzerland

Visit us: www.frontiersin.org
Contact us: info@frontiersin.org | +41 21 510 17 00

REPRODUCIBILITY OF RESEARCH
Support open data and methods to enhance research reproducibility

DIGITAL PUBLISHING
Articles designed for optimal readership across devices

FOLLOW US
@frontiersin

IMPACT METRICS
Advanced article metrics track visibility across digital media

EXTENSIVE PROMOTION
Marketing and promotion of impactful research

LOOP RESEARCH NETWORK
Our network increases your article's readership